# UNRAVELLING EARLY TELEOST RELATIONSHIPS: DIVERSIFICATION AT THE DAWN OF THE MOST SUCCESSFUL FISH RADIATION

**Jake Atterby**

A thesis submitted to the University of Birmingham for the degree of DOCTOR OF PHILOSOPHY

Department of Earth Sciences

School of Geography, Earth and Environmental Sciences

College of Life and Environmental Sciences

University of Birmingham

June 2024

# ABSTRACT

Teleost fishes comprise more than 36,000 living vertebrate species and occupy a wide range of aquatic ecosystems. However, despite their overwhelming success, the anatomy and diversification of extinct Mesozoic taxa outside of the living radiation – stem teleosts – remain poorly understood. The teleost stem includes an abundance of charismatic Mesozoic fossil groups underpinned by centuries of study, such as pholidophorids, aspidorhynchids and pachycormids. But efforts to understand their interrelationships have been limited by several critical areas of uncertainty: key taxa allied to the stem are often omitted from phylogenetic investigations and the concealed potentially phylogenetically valuable internal anatomy of well-preserved specimens is rarely described. Consequently, there are multiple conflicting hypotheses of the phylogenetic arrangement of the teleost stem which obscures character distribution and patterns of diversification. This thesis presents comprehensive redescriptions of remarkably preserved historical specimens of iconic early neopterygian taxa using high resolution CT and synchrotron scanning. This has revealed novel anatomical insights across key taxa, including stem teleosts: *Dorsetichthys bechei* (Dorsetichthyidae) from Jurassic (Sinemurian) Lyme Regis, UK, *Richmondichthys sweeti* (Aspidorhynchidae) from the Cretaceous (Albian) Rolling Downs Group, Queensland, Australia and *Pachycormus macropterus* (Pachycormidae) from the Jurassic (Toarcian) Strawberry Bank Lagerstätte, Somerset, UK and enigmatic holostean taxa, *“Aspidorhynchus”* from the Jurassic (Bathonian) Great Oolite Group, Northamptonshire, UK. The anatomical insight obtained in this project has informed ecological inferences, new taxonomic appraisals of enigmatic specimens and a markedly strengthened phylogeny of the teleost stem and associated groups within Neopterygii.

# ACKNOWLEDGEMENTS

My sincerest thanks are extended to my supervisor, Sam Giles, for enduring me for so many years. Sam was supportive, affirming, especially during lockdown and when I was burned out. I'm immensely proud of the work we have achieved together. I must also thank Ivan Sansom and Martin Brazeau for being such kind Viva examiners. Their feedback was brutal but invaluable.

This project would have also not been possible without Zerina Johanson and Emma Bernard. As my external supervisor, Zerina's guidance and lightning-fast feedback was a godsend, and Emma, curator of fossil fishes at the NHM, made some of the most daunting aspects of this project inviting and accessible. I'd like to also mention Vincent Fernandez and Kathleen Dollman for their work at the ESRF, Matt Williams, curator at BRLSI and keeper of our beloved Strawberry Bank fishies, Graeme Lloyd and Martin Ezcurra for teaching me to run phylogenetic analyses and Matt Friedman for the torture I put him through.

I would like to thank a few lecturers at UoB for their deeply meaningful discussions and encouragement: Sarah Greene, Carl Stevenson, and Stephan Lautenschlager. I would also like to thank Yara Haridy, Donald Davesne, Omar Rafael Regalado Fernández, Jane Reeves, Paulo Brito, Erin Maxwell, and Sam Cooper for their enthusiasm, encouragement and for being a welcoming face at various conferences - basically giving me the opposite of imposter syndrome! I must also thank Dave Marshall and the rest of Palaeocast for providing me the ultimate platform to procrastinate.

I’d also love to thank my fellow staff at the Lapworth Museum: Jon, Andi, Anna, Angela and Josh were very supportive and patient while doing my corrections. Once out of this thesis’ shadow, I cannot wait to see what we accomplish together next!

I’m of course indebted to the unconditional love and support from my family: Max, Maggie, Boris, Vera, and Moira and for them fostering and encouraging my love of science and nature without which this project would have never happened.

My fondest acknowledgements belong to my found family of misfits at UoB: Andi, Anya, Chris, Emma D, Emma H, Gemma, Hazel, Iacopo, Ibrahim, JP, Jordan, Kerys, Lisa, Luke, Marie, Matt, Pam, Phil, Soph, Struan, Terri, Thomas and Richard. I adore them beyond all measure and our near-constant adventures will prove to be the most unforgettable part of my PhD. I would like to especially single out Thomas Clements, Emma Dunne, Lisa Schnetz, Andi Jones and Soph Fasey for providing a safe and supportive environment whenever needed. I owe them all the world.

# CONDEMNATIONS

I would also like to extend my sincerest condemnations to the following people, without which this thesis would have been much easier to complete:

- My landlord
- My next-door neighbour who took up the trombone during lockdown
- The guy at the Royal Society who said “women shouldn’t wear suits to conferences or else they look like staff”
- Starmer.

# ANATOMICAL TERMINOLOGY

Conventional actinopterygian terminology is used throughout to refer to skull roofing bones (i.e., Gardiner & Schaeffer, 1989; Gardiner *et al.,* 2005): frontals, parietals, intertemporals and supratemporals.

# CONTENTS

# 1. INTRODUCTION AND LITERATURE REVIEW

## 1.1 Introduction

Teleost fishes are the most species-rich vertebrate assemblage on the planet, with over 30,000 species of teleost fishes known worldwide. They inhabit a plethora of aquatic ecosystems from terrestrial swamplands to the deep abyssal plane and display an exceptionally disparate range of specialised body plans. They include iconic fishes, such as seahorses, pufferfishes, and anglerfishes, as well as some of the most commercially valuable groups, such as cod, tuna, and mackerel. However, despite the ubiquity, exceptional diversity, and critical ecological and economic value of living teleosts, the evolution of teleosts outside of the living radiation (e.g., Cavin, 2008; Clarke et al., 2016) are scarce and contradictory – especially when compared to their lobe-finned counterparts and other vertebrates (Sallan, 2014).

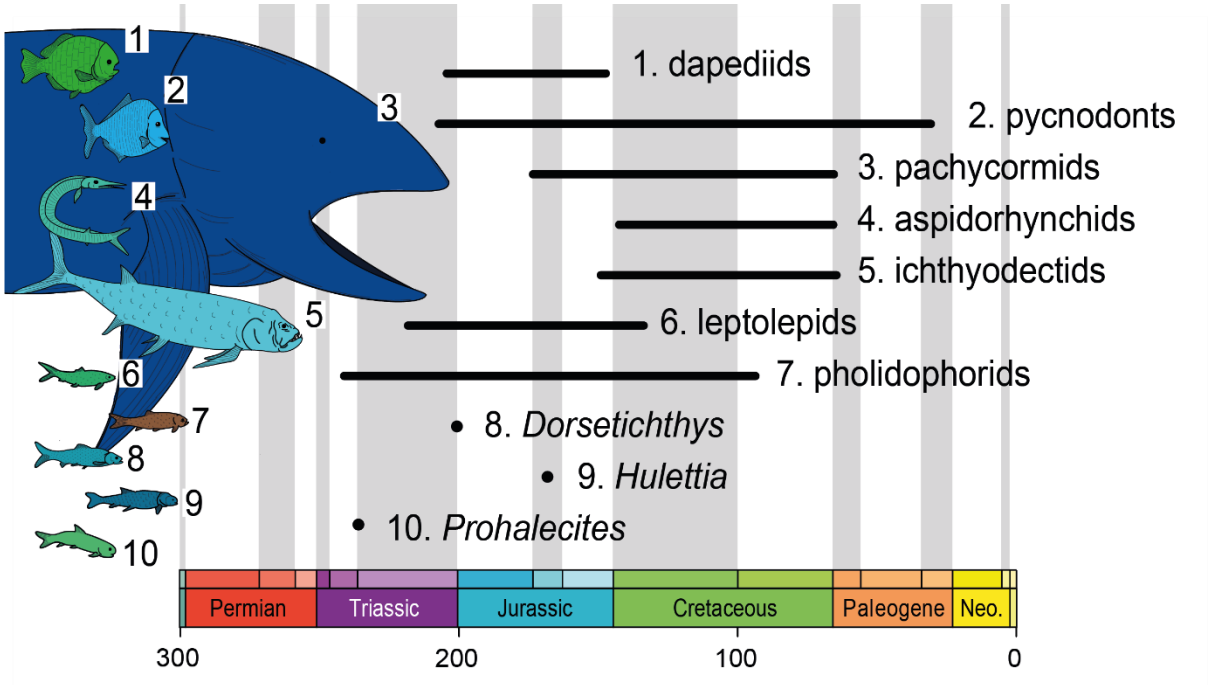


**Figure 1.1: Illustrated examples of taxonomic assemblages associated with the teleost stem and their temporal ranges.** Circles indicate taxa with a single occurrence. Outline 5 from Bogdanov, 2008.

Over the last 150 years, a broad range of extinct groups have been associated with the teleost stem (Fig. 1.1), many of which are represented by exceptionally preserved, three dimensional fossils with compelling morphologies (Fig. 1.2). Fossil taxa associated with the teleost stem include: dapediids and pycnodonts – deep bodied predators known for their unique, rounded teeth adapted for crushing shelled prey; pachycormids – a diverse assemblage of marine fishes most famous for converging on gigantism and suspension feeding; aspidorhynchids - agile and elongate fishes with sharp marlin-like rostrals; ichthyodectids – a disparate range of fanged marine predators*;* pholidophorids and leptolepids – superficially similar to modern herrings; as well as several enigmatic and monotypic genera, such as *Dorsetichthys, Hulettia* and *Prohalecites.* Each of these groups have at one time been resolved on the teleost stem, but their exact placement of each of these groups on the stem remains uncertain.

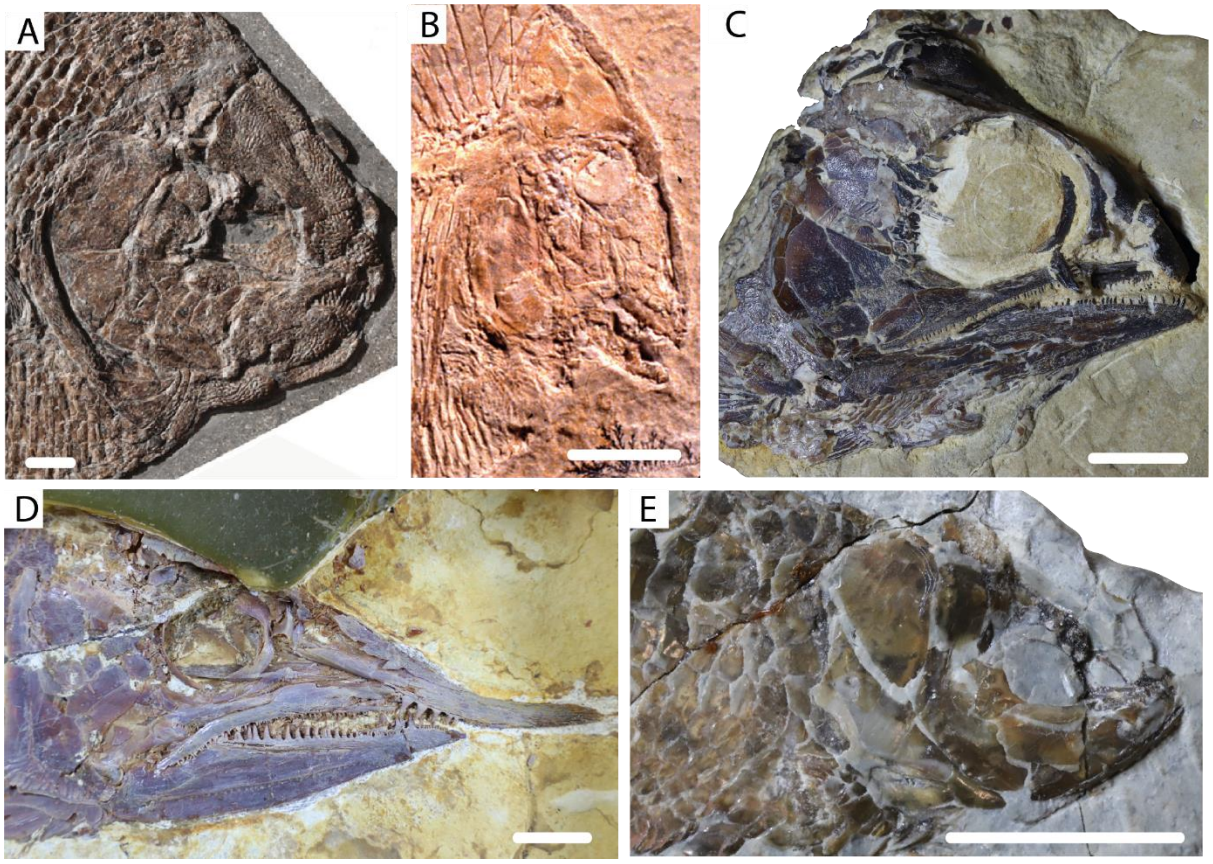

**Figure 1.2: Exceptionally preserved fossils associated with the teleost stem.** (A) *Dapedium pholidotum* UUH 5, (Thies & Waschkewitz, 2016). (B) Turbomesodon relegans NHMUK PV P. 5546, a pycnodont from the Tithonian Lithographic Limestone, Solnholfen Formation, Germany (Poato-Ariza, 2015); (C) *Pachycormus curtus* NHMUK PV 32434, a pachycormid from the Rhaetian Upper Lias Group, France. (D). *Aspidorhynchus acutirostris* NHMUK PV P 973, an aspidorhynchid from the Tithonian Lithographic Limestone, Solnholfen Formation, Germany (image flipped horizontally). (E) *Pholidophorus higginsi* NHMUK PV P 578 from the Rhaetian stromatolitic limestone, Penarth Group, England (image flipped horizontally). Scale = 10 mm.

Despite their record of charismatic fossils, there is a very limited grasp on the anatomy and relationships of these fishes. Perhaps, as only a handful of potential stem teleosts have undergone x-ray imaging, descriptions of potentially phylogenetically significant internal morphology such as the braincase and inner ear, as well as the hyoid arch and gill skeleton (Giles *et al.*, 2015, 2017, 2018; Latimer & Giles, 2018) are lacking relative to the more readily accessible elements of the dermal skeleton. Important, potentially valuable grouping information may not be being captured by existing studies.

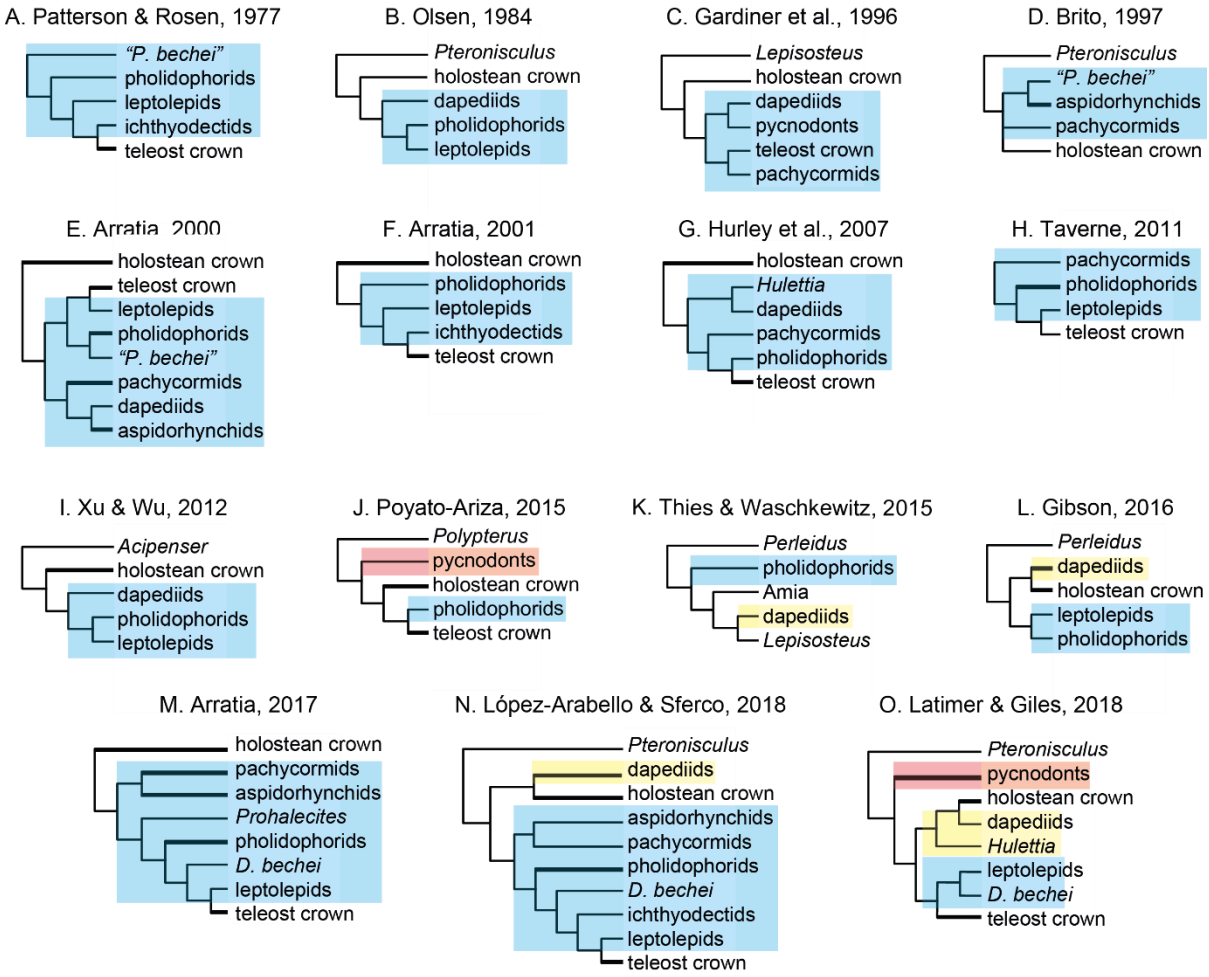


**Figure 1.3: Simplified hypotheses of neopterygian phylogenetic relationships.** Taxa recovered on the teleost stem are highlighted in blue; taxa recovered on the holostean stem are highlighted in yellow; taxa recovered on the neopterygian stem are highlighted in red. Bold lines identify where multiple nodes have been condensed into a single terminal.

These issues have culminated in many conflicting and inconsistent hypotheses for the phylogenetic relationships for taxa associated with the teleost stem. Over the course of the last century, key fossil groups have been resolved in varying positions on the teleost stem, holostean stem, and even occasionally rendered outside crown Neopterygii entirely (Fig. 1.3). Furthermore, existing phylogenetic analyses often do not incorporate the full breadth of potential stem teleost taxa. In addition to relying on a limited anatomical dataset, many analyses focus solely on a single group

(e.g., Poyato-Ariza & Wenz, 2002, Poyato-Ariza 2015; Alvarado-Ortega, 2005; Friedman, 2012), represent entire assemblages with just one specimen (e.g., Hurley *et al.*, 2007; López-Arbarello & Sferco, 2018), use inappropriate outgroups, including the controversial usage of hypothetical outgroups (e.g., Alvarado-Ortega, 2005). Ultimately, there little consensus as to the broad topology of the teleost stem.

Clarifying the interrelationships of the teleost stem is important to understanding the origins of one half of all vertebrate species. Early Teleostei underwent exceptional periods of diversification during the Mesozoic, acquiring a vast array of body plans and innovative feeding mechanisms – seemingly very rapidly (Clarke & Friedman, 2018). However, a lack of consensus as to their interrelationships undercuts investigations into the acquisition of key characters and rates of diversification and speciation, the intrinsic and extrinsic drivers underpinning their radiation, and even the ability to quantify loss and recovery across mass extinctions or the potential role played by teleosts in major faunal turnovers. There is a significant gap in the literature that needs addressing with an improved anatomical investigation and phylogenetic analysis of key taxa associated with the teleosts stem. This chapter reviews the history and current state of stem teleost research, highlighting critical issues and ambiguity in the study of taxa previously allied to the stem.

## 1.2 Wider Diversity Within Living Actinopterygii

### 1.2.1. Actinopterygian Interrelationships

Less than 0.2% of living actinopterygian diversity are non-teleosts: Cladistia, Chondrostei and Holostei. Cladistia, the extant sister group of all other ray-finned fishes (Actinopteri), includes living Polypteriformes (bichirs and ropefish), Actinopteri encompasses Neopterygii and their sister group; the Chondrostei. Chondrosteans are

predominantly cartilaginous, comprising 27 species of Acipenseridae (sturgeons) and as of 2020, only one living species of Polyodontidae (paddlefishes) (Zhang *et al.*, 2020). Finally, holosteans form the small sister group to the vast Teleostei. Comprising just seven species of Lepisosteiformes (garfishes) and a sole survivor of the Amiiformes (bowfins), holosteans are a miniscule proportion of modern neopterygian diversity and their importance is often overlooked (Friedman, 2015).

The interrelationships within Neoptergyii, i.e., the arrangement of Amiiformes and Ginglymodi (Lepisosteiformes) relative to Teleostei has been frequently reworked following changes in attitudes and methods in phylogenetics. Historically, fossil neopterygians were only considered transitional “grades” (e.g., Berg, 1940; Schaeffer, 1955). Today, clades are defined by shared characters in a phylogenetic tree. However, prior to the popular use of cladistics, organisms with shared morphologies in a non-phylogenetic context were considered “grades”. The term “grade” has fallen out of formal use as cladistics provide more precise language (Benton, 2000).

Nelson (1969) originally united bowfins and gars under Holostei as the sister group to Teleostei as they are today, but in 1973, Patterson founded the Halecostomi – a new grouping of bowfin and teleosts to the exclusion of gars. This new model was very well supported, and for several decades while popular with many authors (e.g., Schaeffer & Patterson, 1984; Gardiner *et al.,* 1996) it was contested by others (e.g., Grande & Bemis, 1998; Arratia, 2001). Olsen (1984) and Olsen & McCune (1991) proposed an alternative model – a sister relationship between teleosts and gars based on one supporting character: single jaw articulation due to the detachment of the symplectic from the jaw joint – but this hypothesis was largely dismissed (as reviewed by Friedman, 2015). It was not until Grande (2010) reassessed all fossil and extant Ginglymodi that significant support was found to reunite gars and bowfin under

Holostei on the basis of 13 morphological characters, restoring Nelson's (1969a) model. Furthermore, the widespread use of molecular analyses (e.g., Venkatesh *et al.,* 2001; Inoue *et al.,* 2003; Meyer & Zardoya, 2003; Kikugawa *et al.,* 2004; Hurley *et al.,* 2007) has provided further support for a sister relationship between gars and bowfins to the exclusion of teleosts.

To summarise, the current state of living actinopterygian taxonomy pits the hyper diverse Teleostei alongside its relatively depauperate sister groups. While the species richness of living actinopterygian groups has potentially swayed how their evolution has been perceived, after decades of controversy the broad arrangement of living Actinopterygii has reached a consensus.

### 1.2.2 Teleost Interrelationships, Evolutionary Origins and Successes

Much like Actinopterygii as a whole, crown teleosts are also taxonomically imbalanced. The wealth of teleost diversity, disparity and species richness is confined to Ostariophysi and Acanthomorpha. Acanthomorpha (spiny-rayed fishes) contains almost 17,000 species – approximately one third of all living vertebrates (Friedman, 2010; Eschmeyer & Fricke, 2012) and include the exceptionally diverse Percormopha (Near *et al.*, 2012; Betancur-R *et al.,* 2013). Once described as 'the (cladistic) bush at the top of the tree' by Nelson (1989: pg. 326), percomorphs include a range of disparate taxa, including Tetraodontiformes (pufferfishes and sunfishes), Lophiiformes (anglerfishes), Pleuronectiformes (flatfishes) and Syngnathiformes (seahorses), the majority of which first emerged in the Late Cretaceous and proliferated in the Paleogene. Although the interrelationships of living teleosts are relatively uncontested, the same cannot be said for the extinct members of the teleost stem. It is broadly understood that stem teleost fishes first emerged in the early Triassic and subsequently radiated throughout the Jurassic (Arratia, 1996; Santini *et al*., 2009).

The remarkably species rich living teleosts would suggest that their early radiation was a period of rapid diversification and speciation, especially when compared to their depauperate sister group – living holosteans. The vast gulf in species richness between teleosts and holosteans has been the subject of debate for many decades, and several explanations have been put forwards to explain how teleosts achieved their modern-day diversity and morphological disparity.

For instance, Whole Genome Duplication (WGD) is widely implicated as the main driving factor in the Mesozoic radiation of teleosts (Wittbrodt *et al.,* 1998; Van de Peer *et al.*, 2003; Hoegg *et al.*, 2004; Meyer & Ven de Peer, 2005; Glasauer & Neuhauss, 2014), with an assumption that the initial teleost WGD event occurred shortly after their divergence from Holostei (Amores *et al.*, 1998), and that subsequent WGD events occurred throughout the teleost lineage, e.g., in the Order Salmonidae (Macqueen & Johnston, 2014). Given that the first teleost WGD occurred in extinct fossil fishes, evidence of it occurring has only recently been physically detected in the fossil record. Davesne *et al.* (2021) found that the volume of osteocyte cavities increased in the earliest stem teleosts, likely corresponding to an increased genome size – a timing decoupled from the explosive diversification of teleosts and the acquisition of important characters, such as the mobile premaxilla, which likely aided their successes. This strongly suggests that WGD was not a direct factor behind teleost diversification. It has also been argued that teleosts underwent a more steady, stepwise acquisition of functional characters instead (Near *et al.*, 2014).

While living fishes may be an important proxy for the ecology and biomechanics of fossil fishes, the current makeup of actinopterygian biodiversity does not reflect their evolutionary history. This is complicated further when teleosts are compared to holosteans and other actinopterygians. Combined with their seemingly “primitive”

appearance, Recent Holostei are frequently referred to as “living fossils” (e.g., Wiley & Schultze, 1984). The term “living fossil” was coined by Darwin (1859) to refer to lineages that appear to have undergone comparatively little to no change since their origin in deep time. The term is often regarded as problematic and outdated due to its ambiguity and subjectivity (Werth & Shear, 2014; Lidgard & Love, 2021), as well as the term’s history of being misappropriated in scientific racism (Martin, 2019; Kuljian, 2024). However, recent work by Rosindell *et al.* (2024) has demonstrated that a given taxon’s “living-fossil-ness” may be quantifiable and therefore have merit. It is now understood that despite their relatively low diversity and perception as a “living fossil”, Holostei had already achieved similar if not greater levels of disparity and diversity as Teleostei by the early Mesozoic (Clarke *et al*., 2016). In addition, species-poor lineages such as Acipenserformes (sturgeons) have also undergone WGD (Havelka *et al.*, 2013; Redmond *et al.*, 2023), despite a lack of diversity today. The notion that rapid diversification can only occur as result of WGD does not hold up given the available evidence (Clarke *et al.*, 2016), but rapid speciation events are still likely to have occurred in the teleost lineage through the acquisition of uniquely innovative morphologies, such as protrusible jaws and pharyngeal jaws (Collazo *et al.,* 1994; Collazo, 1996). This exceptional adaptability still enabled teleosts to occupy ecological niches and feeding strategies that were otherwise out of reach for other assemblages extremely rapidly, but it does not convey the full picture.

### 1.2.3 Defining Teleostei

Comparing historic studies of fossil taxa with more recent work is difficult without first highlighting that the understanding of evolution has changed over time. Though the theory of evolution is almost 200 years old, phylogenetic concepts such as stem and crown groups (Abel, 1914) only became popular in recent decades (see

Willman, 2003). The history of teleost research predates the invention of cladistics and evolutionary theory, and living and fossil teleosts were studied completely separately for decades. As a result, there have been several conflicting methods of defining Teleostei, with the most fundamental differences arising from the methods in which phylogenetic taxa are defined:

1. An apomorphy-based approach defines a clade by the presence of one or more shared characters. Taxa in which the apomorphy is present are considered to fall within the clade.

2. A taxon-based or node-based approach defines a clade by determining the earliest diverging member of a group and including within the clade all taxa that branch above the chosen taxon.

3. A crown/stem group-based approach is similar to a node-based approach and defines clades relative to living relationships. Taxa that fall within the living radiation form the crown group, and any taxa that are more closely related to the living radiation than another living radiation are placed on the stem. Collectively, the crown and stem are referred to as the total-group (Sereno, 2005).

As a result of these contrasting approaches, even the definition of what constitutes a teleost has changed over time, leading to taxonomic and nomenclatural confusion. Many authors such as Berg (1940), Greenwood *et al.* (1966, 1973), Nelson (1969a) and Grande (2010) neglected to define Teleostei entirely (as reviewed by Sallan, 2014).

The earliest defined diagnosis of Teleostei by Müller, 1845 was generally unhelpful to palaeontologists, as Müller neglected to consider fossilised taxa. The definition relies purely on soft tissue anatomy, i.e., the optic chiasma, heart valves,

pseudobranch, swimbladder, spiral valve and genital duct. As these features are very unlikely to be retained in the fossil record, it has no application for the overwhelming majority of extinct taxa.

Foundational work by Patterson (1973, 1975, 1977) set in motion the first monophyletic definition of Teleostei through an apomorphy-based approach, establishing a set of anatomical characters with which to assess membership of the clade: caudal uroneurals, seven epurals, a mobile premaxilla separate from the rostral, a parasphenoid bearing a foramen for the internal carotid, and fusion between the propterygium and primary pectoral lepidotrichium. Patterson's seminal papers were among the earliest studies to incorporate both living and fossil teleost taxa. The novelty of introducing fossils to biologists is clear throughout, with Patterson often writing short asides reminding unfamiliar readers about the ordeals of studying incompletely preserved fossil specimens (e.g., Patterson & Rosen, 1977; p.86). Despite this radical leap in stem teleost research, Patterson was most interested in anatomy, and less so relationships and patterns of divergence.

It was not until de Pinna (1996) that a stem-based approach to defining Teleostei was introduced, in which Teleostei were determined by the last common ancestor of the total-group, excluding the now obsolete Halecomorphi and/or Ginglymodi, due to the uncertainty of teleostean synapomorphies. Here, de Pinna also redefined the living teleost crown (osteoglossomorphs, elopomorphs, clupeomorphs and euteleosts) as a monophyletic clade called Teleocephala. In response, Arratia (1999, 2001) attempted to reconcile the Teleostei total group - both the apomorphy defined crown taxa (true teleosts) as well as extinct stem-defined taxa - as Teleosteomorpha. However, Teleosteomorpha is functionally the same as Teleostei *sensu* Patterson & Rosen (1977) and de Pinna (1996). Today, the interrelationships of

the teleost crown are fairly settled, however, the arrangement of fossil taxa recovered as belonging to the teleost stem is highly contentious.

## 1.3 Debated taxa associated with the teleost stem

Throughout the last 150 years of teleost research, numerous fossil taxa have been proposed as belonging to the teleost stem but their phylogenetic position is in fact unsettled and debated. Some groups have been consistently recovered on the teleost stem, but their exact position is variable, such as pachycormids, pholidophorids, aspidorhynchids, *Dorsetichthys* and *Prohalecites.* Other taxa have been occasionally resolved as stem teleosts, though they have also been recovered outside the teleost stem, such as dapediids, pycnodonts and *Hulettia.* And some groups have been assigned to both the crown and stem teleost radiations, such as ichthyodectids and leptolepids. These ongoing disagreements contribute to the teleost stem being poorly resolved.

The earliest descriptions of fossil taxa allied with the teleost stem date back to the late 19$^{th}$ century (e.g., Woodward, 1890, 1895, 1896) and are based primarily on external morphology. Over time, these early investigations were followed by descriptions of new taxa, redescriptions of existing taxa and major taxonomic revisions (e.g., Berg, 1940; Gardiner, 1960; Lehmen, 1966; Patterson, 1973, 1975, 1977; Patterson & Rosen, 1977; Olsen 1984; Arratia, 1999, 2000, 2001, 2013). There is also a long history of anatomical investigations of the braincase and endocast, including thorough descriptions of acid prepared (e.g., Patterson, 1975) and mechanically prepared (e.g., Rayner, 1948) crania, revealing that they contain phylogenetically informative characters. Despite this potential, relatively few CT-based investigations have been carried out on early teleost fossils. It may be that an often-incomplete

understanding of the anatomy of fossil taxa associated with the teleost stem has contributed to a lack of phylogenetic stability.

The history of the phylogenetic debates over key groups previously allied to the teleost stem are outlined below. These taxa represent ideal targets for new improved morphological description and phylogenetic analysis.

**Dapediids:** Dapediids occupied a range of marine and freshwater ecosystems from the late Triassic (Rhaetian) to the late Jurassic (Tithonian) (Lombardo & Tintori, 2005; Szabó & Pálfy, 2020), and are known from fossil localities in North America, Europe, and India. Despite their relatively short temporal range of ~30 million years, at least twenty species have been erected since the discovery of *Dapedium politum* (Leach, 1822), thirteen of which belong to the type genus *Dapedium*. Dapediids are most recognisable for their heterodont dentition and muscular jaws being adapted towards durophagy, i.e., they are equipped to capture, crush, and consume armoured prey such as shelled molluscs, echinoderms and certain arthropods (Thies & Hauff, 2011). This series of adaptions likely enabled their successful radiation following the End-Triassic Extinction, in which prior durophageous ecological niches were suddenly emptied (Smithwick, 2015).

Despite nearly two centuries of research, there is still no consensus on the phylogenetic placement of dapediids. *Dapedium* was originally considered a “semionotid” (Woodward, 1890, 1895) on the basis of four characters, including the deeply fusiform trunk, tritural or styliform teeth and a dorsal fin longer than half the trunk length. At this time, “semionotids” were another example of an evolutionary grade united by simple morphological features like ganoid scales. Today, “semionotids” are best characterised as a paraphyletic, taxonomic wastebasket of early neopterygians

(López-Arbarello & Sferco, 2011; Latimer & Giles, 2018). Their much-needed revision is beyond the scope of this thesis. Lehmen (1966) believed that the deep, circular body of *Dapedium* was morphologically distinct from other "semionotids" to relocate *Dapedium* into its own family – Dapediidae, which was soon adopted by Wenz (1968) and later by Thies & Hauf (2008, 2011). However, Woodward's initial "semionotid" classification maintained some popularity with both Patterson (1973), Tintori & Renesto (1983) and even tentatively as late as López-Arbarello (2012).

*Dapedium* has most frequently been resolved as a stem teleost, initially by Gardiner (1960) and Olsen (1984). Olsen recovered *Dapedium* as the sister taxon to all other teleosts, represented in his analysis only by *Leptolepis* and "*Pholidophorus" bechei,* on the basis of two characters: the internal carotids piercing the parasphenoid and the presence of a median vomer. Gardiner *et al.* (1996) also recovered *Dapedium* as a stem teleost, specifically in a clade alongside *Microdon* (a now invalid pycnodont genus), as supported by six characters, including a curved medial process of the maxilla, a parasphenoid both lacking teeth and contacting the aortic canal, a reduced maxillary tooth row and ridge scales along the dorsal and ventral margins. Dapediids were resolved as stem teleosts by Xu & Wu (2012) – again as sister to *Leptolepis* and "*P. bechei"* and Arratia (1999, 2004, 2013) also proposed a teleost affinity, recovering *Dapedium* in a clade alongside pachycormids. Finally, Giles *et al.* (2017) recovered Dapedidae (represented by *D. pholidotum* and *D. sp.)* as stem teleosts, forming a sister group to a clade containing *Dorsetichthys* on the basis of four characters; a single coronoid, elongate olfactory tracts, the optic lobe being larger than the telencephalon and that the lateral cranial connecting to the cranial cavity anteriorly.

However, a holostean affinity has also been repeatedly suggested for dapediids. Bermúdez-Rochas & Poyato-Ariza (2015) recovered a close sister

relationship between *Dapedium* and Ginglymodi; Thies & Waschkewitz (2015 found comparable results on the basis of four synapomorphies, including the forward extension of the exoccipital around the vagus nerve, the presence of an independent splint-like quadrojugal and a “scale-like” ray at the caudal fin dorsal margin; and Gibson (2016) resolved *Dapedium* and Ginglymodi as sister groups, also based on four synapomorphies, here including a subopercular less than half the depth of the operculum, the presence of a dorsal ridge of scales and again the splint-like quadratojugal. Most recently, López-Arbarello & Sferco (2018) resolved dapediids as stem holosteans on the basis of 15 synapomorphies, and Latimer & Giles (2018) corroborated this position when with an expanded taxon and character list, recovering the same placement with five characters, including the presence of two infradentaries, an anterodorsal process of subopercular, and a parasphenoid with multifid anterior margin.

In summary, the position of *Dapedium* remains controversial, with no consensus to support its monophyly or confirm its affinity with either Teleostei or Holostei. This lack of clarity may be the result of the myriad issues associated with stem teleost research, in this instance using only a composite *Dapedium* genus as a stand in for the entire group. On the other hand, character information regarding internal anatomy is also extremely limited for dapediids, as due to their deep bodies they are typically preserved as laterally compressed, two dimensional fossils (Latimer & Giles, 2018) and their heavily ornamented skulls tend to obscure useful internal characters. Perhaps further investigation into dapediid internal morphology could strengthen support for either phylogenetic placement, but as it stands their position with Neopterygii is unclear.

**Pycnodonts:** Pycnodonts spanned a vast temporal range of ~175 million years; from the Late Triassic (Norian) to the late Eocene (Priabonian) (Voss *et al.,* 2019). They first appeared in the western Tethys and subsequently proliferated almost globally, with fossils found in Asia, North and South America, Western Europe and Africa. Consisting of at least 30 genera, pycnodonts generally possess deep, circular bodies, heterodontous dentition and powerful jaws specially adapted towards durophagy (Kriwet, 2005). However, throughout the Mesozoic, pycnodonts rose to inhabit a wide range of marine, brackish and freshwater ecosystems through a surprising range of body plans. Though they are most well known for being associated with shallow reefs, possessing similar morphological features to modern reef fishes (i.e., manoeuvrable, laterally compressed/ rounded bodies with posteriorly placed dorsal and anal fins), other morphologies were present, including the piranha-like *Piranhamesodon pinnatomus* (Kölbl-Ebert, *et al.*, 2018).

Since Berg (1940) first formally classified the Order Pycnodontiformes as actinopterygians, alongside Aspidorhynchiformes and Pachycormiformes, the phylogenetic position of pycnodonts has varied wildly. Again, it remains unclear whether they are more closely associated with teleosts, holosteans or neither. Pycnodonts were initially found to be closely affiliated with Holostei by Arambourg (1954) and Gardiner (1960). At one stage, it was even suggested that they were more closely related to chondrosteans as opposed to neopterygians (McAllister, 1968). However, once Holostei was temporarily disbanded by Patterson (1973), their phylogenetic position was brought further into question. For several decades, they were considered Neopterygii *incertae sedis.*

Nursall (1996a) was the first to propose that pycnodonts were stem teleosts, but this was not fully supported with a cladistic analysis. Furthermore, while

subsequent studies (e.g., Nursall, 2010) arrived at the same conclusion - only now employing Arratia's (1999) Teleosteomorpha and Pycnodontomorpha, they were again not supported by a cladistic analysis, instead relying on a list of 'ad hoc characters' (Poyato-Ariza, 2015, pg. 300) on a hand-drawn tree. Pycnodonts are rarely included in broader, more exhaustive analyses, with the majority of recent pycnodont studies being expressly focused on genus-level interrelationships within Pycnodontidae and not their position within Actinopterygii (e.g., Kriwet, 2004). The most comprehensive cladistic approach in attempting to reconcile the position of pycnodonts was by Poyato-Ariza (2015), which recovered the novel hypothesis of pycnodonts as stem neopterygians. He argued that apparent similarities between pycnodonts and teleosts – or holosteans – were the result of convergent evolution, and they diverged separately from either group. Subsequently, Latimer & Giles (2018) also resolved pycnodonts as a clade of stem neopterygians, again with the argument that analyses of pycnodont relationships are vulnerable to the effects of convergence, particularly with other deep bodied fishes.

Pycnodont monophyly is exceptionally well supported (Nursall, 1996b; Poyato-Ariza *et al*., 1998; Kriwet, 2000, Poyato-Ariza & Wenz, 2002, 2005, 2015; Kriwet, 2004; Martin-Abad & Poyato-Ariza, 2013, 2015, Ebert & Kölbl-Ebert, 2018). However, there are a host of other issues that limit the potential to better understand their phylogenetic placement. Firstly, they share a similar preservational bias to dapediids, in that knowledge of their internal anatomy is reduced on account of them most often being flattened. Taxa that are known from endoskeletal remains, such as acid-prepared specimens from the Santana Formation Konservat Lagerstätten – (e.g., Brito & Yabumoto, 2011), tend to be nested within the radiation and of limited use in resolving relationships to non-pycnodont outgroups; despite this, they are the terminals most

commonly employed in wider investigations of neopterygian relationships (e.g., *Mesturus*: Hurley *et al.*, 2007; Grande, 2010; and the now invalid *Microdon*: Gardiner *et al.*, 1996). Similarly, despite their long temporal range, very little is understood about the earliest pycnodonts: early- to mid-Jurassic members of this group are known only from partially preserved jaws and isolated teeth (Stumpf *et al.*, 2017).

**Pachycormids:** Pachycormids are a highly speciose assemblage of marine neopterygians, with a temporal range spanning from the early Jurassic (Toarcian) to the late Cretaceous (Maastrichtian; Friedman *et al.*, 2012). Over a dozen genera are formally recognised (Cooper *et al*., 2022), many of which from well-preserved, articulated specimens from renowned Lagerstätten such as the Posidonia Shale (Hauff 1953) and Strawberry Bank (Cawley *et al.*, 2019). Pachycormids occupied a range of ecological niches, with most genera exhibiting dentition consistent with generalist and hyper-carnivorous diets. However, they are most well-known for the iconic giant pachycormids. The largest pachycormid, *Leedsichthys problematicus*, is estimated to have had a maximum body length of 10-12 m (Liston *et al.*, 2013), making it the largest known bony fish to have ever lived. Their large body size, elaborate gill rakers and absence of teeth indicate that giant pachycormids were most likely planktivorous suspension feeders (Friedman, 2010).

Traditionally, pachycormids, as well as all “ganoid” fishes, were thought of as “holosteans” (e.g., Regan, 1923; Rayner, 1941), although use of this term reflected a temporal grade rather than association with the extant holostean radiation. Gardiner (1960) and Lehman (1966) both reported pachycormids, alongside macrosemiids, as a group of highly specialised Amiiformes based on similarities in the shape of the skull, specifically the parasphenoid. However, Patterson (1977) and Patterson & Rosen (1977) both considered the Order Pachycormiforms a group of stem teleosts and

potentially the earliest diverging teleost group, based on the presence of uroneurals. Since 1977, they have been cautiously considered stem teleosts (Gardiner *et al.*, 1996; Arratia & Lambers, 1996; Arratia, 2004; 2013; Kear, 2007; Cawley *et al.*, 2019; Dobson *et al.* 2021), although their placement as the earliest diverging group was countered by Arratia (1999, 2000), who argued that "*Pholidophorus" bechei* was the earliest diverging taxon on the teleost stem. Taverne (2011) reproposed Patterson's original position, but this manual analysis was criticised for its inappropriate characters (Arratia, 2013). Most recently, Arratia (2013, 2017), López-Arbarello & Sferco (2018) and Gouiric-Cavalli & Arratia (2022) recovered pachycormids in a clade alongside aspidorhynchids, as the sister group to all other teleosts.

Pachycormid relationships have confounded researchers for centuries. Although this is due in part to the broad ecological range and morphological disparity displayed by the group, they are consistently represented by just one taxon, *Pachycormus macropterus*, in many analyses. Another unusual issue is that charismatic giant pachycormids like *Leedsichthys* and *Bonnerichthys* have come to be used as a proxy for pachycormids as a whole. Due to their titanic size and weakly ossified skeletons, giant pachycormids easily suffer from disarticulation, hindering their identification: the earliest giant pachycormid discovery, consisting of large plate-like bones, was initially ascribed to a stegosaur (Hulke, 1887) an issue which has reoccurred in surprisingly recent literature (Michelis *et al*., 1996). As a result, there is a scarcity of fossil material suitable for sufficient description and cladistic analysis, giving the sense that giant pachycormids are exceptionally enigmatic. Furthermore, there is yet to be an investigation of the internal anatomy of pachycormids via CT or synchrotron scanning. With the exception of unpublished work by Dobson (2019),

most descriptions are based on externally visible features (Gouiric-Cavalli & Arratia, 2022; Cooper & Maxwell, 2023). Without a complete character set, only a partial insight into their anatomy and ecology is possible and systematic approaches to their phylogeny are limited (Cawley *et al.*, 2019; Dobson *et al.*, 2021).

**Aspidorhynchids:** Aspidorhynchids were first identified by Nicholson & Lydekker (1889). They are a long-ranging assemblage of fishes, with an approximate temporal range of 100 million years, from the late Jurassic (Tithonian) to the late Cretaceous (Maastrichtian), perhaps even the late Palaeocene (Tiffian; Maisey, 1991; Vranken *et al.*, 2019). Today they consist of six genera, however it is unclear how many genera are still valid, as numerous species of *Belonostomus* have since been referred to other groups, such as *Richmondichthys* (Bartholomai, 2004). Aspidorhynchid fossils are staples of the Solnhofen Lägerstatte (late Kimmeridgian to early Tithonian), forming exceptionally well preserved, laterally compressed specimens along the thinly bedded laminae or “plattenkalks” of the lagoonal limestone (López-Arbarello & Schröder, 2014). Aspidorhynchids are also known from France, Italy, Russia, Uzbekistan and North America, including Alberta, North Dakota, Montana and Wyoming. They are characterised by their elongated bodies; most notably with an extended dermethmoid forming a long, snout-like rostral.

Aspidorhynchids have also undergone frequent revision, and though their monophyly is well supported (Brito, 1997; Arratia, 2013), their position within Neopterygii is poorly understood. Traditionally they were considered “holosteans” and assumed to be closely related to Leptolepiformes (modern gars and their kin, e.g., Reis, 1887; Woodward, 1895; Goodrich, 1930). This was unsurprisingly on account of their superficial resemblance to modern alligator gars, i.e., their elongate snouts and sharp, conical teeth. However, they continued to be considered “holosteans”, on

account of their ganoid scales, alongside other groups such as pachycormids (e.g., Danil'chenko, 1967), for several decades (Gouiric-Cavalli, 2016). Though this arrangement is rarely supported in more recent literature, features of the bony labyrinth still point to a holostean affinity for aspidorhynchids (Giles *et al.,* 2018), although this hypothesis is yet to be tested in a phylogenetic context.

Like many taxa in this review, aspidorhynchids were first considered as early diverging teleosts by Patterson (1973, 1977) and Patterson & Rosen (1977). This was on the basis of three morphological characters: modified ural neural arches, propterygium fused with first pectoral ray, and four pectoral radials. Recent phylogenetic analyses continued to find support for aspidorhynchids as stem teleosts, for instance Brito (1997) recovered a clade of *Aspidorhynchus, Belonostomus* and *Vinctifer* as sister to a polytomy of *Ichthyokentema, "Pholidophorus" bechei* and *Leptolepis* based on the absence of a quadratojugal. Arratia (2013, 2017) resolved *Aspidorhynchus* as sister to pachycormids, most recently based on 13 homoplasies, including the presence of one supraorbital bone, the lack of a coronoid process of the lower jaw and modified preural neural arches.

Issues common to the study of stem teleosts also plague aspidorhynchids. Jurassic taxa are particularly poorly preserved; very little to no research has been carried out on their internal anatomy or postcranial skeleton (Gouiric-Cavalli, 2016); and the clade is frequently reduced to a single terminal – *Aspidorhynchus* – in many phylogenetic analyses. There have also been no investigations into the internal anatomy of aspidorhynchids via CT or synchrotron scanning.

**Ichthyodectids:** Ichthyodectids are a family of typically large-bodied fishes known from the middle Jurassic to the late Cretaceous (Crook, 1892) and potentially

early Palaeocene (Boles *et al*., 2024). By the end of the Mesozoic, ichthyodectids had achieved a near-global distribution with marine and estuarine fossil material known across Africa, North America, Antarctica, eastern Asia, Europe and Lebanon (Alvarado-Ortega & Brito, 2010), as well as freshwater examples in South America (Maisey, 1996, 2000). Roughly 50 species have been described, the largest of which being the charismatic, 5m long predator *Xiphactinus* (Vavrek *et al.*, 2014), however almost 50% of ichthyodectid species are based entirely on isolated scales and jaws and are therefore of some uncertain validity (Cavin *et al.*, 2013).

Unlike many other taxa now allied with the teleost stem, several species of ichthyodectids were initially placed in what is now considered Crown Group Teleostei, including living groups such as Clupeiformes (Heckel, 1849. Patterson (1977) and Patterson & Rosen (1977) were the first to confirm the monophyly of ichthyodetids and place them outside of the crown group on the teleosts stem. Subsequently, Taverne (1975), Lauder & Liem (1983) and Arratia (2000) also recovered ichthyodectids as the immediate sister group to crown teleosts. Arratia's (2000) morphological support for this included the absence of a middle pit line groove crossing the dermopterotic, a notch in the dentary dorsal ascending margin, and relatively many epipleural intermuscular bones in the anterior caudal region. This interpretation of ichthyodectid taxonomy is widely accepted throughout the literature (e.g., Alvarado-Ortega & Brito, 2010; Cavin & Berrell, 2019).

Many ichthyodectids are very poorly represented in the fossil record. Their fossils are rarely articulated (Alvarado-Ortega & Brito, 2010) and several genera are known entirely on isolated vertebrae, teeth and scales (Cavin *et al*., 2013). Consequently, understanding of their anatomy is incomplete. Given that they are

frequently resolved proximate to the teleost crown, a better understanding of their position on the stem is key.

**Leptolepids:** Leptolepididae (also spelled Leptolepidae, e.g., Nelson, 2006 and Arratia, 2017) was erected by Nicholson & Lydekker (1889) to contain *Leptolepis bronni.* However, it has since served as a wastebasket taxon, and now encompasses a paraphyletic assemblage of over a dozen stem teleost fishes from the mid Triassic to the early Cretaceous, some of which are very poorly characterised, with fossils known from Europe, Chile and Antarctica (Arratia & Hikuroa, 2010). While most *Leptolepis* fossil material consists primarily of isolated teeth and scales, many articulated specimens are known from the Wealden Supergroup (Ross & Cook, 1995) and isolated otoliths have also been ascribed to *Leptolepis*, providing evidence of ontogenetic variation (Flannery-Sutherland, 2017).

Bronn (1830) was the first to describe the type taxon (as *Cyprinus coryphaenoides*) from the Upper Lias Group of Germany. In 1832, Agassiz renamed and reclassified the specimen as *Leptolepis bronni*, alongside *L. longus* and *L. jaegeri*. Gardiner (1960) included Leptolepididae (spelled Leptolepidae) as an example of a fossil “holostean” and argued that, based on scale microstructure, they could not be ancestral to teleosts unless a reversal had taken place. However, the morphological evidence used by Gardiner is highly ambiguous. Despite his argument, *Leptolepis* was soon associated with various extant teleostean lineages, including osteoglossomorphs (Greenwood *et al.,* 1966) and clupeomorphs (Patterson & Rosen, 1977).

Nybelin (1974), using non-cladistic methods, was the first to argue that leptolepids may lie on the teleost “stem”, although the characters used in his diagnosis are considered inexact and ambiguous by modern standards (Arratia & Thies, 2001).

Olsen (1984) resolved a close relationship between *Leptolepis* and "*Pholidophorus" bechei*, based on seven characters, including membranous outgrowths of the intercalar, the ural neural arches forming uroneurals, two supramaxillae, a median supraethmoid and free lateral dermoethmoids. Stem teleost affinities have also been recovered by Xu & Wu (2012) and Latimer & Giles (2018), with support in both analysis for a sister group relationship between *Leptolepis* and *Dorsetichthys bechei*.

Leptolepids are also illustrative of another issue in stem teleost palaeontology. Arratia (2003) remarks that some museum collections have misidentified many different specimens of small, generic fossil teleosts as *Leptolepis*. It is possible that the species richness within Leptolepidae is not being captured.

**Pholidophorids:** Pholidophoridae was first established by Woodward (1890) to contain *Pholidophorus* – a genus conceived by Agassiz (1832) with two constituent species (*P. pusilus* and *P. latusculus).* Today, pholidophorids encompass a dozen genera of small, fusiform fishes from the Late Triassic (Ladinian; Tintori *et al.*, 2015) to the Late Jurassic (Tithonian), and are known from the UK, including the Lower Lias of Lyme Regis, Italy (Arratia, 2017), Germany, Poland (Konwert & Hörnig, 2018) and China – from which the oldest known fossil pholidophorid and potentially oldest fossil teleost: *Malingichthys* (Upper Ladinian) was recovered (Tintori *et al.*, 2015).

Pholidophorids were initially classified within Isospondyli, an expansive but now defunct suborder which contained several extinct groups (including Leptolepidae) as well as living teleosts like salmon and trout (Berg, 1940). However, by the mid-20$^{th}$ century, pholidophorids were long considered a lineage of "holosteans" (Gardiner, 1960; Danil'chenko & Yakovlev, 1964; Lehman, 1966; Nybelin, 1966), based almost entirely on the presence rhombic ganoid scales. As reviewed in Arratia (2000), several

early Pholidophoridae diagnoses were heavily reliant on vague and ambiguous characters (e.g., Nybelin, 1966; Zembelli, 1986). Nonetheless, the characters were consistent with those of other early diverging teleosts.

Patterson (1977) was the first to formally recover pholidophorids as stem teleosts on the basis of several specialisations of the braincase. Despite the uncertainty of their precise position on the stem, pholidophorids (alongside leptolepids) appear to have the clearest affinity with teleosts. Arratia (1999, 2000) recovered a paraphyletic Pholidophoridae as the sister group to “advanced Teleostei”, making them the earliest diverging taxon followed by *Leptolepis* and *Ichthyokentema.* Arratia (2013, 2017) went on to resolve pholidophorids (and *Eurycormus*) as the monophyletic sister to the teleost crown group on the basis of two uniquely derived characters and 12 homoplasies, including total fusion of the skull roof into a single bony plate, a symplectic in articulation with the lower jaw and the absence of long epineural processes. Beyond the work of Arratia, however, there are very few recent phylogenies that incorporate pholidophorid taxa. López-Arbarello & Sferco (2018) confirmed the monophyly of seven pholidophorid species but conceded that their position relative to other groups, such as aspidorhynchids and pachycormids, was uncertain.

As one of the earliest stem teleost lineages, pholidophorids are key to understanding the early diversification of Teleostei. However, well preserved specimens are uncommon, with the anatomy of early Jurassic taxa being especially poorly known (Konwert & Hörnig, 2018). Though recent analyses have used a wider range of taxa, the majority of analyses also underrepresent pholidophorids through the overreliance on the wastebasket taxa *Pholidophorus.*

***Dorsetichthys:*** The taxonomic history of pholidophorids is complicated further by *Dorsetichthys bechei. Dorsetichthys* is a recently established monotypic genus, endemic to the early Jurassic (early Sinemurian) of Lyme Regis. Arratia (2013) removed "*Pholidophorus" bechei* (Agassiz, 1832) from Pholidophoriformes to a newly erected genus *Dorsetichthys*, after it was found to be more closely related to crown-group teleosts than other pholidophorids, on the basis of seven characters, including the well-developed post-articular process of the lower jaw, absence of a prearticular and a pectoral propterygium fused with the first ray. Since the reappraisal of the morphology of *Dorsetichthys,* and its subsequent referral to its own monotypic order, *D. bechei* has been consistently recovered as a very closely related stem teleost, but in slightly different positions on the stem. Arratia (2013) initially recovered *Dorsetichthys* as sister to a clade containing *Ichthyokentema*, *Leptolepis* and "more advanced teleosts" on the basis of seven synapomorphies, such as the absence of a prearticular bone. Comparable results were recovered by Arratia's later study (2017), albeit with *Dorsetichthys* more proximate to the teleost crown than *Ichthyokentema*. López-Arbarello & Sferco (2018) also recovered *Dorsetichthys* as an early diverging teleost, sister to a clade containing *Siemensichthys*, *Thrissops* (the only ichthyodectiform in the analysis) and Teleocephala (the teleost crown, *sensu* de Pinna, 1996) on the basis of three uniquely derived synapomorphies, including the presence of a urohyal, and two homoplastic synapomorphies, including the presence of supraoccipital bone. (See chapter II for a more detailed history),

***Hulettia:*** The type species of *Hulettia*, *H. americana* is another species that has been reassigned from *Pholidophorus* (Schaeffer & Patterson, 1984). *Hulettia* typifies famous North American Jurassic formations such as the Morrison and Sundance Formations in Wyoming, Montana and South Dakota and the Todilto

Formation in New Mexico. Beyond this, however, very little is understood about the phylogeny or even the ecology of this taxon. Schaeffer & Patterson (1984, pg. 14) argued that its combination of both derived and “primitive” features gave *Hulettia* a ‘generalised’ appearance, obfuscating any obvious relationships to teleosts or holosteans: many of its features, such as the large rostral dividing the nasals, open cranial fissure, endochondral intercalar, lack of supraoccipital, broad parasphenoid perforated by a bucco-hypophysial canal, lack of supramaxilla, intercalary bones in the hyoid arch, diplospondyly and unmodified hypurals are broadly distributed across actinopterygians.

*Hulettia* does, however, exhibit a small number of more derived character states commonly found in crown neopterygians (e.g., nasal process of premaxilla, an antorbital with an elongate rostral process, large and small suborbitals, mobile maxilla, splint-like quadratojugal, reduced arcual tail lobe). Furthermore, Schaeffer & Patterson (1984) noted several similarities between *Hulettia* and *Dapedium*, though it was not until over two decades later that Hurley *et al.* (2007) first recovered *Hulettia* (misspelled as *Hulletia*) and *Dapedium* as sister taxa, forming a novel clade with *Mesturus* based on two compound characters: a free maxilla with short medial processes and a splint-like quadratojugal, free along posterior border of quadrate.

Latimer & Giles (2018) also found support for *Hulettia* and *Dapedium* as sister taxa, albeit as a clade of stem holosteans. This was recognised based on three homoplastic characters: dorsal with basal fulcra, scutes anterior to the anal fin, and the preoperculum being shorter than the operculum. Latimer & Giles (2018) also note that *Hulettia* exhibits a number of character reversals, potentially accounting for the appearance of both derived and “primitive” traits recognised by Schaeffer & Patterson (1984), complicating its phylogenetic affinities even further.

The position of *Hulettia* within Neopterygii is far from resolved, exacerbated by limited knowledge of its internal anatomy (due to the flattened mode of preservation), rare inclusion of the taxon in previous phylogenetic analyses and recent doubt on the validity of "*Hulettia" hawesi* (see Foster *et al*., 2018). However, understanding this taxon is important to constrain character acquisition on the teleost and holostean stems.

***Prohalecites:*** *Prohalecites* (Deecke, 1889) is a mid-Triassic (Ladinian to Carnian) monotypic taxa, found in lagoonal deposits in Italy and Switzerland (Bechly & Stockar, 2011). Its distinctive fossils are naked (lacking scale covering) and usually found in mass death assemblages (Furrer, 1995). Possibly due to its wide skull roof, the skull is most often flattened dorso-ventrally while the trunk is compressed laterally, twisting the body fossil at the shoulder girdle (Tintori, 1989).

Like *Hulettia*, *Prohalecites porroi*, was initially described as a species of *Pholidophorus* (Bellotti, 1857), before being reassigned to its own genus by Deecke (1889). Brough (1939, p. 107) referred to *Prohalecites* as a 'potential sub-holostean' (an outmoded expression referring to an intermediate morphology between Mesozoic holosteans and Palaeozoic palaeoniscoids). However, after this brief mention *Prohalecites* is seemingly absent from the literature for several decades. Patterson (1973) formally determined that *Prohalecites* was at least a neopterygian, although its position within Neopterygii was and remains unclear. This is because much like *Hulettia,* the phylogenetic position of *Prohalecites* is obfuscated by its combination of both "primitive" and derived character states (Arratia & Tintori, 1999). Griffith (1977) and Patterson (1982) were the first to refer to *Prohalecites* as an early teleost, but it was not until Tintori (1989) that this was formally investigated through a phylogenetic analysis. Tintori concluded that *Prohalecites* represents a transitional stage between

Parasemiontidae and the more derived *Dapedium* and Pholidophoridae, though it most closely resembles the latter taxa, in that its quadratojugal is shaped and positioned similarly to that of Pholidophoridae, but is separate to the quadrate, as in *Dapedium*. Arratia (1999, 2013, 2017) also resolved *Prohalecites* as a stem teleost on the basis of a number of homoplastic characters, such as a toothless parasphenoid, an ascending process on the premaxilla and a mid-caudal region with diplospondylous vertebrae. If this arrangement were to find further support, it would indicate that *Prohalecites* represents one of the oldest stem teleosts, alongside *Malingichthys*, implying a substantial ghost lineage between these taxa and the appearance of late Triassic pholidophorids.

## 1.4 Objectives and Outstanding Issues

To summarise, the phylogenetic positions of taxa commonly associated with the teleost stem have undergone decades of debate due to many outstanding issues in their study:

1. Potentially phylogenetically valuable internal anatomy is underappreciated due to preservational biases of laterally compressed specimens and a slow uptake of taxa associated with the teleost stem, e.g. aspidorhynchids and pachycormids, being described via computerised tomography.
2. Existing phylogenetic analyses of the teleost stem do not include a sufficiently broad range of taxa, impacting character distribution.
3. Taxa associated with the teleost stem are laden with historical baggage from over a century of study; wastebasket taxa and groups with generic descriptions and ambiguous diagnoses need revision.

This thesis aims to address these issues with the following aims:

1. Use computed tomographic and synchrotron tomographic techniques to re-examine the anatomy of Mesozoic fossil fishes associated with the teleost stem and reconstruct the internal anatomy, particularly the braincase, gill skeleton and hyoid arch, of taxa historically associated with the teleost stem as well as other neopterygians.
2. Produce an expanded character-by-taxon matrix incorporating newly produced anatomical data in order to generate a more robust phylogenetic hypothesis of the relationships of early Neopterygians, in particular Mesozoic taxa previously allied to the teleost stem.
3. Revise and modernise descriptions of historically significant specimens and diagnoses of key taxa to provide clarity for future work.

To achieve these goals, three dimensionally preserved specimens of iconic fossil neopterygians, particularly those with articulated dermal skeletons and/or complete braincases which were suitably preserved to be examined using CT- or synchrotron tomography were scanned, segmented, and visualised as 3D anatomical models and redescribed in detail. This new anatomical information was then fed into a revised phylogenetic analysis.

Chapter 1 reviews previous research in stem teleost anatomy and diversification and identifies key fossil assemblages that are vital to understanding this group, specifically pholidophorids, aspidorhynchids, and pachycormids. Each of these assemblages forms the focus of the following chapters.

Chapter 2 describes two three-dimensionally preserved, articulated specimens of *Dorsetichthys bechei*, one of which is a new, undescribed specimen, via-CT scanning. The complete cranial and dermal and endocranial anatomy of the taxon

infers a new ecological hypothesis and informs a re-assessment of interrelationships of Pholidophoriformes.

Chapter 3 investigates the braincase and endocast anatomy of two enigmatic, three-dimensionally preserved holostean braincases to better constrain neurocranial anatomical characters within Neopterygii, and presents an updated diagnosis for *“Ionoscopus” cyprinoides* and ‘Rayner’s *“Aspidorhynchus”’.*

Chapter 4 presents the complete anatomy of an exceptionally preserved pachycormid *(Pachycormus macropterus)* from the Strawberry Bank Lagerstätte and redescribes the earliest published aspidorhynchid braincase (*Richmondichthys sweeti*), including the first digital reconstruction of an endocast for both orders. Finally, the new anatomical information acquired in the previous chapters is presented in a novel phylogenetic model of early neopterygian relationships.

# 2. MICRO-CT BASED DESCRIPTION OF *DORSETICHTHYS BECHEI* (ACTINOPTERYGII: TELEOSTEI): CRANIAL ANATOMY OF AN ICONIC EARLY TELEOST

This chapter is a reformatted version of the following paper, submitted to *PeerJ:*

Atterby, J., Friedman, M., and Giles, S., 2024. Micro-CT based description of *Dorsetichthys bechei* (Actinopterygii: Teleostei): cranial anatomy of an iconic early teleost. *PeerJ*. *Biorxiv* doi: https://doi.org/10.1101/2024.05.10.593503

All authors (JA, SG and MF) were involved in revising the manuscript. JA performed segmentation, prepared figures, designed and wrote the manuscript, SG provided guidance throughout and contributed to drawing braincase figures. “We” is used in this chapter to reflect this collaborative effort.

## Abstract

*Dorsetichthys bechei* is an Early Jurassic stem teleost of historic importance. Although *D. bechei* is well described, its proximity to the teleost crown and relationships with other stem teleosts is challenging due to previous associations with the wastebasket assemblage known as “pholidophorids”. Here, a new, three-dimensionally preserved specimen of *Dorsetichthys bechei* from the Blue Lias Formation (Sinemurian) Lyme Regis, UK is described for the first time. High-resolution CT scanning of this specimen plus additional material reveals previously unknown internal morphological information, including of the jaw and palate, hyoid arch, and gill skeleton. Importantly, this previously undescribed articulated specimen permits description of the external dermal skeleton and internal endoskeleton for the same individual, clarifying past

accounts drawing on composite descriptions of two- and three-dimensionally preserved specimens. This chapter confirms the presence of important teleost synapomorphies such as a mobile premaxilla and “quadratojugal process” but contrasting previous accounts, confirms the presence of a prearticular and finds no evidence for a postarticular process of the lower jaw. Furthermore, the presence of a mobile upper jaw, elaborate gill rakers and reduced dentition also support a possible facultative filter feeding ecology. These new anatomical data support removal of *D. bechei* from Pholidophoridae and Pholidophoriformes as currently defined but indicate that finer-scale patterns of relationships among more crownward members of the teleost stem are some way from being resolved.

## 2.1 Introduction

Teleost fishes account for more than half of all extant vertebrate species, but the anatomy and relationships of taxa outside of the living radiation are poorly constrained despite an abundance of well-preserved material. Although past work identifies a broad range of Mesozoic actinopterygians as branching from the teleost stem (Patterson, 1973, 1975; Gardiner *et al.*, 1996; Hurley *et al.,* 2007; Nursall, 2010; Arratia, 1997, 1999, 2013, 2017; Poyato-Ariza, 2015; Latimer & Giles, 2018), the anatomy and relationships of some key taxa are incompletely known (Arratia & Tintori, 1999; Arratia, 2001; Poyato-Ariza, 2015; Latimer & Giles, 2018), despite occasional instances of exquisite preservation (e.g., Frey & Tischlinger, 2012; Cawley et al., 2019) and centuries of anatomical and taxonomic study (Agassiz, 1833 – 1844; Woodward, 1885).

“Pholidophoridae” (*sensu* Woodward, 1890), first established for the genus *Pholidophorus*, is an assemblage of modestly sized stem teleosts with a complicated

taxonomic history. The importance of this group to understanding teleost evolution has been recognised for well over a century, with Woodward (1895) classifying pholidophorids as the earliest members of Isospondyli (early fossil teleosts and extant relatives). They later came to be classed within “holosteans.” A more inclusive group than that currently recognized (Grande, 2010), the “holosteans” of these authors also encompassed many other Mesozoic actinopterygians (e.g., aspidorhynchids, semionotids, pycnodonts) and the lineage leading to *Amia* (Romer, 1945). Although support for a direct link between pholidophorids and extant teleosts mounted (Woodward 1942, Rayner 1948, Saint-Seine, 1949; Gardiner, 1960; Griffith & Patterson, 1963; Nybelin, 1966; Patterson, 1968; Patterson, 1975), the large number of plesiomorphic characters displayed by the assemblage meant that influential figures such as Patterson initially resisted recognising them as teleosts rather than “holosteans” (Patterson 1967, 1968, 1973).

Early diagnoses of *Pholidophorus* largely cite vague and generic neopterygian characters (e.g., Agassiz, 1833-1843; Woodward, 1889; Lehman, 1966; Nybelin, 1966; Zambelli, 1986), leading to a taxonomic quagmire: at one point, the type genus *Pholidophorus* (Agassiz, 1832; 1837 [1833-43]) contained over 40 species, most based on poorly preserved or inadequately described material (e.g., Woodward, 1895). Due in part to their position relative to more crownward parts of the tree, “pholidophorids” became a wastebasket taxon for early teleosts that retained a suite of primitive features such as rhombic ganoid scales (e.g., Patterson, 1975, pg. 281; Arratia, 2013, pg. 2-4). Perhaps understandably, “*Pholidophorus” bechei*, one of the better preserved “pholidophorids”, was erroneously considered the type species by Woodward and later authors (e.g. Rayner 1948, pg. 318; Nybelin 1966, pg. 32; see discussion in Arratia 2000 and Arratia & Schultze 2024), and both its dermal skeleton

and neurocranium were described in detail. The actual type species, *P. latiusculus*, is relatively poorly preserved (Taverne, 2018) Several efforts have been made to revise the taxonomy of Pholidophoridae, with many species being reassigned to new genera (e.g., Deecke, 1889; Woodward, 1941; Nybelin 1966; Gaudant, 1978; Arratia, 2000). Work to tackle this problem culminated in Arratia's (2013) comprehensive anatomical, taxonomic, and phylogenetic reassessment of pholidophorids and associated taxa, which resolved a monophyletic remnant of pholidophorids as sister to *Eurycormus* and all remaining teleosts (Arratia, 2013). Today, Pholidophoridae (*sensu* Arratia, 2013) is restricted to around 15 genera spanning the Late Triassic (Ladinian) of Europe and China.

Significantly, Arratia's revision excluded "*Pholidophorus*" *bechei* from Pholidophoridae, removing it to its own monotypic genus *Dorsetichthys*, within a monotypic Order Dorsetichthyiformes and Family Dorsetichthyidae (Arratia, 2013; 2017). *Dorsetichthys* was recovered as branching closer to the teleost crown than pholidophorids, a placement supported by seven synapomorphies: a skull roof with an orbital region slightly narrower than the postorbital region, small teeth on the parasphenoid, a well-developed postarticular process of the lower jaw, absence of a prearticular, absence of serrated appendages, a pectoral propterygium fused with the first lepidotrich, and three rows of rhomboidal mid-flank ganoid scales between the postcleithra and mid-length of the body (Arratia, 2013). The removal of *Dorsetichthys* from pholidophorids also has implications for interpreting broader patterns of relationships on the teleost stem: this taxon has been effectively emblematic of pholidophorids for more than a century (Arratia, 1999). Because it has been described in the most detail, it is often the only "pholidophorid" taxon included in analyses of teleost or actinopterygian relationships (e.g., Patterson and Rosen, 1977; Olsen, 1984;

Grande and Bemis, 1998; Arratia, 1997, 1999, 2001; Hurley et al., 2007; Xu & Wu, 2012; Poyato-Ariza, 2015; Thies & Waschkewitz, 2015; Gibson, 2016). Consequently, it is unclear to what extent the pholidophorid terminal in some past analyses represents a composite taxon, and to what extent valid pholidophorid taxa are represented.

While the cranial dermal (Nybelin, 1966) and endoskeletal (Patterson, 1975) anatomy of *Dorsetichthys* has been studied in great detail in comparison to most other stem teleosts, these accounts are typically taken from different individual specimens, with less clear aspects of anatomy supplemented by comparison to taxa such or *Leptolepis* (e.g. Rayner, 1948). Rayner (1948) described the dermal skeleton, braincase, hyomandibula and palate and Patterson (1975) the neurocranium from isolated material, the species determination of one braincase (NMHUK PV P 51682) being noted by Patterson (1975: pg. 283) as uncertain due to the lack of other pholidophorids in which the braincase was known. Likewise, accounts of the dermal skeleton made by Nybelin (1966) are based on two-dimensional, laterally compressed specimens in which the endoskeleton is largely unknown, and the internal aspect of many dermal bones cannot be assessed. Most recently, Giles *et al.* (2018) used CT scanning to describe the endocast and bony labyrinth of another isolated braincase of *D. bechei*, NMHUK PV P 51682 (referred to incorrectly by Giles *et al.* as NHMUK PV P 1052), supplementing past preliminary descriptions of the endocranial cavity that were based on sagittal sections (e.g., Patterson, 1975). While our understanding of the anatomy of this taxon is comprehensive, it assumes that these isolated elements scattered across the dermal and endoskeleton belong to the same taxon.

Here, we present a complete, articulated, previously undescribed individual of *Dorsetichthys bechei* and a redescription of a specimen previously studied by Rayner

(1948) and Patterson (1975). Through high resolution CT scanning, we describe both the dermal and endoskeletal anatomy of these specimens. In doing so, we clarify ambiguity regarding the compositing of isolated material and providing new details on its internal morphology. We then consider the consequences of this refined anatomical picture of *Dorsetichthys* for its placement relative to pholidophorids and other stem teleosts.

## 2.2 Materials and Methods

### 2.2.1. Institutional Abbreviations

NHMUK = Natural History Museum, London, UK.

### 2.2.2. Materials

NHMUK PV P 73995 is a heavily pyritised, three-dimensionally preserved specimen, the history of which is poorly known. It was recently located among the cabinets containing specimens from the NHMUK collections as well as borrowed fossils studied by Colin Patterson; this was effectively his “working collection” of material. The specimen was kept with a hand-written note dated 1888 and signed by William Davies, but the stratigraphic origin and provenance of the specimen is unclear. Despite no indication on Davies’ associated note, the matrix and mineralisation are consistent with fossils from the Blue Lias Formation, Lyme Regis, UK (Lord & Davis, 2010). Upon its rediscovery, the specimen was provisionally identified as *Dorsetichthys bechei* and was formally registered and assigned a catalogue number in 2016 (pers comms, E. Bernard, 2020).

NHMUK PV P 1052 is a mechanically prepared braincase from the Early Jurassic (Sinemurian) Charmouth (UK), with some associated dermal elements.

Unlike NHMUK P 73995, NHMUK PV P 1052 has a well-documented history of study and description and has informed several composite reconstructions by Rayner (1948) and Patterson (1975) but has not been described via CT: NMHUK PV P 51682 is incorrectly referred to as NHMUK PV P 1052 by Giles *et al. (*2018). NHMUK PV P 1052 was originally identified as *Pholidophorus bechei*, and later removed to *Dorsetichthys bechei* (Arratia, 2013).

Several additional specimens of *D. bechei* were also examined for comparison of the braincase and dermal skeleton, and to investigate the possibility of intraspecific variation in the circumorbital series: NHMUK OR 19010, NHMUK OR 38107, NHMUK OR 38109, NHMUK OR 39859, NHMUK PV P 3589a, NHMUK PV P 1051, NHMUK PV P 1052a, NHMUK PV P 3586c, NHMUK OR 154, NHMUK OR 38535 and NHMUK OR 1885. Each specimen is attributed to the Lower Lias, most likely corresponding to the Charmouth Mudstone Formation, but their precise provenance is poorly recorded. NHMUK OR 19010 comprises a three-dimensionally preserved cranium and complete body, which also preserves some relief. The braincase and associated cranium can be separated from the rest of the specimen and was previously studied by Patterson (1975). The remaining specimens comprise laterally compressed dermal skeletons of varying completeness which have also previously informed composite descriptions by Rayner (1948) and Nybelin (1966).

### 2.2.3. CT Scanning and Imaging

NHMUK PV P 73995 was scanned at the CTEES Facility, University of Michigan using a Nikon XTH 225 ST with a 0.85 mm Cu filter; current = 180 μA; voltage = 195 kV; exposure = 1000 ms and 4 frames per projection, resulting in a voxel size of 21.68 μm.

NHMUK PV P 1052 was scanned at the Imaging and Analysis Centre, NHMUK using a Zeiss Versa 520 micro-CT scanner with a HE2 filter (unspecified thickness of glass); current = 63 μA; voltage = 160 kV; exposure = 8000 ms and 1 frame per projection, resulting in a voxel size of 20.59 μm.

Resulting image stacks were cropped in ImageJ (Schneider *et al.*, 2012) and segmented in Mimics v.25 (biomedical.materialise.com/mimics; Materialise, Leuven, Belgium). Renders of 3D models were captured using Blender v. 3.3.0 (blender.org) and interpretive drawings were created in Adobe Illustrator (adobe.com/products/illustrator).

## 2.3 Systematic Palaeontology

Osteichthyes Huxley, 1880

Actinopterygii Cope, 1887

Neopterygii Regan, 1923

Teleostei Müller, 1844

Dorsetichthyiformes Nelson, Grande & Wilson, 2016

Dorsetichthyidae Nelson, Grande & Wilson, 2016

*Dorsetichthys* Arratia, 2013

*Dorsetichthys bechei* (Agassiz, 1837)

**Holotype:** PAL-J.003065, Oxford University Museum of Natural History.

**Diagnosis (emended from Arratia, 2013):**

Neopterygian diagnosed by the following unique combination of characters: partially fused skull roof plate; five infraorbital bones between the antorbital and dermosphenotic; one or two suborbital bones; two or three supraorbital bones; thin lateral strut extending across the sub-temporal fossa of the braincase; mobile premaxilla and maxilla articulating with the lateral dermethmoid; four ural neural arches modified as uroneurals; hypurals divided into dorsal and ventral groups.

## 2.4 Description: *Dorsetichthys bechei* (NHMUK PV P 73995)

A

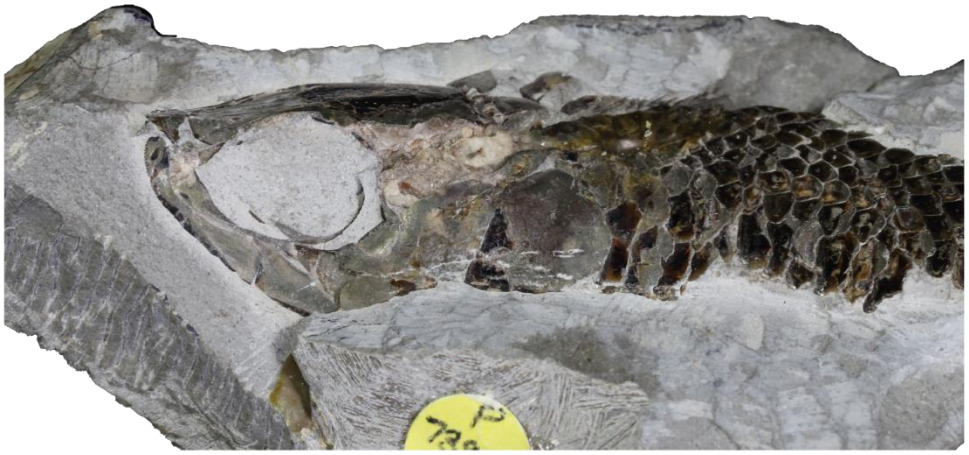

B

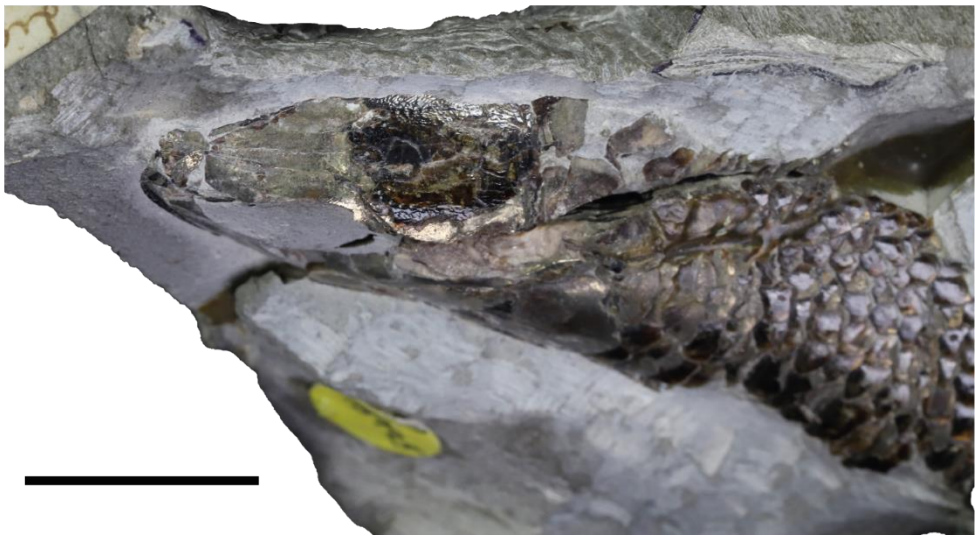

**Figure 2.1: *Dorsetichthys bechei* NHMUK PV P 73995** In (A) left lateral and (B) dorsal view. Scale = 10 mm.

## 2.4.1 General morphology.

NHMUK PV P 73995 (Fig. 2.1) consists of a near-complete skull, as well as a partial postcranium with scales and a pectoral fin. The left side of the skull and the skull roof have been exposed following mechanical preparation, but several bones on the exposed side are displaced and/or damaged. The right side of the skull, however, is preserved within the matrix and almost every dermal bone is present and in articulation. The entire fossil has undergone secondary mineralisation by pyrite, giving most of the specimen a golden, metallic lustre and relatively high contrast in tomograms.

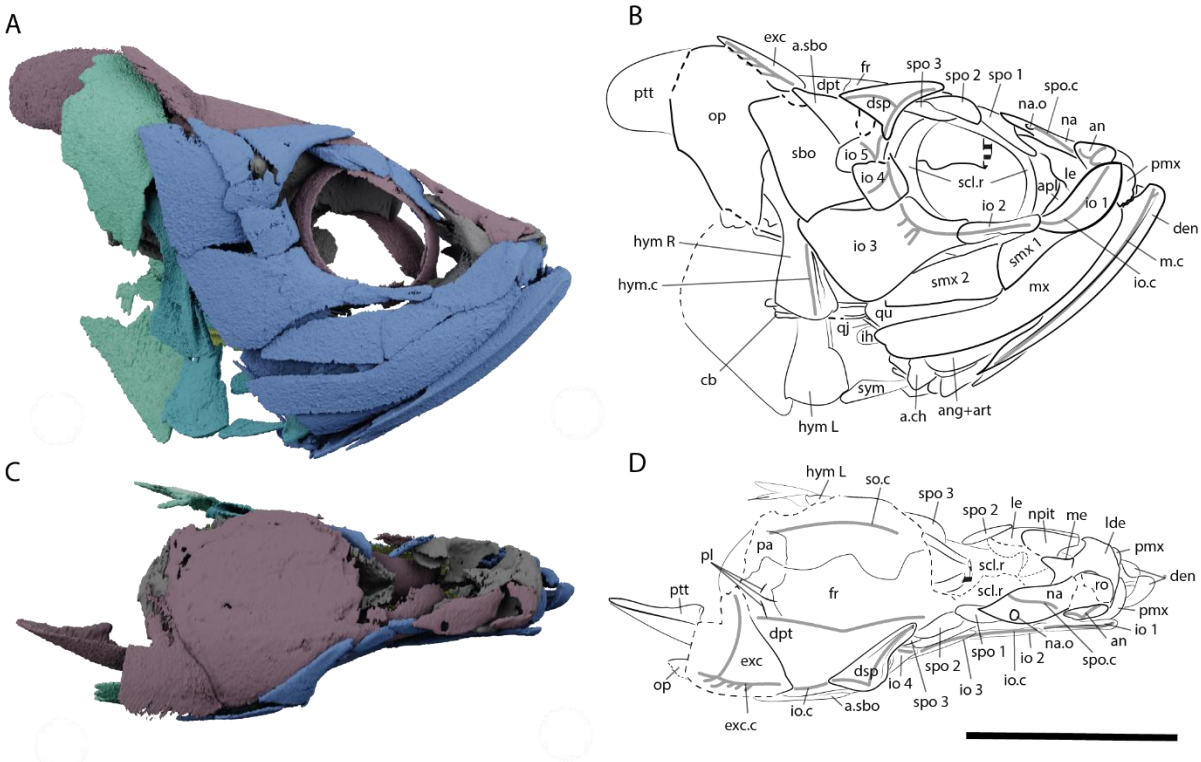

**Figure 2.2: The skull of *Dorsetichthys bechei* NHMUK PV P 73995**. (A) Render and (B) interpretive drawing in right lateral view. (C) Render and (D) interpretive drawing in dorsal view. Colour coding: blue, cheek and jaw; purple, skull roof, dermal shoulder girdle and sclerotic ossicle; grey, braincase; turquoise, hyomandibula; light green, operculogular system; yellow, gill skeleton. Sensory lines indicated in grey. Scale bar = 10 mm. *Abbreviations: an, antorbital; ang+art, fused angular and articular, apl, autopalatine; angular; a.sbo, accessory suborbital; cb, ceratobranchial; a.ch, anterior ceratohyal; den, dentary; dpt, dermopterotic; dsp, dermosphenotic; exc, extrascapular; exc.c, extrascapular canal; fr, frontal; hym, hyomandibula; ih, interhyal; io.c, infraorbital canal; io 1-5, infraorbital bones; le, lateral ethmoid; lde, laterodermethmoid; me, mesethmoid; mx, maxilla; m.c, mandibular canal; na, nasal; na.o, nasal opening; npit, nasal pit; op, opercular; pa, parietal; pl, pit lines; pmx, premaxilla; ptt, posttemporal; qu, quadrate; qj, 'quadratojugal' process; sbo, suborbital; scl.r, sclerotic ring; smx 1-2, supramaxillae; so.c , supraorbital canal; spo 1-3, supraorbital bones; spo.c, supraorbital canal; sym, symplectic*

### 2.4.2 Skull Roof

The dermal plates of the skull roof are partially preserved. Overall, the skull roof is broadest posteriorly, tapering abruptly above the postorbital margin and towards the snout. The broadest section of the skull roof is roughly four times wider than the anterior region. The skull roof comprises paired frontals, parietals and dermopterotics (fr, pa, dpt, Figs. 2.2B,D, 2.6B). Sutures between individual bones are difficult to trace in tomograms but visible on the specimen. They are largely straight, or gently curved with the exception of the strongly sinusoid suture between the midsection of the

frontals (Fig. 2.2B). The broader, posterior portion of the skull roof is damaged on the left side, but the right is well preserved within the matrix, exhibiting anterior, middle, and posterior pit lines (pl, Fig. 2.2D). Enclosed supraorbital canals (so.c, Fig. 2.2D) extend along the full length of the plate to the nasal region and are exposed as moulds anterior to the preserved portion of bone. Each canal opens to the surface via irregularly spaced pores that accommodate simple tubules. The right infraorbital canal (io.c, Fig. 2.2D) is fully enclosed in a ridge on the ventral margin of the skull roof plate, extending along its lateral margin and exiting the posterior margin into the extrascapular (exc, Fig. 2.2B, D).

The right nasal (na, Figs. 2.2B, D, 2.6B) is well preserved, although the left nasal is missing entirely. It is sub-rectangular with a stepped, tapered posterior extension that lies parallel to the supraorbital series. It carries the supraorbital sensory canal (spo.c, Fig. 2B, D) along its entire length and bears the posterior nasal opening (na.o, Figs. 2.2B, D, 2.6B). Though not preserved in this specimen, previous descriptions (Nybelin, 1966; pg. 360) show the frontals separating the left and right nasals. The antorbital (an, Figs. 2.2B, D, 2.6B) is small and triangular, forming the most anterior portion of the orbital margin, partially overlapping the nasal and lying anterodorsally to the first infraorbital. Two or three pores from the infraorbital canal (io.c, Figs. 2.2B, D, 2.6B) open onto the lateral surface of the antorbital. The canal bifurcates within the bone, with a dorsal branch continuing into the nasal, and the ethmoid commissure continuing anteriorly into a small fragment of the right rostral bone (ro, Fig. 2.2D). Despite being poorly preserved, the rostral fragment appears to be *in situ*. The nasal, rostral and antorbital bones all partially overlap in the ethmoid region, and the right nasal bone has partly subsided into the underlying nasal pit.

### 2.4.3 Braincase

The bulk of the braincase consists of a single ossification encompassing the occipital, otic, orbitotemporal and basisphenoid regions; separate ossifications or ossification centres cannot be identified. However, both the orbitosphenoid and ethmoid regions are independently ossified, and entirely separated from the other portions of the braincase that presumably would have been filled by cartilage in life.

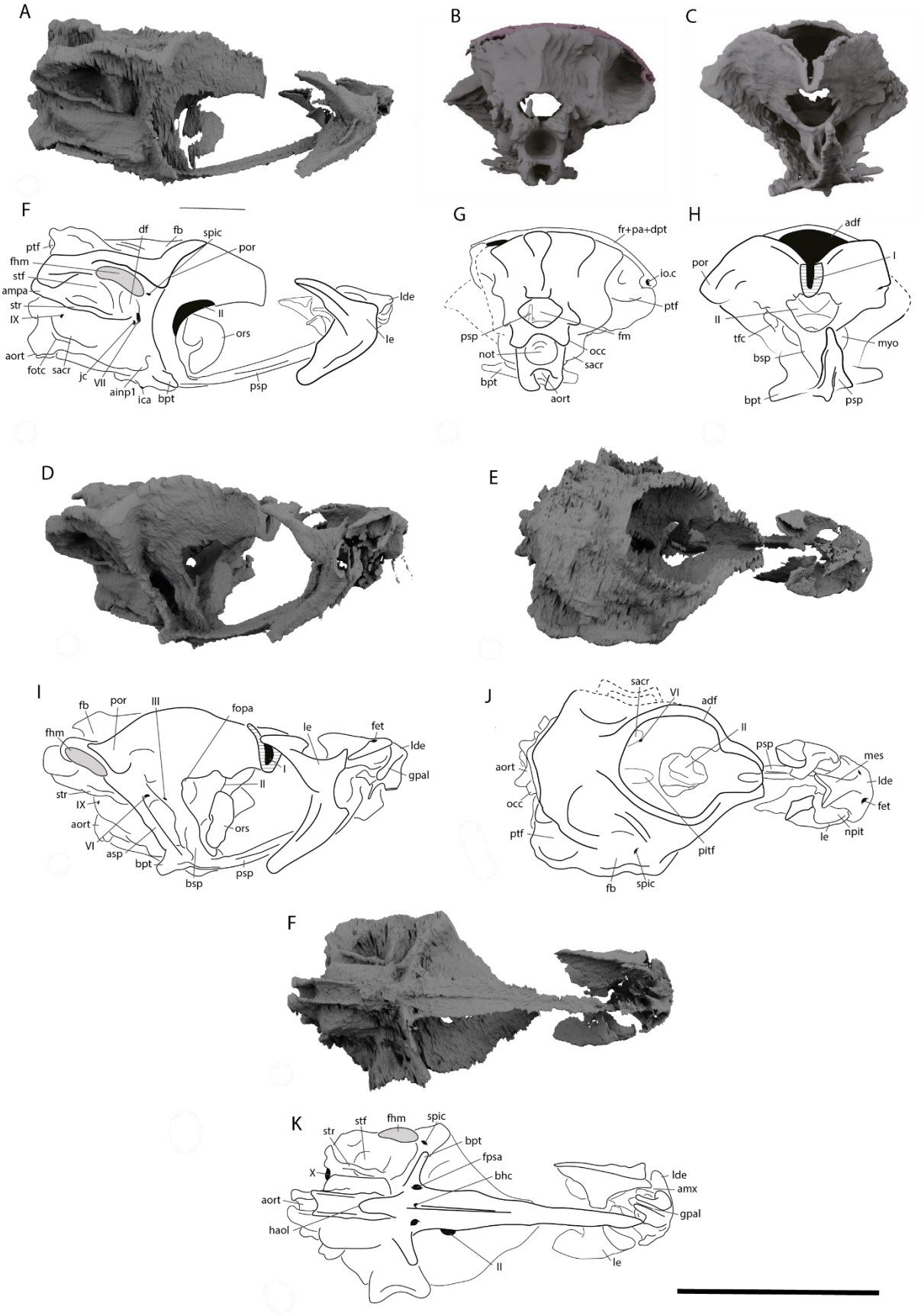
A
B
C
F
df
fb
spic
ptf
por
fhm
stf
ampa
str
IX
II
ors
lde
le
aort
fotc
sacr
jc
VII
ainp1
ica
bpt
psp
G
fr+pa+dpt
io.c
ptf
psp
fm
not
occ
sacr
bpt
aort
H
adf
I
por
II
tfc
myo
bsp
bpt
psp
D
E
I
fb
por
III
fopa
le
fet
lde
fhm
I
gpal
II
str
IX
aort
ors
VI
asp
bpt
psp
bsp
J
sacr
VI
adf
II
psp
mes
aort
lde
occ
fet
ptf
le
npit
pitf
fb
spic
F
K
str
stf
fhm
spic
bpt
fpsa
X
bhc
lde
amx
aort
gpal
haol
II
le

**Figure 2.3: The braincase of *Dorsetichthys bechei* NHMUK PV P 73995.** Renders in (A) right lateral, (B) posterior, (C) anterior, (D) anterolateral, (E) dorsal, and (F) ventral view. Interpretive drawings in (G) right lateral, (H) posterior, (I) anterior, (J) anterolateral, (K) dorsal, and (L) ventral view. Scale bar = 10 mm. Abbreviations*: adf, anterior dorsal fontanelle; ainp, anterolateral process; amx, articular surface for maxilla and premaxilla; aort, aortic notch; asp, ascending process of parasphenoid; bhc, buccohypophysial canal; bpt, basipterygoid process; bsp, basisphenoid; df, dilatator fossa; epsa, efferent pseudobranchial artery; fb, fossa bridgei; fhm, hyomandibular facet; fet, ethmoid fenestrae for articulation with maxilla; fm, foramen magnum; fopa, foramen for optic artery; fotc, otoccipital fissure; gpal, groove for palatine nerve; haol, housing of aortic ligament; ica, internal carotid artery; io.c; infraorbital canal; jc, jugular canal; le, lateral ethmoid; lde, laterodermethmoid; mes, mesethmoid; myo, posterior myodome; not, notochord; npit, nasal pit; ors, orbitosphenoid; pf, pituitary fossa; por, postorbital process; proc, posteroventral process; psp, parasphenoid; ptf, post-temporal fossa; sacr, saccular recess; spic, spiracular canal; sr, skull roof; str, lateral strut; tfr, trigemino-facial recess; I, olfactory nerve*; *II, optic fenestra; VI, foramen of abducens nerve; VII, foramen of facial nerve; IX, foramen for glossopharyngeal nerve; foramen for X, foramen of vagus nerve; X.st, foramen for supratemporal branch of vagus nerve.*

*Occipital Region*. The occipital region is well preserved and relatively well ossified, with a complete lining of perichondral bone and moderate development of endochondral bone posteriorly. However, ossification is insufficient to trace or identify some canals for nerves and vessels. The occipital region is comparatively narrow, and bounded anteriorly by a shallow groove on the lateral margin of the braincase that

marks the closed otoccipital fissure (fotc, Fig. 2.3G). In posterior view (Fig. 2.3H), the region corresponding to the supraoccipital forms a pronounced, hourglass-shaped, vertical ridge of bone flanked by shallow depressions. Contra Patterson (1975, pg. 307), there is no evidence that the medial portion of the “supraoccipital region” has a dermal component as it passes beneath the parietals. An oval opening for the foramen magnum (fm, Fig. 2.3H) lies immediately ventral to the supraoccipital ridge. Its ventral margin is thickened into overhanging posteroventral processes (proc, Fig. 2.3H, K), which likely articulated with the intercalaries of the first vertebra (Patterson, 1975). The inner walls of the foramen magnum narrow anteriorly and appear to lack any distinct foramina. More ventrally, the rounded notochordal opening (not, Fig. 2.3H), extends into the braincase as a conical canal that constricts rapidly and terminates anteriorly at the level of the saccular recess. A C-shaped aortic notch forms the most ventral feature on the posterior face of the occipital region, framing the walls of a deep, open groove for the dorsal aorta (aort, Fig. 2.3H, K, L) that extends along the ventral surface of the basiocciput. In agreement with Patterson (1975), we find no evidence for an enclosed aortic canal. The posterior margin of the aortic notch extends posteriorly to the level of the occipital condyle, forming the basal point of articulation with the vertebrae.

Anterior to the closed otoccipital fissure, a ventrally directed elliptical opening marks the exit of the vagus nerve (X, Fig. 2.3L). The smaller supratemporal branch of the vagus nerve appears to exit anterolaterally (X.st, Fig. 2.3H), although the canal itself is hard to trace internally. A swelling dorsal to the exit of the vagus nerve, in the region formed by the exoccipital, corresponds to the position of the posterior ampulla of the inner ear (ampa, Fig. 2.3G). Foramina for the occipital nerve and posterior cerebral vein cannot be identified. The posterior myodome (myo, Fig. 2.3I, J), which

originates in the posterior orbital wall, extends well into the occipital region, narrowing posteriorly and terminating level with the posterior margin of the saccular cavities. There is no posterior dorsal fontanelle or vestibular fontanelle, and the ventral otic fissure is also closed.

*Otic Region*. The otic region represents the widest portion of the braincase, approximately 1/3 wider than the occipital region. Much of this region is poorly ossified, with only thin perichondral bone forming most margins, and no endochondral development. As with the occipital region, this makes the path of canals difficult to follow. The endocranial roof is almost entirely unossified and is instead open as a large anterior dorsal fontanelle (adf, Fig, 2.3I, K), which extends to the anterior margin of the orbital region. Several fractures disrupt the left side of the otic region, but the right side is well preserved, revealing several fossae. The post-temporal fossa (ptf, Fig. 2.3G, H, K), which opens onto the posterior face of the braincase as a possible muscle insertion point, is wide, rounded, and gradually narrows anteriorly towards the complex fossa bridgei (fb, Fig. 2.3G, J, K). The fossa bridgei is very broad, with a shallow, convex dorsal margin, narrowly separated from the anterior dorsal fontanelle and the endocranial cavity by the housing of the supraorbital canals in the skull roof. The fossa bridgei does not appear to be confluent with the post-temporal fossa, although ossification between them is very thin. Both depressions lack an endocranial roof and are overlain exclusively by the dermal skull roof. At its deepest point, the floor of the fossa bridgei is connected to the dorsal opening of the spiracular canal (spic, Fig. 2.3G, K). The spiracular canal is vertically oriented and enclosed in bone within the postorbital process (por, Fig. 2.3G, I, J), re-emerging ventrally into a groove roughly level with the anterior foramen of the abducens nerve. No bifurcations or branching

rami are resolved as extending from the spiracular canal, consistent with Patterson (1975).

The hyoid facet (fhm, Fig. 2.3G, J, L) and sub-temporal fossa (stf, Fig. 2.3G, L) lie ventral to the post-temporal fossa and fossa bridgei. The hyoid facet is fairly shallow, oriented sub-horizontally, and lined with perichondral bone. Anteroventrally, the sub-temporal fossa forms a considerably deeper recess, partially delineated from the hyomandibular facet and post-temporal fossa by a thick ridge of bone that houses the horizontal semicircular canal. A thin lateral strut (str, Fig. 2.3G, J, L) of endochondral bone extends from the intercalar region across the full length of sub-temporal fossa and reconnects with the braincase on the underside of the utricular recess.

The jugular groove passes ventral to and parallel with the lateral strut. It is shallow without sharply defined margins but appears to extend posteriorly from the glossopharyngeal foramen (IX, Fig. 2.3J, G) and across the external face of the saccular chamber (sacr, Fig. 2.3G, H) before piercing the postorbital process and entering the jugular canal (jc, Fig. 2.3G). The foramen for the facial nerve (VII, Fig. 2.3G) opens laterally into the floor of the jugular groove. The anterior wall of the shallow dilatator fossa (df, Fig. 2.3G) contributes to part of the anterior wall of the otic region. A smooth and rounded swelling, which narrows anteriorly, corresponds the saccular chamber and forms much of the ventral portion of the lateral face of the otic region. A stout, sub-triangular anterolateral process (ainp1, Fig. 2.3G) anterior to the saccular recess represents the articulation point for the infrapharyngobranchial of the first gill arch.

*Orbitotemporal Region*. The orbitotemporal region is relatively narrow and poorly ossified anteriorly. Posteriorly, the orbitotemporal region is separated from the otic region by a steep wall formed by the postorbital process, lateral commissure, and ascending process of the parasphenoid. The posterior orbital wall is well ossified and opens ventrally to the facial recess and median posterior myodome. Several shallow fossae occupy the posterior corner of the orbital cavity. The largest, the trigemino-facial recess (tfc, Fig. 2.3I), forms a short longitudinal tunnel in the wall of the postorbital process. The chamber includes the dorsal openings of the abducens nerve and the palatine branch of the facial nerve (VII, Fig. 2.3J), which exit the cranial cavity to pierce the concave roof of the large, median posterior myodome (myo, Fig. 2.3I, J, K). Though it forms a single median chamber, its anterior opening is bisected medially by the vertical pillar of the basisphenoid (bsp, Fig. 2.3J, K). The basisphenoid is notably reduced but frames the large median optic foramen (II, Fig. 2.3J, K), as well as the subtriangular pituitary fossa (pitf, Fig. 2.3k) which allows the posterior myodome to communicate with the optic foramen above it.

The median optic foramen (II, Fig. 2.3G, I, J, K, L) is large. A small notch on its dorsal margin would likely have accommodated the optic artery (fopa, Fig. 2.3J). The foramen for the trochlear nerve is hard to identify but may be present as a perforation halfway up the left orbital wall (IV, Fig. 2.3K). A small opening adjacent to the optic foramen may represent the oculomotor foramen (III, Fig. 2.3J). There is a short gap between the postorbital ossification and the lateral ethmoids.

**Ethmoid**

The ethmoid region is mostly complete and articulated, although some ossifications have shifted relative to each other. Overall, the ethmoid contributes to a rounded snout, with large paired nasal pits (npit, Figs. 2.3K, 2.4B, D, F). The ethmoid complex

includes partially fused paired lateral dermethmoids (lde, Figs. 2.3J, K, L, 2.4B, D, F, J), lateral ethmoids (le, Fig. 2.4) and a median mesethmoid (mes, Figs. 2.3K, 4B, F, H). Sutures between these ossifications are difficult to identify, even in tomograms. The mesethmoid has a broad, subtriangular dorsal surface, which tapers ventrally to a thick nasal septum (nse, Fig. 2.4B, D) that forms the medial walls of the nasal pits. The ventral surface of the mesethmoid bears a very deep but narrow median groove (gpal, Figs. 2.3L, 2.4H, L). This incision likely transmitted the palatine nerve to the relatively shallower palatine notch (npal, Fig. 2.4B) between the articular surfaces for the maxillae and premaxillae (see below). Although the ethmoid is slightly offset from the remaining braincase, the anterior margin of the parasphenoid or vomer (the latter of which is not preserved) also likely extended into the posterior margin of the groove. The groove is flanked by lateral fossae, which may have accommodated the vomer.

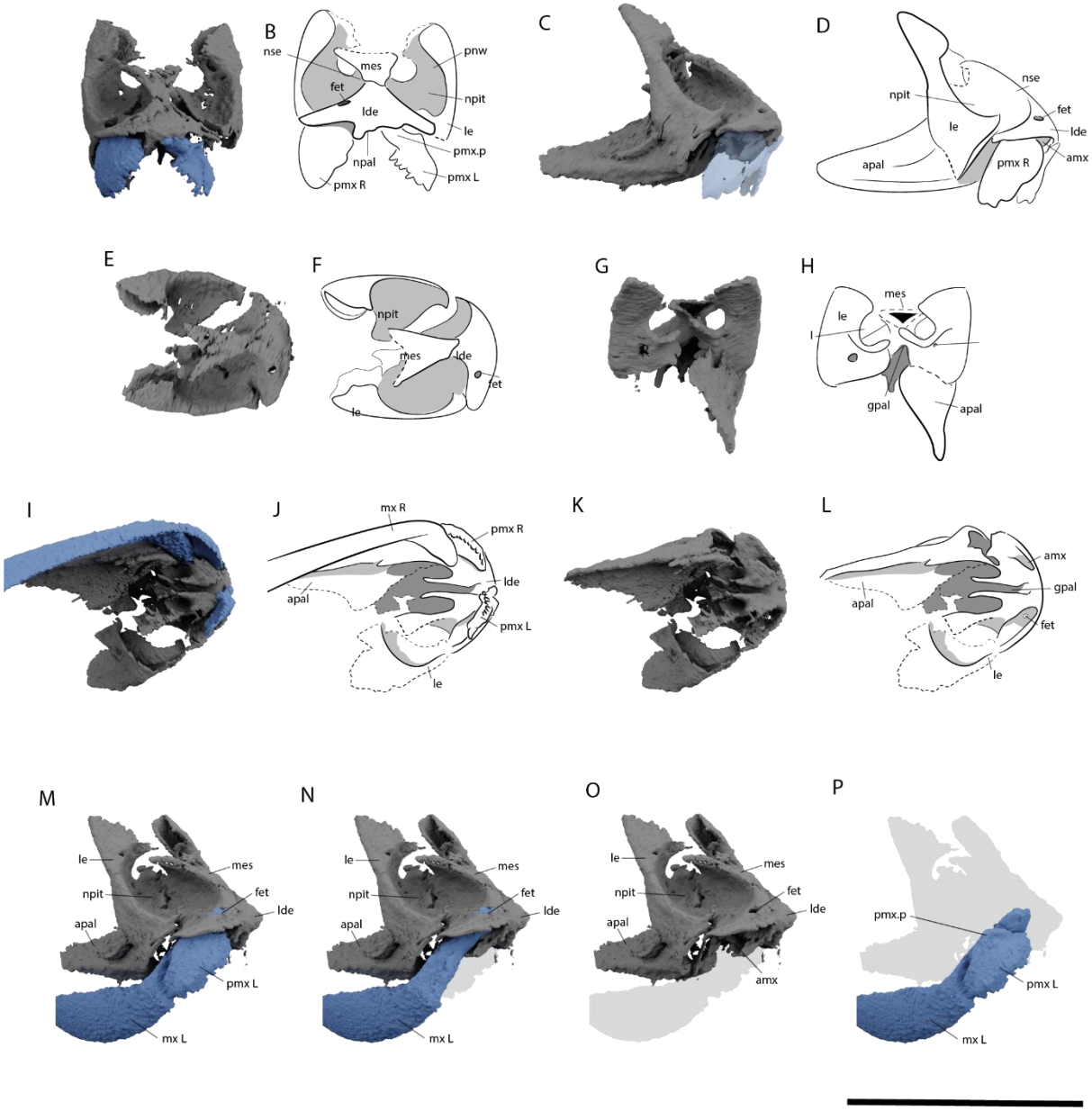
A
B
nse
mes
fet
lde
pnw
npit
le
pmx.p
npal
pmx R
pmx L
C
D
nse
npit
fet
le
lde
amx
apal
pmx R
E
F
npit
mes
lde
fet
le
G
H
mes
le
gpal
apal
I
J
mx R
pmx R
lde
apal
pmx L
le
K
L
amx
gpal
apal
fet
le
M
N
O
P
le
mes
npit
fet
lde
apal
pmx L
mx L
amx
pmx.p

**Figure 2.4: The ethmoid region of *Dorsetichthys bechei* NHMUK PV P 73995.** Renders in (A) anterior, (C) right lateral, (E) dorsal, (G) posterior, (I) ventral view, and interpretive drawings in (B) anterior, (D) right lateral, (F) dorsal, (H) posterior, (J) ventral view. (K) Render of right maxilla articulating with the ethmoid. Colour coding: blue, jaws; grey, braincase. Scale bar = 5 mm. Abbreviations: *adf, anterior dorsal fontanelle; amx, articular surface for maxilla and premaxilla; apal, autopalatine; fet, ethmoid fenestrae for articulation with maxilla; gpal, groove for palatine nerve; lde, laterodermethmoid; le, lateral ethmoid; mes, mesethmoid; mx, maxilla; npal, notch for palatine nerve; npit, nasal pit; nse, nasal septum; pmx, premaxilla; pmx.p, premaxillary process; I, olfactory nerve*.

The lateral dermethmoids are fused along the midline and extend posteriorly to contribute to the floor of the nasal pit and anteriorly beneath the rostral (Fig. 2.2B, F, J) to contribute to the snout. Teeth appear to be absent from this anterior margin. A large, rounded foramen on the anterodorsal face of the lateral dermethmoid (fet, Figs. 2.3J, K, 2.4B, D, F, M, N, O) resembles that previously observed in "*Pholidophorus" germanicus*, where it was described as "an unknown foramen or pit" by Patterson (1975: pg. 477). This opening communicates ventrally with a large socket (amx, Figs. 2.3L, 2.4D, L O), bounded laterally and dorsally by the lateral dermethmoid and medially by the mesethmoid. The more dorsal part of this socket accommodates the anterior process of the maxilla—which extends directly to the foramen on the face of the lateral dermethmoid—and the more ventral the anterior process of the premaxilla, enabling both bones to articulate with the braincase and the upper jaw to protrude (Fig. 2.4M, N, O, P). It is likely that this feature is widely distributed amongst other taxa branching from similar parts of the teleost stem, such as *Ichthyokentema* (Griffith &

Patterson, 1963) and *Leptolepis* (Patterson, 1975). However, dermal bones obscure the position of a potential facet in these examples.

Posteriorly, the lateral ethmoids form the remainder of the floor and walls of the nasal pit, as well as the postnasal wall (and thus the anterior face of the orbits). Multiple small foramina perforate the postnasal wall, and likely correspond to orbitonasal vessels. A much larger, rounded opening, the roof of which is unossified, transmitted the olfactory nerve from the orbit into the nasal capsules (I, Figs. 2.3I, J, 2.4H). This opening may also have been confluent with the anterior myodome.

**Parasphenoid**

The parasphenoid (psp, Fig. 2.3G, I, J, K, L) spans almost the entire length of the braincase, terminating posteriorly just before the occiput and anteriorly beneath the ethmoid. A deep, median groove for the dorsal aorta occupies the ventral surface of the parasphenoid anterior to the aortic notch (aort, Fig. 2.3I). The groove is widest posteriorly, and tapers gradually anteriorly towards a narrow, deep canal for accommodating the aortic ligament (haol, Fig. 2.3J, K, L). Anterior to this opening, the parasphenoid broadens slightly and the dorsal aorta bifurcates; paired, shallow grooves on the ventrolateral face of the parasphenoid carry the lateral dorsal aortae forward. Further anteriorly, the parasphenoid bears a ventral keel, along with ascending processes that extend dorsally to meet the postorbital process. Slender, elongate dermal basipterygoid processes (bpt, Fig. 2.3G, I, J, L) project anterolaterally from the main body of the parasphenoid at a roughly 45° angle. The internal carotids pierce their posterior margin (fica, Fig. 2.3G), while the efferent pseudobranchial arteries (fpsa, Fig. 2.3L) occupy large, rounded foramina near their anterior margin. The ventrally-directed opening of the buccohypophysial canal (bhc, Fig. 2.3L) is positioned directly between the efferent pseudobranchial foramina; it is poorly

preserved in this specimen, but its presence is corroborated by NHMUK PV P 1052. The buccohypophysial canal is surrounded by a raised, rounded rim of well-ossified bone on the ventral surface of the parasphenoid. This forms the posterior margin of a ventral keel that runs along the midline of the anterior corpus, fading out anteriorly. The anterior corpus of the parasphenoid is narrow and elongate, triangular in profile, and extends well anterior to the orbits. Although too poorly resolved to segment, examination of the tomograms suggests the parasphenoid continues ventral to the ethmoid, inserting into the deep groove on the underside of the mesethmoid (gpal, Fig. 2.3J, L, 4H, J). No dentition is visible on the ventral surface, but minute teeth have previously been described in the taxon (Patterson, 1975, pg. 328, 520), and are likely beyond the resolution of the scan.

**Endocast**

Despite poor mineralisation of the walls of the cranial cavity, the medial and right side of the endocast can be reconstructed (Fig. 5). The left side is incomplete due to fractures. Overall, the endocast is short, rounded, and robust. Much of its dorsal surface, from the anterior limit to the level of the crus commune, is open to the anterior dorsal fontanelle.

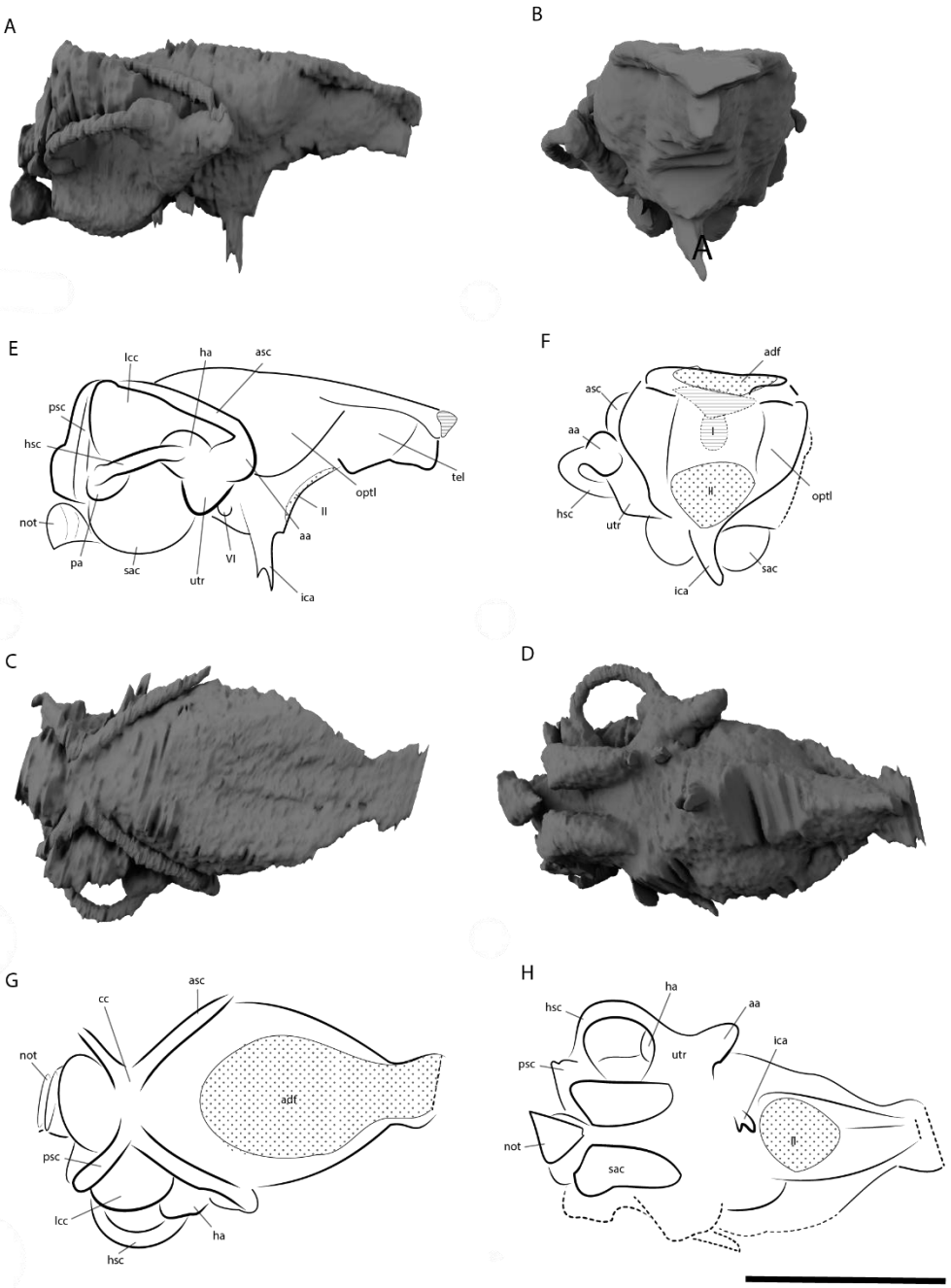
A
B
A
E
lcc
ha
asc
psc
hsc
tel
optl
II
not
aa
pa
sac
VI
utr
ica
F
adf
asc
aa
I
II
optl
hsc
utr
sac
ica
C
D
G
asc
cc
not
adf
psc
lcc
ha
hsc
H
ha
hsc
aa
ica
utr
psc
not
II
sac

**Figure 2.5: The endocast of *Dorsetichthys bechei* NHMUK PV P 73995.** Renders in (A) right lateral, (B) anterior, (C) dorsal and (D) ventral view. Interpretive drawings in (E) right lateral, (F) anterior, (G) dorsal, and (H) ventral view. Scale bar = 5 mm. Abbreviations*: aa, anterior ampulla; asc, anterior semicircular canal; cc, crus commune; ha, horizontal ampulla; hsc, horizontal semicircular canal; ica, internal carotid artery; lcc, lateral cranial canal; not, notochordal canal; optl, optic lobe; pa, posterior ampulla; psc, posterior semicircular canal; sac, saccular; tel, telencephalon; utr, utricular; II, optic nerve; VI, abducens nerve.*

The hindbrain region occupies around a third of the length of the endocast and has a mineralised roof. It is shallower than the rest of the endocast and restricted ventral to the anterior semicircular canal. The cerebellar auricles are very small, and difficult to distinguish from the rest of the endocavity. The root of the vagus nerve is oval, and exits the endocranial cavity ventrally. It is initially confluent with the posterior ampulla, but becomes separated by a very thin sheet of bone more distally from the endocranial cavity. There is no distinct cerebellar corpus.

Almost the entire midbrain region of the endocast is occupied by the optic tectum. The paired swellings for the optic lobes (optl, Fig. 2.5E, F) are deep and rounded, and wider than both the cerebellar and telencephalic (tel, Fig. 2.5E, F, H) regions of the endocast. However, the dorsal margin of the optic lobes is unclear on account of the open anterior dorsal fontanelle. The abducens nerve (VI, Fig. 2.5E) leaves the cranial cavity in this region, piercing the postorbital process before opening ventrally into the roof of the myodome. Cerebellar auricles appear to be absent.

Very little of the region corresponding to the forebrain can be described, largely due to poor mineralisation of the orbital walls of the endocavity. The area for the forebrain is the narrowest portion of the endocast, with convex lateral walls. Its anteroventral margin is continuous with the large, median optic foramen (II, Fig. 2.5E, F, H). Ventral to the optic nerve is a narrow canal for the internal carotid artery (ica, Fig. 5E, F, H), which enters the basisphenoid via the pituitary fossa (pitf, Fig. 2.3L). The proportions of the skull suggest elongated olfactory tracts, but no other features can be inferred.

All three semicircular canals are preserved and fully enclosed in bone. The canals are all equally narrow gauge, but of varying lengths. The anterior semicircular canal (asc, Fig. 2.5E, G) is long and mostly straight, and closely applied to the cerebellar region of the endocranial cavity. The horizontal semicircular canal (hsc, Fig. 2.5E, G, H) is tightly curved, forming a half circle that enters the vestibular region via a swelling level with, but continuous with, the ampulla for the posterior canal. The posterior semicircular canal (psc, Fig. 2.5E, G) is steeply inclined, almost vertical, and is the shortest of the three. Each canal terminates at a large, bulbous ampulla (aa, ha, pa, Fig. 2.5) roughly a third to a quarter of the length of each canal. All ampullae are confluent with the cranial cavity and fully enclosed in bone.

A sub-triangular utriculus (utr, Fig. 2.5E, F) lies immediately ventral to the anterior and horizontal ampullae. Both the posterior ampulla and utriculus join the deep, rounded saccular chamber (sac), which is only narrowly divided from its counterpart by the parachordal plates.

Both pairs of anterior and posterior semicircular canals meet at the crus commune (cc, Fig. 2.5G), which is narrowly separated from its antimere on the midline.

The crus commune is inset into the dorsal surface of the endocast, ventral to the endocranial roof. A large lateral cranial canal (lcc, Fig. 2.5E, G) protrudes from the cranial cavity between the semicircular canals, although due to weak endochondral mineralisation, its posterior extent is poorly resolved. The lateral cranial canal is connected to the cranial cavity anteriorly and posteriorly through the loops of the semicircular canals and extends dorsally above the endocranial roof. It lacks a connection with either the posttemporal fossa or fossa bridgei.

### 2.4.4 Cheek

The orbit is very large, extending almost a third of the length of the entire skull. The right circumorbital series is completely preserved, and consists of numerous bones: three supraorbitals, the dermosphenotic, two suborbitals (including an accessory suborbital, following the terminology of Arratia, 2013), five infraorbitals, and the antorbital. Only the second and third supraorbitals are present on the left side of the skull. Although the individual circumorbital bones are in almost continuous contact with each another, they do not form a complete ring, as supraorbital 1 (spo 1, Figs. 2.2B, D, 2.6B) and the antorbital (an, Figs. 2.2B, D, 2.6B) are interrupted by the nasal (na, Figs. 2.2B, D, 2.6B) and laterodermethmoid.

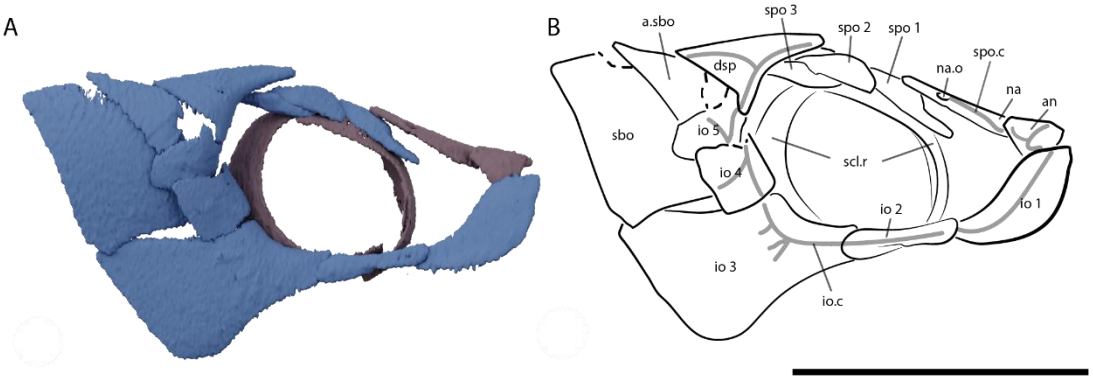

**Figure 2.6: The circumorbital series of *Dorsetichthys bechei* NHMUK PV P 73995.** (A) Render and (B) interpretive drawing in right lateral view. Colour coding: blue, cheek; purple, skull roof. Scale bar = 10 mm. Abbreviations*: a.sbo; accessory suborbital; an, antorbital; dsp, dermosphenotic; io 1-5, infraorbital bones; io.c, infraorbital canal; na, nasal; na. o, nasal opening; sbo, suborbital; scl.r, sclerotic ring; spo 1-3, supraorbital bones.*

The three anamestic supraorbitals contact each other in sequence. Supraorbital 1 (spo 1, Figs. 2.2B, D, 2.6B) is elongate, with a narrow projection extending anteriorly beneath the nasal. Supraorbital 2 (spo 2, Figs. 2B, D, 6B) is broader, gently tapering posteriorly where it rests on top of supraorbital 3. Supraorbital 3 (spo 1, Figs, 2.2B, D, 6B) is irregularly shaped, with a small shelf-like overlap area to accommodate supraorbital 2.

The infraorbitals also form a continuous, uninterrupted series. Infraorbital 1 (io 1, Figs. 2.2B, 2.6B) is a large, smooth, curved plate which partially overlaps supramaxilla 1, the maxilla and the antorbital (an, Fig. 2.2B). Infraorbital 2 (io 2, Figs. 2.2B, 2.6B) is narrow and sub-rectangular, overlapping both neighbouring infraorbitals. Infraorbital 3 (io 3, Figs. 2.2B, 2.6B) is by far the largest of the circumorbital series, with a concave anterodorsal margin framing the posterior limit of the orbit. It broadens posteriorly into a roughly rectangular plate, and its anterior margin is embayed for articulation with infraorbital 2. Infraorbitals 4 and 5 (io 4, 5, Figs. 2.2B, 2.6B) are roughly square and almost equal in size, with narrow projections at their anterodorsal margins. Infraorbital 4 overlaps a significant portion of infraorbital 5. The infraorbital sensory canal (io.cl, Fig. 2.6B) is transmitted through each infraorbital, with at least

three posterior ramifying branches in the third infraorbital and one in the fourth infraorbital.

Two suborbital (sbo, Figs. 2.2B, 2.6B) bones are present, partially overlapped by the infraorbitals. The smaller, accessory suborbital is triangular, with a straight dorsal margin roughly parallel with the edge of the skull roof. It overlaps the much larger, ventral suborbital, which forms a tall, sub-rectangular plate with an angled dorsal margin.

The dermosphenotic (dsp, Figs. 2.2B, D, 2.6B) is triangular, tapering to rounded points anteriorly, posteriorly, and ventrally. It has been slightly displaced to project above the supraorbitals and skull roof, but its short ventral ramus remains in contact with the fifth infraorbital. It houses the junction of the infraorbital canal between the infraorbital series and skull roof. An anterior branch of the canal is also transmitted above the orbit.

Finally, the sclerotic ring (scl.r, Figs. 2.2B, 2.6B) is formed of two ossicles, both of which are completely preserved on the right side of the skull. They contact dorsally but are offset by a gap ventrally, failing to form a continuous ring. Only displaced fragments of the left sclerotic ring are preserved.

### 2.4.5 Dorsal Shoulder Girdle

The shoulder girdle is incomplete, with only the right extrascapular and posttemporal completely preserved within the matrix. The cleithrum is difficult to resolve in the CT data and not fully visible on the surface of the specimen.

The posterior margin of the skull roof is overlapped by a single large, triangular extrascapular (exc, Figs. 2.2B, D). It is thin and narrows considerably towards the

midline, with the thicker lateral margin carrying the lateral line canal and at least five short, laterally directed branches. There is a distinct medial commissure of the lateral line canal within the extrascapular. The extrascapular appears to extend beyond the lateral margin of the skull roof, creating an overhang above the operculum. A large, strongly curved posttemporal lies posterior to the extrascapular, although it has been displaced somewhat ventrally. Its anterior margin is concave to match the convex posterior margin of the extrascapular. The posttemporal has a thickened ventral lateral margin to accommodate the lateral line canal, and several small branches extend medially from the main trunk to open in pores on the surface.

### 2.4.6 Upper Jaw

The articulated right upper jaw includes the premaxilla, maxilla and two supramaxillae, while the left side preserves only a fragmentary premaxilla, displaced maxilla and the remnants of one supramaxilla (Figs. 2.2, 2.7).

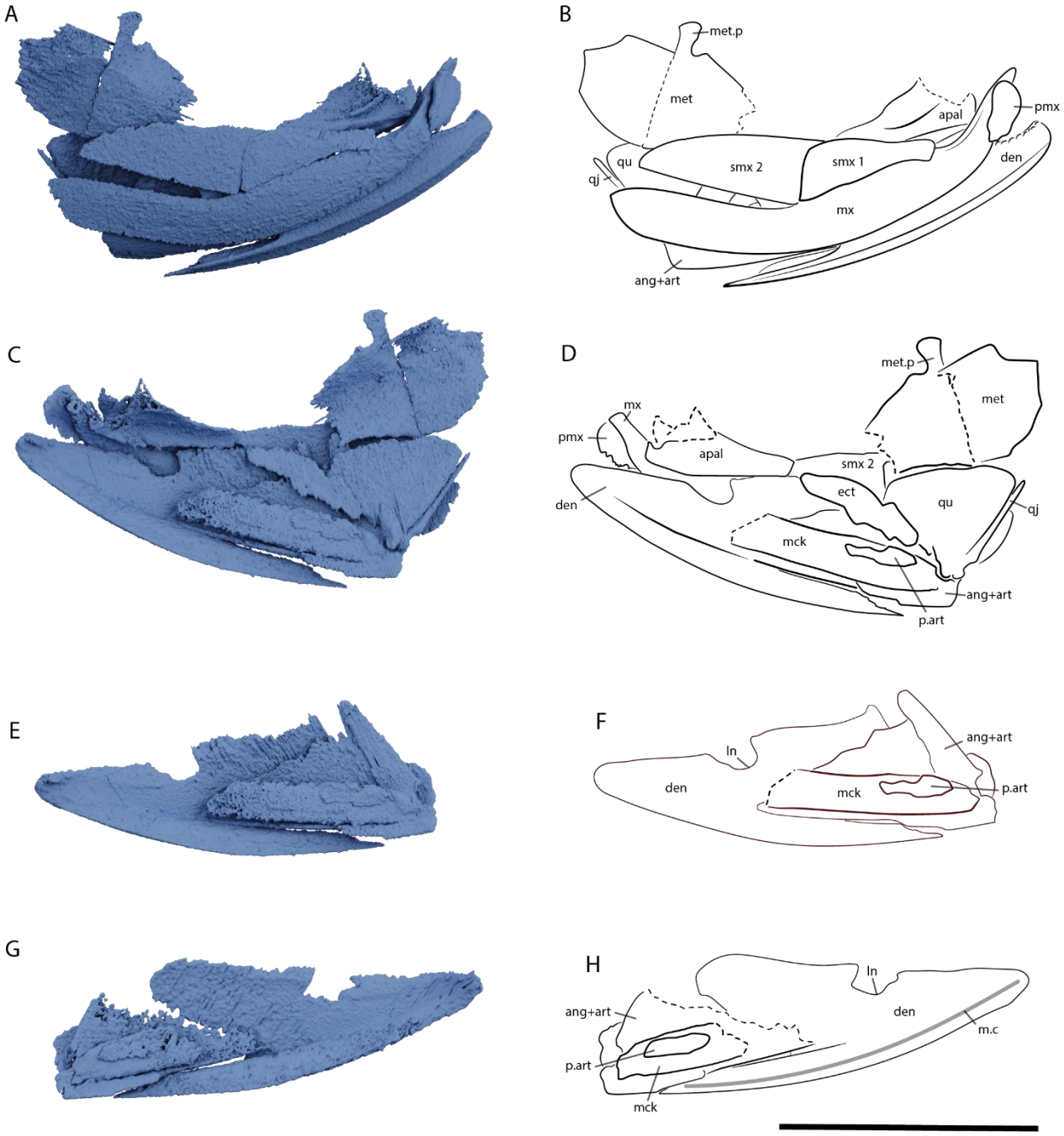
A
B
met.p
met
apal
pmx
qu
smx 2
smx 1
den
qj
mx
ang+art
C
D
met.p
met
mx
pmx
apal
smx 2
ect
qu
qj
den
mck
ang+art
p.art
E
F
ang+art
ln
den
mck
p.art
G
H
ln
ang+art
den
m.c
p.art
mck

**Figure 2.7: The jaws of *Dorsetichthys bechei* NHMUK PV P 73995.** (A) Render and (B) interpretive drawing of right upper and lower jaw in lateral view. (C) Render and (D) interpretive drawing of right upper and lower jaw in medial view. (E) Render and (F) interpretive drawing of right lower jaw in medial view. (G) Render and (H) interpretive drawing of left lower jaw in medial view. Scale bar = 10 mm. Abbreviations: *apal, autopalatine; ang+art, fused angular and articular; den, dentary; ; mck, Meckel's cartilage; m.c, mandibular canal; met, metapterygoid; met.p, metapterygoid process; mx, maxilla; p.art, prearticular; pmx, premaxilla; qj, 'quadratojugal process'; qu, quadrate; smx, supramaxilla,.*

The premaxilla (pmx, Figs. 2.4M, P, 2.7B, D) is small and sub-triangular, bearing a single row of approximately six small teeth. Each tooth is small, blunt and peg-like, and directed medially. The left premaxilla bears a short premaxillary process (pmx.p, Fig. 4P) which articulates with a small socket on the anterior face of the lateral dermethmoid (amx, Fig. 4D, L, M, N O), indicating that the premaxillae were capable of rotational movement. Its inner surface bears a ridge, above which rests the peg-like anterior process of the maxilla.

The maxilla (mx, Figs. 2.4M, N, P, 2.7B, D) is gently curved, elongate and substantially overlaps the mandible over its entire length. A single row of minute teeth appears to be present along the ventral margin of the bone. These are at the limit of scan resolution and their number and geometry cannot be accurately discerned. The outer surface bears ridged ornament that is subparallel to the long axis of the bone, while the inner surface is relatively smooth, although the dorsal half of the bone is thicker than the ventral half. Anteriorly, the maxilla narrows and projects towards the midline and somewhat dorsally behind the premaxilla. The anterior process of the

maxilla forms a narrow peg that articulates with the ethmoid, terminating in a foramen in the lateral dermethmoid (fet, Fig. 4M, N, O, P).

Two thin supramaxillae are preserved on the right side of the specimen. The posterior supramaxilla (smx 2, Fig. 2.7B, D) is twice as large as the anterior supramaxilla (smx 1, Fig. 7B, D). Supramaxilla 1 is sub-rectangular and tapers anteriorly, partially overlapping the maxilla, while supramaxilla 2 is more elongate, with a straight ventral margin and a curved dorsal margin, tapering to a point posteriorly. A narrow anterodorsal projection of supramaxilla 2 extends beneath the posterodorsal margin of supramaxilla 1. A gap between supramaxilla 2 and the maxilla suggests with that the supramaxilla is displaced or its ventral margin is too thin to be resolved in the tomograms.

### 2.4.7 Palate

The palate includes the quadrate, metapterygoid, ectopterygoid, entopterygoid and autopalatine. The quadrate (qu, Figs. 2.7B, D, 2.8B, D, F) is broadly triangular with a thickened, well ossified posteroventral margin, developed as two cotyles to articulate with the lower jaw. A long, splint-like process, sometimes referred to as the “quadratojugal” process (qj, Figs. 2.7B, D, 2.8B, D, F), projects posterodorsally from the body of the quadrate. The process lies parallel to the posterior margin of the bone, and tapers to a point.

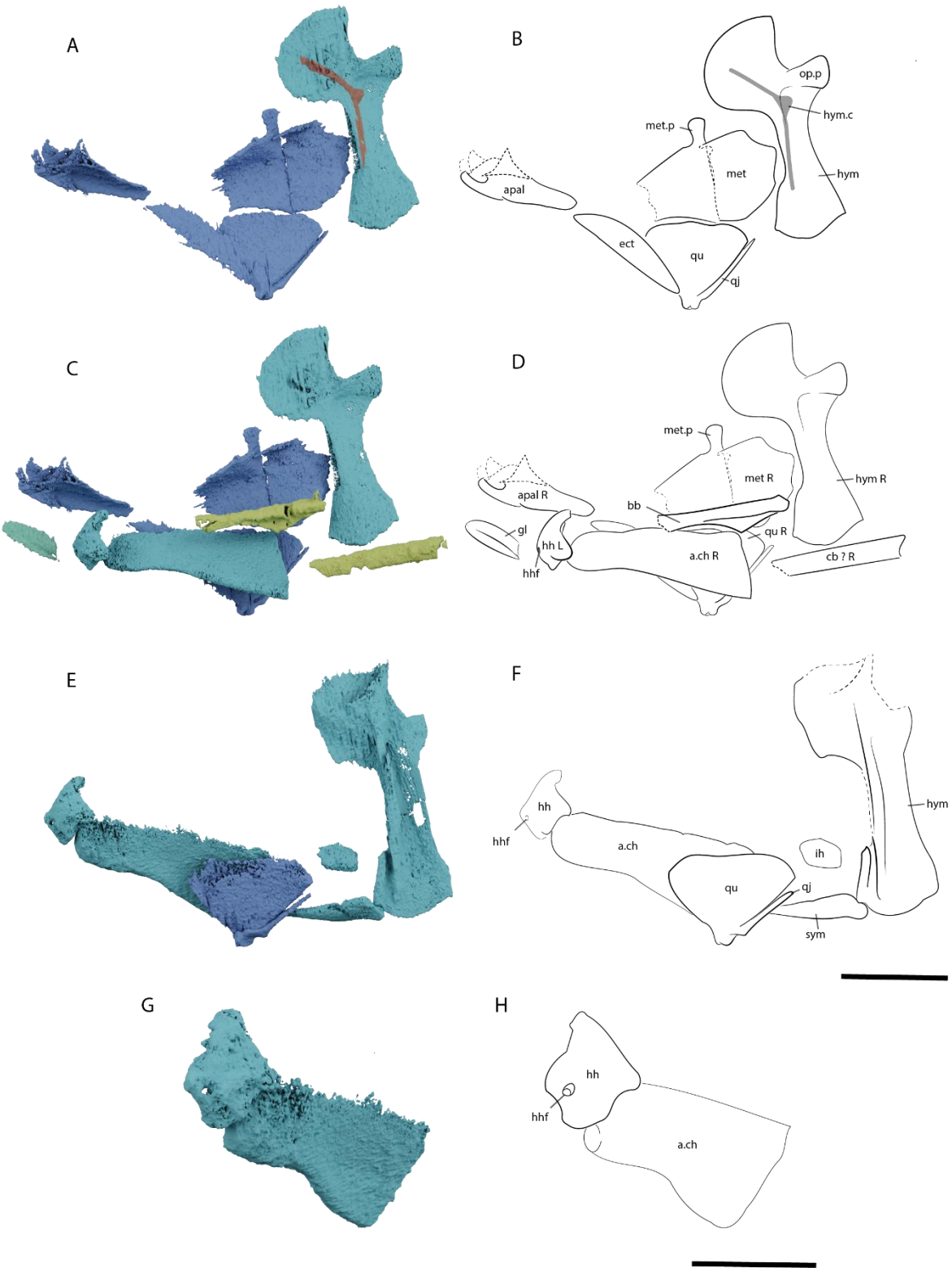
A
B
op.p
hym.c
met.p
met
hym
apal
ect
qu
qj
C
D
met.p
met R
hym R
apal R
bb
gl
hh L
qu R
a.ch R
cb ? R
hhf
E
F
hh
hym
hhf
a.ch
ih
qu
qj
sym
G
H
hh
hhf
a.ch

**Figure 2.8: The palate and hyoid arch of *Dorsetichthys bechei* NHMUK PV P 73995.** (A) Render and (B) interpretive drawing of right palate and hyoid arch in medial view. (C) Render and (D) interpretive drawing of right palate and elements of hyoid gill skeleton in medial view. (E) Render and (F) interpretive drawing of left palate and hyoid arch in right lateral view. (G) Render and (H) interpretive drawing of left hypohyal and anterior ceratohyal in anteroventral view Scale bar = 5 mm. Colour coding: blue, cheek and jaw; turquoise, hyoid arch; yellow, gill skeleton. Abbreviations: *apal, autopalatine; bb, basibranchial; cb, ceratobranchial; a.ch, anterior ceratohyal; ect, ectopterygoid; gl, gular plate; hh, hypohyal; hhf, efferent hyoidean artery; hym, hyomandibula, hym.c, hyomandibular canal; ih, interhyal; met, metapterygoid; met.p, metapterygoid process; op.p opercular process; qj, quadratojugal process; qu, quadrate; sym, symplectic.*

The large metapterygoid (met, Figs. 2.7B, D, 2.8B, D) lies dorsal to the quadrate, with an anterior face that curves medially and bears a well-developed metapterygoid process (met.p, Figs. 2.7B, D, 2.8B, D). It is incompletely ossified anteriorly. The ectopterygoid (ect, Fig. 2.7D, 2.8B) is elongate and rectangular. It does not appear to be tooth-bearing, is extremely reduced, and projects anterodorsally from the jaw joint. The entopterygoid, like the anterior portion of the metapterygoid, is too weakly mineralised to be accurately segmented, but it most likely extended to meet the posterior margin of the autopalatine.

The autopalatine (apal, Figs. 2.7B, D, 2.8B, D) is robustly ossified and tightly bound fused to the lateral ethmoid; together, these floor the anterior corner of the orbit. Its dorsal surface is smooth and gently concave, with a thickened lateral margin.

### 2.4.8 Lower jaw

The lower jaw (Fig. 2.7) consists of the dentary, Meckel's cartilage, and a fused angular and articular. Both the left and right dentaries (den, Fig. 2.7) are well preserved, although slightly out of alignment. The dentary is curved and elongate, with an anterior portion that curves strongly towards the midline. A deeply embayed posterior margin of the dentary accommodates the angular. Pyrite lines the dorsal margin of the dentary, making the presence or absence of teeth difficult to determine. There may be some teeth close to the anterodorsal margin. Approximately halfway along the dorsal margin of the dentary, which slopes anteroventrally, is a wide, sub-rounded indentation: the so-called "leptolepid notch" (ln, Fig. 2.7F, H). Both the outer and inner surface of the dentary are smooth. Ventrally, the dentary thickens into a lateral ridge, with a distinct ventromedially directed flange. The mandibular canal (m.c, Fig. 2.7H) is housed within the bone at the junction of this ridge and flange. It extends from the anterodorsal tip of the dentary to its posterior margin, after which it passes into the angular. At least half a dozen small, equally spaced pores, infilled with pyrite, connect the mandibular canal to the external surface of the dentary.

The large, triangular angular is significantly overlapped by the dentary, with its anterior apex reaching to the level of the "leptolepid notch". A thickened ridge along the ventral margin of the angular houses the mandibular canal. Its dorsal margin is approximately level with that of the dentary, and together these form a modest coronoid process. There is no independent surangular. At its posteroventral corner, the angular is fused to the articular (and possibly a fused retroarticular; ang+art, Fig. 2.7); the posterior margin of this compound ossification bears two articulation facets to receive the condyles of the quadrate. An independent retroarticular ossification is

not present. Meckel's cartilage (mck, Fig. 2.7D, F, H) is ossified anterior of the articular to the level of the "leptolepid notch". It is rectangular and lies parallel to the dentary, with slightly thickened dorsal and ventral margins. Although its anterior extent is difficult to determine due to poor ossification, there is no indication of an independent anterior mentomeckelian ossification. A thin, rectangular element that is challenging to segment lies closely applied and parallel to the medial surface of the upper portion of Meckel's cartilage on both jaws (p.art, Fig. 2.7D, F, H). Comparison to the better-resolved lower jaws of NHMUK PV P 1052 indicates that this ossification is a prearticular. It does not appear to be tooth-bearing, but this may be a limit of the scan resolution. Coronoids are absent. The posteroventral corner of the lower jaw barely extends posterior to the articular facets, and there is no evidence of a well-developed postarticular process.

### 2.4.9 Hyoid Arch

The hyoid arch comprises the hyomandibula, ceratohyal, hypohyal, symplectic, and a displaced element we interpret as an interhyal. Both the right (hym, Fig. 2.8B, D) and left hyomandibula (hym, Fig. 2.8F) are preserved, but the right is significantly better preserved and *in situ*, in articulation with the hyomandibular facet on the braincase. The hyomandibula is broad, with an upright ventral limb and large anterior head that lies at an acute angle to the rest of the ossification. Both the ventral and anterodorsal margins are convex, and a stout opercular process is present on the posterior margin. A pronounced ridge, which flares dorsally, runs down the lateral face of the hyomandibula. A corresponding, although much fainter, ridge is present on the medial face. The hyomandibular branch of the facial nerve (hym.c, Fig 2.8B) pierces the medial face of the hyomandibula anterodorsal to the conjunction of the vertical ridge

and opercular process, exiting the lateral face posteroventrally and continuing in a groove on the posterior margin of the ridge.

The symplectic (sym, Fig. 8F) is elongate, extending medial to the quadrate. It articulates with the hyomandibula posteriorly and is not involved in the lower jaw joint. A distinct gap, approximately equal to the length of the symplectic, separates the hyomandibula from the preserved ceratohyal element; it is likely that the posterior ceratohyal was not ossified and was instead cartilaginous. The anterior ceratohyal (a.ch, Fig. 2.8D, F, H) has a straight posterior margin, a thickened, rounded ventral margin, and is poorly ossified along its dorsal margin. Unusually, it lacks a groove for the afferent hyoidean artery. Both the left and right anterior ceratohyal are well preserved, although the right ceratohyal is significantly displaced and overturned. A small, sub-rounded element that is substantially shorter and shallower than the gap between the hyomandibula and anterior ceratohyal lies a little way dorsal and medial to the left symplectic. It is perichondrally lined along much of its upper and lower margins, and does not appear to be a broken portion of a larger element. As such, and by comparison to NHMUK PV P 1052 (see below), we interpret this as a displaced interhyal (ih, Fig. 2.8F), although it is difficult to tell whether it derives from the left or right hyoid arch. Anterior to the preserved ceratohyal, the hypohyal (hh, Fig. 2.8D, F, H) forms a single ossification on each side, as opposed to dorsal and ventral ossifications. It is very weakly ossified and is pierced by the efferent hyoidean artery via a foramen on the ventral margin (hhf, Fig. 2.8D, F, H).

### 2.4.10 Gill skeleton

The gill skeleton is very poorly mineralised in this specimen; several elements appear faintly in tomograms, but only a basibranchial and fragment of a ceratobranchial can

be segmented. The basibranchial (bb, Fig. 2,8D) lies directly ventral and parallel to the parasphenoid. It is elongate, with a shallow, triangular ridge along its ventral margin and a flared anterior margin. The ceratobranchial (cb, Fig. 2.8D) is present ventrolateral to the braincase. It is narrow, with a U-shaped trough along its ventral margin. Other bones posterior to the braincase might also represent fragments of gill skeleton, but they are too faintly ossified to be accurately segmented.

### 2.4.11 Operculogular Series

Elements of both the left and right opercular series are present. Only the opercle (op, Fig. 2.2B) can be resolved in tomograms, although other elements are visible externally. The left preopercular is expanded ventrally and narrows dorsally. Its anterior margins are overlapped by the suborbitals. The path of the preopercular canal and any associated rami is not externally visible. The opercle forms a large, ovoid plate, the anterior margin of which appears to abut the preopercle. The posterior margin of the opercle is well-rounded. No other elements of the opercular skeleton can be described. A thin, ovoid median gular plate (gl, Fig. 2.8D) appears to be present, lying between the left and right dentaries.

## 2.5 Description: *Dorsetichthys bechei* (NHMUK PV P 1052)

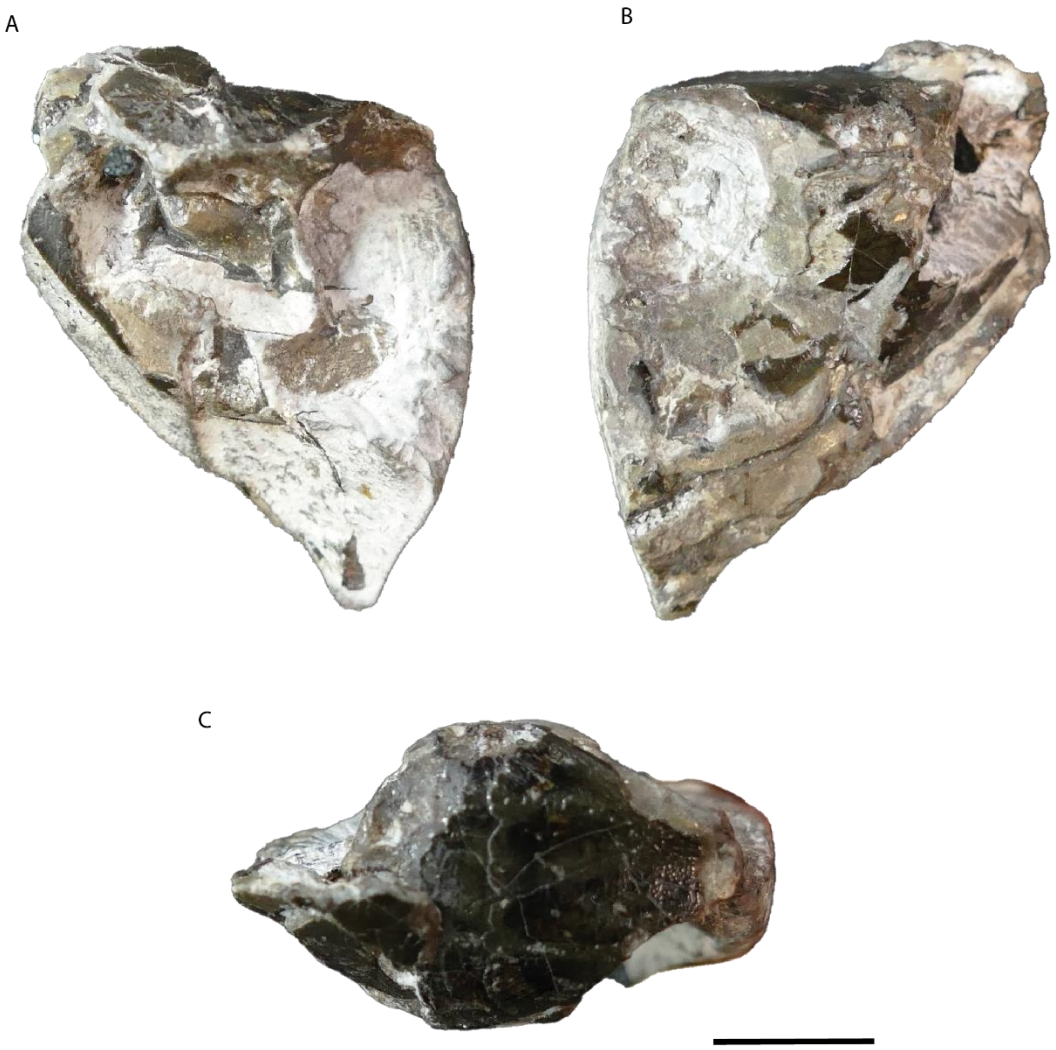


**Figure 2.9: *Dorsetichthys bechei* NHMUK PV P 1052** in (A) right lateral, (B) left lateral and (C) dorsal view. Scale = 10 mm.

### 2.5.1 General morphology

NHMUK PV P 1052 (Fig. 2.9) includes an almost complete braincase lacking only the ethmoid region, as well as partially preserved elements of the skull roof, gill skeleton, cheek, circumorbital series, palate, and lower jaw, all partly encased in matrix. The

anterior portion of the specimen, beyond the orbit, is missing. Many dermal plates have been also displaced or lost.

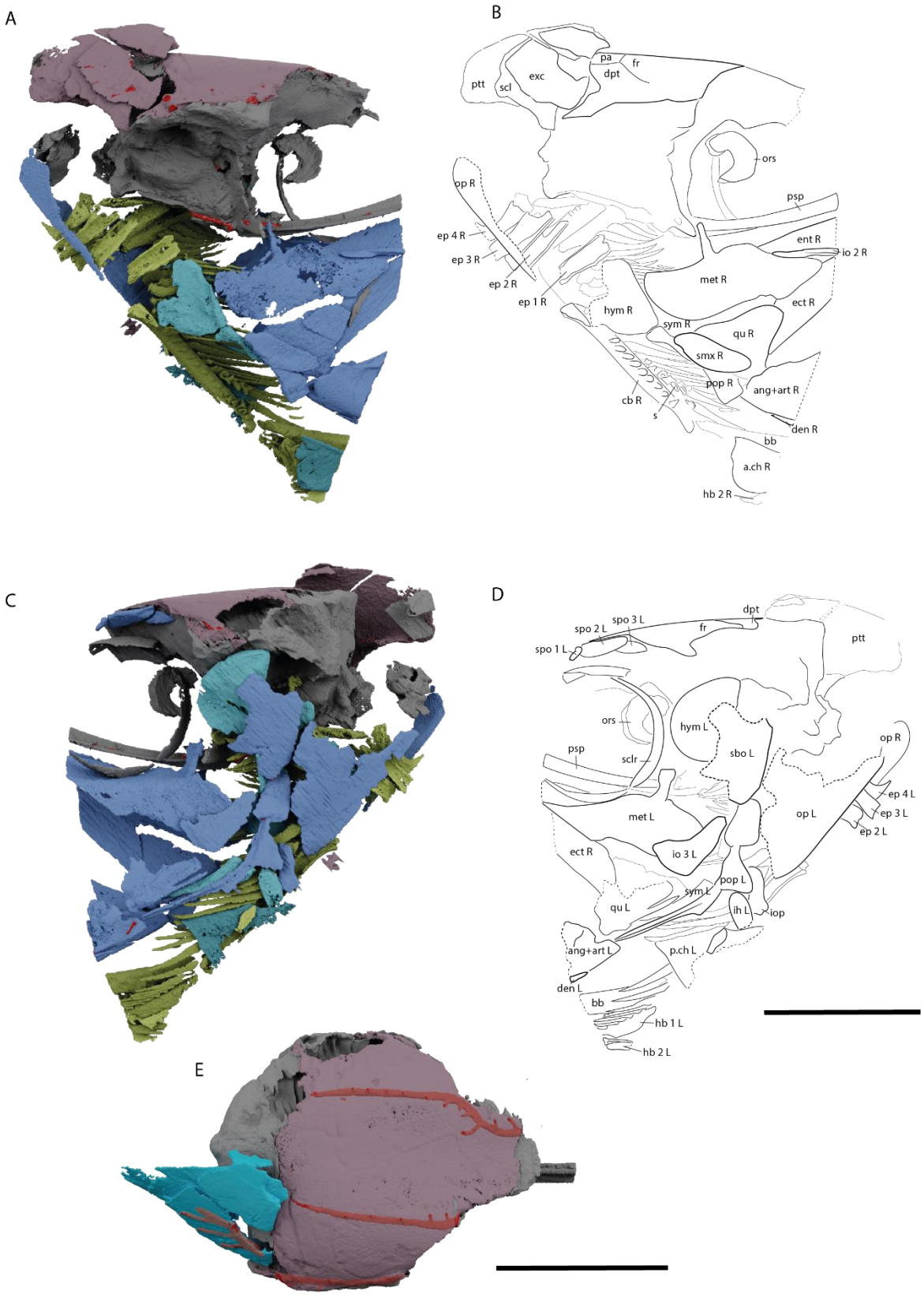

**Figure 2.10: *Dorsetichthys bechei* NHMUK PV P 1052** (A) render and (B) interpretive drawing in right lateral view, (C) render and (D) interpretive drawing in left lateral view, render (E) in dorsal view. Colour coding: blue, cheek and jaw; purple, skull roof, dermal shoulder girdle and sclerotic ossicle; grey, braincase; turquoise, hyomandibula; light green, operculogular system; yellow, gill skeleton. Sensory lines in grey Scale = 10 mm.
Abbreviations: *ang+art, fused angular and articular; bb, basibranchial; a.ch, anterior ceratohyal; p.ch, posterior ceratohyal; cb, ceratobranchial; den, dentary; dpt, dermopterotic; ect, ectopterygoid; ent, entopterygoid; ep, epibranchials; exc, extrascapular; fr, frontal; hb, hypobranchial, hym, hyomandibula; ih, interhyal; io, infraorbital; iop, interoperculum; met, metapterygoid; op, opercular; ors, orbitosphenoid; pa, parietal; pop, preopercular; psp, parasphenoid; ptt, posttemporal; qu, quadrate; s, gill raker posterior socket; sbo, suborbital; sclr, sclerotic ring; smx, supramaxilla; spo, supraorbital; sym, symplectic.*

The anatomy of NHMUK PV P 1052 is largely similar to that of NHMUK PV P 73995, including the braincase and skull roof (Figs. 2.10, 2.11). As such, we do not redescribe these elements here, and instead focus on differences in anatomy or features that cannot be described in NHMUK PV P 73995. Furthermore, although the braincase of NHMUK PV P 1052 is more complete, its internal endocranial walls are poorly mineralised, and the endocast is difficult to segment accurately (Fig. 2.12) and it is therefore not described in detail.

### 2.5.2 Braincase

The braincase of this specimen has already been described by Rayner (1948) and Patterson (1975) on the basis of external examination, and we have little to add to

their comprehensive descriptions. Most of the braincase is ossified as a single unit comprising the occipital, otic, orbitotemporal and basioccipital regions, with the exception of the separate orbitosphenoid. The ethmoid region is not preserved as the specimen is incomplete anteriorly. Grooves on the posterior face of the occiput have been interpreted as delimiting the epioccipitals, exoccipitals and supraoccipital (Patterson 1975, fig. 55), but these cannot be traced as separate ossifications extending into the neurocranium in tomograms.

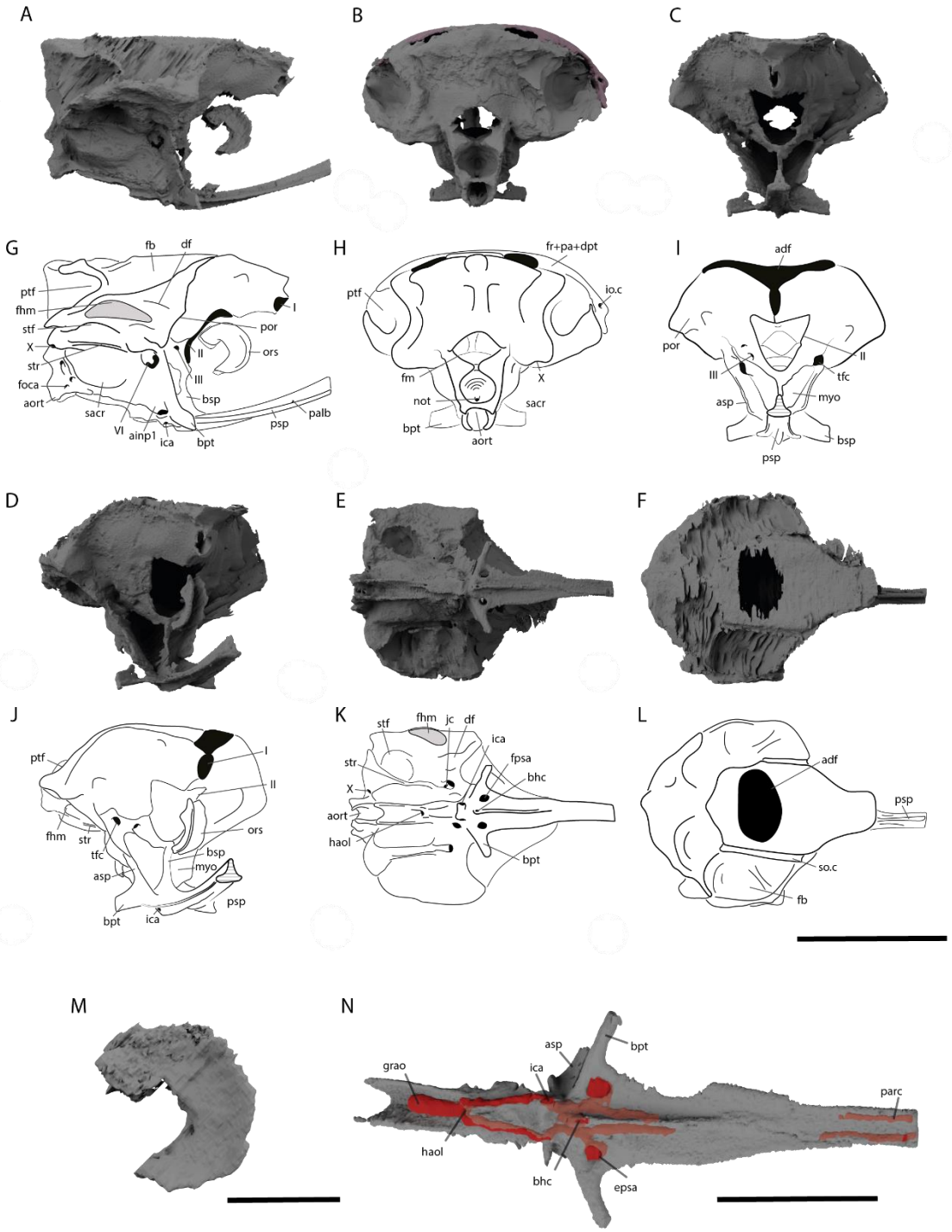
A
B
C
G
fb
df
ptf
fhm
stf
X
str
foca
aort
I
por
II
ors
III
bsp
sacr
VI
ainp1
ica
bpt
psp
palb
H
fr+pa+dpt
ptf
io.c
fm
X
not
sacr
bpt
aort
I
adf
por
II
III
tfc
asp
myo
bsp
psp
D
E
F
J
ptf
I
II
fhm
str
tfc
ors
bsp
asp
myo
psp
bpt
ica
K
stf
fhm
jc
df
ica
str
fpsa
bhc
X
aort
haol
bpt
L
adf
psp
so.c
fb
M
N
grao
asp
bpt
ica
parc
haol
bhc
epsa

**Figure 2.11: The braincase of *Dorsetichthys bechei* NHMUK PV P 1052**. Renders in (A) right lateral, (B) posterior, (C) anterior, (D) anterolateral, (E) ventral and (F) dorsal view. Interpretive drawings in (G) right lateral, (H) posterior, (I) anterior, (J) anterolateral, (K) ventral and (L) dorsal view. Scale bar = 10 mm. (M) Render of orbitosphenoid in right lateral view. Scale bar = 2.5 mm (N) Render of parasphenoid in ventral view. Scale bar = 5 mm Orbitosphenoid not rendered in panels C and I. Abbreviations*: adf, anterior dorsal fontanelle; aort, aortic notch; bhc, buccohypophysial canal; bpt, basipterygoid process; bsp, basisphenoid; df, dilatator fossa; dsp, dermosphenotic; epsa, efferent pseudobranchial artery; fb, fossa bridgei; fhm, hyomandibular facet; fm, foramen magnum; foca; foramen for occipital artery; grao, aortic groove; haol, housing of aortic ligament; ica, internal carotid artery; io.c, infraorbital canal; myo, posterior myodome; not, notochord; parc, parabasal canal; por, postorbital process; psp, parasphenoid; ptf, post-temporal fossa; sacr, saccular recess; sr, skull roof; str, lateral strut; tfr, trigemino-facial recess; I, olfactory nerve; II, optic fenestra; III, oculomotor nerve; VII, foramen of facial nerve X, foramen of vagus nerve.*

In most aspects, the braincase is identical to that of NHMUK PV P 73995. The separate orbitosphenoid ossification is well mineralised, and can be described in detail (Fig. 2.11M). It resembles a backwards ‘C’, and occupies less than a quarter of the orbit. Although the orbitosphenoid forms a single median ossification, it appears to comprise two plates that join posteriorly and diverge anterolaterally. A deep notch in the posterior margin opposes the opening of the optic nerves into the orbit.

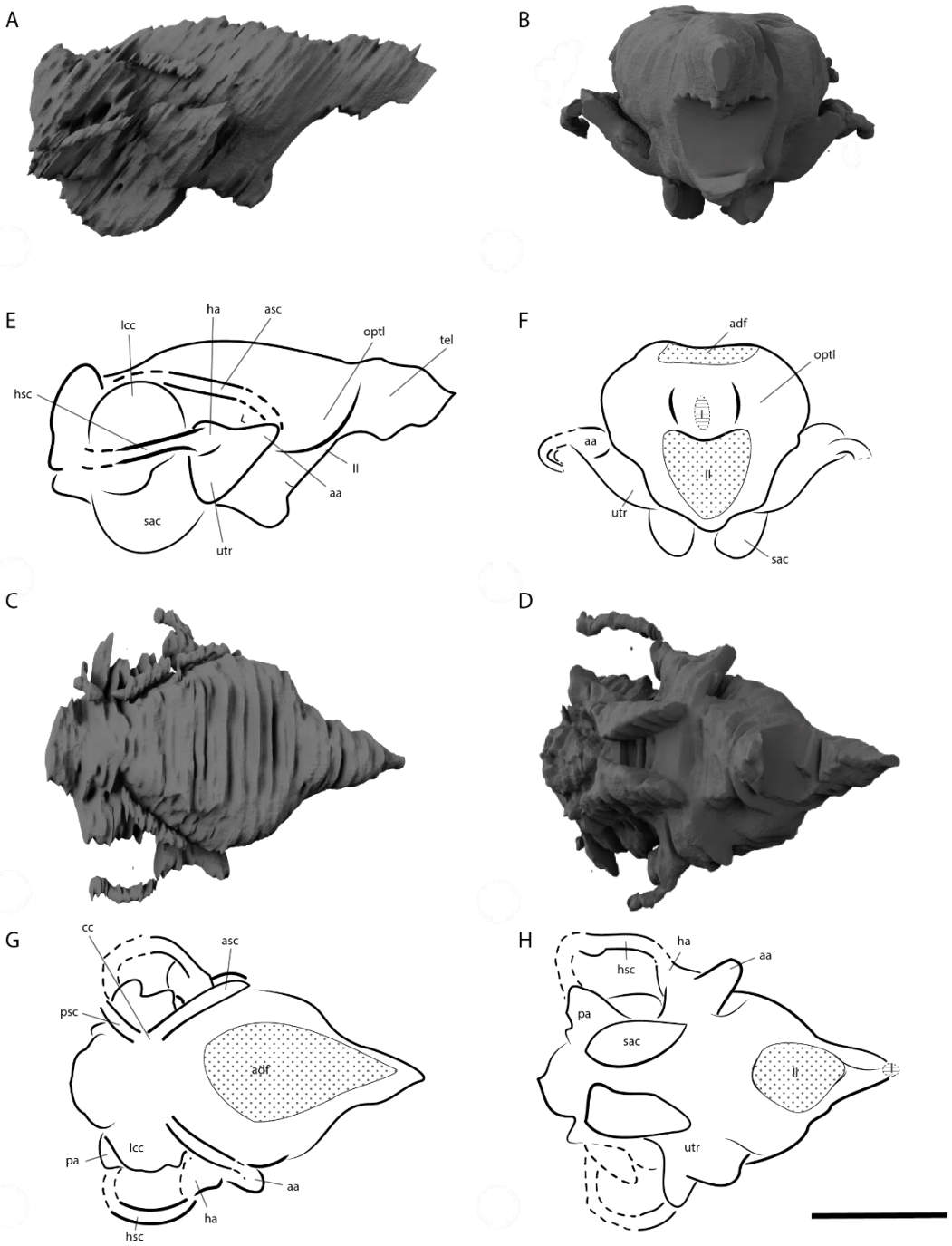
A
B
E
lcc
ha
asc
optl
tel
hsc
ll
aa
sac
utr
F
adf
optl
aa
ll
utr
sac
C
D
G
cc
asc
psc
adf
lcc
pa
aa
ha
hsc
H
ha
hsc
aa
pa
sac
ll
utr

**Figure 2.12: The endocast of *Dorsetichthys bechei* NHMUK PV P 1052.** Renders in (A) right lateral, (B) anterior, (C) dorsal and (D) ventral view. Interpretive drawings in (E) right lateral, (F) anterior, (G) dorsal and (H) ventral view. Scale bar = 5 mm. Abbreviations*: aa, anterior ampulla; adf, anterior dorsal fontanelle; asc, anterior semicircular canal; cc, crus commune; ha, horizontal ampulla; hsc, horizontal semicircular canal; lcc, lateral cranial canal; optl, optic lobe; pa, posterior ampulla; psc, posterior semicircular canal; sac, saccular; tel, telencephalon; utr, utricular; I, olfactory nerve; II, optic nerve.*

**Parasphenoid**

The parasphenoid (Fig. 2.11N) is very well preserved, allowing the route of the basicranial circulation to be reconstructed. The parasphenoid is applied directly to the underside of the basiocciput, with the convex form of the posterior stalk of the parasphenoid fitting into a corresponding concave surface on the base of the braincase. The dorsal aorta extended along the deep aortic groove (grao, Fig. 2.11N) which terminates at the median, cup-like housing of the insertion of the aortic ligament (haol, Fig. 2.11N). The dorsal aorta bifurcates around the opening, continuing in shallow grooves on the lateral face of the parasphenoid before entering laterally directed foramina for the internal carotid arteries (fica, Fig. 2.11N). The foramina for the internal carotids are housed in a ventral pedestal. The internal carotids emerge on the dorsal surface of the parasphenoid and briefly run along shallow grooves before bifurcating once again. One branch flows laterally and enters the wide, paired openings of the efferent pseudobranchial arteries (epsa, Fig. 2.11N), while the other continues anteriorly along the median crest of the parasphenoid, following the parabasal canal (parc, Fig. 2.11N). The median, ventral opening of the buccohypophysial canal (bhc, Fig. 2.11N) is also present and positioned directly

between the openings of the left and right foramina of the efferent pseudobranchial arteries. It has a rounded, well ossified rim and forms part of the ventral keel of the anterior corpus of the parasphenoid. As with NHMUK PV P 73995, teeth are not visible, but this may be an artefact of scan resolution.

### 2.5.3 Cheek

The cheek is incomplete. Most dermal plates are disarticulated or heavily prepared and thus indistinguishable in tomograms, with only the preoperculum, one suborbital, two infraorbitals and two or three supraorbitals present. Other, smaller fragments of dermal bone cannot be identified.

One infraorbital (io 2, Fig. 2.10B, D) is present on the right side. It is very well preserved and morphologically identical to the second infraorbital of NHMUK PV P 73995. However, it has been displaced ventrally to lie on the palate. A fragment of infraorbital 3 can also be identified on the left side of the specimen (io 3, Fig. 2.10B). A large, plate-like suborbital (sbo, Fig. 2.10D) is present on the left side of the specimen and can be identified by its position relative to the orbit and the absence of a canal. At least two complete supraorbital bones (spo 1-3, Fig. 2.10D), identical to those of NHMUK PV P 73995, are preserved *in situ* on the left side. A small fragment of bone anterior to the two complete supraorbitals likely represents a part of the first supraorbital, giving NHMUK PV P 1052 a total of three supraorbitals matching NHMUK PV P 73995.

### 2.5.4 Operculogular Series

A partial preoperculum (pop L, Fig. 2.10D) can be identified on the left side of the specimen. Its posterior margin is difficult to discern, and the preopercular sensory canal, which extends along the anterodorsal margin, occupies the most complete portion. On the right side, only the rounded anteroposterior margin of the preoperculum is preserved within the matrix (pop R, Fig. 2.10B). The preopercular canal is transmitted through this into the back of the lower jaw, which it abuts. Similarly, only a portion of the large, left operculum (op, Fig. 2.10B, D) can be identified. Several short, posteriorly-projecting filaments line the medial face of the operculum. A very small portion of the interoperculum (iop, Fig. 2.10D) is preserved posterior to the preoperculum, but it is truncated by the specimen break, and little can be said of its morphology.

### 2.5.5 Upper Jaw

The dermal portions of the upper jaw are largely missing, with only one supramaxilla preserved on the right side, lateral to the quadrate (smx R, Fig 2.10B). It is lenticular in shape and exposed at the surface, where the specimen is incomplete posteriorly.

### 2.5.6 Palate

The palate is very well ossified and preserved in articulation, comprising the metapterygoid, entopterygoid, ectopterygoid and quadrate. Its morphology largely matches that of NHMUK PV P 73995. The metapterygoid (met, Figs. 2.10B, D, 2.13B, D, E) is a large, sheet-like ossification with a rectangular lateral face and a triangular medial face that extends towards the parasphenoid. This medial face tapers anteriorly, substantially overlapping the posterior portion of the entopterygoid and, to a lesser

extent, the ectopterygoid. A well-developed metapterygoid process (met.p, Figs. 2.10B, D, 2.13B, D, E) extends dorsally from the junction between these faces to articulate with the anterior margin of the basipterygoid process. The preserved portion of the entopterygoid (ent, Figs. 2.10B, D, 2.13B, D) is large and ovoid, and contacts its antimere on the midline anteriorly, excluding most of the parasphenoid from the oral cavity except for the posterior portion of the narrow ventral ridge. As in NHMUK PV P 73995, the quadrate (qu, Figs. 2.10B, D, 2.13B, D, E) is sub-triangular, with an elongate splint-like posterodorsal process. Anteroventrally, the quadrate is expanded into condyles that articulate with the lower jaw. The palate appears to be edentulous, with smooth medial surfaces.

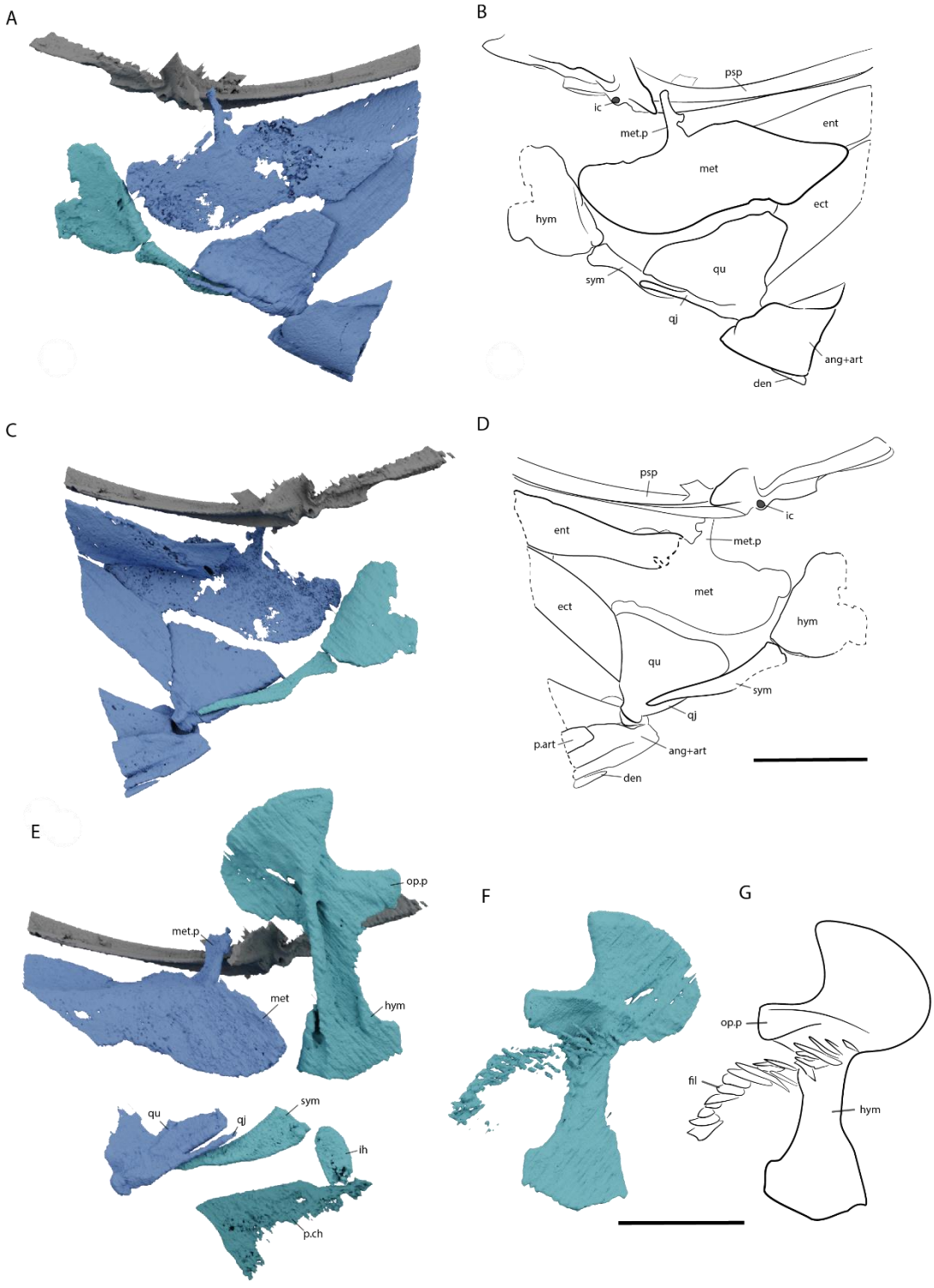
A
B
psp
ic
met.p
ent
met
ect
hym
qu
sym
qj
ang+art
den
C
D
psp
ic
ent
met.p
met
ect
hym
qu
sym
qj
p.art
ang+art
den
E
op.p
met.p
met
hym
qu
qj
sym
ih
p.ch
F
G
op.p
fil
hym

**Figure 2.13: The palate and hyoid arch of *Dorsetichthys bechei* NHMUK PV P 1052.** (A) Render and (B) interpretive drawing of right palate and hyoid elements in lateral view. (C) Render and (D) interpretive drawing of right palate and hyoid arch in medial view. (E) Render of left palate and hyoid arch in lateral view. (F) Render and (G) interpretive drawing of left hyomandibular and associated filaments in medial view. Colour coding: blue, cheek and jaw; grey, parasphenoid; turquoise, hyomandibula. Scale bar = 5 mm. Abbreviations*: ang+art, fused angular and articular; a.ch, anterior ceratohyal; den, dentary; ect, ectopterygoid; ent, entopterygoid; fil, filaments; hym, hyomandibula; ih, interhyal; met, metapterygoid; met.p, metapterygoid process; op.p, opercular process; p.art, prearticular; psp, parasphenoid; qj, 'quadratojugal' process; qu, quadrate; sym, symplectic*

### 2.5.7 Lower Jaw

A short portion of the angular and articular are preserved in articulation (Figs. 2.10B, D, 2.14). The angular is narrow and carries the mandibular sensory canal along its ventral margin. The articular and angular are fused (ang+art, Figs. 2.10B, D, 2.14), and the posterodorsal surface of the articular forms a deep articulation facet for the quadrate. Ossification of the Meckel's cartilage continues anteriorly until the specimen break. A rectangular plate, which we identify as the prearticular (p.art, Fig. 2.14), lies along the dorsal portion of the medial face of the mandible. Only a tiny fragment of the posteroventral margin of the dentary (den, Figs. 2.10B, D, 2.14) is preserved.

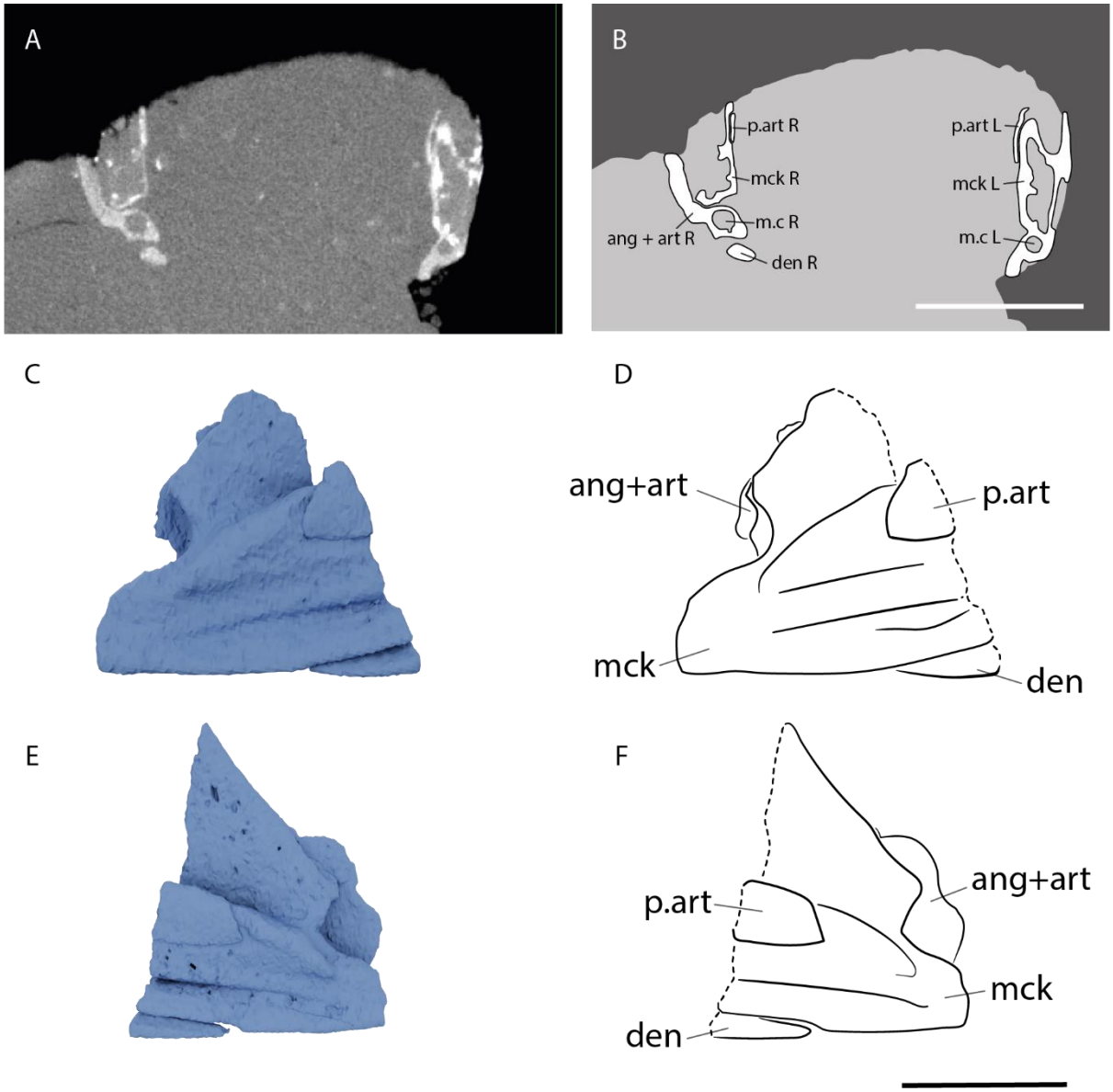


**Figure 2.14: The lower jaws of *Dorsetichthys bechei* NHMUK PV P 1052.** (A) Tomograph (frontal section) of lower jaws with (B) interpretive drawing. Scale bar = 2.5 mm. (C) Render and (D) interpretive drawing of right lower jaw in lateral view. (E) Render and (F) interpretive drawing of right lower jaw in medial view. Scale bar = 5 mm. *Abbreviations: ang + art, fused angular and articular; den, dentary; mck, Meckel's cartilage; m.c, mandibular canal; p.art, prearticular.*

### 2.4.8 Hyoid arch

The hyoid arch includes a hyomandibula, ceratohyal and symplectic. The left interhyal is also preserved. The left hyomandibula (hym, Figs. 2.10D, 2.13E, G) is fully intact, while only a fragment of the right hyomandibula (hym, Fig. 2.13B, D) is present. Its gross morphology appears to match that of NHMUK PV P 73995. In addition, a series of sinuous, posteriorly directed filaments (gf, Figs. 2.13G, 2.15B) are present on the medial surface of the left hyomandibula, ventral to the opercular processes. They form a continuous series with the filaments borne on the posterodorsal margin of epibranchial 1, and may represent evidence of a pseudobranch, functioning alongside the spiracular canal (Laurent & Dunel-Erb, 1984).

Only a small portion of the right anterior ceratohyal (a.ch, Figs. 2.10B, 2.15D) is preserved due to a break in the specimen, positioned ventral to the braincase along with the ventral gill skeleton. It is narrow and roughly rectangular in axial section, with a thickened ventral margin. The left posterior ceratohyal (p.ch, Fig. 2.13E) is near complete, though exposed on the surface ventrally. It bears a broad notch on its dorsal surface to accommodate the interhyal (ih, Fig. 2.13E), and is not attached to any associated branchiostegals. The symplectic (sym, Fig. 2.13B, D, E) is identical to that of NHMUK PV P 73995. The right symplectic (sym, Fig. 2.13B, D, E) is partially exposed on the surface of the specimen, and a portion of its verntral margin is incomplete, but is preserved in articulation with the hyomandibula posteriorly. Both the left and right symplectic terminate anteriorly against the inner surface of the quadrate, lying parallel to the “quadratojugal” process (qj, Fig. 2.13B, D, E)

### 2.4.9 Gill skeleton

Unlike in NHMUK PV P 73995, much of the gill skeleton of NHMUK PV P 1052 is preserved and articulated (Figs. 2.15, 2.16), and thus can be described in detail. The ventral gill series is incomplete on both sides, but includes ceratobranchials, hypobranchials and a basibranchial ossification. The dorsal gill series includes four epibranchials, infra- and suprapharyngobranchials in the first two arches, and an infrapharyngobranchial in the third arch. Due to the way the specimen is preserved, dorsal components on the right side of the specimen are incomplete anteriorly. An array of rakers and filaments are also present on both sides. Though they are slightly displaced, rakers appear to form an uninterrupted orderly sequence across the dorsal and ventral component of the gill arch.

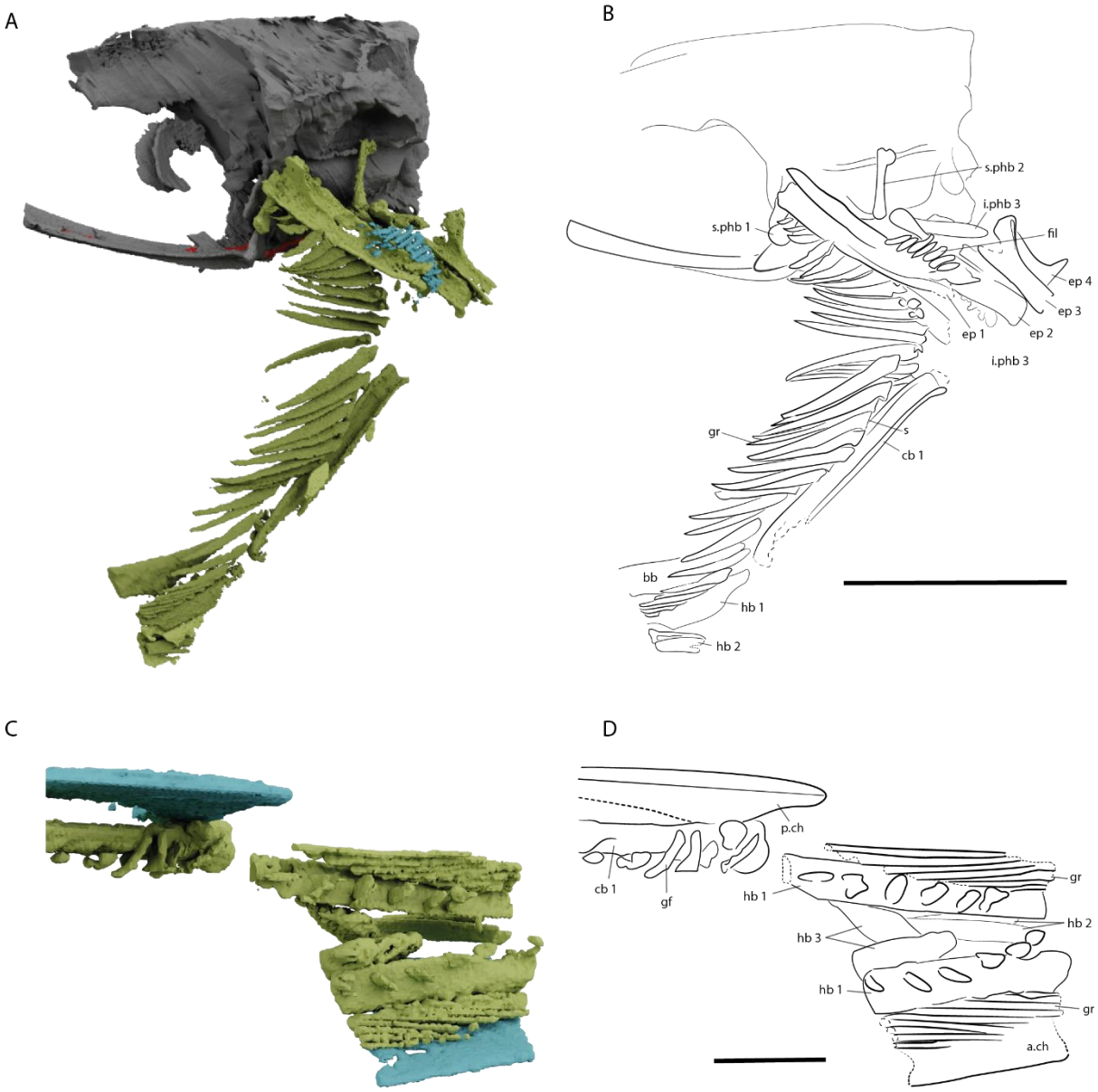
A
B
s.phb 2
i.phb 3
s.phb 1
fil
ep 4
ep 3
ep 1
ep 2
i.phb 3
gr
s
cb 1
bb
hb 1
hb 2
C
D
p.ch
cb 1
gf
hb 1
gr
hb 2
hb 3
hb 1
gr
a.ch

**Figure 2.15: The gill skeleton of *Dorsetichthys bechei* NHMUK PV P 1052.** (A) Render and (B) interpretive drawing of gill skeleton in left lateral view. Scale bar = 10 mm. (A) Render and (B) interpretive drawing of ventral gill skeleton and hyoid arch in dorsal view. Scale bar = 2.5 mm. Abbreviations: *bb, basibranchial; cb, ceratobranchial; a.ch, anterior ceratohyal; p.ch, posterior ceratohyal; ep 1-4, epibranchials; fil, filaments (hyoid); gf, gill filaments; gr, gill rakers; hb 1-3, hypobranchials; i.phb3, infraphyrangobranchial, s, gill raker posterior socket; s.phb 1-2, suprapharyngobranchials.*

Only a single basibranchial (bb, Fig. 15B) is present. It is broader anteriorly and narrows somewhat posteriorly, although the anterior margin is incomplete. The dorsal surface is smooth and flat, and the ventral surface is developed into a broad median ridge. Paired articulation facets are preserved on either side of the ventral ridge, which would have articulated with the hypobranchials in life.

Only a single ceratobranchial is preserved, and its length and position immediately medial to the hyomandibula suggests it belongs to the first arch (cb, Fig. 2.15). It is complete on the left side of the specimen, but only a small fragment is present on the right. The ceratobranchial is elongate, with a slight medial deflection at the distal end, and a groove running along its entire ventrolateral surface. Its dorsal margin bears a row of at least eleven, smooth, elliptical nodes, angled obliquely to the long axis of the cerotobranchial. 13 anteriorly-directed gill rakers (gr, Figs. 2.15B, 2.16A, B) are preserved in articulation with the ceratobranchial, and the base of each raker articulates with the lateral margin of a ceratobranchial node. Each raker is elongate and triangular, tapering anteriorly, with a concave dorsal margin and convex ventral margin. The base of each, at its posterior margin, is thickened into a shallow,

cup-shaped socket (s, Fig. 2.16A, B) for articulation with a corresponding node (gn, Fig. 2.16A) on the host ceratobranchial. In addition to nodes and rakers, the ventral quarter of the ceratobranchial bears a row of fine, undulous gill filaments, positioned medial to the nodes. Although the right ceratobranchial is mostly missing, some of its associated rakers are still present. Rakers of the ventral gill arch are largest nearer the posterior end of the ceratobranchial, and each overlaps the next in sequence slightly at its proximal end.

Three pairs of hypobranchials (hb, Fig. 2.15) articulate with the ventral face of the basibranchial, although the arch to which they belong cannot be determined with confidence. The more anterior pair are elongate, straight, and C-shaped in cross section, with a groove along the ventral margin, although are truncated anteriorly and posteriorly where the specimen is broken. The left aligns with the complete ceratobranchial, and therefore may represent hypobranchial 1 (hb1; Fig. 2.15). A series of elongate rakers, continuous with those of the ceratobranchial, articulate with the lateral surface of the hypobranchial, and short, stubby filaments are borne along its entire dorsal surface. A second pair of ossifications, preserved somewhat ventral to the others, resemble shorter, slightly flattened versions of the first pair, and may belong to the second gill arch (hb2 ; Fig. 2.15). The most posterior pair are fully enclosed within matrix and thus complete. They are short and gently curved, with no distinct groove, and are tentatively identified as hypobranchial 3 (hb3 ; Fig. 2.15). Rakers and filaments appears to be absent from the putative second and third hypobranchials.

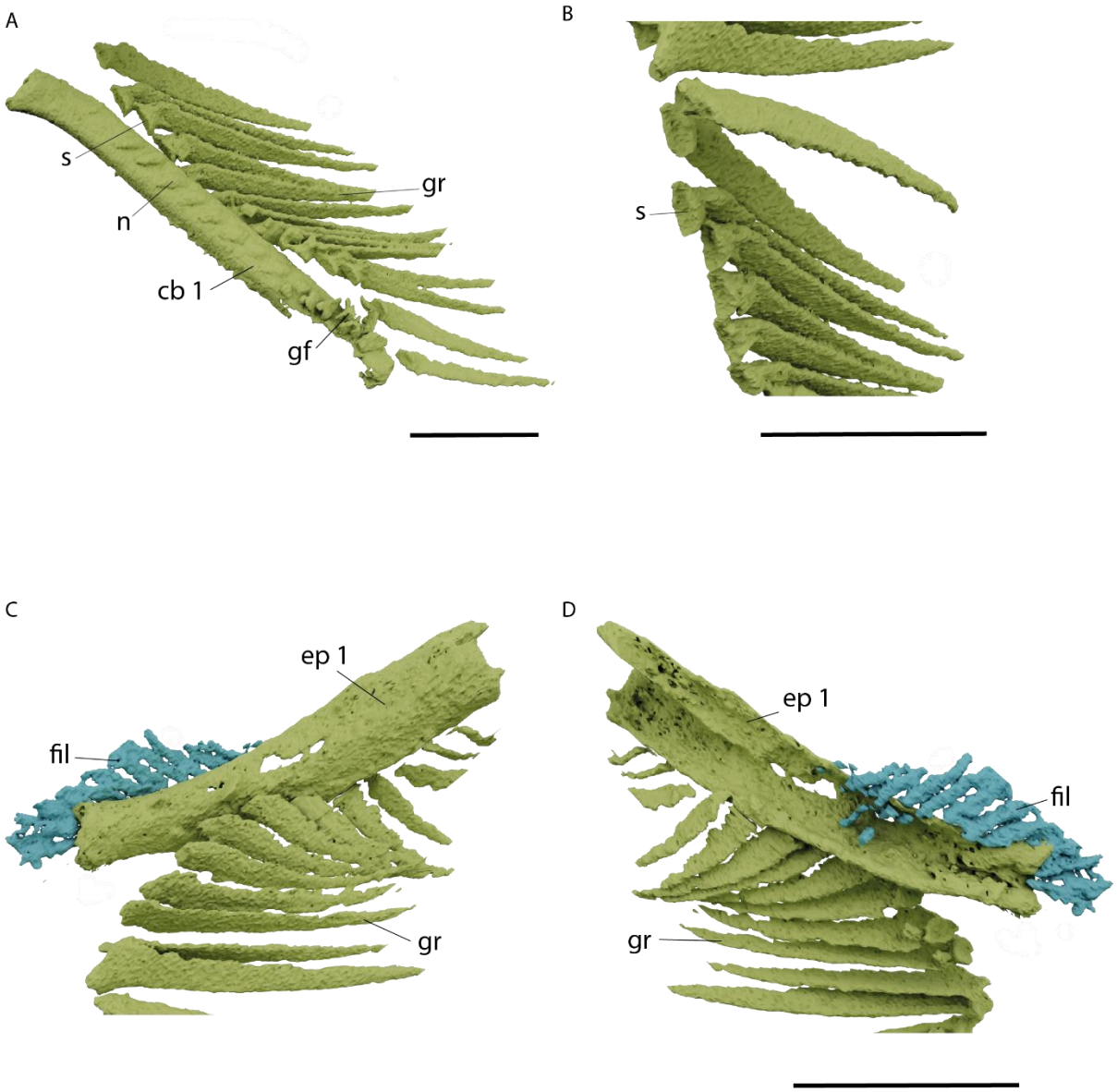


**Figure 2.16: The upper gill skeleton of *Dorsetichthys bechei* NHMUK PV P 1052.** (A) Render of left ceratobranchial and rakers in medial view, (B) render of gill rakers in posterior view, Render of epibranchial 1 and rakers in (C) lateral view and (D) medial view. Scale bar = 5 mm. *Abbreviations: cb, ceratobranchial; ep 1, epibranchial; fil, filaments (hyoid arch); gd, gill nodes; gf, gill filaments; gr, gill rakers.*

Four epibranchials (ep 1-4, Figs. 2.15B, 2.16C, D) are preserved on each side. Epibranchial 1 is the largest of the four, and shows a slight medial curve toward its distal end. Its dorsolateral face is grooved, and the anterodorsal corner is developed as a modest uncinate process. At least 14 gill rakers articulate with its medioventral margin via small nodes. The rakers are morphologically similar to those found on the ceratobranchial, although somewhat shorter, tapering anteriorly. At least twelve short, stout, straight elements in contact with the posterodorsal and posterior margin of the epibranchial likely represent gill filaments. Infrapharyngobranchial 1 and suprapharyngobranchial 1 are short, stout elements that near the anterior margin of the epibranchial; the infrapharyngobranchial is curved and the suprapharyngobranchial straight. Epibranchial 2 is only slightly shorter than the first, but is otherwise morphologically similar, also supporting two pharyngobranchials. Infrapharyngobranchial 2 (i.phb2, Fig. 2.15B) is around a third of the length of the epibranchial, straight, and without a groove, but bifurcates anteriorly to form a short dorsally directed process. Suprapharyngobranchial 2 (s.phb2, Fig 2.15B) is narrow and rod-like. Approximately five short rakers project anterolaterally from the lateral face of epibranchial 2, and around eight very short filaments sit on its dorsomedial face, with a smaller number arranged in a ventromedial series. Epibranchials 3 and 4 are much shorter, straight, and do not seem to have associated rakers or filaments. The third epibranchial is U-shaped in cross section, and bears an uncinate process; the process on epibranchial 3 is proportionately the largest of all. Only one pharyngobranchial element is associated with this arch. Infrapharyngobranchial 3 is elongate, approaching the length of the second epibranchial, and laterally compressed. It also bifurcates anteriorly, and the anterior process is longer than the dorsal. Epibranchial 4 lacks a groove, has a very small uncinate process, and bears a

short dorsal projection at its posterior end. A series of minute, scattered elements are present around the posterior portions of epibranchials 3 and 4, but it is impossible to tell whether these are rakers or filaments. The arrangement of the epibranchials and pharyngobranchial in life position is estimated in Figure 2.17.

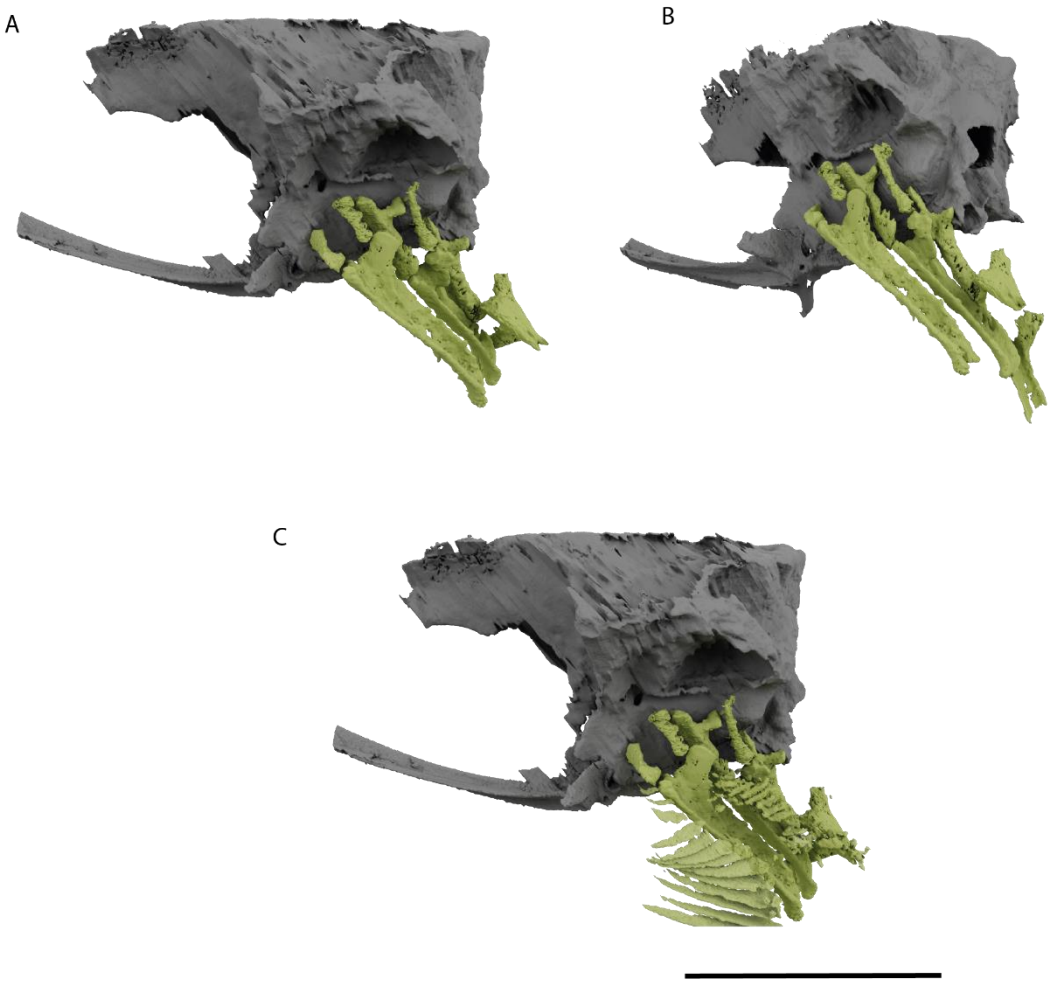


**Figure 2.17: The rearticulated upper gill skeleton of *Dorsetichthys bechei* NHMUK PV P 1052.** Render in (A) left lateral, (B) posteroventral view. (C) Render in left lateral view, with gill rakers and filaments shown. Scale bar = 10 mm.

## 2.6 Discussion

### 2.6.1 Taxonomic coherence of *Dorsetichthys bechei*

Although a key taxon in many investigations of early teleost and neopterygian relationships, the cranial skeleton of *Dorsetichthys* is most often described from an amalgam of three-dimensional but isolated braincase material (Rayner 1948; Patterson, 1975) and abundant but laterally compressed dermal skeletons (Rayner 1948; Nybelin, 1966). Based on comparison to specimens conforming to these disparate modes of preservation, we confirm the identity of NHMUK PV P 73995 as a new specimen of *Dorsetichthys bechei*. The association of external and internal dermal and endoskeletal elements in a single, articulated specimen provides some confidence that past work based on a composite of specimens yielded an accurate picture of anatomy in *Dorsetichthys*. However, there are some anatomical inconsistencies between the material described here and that in past descriptions. For example, the anterior ceratohyal is ungrooved and the posterior ceratohyal does not host branchiostegals, contrasting with conditions in other specimens described by Rayner (1948) and Nybelin (1966). This hints at possible morphological and taxonomic diversity within the material currently referred to *Dorsetichthys bechei*. Future work should target complete specimens that preserve both endoskeletal and dermal elements, and may prove amenable to CT scanning, to investigate further evidence of variation.

### 2.6.2 New anatomical insights

CT scanning permits a comprehensive description of the internal and external anatomy of *Dorsetichthys bechei*, allowing us to clarify the specific diagnosis, revise

previous descriptions, and provide new insights into its ecology. These updates are spread across the cranium but are particularly concentrated in the upper jaw and palate, lower jaw, and hyoid and branchial arches, and we review these below.

**Upper jaw and palate.** In previous descriptions of *D. bechei*, the premaxillae are either described as lacking an anterior connection to the braincase (Rayner, 1948, pg. 40), or the presence or absence of this feature is not remarked upon (Nybelin, 1966; Patterson, 1975). Similarly, descriptions of the ethmoid region (Rayner. 1948; Nybelin, 1966; Patterson, 1975) refer only to partially exposed lateral dermethmoids in two-dimensionally preserved specimens in which internal anatomy cannot be observed or rely on reference to better-preserved ethmoid regions in pholidophorids or leptolepids. Arratia recovers a mobile premaxilla as an unambiguous synapomorphy uniting *Dorsetichthys bechei* with more “advanced teleosts” (Arratia, 1999, pg. 289; Arratia, 2000, pg. 163), although this appears to be based on an inferred presence in *D. bechei*.

CT scanning of NHMUK PV P 73995 reveals an *in-situ* ethmoid and upper jaw. Both the maxilla and premaxilla have narrow anterior processes that articulate with the ethmoid region to allow protrusion of the dermal elements and mobility of the upper jaw complex. Although three-dimensional braincase material is lacking in pholidophorids *sensu* Arratia (2013), premaxillae appear to be immobile. A fenestra in the ethmoid of “*Pholidophorus” germanicus* (Patterson, 1975, pg. 477), recovered as a possible ankylophorid by Arratia (2017), resembles that seen in *D. bechei* and most likely also permitted movement of the entire upper jaw.

Previous descriptions of the quadrate of *Dorsetichthys bechei* (e.g., Rayner, 1948, Fig. 27A) do not figure or describe any form of process along the posterior

margin of this element. Such a process is sometimes referred to as the “quadratojugal” or “quadratojugal process”, although we note that the naming and homology of this is controversial (see Arratia & Schultze, 1991; Arratia, 2013; Arratia, 2015; Taverne, 2018). Despite a lack of direct description, it is coded as present in *D. bechei* in Arratia’s analysis (2013, ch. 78; see discussion in Taverne, 2018) and later included as a diagnostic feature of Dorsetichthyiformes (Arratia, 2017, pg. 22). Here, we confirm the presence of this process in *D. bechei*.

**Lower jaw.** The presence of a surangular was included as a diagnostic character of Dorsetichthyiformes by Arratia (2017, pg. 22), despite widespread possession of a surangular in many neopterygians. Curiously, a surangular has not previously been explicitly described as present in *Dorsetichthys bechei*: Rayner (1948, pg. 40) describes the outer surface of the lower jaw as comprising a dentary and angulo-articular, while Nybelin (1966, pg. 363) reports an angulo-supra-angular that cannot be differentiated from the dentary. We find no evidence for a surangular in *D. bechei* and have emended the diagnosis accordingly.

A well-developed postarticular process of the lower jaw is also cited as present in *D. bechei*, and indeed one of the features uniting it with more derived teleosts (Arratia 2013, 2017). However, the anatomical condition more closely resembles that seen in pholidophorids (e.g. Arratia, 2013, pg. 68, fig. 52; pg. 95, fig. 77C), where it is considered absent. We consider the postarticular process to be absent in *D. bechei*.

Previous evidence concerning the presence or absence of a prearticular in *D. bechei* is conflicting. Rayner (1948) states that it is present, although does not figure or illustrate the lower jaw in medial view, whereas Nybelin (1966) reports its absence.

Although the internal surface of the lower jaw does not seem to be explicitly described, Arratia considers the prearticular absent in *D. bechei* and codes it as such in phylogenetic analyses (e.g. Arratia 2013, 2015, 2017). Absence of a prearticular is therefore one of the characters recovered as supporting a close relationship between *D. bechei* and more crownward teleosts to the exclusion of pholidophorids. Although the inner surface of the lower jaw is unknown in many pholidophoriforms, a narrow, rectangular prearticular is present in *Pholidorhynchodon* (Arratia 2013, fig. 48). Here, we describe a prearticular in the lower jaws of both NHMUK PV P 73995 and NHMUK PV P 1052, which appears reduced relative to that seen in pholidophorids and earlier diverging actinopterygians.

**Hyoid and branchial arches.** Only limited aspects of the hyomandibula and ceratohyal have previously been described. We describe these elements plus the interhyal, symplectic, and hypohyal in more detail. In both specimens, the anterior ceratohyal is smooth, and in NHMUK PV P 1052, the posterior ceratohyal does not appear to support branchiostegals. This contrasts with previous descriptions, where grooved ceratohyals bearing branchiostegals have been reported and figured (Rayner 1948, Nybelin, 1966: pl. 3, fig. 5); the significance of this variation is not yet known.

A subset of teleosts possess paired dorsal and ventral hypohyals. Arratia (1999 pg..292–293) mentions that only a single hypohyal is present in *D. bechei*, and that it is unknown whether it is pierced by the hyoidean artery. However, subsequent matrices indicate an inapplicable condition for this character in *D. bechei* (Arratia 2013, ch. 82; Arratia 2017, ch. 91; functionally equivalent in PAUP to a '?' coding), leading to paired dorsal and ventral hypohyals being optimised as a synapomorphy uniting some

subset of “advanced teleosts” and *Dorsetichthys*. We find evidence for only a single pair of hypohyals in *D. bechei*, which are pierced by the hyoid artery.

**Circumorbital series.** NHMUK PV P 73995 and NHMUK PV P 1052 provide some evidence for intraspecific variation in the circumorbital series of *Dorsetichthys*. A second (accessory) suborbital is present posterior to the dermosphenotic in NHMUK PV P 73995, and both NHMUK PV P 73995 and NHMUK PV P 1052 possess three supraorbital bones, rather than the previously reported two; although a third supraorbital was recognised in NHMUK PV P 1052 by Nybelin, it was interpreted as damage sustained during ontogenetic development (Nybelin, 1966, pg. 360). Similar variations in the circumorbital series have been recorded in multiple genera of pholidophorids: some specimens of *Pholidorhynchodon malzannii* and *Parapholidophorus nybelini* possess either two or three supraorbitals; the number of supraorbitals may even vary on the left and right sides of the same specimen in *P. nybelini*. Furthermore, a second (accessory) suborbital is also found in some individuals of *P. malzannii, P. nybelini*, and *P. gervasuttii* (Arratia, 2013).

### 2.6.3 Feeding ecology in early teleosts

Both dorsal and ventral components of the gill skeleton of *D. bechei* support an array of fine rakers and filaments. Similar structures associated with the hyomandibula provide evidence of a pseudobranch. The presence of reduced teeth on the dentary and maxilla in combination with these elaborate gill rakers suggest that *D. bechei* was capable of suspension feeding facilitated by the mobile upper jaw, an ecology first alluded to by Rayner (1948). While this feeding mode in stem teleosts is more

commonly associated with the giant suspension feeding pachycormids (Friedman *et al.,* 2010, 2013; Schumacher *et al*., 2016; Gouiric-Cavalli, 2017) *Dorsetichthys* may have been analogous to small-bodied suspension feeders such as herring and menhaden. Herring exhibit both particle biting (selective capture of individual particles) and filtering (nonselective, passive feeding on any particles in their path), depending on the concentration of prey (Gibson & Ezzi, 1990). As a limited number of small teeth are present on the anterior portion of the dermal jaws of *D. bechei*, a similar facultative suspension feeding ecology seems likely.

The feeding ecology of early teleost fishes was recently reviewed by Arratia & Schultze (2024). Many of the earliest teleosts appear to exhibit filter feeding to a greater or lesser degree, and although gill morphology is not known in other taxa, *D. bechei* typifies at least the external morphology. An obligate suspension-feeding ecology, employing slightly different adaptations, appears to be present in the Triassic teleosteomorph *Marcopoloichthys* (Arratia 2022). These fishes display long, narrow, edentulous premaxillae lacking an anterior process, which presumably had a ligamentous connection to the ethmoid region. Suction feeding in these fishes was facilitated by antero-posterior extension and dorso-ventral flattening of the cranium, braced against an expanded vertebral column element termed a ‘supraneural carrier’ (Arratia 2022). As noted by Arratia & Schultze (2024), however, carnivory was also employed by some of the earliest teleosts, including the sharp-toothed *Prohalecites* (Tintori 1990) and long-mandibled *Pholidorhynchodon* (Arratia 2013, 2017).

## 2.6.4 Implications for relationships

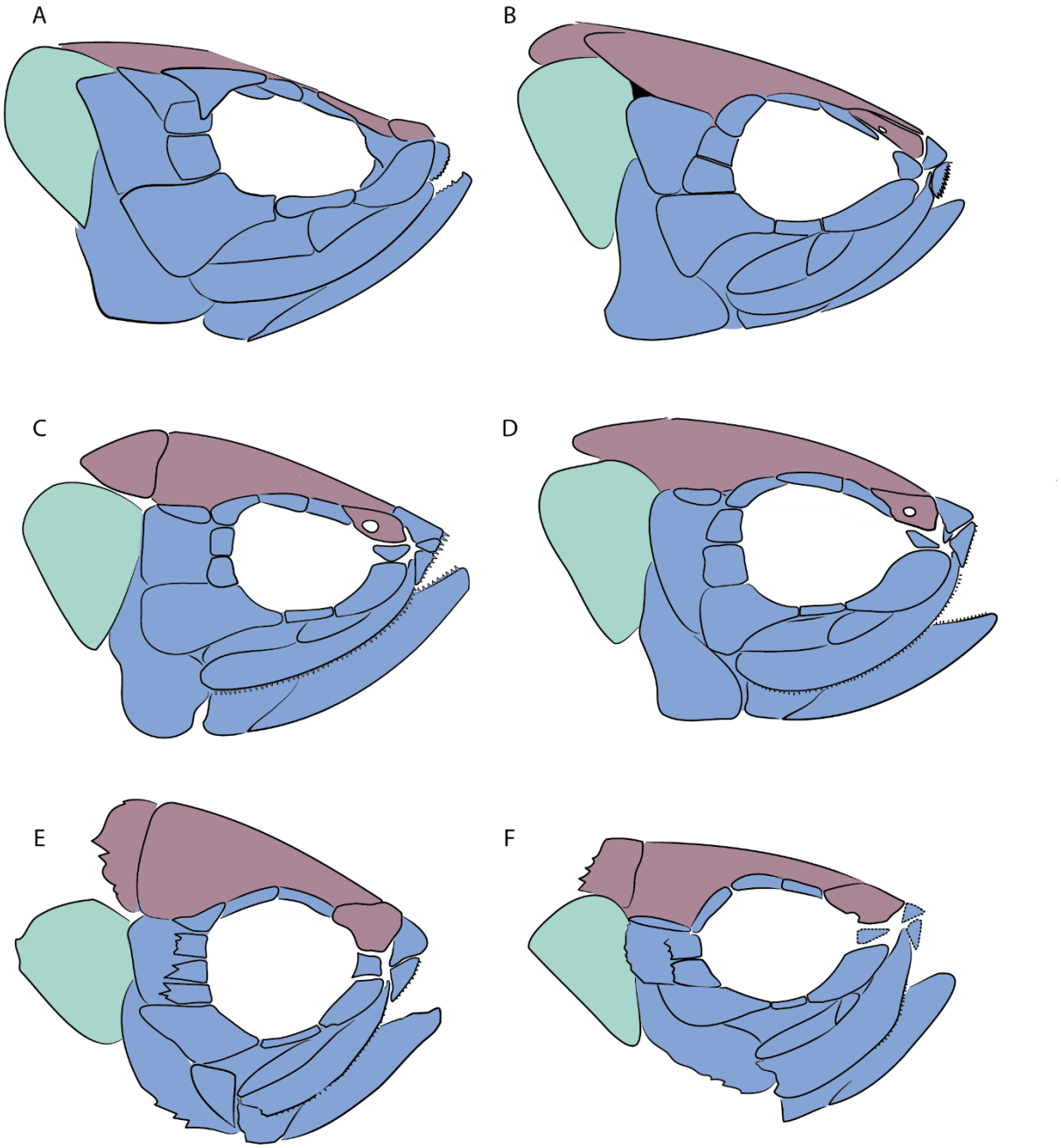

**Figure 2.18: Cranial dermal skeleton comparison in *Dorsetichthys bechei* and pholidophorifoms.** (A) *Dorsetichthys bechei,* reconstructed based on NHMUK PV P 73995 and NHMUK PV P 1052; (B) *Dorsetichthys bechei,* after previous reconstruction by Nybelin (1966, Fig. 1);
(C) *Pholidorhynchodon malzannii* (after Arratia, 2013, Fig. 98);
(D) *Parapholidophorus nybelini,* (after Arratia, 2013, Fig. 98);
(E) *Pholidoctenus serianus* (after Arratia, 2013, Fig. 7) and (F) *Pholidoctenus sanpellegrinensis* (after Arratia, 2013, Fig. 7). Anterior to right. Not to scale.

***Dorsetichthys bechei* and Pholidophoridae:** The wastebasket status of" pholidophorids" (*sensu* Woodward) has presented a significant barrier both for accurate taxonomy and reconstructing patterns of relationships on the teleost stem (Patterson, 1977; Arratia, 2000). Arratia's (2013) detailed monographic work established a revised diagnosis and set of phylogenetically derived characters upholding the monophyly of a subset of the assemblage. Pholidophoridae (*sensu* Arratia) (Fig. 2.18) is diagnosed by a combination of 17 characters, of which six are considered autapomorphic: absence of an interfrontal suture; tendency for all skull roofing bones to form a fully fused plate; supraorbital and otic canals with tubules that may open to the surface; preopercle with a notched anteroventral margin; long serrated appendage or interclavicular element covering medial surface of cleithrum; clavicle suturing with anteroventral margin of cleithrum; and elongate, leaf like axillary process. Of these proposed autapomorphies, *D. bechei* possesses cephalic sensory canals with small tubules that typically connect to the surface of the bone (e.g. NHMUK PV P 73995, NHMUK PV P 1052), and a notch on the anteroventral margin of the

preoperculum is visible in some specimens of *D. bechei* in which this region is unobscured by other ossifications (e.g. NHMUK PV P 38109, NHMUK PV P 3586). The dermal shoulder girdle is poorly preserved and described in *D. bechei*, and the condition of any clavicle or serrated organ is currently unknown.

Monophyly of Pholidophoridae in a phylogenetic context is upheld by two uniquely derived characters: a skull roof with all bones fused into a single plate, and an extrascapular with a large, rollover bony layer at the anterior margin (Arratia 2013, 2017), features both absent in *D. bechei*. The clade is further supported by a large number of homoplastic characters (Arratia 2013: seven; Arratia 2017: 12), a handful of which are present in *D. bechei* and a wider sample of teleosts and neopterygians. These variable characters include an orbital region of the skull roof narrower than the postorbital region (note the difference in orbital vs postorbital skull roof width in NHMUK PV P 73995 (Fig. 2.1) resembles that seen in pholidophorids), a bony ridge on the dentary separating the splenial and post-splenial regions, pelvic axillary processes, and diplospondyly in the mid-caudal vertebrae. As we find no evidence for a surangular in *D. bechei*, the condition of the coronoid process being contributed to by both the surangular and dentary is no longer shared by *D. bechei* and pholidophorids.

Overall, we find evidence to uphold the removal of *D. bechei* from pholidophorids, and also suggest that the diagnosis of Pholidophoridae be revised to clarify characters that are not autapomorphic for the clade, particularly when they are shared with *D. bechei*.

***Dorsetichthys bechei* and Pholidophoriformes:** Arratia's (2017) review of pholidophorids finds evidence for *Eurycormus* as the sister taxon to Pholidophoridae, together comprising the Order Pholidophoriformes, the monophyly of which is supported by a single unique character and six homoplastic ones. The condition of the uniquely derived character, a clavicle articulating with the anteroventral margin of cleithrum, is unclear in *D. bechei* (see above), but is coded as inapplicable in the matrix of Arratia (2017) and optimised as absent by the parsimony analysis. For all other characters that can be assessed, *D. bechei* displays the contrasting state to Pholidophoriformes. On this basis, we agree with the exclusion of *D. bechei* from Pholidophoriformes.

***Dorsetichthys bechei* and crownward teleosts**: The position of *D. bechei* relative to more crownward teleost nodes is more difficult to determine, with conflicting evidence to support previous hypotheses. All teleosts crownward of Pholidophoriformes (sensu Arratia 2017) are recovered in a trichotomy by Arratia (2017), which represents the most recent phylogenetic analysis to include a substantial assemblage of crown and stem teleosts inclusive of pholidophoriforms. This trichotomy subtends the node uniting *Ichthyokentema*, Ankylophoridae and *D. bechei* plus all remaining teleosts, with *Ichthyokentema* assuming different positions in different most parsimonious trees (Arratia 2017). In Arratia's strict consensus tree, two uniquely derived characters support this node: presence of a supraoccipital ossification in the braincase (Arratia 2017, ch. 16) and presence of an elongate posterodorsal/posteroventral process of the quadrate (Arratia, 2017, c: 86). *D. bechei* shows both of these anatomical states. Seven additional homoplastic characters are also recovered at this node. The anatomy in *D. bechei* is consistent with three of these states (Arratia 2017, ch. 87, ch. 151, ch.

187), variably consistent with one (Arratia 2017, ch. 149), conflicts with two (Arratia 2017, ch. 167, ch. 171), and the condition of one character is unknown (Arratia 2017, ch. 123). The updated anatomical description of NHMUK PV P 73995 and NMHUK PV P 1052 does little to change our understanding of these characters in *D. bechei*, other than to confirm the presence of a posterodorsal process of the quadrate (Arratia 2017, ch. 86), separated from the main body of the bone by a distinct notch (Arratia 2017, ch. 87).

Several additional characters previously reported by Arratia (2013) as having a bearing on stem teleost interrelationships are not optimised in the later strict consensus tree, but can be examined in individual most parsimonious trees (Arratia 2017, fig. 10). Many of these characters are homoplastic, but several are particularly pertinent. Absence of a prearticular in the lower jaw (Arratia 2017, ch. 76) is recovered as supporting either all teleosts crownward of Pholidophoriformes (Arratia 2017, fig. 10A) or *Ichthyokentema* plus all remaining teleosts (Arratia 2017, fig. 10B); in the latter tree, it is a uniquely derived character. However, we find evidence for a prearticular in *D. bechei* (contra Arratia). A posttemporal with a distinct process to articulate with the cranium (Arratia 2017, ch. 119) is also recovered as a uniquely derived character in the latter tree (coded as inapplicable in Arratia 2013, ch. 105; and inapplicable in Arratia 2017, ch. 119; as an 'inapplicable' code is functionally equivalent to an 'unknown', it is optimised as present in the parsimony analysis), but we confirm the absence of this process in *D. bechei*. Other characters are variable, although we report that a surangular is absent in *D. bechei*; this character, which was previously considered to be present in *D. bechei*, is recovered as supporting the clade comprising *Ichthyokentema* and *D. bechei* plus all remaining teleosts (Arratia 2013, 2017).

The placement of *Dorsetichthys* as sister taxon to *Leptolepis*, Ascalaboidae, Varasichthyidae and crown teleosts (Arratia, 2017, fig. 9) is supported by five homoplastic characters. Our revised description challenges current understanding of the condition of two of these in *D. bechei*. We find no evidence for a well-developed postarticular process of the lower jaw (coded as present in Arratia 2013, ch. 64 and 2017, ch. 72). We also find evidence for a single hypohyal, rather than the dorsal and ventral hypohyals optimised at this node in previous analyses (Arratia 2013, 2017). Furthermore, two of the remaining homoplastic characters, the posterior region of infraorbital 3 extending below the suborbital bone to reach the anterior margin of the preopercle (Arratia 2017, ch. 47) and a pelvic axillary process (Arratia 2017, ch. 133), both occur in pholidophorids.

This uncertainty reflects broader instability in patterns of relationship on the teleost stem, as well as difficulties in recovering a monophyletic teleost total group encompassing both extant and fossil taxa on the basis of skeletal characters (e.g. Bardack, 1965; Lehman,1966; Patterson, 1977; Patterson & Rosen, 1977; de Pinna, 1996; Arratia & Schultze, 1990; Arratia, 2001, 2016; Grande, 2010; López-Arbarello & Sferco 2018). CT-based redescriptions of key taxa are one way to addressing this issue as a way of uncovering internal anatomy, including of the neurocranium, palate, and gill skeleton. These techniques are yet to be applied to many stem teleost taxa, most notably aspidorhynchids, pachycormids (but see Dobson et al. 2021) and pholidophorids. Targeted description of these taxa, with a focus on identifying new, robust characters, should be a priority for future investigations, as well as a revised and expanded phylogenetic analysis.

## 2.7 Conclusions

This paper presents a new, previously undescribed specimen of *Dorsetichthys bechei.* Through high-resolution CT scanning, we present a detailed description of both the external dermal skeleton and internal endoskeleton from the same individual for the first time for this important genus. We have identified several anatomical features contrasting with previous descriptions, such as an anterior ceratohyal lacking a groove for the afferent hyoid artery, absence of a surangular, and additional elements of the circumorbital series. We have also confirmed the presence of undescribed but presumed traits, including a mobile premaxilla and "quadratojugal" process. The presence of elaborate gill rakers, in combination with reduced dentition of the jaws, also supports an ecological interpretation for *D. bechei* of facultative filter feeding. Our new anatomical data support a non-pholidophorid affinity for *D. bechei*. However, the absence of key features that support more crownward nodes on the teleost stem, such as a well-developed postarticular process of the lower jaw, dorsal and ventral hypohyals, and loss of the prearticular, indicate that the position of *D. bechei* relative to the teleost crown is still uncertain. These data pave the way for future expanded phylogenetic reanalyses interrogating patterns of relationship on the teleost stem.

# 3. CT AND SYNCHROTRON BASED RE-EVALUATION OF RAYNER'S "*ASPIDORHYNCHUS*" AND *"IONOSCOPUS" CYPRINOIDES* (IONOSCOPIDAE)


## Abstract

NHMUK PV P 9843 and NHMUK PV P 9843 from the Jurassic (Bathonian) Great Oolite Group, Northamptonshire, UK, are isolated, three dimensionally preserved braincases. First described in 1918 and misidentified as *Aspidorhynchus*, they represent some of the first fossil braincases associated with the teleost stem to be described in detail. However, both specimens still lack a formal identification and have not been introduced to a phylogenetic analysis. Consequently, their potential value to understanding the diversification and interrelationships of Mesozoic neopterygian is yet to be fully explored. Here, both specimens are re-described via high-resolution CT and synchrotron scanning, revealing external and internal anatomical features. Both specimens are recovered within Ionoscopidae, having confirmed the presence of an elongate dermopterotic and the sensory canal bearing innerorbital flange of the dermosphenotic, and sister taxa to *"Ionoscopus" cyprinoides*, as opposed to *Oshunia brevis* as suggested by previous work, based the shared presence of a pterotic bone, the distal position of the innerorbital flange and a posterior diverticulum on the posterior semi-circular canal. Though the interrelationships of Ionoscopidae is not fully resolved, due to a lack of overlapping anatomy, these new anatomical data support the establishing of a new genus, and help optimise the diversification of the endocast within Mesozoic Neopterygii.

## 3.1 Introduction

Neopterygians are an immensely diverse assemblage of ray-finned fishes which comprise over 36,000 living species, divided into teleosts and holosteans. Today, these two groups are extremely taxonomically imbalanced (Nelson *et al.,* 2016), but this belies the diversity of their fossil record: during the Mesozoic, holostean diversity outweighed that of teleosts (Clarke *et al.*, 2016). Early neopterygians are well represented in the fossil record, including by numerous three-dimensionally preserved braincases, many of which are isolated (Rayner, 1948; Patterson, 1975; Latimer & Giles, 2018). The mismatch between rare but comprehensively described braincases and abundant but phylogenetically less informative dermal skeletons has historically led to difficulty in constraining the taxonomic affinity of isolated braincase material, obfuscating both patterns of character diversification and early teleost and holostean relationships (Gardiner *et al.,* 1996).

NHMUK PV P 9843 (Fig. 3.1) and NHMUK PV P 9844 (Fig. 3.2) are two historically important isolated neurocrania from the Jurassic (Bathonian) Great Oolite Group, Kingsthorpe, Northamptonshire, UK. Woodward (1918, pg. 96) was the first to briefly described these specimens and identify them as belonging to the aspidorhynchid genera *Aspidorhynchus* or *Belonostomus*. Aspidorhynchids are elongate Mesozoic neopterygians with an uncertain phylogenetic position; originally referred to as “holosteans”, they are currently considered early diverging members of the teleost stem (Patterson, 1973; 1977; Patterson & Rosen, 1977; Brito, 1997; Arratia, 2013; 2017) though their exact relation to other key assemblages is inconsistently resolved (see following chapter). *Aspidorhynchus* (Agassiz, 1833), the type genus, and *Belonostomus* (Agassiz 1834) are two of potentially six valid genera known primarily from flattened remains recovered from Europe and North America. Three

dimensionally preserved remains, i.e., specimens which preserve braincases, are typically restricted to genera from South America and Australia, i.e., *Vinctifer* and *Richmondichthys*, which were poorly known at that time. Woodward's justification for associating these new specimens with aspidorhynchids is limited only to noting a similarity in the arrangement of the cranial bones. Later, Rayner's (1948) comprehensive investigation of known Jurassic fish neurocrania revisited both specimens, which by then had undergone acid and mechanical preparation. This detailed treatment is recognised by subsequent use of the moniker 'Rayner's *"Aspidorhynchus"'* (e.g., Patterson 1975, p. 286; Maisey, 1999, pg. 24) to refer to NHMUK PV P 9843 and 9844. Rayner retained the isolated braincases within the Aspidorhynchidae, and indeed they are the only aspidorhynchid braincases she described, as limited comparative material was known at the time (Etheridge & Woodward, 1891; Bartholomai, 2004).

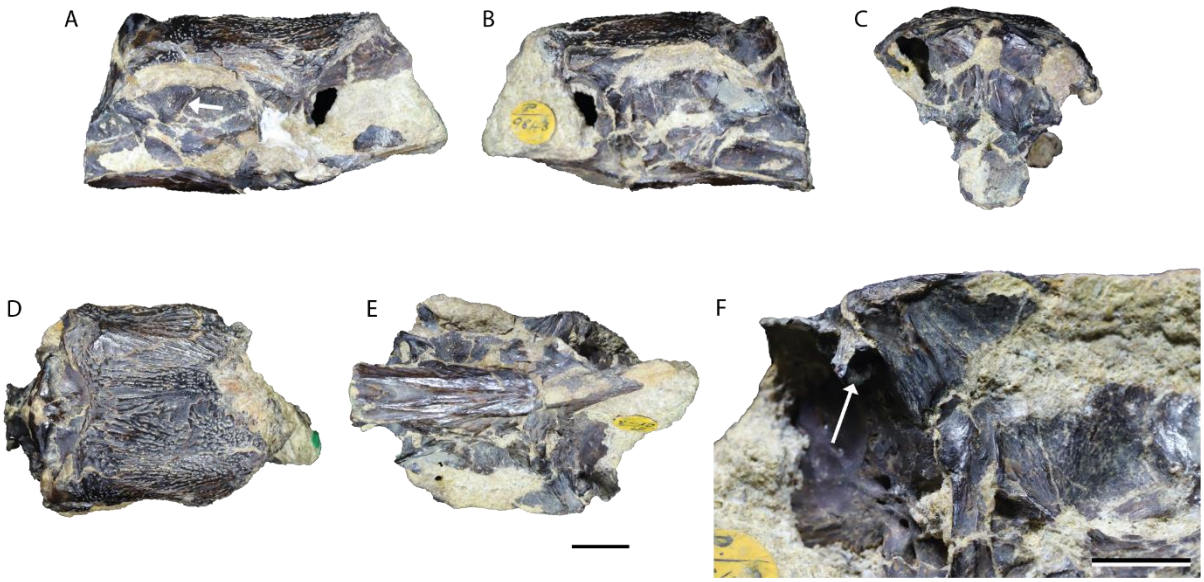

**Figure 3.1: NHMUK PV P 9843** in (A) right lateral, with suture between opisthotic and prootic indicated by arrow (B) left lateral (C) posterior (D) dorsal and (E) ventral view. (F) Closeup of orbital region in left ventrolateral view, with innerorbital flange indicated by arrow. Scale bar = 10 mm

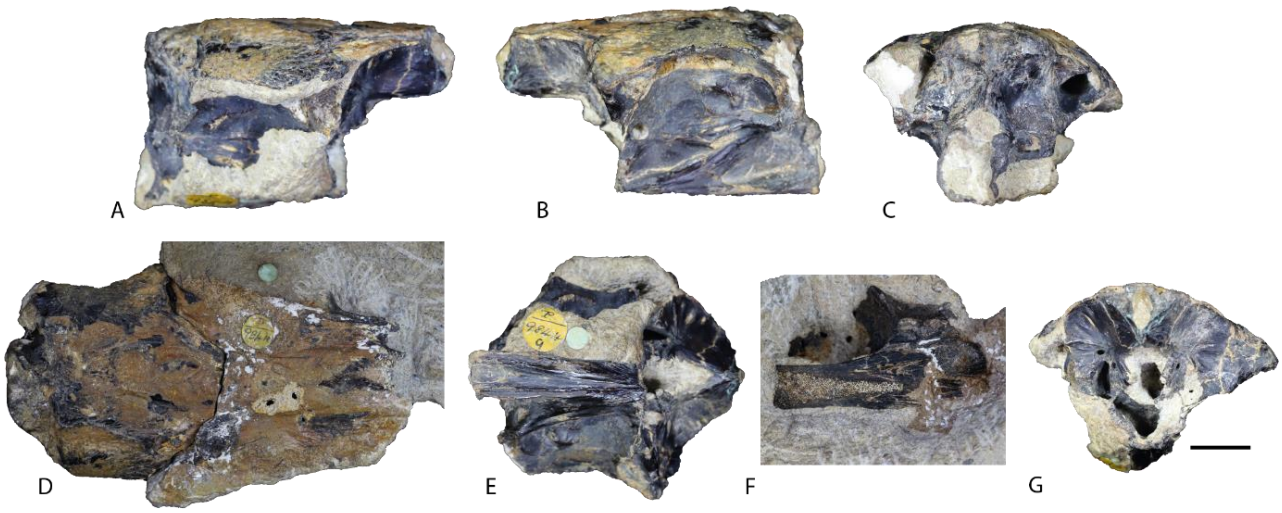


**Figure 3.2: NHMUK PV P 9844** in (A) right lateral (B) left lateral (C) posterior (D) dorsal, (E) ventral (braincase), (F) ventral (ethmoid region) and (G) anterior view. Anterior region of braincase containing ethmoid region also figured in (D). Scale bar = 10 mm.

Doubt over the aspidorhynchid identity of NHMUK PV P 9843 and NHMUK PV P 9844 was first voiced in Patterson's (1973) assessment of the interrelationship of "holosteans", citing unpublished work by Keith Mitchell (Patterson 1973, p. 273). Following comparison with *Heterolepidotus, Caturus* and *Macrepistius*, Patterson (1975, pg. 286) argued that the braincases belonged to a new taxon of caturid (a term broadly synonymous with early halecomorphs) but maintained the name *"Aspidorhynchus"* so that Rayner's detailed description could still be easily associated with them. Subsequent work upheld recognition of a non-aspidorhynchid identity when referring to the specimens, although maintained the use of open nomenclature. Maisey (1991, pg. 162) and Gardiner *et al.* (1996, pg. 120) observed similarities in braincase

ossification patterns between ‘Rayner’s “*Aspidorhynchus*”’ and the halecomorph ionoscopids *Oshunia* and *Ionoscopus*, but no formal taxonomic ranking was given and inclusion of the braincases in phylogenetic analyses was uninformative. Maisey (1999, pg. 24) reiterated that ‘Rayner’s “*Aspidorhynchus*”’ were profoundly different to other aspidorhynchid braincases and, following further comparison with *Oshunia*, proposed that they may represent a new genus of Oshuniidae. Giles *et al.* (2018) manually placed NHMUK PV P 9844 in a nested position within holosteans as sister to the indeterminate halecomorph BRLSI M.1288A. This position was corroborated by the identification of multiple holostean and halecopmorph features in the endocast and inner ear of NHMUK PV P 9844, including the presence of a dorsoventrally deep utriculus, an anteroposteriorly long vagus root and a wide separation between the lateral cranial canal and cranial cavity.

Despite more than 100 years of study and several comprehensive descriptions, both NHMUK PV P 9843 and NHMUK PV P 9844 are yet to be given a formal taxonomic rank or recovered in a stable position within a phylogenetic analysis.

In addition, the taxonomic content of ionoscopids has recently been called into question, with higher ranks such as Oshuniidae disbanded (Alvarado-Ortega & Espinosa-Arrubarrena, 2008) and the generic identification of *“Ionoscopus” cyprinoides* challenged (Taverne & Capasso, 2016; Ebert, 2018; el Hossney *et al.* 2020). Furthermore, the aim of thesis is to investigate the relationships of the teleost stem by using CT data to describe the often underappreciated internal (i.e., endocranial) anatomy of stem teleost specimens. However, in order to better constrain trends in stem teleost evolution, it is also vital to grasp the braincase anatomy of their holostean counterparts also. Due to their three-dimensional preservation, and historical association with both teleost and holostean lineages, they represent ideal

candidates for study. This chapter revisits these notable specimens using micro-computed tomography and synchrotron tomography and seek to: 1) clarify the taxonomic affinity of NHMUK PV P 9843 and NHMUK PV P 9844; 2) present a revised diagnosis and an updated taxonomic identification for "*Ionoscopus" cyprinoides;* 3) investigate patterns of anatomical change in the bony labyrinth of early neopterygians.

## 3.2 Materials and Methods

### 3.2.1 Institutional Abbreviations

**AMNH**, American Museum of Natural History, New York, USA; **BRLSI**, Bath Royal Literary and Scientific Institution, **CLC,** Luigi Capasso registered collection, Chieti; **CMNH**, Carnegie Museum of Natural History, Pittsburgh, USA; **ESRF**, European Synchrotron Radiation Facility, Grenoble, France; **IVPP**, Institute of Vertebrate Palaeontology and Palaeoanthropology, Beijing, China; **JME**, Jura-Museum Eichstätt, Eichstätt, Germany; **MPUN,** Paleontology of the Università degli Studi di Napoli Federico II; **MVP**, Museum Victoria, Melbourne, Australia; **NHMUK**, Natural History Museum, London, UK;

### 3.2.2 Materials

**NHMUK PV P 9843** and **NHMUK PV P 9844**: two isolated crania from the Jurassic (Bathonian) Great Oolite Group, Kingsthorpe, Northamptonshire, UK (Woodward, 1918, Pg. 96). Both specimens were prepared by Rayner (1948), before further mechanical and acid preparation by Patterson (1975, pg. 286, 532) to expose the internal structure of key foramina. NHMUK PV P 9844 is broken into two parts: the orbitotemporal, otic and occipital portion of the braincase is separated from the orbitosphenoid and ethmoid, and the parasphenoid is split between the two blocks.

***"Ionoscopus" cyprinoides*: NHMUK PV OR 37795a**: a heavily acid prepared braincase from the Jurassic (Kimmeridgian) Solnhofen Limestone, Germany. The braincase is preserved in partial articulation with several dermal elements and a short length of the vertebral column within a resin block. Prior to acid preperation, this portion of the specimen was separated from NHMUK PV OR 37795, which comprises the

remaining dermal and caudal skeleton set in a plaster block in a wooden frame. The seperation from the main block (NHMUK PV OR 37795) and acid preperation of NHMUK PV OR 37795a was performed by Robert Evander (NHMUK) for Maisey (1999).

### 3.2.3 CT and Synchrotron Scanning and Imaging

NHMUK PV P 9844 and NHMUK PV OR 37795a were CT scanned in 2015 at the Imaging and Analysis Centre, NHMUK, using a Metris X-Tek HMX ST 225 CT System with a 2,000 x 2,000 pixel detector, tungsten reflection target. NHMUK PV P 9843 was scanned in 2021 at the ESRF in Grenoble, France, in October 2021. The scan was at a voxel size of 21 µm. Image stacks from CT scanning and synchrotron tomography were cropped in ImageJ and segmented in Mimics v.23 (biomedical.materialise.com/mimics; Materialise, Leuven, Belgium). Renders of 3D models were captured using Blender v.3.3.0(blender.org) and interpretive drawings were created in Adobe Illustrator (adobe.com/products/illustrator).

### 3.2.4 Phylogenetic Analysis

In order to investigate the phylogenetic relationships of mid-late Mesozoic taxa, the character matrix of Giles *et al*., 2023 was heavily reworked. The new matrix comprises a total of 108 taxa and 249 characters. 56 taxa were removed from the original matrix, including most Palaeozoic osteichthyans and the original non-osteichthyan outgroup, though several Palaeozoic taxa were retained to allow character polarity to be accurately determined (Maddison *et al*., 1984). Likewise, 103 characters were also removed as they were less relevant to Mesozoic taxa. 50 taxa were introduced to the matrix, as well as 60 characters – some novel and others adapted from existing

literature (Maisey, 1999; Cavin *et al.,* 2013; Arratia, 2017). A complete updated taxon and character list can be found in the Appendices (A1, 2, 3).

For this chapter, the following ionoscopiform taxa were introduced to the matrix: "*Aspidorhynchus*" – NHMUK PV P 9843 and NHMUK PV P 9844 coded within a single terminal – *"Ionoscopus" cyprinoides, Ionoscopus petrarojae, Oshunia brevis, Robustichthys luopingensis* and *Spathiurus* dorsalis, and the following characters were also added to provide grouping information for Ionoscopiformes: c.232, Innerorbital flange of dermosphenotic bearing sensory canal tube [0] absent [1] present (Gardiner *et al.*, 1996; Grande & Bemis, 1998); c. 233, Descending lamina of dermosphenotic (innerorbital flange) [0] fused to sphenotic/ preorbital wall [1] free distally (new); c.234 Ventral surface of (sub)infraorbital bones intensely pitted [0] absent [1] present (López-Arbarello & Sferco, 2018); c.238, Posterior notch of second infraorbital for supramaxilla [0] absent [1] present (Xu *et al.*, 2014); c.239 Lateral line in maxilla [0] absent [1] present (Grande & Bemis, 1998; Alvarado-Ortega & Espinosa-Arrubarrena, 2008); c.240 Lachrymal [0] significantly smaller than orbit [1] equal in size to orbit (Grande & Bemis, 1998; López-Arbarello & Sferco, 2018); c.245 Posterior semicircular canal with posterior diverticulum [0] absent [1] present (new). c.249. dermopterotic significantly more elongate than parietal [0] absent [1] present (Taverne & Capasso, 2016).

An equally weighted parsimony analysis was conducted in TNT v. 1.5 (Boloboff & Catalano, 2016). using a heuristic search utilising Sect. Search, Ratchet, Drift and Tree Fusing algorithms with the following settings: hold 100,000; xmult = level 10; bbreak = fillonly (A.4.1). Trees were rooted by a constrained outgroup of Palaeozoic taxa: *(Moythmasia durgaringa (Mimipiscis bartrama, Mimipiscis toombsi)).* Four characters were ordered following Giles *et al.* (2023): c.51 c.97 c.98 c.121. A strict

consensus tree was produced from the resulting 33480 trees. Trees were visualised in Macclade v. 3.05 (Madidson & Maddison, 1992) in order to describe character distribution and measure consistency indices.

## 3.3 Systematic Palaeontology

Osteichthyes Huxley, 1880

Actinopterygii Klein, 1885

Neopterygii Regan, 1923

Holostei Müller, 1846

†Ionoscopiformes Grande & Bemis, 1998

†Ionoscopidae Lehman, 1966

†*Ionoscopus* Costa, 1853

**Holotype:** MPUN N° M 507

**Other Material:** CLC A-7

**Locality and Horizon:** Pietraroja Plattenkalk, Albian

**Diagnosis (emended from Taverne & Capasso, 2016):** Triangular dermethmoid crossed by rostral sensory commissure, square shaped parietal, posterior margin of infraorbital 3 confined anterior to the suborbital, ventral surface of infraorbital bones intensely pitted, leading margin of paired fins without fringing fulcra, 56 (24 + 32) monospondylous vertebrae.

**Remarks:** *I. petrarojae* is now the only valid species of *Ionoscopus*. The diagnosis of *Ionoscopus* and *I. petrarojae* are considered equivalent. Taverne & Capasso (2016) also refer a destroyed, unaccessioned specimen to *I. petrarojae*.

† *gen. nov.*

**Holotype:** NHMUK PV OR 37795

**Referred Material:** NHMUK PV P 9843, NHMUK PV P 9844, CMNH 4036.

**Locality and Horizon:** Solnhofen, Germany, L. Kimmeridgian.

**Diagnosis:** Braincase with independently ossified pterotic. Parasphenoid not pierced by internal carotid artery. Spiracular enclosed in canal. Posterior semicircular canal with short posteriorly directed diverticulum. Dermosphenotic with long innerorbital process bearing the infraorbital sensory canal and free distally from the postorbital process. Dermethmoid reduced to a bony tube carrying the rostral commissure. Reduced rectangular parietal. Jaw articulation posterior to orbit. Pectoral fins short. Vertebral column with 62 – 63 centra, 22 supraneurals, and 5 – 8 epurals.

† *gen. nov. cyprinoides*

**Etymology:** Original species name maintained from Wagner, 1863.

**Holotype:** NHMUK PV OR 37795

**Referred Material:** CMNH 4036

**Remarks:** JME-ETT86, another isolated braincase associated with *Ionoscopus*, is not referred to *gen nov.* here, as Ebert (2018) noted it exhibits numerous differences to NHMUK PV OR 37795a, including absence of the innerorbital flange. *Gen nov.*

*cyprinoides* is formally removed from *Ionoscopus*, but is referred to as "*Ionoscopus" cyprinoides* throughout.

**Diagnosis (emended from Wagner, 1863):** Exoccipital extends anterior to the vagus foramen. Innerorbital flange is free, and distal to the preorbital wall.

† *sp. nov.*

**Holotype:** NHMUK PV P 9843

**Referred Material:** NHMUK PV P 9844

**Remarks:** Previously assigned to *Aspidorhynchus* sp. (Woodward, 1918; Rayner, 1948). Known only from isolated braincase material.

**Diagnosis:** Anterior limit of exoccipital level with the vagus foramen. Innerorbital flange is free but close to the preorbital wall.

## 3.4 Description: NHMUK PV P 9843

### 3.4.1 General Morphology

**NHMUK PV P 9843** (Figs 3.1, 3.3, 3.4, 3.5) is an isolated, well ossified neurocranium partially embedded in sediment. It comprises a skull roof, braincase and parasphenoid and is incomplete anterior to the midpoint of the orbit. Its exterior anatomy was originally described by Rayner (1948) after initial mechanical preparation, and, following further mechanical and acid preparation, by Patterson (1975).

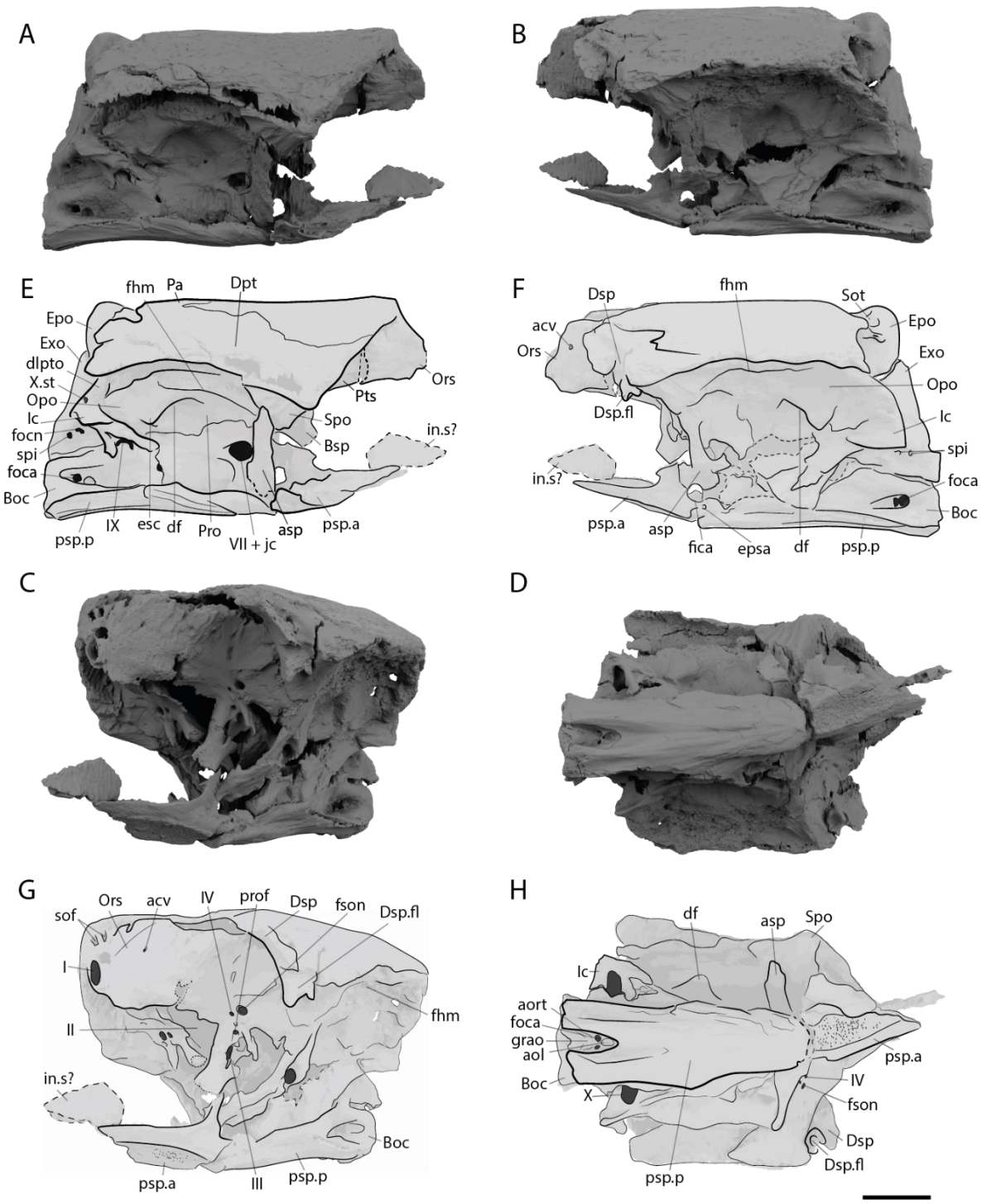
A
B
E
fhm
Pa
Dpt
Epo
Exo
dlpto
X.st
Opo
Ic
focn
spi
foca
Boc
Ors
Pts
Spo
Bsp
in.s?
psp.p
IX
esc
df
Pro
VII + jc
asp
psp.a
F
Dsp
fhm
Sot
acv
Ors
Epo
Exo
Opo
Dsp.fl
Ic
spi
in.s?
foca
Boc
psp.a
asp
fica
epsa
df
psp.p
C
D
G
Ors
acv
IV
prof
Dsp
fson
Dsp.fl
sof
I
II
fhm
in.s?
Boc
psp.a
III
psp.p
H
df
asp
Spo
Ic
aort
foca
grao
aol
psp.a
Boc
X
IV
fson
Dsp
Dsp.fl
psp.p

**Figure 3.3: Braincase of NHMUK PV P 9843.** Renders in (A) right lateral (B) left lateral (C) left anterolateral, (D) ventral, Interpretive drawings in (E) right lateral (F) left lateral (G) left anterolateral, (H) ventral. Scale bar = 10 mm. *Abbreviations*: *acv, anterior cerebral vein; aol, area of origin of arotic ligament; aort, aortic notch; asp, ascending process of the parasphenoid; Boc, basioccipital; Bsp, basisphenoid; df, dilatator fossa; dlpto, descending lamina of dermopterotic; Dpt, dermopterotic; Dsp, dermosphenotic; Dsp.fl, innerorbital flange of the dermosphenotic; Epo, epioccipital; epsa, foramen for efferent pseudobranchial artery; esc, ridge externally marking the semicircular canal; Exo, exoccipital; fhm, hyomandibular facet; fica, foramen for internal carotid artery; foca, foramen for occipital artery; focn, foramen for occipital nerve; fson, foramen for superficial ophthalmic nerves; grao, groove for dorsal aorta; Ic, intercalar; jc, foramen for jugular vein; in.s? possible innerorbital septum; Opo, opisthotic; Ors, orbitosphenoid; Pa, parietal; Pro, prootic; prof, foramen for profundus nerve; psp.a, anterior portion of parasphenoid; psp.p, posterior portion of parasphenoid; Pts, pterosphenoid; sof, supraorbital fossa; Sot, supraotic; spi, spino-occipital nerves; Spo, sphenotic; I, foramen for olfactory nerve; II, foramen for optic nerves; III, foramen for oculomotor nerve; IV, foramen for trochlear nerve; VII, foramen for facial nerve; IX, foramen for glossopharyngeal nerve; X, foramen for vagus nerve. X. st, foramen for supratemporal branch of the vagus nerve.*

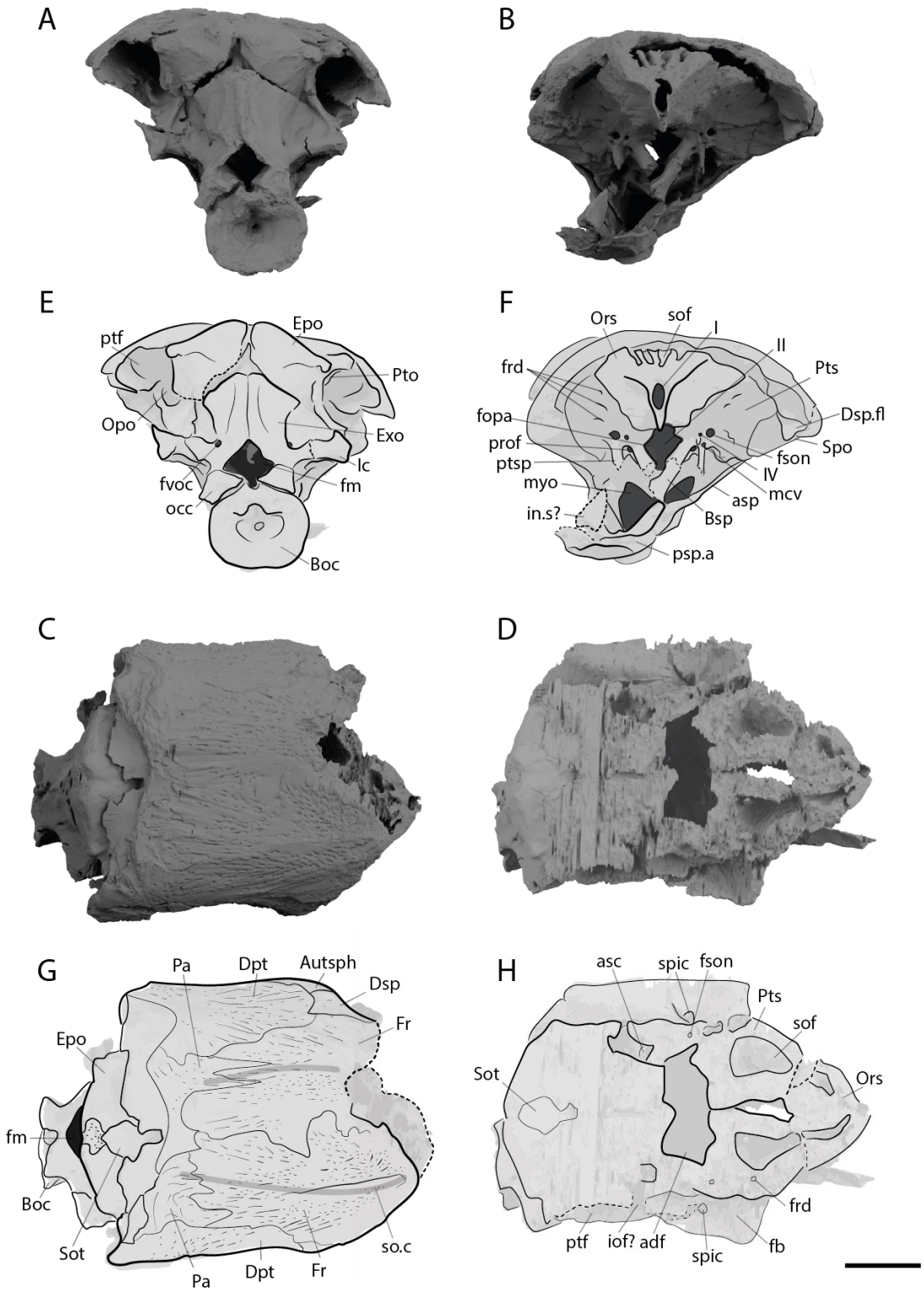
A
B
E
ptf
Epo
Pto
Opo
Exo
Ic
fvoc
fm
occ
Boc
F
Ors
sof
I
II
frd
Pts
Dsp.fl
fopa
prof
Spo
ptsp
fson
IV
myo
mcv
asp
in.s?
Bsp
psp.a
C
D
G
Pa
Dpt
Autsph
Dsp
Fr
Epo
fm
Boc
Sot
Pa
Dpt
Fr
so.c
H
asc
spic
fson
Pts
sof
Sot
Ors
frd
ptf
iof?
adf
spic
fb

**Figure 3.4: Braincase of NHMUK PV P 9843.** Renders in (A) posterior, (B) anterior, (C) dorsal view and (D) dorsal view with skull roof removed. Interpretive drawings in (E) posterior, (F) anterior, (G) dorsal view and (H) dorsal view with skull roof removed. Scale bar = 10 mm. *Abbreviations*: *acv, anterior cerebral vein; adf, anterior dorsal fontanelle; asp, ascending process of the parasphenoid; asc, cavity occupied by anterior semicircular canal; Autsph, autosphenotic; Boc, basioccipital; Bsp, basisphenoid; Dpt, dermopterotic; Dsp, dermosphenotic; Dsp.fl, innerorbital flange of the dermosphenotic; Epo, epioccipital; epsa, foramen for efferent pseudobranchial artery; Exo, exoccipital; fb, fossa bridgei; fm, foramen magnum; Fr, frontal; frd, foramen for ascending branch of superficial ophthalmic nerves; fopa, foramen/ notch for occipital artery; fson, foramen for superficial ophthalmic nerves; fvoc, foramen for tributary of posterior cerebral vein in exoccipital; Ic, intercalar; iof?, possible inferior orbital fissure; in.s? possible innerorbital septum; mcv, middle cerebral vein; occ, occipital condyle; myo, posterior myodome; Opo, opisthotic; Ors, orbitosphenoid; Pa, parietal; prof, foramen for profundus nerve; psp.a, anterior portion of parasphenoid; ptf, post-temporal fossa; Pto, pterotic; Pts, pterosphenoid; ptsp, pterosphenoid pedicle; so.c, supraorbital canal; sof, supraorbital fossa; Sot, supraotic; spic, spiracular canal; I, foramen for olfactory nerve; II, foramen for optic nerves; IV, foramen for trochlear nerve.*

### 3.4.2 Skull Roof

The skull roof is incomplete anteriorly, with the frontal and the right autosphenotic cut off by an irregular fracture. Rostral, nasal and circumorbital bones are lost. The remaining plates are very well preserved, comprising paired parietals (Pa), dermopterotics (Dpto), autosphenotics (Autsph) and frontals (Fr). Each element of the skull roof is distinctly ossified, but tightly sutured to those surrounding it (Figs. 3.3E, D, G, 3.4G).

The posterior margin of the skull roof is broadly notched to form an overlap area for the extrascapulars, which are not preserved, exposing the underlying braincase (Fig. 3.4G, H). The parietals are sutured along the midline and are irregularly shaped, interdigitating with the posterior margin of the frontals via long, asymmetric processes. The dermopterotic lies lateral to the parietal and frontal and is the second largest of the roofing bones. It is elongate and sub-rectangular, with a smooth margin. The anterior extent of the autosphenotic is unclear but it appears very reduced; it is the

smallest element of the skull roof. Anteriorly, the frontals are cut off, but would likely be the largest and longest roofing element. They are sutured along the midline and do not appear to taper for the length they are preserved. The dermosphenotic (Dsp, Figs. 3.3F, G 3.4G) is very large relative to the other roofing bones and is partially fused to the frontal; consequently, the suture is difficult to fully visualise. On the left side, where it is enclosed within the matrix, the dermosphenotic bears a cylindrical ventral innerorbital flange (Dsp.fl, Figs. 3.1F; 3.3F, G, H, 3.4F) which, alongside the autosphenotic, contributes to the postorbital process. The flange carries a branch of the infraorbital canal, which exits from its lateral margin, and the ventral surface of the innerorbital flange is concave.

The entire dorsal surface of the skull roof is ornamented by deep longitudinal grooves and scours. Rayner (1948) noted that this heavy ornamentation obscures the tubules of the sensory canals. Likewise, the middle and posterior pit lines are hard to identify. Tomographic data partially reveals the route taken by the supraorbital sensory canal (so.c, Fig. 3.4G) – extending through the centre of the parietal and frontal–-but it does not appear to be associated with branching tubules and are instead fully housed within projections on the ventral underside of the skull roof. The otic canal is difficult to identify.

### 3.4.3 Braincase

The braincase of PV P 9843 (Figs. 3.3, 3,4) is deep and elongate. Not every suture can be easily identified in tomograms, but the braincase is not continuous and comprises discrete ossifications. The specimen appears to have undergone slight post-mortem breakage and compaction, and some of this has exploited existing sutures. However, the overall morphology remains mostly intact.

**Occipital Region*:*** The occipital region (Fig. 3.4E) is narrow and is the deepest region of the braincase. It comprises a median supraotic (Sot), paired epioccipitals (Epo), paired exoccipitals (Exo), paired intercalars (Ic) and a median basioccipital (Boc) separated by distinct sutures. The posterior margin of the occipital region does not form a vertical wall, but slopes anteriorly dorsal to the foramen magnum (Fig. 3.3E, F).

The supraotic (Sot, Fig. 3.4G) is a small, median endochondral element between the epioccipitals. The edges of the ossification are visible on the external surface of the specimen (Fig. 3.1D), but are barely discernible in tomograms, and the margins of the supraotic cannot be traced internally. As previously remarked by Rayner (1948, pg. 315) and Patterson (1975, pg. 436, 471), the supraotic is only visible in dorsal view, not in posterior view. Viewed dorsally, the supraotic is elliptical with an anterior extension which is partly overlapped by the parietals. The supraotic lacks membranous outgrowths and does not appear to contact the exoccipitals or extend far enough anteriorly to form part of the wall of the bony labyrinth.

The epioccipital (Epo, Figs 3.3E, F, 3.4E, G) forms the dorsal portion of the posterior face of the braincase and contributes to the inner wall of the post-temporal fossa (ptf, Fig. 3.4E). It projects dorsally above the skull roof, obscuring the supraotic in posterior view, and is separated from its antimere on the midline by a narrow gap that broadens ventrally. Beneath the epioccipital, the exoccipital (Exo, Figs. 3.3E, F, 3.4E) is broad, concave, and is pierced by a deep, ventrally directed foramen for the tributary of the posterior cerebral vein (fvoc, Figs. 3.3E, F, 3.4E). This canal bifurcates within the exoccipital and remerges in the foramen for an occipital nerve (focn) beneath the intercalar (Fig. 3.3E). The left and right exoccipitals are fused along the midline, with the join obscured beneath a thick ridge of perichondral bone. Ventrally,

the exoccipital bounds the diamond shaped foramen magnum (fm, Fig. 3.4E, G), which is bounded on either side by short ventrolateral processes likely homologous to the occipital condyle (occ, Fig. 3.4E). The epioccipital also forms the medial margin of the opening of the posttemporal fossa (ptf, Fig. 3.4E).

Lateral to the exoccipital lies the extensive intercalar. The intercalar (Ic, Figs. 3.3E, F, H, 3.4E) forms the posteroventral corner of the post-temporal fossa (ptf) but also emits an elongate, membranous outgrowth which extends anteroventrally into the otic region, contacting the parasphenoid. Lateral to the foramen magnum, the intercalar and exoccipital frame the ovoid, ventrally directed foramen of the vagus nerve (X, Fig. 3.3H). The supratemporal branch of the vagus nerve (X.st, Fig. 3.3E) emanates from its lateral margin and exits through the dorsal margin of the intercalar. Anterior to the exit of the vagus nerve, a ventral splint of the intercalar contacts the basioccipital.

The basioccipital (Boc, Figs. 3.3E, F, G, 3.4E, G) forms the most ventral component of the occipital region, and projects further posteriorly than the exoccipitals and epioccipitals. It contributes to the notochordal opening, which forms a vast, concave dish with a wide, flared margin, accounting for approximately one third of the total height of the occipital region. It is elongate but does not appear to be fused to the first vertebral element. The ventral surface of the basiocciput bears a deep midline notch, which lies posterior to a corresponding notch on the parasphenoid. A small foramen on the anterolateral wall of the notch accommodates an opening of the occipital artery (foca, Fig. 3.3E, F). Anteriorly, near the apex of this notch, a deep median depression surrounded by a posterior rim likely housed the aortic ligament (aol, Fig. 3.3H).

**Otic Region:** The otic region is the widest portion of the braincase. It comprises paired pterotic opisthotic (Opo), prootic (Pro) and sphenotic (Spo) ossifications (Fig. 3.3A, B), and is also contributed to by the paired dermopterotic (Dpto).

The endocranial roof is extensive and generally well ossified, except in the region of the anterior dorsal fontanelle and fossa bridgei. The anterior dorsal fontanelle (adf, Fig. 3.4H) has an anterior and posterior component, partially separated by the pterosphenoid (Pts, Fig. 3.4H), which contacts its antimere – but is not fused to it – in the region of the midbrain endocast. The fossa bridgei (fb, Fig. 3.4H) lies lateral to the anterior dorsal fontanelle in the form of two depressions which are overlain directly by the skull roof. The posterior depression lies within the prootic bone, and the anterior spans the pterosphenoid and partly the sphenotic. The floor of the fossa bridgei is thinly ossified, and the dorsalmost part of the anterior semicircular canal loop (asc, Fig. 3.4H) is briefly continuous with the fossa bridgei. At the deepest point of the fossa bridgei, the spiracular canal (spic, Fig. 3.4H) descends into the postorbital process between the pterosphenoid and autosphenotic.

Immediately posterior to the fossa bridgei is the post-temporal fossa (ptf, Fig. 3.3N, P). Although the fossa bridgei and post-temporal fossa are largely separate, they are connected via a short groove, possibly the inferior orbital fissure (iof?, Fig. 3.4H), though it is poorly resolved. The post-temporal fossa forms a long, deep cavity that narrows anteriorly. It is partially roofed with endochondral bone. The dermopterotic forms the remainder of its roof, and the descending lamina of the dermopterotic (dlpto, Fig. 3.3E) its lateral wall. The floor of the post-temporal fossa is contributed to by the intercalar and opisthotic.

The pterotic lies anterior to the epioccipital, but is obscured laterally by the opisthotic (Pto, Fig. 3.4E). It forms the medial wall of the posttemporal fossa and is delimited by a conspicuous suture. It is difficult to fully distinguish the opisthotic (Opo) and prootic (Pro) in the tomograms (or the resulting segmented model; Fig. 3.3I), although the suture that separates them can be traced on the specimen (Fig. 3.1A). The prootic is more than double the size of the opisthotic; while the prootic spans the lateral wall of the braincase, the opisthotic is confined anteriorly. The lateral wall of the prootic bears a deep depression, which is most likely the dilatator fossa (df, Fig. 3.3E, H). It has a curved dorsal margin, with a deep, overhanging roof which houses the horizontal semicircular canal (esc, Fig. 3.3E). The left side of the braincase is broken ventral to this depression. Near the posterior wall of the depression, just anterior to the boundary between the opisthotic and prootic, is a slight swelling (the ‘knob’ of Patterson 1975: p. 396, 438) to which the branchial levator muscles attach. The glossopharyngeal nerve exits the braincase slightly ventral to the swelling (IX, Fig. 3.3I), dorsal to the intercalar, and the jugular groove (jg) can be traced anterior to the glossopharyngeal foramen. A large foramen near the anterior limit of the otic region transmits the jugular canal into the orbit, alongside the facial (VII) and trigemino (V) nerves, forming the trigemenofacial chamber (Figs. 3.3E, 3.4F). As it is not possible to trace their individual paths clearly within this junction, the facial and jugular nerves are combined into a single label (VII + jg).

**Orbitotemporal Region:** The otic and orbitotemporal region are separated by the postorbital process, an expanse of bone contributed to by the pterosphenoid (Pts, Fig. 3.4F), sphenotic (Spo, Figs. 3.3E, H, M, 3.4F) and ascending process of the parasphenoid (asp, Figs. 3.3E, H, 3.4F). The postorbital process is barely wider than the otic region, and the postorbital wall, which forms its anterior margin, is almost flat.

Anterior to the orbital wall, the braincase narrows rapidly towards the orbitosphenoid (Ors, Figs. 3.3E, F, G, 3.4F, H), which is broken anteriorly. The pterosphenoid forms a narrow pterosphenoid pedicle (ptsp, Fig. 3.3O), which extends some way ventrally into the orbital cavity and may transmit a canal. The pedicle does not reconnect to the braincase ventrally.

The postorbital wall bears multiple foramina and nerve openings, the largest being the median opening for the optic nerve (II, Figs. 3.3G, 3.4F). The ventral half of the optic nerve opening is bounded by the basisphenoid (Bsp, Figs. 3.3E, 3.4F), which forms a robust V-shaped element, although part of the right limb is broken. The basisphenoid is pierced laterally by the elongate opening of the oculomotor nerve (III, Fig. 3.3G), which also extends across the ventral portion of the pterosphenoid.

A notch at the extreme lateral margin of the optic foramen identified as transmitting the ophthalmic artery (opa, Fig. 3.4F). Lateral to the optic nerve are several smaller, paired openings spaced closely together (Fig. 3.4F). The largest and most lateral (i.e. furthest from the optic foramen) is the foramen for the superficial ophthalmic nerve (fson, Fig. 3.4F). It is transmitted a short distance through the pterosphenoid before intercepting the trigemenofacial chamber. Directly ventral to the anterior opening of the superficial ophthalmic nerve is the foramen for the middle cerebral vein (mcv). The middle cerebral vein enters the pterosphenoid above the dorsal terminus of the pterosphenoid pedicle, before also entering the trigemenofacial chamber. Medial to the anterior foramen of the superficial ophthalmic nerve is the foramen for the trochlear nerve (IV, Fig. 3.4F). The trochlear nerve canal is very narrow and enters the orbit directly from the endocranial cavity. The paired, ventrally directed foramen for the profundus nerve (prof, Fig. 3.4F) lies alongside the strut of the

basisphenoid (see below), in the notch between where the basisphenoid and pterosphenoid pedicle meet.

Finally, the upper part of the postorbital wall is pierced by two to three foramina, identified by Patterson as ascending branches of superficial ophthalmic nerves (frd, Fig. 3.4F, H). These branches emanate from a pair of openings in the roof of the braincase, lateral to the posterior supraorbital fossa.

Although slightly fractured, the basisphenoid does not appear to have had a posterior component that extended towards the posterior myodome. The posterior myodome (myo, Fig. 3.4F) extends only a short way into the braincase, terminating approximately level with the posterior opening of the jugular canal. It is continuous with the cranial cavity dorsally.

Dorsal to the optic nerve opening is the orbitosphenoid ossification. The orbitosphenoid carries the olfactory nerve via a median canal (I, Fig. 3.4F). The foramen for the anterior cerebral vein (acv, Fig. 3.3F). The canal arches into the orbitosphenoid directly into the endocranial cavity. The dorsal surface of the orbitosphenoid is excavated beneath the skull roof by several paired deep grooves, most likely representing supraorbital fossa (sof, Fig. 3.4F, H).

A fragmentary piece of bone, forming a vertical plate ventral to the orbitosphenoid, may represent a fragment of the interorbital septum (in.s?, Figs. 3.3E, F, 3.4F, G). However, it is not clear if it was part of the orbitosphenoid or basisphenoid.

**Parasphenoid**

The parasphenoid is split into two major parts by a large fracture level with the posterior margin of the orbit. The portion of the parasphenoid posterior to the fracture (psp.p, Fig. 3.3) is well preserved in life position relative to the braincase. It is closely

applied to the underside of the braincase and floors much of the posterior myodome. Posteriorly, it reaches the posterior margin of the basioccipital, where it is deeply notched (Fig. 3.3H) and concave along the midline. The ventral surface of this part of the parasphenoid is smooth, with ridges that radiate from the anterior margin, and does not bear teeth. Level with the anterior margin of the basiocciput, the parasphenoid increases in depth to extend some way up the lateral face of the braincase. A narrow strut extends dorsolaterally from the parasphenoid to meet the membranous outgrowth of the intercalar.

The portion of the parasphenoid anterior to the fracture has been displaced slightly dorsally relative to life position (psp.a, Figs. 3.3, 3.4F), and is incomplete anterior to the midpoint of the orbit. It is broader than the posterior portion of the parasphenoid, and bears a raised, ovoid patch of minute teeth. Other than a slight dorsal crest, the parasphenoid is exceptionally broad and flattened. An elongate ascending process with a complex shape extends from the lateral margin of the toothpatch, although this is largely incomplete on the left side. Immediately after separating from the main body of the parasphenoid, the posteroventral margin of the process is notched for the internal carotid artery (fica, Fig. 3.3F), and the efferent pseudobranchial leaves through a smaller notch on the anterior margin of the process (epsa, Fig. 3.3F). The ascending process broadens dorsally, with a small posterior process buttressing the posterior opening of the jugular canal, and a slender extension up the postorbital process.

The dorsal surface of the parasphenoid is raised into a modest median crest, terminating posteriorly in a raised platform between the base of the ascending processes. A deep groove along the lateral surface of this crest pierces the parasphenoid near its preserved anterior limit.

## Endocast

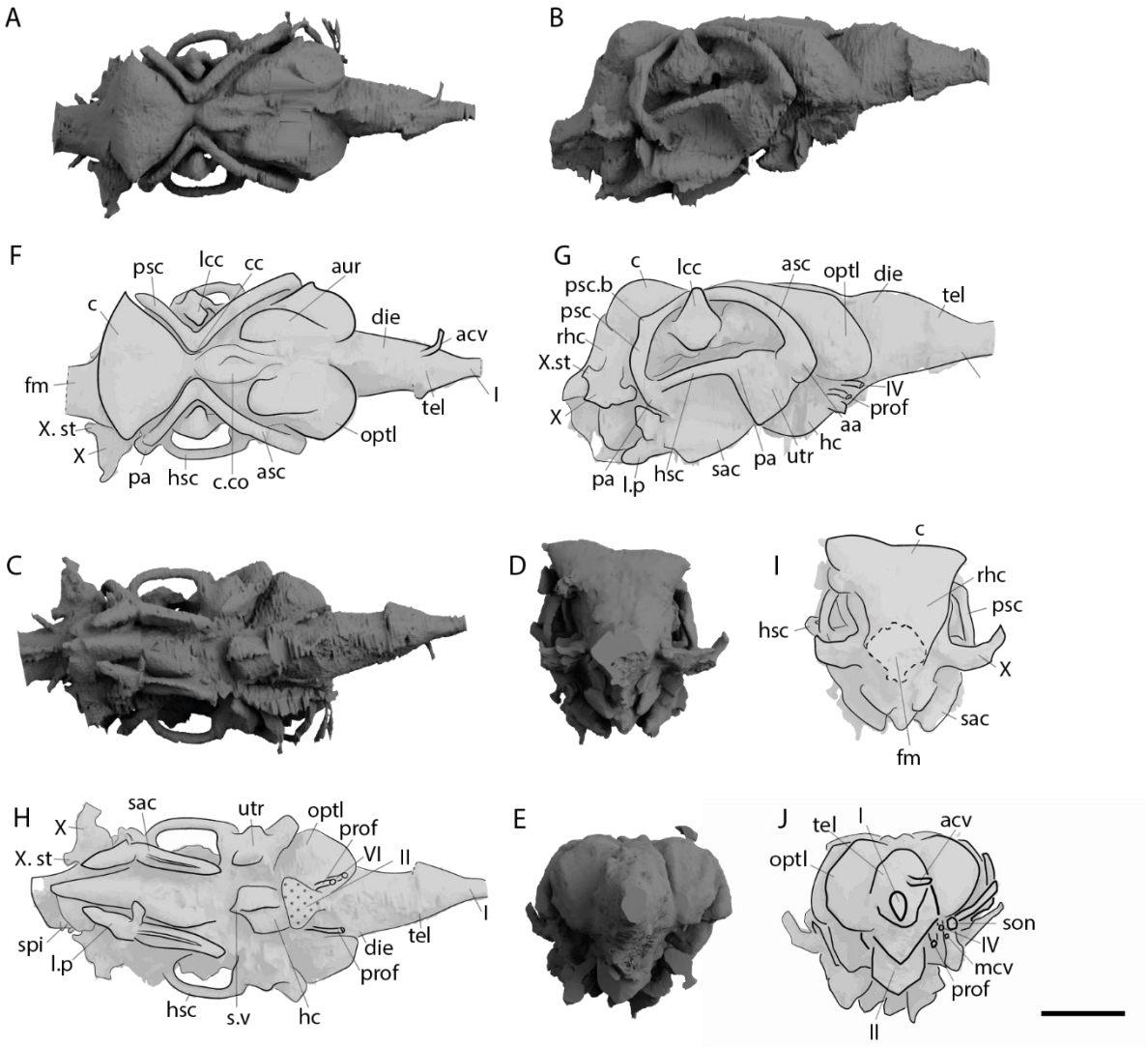
A
B
F
psc
lcc
cc
aur
c
die
acv
fm
tel
I
X. st
optl
X
pa
hsc
c.co
asc
G
c
lcc
asc
optl
die
tel
psc.b
psc
rhc
X.st
IV
prof
X
aa
hc
pa
l.p
hsc
sac
pa
utr
C
D
I
c
rhc
psc
hsc
X
sac
fm
H
X
sac
utr
optl
prof
X. st
VI
II
I
spi
l.p
die
tel
prof
hsc
s.v
hc
E
J
tel
I
acv
optl
son
IV
mcv
prof
II

**Figure 3.5: Endocast of NHMUK PV P 9843.** Renders in (A) dorsal (B) right lateral (C) ventral (D) posterior and (E) anterior view. Interpretive drawings in (F) dorsal (G) right lateral (H) ventral (I) posterior and (J) anterior view. Scale bar = 10 mm. *Abbreviations*: *aa, anterior ampulla; acv, anterior cerebral vein; asc, anterior semicircular canal, aur, cerebellar auricle; c, cerebellar; c.co cerebellar corpus; cc, crus commune, die, diencephalon; fm, foramen magnum; hc, hypophyseal canal; hsc, horizontal semicircular canal lcc, lateral cranial canal; l.p, lagenar pouch; mcv, middle cerebral vein; optl, optic lobes; pa, posterior ampulla; prof, profundus nerve; psc, posterior semicircular canal; psc.b, diverticulum of the posterior semicircular canal; rhc, rhombencephalon; sac, saccular chamber; son, superficial ophthalmic nerve; spic, spiracular canal; s.v, saccus vasculosus; son, superficial ophthalmic nerve; spi, spino-occipital nerve; tel, telencephalon; utr, utricular; I, olfactory nerve; II, optic nerve; IV, trochlear nerve; X, vagus nerve; X.st, supratemporal branch of the vagus nerve.*

The internal walls of the cranial cavity are well ossified, except in the region of the anterior dorsal fontanelle, and a complete endocast and bony labyrinth can therefore be described for NHMUK PV. P 9843 (Fig. 3.5). Overall, the endocast is quite elongate, with many bulbous features.

***Hindbrain*:** The hindbrain portion of the endocast is dominated by a broad and triangular cerebellum (c, Fig. 3.5F, G, I). It contributes to around a quarter of the total length of the segmented endocast. The cerebellum overlies the rhombencephalon (rhc, Fig 3.5G, I) which is deep and narrows slightly towards its ventral margin. The lateral walls of the rhombencephalon are dominated by the large root of the vagus nerve (X, Fig. 3.5F, G, H, I). The vagus nerve canal is exceptionally broad, with a dorsally reflexed distal tip preserved on the right side. It also exhibits a posteriorly directed supratemporal branch (X.st, Fig. 3.5F, G). The root of the vagus nerve is level with the extremely robust medulla oblongata, where the rhombencephalon transitions into the spinal cord within the foramen magnum. This region emits several branches of spino-occipital nerves (spi, Fig. 3.5H).

***Midbrain*:** The endocranial roof covers most of the cranial cavity, allowing the dorsal surface of the endocast to be well-defined without interruption from the anterior dorsal fontanelle. The cerebellar corpus is extremely small. It forms a medial protrusion situated posterior to the cerebellar auricles (aur, Fig. 3.5F); these are only faintly developed and lie lateral to the optic lobes. The bulbous optic lobes (optl, Fig. 3.5F, G, H, J) are very large, contributing to the widest portion of the endocast. They gradually taper posteriorly and are divided by a very wide and deep groove. The trochlear nerve (IV, Fig. 3.5G, H, J) emanates from the ventral margin of the optic lobe.

***Forebrain*:** The diencephalon (die, Fig. 3.5F, G, H) region of the endocast is fully continuous with the telencephalon region (tel, Fig. 3.5F, G, H, J). The telencephalon narrows to around 1/3 of its original width at the base of the olfactory nerve. The olfactory nerve (I, Fig. 3.5F, G, H, J) appears to form a single tract, though its anterior extent is not preserved. The left side of the telencephalon also emits a canal for the anterior cerebral vein (acv, Fig. 3.5F, J). Its root is directed anteriorly, before arching 90$^{o}$ and exiting on the lateral wall of the orbitosphenoid. The hypophyseal canal (hc, Fig. 3.5G, H) extends ventrally from the forebrain endocast beneath the optic lobes. It is shallow, though the morphology of its anterior margin – including the pituitary vein - is not preserved. It lies directly over the posterior myodome and bears a short posteriorly directed saccus vasculosus (s.v, Fig. 3.5H). The abducens nerve (VI) appears to emerge from the anterior medial margin of the sacculus, however its margins are faint. The large root of the optic nerve (II, Fig. 3.5G, H, J) is positioned directly anterodorsal to hypophyseal canal. It is tapered ventrally and along its lateral flanks is an elongate root for the profundus nerve (prof, Fig. 3.5G, H), which runs ventrally and parallel to the trochlear nerve (IV, Fig. 3.5G, H).

***Bony Labyrinth*:** All three semicircular canals are fully preserved on both sides of the braincase and are almost completely enclosed in bone, except where the dorsalmost part of the anterior semicircular canal is continuous with the posterior depression of the fossa bridgei (Fig. 3.4H). Each semicircular canal is roughly equal in width, and the anterior and posterior canals are of similar length. The anterior semicircular canal (asc, Fig. 3.5F, G) is long and curves from the anterior ampulla (aa, Fig. 3.5G) to extend slightly dorsally above the roof of the endocranial cavity. The horizontal semicircular canal (hsc, Fig. 3.5F, G, H, I) is the shortest canal (Fig. 4G). Posteriorly, it is continuous with the ampulla of the posterior semicircular canal; its posterior connection with the cranial cavity is lower than its anterior ampulla. The posterior semicircular canal (psc, Fig. 3.5F, G, I) is also long and is gently curved. It bears a small, posteriorly directed diverticulum (psc.b, Fig. 3.5G) at its apex. The anterior and posterior semicircular canal meet in a crus commune that is set ventral to the cranial roof and broadly separated from its antimere (cc, Fig. 3.5F). Each canal terminates in a well-developed ampulla. The ampullae of the anterior and horizontal semicircular canals are broadly separated but confluent with a deep, triangular utriculus (utr, Fig. 3.5G, H).

The lateral cranial canal (lcc, Fig. 3.5F, G) is extensive. It is deep, with a large dorsal lobe that projects dorsal to the crus commune of the anterior and posterior semicircular canals, and re-joins the main cranial cavity anteriorly, posterior to the cerebellar auricles. There is moderate separation between the canal and the main cranial cavity, and it is almost entirely surrounded by bone, however there is one small connection to the medial wall of the posttemporal fossa. The sacculus (sac, Fig. 3.5G, H, I) is deep, anteroposteriorly elongate and very thin and narrow. The ventral margin features a short, tapered edge. The sacculus is also continuous with a distinct,

elongate lagenar pouch (l.p, Fig. 3.5G, H). The lagenar pouch tapers posteriorly and also appears to exhibit a dorsally directed connection towards the root of the vagus nerve. Finally, there is an elongate, rounded, medial cavity which forms a connection between the medial wall of the sacculus and the main cranial cavity. No otoliths are observed anywhere in the saccular or lagenar chambers.

## 3.5 Description: NHMUK PV P 9844

### 3.5.1 General morphology

**NHMUK PV P 9844** (Figs. 3.2, 3.6, 3.7, 3.8) is an isolated neurocranium comprising a partial skull roof, braincase, parasphenoid and ethmoidal region. As with NHMUK PV P 9843 it was originally described by Rayner (1948), with additional details provided by Patterson (1975) following further preparation. The endocast has also been described by Giles *et al.* (2018) using CT scanning. Overall, the specimen is very similar to NHMUK PV P 9843 so to avoid repetition this chapter only reports key features and notable differences in morphology.

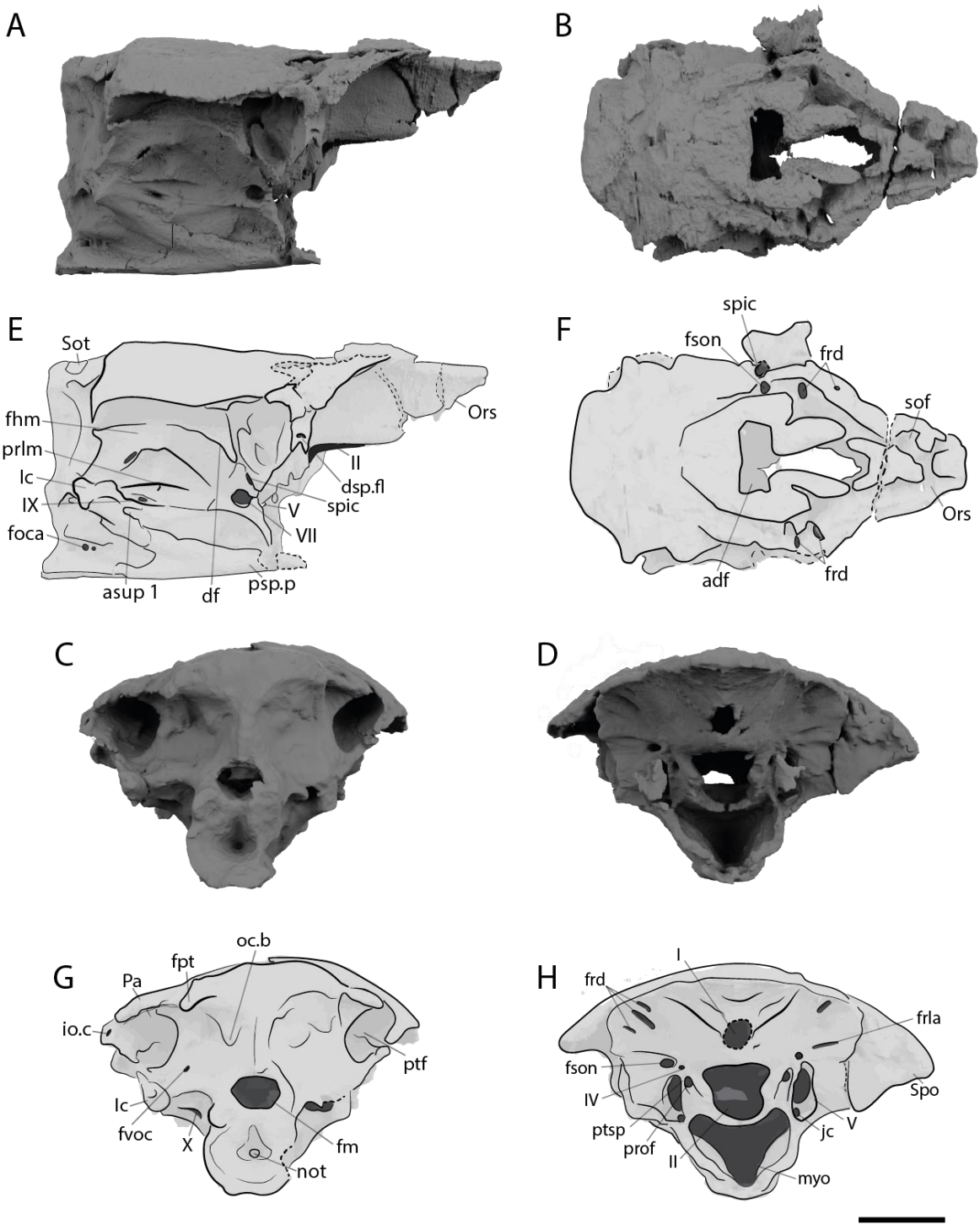
A
B
E
Sot
fhm
prlm
lc
IX
foca
asup 1
df
psp.p
II
dsp.fl
V
spic
VII
Ors
F
spic
fson
frd
sof
Ors
adf
frd
C
D
G
oc.b
fpt
Pa
io.c
ptf
lc
fvoc
X
fm
not
H
I
frd
frla
fson
IV
Spo
ptsp
prof
II
jc
V
myo

**Figure 3.6: Braincase of NHMUK PV P 9844**. Renders in (A) right lateral (B) dorsal (without skull roof) (C) posterior (D) anterior. Interpretive drawings in (E) right lateral (F) dorsal (without skull roof) (G) posterior (H) anterior. Scale bar = 10 mm. *Abbreviations*: adf, anterior dorsal fontanelle; *asup 1,* a*rticular facet for first suprapharyngobranchial; df, dilator fossa; Dsp.fl, innerorbital flange of the dermosphenotic, fm, foramen magnum; fpt, facet for ligament to post-temporal; fhm, hyomandibular facet; foca, foramen for occipital artery; frd, foramen for ascending branch of superficial ophthalmic nerves; fson; foramen for superficial ophthalmic nerves; fvoc, foramen for tributary of posterior cerebral vein in exoccipital; Ic, intercalar; io.c, infraorbital canal; jc, foramen for jugular vein; myo, posterior myodome; not, notochord; oc.b, exoccipital bulge; Ors orbitosphenoid; Pa, parietal prlm, process on prootic giving origin to branchial levator; prof, foramen or canal for profundus nerve; psp.p, posterior portion of parasphenoid; ptf, post-temporal fossa; ptsp, pterosphenoid pedicle; Sot, supraotic; sof, supraorbital fossa; spic, foramen for spiracular canal; Spo, sphenotic; I, foramen for olfactory nerve; II, foramen for optic nerves; IV, foramen for trochlear nerve; V, foramen for trigeminal nerve; VII, foramen for facial nerve; IX, foramen for glossopharyngeal nerve; X, foramen for vagus nerve.*

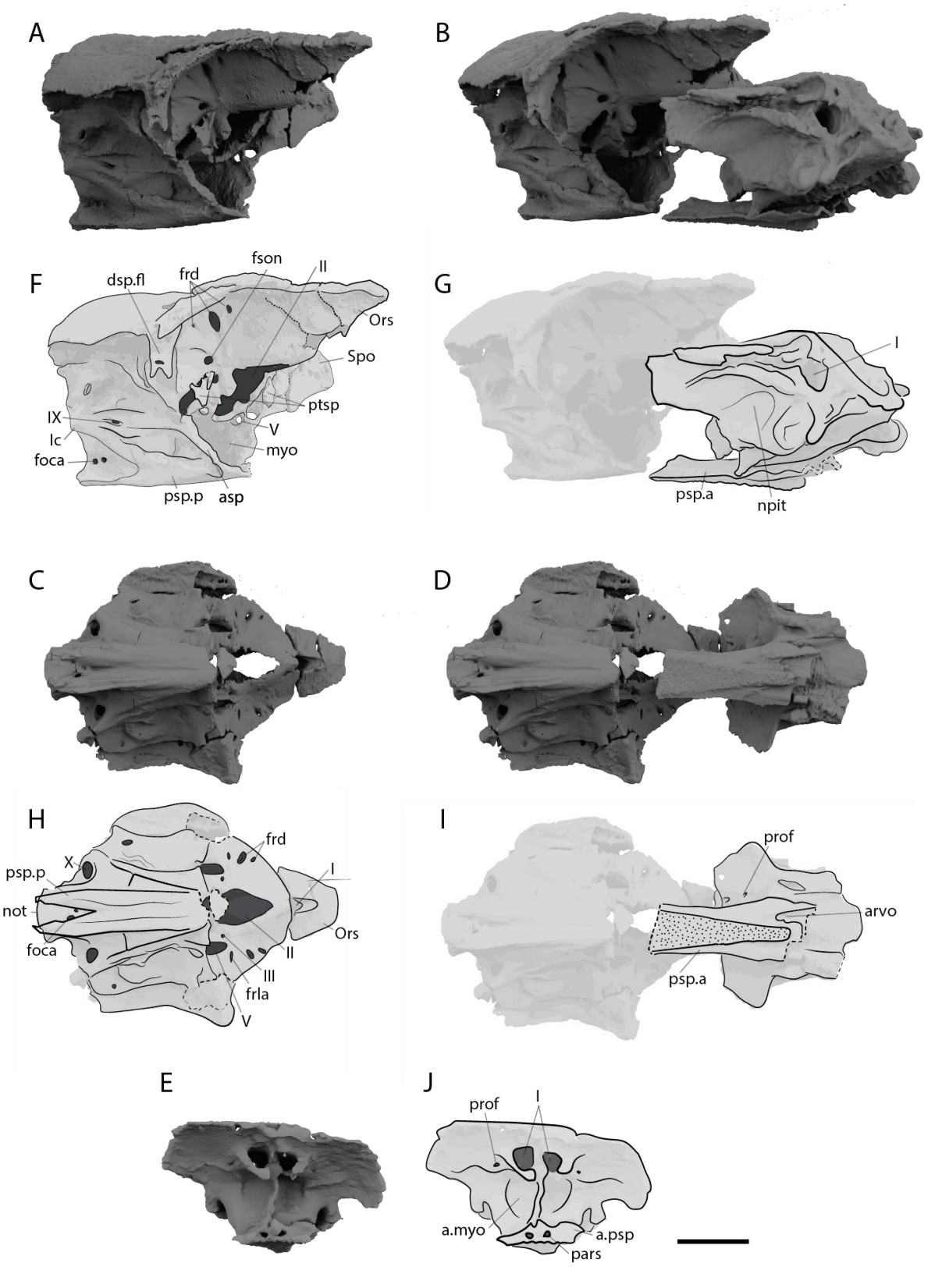
A
B
F
dsp.fl
frd
fson
II
Ors
Spo
ptsp
IX
V
Ic
myo
foca
psp.p
asp
G
I
psp.a
npit
C
D
H
frd
psp.p
X
I
not
Ors
foca
II
III
frla
V
I
prof
arvo
psp.a
E
J
prof
I
a.myo
a.psp
pars

**Figure 3.7: Braincase of NHMUK PV P 9844**. Renders in (A) right anterolateral (B) right anterolateral (with ethmoid) (C) ventral, (D) ventral (with ethmoid) (E) posterior view (ethmoid only). Interpretive drawings in (F) right lateral (G) right anterolateral (with additional length of the pterosphenoid pedicle) (H) ventral (I) ventral (with ethmoid), (J) posterior view (ethmoid only). Scale bar = 10 mm. *Abbreviations*: *a.myo, anterior myodome; arvo, area obscured by vomer; asp, ascending process of the parasphenoid; Dsp.fl, innerorbital flange of the dermosphenotic, oc.b, exoccipital bulge; foca, foramen for occipital artery; foca, foramen for occipital artery; frd, foramen for ascending branch of superficial ophthalmic nerves; frla, foramen for ramus lateralis accessorius; Ic, intercalary; myo, posterior myodome; not, notochord; npit, nasal pit; Ors, orbitosphenoid; pars, parabasal canal; prof, foramen or canal for profundus nerve; psp.a, anterior portion of parasphenoid; psp.p, posterior portion of parasphenoid; ptsp, pterosphenoid pedicle; Spo, sphenotic; I, foramen for olfactory nerve; II, foramen for optic nerves; III, foramen for oculomotor nerve; V, foramen for trigeminal nerve; IX, foramen for glossopharyngeal nerve; X, foramen for vagus nerve.*

### 3.5.2 Skull Roof

Although the skull roof is more anteroposteriorly complete (Fig. 3.2D), it has been heavily prepared. As a result, it cannot be resolved in tomograms anterior to the postorbital processes. The ventral flange of the dermosphenotic (dsp.fl, Figs. 3.6E, 3.7F) is preserved within the matrix on both sides of the specimen, although is separated from the main portion of the dermosphenotic by a fracture. It is slightly longer and slenderer than the process in NHMUK PV P 9843.

### 3.5.3 Braincase

This braincase is similar in gross morphology to that of NHMUK PV P9843. However, it is more completely ossified. Most sutures between braincase ossifications are difficult or impossible to trace in tomograms or on 3D models, although this may be in part because most of the specimen was investigated via CT scanning rather than synchrotron tomography, resulting in lower contrast in tomograms. Some sutures are visible on the external surface of the specimen.

**Occipital Region*:*** Overall, the occipital region is very well preserved (Fig. 3.6G). It is the deepest and narrowest part of this braincase, but it is somewhat squatter (shorter and wider) than the occipital region of NHMUK PV P 9843. The posterior surface of the occipital region also forms a distinctly stepped vertical wall (Fig. 3.6E), as opposed to the gradually sloping posterior face in NHMUK PV P 9843.

A low crest, flanked by a shallow depression, extends along the midline of the occipital region above the foramen magnum. A distinctive, rounded bulge is developed on the medial wall of this depression (oc.b, Fig. 3.6G); it does not correspond with any feature in the underlying cranial cavity. Dorsolateral to the depression, the occiput also forms a pronounced overhang (fpt, Fig. 3.6G), corresponding with the ligament attachment of the post-temporal bone. In other respects, the occipital region resembles that of NHMUK PV P 9843.

**Otic Region:** The otic region forms the widest portion of the braincase. Except for the anterior dorsal fontanelle, the otic region is also very well ossified. Consequently, sutures between individual braincase ossifications are again difficult to identify. The anterior dorsal fontanelle (adf, Fig. 3.6F) is elongate, with a wide posterior portion that narrows abruptly before broadening slightly above the orbits. As the roof of the braincase is exposed on the surface and has been subject to some level of preparation, the original depth of the fossa bridgei is unclear. The portion that is preserved appears to be narrow and not particularly deep. Near its anterior limit, it is continuous ventrally with the spiracular canal (spic, Fig. 3.6F). As in NHMUK PV P 9843 the spiracular descends ventrally into the postorbital process, remerging in dorsal to the posterior opening of the facial nerve (spic, Fig. 3.6E) The post-temporal fossa is like that of NHMUK PV P 9843 although slightly smaller and clearly separated

from the fossa bridgei by well-ossified endochondral bone; no canals connect the two cavities.

The lateral wall of the otic region shows a small number of differences to that of NHMUK PV P9843. The region corresponding to the membranous outgrowth of the intercalar (Ic, Figs. 3.6E, G, 3.7F) is very distinct. It forms the anterior margin of the vagus nerve (X, Figs. 3.6G, 3.7H) and extends anteroventrally to the parasphenoid, forming a posterior process, like the condition in NHMUK PV P 9843. However, the deep, narrow opening of the supratemporal branch of glossopharyngeal nerve (IX, Figs. 3.6E, G, 3.7F) pierces the intercalar in PV P 9844. The anterior margin of the intercalar is also notched to accommodate the articular facet for the suprapharyngobranchial (asup 1, Fig. 3.6E). Dorsal to the anterior arm of the intercalar, the attachment area for the branchial levator muscles (prlm, Fig. 3.6E) is much more robust, and developed as a sub-triangular protrusion.

**Orbitotemporal Region:** The orbitotemporal region broadly resembles that of NHMUK PV P 9843 but is overall wider and shorter. It is also better preserved, without any fractures disrupting the orbital wall, and so the multiple foramina that pierce this surface can be fully described.

At least three elongate foramina for the ascending branch of superficial ophthalmic nerves (frd, Figs. 3.6F, 3.7F, H) are clustered in the posterodorsal corner of the orbit, as in NHMUK PV P 9843. Slightly ventral to these are two additional canals: a narrow, slot-like opening (frla, Fig. 3.7H), which likely corresponds to the recurrent branch of the facial nerve; and a rounded foramen for the superficial ophthalmic nerve (fson, Fig. 3.6F). The narrow, ovoid trigeminofacial chamber is dorsoventrally elongate and transmits the jugular canal (jc) and trigeminal nerve (V)

into the orbit. It is separated from the more medial opening of the profundus nerve (prof) by a ventrally extensive pterosphenoid pedicle (ptsp, Fig. 3.6H). Disconnected, anterior to the braincase is a process of the pterosphenoid pedicle (ptsp, Fig. 3.7F) obscured by the matrix.

Despite some fracturing, the orbitosphenoid (Ors, Figs. 3.6E, F, 3.7F, H) is well ossified and is completely preserved. It becomes narrower and shallower anterior to the opening for the optic nerve. It surrounds the ovoid forebrain cavity for most of its length. A single canal for the anterior cerebral vein exits the cranial cavity on the left of the orbitosphenoid. Only a short portion of the median olfactory nerve tract (I, Fig. 3.7H) is contained within the orbitosphenoid, and it is unfloored (Fig. 3.7H). As opposed to the rounded depressions of the supraorbital fossae in NHMUK PV P 9843 here they form deep, irregular grooves which incise the dorsal surface of the orbitosphenoid (sof, Fig. 3.6F), converging anteriorly. Between the ethmoid and braincase, above the parasphenoid, is a short fragment of the interorbital septum. It is thickened ventrally.

### 3.5.4 Ethmoid

NHMUK PV P 9844 includes a well-preserved ethmoid region and nasal capsule (Fig. 3.7G, I, J), separated from the more posterior region of the braincase by a short gap presumably filled by cartilage in life. It is robustly ossified as a single element extending from the preorbital wall to the front of the snout.

The preorbital wall is gently concave, with a shallow median preorbital septum. Although the preorbital process is laterally expansive, matching the postorbital process in width, it does not extend far posteriorly. A shallow pit for the ventral anterior

myodome (a.myo, Fig. 3.7J) lies approximately halfway up the preorbital wall. Few features or foramina mark the preorbital walls lateral to the myodome. The olfactory nerves (I, Fig. 3.7J) enter the nasal capsule via paired tracts with irregularly mineralised floors, and barely diverge within the nasal capsule before opening onto its anterior surface (I, Fig. 3.7G). A smaller foramen for the profundus nerve flanks the olfactory tract laterally (prof, Fig. 3.7I, J).

The lateral walls of the ethmoid include the smooth, rounded medial walls of the nasal pit (npit, 3.7G). Ventrally, paired, deep, irregular grooves mark the path of the palatine nerve. Posteriorly, paired depressions line the ventral surface of the ethmoid and the correspond to equally sized depressions on the ventral surface of the parasphenoid. These depressions would have accommodated the vomers (arvo, Fig. 3.7I).

### 3.5.5 Parasphenoid

The parasphenoid is near-complete in NHMUK PV P 9844, except for the portion underlying the posterior half of the orbit. Posterior to the postorbital process, the parasphenoid is closely applied to the braincase and identical to that of NHMUK PV P9843, albeit proportionately shorter to correspond with the dimensions of the braincase. It forms the central portion of the floor of the posterior myodome, and an angular ridge projects into the myodome from its dorsal surface.

The anterior portion of the parasphenoid (psp.a, Fig. 3.7G, I, J) is very broad. The large field of teeth on its ventral surface widens to the full width of the parasphenoid before tapering anteriorly to a rounded point. The anterolateral margins of the parasphenoid form short wings that widen anteriorly, creating triangular grooves

into which the paired vomers (not preserved) would have been situated (arvo, Fig. 3.7I). On the dorsal surface of the parasphenoid, a deep groove midline groove broadens and deepens anteriorly. It is flanked by a shallow, rounded ridge. A median keel is not observed. The anterior portion of the parasphenoid carries the paired parabasal canal along its full length (pars, Fig. 3.7J). The parabasal canal lies within the lateral margins of the parasphenoid, diverging further from the midline as the parasphenoid widens near the ethmoid. As the left and right parabasal canals diverge, a subsidiary branch emerges closer to the midline. The lateral walls of these canals are weakly mineralised, so that they are confluent for much of their length.

## 3.5.6 Endocast

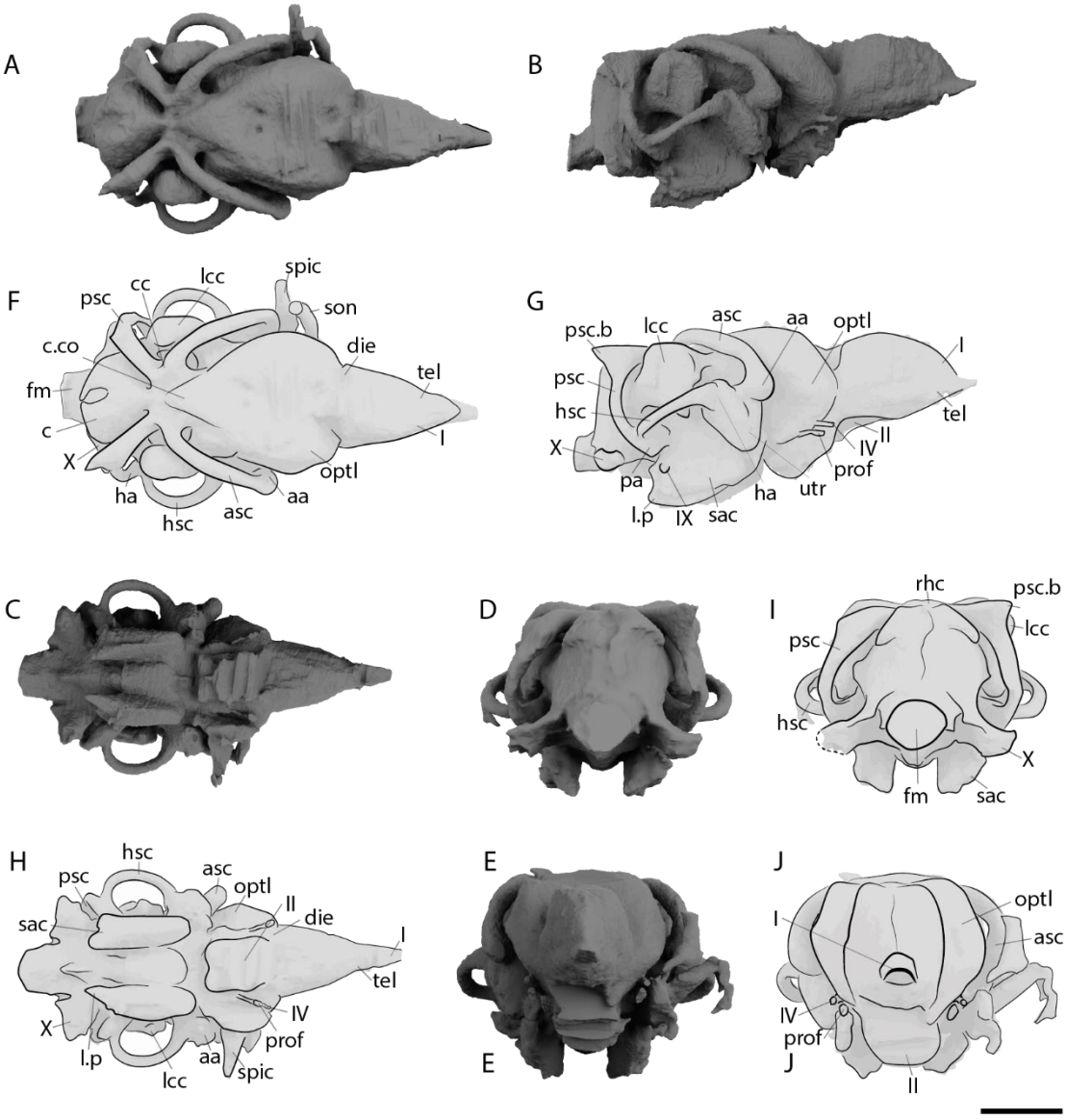


**Figure 3.8: Endocast of NHMUK PV P 9844**. Renders in (A) dorsal (B) right lateral (C) ventral (D) posterior and (E) anterior view. Interpretive drawings in (F) dorsal (G) right lateral (H) ventral (I) posterior and (J) anterior view. Scale bar = 10 mm. *Abbreviations*: *aa, anterior ampulla; asc, anterior semicircular canal, aur, auricles; c, cerebellum; cc, crus commune; c.co, cerebellar corpus; die, diencephalon; fm, foramen magnum; ha, horizontal ampulla; hc, hypophysial canal; hsc, horizontal semicircular canal; lcc, lateral cranial canal; l.p, lagenar pouch; optl, optic lobes; pa, posterior ampulla; prof, profundus nerve; psc, posterior semicircular canal; psc.b, diverticulum of the posterior semicircular canal; rhc, rhombencephalon; sac, saccular chamber; son, superficial ophthalmic nerve; spic, spiracular canal; tel, telencephalon; utr, utricular; I, olfactory nerve; II, optic nerve; IV, trochlear nerve; IX, glossopharyngeal nerve; X, vagus nerve.*

The endocast of NHMUK PV P 9844 (Fig. 3.8) has previously been described by Giles *et al. (*2018); this study only focuses on notable differences it displays to the endocast of NHMUK PV P 9843.

**Hindbrain:** The cerebellar region of the endocast (c, Fig. 3.8F, I) is shorter and considerably narrower than in NHMUK PV P 9843 and lacks the lateral triangular extensions. It also bears a deep, medial groove, continuous with the ventral margin, dividing the hindbrain endocast into two distinct lobes.

**Midbrain:** The midbrain region of the endocast is mostly similar to that of NHMUK PV P 9843. The cerebellar auricle is not as distinct and appears mostly confluent with the optic lobes (optl, Fig. 3.8F, G, H, J). The optic tectum is also slightly narrower and is barely wider than the cerebellar region.

**Forebrain:** The forebrain region of the endocast is slightly wider, and a modest constriction may mark the separation between the diencephalic (die, Fig. 3.8F, G, H) and telencephalic (tel, Fig. 3.8F, G, H) regions. As in NHMUK PV P9843, the olfactory tracts leave the forebrain via a single tract, but the preserved ethmoid region of NHMUK PV P 9844 shows that the tracts separate and diverge anterolaterally near the anterior margin of the parasphenoid (I, Fig. 3.7J).

**Bony Labyrinth*:*** All three semicircular canals are completely preserved and enclosed in bone, alongside their associated ampulla. They are also proportionally longer and spaced more distally from the walls of the endocast. Consequently, the anterior semicircular canal (asc, Fig. 3.8F, G, H) is not set into the lateral margin of the optic lobe. Likewise, the anterior semicircular canal extends further dorsally above the endocranial roof. The horizontal semicircular canal (hsc, Fig. 3.8F, G, H, I) is more steeply inclined than in NHMUK PV P 9843. The crus commune (cc, Fig. 8F) is more

anteroposteriorly elongate, and is raised from the endocranial roof. The lateral cranial canal also has both anterior and posterior connections, although the dorsal projection is much shorter and more bulbous. The sacculus (sac, Fig. 3.8G, H, I) is considerably wider, but is still associated with a thin, tapered, ventral edge and a relatively shorter lagenar pouch (l.p. Fig. 3.8G, H). The medial pouch between the left and right sacculus is also present.

## 3.6 Phylogenetic Results

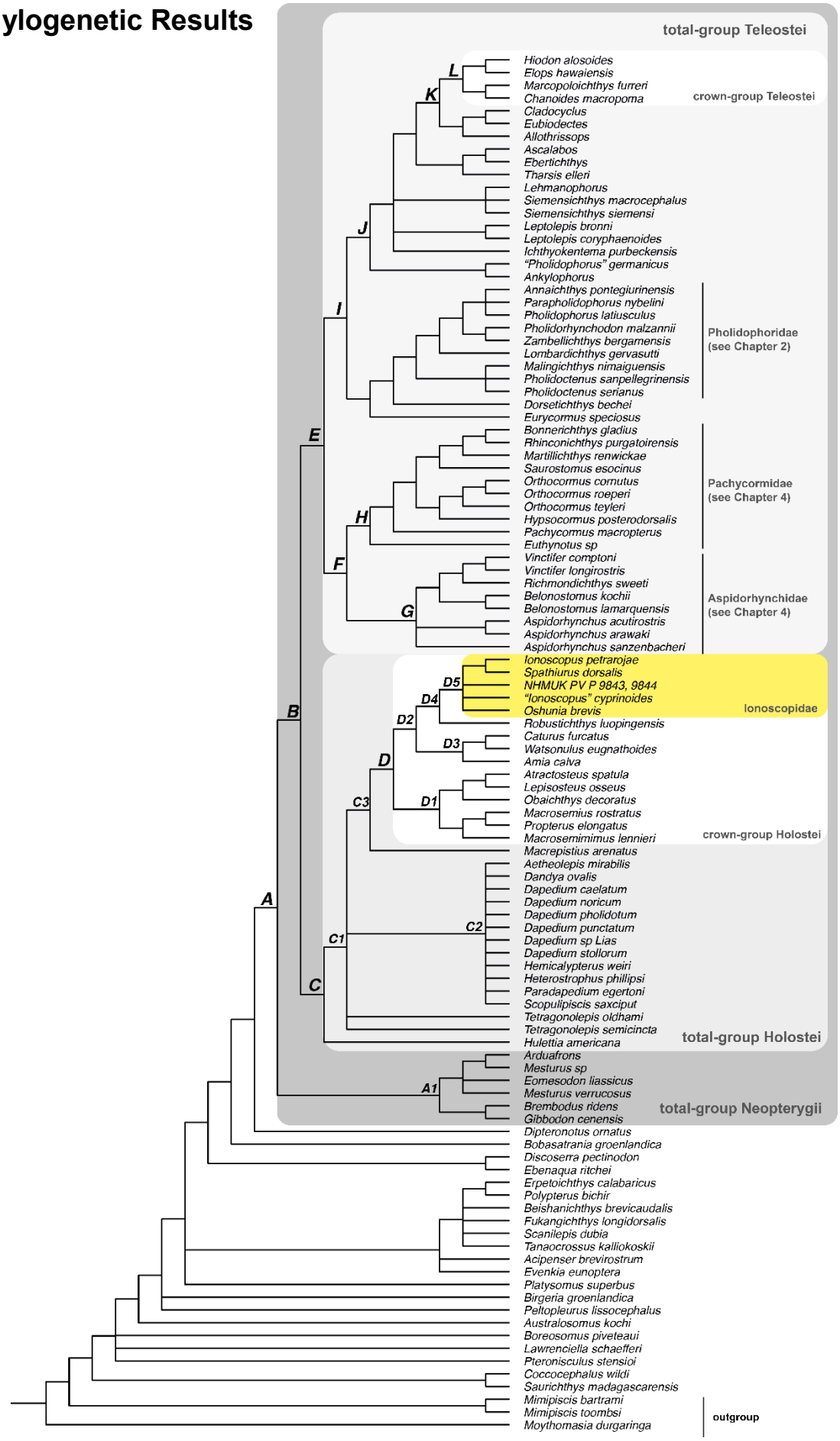

**Figure 3.9: Hypothesis of phylogenetic relationships of neopterygians**. Strict consensus tree of 38448 most parsimonious trees. Ionscopidae highlighted in yellow.

Character optimisations: **Node A:** The neopterygian total group is supported by four homoplastic characters (c.45, peg like anterior process of maxilla; c.78, preoperculum with pronounced ventral limb; c.127, parasphenoid pierced by efferent pseudobranchial artery; c.213, jaw articulation ventral to orbit). **Node B:** The neopterygian crown group (the divergence of the holostean and teleost total groups) is supported by four homoplastic characters (c.57, coronoid process contributed to by dentary plus predentaries; c.80, infraorbitals and suborbitals broadly overlap preoperculum; c.82, interopercle; c.220, ossified centra). **Node C**: The holostean total group, which includes *Hulettia*, Dapediidae, *Macrepistus* and all other holosteans, is supported by four homoplastic characters (c.53, two infradentaries - angular and surangular; c.75, anterodorsal process of suboperculum; c.128, aortic notch in parasphenoid absent; c.132, middle pit line on parietal; c.198, posteriormost proximal radial of dorsal fin present). **Node C1:** Holosteans crownward of *Hulettia* are supported by four homoplastic characters (c.21, anterior branch of infraorbital sensory canal; c.97, occipital fissure closed; c.211, suborbitals extend ventral to orbit; c.223, enlarged vomerine teeth; **Node C2:** Dapediidae (including *Tetragonolepis*, which is not recovered in a clade with other dapediids in the strict consensus tree) are united by four homoplastic characters (c.17, parietals rectangular; c.103, braincase ossifications undifferentiated; c.200, posterior margin of caudal fin unforked; c.217, 'hem-like' median fins). **Node C3:** *Macrepistius* and the holstean crown are united by three homoplastic characters (c.8, olfactory nerve pierces premaxilla; c.29, tube-like canal bearing arm of antorbital; c.37, supraorbitals contact infraorbitals, closing the orbit). **Node D**: The holostean crown group is supported by six homoplastic characters: (c.1, skull roofing bones partially fused; c.125, small parasphenoid teeth; c.126, parasphenoid not pierced by internal carotid artery; c.128, aortic notch in parasphenoid; c.214, parasphenoid wings around basiocciput absent). **Node D1:** Ginglimodi are united by one uniquely derived character (c.36, three or more lachrymals) and four homoplastic characters (c.9, nasal process of maxilla reaches skull roof; c.104, basisphenoid absent or reduced; c.108; forward extension of exoccipital around the vagus nerve; c.112 intercalar absent). **Node D2**: "Halecomorphs" (Amiidae, *Watsonulus* and Ionoscopidae) are united by six homoplastic characters (c.47, one supramaxilla; c.62. symplectic involved in jaw joint; c.145, junction between ampulla of posterior semicircular canal and cranial cavity separated by a short length of canal; c.154 scale with peg and socket articulation absent; c.167 symplectic hatchet shaped; c.181 posttemporal with a distinct dorsal process to articulate with the cranium**. Node D3:** *Amia*, *Caturus* and *Watsonulus* are united by six homoplastic characters (c.33, suborbitals absent; c.46, posterior maxillary notch; c.157 leading margin of paired fins without fringing fulcra; c.158, leading margin of dorsal and anal fins without fringing fulcra; c.159, leading margin of caudal fin without fringing fulcra; c.213 jaw articulation ventral to orbit absent). **Node D4**: Ionoscopiformes (*Robustichthys* + Ionoscopidae) are united by one uniquely derived characters (c.233, innerorbital flange of dermosphenotic bearing sensory canal tube and five homoplastic characters (c.15 mesial margin of nasal notched; 17 parietals rectangular; 32 posterior margin of infraorbital 3 confined anterior to the suborbital; c.37 supraorbitals do not contact infraorbitals at anterior rim of circumorbital ring; c.80 infraorbitals abut preopercular; c.156, small scales below dorsal fin)

(Figure 3.9 cont.) **Node D5**: Ionoscopidae is united by five uniquely derived characters (c.235, ventral surface of infraorbital bones intensely pitted; c.238, notch in second infraorbital to accommodate supramaxilla; c.239, maxillary canal; c.240, lachrymal equal in size to orbit; c.249, dermopterotic double the length of the parietal). **Node D5:** NHMUK PV P 9833, 9844 + "*Ionoscopus" cyprinoides* and *Ionoscopus petrarojae* + *Spathiurus dorsalis* form a clade. Characters are not optimised in the strict consensus tree, but they are united by the presence of the pterotic (c.111). *Oshunia* also undergoes six additional homoplastic character changes (c.34, supraorbitals absent; c.88, anterodorsal myodome paired; c.90, spiracular canal open c.126, parasphenoid pierced by internal carotid artery; c.127, parasphenoid pierced by efferent pseudobranchial artery c.210, suborbitals fragmented). **Node D7**: *Ionoscopus petrarojae* and *Spathiurus dorsalis* form a clade united by two homoplastic characters (c.17 parietals quadrate; c.157 leading margin of paired fins without fringing fulcra). **Node D8:** NHMUK PV P 9833, 9844 + "*Ionoscopus" cyprinoides* form a clade united are united* by two uniquely derived characters (c.233 descending lamina of innerorbital flange free distally; c.245 Posterior semicircular canal with posterior diverticulum)**.** **Node E:** The teleost total group is supported by four homoplastic characters (c.114 supraoccipital bone; c.116 median supraotic absent; 205 hypural diastema; c.214 parasphenoid wings around basioccipiut absent). Teleost nodes explored in subsequent chapter.

The topology of the strict consensus tree is presented in Fig. 3.9. Character optimisations are given in the figure caption. A comparison of the alternative topologies within Ionoscopidae is found in Fig. 3.7.1.

## 3.7 Discussion

### 3.7.1 Clarifying the status of "*Aspidorhynchus*" and "*Ionoscopus*" *cyprinoides*

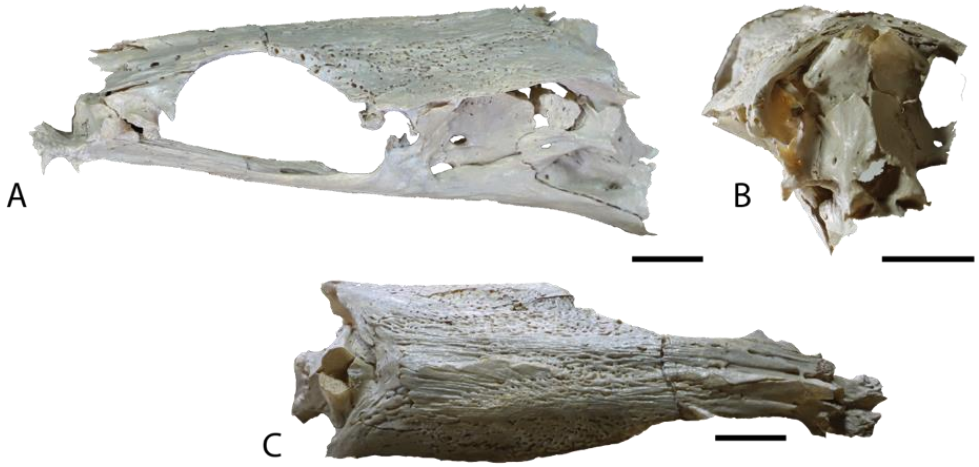


**Figure 3.10: Skull roof and braincase of "*Ionoscopus" cyprinoides* NHMUK PV OR 37795a** braincase in (A) left lateral, (B) posterolateral, and (C) dorsal view. NB photograph angles limited by how the specimen is mounted. Scale bar = 10 mm.

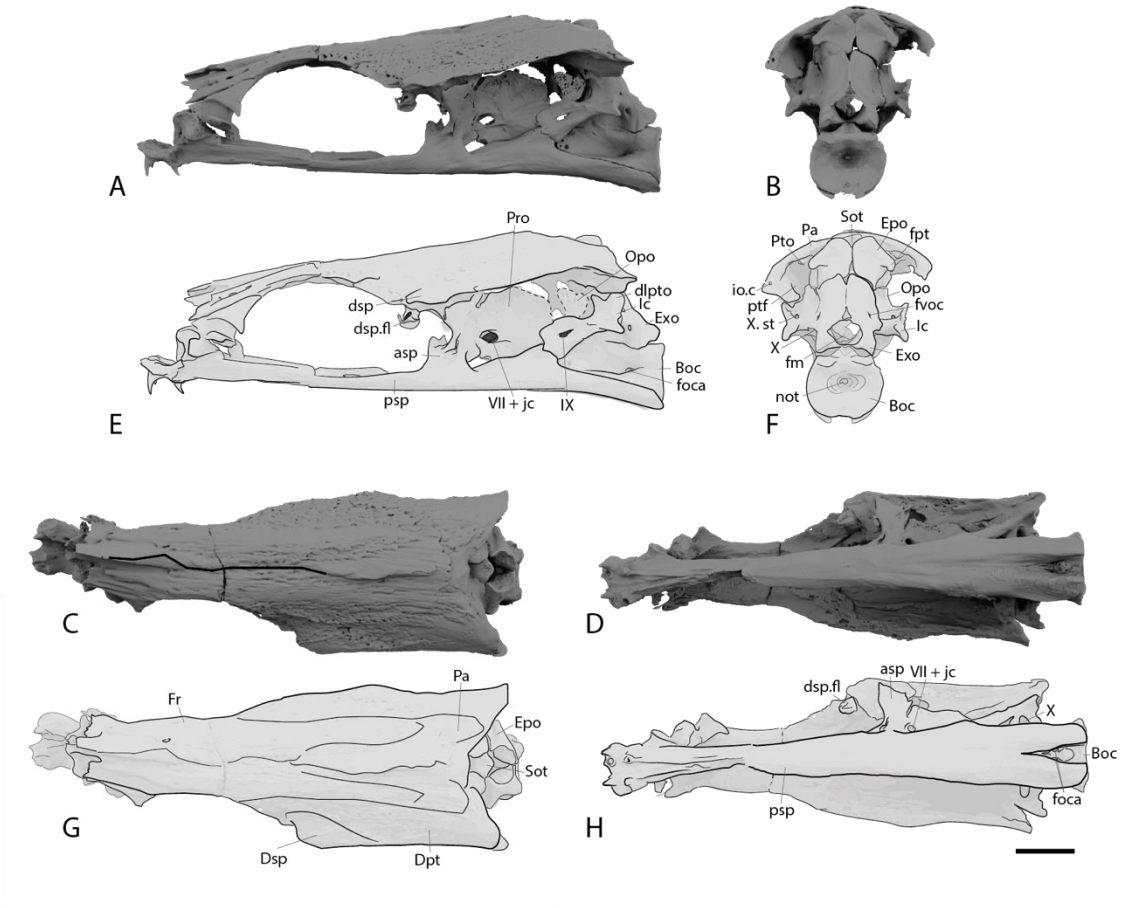


**Figure 3.11: Skull roof and braincase of "*Ionoscopus" cyprinoides* NHMUK PV OR 37795a.** Renders in (A) left lateral, (B) posterior, (C) dorsal and (D) ventral view. Interpretive drawings in (E) left lateral, (F) posterior, (G) dorsal and (H) ventral view. Scale bar = 10 mm. *Abbreviations*: *asp, ascending process of the parasphenoid; Boc, basioccipital; dlpto, descending lamina of the dermopterotic; Dsp, dermosphenotic; Dsp.fl, innerorbital flange of the dermosphenotic; Epo, epioccipital; Exo, exoccipital; fm, foramen magnum; foca, foramen for occipital artery; fpt, facet for ligament to post-temporal; fvoc, foramen for tributary of posterior cerebral vein in exoccipital; Ic, intercalar; io.c, foramen for infraorbital canal; jc, foramen for jugular vein; Opo, opisthotic; not, notochordal opening; Pa, parietal; Pro, prootic; ptf, post-temporal; Pto, pterotic; psp, parasphenoid; Sot, supraotic; VII, foramen for facial nerve; IX, foramen for glossopharyngeal nerve; X foramen for vagus nerve; fo X. st, foramen for supratemporal branch of the vagus nerve.*

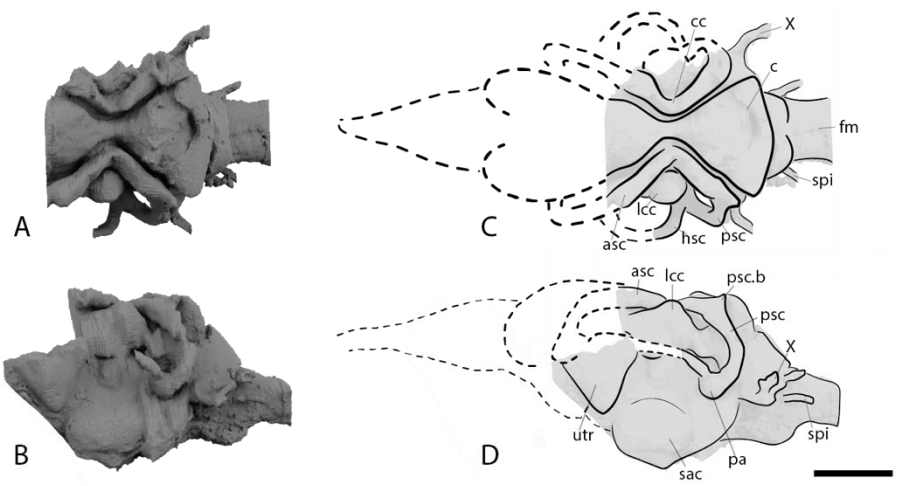


**Figure 3.12: Partial endocast of "*Ionoscopus" cyprinoides* NHMUK PV OR 37795a.** Renders in (A) dorsal and (B) left lateral view. Interpretive drawings in (C) dorsal and (D) left lateral view. Dashed lines indicate inferred shape of unresolved endocast based on NHMUK PV P 9843 and 9844. Scale bar = 10 mm. *Abbreviations*: *asc, anterior semicircular canal; c, cerebellum; cc, crus commune; fm, foramen magnum; hsc, horizontal semicircular canal; lcc, lateral cranial canal; optl, optic lobes; pa, posterior ampulla; psc, posterior semicircular canal; psc.b, diverticulum of the posterior semicircular canal; sac, saccular chamber; spi, spino-occipital nerve; utr, utricular; X, vagus nerve.*

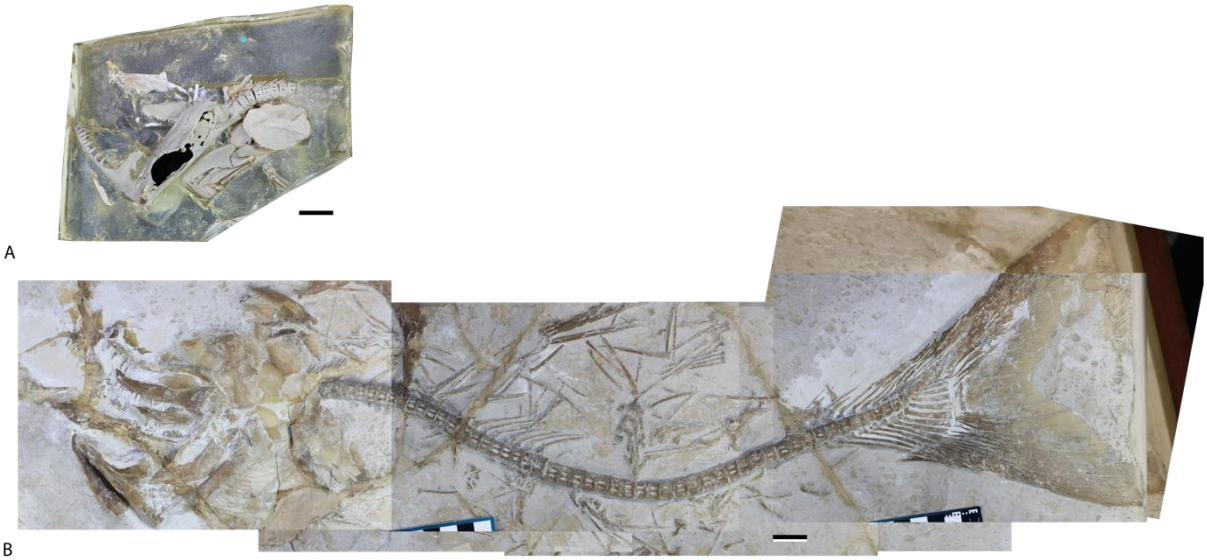


**Figure 3.13: "Ionoscopus" cyprinoides NHMUK PV OR 37795 A and B (counterparts).** (A) photograph of acid prepared resin block (NHMUK PV OR 37795a) in dorsal view. (B) Photograph of counterpart (NHMUK PV OR 37795) in dorsal view. Scale bar = 20 mm.

Based on shared features of the braincase and dermal skull roof, such as the narrow otic region, elongate dermopterotic (c.249), relative proportions of the prootic and opisthotic (c.105) and crucially the innerorbital flange of the dermosphenotic

carrying a branch of the infraorbital sensory canal (c.233), NHMUK PV P 9843 and NHMUK PV P 9844 can be confidently placed with halecomorphs, specifically ionoscopids. Characters are discussed in more detail below. This conclusion agrees with formal and informal arguments made in previous work (Patterson 1973; Patterson 1975; Maisey 1991, 1999; Gardiner *et al.,* 1996) proposed a close relationship with "*Ionoscopus" cyprinoides* (Fig. 3.10-3.13) and *Oshunia brevis* due to multiple similarities in the occipital region, provisionally placing NHMUK PV P 9843 and 9844 in the now disbanded family Oshuniidae. As the taxonomic content and status of Ionoscopiformes and the families contained within it has changed substantially in the last few decades, these must be reviewed before a more precise placement for NHMUK PV P 9843 and 9844 can be determined.

The monophyly of Ionoscopiformes (*sensu* Grande & Bemis, 1998, pg. 603) was established based on two synapomorphies: c. 18, frontals relatively long, and c. 63, innerorbital flange of the dermosphenotic bearing a sensory canal tube. Other synapomorphies have since been proposed, such as the presence of a maxillary branch of the infraorbital sensory canal within the maxilla (e.g., Alvarado-Ortega & Espinosa-Arrubarrenach, 2008, ch. 5). Ionoscopiformes contains the Ophiopsidae and Ionoscopidae. These characters can only be coded from three dimensionally preserved crania. Ionoscopidae are characterised by an elongate dermopterotic longer than the parietal, fifteen or more supraneurals (Taverne & Capasso, 2016); the ventral surface of subinfraorbital bones being intensely pitted (López-Arbarello & Sferco, 2018, ch.128), the absence of caudal diplospondyly (e.g., Gardiner *et al.*, 1996, ch.11) and the presence of a quadratojugal (e.g., López-Arbarello *et al.,* 2020, ch. 98). These characters can be preserved from flattened caudal skeletons.

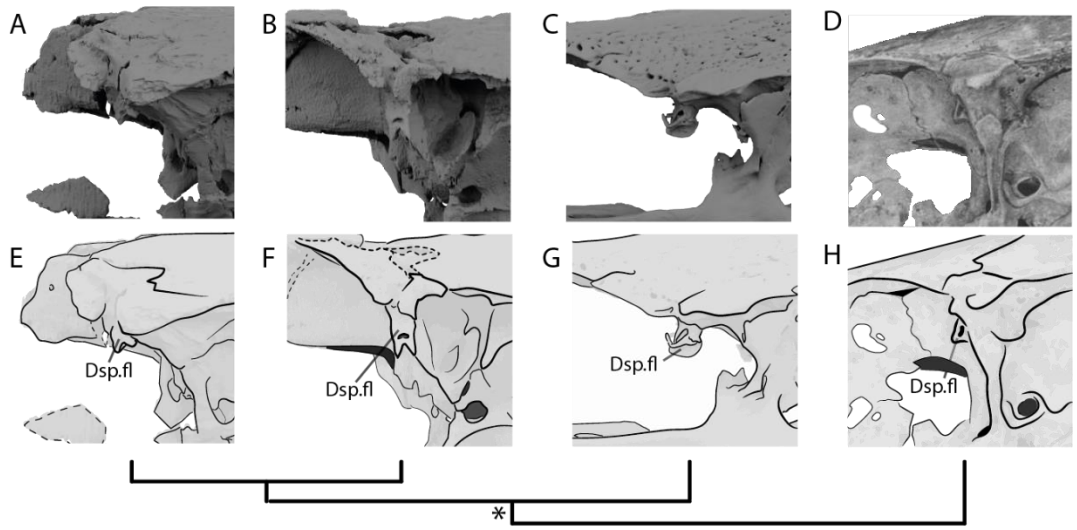


**Figure 3.14: Handdrawn cladogram of the position of the canal-bearing innerorbital flange in ionoscopids relative to the postorbital wall.** Render of canal-bearing innerorbital flange in (A) NHMUK PV P 9843 (B) NHMUK PV P 9844 (flipped) and (C) *"Ionoscopus" cyprinoides* NHMUK PV OR 37795a. (D) Photograph of canal-bearing innerorbital flange in *Oshunia brevis* AMNH 12793 (Maisey, 1999). Interpretive drawing of canal-bearing innerorbital flange in (A) NHMUK PV P 9843 (B) NHMUK PV P 9844 (flipped), (C) "*Ionoscopus" cyprinoides* NHMUK PV OR 37795a and (D) *Oshunia brevis* AMNH 12793. NHMUK PV P 9843, NHMUK PV P 9844 and "*Ionoscopus" cyprinoides* NHMUK PV OR 37795a form a clade (*) to the exclusion of *Oshunia brevis* by the canal-bearing innerorbital flange being free distally from the postorbital wall. Not to scale.

The presence of an innerorbital flange of the dermosphenotic carrying a branch of the infraorbital sensory canal is unique and consistent among Ionoscopiformes (e.g., Gardiner *et al.,* 1996, ch. 33; Grande & Bemis, 1998, ch. 63; Alvarado-Ortega & Espinosa-Arrubarrena, 2008, ch. 1; Sun *et al.*, 2016). The flange is best seen in *"Ionoscopus" cyprinoides* (Grande & Bemis, 1998: fig. 410, CMNH 4036; Maisey, 1999: figs. 1A, 8, 14: NHMUK PV OR 37795a), *Oshunia brevis* (Maisey, 1999: fig. 1B, AMNH 12793) and *Robustichthys luopingensis* (Xu *et al.*, 2014: fig. 1, IVPP V18571). Presence of this feature was also noted by Maisey (1991, pg. 159) and Gardiner *et al. (*1996, pg. 125) in 'Rayner's *"Aspidorhynchus"',* referring to Patterson's (1975; fig. 39, 101) detailed figures, where the flange is visible but unlabelled. This study confirms the presence of the flange in Rayner's *"Aspidorhynchus"* (Fig. 3.3F, G, H, 3.4F, 3.6E, 3.7F, 3.14A, B), as well as an internal sensory canal, providing strong support for the

placement of ‘Rayner’s *“Aspidorhynchus”’* within Ionoscopiformes. NHMUK PV P 9843 and NHMUK PV P 9844 also display an elongate dermopterotic longer than the parietal, as previously recognised by Rayner (1948, fig. 19) and Patterson (1975, fig. 99). This feature further affirms their placement within Ionoscopidae as opposed to Ophiopsidae.

Of note, Ebert (2018) cast doubt upon the reliability of the innerorbital flange as a useful synapomorphy, contrasting previous studies, because the feature is absent in JME-ETT86. JME-ETT86 is a fossil braincase also referred to *Ionoscopus* which is better preserved than NHMUK PV OR 37795a as it has not been acid prepared. Furthermore, Ebert argues that NHMUK PV OR 37795a cannot be reliably diagnosed as *“Ionoscopus” cyprinoides* because it is only associated with a few dermal elements and not the diagnostic caudal skeleton. However, Ebert’s argument likely stems from confusion over the history of NHMUK PV OR 37795a, which this study will now attempt to clarify. The acid prepared portion of the specimen – NHMUK PV OR 37795a (Figs. 3.10, 3.13A), comprising the braincase (figured by Maisey 1999), the anterior most vertebrae and disarticulated dermal elements – is the counterpart to NHMUK PV OR 37795 (Fig 13B) which comprises the remaining body, including the skull, vertebral column and caudal fin, which has been previously illustrated by Patterson (1973, pg. 289). It appears that the portion containing the braincase was mechanically removed from the main specimen, flipped over, then re-mounted adjacent to the remaining block in a framed plaster display. After some time in this arrangement, the portion containing the braincase was removed again, flipped back into its original orientation, and acid prepared for description by Maisey (1999). Over time, the two parts of the specimen drifted apart in the NHMUK collections (pers comm, E Bernard, 2024). Having studied both portions of the specimen, it is evident that they belong to a single, articulated,

near-complete individual and a composite restoration of NHMUK PV OR 37795 and NHMUK PV OR 37795a has been attempted, and can be found in the Appendices (A.5). Contrary to Ebert, 2018, the complete specimen confirms that its anatomy is consistent with other specimens of *“Ionoscopus” cyprinoides* (e.g., CMNH 4036). Furthermore, CMNH 4036 (Grande & Bemis, 1998, pg. 614), which preserves only a partially compressed but fully articulated dermal skeleton, also appears to exhibit a canal-bearing innerorbital flange of the dermopterotic. Additionally, the absence of this feature in JME-ETT86 strongly suggests that JME-ETT86 belongs to a taxon outside of Ionoscopiformes and that the robustness of the character as an ionoscopiform synapomorphy is upheld.

Ionoscopid taxonomy is further complicated by the possible paraphyly of the genus *Ionoscopus*, with the inclusion of the species *“Ionoscopus” cyprinoides* being called into question. Maisey (1999) recognised a greater number of similarities between the dermal skeletons of *Oshunia brevis* and *I. petrarojae*, for example a short maxilla, than between *I. petrarojae* and *“I.” cyprinoides*. In their redescription of the type species, Taverne & Capasso (2016) identified further differences across the cranial, appendicular and axial skeleton of *I. petrarojae* and *“I.” cyprinoides*, considering these significant enough to warrant the erection of a new genus for *“I.” cyprinoides*. This was supported by Ebert (2018), who also noted the difficulty in identifying differences due to the poor preservation of *I. petrarojae*. Most recently, a redescription and phylogenetic evaluation of *Spathiurus dorsalis* from the Cenomanian of Lebanon (Hossney *et al.*, 2020) recovered a sister taxon relationship between *I. petrarojae* and *S. dorsalis*, to the exclusion of *“I.” cyprinoides*.

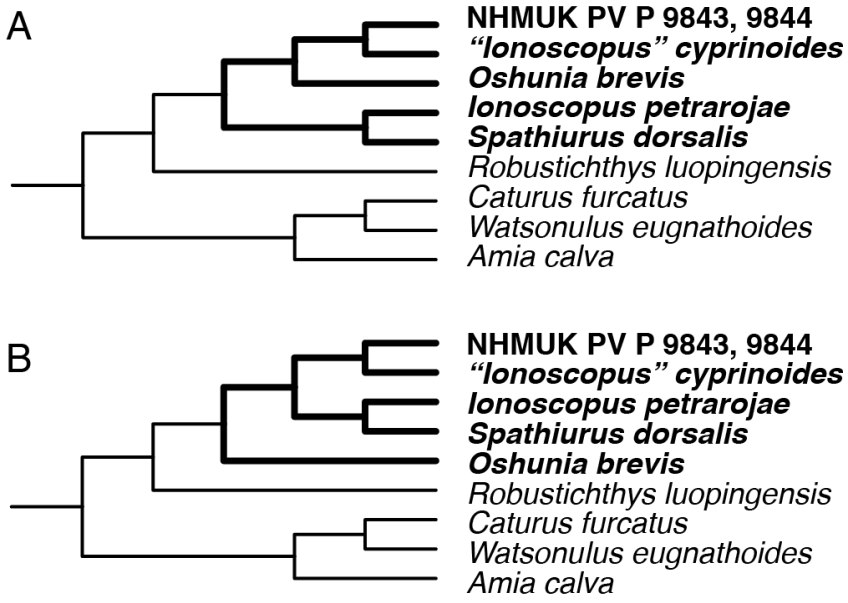


**Figure 3.15: Alternate topologies for Ionoscopidae recovered from phylogenetic analysis.** (A) NHMUK PV P 9843 9844 and *"I" cyprinoides* are sister to *Oshunia brevis* (B) NHMUK PV P 9843 9844 and *"I" cyprinoides* are sister to *I. petrarojae* and *S. dorsalis*.

The phylogenetic placement of NHMUK PV P9834 and NHMUK PV P 9844 (Fig. 3.9) is supported within ionoscopiforms by one uniquely derived character (c.232, innerorbital flange of dermosphenotic bearing sensory canal tube) and ionoscopids by one homoplastic character (c.248, elongate dermopterotic longer than the parietal). However, relationships are difficult to resolve between the ionoscopids due to the limited overlap between the preserved anatomy. *"I." cyprinoides* and *O. brevis* are relatively well known from dermal skeletons in various states of articulation, three-dimensionally preserved braincases and complete vertebral columns and caudal skeletons, but NHMUK PV P 9843 and NHMUK PV P 9844 are represented by isolated braincases and therefore can only be coded for characters of the cranial skull roof, neurocranium and endocast. All other ionoscopids are known primarily from disarticulated dermal skeletons. Here, ionoscopids form a polytomy (Fig. 3.9) reflecting two contrasting topologies, entirely a result of the conflicting placement of *O. brevis*:

either as sister taxon to NHMUK PV P 9843 and NHMUK PV P 9844 and *"I" cyprinoides* to the exclusion to a clade comprising *I. petrarojae* and *S. dorsalis* (Fig. 3.15A), or as sister taxon to a clade comprising NHMUK PV P 9843 and NHMUK PV P 9844 and *"I" cyprinoides* and *I. petrarojae* + *S. dorsalis* (Fig. 3.15B).

Previous work (Maisey, 1991, 1999) has suggested a closer relationship between NHMUK PV P 9843 and NHMUK PV P 9844 to *O. brevis* based on features such as a membranous outgrowth of the intercalar contacting the parasphenoid. However, these characters are distributed across ionoscopids, and do not exclusively support a relationship between *O. brevis* and any single other taxon.

In either scenario reflected in the polytomy in the strict consensus tree (Fig. 3.9), "*Ionoscopus" cyprinoides* and NHMUK P 9843 + NHMUK P 9844 form a clade distinct from *Ionoscopus petrarojae*, supported by, several features of the braincase and skull roof**.** The innerorbital flange of the dermosphenotic in NHMUK PV P 9843 and NHMUK PV P 9844 lies close to the postorbital wall but is not in direct contact with it, as in *"I." cyprinoides* (also observed by Gardiner *et al.,* 1996, pg. 125). In contrast, in *O. brevis*, the flange and the postorbital wall are in direct contact (Fig. 3.14).

Other similarities with *"I." cyprinoides* to the exclusion of *O. brevis* include the presence of a pterotic. Loss of the pterotic has previously been interpreted as a synapomorphy of amiids, due to uncertain homology with the braincase ossification of other neopterygians (Grande & Bemis, 1998, pg. 612), and later as a holostean synapomorphy (Grande 2010, pg. 800). As the braincase is unknown in many early holosteans – including other ionoscopids – the presence of the pterotic is poorly optimised in this chapter's phylogenetic analysis, i.e., as this character's occurrence

is uncertain in most taxa, it is difficult to trace its acquisition along the stem. However, it is most likely that the pterotic was retained by "*I." cyprinoides*, NHMUK PV P 9843 and NHMUK PV P 9844 as an ancestral state. The parasphenoid of "*I." cyprinoides*, NHMUK PV P 9843 and NHMUK PV P 9844 lacks a basipterygoid process, which is present in *Oshunia*. Similarly, the parasphenoid of "*I." cyprinoides*, NHMUK PV P 9843 and NHMUK PV P 9844 is not pierced by the internal carotid artery, contrary to the condition in *O. brevis*. Although the endocast of *O. brevis* is unknown, numerous features are shared between the endocast and bony labyrinth of NHMUK PV P 9843 and NHMUK PV P 9844 and "*Ionoscopus*" *cyprinoides*. These include a deep utricular, an elongate anterior semicircular canal, and wide cerebellum, which is distinctly triangular in NHMUK PV P 9844 and *"I" cyprinoides*. Finally, the short posterior diverticulum of the posterior semicircular canal appears to represent a uniquely derived feature shared by NHMUK PV P 9843 NHMUK PV P 9844 and *"I." cyprinoides*.

In agreement with Taverne & Capasso (2016), Ebert (2018) and Hossney *et al. (*2020), this chapter supports the exclusion of *"I" cyprinoides* from *Ionoscopus* and erect a new genus to contain it, alongside NHMUK PV P 9843 and NHMUK PV P 9844.

### 3.7.2 Intraspecific variation between NHMUK PV P 9843 and NHMUK PV P 9844

NHMUK PV P 9843 and NHMUK PV P 9844 are consistently regarded as the same species, however some differences in anatomy have been noted, such as the greater degree of ossification in NHMUK PV P 9844 (Patterson, 1975, pg. 438), the presence of a distinct supraotic and independent prootic and epiotic ossifications in NHMUK PV P 9843 and the difference in development of the margin of the vagus nerve within the intercalar (Rayner, 1948, pg. 315). This chapter notes some additional

variation between the two specimens. The basioccipital is more elongate in NHMUK PV P 9843 resulting in a more steeply inclined occipital surface when compared to the more vertical occiput of NHMUK PV P 9844 (Figs. 3.3E, 3.6E). Other variation is observed within the endocast: NHMUK PV P 9843 displays a much larger cerebellum than that of NHMUIK PV P 9844 (Figs. 3.5F, 3.8F), and a considerably narrower saccular chamber (Figs. 3.5H, 3.8H). Most investigations of the braincase and endocast in early neopterygians are limited to a single individual (Rayner, 1948; Griffith & Patterson, 1963; Patterson, 1975; Berrel *et al.,* 2014; Giles *et al.,* 2016 and Latimer & Giles, 2018) so the extent of intraspecific variation in taxa is poorly understood. It is most likely that some of these variations can be attributed to post-mortem deformation. Given the overall similarity between the two braincases, and in the absence of additional dermal comparative material, it is not especially useful to the overall aims of the thesis or helpful for readers to refer each specimen to separate taxa.

### 3.7.3 Broad patterns of bony labyrinth anatomy within Neopterygii

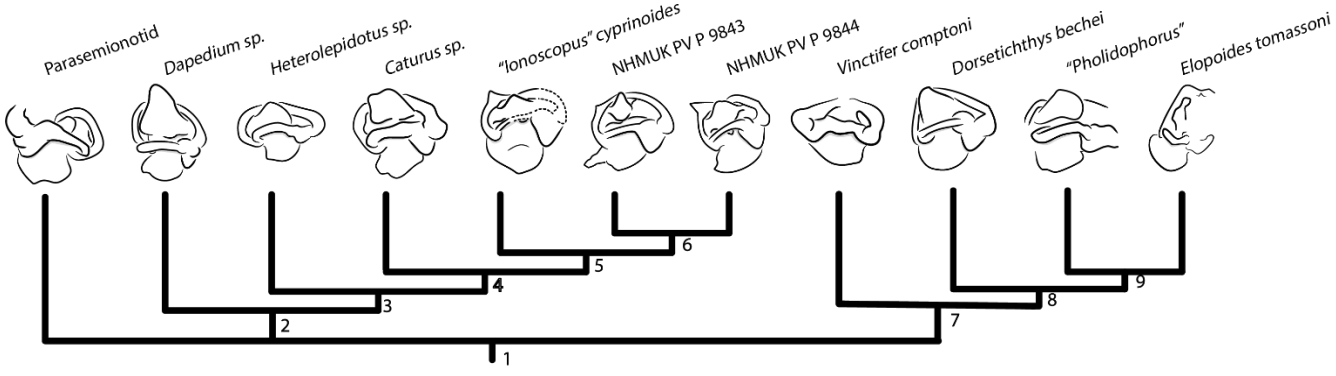

**Figure 3.16: Hand-drawn cladogram of character evolution in the bony labyrinth in early neopterygians, updated from Giles *et al.* (2018).**

Character optimisations: **Node 1:** semicircular canals fully invested in bone, long axis of anterior ampulla orientated vertically, horizontal semicircular canal joins vestibular region level with ampulla for the posterior semicircular canal, lateral cranial canal has anterior and posterior connection to cranial cavity, root of vagus (CN X) nerve rounded, wide separation between lateral cranial canal and cranial cavity, shallow utriculus, sacculus posterior notch absent, horizontal canal curved isoclinally absent, posterodorsal diverticulum on posterior semicircular canal absent, saccular lagenar reduced or absent, crus commune dorsal to endocranial roof, hypophyseal chamber projects ventrally, optic lobes wider than cerebellum, optic lobes divided into bilateral halves. **Node 2 – Holostei Total Group:** utricular deep, root of vagus (CN X) nerve large and anteroposteriorly long. horizontal semicircular canal joins vestibular region dorsal to ampulla for the posterior semicircular canal. **Node 3:** horizontal semicircular canal joins vestibular region level to ampulla for the posterior semicircular canal, long axis of anterior ampulla oriented horizontally **Node 4:** posterior portion of horizontal canal completely engulfed by posterior ampulla; narrow separation between lateral cranial canal and cranial cavity; sacculus posterior notch. **Node 5 - Ionoscopidae:** posterior semicircular canal with posterodorsal diverticulum. **Node 6 - NHMUK PV P 9843 and 9844:** elongate saccular lagenar. **Node 7 - Teleostei Total Group:** posterior portion of horizontal canal completely engulfed by posterior ampulla **Node 8:** horizontal semicircular canal joins vestibular region level to ampulla for the posterior semicircular canal. **Node 9:** semicircular canals partially invested in bone, long axis of anterior ampulla orientated vertically. Not to scale.

Including *“l.” cyprinoides* and NHMUK PV P 9843 to an existing hand drawn cladogram (Fig. 3.16) further illustrates patterns of diversification of the bony labyrinth within holosteans and highlights the unique specialisations acquired by the new genus erected here. Ionoscopids (Fig. 3.16, Node 5) are found to be characterised by a novel anatomical feature in the bony labyrinth: a posterodorsally directed diverticulum of the posterior semicircular canal. Furthermore, neopterygians (Fig. 3.16, Node 1) are typically characterised by a reduced or absent lagenar pouch, but NHMUK PV P 9843 and 9844 (Fig. 3.16, Node 6) appear to develop a larger, elongate lagenar pouch.

## 3.8 Conclusion

This chapter presents a re-evaluation of historical and enigmatic specimens of three-dimensionally preserved neopterygian braincases. Through high resolution CT and synchrotron scanning, this chapter presents a detailed description of the braincase and endocast of “Rayner’s ‘*Aspidorhynchus*’”, using this information to erect a formal taxonomic placement for the specimens within Ionoscopidae. This chapter also presents an updated diagnosis for Ionoscopidae and identify a new genus for *“Ionoscopus” cyprinoides* and “*Aspidorhynchus”*.

# 4. CT AND SYNCHROTRON BASED INVESTIGATION OF ICONIC STEM TELEOST TAXA: *RICHMONDICHTHYS SWEETI* (ASPIDORHYNCHIDAE) AND *PACHYCORMUS MACROPTERUS* (PACHYCORMIDAE)


## Abstract

Aspidorhynchids and pachycormids are both historically considered early diverging members of the teleost stem, but their precise placement on the stem and their interrelationships remain uncertain. Recent studies have proposed an unusual coupling of Aspidorhynchids and pachycormids, forming a novel clade: Aspidorhynchoidei. However, there is little support for this clade, their relationships are contested, and existing anatomical descriptions are incomplete. Here, an exceptionally preserved representative of both Aspidorhynchidae and Pachycormidae are described. The braincase of *Richmondichthys* (Aspidorhynchidae) Toolebuc Formation (Albian), Queensland, Australia is described via CT scanning for the first time, forming the first digital reconstruction of an aspidorhynchid braincase and endocast. This study identifies key characters transitions such as the loss of the lateral cranial canal. This study also presents an exceptionally preserved, fully articulated and three dimensional *Pachycormus* (Pachycormidae) from the Strawberry Bank Lagerstätte (Toarcian) Somerset, UK. High resolution synchrotron scanning reveals a partially ossified braincase, elaborate gill skeleton, evidence of soft tissue preservation, and the first three-dimensional, digitised visualisation of the endoskeletal pectoral fin and axial skeleton of *Pachycormus*. This extraordinary insight has clarified previous descriptions, such as the total number of infraorbitals and coronoids and the

life position of often disarticulated tooth plates – all of which are typically lost during preparation. This study also finds an inflated anterior coronoid and large fang-like teeth on the anterior dermopalatines and coronoids, suggesting a closer link to the macrophageous toothed clade. These data were introduced to a revised phylogenetic model of early Neopterygii, revealing very limited support for Aspidorhynchoidei.

## 4.1 Introduction

Numerous notable fossil assemblages are associated with the teleost stem, such as aspidorhynchids and pachycormids. Despite disparate morphologies and ecologies, these groups show morphological affinities with other early teleost assemblages, such as pholidophorids and leptolepids (Arratia, 2013, 2017; López-Arbarello & Sferco, 2018). Although historically considered distinct clades on the teleost stem, with aspidorhynchids generally considered to branch closer to other teleosts (e.g., Gardiner, 1960; Patterson, 1977; de Pinna, 1996; Brito, 1997), in recent years support has been growing for aspidorhynchids and pachycormids to form a clade [Arratia, 2013, 2017; López-Arbarello & Sferco, 2018; Gouiric-Cavalli & Arratia, 2022) which has knock on impacts for the

Aspidorhynchids (Bathonian to Maastrichtian; Brito, 1997; Brito & Suàrez, 2003) exhibit a suite of morphological specialisations resulting in a superficial resemblance to elongate extant fishes such as garfish and needlefishes. They have distinctively long, toothed snouts contributed to by an immobile premaxilla and apomorphic predentary bone, as well as elongate bodies with distally positioned dorsal and anal fins. Aspidorhynchids are known from both flattened, two-dimensionally preserved specimens, such as from the Jurassic (Tithonian) Solnhofen Limestone, Germany (e.g., Frey & Tischlinger, 2011; López-Arbarello & Schröder, 2013) and

three-dimensionally preserved specimens, such as from the Cretaceous (Aptian) Araripe Basin, Brazil (e.g., Maisey, 1991; Brito & Yabumoto 2011; Silva *et al.,* 2023).

In addition to articulated material, a number of isolated aspidorhynchid braincases have also been reported. The first aspidorhynchid braincase described in the literature, NHMUK PV P 62533a, has a complex taxonomic history. This specimen, from the Albian Rolling Downs Group, Queensland, Australia had been previously referred to "*Belonostomus" sweeti* (Etheridge & Woodward, 1891), "*Aspidorhynchus" sweeti* (Agassiz, 1833) and "*Vinctifer" sweeti* (Jordan, 1919; Brito, 1997), before Bartholomai (2004) comprehensively revaluated Australian aspidorhynchid material and erected the new genus *Richmondichthys* to contain it. For a century, *Richmondichthys* represented the sole insight into aspidorhynchid neurocranial anatomy, until Maisey's (1991: pg. 170) description of acid prepared neurocrania belonging to *Vinctifer* from the Santana Formation. Brito (1992, 1997) described the braincase of multiple genera of aspidorhynchid, including *Aspidorhynchus*, *Belonostomus* and *Vinctifer* (nb. *"Vinctifer" sweeti* (Rb 7321-2) was later reassigned to *R. sweeti* by Bartholomai, 2004: pg. 522) and Bogan *et al. (*2011) described an isolated braincase (associated with a predentary – an aspidorhynchid synapomorphy) assigned to *Belonostomus lamarquensis*. Despite a growing understanding of the braincase, the aspidorhynchid endocast is known only from non-digital interpretation of several specimens of one species: *Vinctifer comptoni* (Brito, 1992). The phylogenetic placement of aspidorhynchids remains relatively uncertain, in part due to their highly specialised anatomy and poor fossil record of early members of the clade. This issue is shared with pachycormids.

Pachycormids (Toarcian; Lehman, 1949 to Maastrichtian; Friedman, 2012) are another clade of iconic, highly specialised stem teleosts. Numbering ~50 species

(Cooper & Maxwell, 2022), they exhibit a highly disparate range of body plans, encompassing macrophagous predators such as *Hypsocormus* and the swordfish-like *Protosphyraena* (Amalfitano *et al.*, 2017) to giant suspension filter feeders such as *Martillichthys* and *Leedsichthys* (Friedman *et al.*, 2010). Although finer patterns of relationships are often confounded by these diverging morphologies, pachycormids are united by a median, compound rostrodermethmoid between the nasals and immobile premaxillae and a fused hypural plate in the caudal fin. The eponymous genus *Pachycormus* is now considered to contain only a single valid species, *P. macropterus* (Wretman *et al.*, 2016), from the Jurassic (Toarcian) from the UK, France and Germany (Cawley *et al.*, 2019).

Pachycormids are comprehensively represented in the fossil record by both flattened, two-dimensional specimens (Weitzel, 1930; Lambers, 1988; Arratia & Schultze, 2013; Cooper & Maxwell, 2022) and articulated, three-dimensional specimens (Woodward 1897; Patterson, 1975; Mainwaring, 1978; Cawley *et al.*, 2019). The endoskeleton is also known in some specimens but tends to be disarticulated or incomplete (e.g., Rayner, 1948; Cooper *et al.*, 2022). Acid-preparation of specimens allows a comprehensive description of these internal elements (e.g., Patterson, 1975; Mainwaring, 1978), although delicate structures and key positional information can be lost during the process (e.g., Gardiner, 1984; Choo *et al.,* 2009. Through a combination of disarticulated specimens and mechanical and acid preparation the braincase anatomy of *Pachycormus* is moderately well-known in specimens from the Upper Lias of Whitby, UK (Lehman, 1949; Mainwaring, 1978: pg. 44); Normandy, France (Patterson, 1975) and the Solnhofen Limestone, Germany (Holmgren & Stensiö, 1936; Rayner, 1948). Several other pachycormid braincases have also been described in greater or lesser amounts of detail (e.g., Rayner 1948,

Dobson *et al.,* 2021), although the trend for reduced ossification in pachycormids limits the amount of information that can be gathered (Giles *et al.*, 2016), and the anatomy of the endocast is entirely unknown (Friedman & Giles, 2016: pg. 36).

Like many other taxa now associated with the teleost stem, aspidorhynchids and pachycormids were historically interpreted as “holosteans” for over a century (Woodward, 1895). As previously explored in this thesis, this historical interpretation of “holostean” is not equivalent to the modern interpretation (*sensu* Grande, 2010), but referred to a structural grade of taxa of typically Mesozoic age possessing plesiomorphic features such as ganoid scales. Over time, groups such as pholidophorids and leptolepids were gradually reconsidered as early diverging teleosts. However, a holostean affinity was maintained for aspidorhynchids and pachycormids for many more decades (e.g., Lehman, 1949; Gardiner, 1960, Romer, 1966).

Although Rayner (1941) argued that pachycormids were too specialised to be placed in a group with certainty, her subsequent detailed description of pachycormid neurocrania (Rayner 1948) allowed Gardiner (1960: pg. 344) to highlight evidence for a halecomorph placement for pachycormids. Gardiner cited similar ossification patterns between *Pachycormus*, *Orthocormus* and *Heterolepidotus*, such as the presence of an opisthotic and the absence of a supraoccipital, as indicative of a close relationship between pachycormids and relatives of the extant *Amia*. Affinities of aspidorhynchids were less clear, partly due to confusion stemming from uncertain homologies between the braincase ossifications in ‘Rayner’s “*Aspidorhynchus*”’ – NHMUK PV P 9843 and NHMUK PV P 9844, now established to be ionoscopids (Rayner 1948; see Chapter 3) – and those of pholidophorids and leptolepids.

However, in 1973, Patterson proposed the first synapomorphy-based definition for a monophyletic teleost group comprising both fossil and living taxa. Patterson argued for the first time that pachycormids and aspidorhynchids lacked key features associated with the lineage leading to *Amia*, and were better placed as stem teleosts (Patterson 1973, p. 276; 1977, fig. 19). This novel interpretation was not universally adopted. As reviewed by Arratia (1999), Carroll (1988) and Nelson (1994) argued that while pholidophorids and leptolepids could be evidenced as early members of the teleost lineage, pachycormids and aspidorhynchids could only be confidently resolved as early neopterygians. It was not until de Pinna (1996) that further support was found for Patterson's hypothesis of relationships. Affiliation with the teleost stem has continued to characterise both aspidorhynchids and pachycormids since the development of modern phylogenetic analyses (de Pinna, 1996; Brito, 1997; Friedman, 2011; Arratia, 2013; 2017; López-Arbarello & Sferco, 2018), However, their placement on the teleost stem is not robust under the manipulation of outgroup taxa (Arratia, 1999; Arratia *et al.*, 2021).

Arratia (1999; 2001; 2004) recovered aspidorhynchids and pachycormids as sister taxa under some phylogenetic schemes; this clade, alongside dapediids and pycnodonts, represented the sister group to Teleostei. However, the sister relationship between aspidorhynchids and pachycormids is not discussed in the text, and while Arratia clearly considers the teleost affinity of pachycormids as secure, she is more equivocal about the placement of aspidorhynchids. It is not until Arratia (2013, 2017) that this clade (Aspidorhynchoidei: Nelson *et al.*, 2016) is considered to have merit. In Arratia's 2013 analysis, the clade is supported by three uniquely derived characters: the supramaxilla lies posterior to the maxilla; the coronoid process is extremely reduced/ absent, and the postcliethrum is absent (optimised as a uniquely derived

character but coded as missing in pachycormids in the underlying matrix). By Arratia's 2017 analysis, the clade is only supported by one uniquely derived character: the position of the supramaxilla, with other characters used to previously unite the clade being recovered as homoplastic. Aspidorhynchoidei is also recovered by López-Arbarello & Sferco (2018). This is noteworthy, as the character matrix for this analysis incorporates a very broad range of taxa and characters, including non neopterygians. However, in their analysis, aspidorhynchids and pachycormids are only represented by a single species each: *Aspidorhynchus acutirostris* and *Pachycormus macropterus*. Regardless, Aspidorhynchoidei is united by two uniquely derived characters: the posterior placement of the supramaxilla and the absence of epural bones, in addition to eleven homoplastic characters. Epurals are indeed absent in aspidorhynchids (Arratia, 2008a; 2008b), while "epurals", which are not considered homologous to the epural bones of other neopterygians, are present in pachycormids (Arratia & Schultze, 1992). Most recently, Gouiric-Cavalli & Arratia (2022) also recovered Aspidorhynchoidei, but even with a broader range of pachycormids only found limited support for the clade, with one uniquely derived character (the posterior placement of the supramaxilla) and four homoplastic characters.

Very few analyses of neopterygian relationships incorporate both a broad range of aspidorhynchid and pachycormid taxa and a large number of other actinopterygians. For pachycormids, more emphasis has been placed on interrelationships within the group (e.g., Lambers, 1988; Friedman *et al.*, 2010; Friedman, 2012; Wretman, 2016, Cooper & Maxwell, 2020). There is a broad consensus that pachycormids are generally split into two major clades: the macrophageous toothed clade (e.g., *Orthocormus*, *Hypsocormus*) and the highly specialised edentulous suspension filter feeding clade (e.g., *Bonnerichthys*, *Leedsichthys*). Other taxa, such as *Saurostomus*,

are identified as transitional suspension feeders (Cooper & Maxwell, 2022) (see 4.6.3). *Pachycormus* is typically perceived as representative of pachycormids as it exhibits a combination of traits from both major groupings. However, this mix of anatomical traits means its position within Pachycormidae is not settled. Liston (2012) recovers *Pachycormus* as forming a clade with *Saurostomus*, sister to the suspension feeding clade. Friedman *et al. (*2010) finds the position of *Pachycormus* uncertain, forming a polytomy with both the suspension feeding clade and macrophageous clade. Friedman (2012) recovers it as the sister to a clade comprising *Saurostomus* and the suspension filter feeding clade. Gouiric-Cavalli (2016) – which features a very wide range of taxa comparable to this analysis – finds *Pachycormus* within the macrophageous toothed pachycormid clade as an early diverging member. Finally, Cooper & Maxwell (2022) recover *Pachycormus* as sister to both the transitional suspension feeding clade and suspension feeding clade, similar to the results of Friedman (2012).

In contrast, phylogenetic relationships within Aspidorhynchidae have recovered comparatively less attention (Brito, 1999; López-Arbarello & Schröder, 2014), though there are some studies which examine character distribution across major genera (e.g., Bartholomai, 2004: table 3; Ebert, 2014: table 2). And, as has been seen with other stem teleost radiations, broader phylogenetic analyses that do encompass aspidorhynchids and pachycormids tend to include just *Pachycormus* and *Aspidorhynchus* (e.g., Gardiner *et al.,* 1996; Arratia, 2004; Hurley *et al.*, 2007; López-Arbarello & Sferco 2018), Consequently, the distribution of characters within and across these specialised groups is not fully captured.

Ultimately, the highly specialised morphologies of aspidorhynchids and pachycormids acts as a barrier to resolving relationships to each other and other early teleost – and indeed neopterygian – lineages. The purported earliest diverging pachycormid, *Euthynotus* (Wenz 1968), is known less comprehensively than taxa such as *Pachycormus*, and as such is rarely included in analyses outside of those that focus on pachycormids. Similarly, early Jurassic aspidorhynchids that exhibit a more generalised appearance (Brito & Ebert, 2009) are rarely included in phylogenetic analyses. Consequently, aspidorhynchids and pachycormids appear almost isolated in most phylogenetic analyses, with a 50 million year long ghost lineage extending to the early Triassic (Gouiric-Cavalli & Arratia, 2022).

Here, this study aims to build a more comprehensive picture of the internal three-dimensional anatomy in key examples of Aspidorhynchidae and Pachycormidae to produce a revised hypothesis of their relationships. This chapter redescribes the braincase of *Richmondichthys sweeti* (NHMUK PV P 62533a) via CT scanning and present the first digitally reconstructed aspidorhynchid endocast. This study also describes an exceptionally preserved, articulated *Pachycormus macropterus* (BRLSI M1311) from the Strawberry Bank Lagerstatte, Ilminster, Somerset, UK. This is in order to visualise and identify novel, previously concealed anatomical information in both specimens via CT and synchrotron scanning, allowing for a more complete character coding for both taxa. Anatomical information derived from these data inform a revised phylogenetic hypothesis of relationships for early Neopterygii.

## 4.2 Materials and Methods

### 4.2.1 Institutional Abbreviations

**BRLSI**, Bath Royal Literary and Scientific Institution; **ESRF**, European Synchrotron Radiation Facility, Grenoble, France; **QMF**, Queensland Museum Fossil Collection, Brisbane, Australia; **NHMUK**, Natural History Museum, London, UK.

### 4.2.2 Materials

***Richmondichthys sweeti*: NHMUK PV P 62533a** (formally QMF13412): an isolated braincase collected from the Cretaceous (Albian) Toolebuc Formation, Rolling Downs Group, Porcupine, north-west Queensland, Australia. The braincase is also associated with NHMUK PV P 62533: a collection of disarticulated elements, including parts of the gill skeleton, hyoid arch and fins, likely separated from the braincase during acid prepartion. These are not described here. It is important to note that this specimen was collected under British colonial rule (1859 – 1901) by English palaeontologists Etheridge and Woodward (1891).

***Pachycormus macropterus:* BRLSI M1311:** a near-complete three-dimensionally preserved and articulated specimen comprising the cranium, pectoral fins, and flanks, incomplete posterior to the middle of the body. The specimen derives from the Jurassic (Toarcian) Beacon Limestone Formation, Upper Lias Group, Strawberry Bank Lagerstätte, Ilminster, Somerset, UK. It is preserved within a calcareous concretion and has been mechanically prepared by Lorie Barber. This work was conducted between 2010 and 2013 as part of the Jurassic Ecosystem of Strawberry Bank Ilminster (JESBI) project with the Bristol Museum (pers comm, M. Williams, 2025). BRLSI M1311 is one of several pachycormid specimens collected by Charles Moore before the closure of the quarry in 1861. The Strawberry Bank site represents an early Jurassic (Toarcian) shoreline and has yielded a wealth of exceptionally preserved

specimens preserved inside calcareous concretions, reducing the opportunity for diagenetic flattening (Caine & Benton, 2011; Williams *et al.*, 2015; Cawley *et al.*, 2019).

### 4.2.3 CT and Synchrotron Scanning and Imaging

NHMUK PV P 62533a was CT scanned at the Imaging and Analysis Centre, NHMUK, using a Metris X-Tek HMX ST 225 CT System with a 2,000 x 2,000 pixel detector, tungsten reflection target, and 3,142 projections, and a voxel size of 74.2 µm.

BRLSI M1311 was imaged on Beamline BM18 at the ESRF, Grenoble, France in October 2021. The scan was at a voxel size of 21 µm. Due to the enormous file size of BRLSI M1311, the data was cropped into several regions of interest and recompiled in blender.

Resulting tomograms were cropped in ImageJ and segmented in Mimics v.25 (biomedical.materialise.com/mimics; Materialise, Leuven, Belgium). Renders of 3D models were captured using Blender v. 3.3.0 (blender.org) and interpretive drawings were created in Adobe Illustrator (adobe.com/products/illustrator).

### 4.2.4 Phylogenetic analysis

In order to investigate the phylogenetic relationships of aspidorhynchids and pachycormids, *Aspidorhynchus acutirostris, A. arawaki, A. sanzenbacheri, Belonostomus kochi, B lamarquensis, Richmondichthys sweeti* (based on redescription of NHMUK PV P 62533a)*, Vinctifer comptoni* and *V. longirostris* (Aspidorhynchidae); *Bonnerichthys gladius, Euthynotus sp., Hypsocormus posterodorsalis, Martillichthys renwickae, Orthocormus cornutus, O. roeperi, O. teyleri. Pachycormus macroptertus* (based on description of BRLSI M1311)*, Rhinconichthys purgatoirensis* and *Saurostomus esocinus* (Pachycormidae) were introduced to a modified version of the character matrix of Giles *et al*. (2023) (see

3.2.4). An equally weighted parsimony analysis was conducted in TNT v. 1.5 (Boloboff & Catalano, 2016). using a heuristic search utilising Sect. Search, Ratchet, Drift and Tree Fusing algorithms with the following settings: hold 100,000; xmult = level 10; bbreak = fillonly. Trees were rooted by a constrained outgroup of Palaeozoic taxa: : *(Moythmasia durgaringa (Mimipiscis bartrama, Mimipiscis toombsi)).* Four characters were ordered following Giles *et al.* (2023): c.51 c.97 c.98 c.121. A strict consensus tree was produced from the resulting 33480 trees. Trees were visualised in Macclade v. 3.05 (Madidson & Maddison, 1992) in order to describe character distribution and measure consistency indices.

## 4.3 Description: *Richmondichthys sweeti* (NHMUK PV P 62533a)

### 4.3.1 General Morphology

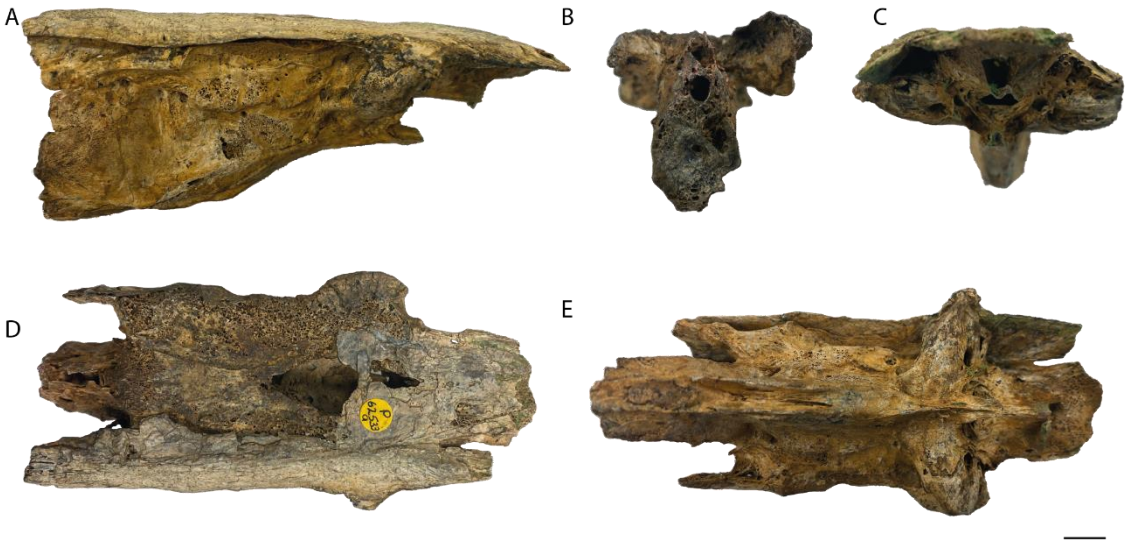


**Figure 4.1:** ***Richmondichthys sweeti*** **NHMUK PV P 62533a** in (A) right lateral, (B) anterior, (C) posterior, (D) dorsal and (E) ventral view. Scale = 10 mm.

**NHMUK PV P 62533a** (Fig. 4.1, 4.2, 4.3) is an acid prepared neurocranium that is incomplete anterior to the midpoint of the orbit. It comprises remnants of the skull roof,

braincase, and a partial parasphenoid; the latter is only preserved behind the orbit. Overall, the braincase is elongate and deepens posteriorly. It appears very well ossified with few visible sutures: only the median supraoccipital (Soc) and paired intercalars (Ic) and autosphenotics (Autsph) can still be identified as independent ossifications, with all other braincase elements co-ossified.

### 4.3.2 Braincase

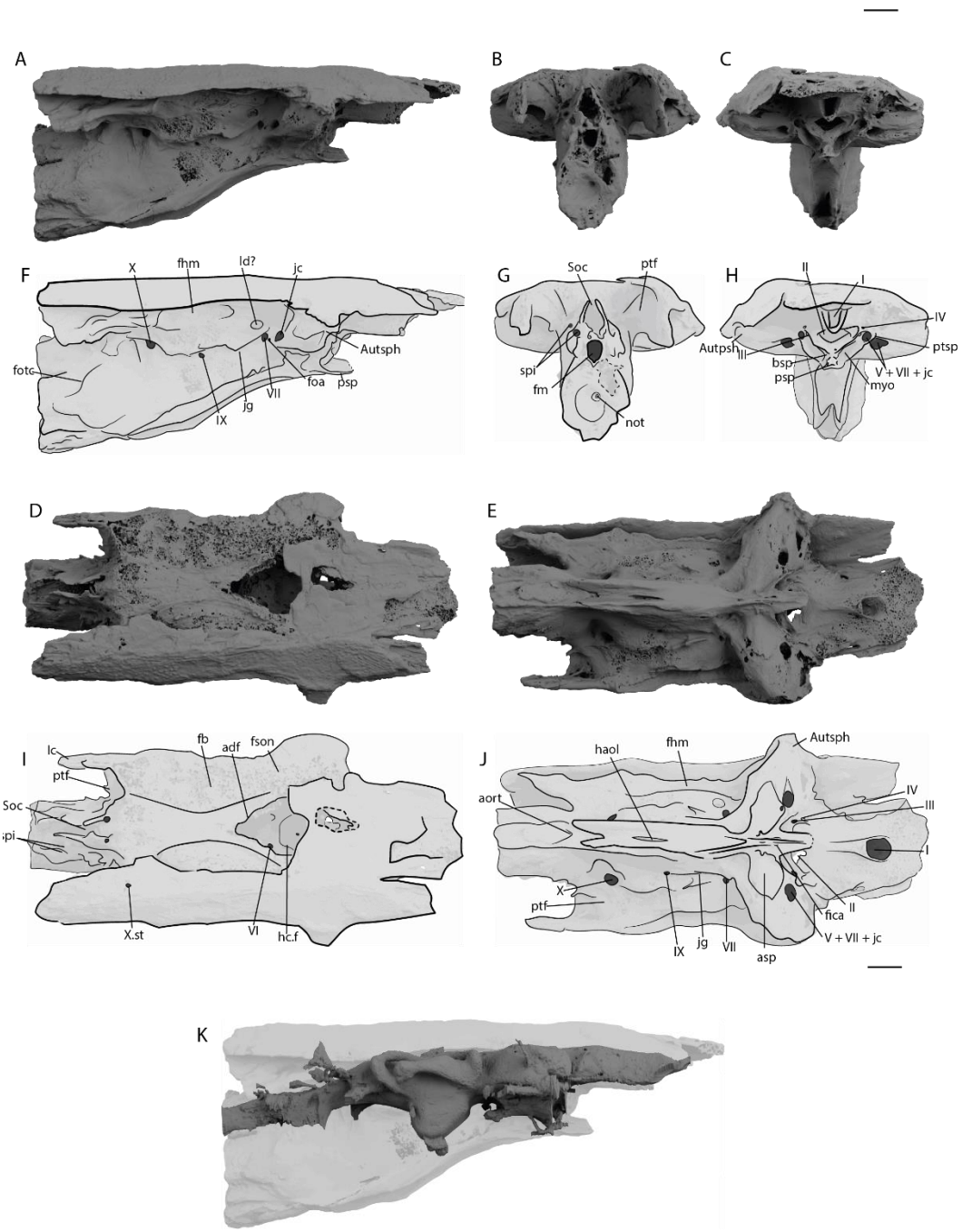

**Figure 4.2: Braincase of *Richmondichthys sweeti* NHMUK PV P 62533a**. Renders in (A) right lateral (B) posterior (C) anterior (D) dorsal, and (E) ventral view. Interpretive drawings in (F) right lateral (G) posterior (H) anterior (I) dorsal, and (J) ventral view. (K) Braincase in right lateral view rendered transparent to show position of endocast. Scale bar = 10 mm. *Abbreviations*: adf, anterior dorsal fontanelle; aort, aortic notch; asp, ascending process of the parasphenoid; Autsph, autosphenotic; bsp, basisphenoid; fb, fossa bridgei; fhm, hyomandibular facet; fm, foramen magnum; foa, foramen for orbital artery; fotc, otoccipital fissure; fson, foramen of superficial ophthalmic nerves; haol, housing of aortic ligament; hc.f, foramen for hypophysial canal; Ic, intercalar; fica, foramen for internal carotid artery; jc, foramen for jugular canal; jg, jugular groove; ld?, lateral depression; myo, posterior myodome; not, notochordal opening; psp, parasphenoid; ptf, post-temporal fossa; ptsp, pterosphenoid pedicle; Soc, supraoccipital; spi, spino-occipital nerves; I, foramen for olfactory nerve; II, foramen for optic nerves; III, foramen for oculomotor nerve; IV, foramen for trochlear nerve; V, foramen for trigeminal nerve; VI, foramen for abducens nerve; VII, foramen for facial nerve; IX, foramen for glossopharyngeal nerve; X, foramen for vagus nerve; X. st foramen for supratemporal branch of the vagus nerve.

*Occipital Region:* The occipital region is relatively narrow and extremely elongate. Except for the supraoccipital, individual occipital ossifications cannot be identified, a condition shared by most aspidorhynchid genera with the exception of *Aspidorhynchus* (Bartholomai, 2004). The occipital region is delimited anteriorly by a shallow groove, corresponding to the closed otoccipital fissure (fotc, Fig. 4.2F).

The supraoccipital (Soc, Fig. 4.2G, I) forms a small, median protrusion. It has a thick perichondral shell and is flanked on either side by well ossified endochondral bone, which extends laterally to form the wide, concave anterior limit of the post-temporal fossa (ptf, Fig. 4.2G, I, J). Ventral to the supraoccipital region, the occiput extends some way posterior to the medial portion of the skull roof. The medial walls of the occiput are relatively smooth but bear several openings for spino-occipital nerves (spi, Fig. 4.2G, I).

Further ventrally, the opening of the foramen magnum (fm, Fig. 4.2G) is tall and rounded, narrowing slightly ventrally; internally, it is almost heart shaped in axial

section. The inner walls of the foramen magnum are pierced by several foramina for the spinal nerves, some of which connect to the post-temporal fossa. The basioccipital region is well ossified, elongate and almost cylindrical, terminating posteriorly in a wide circular dish around the narrow notochordal opening (not, Fig. 4.2F, G, J). It comprises almost half of the height of the occipital region in posterior view. In most aspidorhynchids (Maisey. 1991: pg. 186), the first vertebra appears to be fused to the basioccipital. The same condition has been previously described to be present in *Richmondichthys* (Bartholomai, 2004). The basioccipital region in this specimen is extremely elongate, although it is difficult to confidently assess whether this is the result of fusion with the first vertebra because of the specimen is very well ossified. A deep, concave notch along the ventral surface of the basiocciput accommodates the posterior stalk of the parasphenoid. Lateral basioccipital processes are not observed.

*Otic region:* The otic region is the longest portion of the braincase. Although wide dorsally, it becomes very narrow ventrally. The dorsolateral corner of the otic region and skull roof, which includes the dermopterotic and intercalar, extends posterior to the occipital region as a wing-like projection. This forms the lateral wall of the expanded post-temporal fossa (ptf, Fig. 4.2J). The post-temporal fossa is open both dorsally and ventrally, suggesting that the muscles which occupied the fossa were very deep.

The roof of the otic region has been heavily prepared, almost fully exposing the anterior dorsal fontanelle (adf, Fig. 4.2I). The anterodorsal fontanelle is fairly elongate with tapered posterior and anterior margins. The anterior portion of the anterior dorsal fontanelle is markedly narrower. Lateral to the anterior dorsal fontanelle is the fossa bridgei, which is extremely shallow and very elongate. Its floor appears densely pitted in dorsal view because it is not lined with perichondral bone, instead the honeycomb

structure of the underling endochondral bone is exposed. It is associated with the dorsal opening of the foramen of superficial ophthalmic nerves (fson, Fig. 4.2I). The canal extends ventrally into the neurocranial roof, intercepting the dorsal root of the trigeminofacial chamber.

The opening for the vagus nerve is large and dorsally positioned (X, Fig. 4.2F, J). It is internally confluent with a smaller canal, which carried the supratemporal branch of the vagus nerve. This travels through the intercalar and appears to exits thorough the cranial roof (X.st, Fig. 4.2I). Much of the dorsal margin of the lateral wall of the otic region is occupied by the long, narrow hyomandibular facet (fhm, Fig. 2F, J). Several features of interest are found ventral to the facet. The most dorsal of these, a rounded, unfinished surface, may represent an articular surface, although it is only identifiable on the right side (?, Fig. 4.2F). Immediately ventral, an oval opening for the facial nerve (VII, Fig. 4.2F, J) lies at the anterior of the jugular groove (jg, Fig. 4.2JF), which runs roughly parallel to the hyomandibular facet. The opening of the glossopharyngeal nerve (IX, Fig. 4.2F, J) sits at the posterior margin of the jugular groove. In the anteroventral corner of the foramen for the facial nerve is the small foramen of the orbital artery (foa, Fig. 4.2F). It is best preserved on the right side. Finally, the anterior most foramen in the otic region is the posterior opening of the jugular vein (jg, Fig. 4.2F), which enters the postorbital process and into the trigeminofacial chamber.

*Orbitotemporal Region:* The orbitotemporal region is the widest portion of the braincase. The triangular autosphenotic (Autsph, Fig. 4.2F, H, J) is delineated by a jagged suture and forms the lateralmost margin of the postorbital wall.

A broad albeit squat postorbital process is formed by the autosphenotic, other braincase ossifications, and ascending processes of the parasphenoid (asp, Fig. 4.2H, J). It is well ossified and extends almost laterally from the parasphenoid, with little anterior or dorsal inflection. Its anterior surface is flat and perforated by multiple openings and foramina. The median foramen of the optic nerve (II, Fig. 4.2H, J) is the largest, formed as a short oval, and with a distinct rim around its margins. Immediately anterolateral to the optic foramen is the small opening of the trochlear nerve (IV, Fig. 4.2H, J). Ventral to the trochlear nerve is the larger opening of the oculomotor nerve (III, Fig. 4.2H, J), which is almost parallel to the route of the trochlear.

The pterosphenoid forms a thin, medioventrally directed pedicle (ptsp, Fig. 4.2H) lateral to the oculomotor and trochlear nerves, and cuts across the anterior opening of the trigemenofacial chamber. The trigemenofacial chamber contains the junction of the trigeminal (V) and facial (VII) nerves and the jugular canal (jc).

The basisphenoid is reduced to a short strut ventral to the foramen of the optic nerve (bsp, Fig. 4.2H). It extends a short way into the floor of the posterior myodome and anteriorly above the anterior corpus of the parasphenoid. As a result of this reduced ossification, the roof of the posterior myodome (myo, Fig. 4.2H) is almost entirely unossified, and its floor and lateral walls are contributed to by the parasphenoid. Consequently, the abducens nerve (VI) pierces the myodome via a deep, recessed foramina in the dorsolateral corner of the posterior wall in the otic portion of the braincase. It is not visible externally. A median recess at the back of the posterior myodome extends between the braincase and the parasphenoid and housed the saccus vasculosus.

Anterior to the opening for the optic nerves, the braincase narrows to form the dorsal portion of the preorbital wall and the roof of the orbit. It primarily houses the olfactory nerve (I, Fig. 4.2H, J). For the preserved length of the braincase, the olfactory nerve is carried in a single tract. This region also houses the paired anterior cerebral vein, which arches ventrally from the right side of the endocranial wall lateral to the telencephalic endocast. Elongate, paired openings along the dorsolateral margins of the telencephalic endocast may have carried the supraorbital sensory canal, but it is not possible to trace their route posteriorly.

### 4.3.3 Parasphenoid

The parasphenoid (psp, Fig. 4.2F, H, J) is thickened along its sagittal axis and is frequently vascularised. It is separated from the underside of the braincase by a narrow gap. The parasphenoid appears to terminate just posterior to the anterior margin of the basioccipital. Anteriorly, it is broken and not preserved beneath the orbit. The posterior margin of the parasphenoid forms a deep, V-shaped notch, which extends into a groove for the dorsal aorta (aort, Fig. 4.2J). The groove tapers anteriorly towards the extremely elongate housing of the aortic ligament (haol, Fig. 4.2J). Here, the dorsal aorta bifurcates and traverses anteriorly along shallow lateral grooves towards the very small opening of the internal carotid artery (ica, Fig. 4.2J). The foramen for the internal carotid artery is ventrally directed, very narrow and close to its antimere on the midline. There is no basipterygoid process, but the parasphenoid forms a broad ascending process at the level of the postorbital process (asp, Fig. 4.2H, J). The ascending process fans laterally, underlying the postorbital wall and almost reaching the autosphenotic. Bartholomai (2004) previously noted that the openings of

the efferent pseudobranchial canal may be present in the ascending process, but they cannot be identified here.

## 4.3.4 Endocast

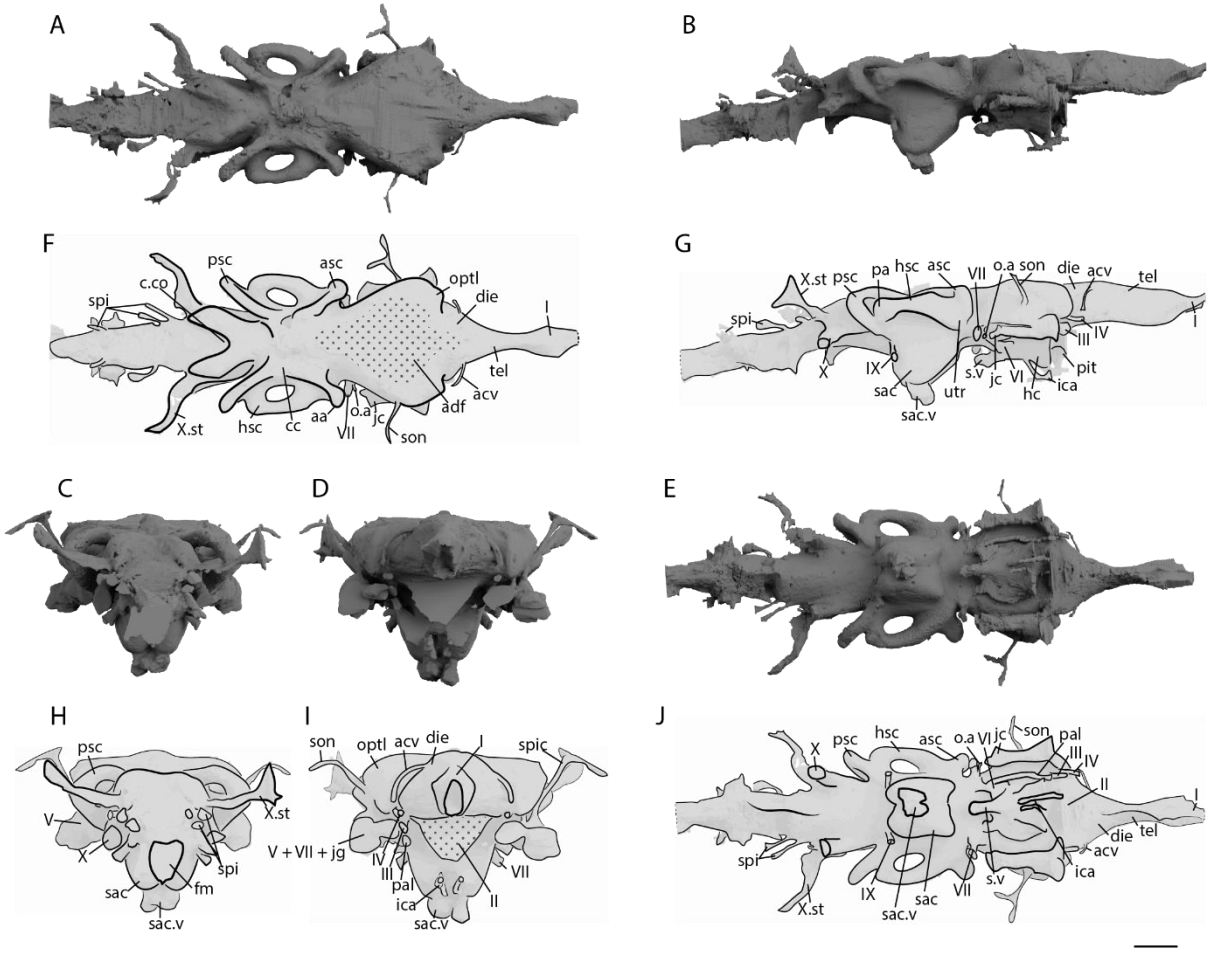

**Figure 4.3: Endocast of *Richmondichthys sweeti* NHMUK PV P 62533a**. Renders in (A) dorsal, (B) right lateral, (C) posterior, (D) anterior, and (E) ventral view. Interpretive drawings in (F) dorsal, (G) right lateral, (H) posterior, (I) anterior, and (J) ventral view. Scale bar = 10 mm. *Abbreviations: aa, anterior ampulla; acv, anterior cerebral vein; adf, anterior dorsal fontanelle; asc, anterior semicircular canal; cc, crus commune; c.co, cerebellar corpus; die, diencephalon; fm, foramen magnum; hc, hypophysial canal; hsc, horizontal semicircular canal; ica, internal carotid artery; o.a, orbital artery; optl, optic lobes; pa, posterior ampulla; pal, palatine nerve; pit, pituitary canal; psc, posterior semicircular canal; sac, saccular chamber; sac.v, posteroventral component of saccular; son, superficial ophthalmic nerve; spi, spino-occipital nerves; s.v, saccus vasculosus; tel, telencephalon; utr, utricular; I, olfactory nerve; II, optic nerve; III, oculomotor nerve; IV, trochlear nerve; V, trigeminal nerve; VI, abducens nerve, VII, facial nerve; IX, glossopharyngeal nerve; X, vagus nerve; X.st, supratemporal branch of the vagus nerve.*

The internal walls of the endocavity are well mineralised, and as a result the endocast can be fully segmented. It is similar in overall shape to the reconstruction of the endocast for *Vinctifer comptoni* Brito (1992), and it is possible to resolve the paths of the cranial nerves. The endocast is confined within the dorsal portion of the braincase (Fig. 4.2K).

The endocast is extremely elongate and narrow. The region corresponding to the hindbrain, particularly the rhombencephalon, is very long posteriorly, with three pairs of spino-occipital nerves (spi, Fig. 4.3F, J) emanating from its lateral margins. Anterior to these, the vagus nerve (X, Fig. 4.3G, J) is very short and broad, while the supratemporal branch of the vagus nerve (X.st, Fig. 4.3F, G, H, J) is much longer, and extends postero-dorsolaterally towards the cranial roof. The cerebellar portion of the endocast is under half the length of the rhombencephalar region. The corpus cerebellum (c.co, Fig. 4.3F) is barely distinguished, and a flattened portion posterior to it likely represents the fourth ventricle of the brain. Cerebellar auricles are absent.

The region corresponding to the midbrain forms the broadest portion of the endocast. The midbrain endocast is formed primarily of the wide optic tectum (optl,

Fig. 4.3F, G, I), which extends laterally slightly beyond the lateral limit of the bony labyrinth, giving the mesencephalon a heart shape in dorsal view. The central region is open to the anterior dorsal fontanelle (adf, Fig. 4.3F). The facial exits the lateral wall of the cranial cavity in a short canal, which also emits a small branch of the orbital artery (o.a, Fig. 4.3G. J), best visualised on the right side. A very broad canal carries the jugular vein (jg, Fig. 4.3F) where it forms part of the trigeminofacial chamber (V + VII + jg, Fig. 4.3F, G, H, J).

The root of the abducens nerve (VI, Fig. 4.3G, J) is relatively short, only briefly leaving the main cranial cavity posterior to the optic lobes, before immediately entering the roof of the posterior myodome, where it becomes confluent with the hypophysial canal (see below). The abducens nerve also appears to be associated with an elongate branch of the palatine nerve (pal, Fig. 4.3J), which extends anteriorly, lateral to the posterior myodome and separate to the main cranial cavity, although the roof of the canal is weakly ossified.

Anterior to the optic tectum, the endocast narrows considerably into the forebrain region. It is difficult to differentiate between diencephalic (die) and telencephalic (tel) portions, at least dorsally, although a slight constriction might represent a boundary between the two (Fig. 4.3F, G, J). There is no indication of distinct swellings corresponding to olfactory bulbs confluent with the forebrain region of the endocast. A deep, median tract for the olfactory nerve (I, Fig. 4.3F, G, I, J) extends anteriorly but is broken, so its full morphology cannot be described. Beneath the olfactory tract, the diencephalic region of the endocast extends ventrally and some way posteriorly.

Several nerve canals exit from the anterior face of the midbrain/forebrain endocast. Much of the midline is open to the wide, oval optic nerve (II, Fig. 4.3I, J). A short, paired, relatively thickened canal for the oculomotor nerve (III, Fig. 4.3I, J) emanates from the floor of the optic lobe. It travels anteroventrally into the orbit. The root of the trochlear nerve (IV, Fig. 4.3G, I, J) is extremely narrow, and projects anterodorsally to the oculomotor nerve, projecting from the posteriormost region of the diencephalon, medial to the optic lobe, and projecting into the orbit subparallel to the oculomotor nerve. The telencephalon also emits the paired anterior cerebral vein.

The hypophysial fossa is extremely wide and almost fully confluent with the posterior myodome. The hypophysial canal (hc, Fig. 4.3G) is therefore resolved as extremely broad, extending ventrally, just posterior to the optic nerve. It is relatively shallow, due to the highly reduced basisphenoid bone. However, the basisphenoid also carries a length of the pituitary vein (pit, Fig. 4.3J). It enters the basisphenoid via the small pituitary fenestra before quickly exiting ventral to the optic nerve.

The saccus vasculosus (s.v, Fig. 4.3G, J) extends very far posteriorly, between the left and right abducens verves, into an open cavity dorsal to the parasphenoid. Directly ventral to the hypophysial canal, the internal carotid enters the parasphenoid. Due to the heavy vascularisation of the parasphenoid the exact route taken by the internal carotid is difficult to follow, however, it appears to travel through the parasphenoid into the floor of the posterior myodome. It then extends a short length anteriorly, before re-entering and travelling anteriorly along the dorsal margin of the parasphenoid.

*Bony Labyrinth:* All three semicircular canals are preserved as they are fully enclosed in bone, and the overall morphology of the bony labyrinth resembles that described for *Vinctifer comptoni* (Brito, 1992). The canals are stout and do not extend far from the cranial cavity, nor project dorsally above its roof. The anterior semicircular canal is the shortest and narrowest canal. It remains confluent with the anterior ampulla for much of its length. The horizontal semicircular canal (hsc, Fig. 4.3F, G, J) is the most robust, and is almost as wide as its associated ampullae. The posterior semicircular canal (psc, Fig. 4.3F, G, H, J) is the longest of the three and curves tightly the meet the posterior ampulla (pa, Fig. 4.3G). The crus commune is very shallow relative to the endocranial roof, and there is no sinus superior. A lateral cranial canal is absent, and the utricular is so small as to be barely developed.

The narrow triangular saccular chamber is deep posteriorly and tapers anteriorly (sac, Fig. 4.3G, H, J). Each is confluent with its antimere along the midline; this arrangement limits the posterior extent of the posterior myodome. An additional, irregular cavity is continuous with the posteroventral component of both saccular chambers (sac.v, Fig. 4.3G, H, I J). There is no lagenar pouch. The root of the glossopharyngeal nerve, which was not observed by Brito (1992) in *Vinctifer*, projects almost laterally from the posterodorsal corner of the saccular cavity (IX, 4.3G, J).

## 4.4 Description: *Pachycormus macropterus* (BRLSI M1311)

### 4.4.1 General Morphology


**Figure 4.4: *Pachycormus macropterus* (BRLSI M1311) in right lateral view.** Scale = 10 mm. (photo by M. Williams, BRLSI)

**BRLSI M1311** is a mechanically prepared concretion containing the complete skull, pectoral girdle, and a significant portion of the postaxial skeleton (Fig 4.4). The portion of BRLSI M1311 (Fig. 4.5) captured in the tomographic scan encompasses all of these regions. The fossil is preserved within a carbonate concretion, and has been manually prepared to expose the skull, girdle and left pectoral fin. It is fully articulated, and most elements are preserved in life position.

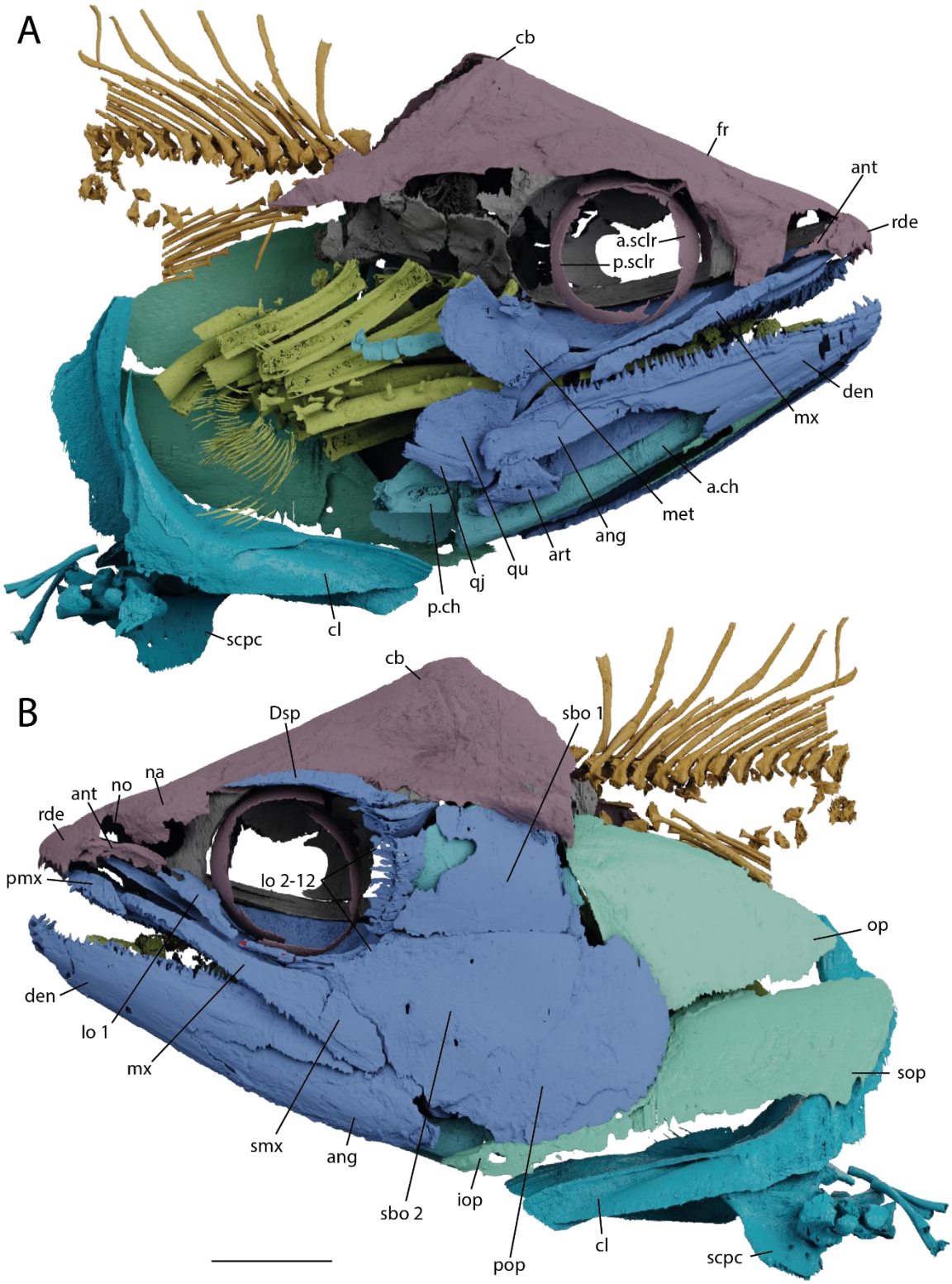
A
cb
fr
ant
rde
a.sclr
p.sclr
den
mx
a.ch
met
ang
art
qu
qj
p.ch
cl
scpc
B
cb
Dsp
sbo 1
na
no
ant
rde
pmx
lo 2-12
op
den
lo 1
mx
sop
smx
ang
sbo 2
iop
cl
pop
scpc

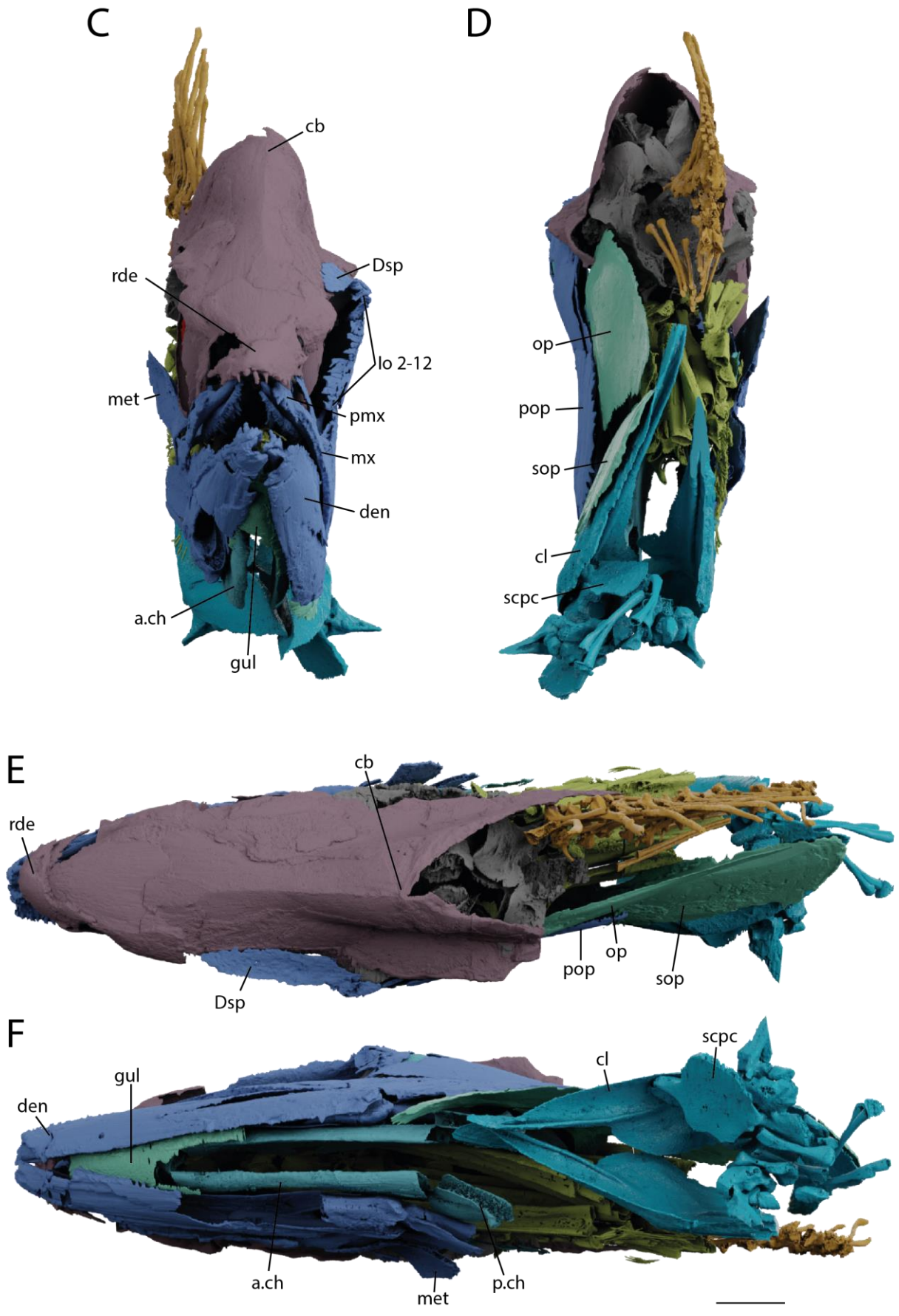
C
cb
Dsp
rde
lo 2-12
met
pmx
mx
den
a.ch
gul
D
op
pop
sop
cl
scpc
E
cb
rde
Dsp
pop
op
sop
F
scpc
cl
gul
den
a.ch
met
p.ch

**Figure 4.5: *Pachycormus macropterus* (BRLSI M1311).** Renders in (A) right lateral, (B) left lateral, (C) anterior, (D) posterior, (E) dorsal, (F) ventral view. Colour coding: blue, cheek and jaw; purple, skull roof and sclerotic ossicles; grey, braincase; light turquoise, hyoid arch; light green, operculogular; yellow, gill skeleton; dark turquoise, shoulder girdle; orange, axial skeleton. Scale bar = 10 mm. *Abbreviations: ch, anterior ceratohyal; a.sclr, anterior ossicle of sclerotic ring; ang, angular; ant, antorbital; art, articular; cb, cranial boss; cl, cleithrum; den, dentary, Dsp, dermosphenotic; Fr, frontal; gul, median gular plate; io 1-12, first to twelfth infraorbital bone; iop, interopercular; met, metapterygoid; mx, maxilla; na, nasal; no, nasal opening; op, operculum; p.ch, posterior ceratohyal; p.sclr, posterior ossicle of sclerotic ring; pmx, premaxilla; pop, preoperculum; qj, quadratojugal process; qu, quadrate; rde, rostrodermethmoid; sbo 1-2, first to second suborbital bone; scpc, scapulacoracoid; smx, supramaxilla; sop, suboperculum*

## 4.4.2 Skull Roof

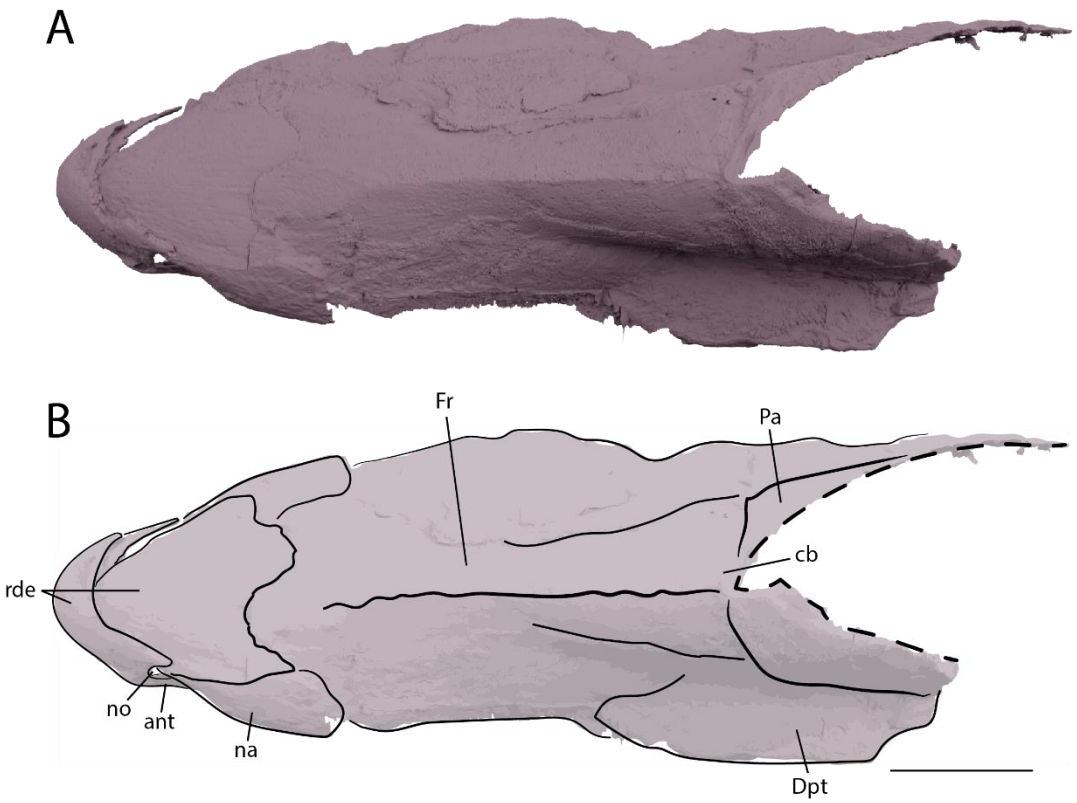


**Figure 4.6: Skull roof of *Pachycormus macropterus* (BRLSI M1311).** (A) Render and (B) interpretive drawing in dorsal view. Scale = 10 mm. *Abbreviations: ant, antorbital; cb, cranial boss; Dpt, dermopterotic; Fr, frontal; na, nasal; no, nasal opening; Pa, parietal; rde, rostrodermethmoid.*

The skull roof (Fig. 4.6B) is completely preserved and contains discrete ossifications: paired parietals (Pa), dermopterotics (Dpt), dermosphenotics (Dsp) and frontals (Fr). Overall, the skull roof is of a fairly consistent width. Posteriorly, the skull roof forms a steep cranial “boss” (cb). (Nb. The term ‘cranial boss’ is widely used to describe the prominent medial eminence on the skull roof of pachycormids (e.g., Lehman, 1949; Mainwaring, 1978; Lambers, 1988; Cawley, 2019) and is a commonly used autapomorphy in phylogenetic analyses (e.g., Friedman *et al.*, 2010; Gouiric-Cavalli & Arratia, 2022). Throughout this chapter, “boss” is written in scare quotes because the term boss in other vertebrates typically refers specifically to a robust thickening of the skull roof. In BRLSI M1311, the thickness of the skull roof is consistent and beneath the cranial “boss”, the skull appears to be hollow. For cohesion with existing work, the feature is not renamed but attention is drawn to a possible issue).

The parietal is the smallest roofing element and is sub-rectangular. They do not contact at the midline as they are interrupted by the cranial boss which is formed by the frontals. The frontals are elongate, extending more than half the total length of the skull roof. They are sutured along the midline, though the medial margin is highly irregular. The dermosphenotic (Dsp, Fig. 4.5C, E) forms a thickened, horizontal plate which tapers anteriorly and posteriorly. Pachycormids lack supraorbitals, instead the dermosphenotic contributes to the dorsal margin of the orbit. Finally, the dermopterotic (Dpt, Fig. 4.6B) forms the posterolateral corner of the skull roof. It is thickened ventrally around the housing of the infraorbital canal, which it carries for almost its entire length. Pit lines are not observed and there is no visible ornamentation bar some slight striations parallel to the midline. It is possible that subtle features on the surface of the skull roof were lost during preparation.

### 4.4.3 Snout (dermal)

The snout comprises paired nasals (na), paired antorbitals (ant) and a median rostrodermethmoid (rde). Much of the snout is incompletely segmented and is rendered as a single unit, due to the difficulty in distinguishing individual ossifications in tomograms beneath the faint suture lines visible on the surface of the snout.

The nasal (na, Figs. 4.5B, 4.6B) is a thin, sub-triangular plate, with a thickened ventral margin to accommodate the nasal canal. The left and right nasal do not contact at the midline, as the rostrodermethmoid separates them. The nasal plate forms a wide nasal opening in its anteroventral corner. The ventral margin of the nasal opening (no, Figs. 4.5B, 4.6B) is formed by the antorbital.

The antorbital (ant, Figs. 4.5A, B, 4.6B) is small and elongate. It lies directly ventral to the nasal and is positioned anterior to the lachrymal (io 1, Figs. 4.5B, 4.10B) where it carries the anterior portion of the infraorbital canal.

The rostrodermethmoid (rde, Fig. 4.5A, B, C, E, F) representing the fused dermethmoid and rostral plate, forms a convex cap over the dorsal oral margin. A faint suture between the medial rostral and the dermethmoid is visible in tomograms: the rostral portion is broad with an irregular posterior margin and a tapered anterior margin; the dermethmoid region is tooth-bearing along its anterior ventral margin.

## 4.4.4 Braincase

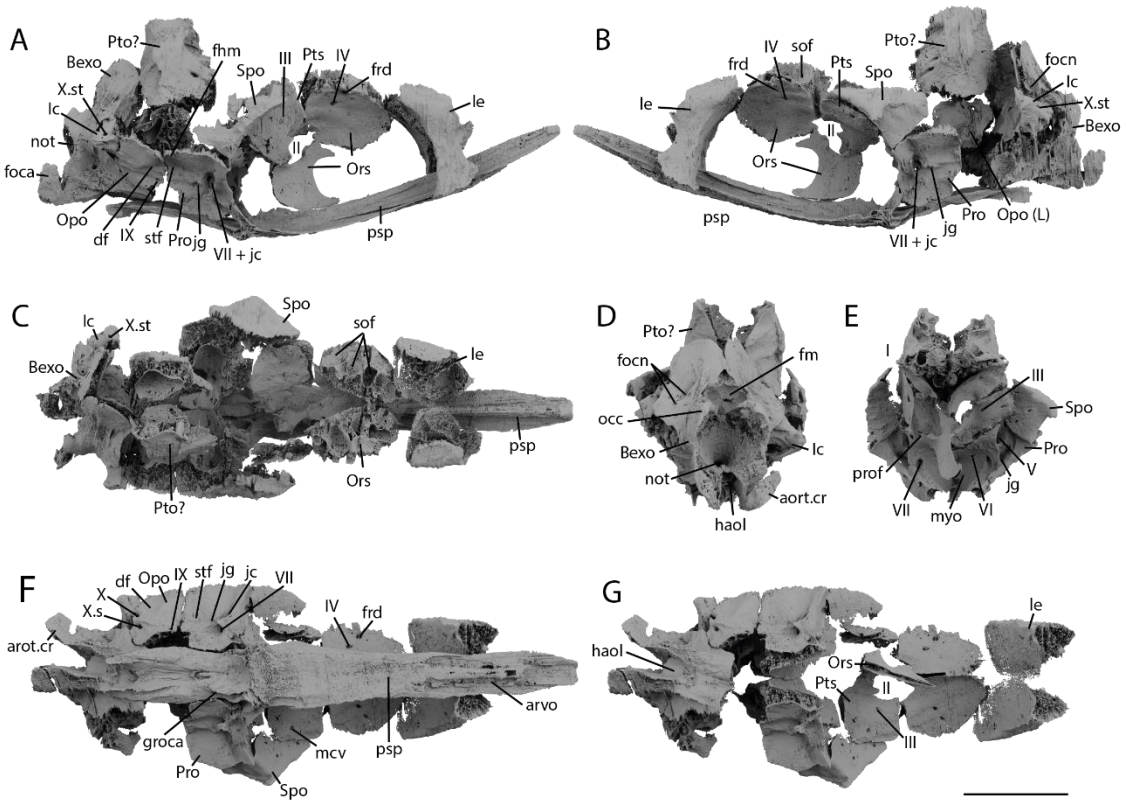


**Figure 4.7: Braincase of *Pachycormus macropterus* (BRLSI M1311).** Renders in (A) right lateral (B) left lateral (C) dorsal (D) posterior (E) anterior (without parasphenoid) (F) ventral (with parasphenoid) and (G) ventral (without parasphenoid). Scale = 10 mm. *Abbreviations; aort.cr, aortic crest; arvo, area covered by vomer; Bexo, basi-exooccipital; df, dilatator fossa; fm, foramen magnum; foca, foramen for occipital artery; focn, foramen for occipital nerve; frd, foramen for ascending branch of superficial ophthalmic nerve; groca, groove for occipital artery; haol, housing of aortic ligament; Ic, intercalar; jc, foramen for jugular canal; jg, jugular groove; le, lateral ethmoid; myo, posterior myodome; not, notochordal opening; occ, occipital condyle; Opo, opisthotic; Ors, orbitosphenoid; Pro, prootic; prof, foramen for profundus nerve; psp, parasphenoid; Pto?, pterotic?; Pts, pterosphenoid; sof, supraorbital fossa; Spo, sphenotic; stf, subtemporal fossa; I, foramen for olfactory nerve; II, foramen for optic nerve; III, foramen for oculomotor nerve; IV, foramen for trochlear nerve; V, foramen for trigeminal nerve; VII, foramen for facial nerve; IX, foramen for glossopharyngeal nerve; X, foramen for vagus nerve; X.s, foramen for subsidiary branch of vagus nerve; X.st, foramen for supratemporal branch of vagus nerve.*

The braincase (Fig. 4.7) is well preserved; but it is very weakly mineralised with very wide gaps between ossifications that would have been filled by cartilage in life. As a result of these large gaps, several ossifications have shifted relative to each other.

*Occipital Region.* The occipital region is relatively well ossified. It comprises paired epioccipitals (epi), intercalars (ic) and a co-ossified basi-exoccipital (Bexo), each lined by perichondral bone. A supraoccipital is not observed (Fig. 4.7C).

The occiput is formed from a single element previously interpreted as a basi-exoccipital (Bexo, Fig. 4.7A, B, C, D) - fused basioccipital and exoccipitals (Patterson, 1975; Mainwaring, 1978). A residual midline suture, which widens dorsally and ventrally, can be identified between the left and right ossifications of the “exoccipital”. The surface of the basi-exoccipital is lined by ventro-laterally aligned grooves, separated by thin ridges. At their deepest points, the grooves hold foramina for occipital nerves (focn, Fig. 4.7D). The occipital nerves bifurcate within the basi-exoccipital, emerging from the medulla oblongata in the walls of the foramen magnum (foca, Fig. 4.7A).

The foramen magnum (fm, Fig. 4.7D) forms a wide, oval-shaped opening in the centre of the basi-exoccipital. It is unossified along its ventral margin, forming a deep notch. Directly ventral to the foramen magnum is the wide notochordal opening (not, Fig. 4.7D), which forms an anteriorly-narrowing funnel through the entire length of the basi-exoccipital. The dorsal margin of the notochordal opening is bounded by a well ossified occipital condyle (occ, Fig. 4.7D).

The intercalar (Ic, Fig. 4.7A, B, C, D) is preserved but both the left and right ossification have been shifted and rotated in place. The intercalar lacks large membranous outgrowths of the kind common in stem teleosts and holosteans such as

*Dorsetichthys* and *Heterolepidotus* (Patterson, 1975). It appears to the frame the posterior margin of the vagus nerve (X, Fig. 4.7F) and carries a supratemporal branch of the vagus nerve (X.st, Fig. 4.7A, B, C, F), but their complete route from the main cranial cavity is not possible to fully visualise due to the disarticulation of the intercalar.

The opening of the aortic groove is bounded by deep, posteriorly projected longitudinal aortic crests (aort.cr, Fig. 4.7D, F). The lateral wall of the dorsal aorta contains an opening for the occipital artery, which continues dorso-laterally, remerging along the occipital artery groove (groca, Fig. 4.F) in the ventral portion of the basiocciput.

*Otic Region:* The otic region is very poorly ossified; it is not possible to describe several features, including the post-temporal fossa or fossa bridgei. The otic region comprises paired opisthotics (Opo), prootics (Pro) and a possible pterotic (Pto?). These discrete ossifications contribute to the lateral wall of the braincase and are divided by clear sutures. Each bone is partly disarticulated.

The putative pterotic (Pto?, Fig. 4.7A, B, C, D) appears to have been shifted dorsally into the hollow space below the cranial boss. It contains a deep rounded cavity with distinctly ossified edges which likely accommodated the cerebellum (Fig. 4.7C).

The opisthotic (Opo, Fig. 4.7A, B, F) forms the posterior ossification of the lateral wall of the braincase. The right opisthotic is relatively *in situ*, however the left opisthotic bone appears to have fallen into the cranial cavity, rotated and landed on the inner wall of the opposite side of the braincase (Fig. 4.7B). The opisthotic forms the anterior margin of the foramen for the vagus nerve, with the suture between the opisthotic and intercalar extending inside the foramen itself. The opisthotic also carries a ventrally directed subsidiary branch of the vagus nerve (X.s, Fig. 4.7C), which forms

a shallow groove. Much of the lateral surface of the opisthotic forms a shallow dilatator fossa (df, Fig. 4.7A, F). At the anterior margin of the bone, the opisthotic carries the glossopharyngeal nerve (IX, Fig. 4.7A, F). Posteroventrally, the opisthotic contacts the basi-excoccipital. They are separated by a deep suture representing the occipital fissure.

The prootic (Pro, Fig. 4.7A, B, E, F) lies directly anteriorly to the opisthotic. There is a relatively deep fossa which spans both elements - likely the subtemporal fossa (stf, Fig. 4.7A, F). Dorsal to the subtemporal fossa, the edge of the hyomandibular facet (fhm, Fig. 4.7A) is partially ossified. Ventral to the fossa, in the centre of the opisthotic, is a diagonally oriented ridge. This ridge appears to extend to the opening of the glossopharangyeal nerve, suggesting it forms the roof of the jugular groove (jg, Fig. 4.7B, F). At the anterior end of the jugular groove is the large, circular opening for the facial nerve (VII) and jugular vein (jc) (Fig. 4.7A, B, F).

*Orbitotemporal Region:* The orbitotemporal region is the broadest part of the braincase. It comprises the paired sphenotic (Spo), pterosphenoid (Pts), and orbitosphenoid (Ors), and the median basisphenoid (Bsp). The orbitotemporal region is bounded posteriorly by the postorbital wall, which is contributed primarily to by the sphenotic and pterosphenoid, as well as the ascending processes of the parasphenoid, but also the prootic. As is the case for the remainder of the braincase, each ossification in the orbitotemporal region is distinct, bounded by a deep suture, and has been somewhat displaced.

The postorbital wall is punctured by numerous foramina; the optic foramen (II, Fig. 4.7A, B, G) is the most readily identifiable as the largest median opening. The margins of the optic foramen are well ossified but have been marginally displaced. The

opening of the optic nerve is irregular, interrupted by a deep notch for the optic artery (fopa). Lateral to the foramen for the optic nerve, the pterosphenoid forms a large foramen, likely for the oculomotor nerve (III, Fig. 4.7E, G). It is fairly short and appears to emerge anteriorly from the ventral surface of the optic lobe. Dorsally, there is a smaller opening for the middle cerebral vein (mcv, Fig. 4.7F).

The prootic forms the lateral, ventral margins of the postorbital wall and contains the trigeminofacial chamber and the posterior myodome (myo, Fig. 4.7E). At its dorsal margin, the prootic also carries the profundus nerve (prof, Fig. 4.7E) into the orbit. The posterior myodome opens medially. It is fairly shallow and contained entirely within the prootic. It narrows posteriorly and terminates anterior to the basi-exoccipital. The roof of the posterior myodome is well ossified posteriorly by the left and right prootic bones. Here, the roof is also pierced by the foramen of the abducens nerve (VI, Fig. 4.7E). Anteriorly, the roof is deeply notched by the hypophysial foramen – the anterior margins of which are heavily displaced. The floor of the posterior myodome is entirely unossified.

The trigeminofacial chamber is very well resolved (Fig. 4.7A). The facial nerve (VII) exits the cranial cavity anterolateral to the abducens nerve, and travels anteroventrally within the prootic in the walls of the posterior myodome. At its anterior limit, the canal bifurcates, with a medially directed opening transmitting into the walls of the posterior myodome and a laterally directed opening intercepting the trigeminofacial chamber. The trigeminal nerve (V) exits the cranial cavity anterodorsal to the facial nerve. The wide canal opens anteriorly, directly into the trigeminofacial chamber. Finally, the jugular vein (jc) joins the trigeminofacial chamber via a large, posteriorly directed opening in the preorbital wall. The chamber transmits anteriorly

into the orbit, but there is also, a small ventromedially directed opening in the floor of the chamber, towards the ascending process of the parasphenoid.

The orbitosphenoid (Ors, Fig. 4.7A, B, C, E, G) is dorsally extensive, forming the upper portion of the interorbital septum, but is weakly ossified anteriorly. Its dorsal surface is lined by at least six pairs of deep, rounded supraorbital fossae (sof, Fig. 4.7C). Laterally, the left side of the orbitosphenoid is pierced by a large foramen for the trochlear nerve (IV), which passes directly into the telencephalic chamber (tel). Dorsal to this opening is the foramen for the ascending branch of the superficial ophthalmic nerves, which pass dorsally into the endocranial roof. The orbitosphenoid also forms an elaborate, c-shaped median ossification on the midline of the orbits. It has a thickened dorsal margin, which frames the opening of the optic foramen both laterally and medially. At its widest point, in the posterodorsal region, it forms paired wings which contacted the pterosphenoid to frame the dorsal margin of the optic foramen.

### 4.4.5 Ethmoid

The posterior portion of the paired lateral ethmoid (le, Fig. 4.7A, B, C, G), which forms the preorbital wall, is preserved. No foramina are observed and there is no distinct anterior myodome. However, the posterior surface of the right lateral ethmoid bears a sinuous structure. Anteromedially, the lateral ethmoid very weakly ossified.

### 4.4.6 Parasphenoid

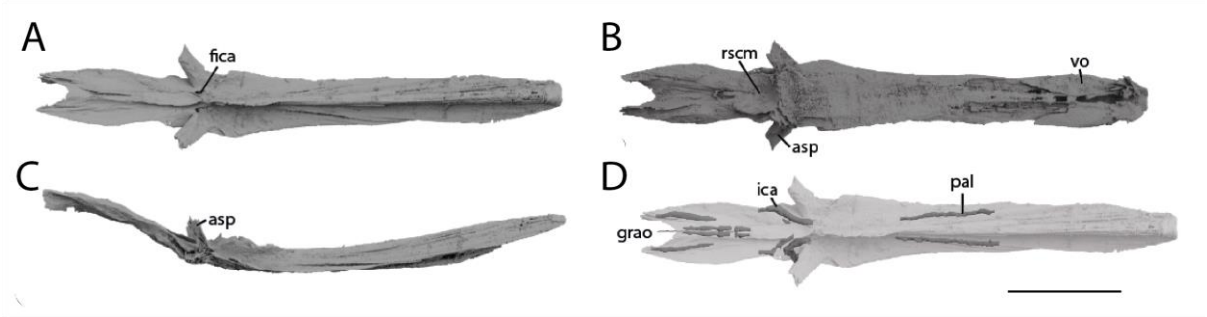

**Figure 4.8: Parasphenoid of *Pachycormus macropterus* (BRLSI M1311).** Renders in (A) dorsal, (B) ventral (with vomers) and (C) lateral view. (D) Parasphenoid rendered partially transparent to show path of canals. Scale = 10 mm. *Abbreviations: asp, ascending process; fica, foramen for internal carotid artery; grao, groove for dorsal aorta; ica, internal carotid artery; pal, palatine nerve; rscm, recess on parasphenoid housing origin of subcephalic muscles; vo, vomers*). Scale = 10 mm.

The parasphenoid (Fig. 4.8) is very well ossified and preserved in its entirety. It terminates posteriorly around the aortic notch and extends anteriorly across the entire orbit, terminating near the rostrodermethmoid. It is a near-consistent width, narrowing only slightly anterior to the orbit. The relationship with the rostrodermethmoid is unclear. A median crest runs along the dorsal surface, from the anterior margin to the anterior portion of the aortic notch. Small ascending processes (asp, Fig. 4.8A, B, C) are present, steeply inflected upwards and closely applied to the postorbital wall. The internal carotid arteries pierce the parasphenoid via a pair of very small antero-dorsally directed foramina (fica, Fig. 4.8A) positioned adjacent to the ascending processes. There is no basipterygoid process.

Posteriorly, the parasphenoid forms a deep, V-shaped notch around the aortic canal. At the apex of the notch, a large, rounded, concave recess housed the subcephalic muscles (rscm, Fig. 4.8B). Anterior to this recess is a broad toothplate. At the anterior end of the parasphenoid, there are paired depressions for the vomers (arvo, Fig. 4.7F).

## 4.4.7 Endocast

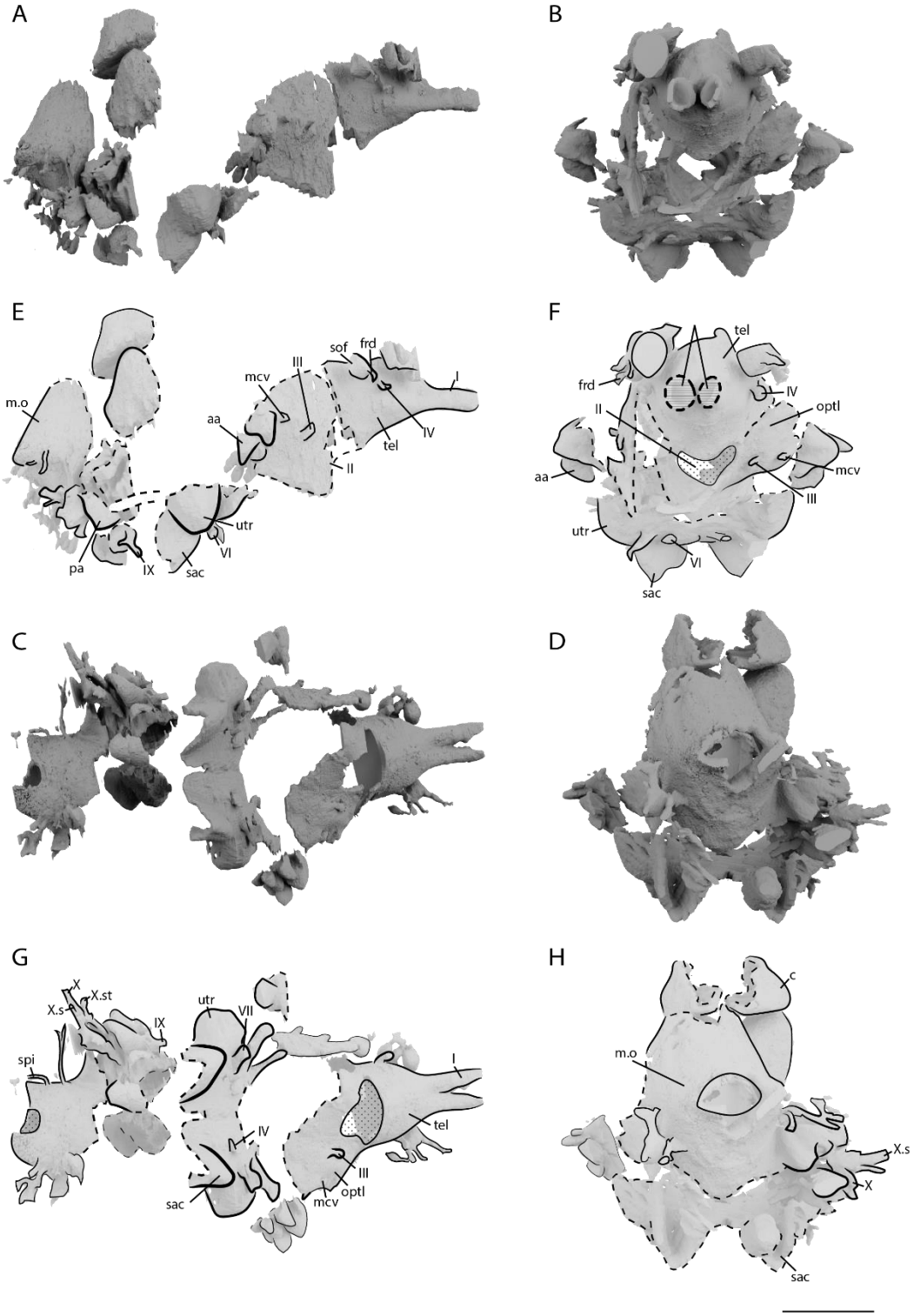

**Figure 4.9: Partial endocast of *Pachycormus macropterus* (BRLSI M1311).** Renders in (A) lateral, (B) anterior, (C) ventral, (D) posterior view. Interpretive drawing in (E) lateral, (F) anterior, (G) ventral, (H) posterior view. Scale = 10 mm. *Abbreviations: aa, anterior amuplla; c, cerebellum; frd, ascending branch of superficial ophthalmic nerve; m.o, medulla oblongata; mcv, middle cerebral vein; optl, optic lobe; pa, posterior ampulla; sac, sacculus; sof, supraorbital fossa; spi, spinal nerves; tel, telencephalon; utr, utricular; I, olfactory nerve; II, optic nerve; III, oculomotor nerve; IV, trochlear nerve; V, trigeminal nerve; VI, abducens nerve; VII, facial nerve; IX, glossopharyngeal nerve; X, vagus nerve; X.s, subsidiary branch of vagus nerve; X.st, supratemporal branch of vagus nerve.*

The braincase is incompletely ossified; therefore, it is not possible to render a complete endocast. However, certain elements of the endocast (Fig. 4.9) are possible to visualise. Overall, the endocast is very wide and fairly short.

***Hindbrain:*** The hindbrain region of the endocast is short and fairly narrow with protuberant lateral margins, however the cerebellum is poorly resolved due to the displacement of the pterotic. Due to the well ossified basi-exoccipital, the rhombencephalon is very well resolved. It forms a convex medulla oblongata (m.o, Fig. 4.9H). Lateral to the foramen magnum are the occipital nerve canals. Anterolaterally is the vagus nerve (X, Fig. 4.9G, H), though its exact exit from the cranial cavity is unclear due to the disarticulation of the intercalars. The vagus nerve forms three branches. Ventrally emitting the subsidiary branch (X.s, Fig. 4.9G, H), and anteriorly emitting a sub parallel supratemporal branch (X.st, Fig. 4.9G). The endocranial roof is entirely unossified, it is not possible to render the corpus cerebellum.

***Midbrain:*** The midbrain region of the endocast is discontinuously resolved; posteriorly the lateral walls of the midbrain are not resolved and the endocranial roof is also missing. The root of the abducens nerve (VI, Fig. 4.9F, G) is short, briefly exiting the cranial cavity anterior to the sacculus into the roof of the myodome. The endocast

expands anteriorly forming the paired optic lobes (optl, Fig. 4.9G). Only the lateral wall of the optic lobe is preserved. It emits the short anteriorly directed oculomotor nerve (III, Fig. 4.9A, B, C) and the laterally directed middle cerebral vein (mcv, Fig. 4.9A, B, C).

***Forebrain:*** Anteriorly, the forebrain region of the endocast narrows only slightly to forms the relatively broad telencephalon (tel, Fig. 4.9A, B, C). The telencephalon emits the paired anterolaterally directed trochlear nerve (IV, Fig. 4.9A, B). Anteriorly, the telencephalon immediately narrows and forks into the paired tracts of the olfactory nerve (I, Fig. 4.9E, F, G).

**Bony labyrinth:** Much of the bony labyrinth is not resolved, including the semicircular canals. There is a possible posterior ampulla (pa, Fig. 4.9E) preserved within the opisthotic. The anterior portion of the saccular chamber is well resolved. The left and right sacculae are spaced far apart, positioned on either side of the posterior myodome. Anteriorly, the utricular is very bulbous.

### 4.4.8 Cheek

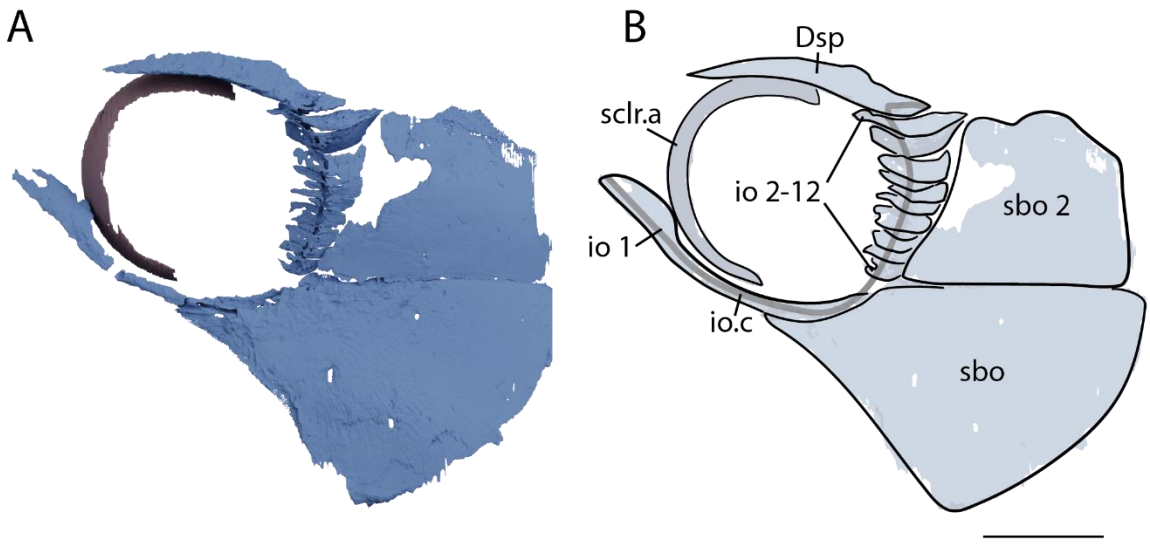


**Figure 4.10: Circumorbital series of *Pachycormus macropterus* (BRLSI M1311).** (A) Render of left circumorbitals in lateral view. (B) Interpretive drawing of left circumorbitals in lateral view. Scale = 10 mm. Light grey indicates path of sensory canal. *Abbreviations: Dsp, dermosphenotic; io 1-12, first to twelfth infraorbital; sbo 1-2, first to second suborbital; sclr.a, anterior ossicle of sclerotic ring.*

A complete circumorbital series (Fig. 4.10) is preserved on both sides of the skull, comprising at least twelve discrete infraorbitals (io), as well as the dermosphenotic (dsp) and two suborbitals (sbo). It lacks supraorbital bones. The infraorbitals form a discontinuous sequence, contributing only to the ventral and posterior margins of the orbit. The first infraorbital (=lachrymal) (io, Fig. 4.10B) forms the ventral margin of the orbit. It is by far the largest infraorbital and has a highly irregular anterior margin. Forming a straight narrow tube around the infraorbital canal, it is broken approximately one third of the way along its length but would form a continuous ossification. Posteriorly, it terminates medially to the second suborbital (sbo 2, Fig. 4.10B), where it expands to form the posteroventral corner of the orbit. The remaining infraorbital series comprises a ladder of eleven small, vertically

arranged plates along the posterior margin of the orbit (io 2-12, Fig. 4.10B). The infraorbital canal (io.c, Fig. 4.10B) travels vertically through the sequence of infraorbitals and appears exposed to the surface as a groove – though this may be worn away through preparation.

Two suborbital bones (sbo, Fig. 4.10B) are present. The anterior margin of the upper suborbital (sbo 1) is partially lost, but it appears trapezoid shaped, widening ventrally. The larger, ventral suborbital (sbo 2) is better preserved. It projects a curved arm anteriorly and broadens posteriorly, to form a large plate. It extends anteriorly beneath the lachrymal. As supraorbitals are absent, the dermosphenotic (Dsp, Figs. 4.5B, E, 4.10B) forms the dorsal margin of the orbit. It briefly carries the infraorbital canal and partially overlaps the nasal anteriorly.

The preoperculum (pop, Fig. 4.5B, E, C) has a large, plate-like ventral process which extends ventral to the suborbital bones. In addition, the preoperculum features a very narrow, vertical dorsal process which has fractured into, or developed as, two splints distinct from the ventral plate. The preopercular canal lies within the anterior margin of the bone.

## 4.4.9 Upper jaw

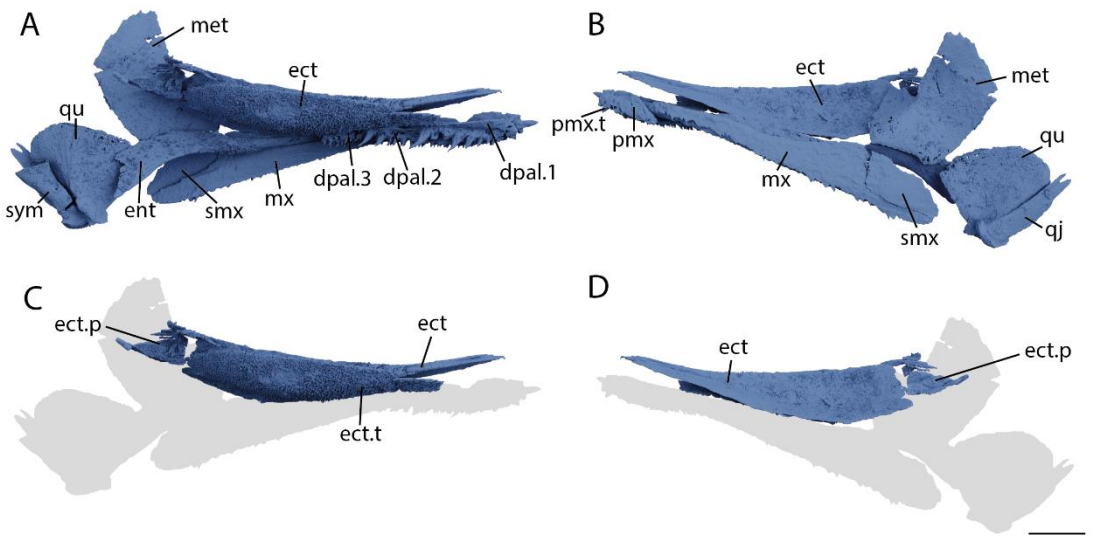


**Figure 4.11: Upper jaw and palatoquadrate of *Pachycormus macropterus* (BRLSI M1311).** Render of complete upper jaw and palatoquadrate in (A) medial and (B) lateral view. Render of Ectopterygoid in (C) medial and (D) lateral view. Scale = 10 mm. *Abbreviations: art, articular; dpal.1-3, first to third dermopalatine; dpal.t, dermopalatine teeth; ect, ectopterygoid; ect.p, posterior elements of ectopterygoid; ect.t, ectopterygoid toothplate; ent, entopterygoid; met, metapterygoid; pmx, premaxilla; pmx.t, premaxilla teeth; qj, quadratojugal process; qu, quadrate; smx, supramaxilla; sym, symplectic.*

The upper jaw (Fig. 4.11) comprises a premaxilla (pmx), maxilla (mx), and a single supramaxilla (smx), with the rostrodermethmoid (rdm) also contributing substantially to the upper oral cavity. Laterally, the premaxilla (pmx, Fig. 4.11B, G, H) is robust and ovoid shaped. In profile, the premaxilla is sub-triangular, tapering at its anterior and posterior margin. The ventral margin is broad to accommodate a row of many small teeth (pmx.t, Fig. 4.11B). The left and right premaxillae do not contact at the midline, as they are separated by the rostrodermethmoid. The maxilla (mx, Fig. 4.11A, B) is exceptionally narrow and elongate, extending the full length of the jaw from beyond the posterior margin of the orbit and reaching the anterior margin of the parasphenoid – narrowly anterior to the premaxilla, and deepening and thinning at its

posteroventral corner to accommodate the supramaxilla. The highly pointed anterior margin of the maxilla curves medially around the premaxilla. The maxilla also carries a single row of small, roughly equally sized teeth. The single supramaxilla (smx, Fig. 4.11A, B) Is parallelogram shaped and overlaps the maxilla and ventral suborbital. It is smooth on both its lateral and medial surface.

### 4.4.10 Palatoquadrate

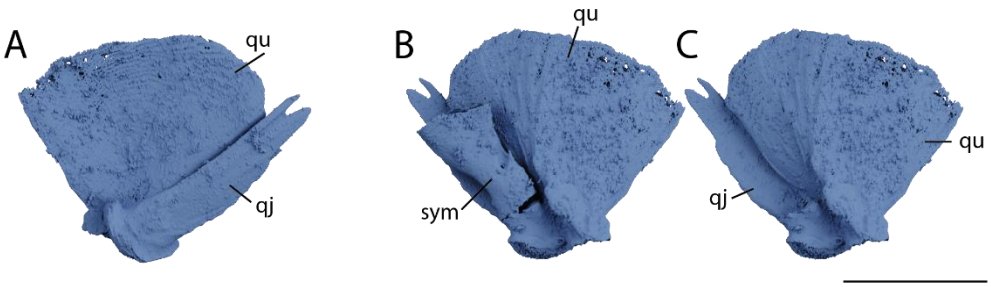


**Figure 4.12: Quadrate and symplectic of *Pachycormus macropterus* (BRLSI M1311).** Render of quadrate in (A) lateral view, (B) medial view (with symplectic) and (C) lateral view. Scale = 10 mm. *Abbreviations: sym, symplectic; qj, quadratojugal process; qu, quadrate.*

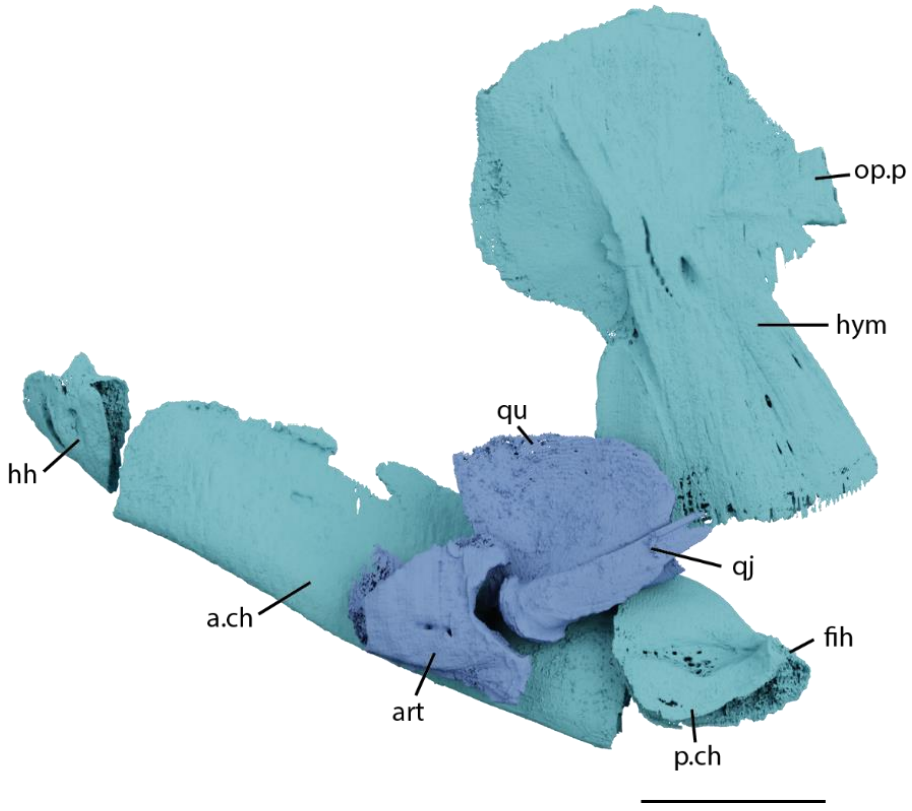

**Figure 4.13: Jaw and hyoid arch articulation of *Pachycormus macropterus* (BRLSI M1311).** Render of left jaw joint and hyoid arch in lateral view. Scale = 10 mm. *Abbreviations: a.ch, anterior ceratohyal; art, articular; fih, facet for interhyal; hh, hypohyal; hym, hyomandibula; op.p, opercular process; p.ch, posterior ceratohyal; qj, quadratojugal; qu, quadrate.*

The palatoquadrate (Figs. 4.11; 4.12; 4.13; 4.14) is made up of discrete ossifications, including the quadrate (qu), metapterygoid (met), ectopterygoid (ect) and several dermopalatines (dpal 1-3). The quadrate qu, (Figs. 4.11A, B; 4.12; 4.13) is large and fan shaped with a slightly concave lateral margin. The dorsal margin is relatively weakly ossified while the ventral is very strongly ossified, forming a robust articulation condyle which corresponds to an equivalent cotyle in the posterior margin of the articular (art, Fig. 4.13). The quadratojugal process (qj, Figs. 4.11A, B; 4.12A, C; 4.13) is thin and blade-like with a rounded dorsal margin, fused ventrally to the quadrate. The quadrate does not directly contact the articulator and appears to have been displaced posteriorly.

The metapterygoid (met, Fig. 4.11A, B) is positioned anterodorsally to the quadrate. It is weakly ossified anteriorly but more robust and concave laterally. Anteriorly, a medially directed flange closely overlaps the ectopterygoid. The ectopterygoid (ect, Fig. 4.11A, B, C, D) is highly elongate, tapering towards the snout. It has a deeply concave lateral margin, which forms the ventral margin of the orbit. The anterior margin is pointed, but the posterior margin fragmented into a series of small plates (ect.p, Fig. 4.11C, D).

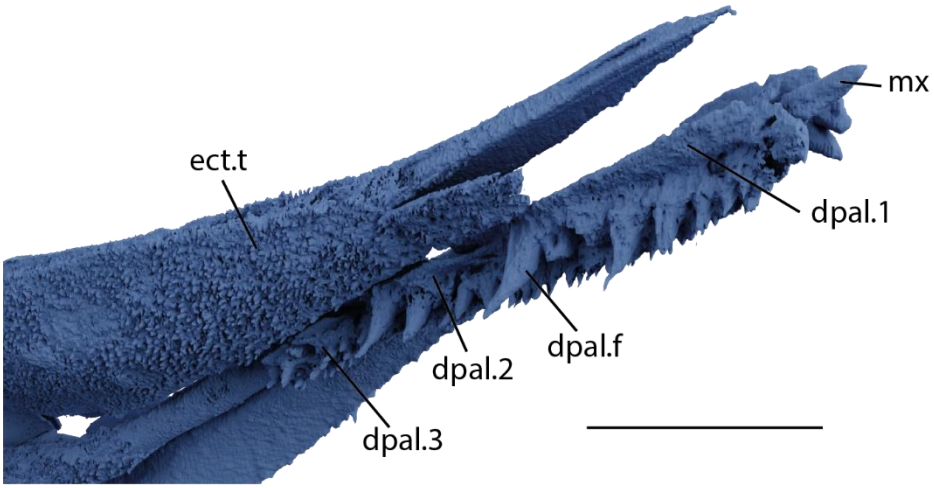


**Figure 4.14: Dermopalatine teeth of *Pachycormus macropterus* (BRLSI M1311).** Render of left palate in medial view. Scale = 10 mm. *Abbreviations: ect.t, ectopterygoid toothplate; dpal.1-3, first to third dermopalatine, dpal.f, dermopalatine fang; mx, maxilla.*

The anteriormost dermopalatine (dpal.1, Figs. 4.11A, B; 4.14) lies parallel to the maxilla and bears a row of conical teeth of varying sizes - some of which are elongate fangs and the largest teeth in the upper jaw (dpal.f, Fig. 4.14).

The snout also includes paired vomers, developed as relatively broad, blade-like plates with a slightly concave dorsal surface. The left and right vomers lie on either side and parallel to the parasphenoid (vo, Fig. 4.8B) interrupted from contacting at the midline. They are separate from the rostrodermethmoid.

## 4.4.11 Lower jaw

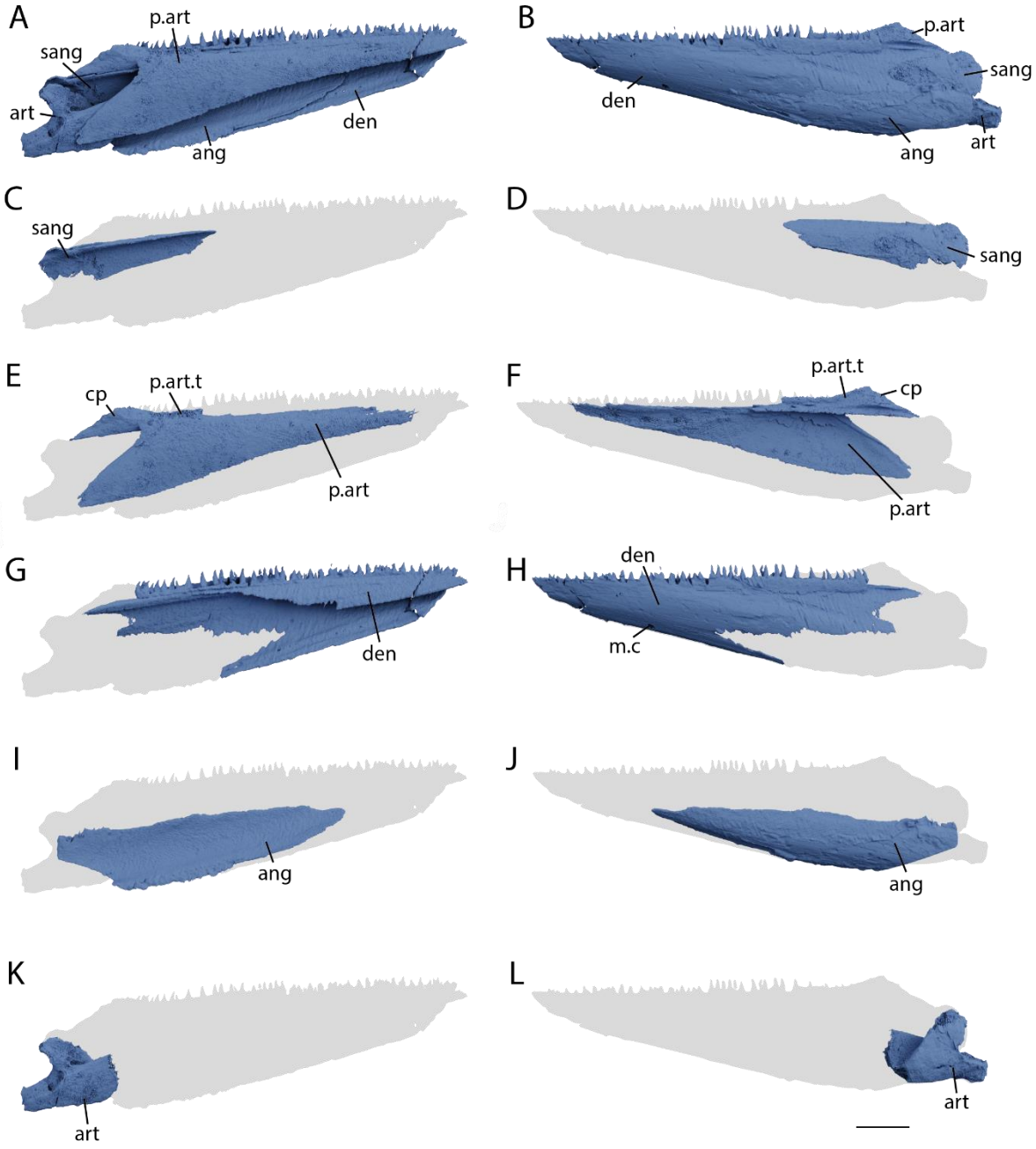


**Figure 4.15: Lower jaw of *Pachycormus macropterus* (BRLSI M1311).** Render of complete lower jaw in (A) medial and (B) lateral view. Remaining panels show most ossifications rendered partially transparent to highlight surangular in (C) medial and (D) lateral view, prearticular in (E) medial and (F) lateral view, dentary in (G) medial and (H) lateral view, angular in (I) medial and (J) lateral view, and articular in (K) medial and (L) lateral view. Scale = 10 mm. *Abbreviations: ang, angular; art, articular; cp, coronoid process; den, dentary; p.art, prearticular; p.art.t, prearticular toothplate; sang, surangular.*

The lower jaw (Fig. 4.15) comprises a dentary (den), angular (ang), surangular (sang), prearticular (p.art), articular (art) and a series of coronoids (cor).

The dentary (den, Fig. 4.15A, B, G, H) is the largest element of the lower jaw. It is elongate and robust, and thickened ventrally around the housing of the mandibular canal, which forms a small lateral opening halfway along the ventral margin (m.c, Fig. 4.15H). The left and right dentaries do not appear to contact along the ventral midline and are instead interrupted by the gular plate (see below). The dentary is lined by a single row of conical teeth. Each dentary tapers anteriorly. Posteriorly, there is a very deep triangular notch to accommodate the predentaries.

The angular (ang, Fig. 4.15A, B, I, J) lies parallel to the dentary, and is visible externally, forming the posteroventral margin of the lower jaw. It is elongate and carries the posterior portion of the mandibular sensory canal. The surangular (sang, Fig. 4.15A, B, C, D) appears to be fused to the dorsal margin of the angular. It is the smallest component of the lower jaw. The articular (art, Fig. 4.15A, B, K, L) is small and very robust, endochondrally ossified very similarly to the quadrate. It is positioned between the angular and prearticular. Posteriorly, the articular bears a large articulator facet, which corresponds to the quadrate (see above). Dorsally, the prearticular (p.art, Fig. 4.15A, B, E, F) exclusively forms the extremely reduced coronoid process (cp, Fig. 4.15E, F), which barely extends above the rest of the mandible. The prearticular forms much of the medial surface of the lower jaw. It is also highly elongate, lying parallel to the dentary, and bears a very deep triangular posterior notch around the adductor fossa. Of note, there is a small, raised patch of small conical teeth (p.art.t, Fig. 4.15E, F) on its posterior dorsal margin.

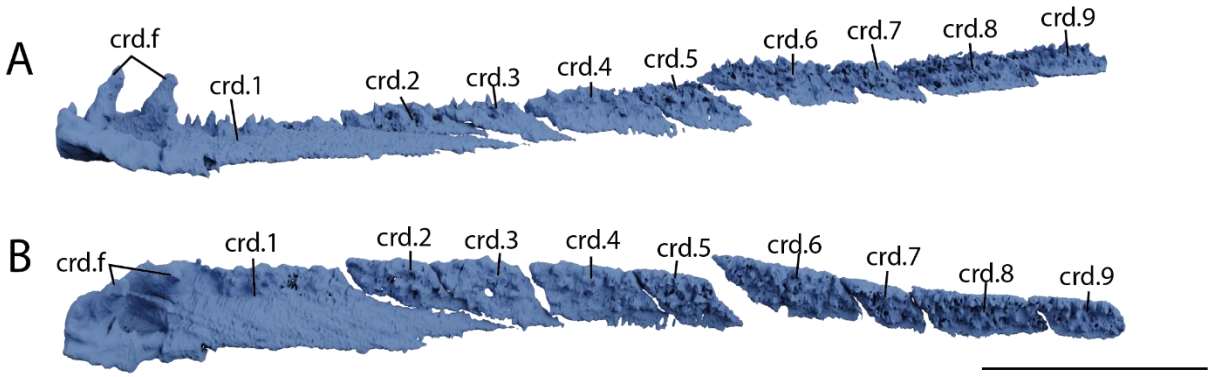


**Figure 4.16: Coronoids of *Pachycormus macropterus* (BRLSI M1311).** Render of right coronoids in (A) medial and (B) dorsal view. Scale = 10 mm. *Abbreviations: crd.1-9, first to ninth coronoid; crd.f, coronoid fang.*

Medial to the tooth row, the dentary is overlain by a row of coronoid plates (Fig. 4.16). On the right side of the specimen, a complete sequence of nine coronoids is preserved. Each plate bears an irregular patch of small, conical teeth. Each successive coronoid is irregular in length. However, each coronoid bears a medial, posterior process which underlies the preceding plate. These processes decrease in length posteriorly. The anteriormost coronoid (crd.1, Fig. 4.16) is considerably larger than the other plates, and its posterior process extends past the second plate. Anteriorly, it bears three large conical fangs (crd.f, Fig. 4.16) with an empty socket where a fourth would have been housed. The fangs are four times the height of the other coronoid teeth, and the widest teeth in the lower jaw.

## 4.4.12 Hyoid arch

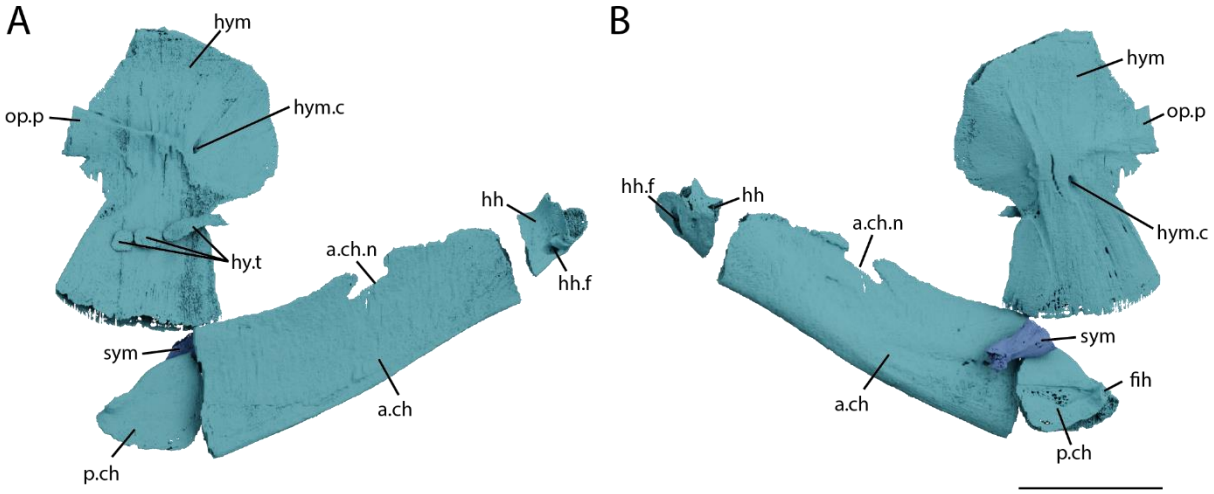


**Figure 4.17: Hyoid arch of *Pachycormus macropterus* (BRLSI M1311).** (A) Render of left hyoid arch in lateral view. (B) Render of left hyoid arch in medial view. Scale = 10 mm. *Abbreviations: a.ch, anterior ceratohyal; fih, facet for interhyal; hh, hypohyal; hh.f, efferent hyoidean artery; hym, hyomandibula, hym.c, hyomandibular canal; hy.t, hyomandibular tooth plate; op.p, opercular process; p.ch, posterior ceratohyal, sym, symplectic.*

The hyoid arch (Figs. 4.13; 4.17) comprises a hyomandibula, hypohyal, and anterior and posterior ceratohyals. An interhyal is not observed.

The hyomandibular (hym, (Figs. 4.13; 4.17) is extremely broad, with flared dorsal and ventral margins, narrowing slightly at its midpoint. A short, posteriorly directed opercular process (op.p, Fig. 4.17) with straight margins is present on the posterior margin. The hyomandibular canal (hym.c) is near vertical, emerging from a dorsally directed foramen on the inner surface, and a ventrally directed foramen on the outer surface (hym.c, Fig. 4.17).

The posterior ceratohyal (p.ch, Fig. 4.13; 4.17) is small and triangular, and an unfinished facet on its dorsal margin may represent an articulation surface for the interhyal (fih, Figs. 4.13; 4.17B) which is otherwise not preserved. The anterior ceratohyal (a.ch, Figs. 4.13; 4.17) is elongate with a thickened ventral margin. The

anterior margin is notched (a.ch.n, Fig. 4.17); anteriorly the notch has a vertical margin, posteriorly it embeds beneath the dorsal margin. The groove for the efferent hyoidean artery is extremely shallow.

The symplectic (sym, Fig. 4.17A, B) is broad and cylindrical, lying postero-ventrally and articulated with the quadrate, parallel to the quadratojugal process. Its dorsal margin is weakly ossified.

The hypohyal (hh, Figs. 4.13; 4.17) is relatively small, with a deeply concave medial lateral margin. It is pierced by the dorsolaterally directed canal for the efferent pseudobranchial artery (hh.f, Fig. 4.17). This forms a very deep groove on the outer surface of the bone. The inner surface of the hypohyal forms a broad rounded depression which likely accommodated the hypobranchial.

A single row of small tooth plates are associated with the medial face of the hyomandibula (hy.t, Fig. 4.17A). The anterior tooth plate is elongate, while the remaining are square shaped with rounded corners.

## 4.4.13 Gill skeleton

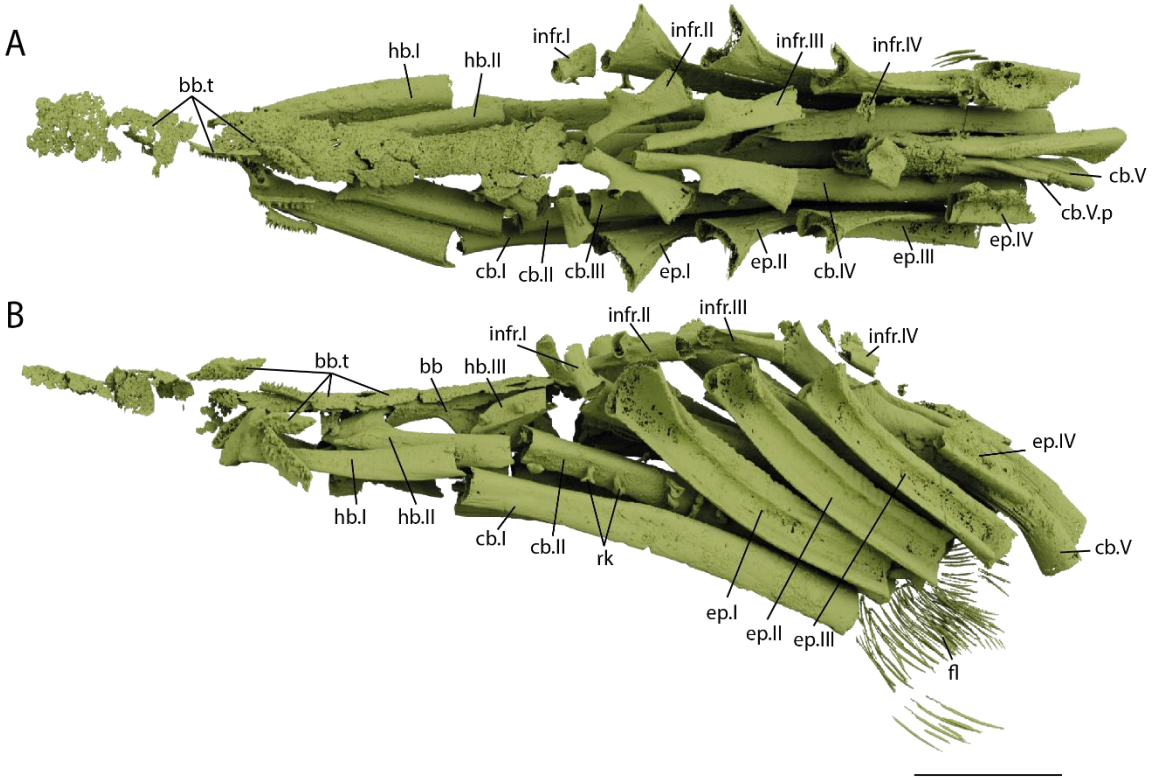


**Figure 4.18: Complete gill skeleton of *Pachycormus macropterus* (BRLSI M1311).** Renders *in situ* in (A) dorsal, (B) left lateral view. Scale = 10 mm. *Abbreviations Bb.III+IV, third basibranchial; Bb.t; basibranchial toothplate; Cb.I-V, first to fifth ceratobranchials; Cb.V.p; process on fifth ceratobranchial; Ep.I-IV, first to fourth epibranchial; fl, gill filaments; Hb.I-IV, first to fourth hypobranchial; Infr.I-IV, first to fourth infrapharyngobranchials; rk, gill rakers.*

The gill skeleton (Figs. 4.18; 4.19; 4.20; 4.21; 4.22; 4.23; 4.24; 4.25) is very well mineralised, well-articulated and equally complete on both the left and right sides. The ventral gill series includes five paired ceratobranchials (cb.I-V), four paired hypobranchials (hb,I-IV) and a median basibranchial (bb.III+IV). The dorsal gill series includes four paired epibranchials (ep.I-IV) and four paired infraphyrangobranchials (infr.I-IV). A complex nest of loose gill filaments (fl) and rakers (rk) is also preserved, and the basibranchial is associated with an extensive dorsal median toothplate (bb.t).

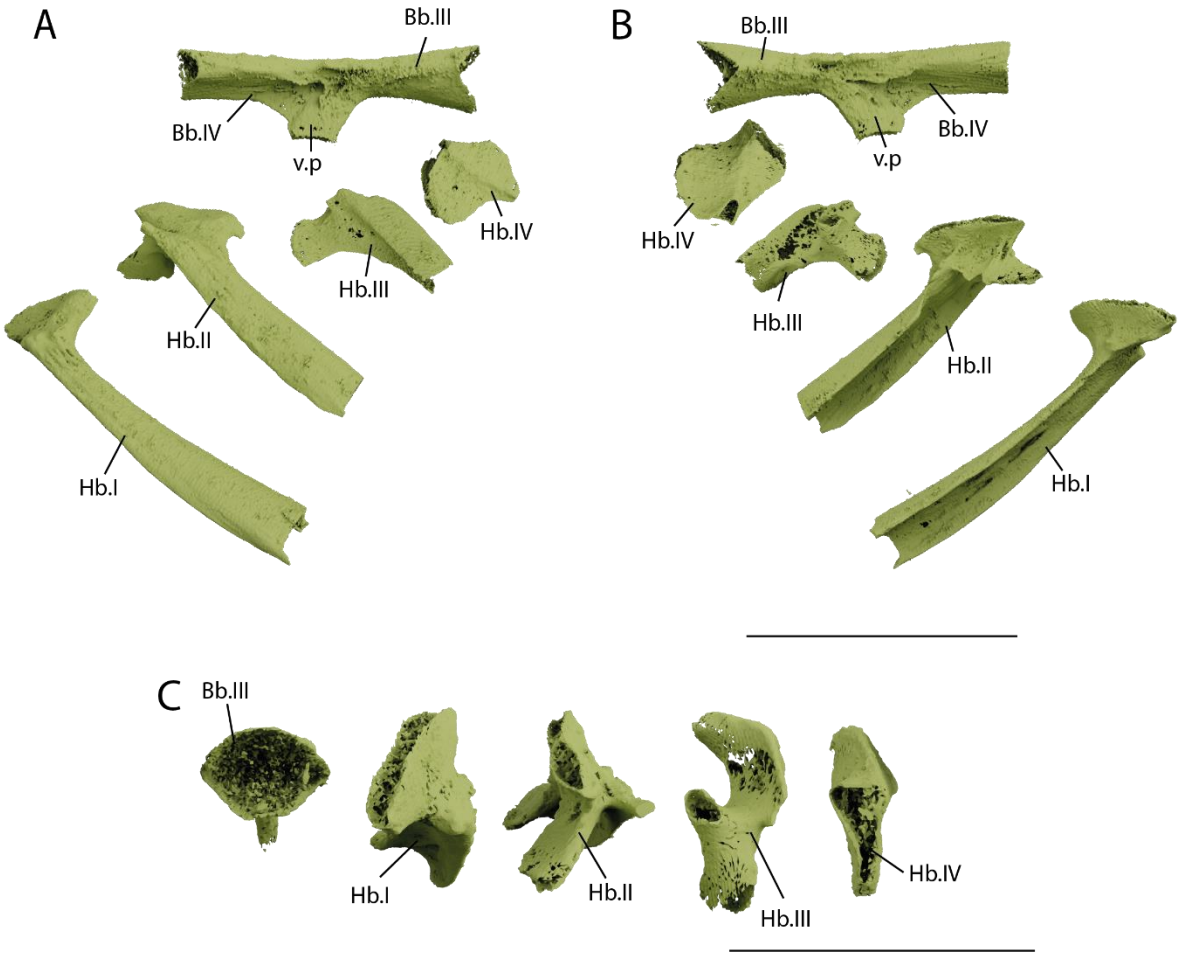


**Figure 4.19: Left hypobranchials and median basibranchial of *Pachycormus macropterus* (BRLSI M1311).** Renders of elements arranged in (A) left lateral view, (B) medial view, (C) anterior view. Scale = 10 mm. *Abbreviations: Bb.III, third basibranchial; Hb.I-IV, first to fourth hypobranchial; v.p, ventral process.*

The third and fourth basibranchials are fused to form a single copula (sensu, Nelson, 1969b) (bb III+IV, Figs. 4.18; 4.19; 4.24) is preserved. In cross section, the basibranchial copula is oval shaped, constricting at its approximate halfway point. Dorsally, the basibranchial copula is smooth and flat, but ventrally it projects a large, deep median process (v.p, Fig. 4.19). The anterodorsal corner of the ventral process is thickened slightly around paired posteroventrally directed articulation facets for the hypobranchials. The basibranchial copula is overlain by a broad and elongate median

tooth plates (Fig. 4.18), which continues above the inferred position of the anterior, unmineralised basibranchials.

Four pairs of hypobranchials (Hb.I-IV) are present, with successive pairs decreasing in length and complexity posteriorly. Each hypobranchial bears an elaborate anterior head for articulation with the corresponding facet on the basibranchial, although the third hypobranchial and basibranchial are slightly out of life position. The left and right of each hypobranchial pair meet anteriorly at the midline.

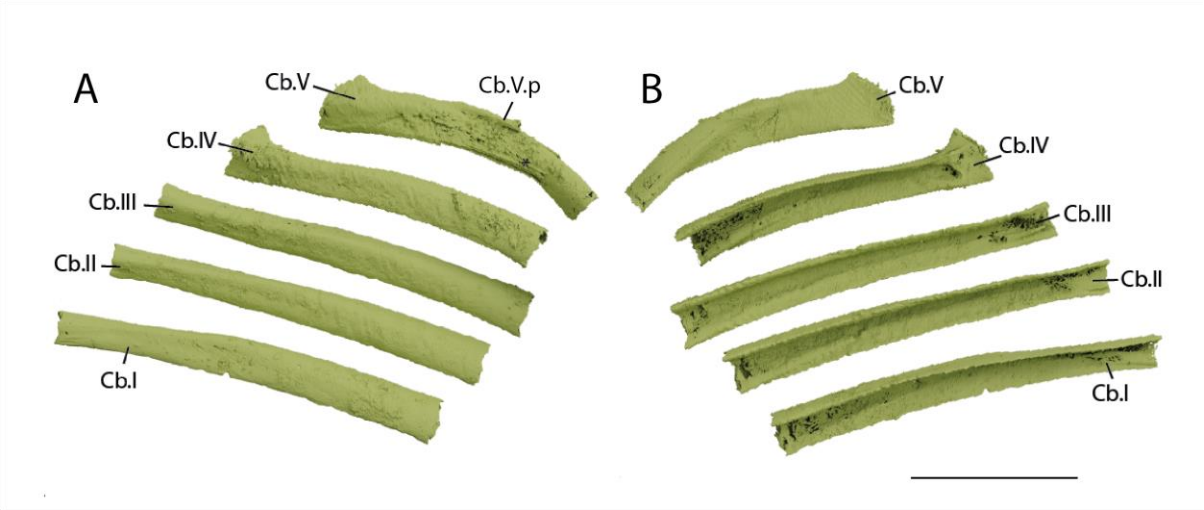


**Figure 4.20: Ceratobranchials of *Pachycormus macropterus* (BRLSI M1311).** Renders of elements arranged in (A) left lateral view, (B) medial view. Scale = 10 mm. *Abbreviations: Cb.I-V, first to fifth ceratobranchials; Cb.V.p; process on fifth ceratobranchial.*

Five pairs of ceratobranchials (cb.I-V, Figs. 4.18; 4.20; 4.21; 4.24) are present. The first four ceratobranchials (Cb.I-IV) are “C” shaped in cross section, with the convex margin facing laterally. The fifth ceratobranchial (Cb.V) is relatively straight with a thickened posterior end. The left fifth ceratobranchial bears an elongate tube part way along its dorsal surface (Cb.V.p, Figs. 4.20, 4.24). This novel feature is

asymmetric, and not present on the corresponding ceratobranchial on the right side of the specimen.

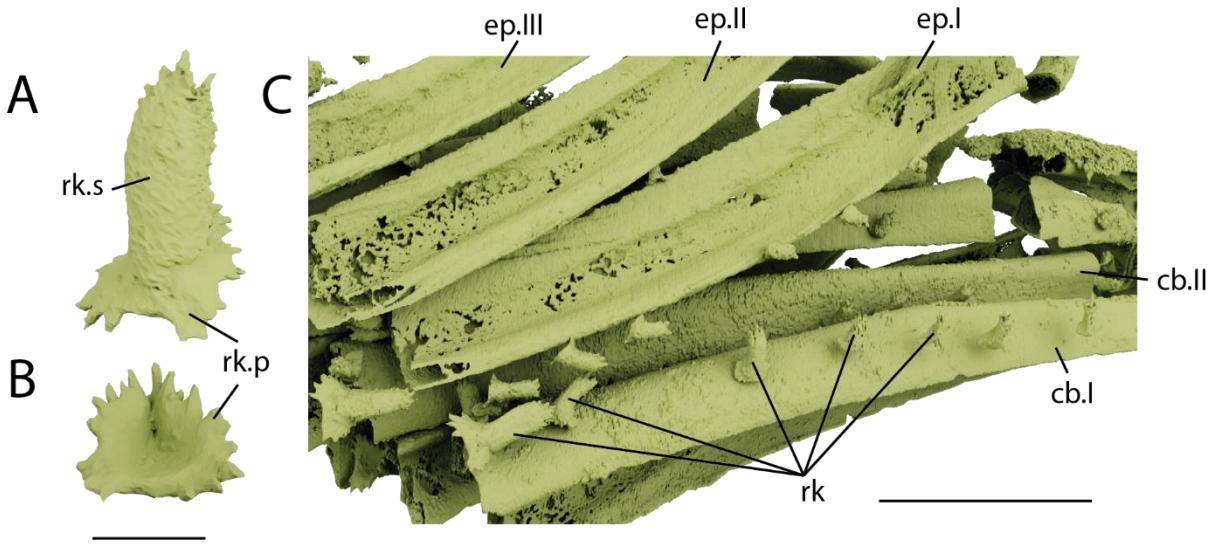


**Figure 4.21: Gill rakers of *Pachycormus macropterus* (BRLSI M1311).** Posteriormost gill raker rendered in (A) lateral and (B) ventral view. Scale = 1 mm. Rakers *in situ* in (C) lateral view. Scale = 5 mm. *Abbreviations: cb.I-II, first to second ceratobranchial; ep.I-III, first to third epibranchial; rk, gill rakers, rk.p, gill raker articular surface, rk.s, gill raker stalk.*

Gill rakers (rk, Figs. 4.18B, 4.21) line the lateral surfaces of the ceratobranchials and epibranchials. Each raker is moderately elongate, comprising a robust cylindrical stalk (rk.s, Fig. 4.21A) which inflects slightly dorsally. Each raker has a rounded distal surface and a flared proximal articulator surface with a serrated margin (rk.p, Fig. 4.21A, B). The gill rakers appear to increase in size posteriorly; the posteriormost rakers are extremely large with a very wide articulator surface. Many of the rakers are separated from their respective gill element, especially the larger examples. Those that are in articulation are directed laterally. Fine gill filaments (fl, Fig. 4.18B) are also preserved along the gill bars, and disarticulated filaments can also be found throughout the specimen – an example of several filaments have been segmented.

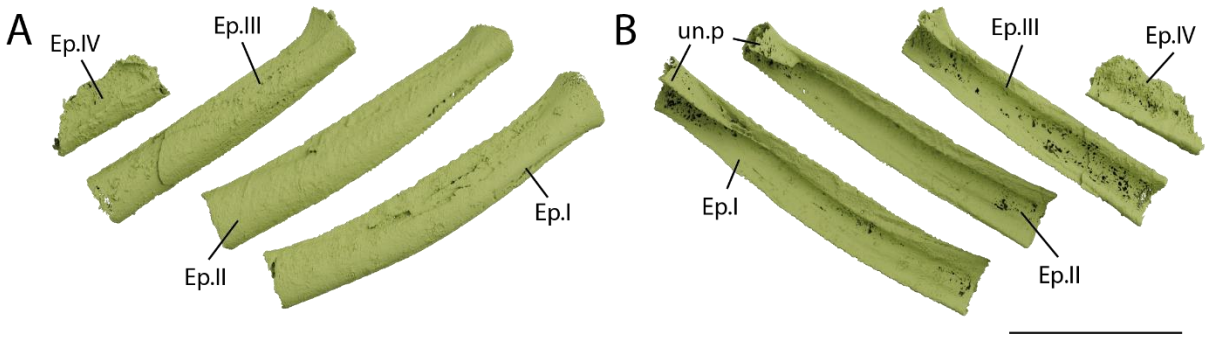


**Figure 4.22: Epibranchials of *Pachycormus macropterus* (BRLSI M1311).** Renders of elements arranged in (A) left lateral view, (B) medial view. Scale = 10 mm. *Abbreviations: Ep.I-IV, first to fourth epibranchial; un.p, uncinate process.*

Four pairs of epibranchials (Ep.I-IV, Figs. 4.18; 4.21; 4.22) are present. They are elongate and curved dorsally; resulting in a “C” shaped in cross section, with their convex margin facing medially. The anterior margin is flared into a robust uncinate process (un.p, Fig. 4.22) for articulation with the infraphyrangobranchials. The fourth epibranchial (ep.IV) is considerably shorter, and less convex. It is roughly quadrate in shape, and bears no articulator processes. It is also preserved posterior to the parasphenoid (Fig. 4.25).

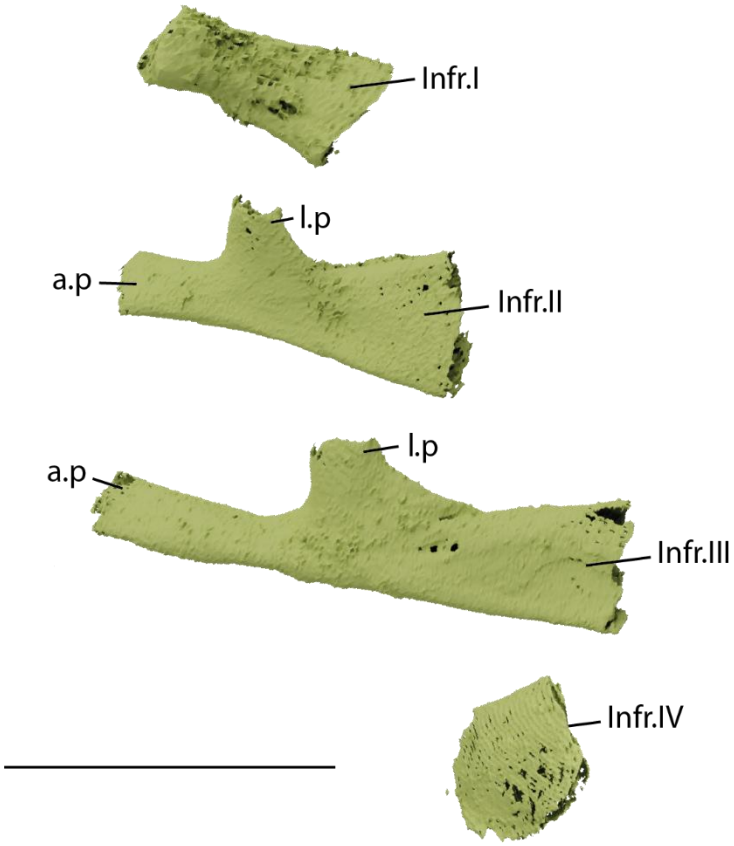


**Figure 4.23: Infrapharyngobranchials of *Pachycormus macropterus* (BRLSI M1311).** Renders of elements arranged in dorsal view. Scale = 10 mm. *Abbreviations: a.p, anterior process; l.p, lateral process; Infr.I-IV, first to fourth infrapharyngobranchials.*

Four pairs of infraphyrangobranchials (nfr.I-IV, Figs. 4.18; 4.23; 4. 25) are preserved. The first pair (Infr.I) are simple cylindrical elements with no processes. The second (Infr.II) and third Iinfr.III) pairs are more complex and very similar in shape, though the third is more elongated. Each pair forms a narrow anterior process (a.p, Fig. 4.23), where it articulates with the parasphenoid and braincase, and project a robust laterally directed articulator process (l.p, Fig. 4.23) which appears to affix with the associated epibranchial. The fourth pair (Infr.IV) are very small and may not be complete/ ossified anteriorly. The left fourth infraphyrangobranchial forms an oval-shaped plate which broadens posteriorly (Infr.IV, Fig. 4.23). The right fourth

infraphyrangobranchial (Infr.IV, Fig. 4.18) is only represented by a small fragment. No suprapharyngobranchials are known.

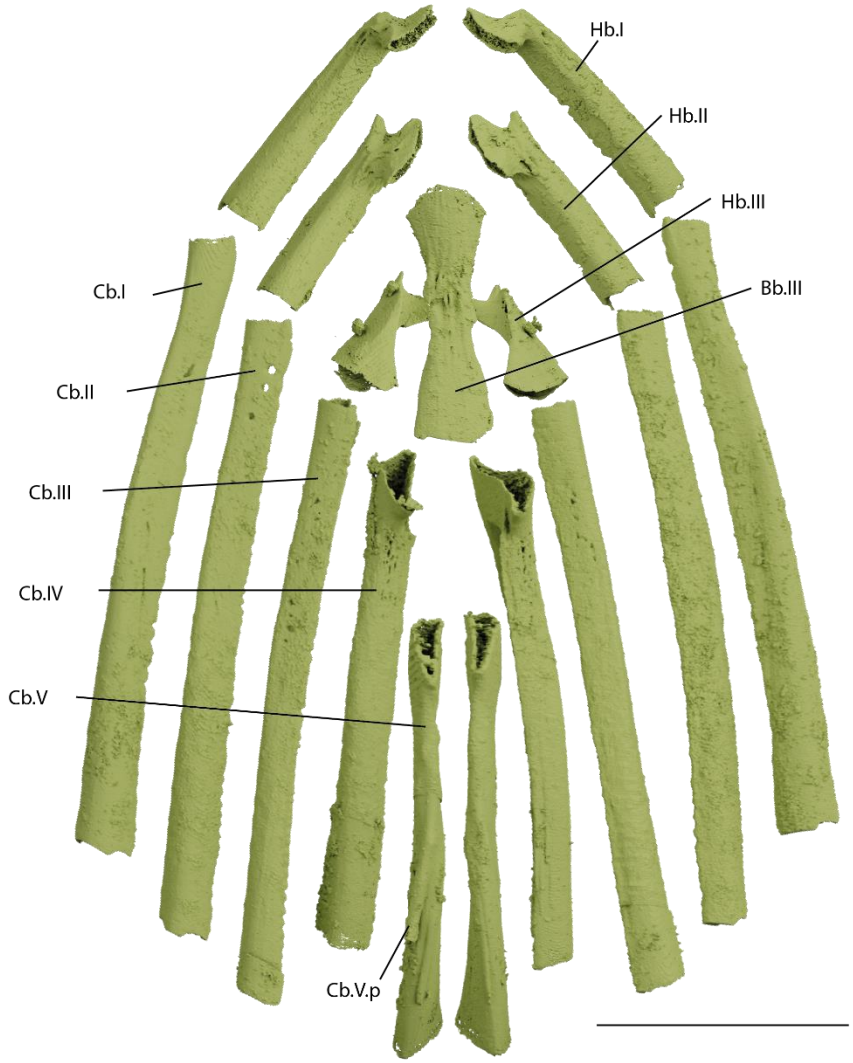


**Figure 4.24: Idealised reconstruction of the ventral gill arch of *Pachycormus macropterus* (BRLSI M1311).** Render of elements arranged in dorsal view. Scale = 10 mm. *Abbreviations: Bb.III, third basibranchial; Cb.I-V, first to fifth ceratobranchials; Hb.I-III, first to third hypobranchial.*

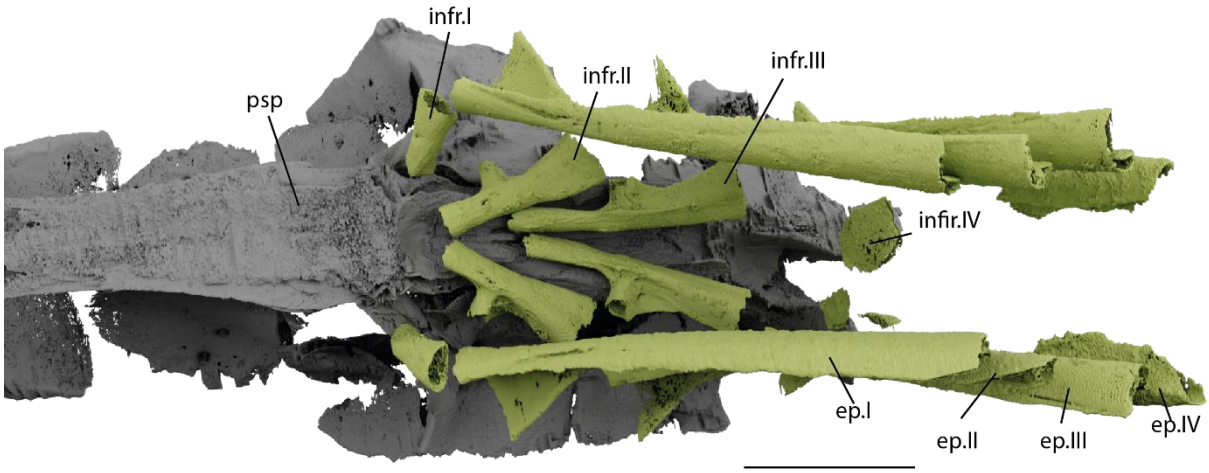


**Figure 4.25: Articulation of infrapharyngobranchials and braincase in *Pachycormus macropterus* (BRLSI M1311).** Render in ventral view. Scale = 10 mm. *Abbreviations: infr.I-IV, first to fourth infrapharyngobranchials; ep.I-IV, first to fourth epibranchial, psp, parasphenoid.*

## 4.4.14 Opercular gular

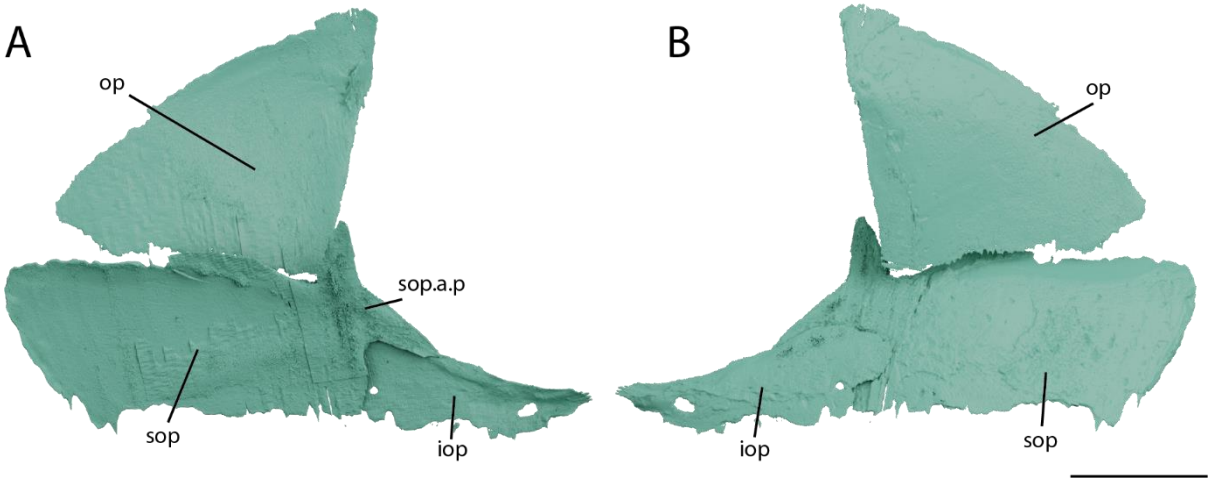


**Figure 4.26: Opercular series of *Pachycormus macropterus* (BRLSI M1311).** Render of left opercular series in (A) medial view and (B) lateral view. Scale = 10 mm. *Abbreviations: iop, interoperculum; op, operculum; sop, suboperculum. sop.a.p, subopercular process.*

The opercular series (Figs. 4.5B, D, E; 4.26) includes the operculum (op), interoperculum (iop), suboperculum (sop) and median gular plate (gul, Fig. 4.5C, F).

The operculum (op, Fig. 4.26) is roughly triangular shaped with smooth margins. It is wider but shorter than the preoperculum. The suboperculum (sop, Fig. 4.25) is rhomboidal and bears an elaborate anterodorsal process (sop.a.p, Fig. 4.26). The process is forked anteriorly, matching the curvature of the preoperculum. The interoperculum (iop, Fig. 4.26) is elongate and overlapped by the preoperculum. A median gular plate (gul, Fig. 4.5C, F) lies directly between the left and right dentaries the underlie the ventral part of the mouth. It is convex ventrally. It is very weakly ossified posteriorly. Lateral gulars are not observed and believe to be absent.

### 4.4.15 Pectoral girdle

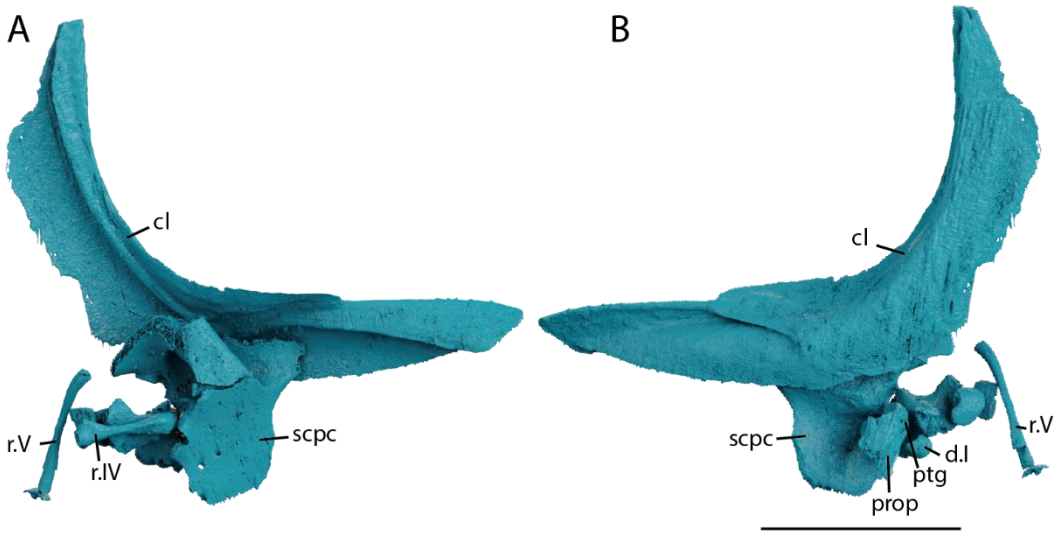


**Figure 4.27: Pectoral girdle of *Pachycormus macropterus* (BRLSI M1311).** Render of left pectoral girdle in (A) medial view and (B) lateral view. Scale = 10 mm. *Abbreviations: cl, cleithrum; ptg, propterygium; r.II, second radial; r.III, third radial; r.IV, fourth radial; lep, lepidotrichia; mtg, metapterygium.*

The pectoral girdle (Figs. 4.27; 4.28; 4.29) is also well preserved and partially articulated. It includes the cleithrum (cl), scapulacoracoid (scpc) and fin radials (ptg, r.I-IV, mtg). The cleithrum (cl, Fig. 4.27) is crescent shaped, with a steeply curved, almost vertical dorsal limb, and a horizontal ventral limb that extends anteriorly level

to the hypohyal. The cleithrum has an expanded, medial wing which meets its antimere on the midline.

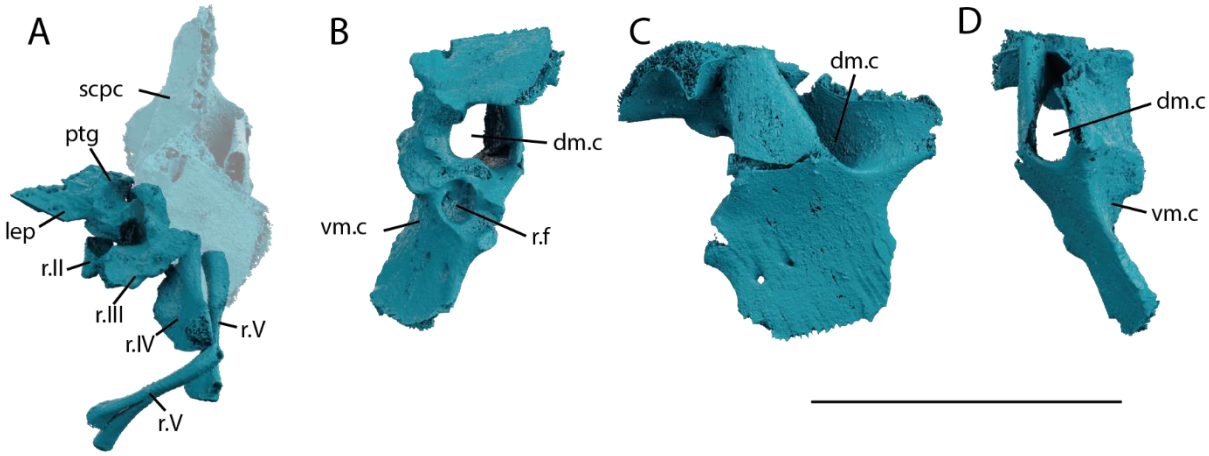


**Figure 4.28: Scapulocorocoid of *Pachycormus macropterus* (BRLSI M1311).** Render of left scapulocoroid and radials *in situ* in (A) dorsal, (B) posterior, (C) medial, (D) anterior view. Scale = 10 mm. *Abbreviations: dm.c, dorsal muscle canal; lep, lepidotrichia; ptg, propterygium; r.II, second radial; r.III, third radial; r.IV, fourth radial; mtg, metapterygium; r.f, rounded facet; vm.c, ventral muscle canal.*

Endochondral elements of the pectoral shoulder girdle are continually ossified into a single scapulocoracoid element (scpc, Figs. 4.27; 4.28), although a fracture along the dorsomesial margin of the left scapulocoracoid indicates the likely position of the mesocoracoid element (Fig. 4.28B). The girdle attaches to the cleithrum in a ventral position. Dorsally, the scapulocoracoid forms a large, arched opening for the dorsal muscle canal (dm.c, Fig. 4.28B, C, D). The canal is not fully closed along the dorsal margin. Ventral to the posterior opening of the dorsal muscle canal is a subhorizontal facet for the articulation of the pectoral radials. a large, circular, radial facet (r.f, 4.28B). Lateral to the radial facet are shallower articulation surfaces for additional radials. Further ventrally, the scapulocoracoid forms a wide, plate like process. The process is curved on its lateral margin to accommodate the ventral muscle canal (vm.c, 4.28B, D).

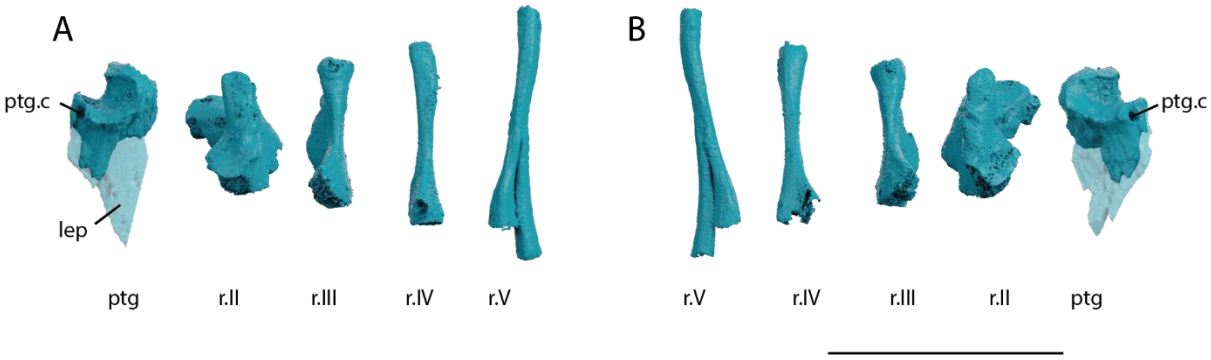


**Figure 4.29: Radials of *Pachycormus macropterus* (BRLSI M1311).** Renders of left radials arranged in dorsal view (A), render of right radials arranged in dorsal view (B). Scale = 5 mm. *Abbreviations:lep, lepidotrichia; ptg, propterygium; r.II, second radial; r.III, third radial; r.IV, fourth radial; mtg, metapterygium.*

Five proximal radials and three distal radials are recovered. The first proximal radial is the propterygium (ptg, Figs. 4.28A; 4.29). It has a rounded, proximal margin for articulation with the scapulocoracoid, and a triangular distal process fused to the proximal lepidotrichia (lep, Figs. 4.28A; 4.29). The propterygium is perforate, pierced by the propterygial canal (ptg.c, Fig. 4.29). The next radial (r.II, Figs. 4.28A; 4.29) is extremely robust and is the largest and most elaborate. It bears a deep, ventral process, which is also perforate and a curved lateral margin around the propterygium and the first distal radial. The third proximal radial (r.III, Figs. 4.28A; 4.29) is smaller. It also has a convex lateral margin, also associated with a distal radial, but bears a shallower ventral process. The fourth proximal radial (r.IV, Figs. 4.28A; 4.29) is long and narrow and bifurcates distally. The fifth proximal radial (r.V, Figs. 4.28A; 4.29) has flared proximal and distal ends. It may represent the metapterygium (mtg, Figs. 4.2B). The distal radials are slightly flattened, with a concave posterior margin for articulation with the proximal radials. Each distal radial is similar in size.

### 4.4.16 Axial skeleton

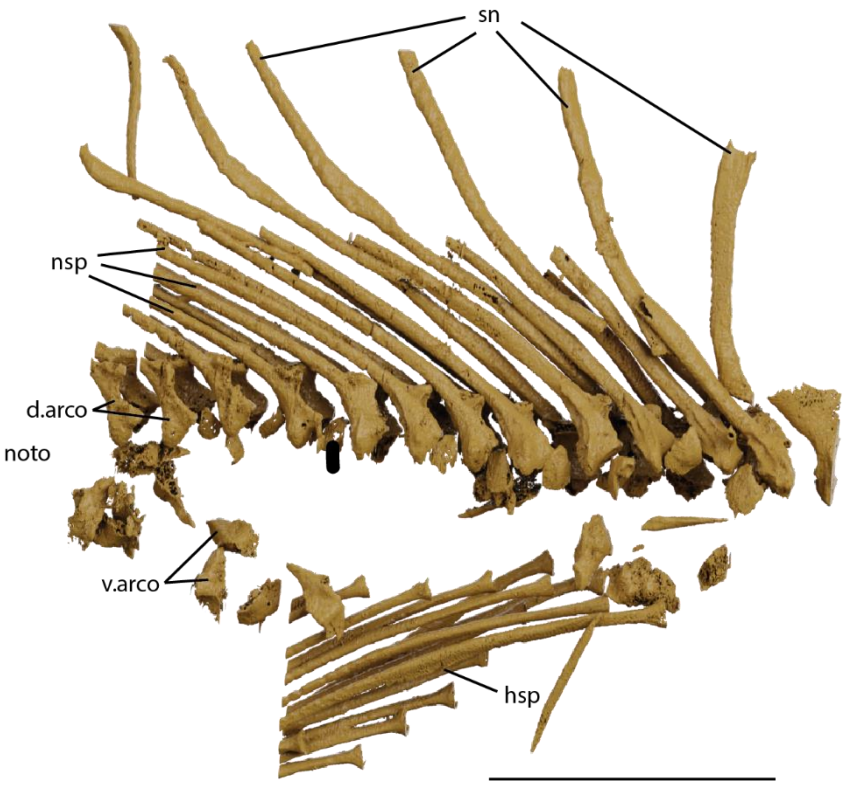


**Figure 4.30: Axial skeleton of *Pachycormus macropterus* (BRLSI M1311).** Render of axial skeleton in right lateral view. Scale = 10 mm. *Abbreviations; d.arco, dorsal arcocentra; hsp, haemal spines; nsp, neural spines; noto, space for notochord; snsp, supraneural spines; v.arco, ventral arcocentra.*

The axial skeleton is also preserved and articulated with the braincase. a short length has been segmented; the first thirteen anterior neural arches (Fig. 4.30). Vertebral centra are not ossified, and the notochord is continuous. The neural arches comprise paired ossifications. The neural arches are developed distally into a narrow, elongate neural spine, which curves steeply (~60º) posteriorly. Each arch also supports a supraneural which form a single median row. Ventral to the vertebrae is a row of haemal spines. They are elongate and very narrow, the proximal surface of each element forms a concave, cup-like surface. Several ventral arcocentra (v.arco, Fig. 4.30) are also preserved; they are better articulated anteriorly. Each is smooth, taper anteriorly and broaden posteriorly.

### 4.4.17 Soft tissue

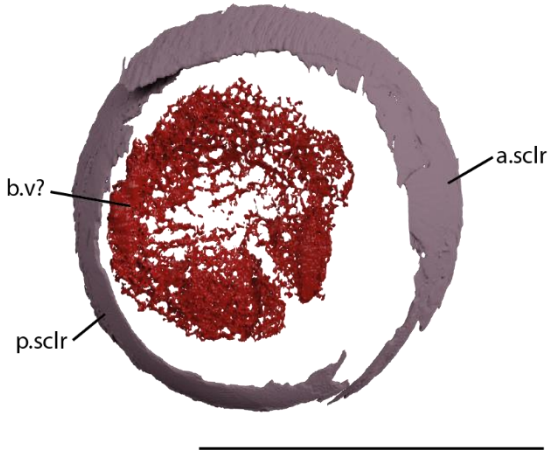


**Figure 4.31: Soft tissue preservation in the orbit of *Pachycormus macropterus* (BRLSI M1311).** Render in right lateral view. Scale = 10 mm. *Abbreviations: a.sclr, anterior ossicle of sclerotic ring; b.v, preserved blood vessels; p.sclr, posterior ossicle of sclerotic ring.*

There are numerous traces of exceptionally preserved soft tissue throughout the specimen, including traces of multiple internal organs and musculature. There is also a concave ring of high density, branching tissue in the orbit, with a depressed divot in the centre (b.v?, Fig. 4.31). It closely resembles the dense network of blood vessels which cover the back of the eyeball, responsible for rapidly delivering blood to the receptor cells (Ather Ali & Anctil, 1976). This could represent the oldest example of the retinal network preserved in the actinopterygian fossil record. Consideration of the soft tissue, or the evolutionary significance of this find (i.e., Damsgaard *et al.,* 2019) is beyond the scope of this thesis.

## 4.5 Phylogenetic Results

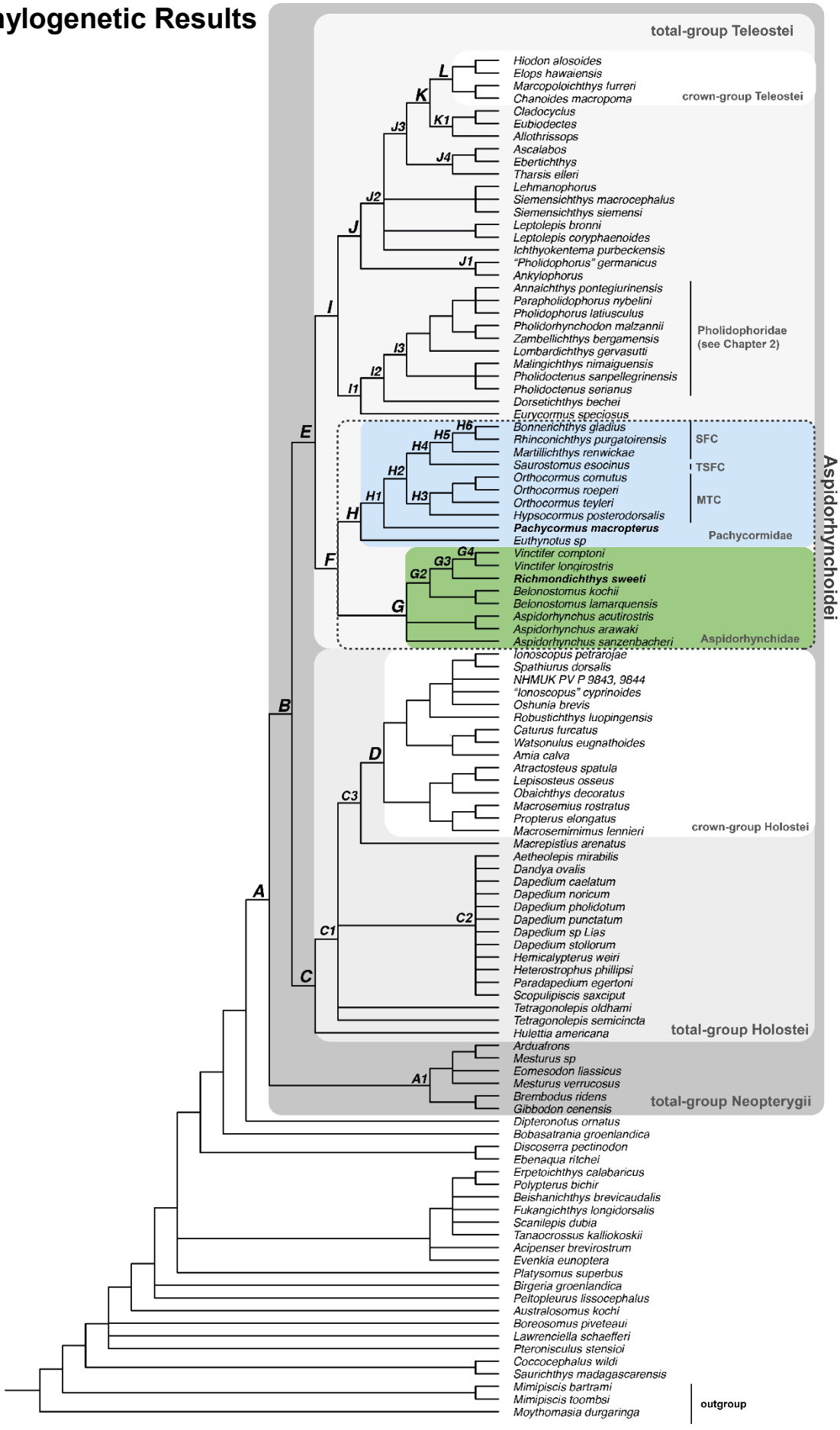

**Figure 4.32: Hypothesis of phylogenetic relationships of neopterygians**. Strict consensus tree of 38448 most parsimonious trees. Pachycormidae highlighted in light blue, Aspidorhynchidae highlighted in green

Character optimisations: **Node A:** The neopterygian total group is supported by four homoplastic characters (c.45, peg like anterior process of maxilla; c.78, preoperculum with pronounced ventral limb; c.127, parasphenoid pierced by efferent pseudobranchial artery; c.213, jaw articulation ventral to orbit). **Node A1:** Pycnodonts are supported two uniquely derived synapomorphies (c.225 prearticular symphysis present; c.229, parasphenoid inflected ventrally below orbit) and eleven homoplastic characters c.19 0; c.23 1; c.183 0; c.190 1; c.200 1; c.215 1; c.219 1; c.222 1; c.223 1; c.224 1; c.227 1). **Node B:** The neopterygian crown group (the divergence of the holostean and teleost total groups) is supported by four homoplastic characters (c.57, coronoid process contributed to by dentary plus predentaries; c.80, infraorbitals and suborbitals broadly overlap preoperculum;p c.82, interopercle; c.220, ossified centra). One character (c.57) has a high consistency index (>0.9) and only reverses once, in a clade comprising *Tharsis, Ascaolobus* and *Erbertichthys.* **Nodes C, D**: Character transformations within Holostei are described in detail in Chapter 3. **Node E:** The teleost total group is supported by four homoplastic characters (c.114 supraoccipital bone; c.116 median supraotic absent; 205 hypural diastema; c.214 parasphenoid wings around basiocciput absent). **Node F:** Aspidorhynchids and pachycormids form a clade supported by one uniquely derived character (c.235 epural bones absent) and seven homoplastic characters (c.105 opisthotic larger than pterotic; c.108 forward extension of the exoccipital around the vagus nerve; c.158 leading margin of dorsal and anal fins without fringing fulcra; c.162 anterior ceratohyal with no medial constriction; c.183 anterior rays do not embrace propterygium; c.211 suborbitals extend ventral to orbit; c.231 supramaxillae positioned posterior to maxilla). **Node G:** Aspidorhynchids are supported by one uniquely derived character: c.61 predentary, and twelve homoplastic characters (c.4 1; c.23 1; c.28 0; c.31 0; c.40 1; c.54 1; c. 69 1; c.80 0; c.160 0; c.165 0; c.192 0; c.221 1). **Node G1** *Aspidorhynchus sanzenbacheri, A. acutirostris* and *A. arawaki* do not form a clade in the strict consensus tree **Node G2** *Belonostomus, Richmondichthys* and *Vinctifer* form a clade, united by four homoplastic characters (c.37, suborbitals contact infraorbitals; c.45, peg-like anterior process of maxilla; c.82, interopercle absent; c.104, braincase ossifications undifferentiated). **Node G3** *Richmondichthys* and *Vinctifer* form a clade united by three homoplastic characters (c.6 teeth on premaxillae absent; c.56 coronoid process of lower jaw absent or reduced; c.97 otoccipital fissure closed). **Node G4** *Vinctifer comptoni* and *V. longirostris* form a clade united by two homoplastic characters: c.32 posterior margin of infraorbital 3 extending beyond the suborbital and c. 62 symplectic involvement in jaw joint.

(figure 4.31 cont.) **Node H:** Pachycormids are supported by two uniquely derived characters (c. 129 large compound rostrodermethmoid; c. 243 hypural plate) and six homoplastic characters (c.34 supraorbital absent; c.56 coronoid process reduced or absent; c.154 scales with peg and socket articulation absent; c.193 median fin rays more numerous than radials; c.196 proximal and middle radials of similar size; c.213 jaw articulation ventral to orbit absent). **Node H1:** *Pachycormus* and all other pachycormids are supported by one uniquely derived character (c.246 posterior boss present) and one homoplastic character (c.199 caudal fin lobe short). **Node H2:** the suspension feeding clade (SFC), *Saurostomus* and microphagous toothed clade (MTC) (*sensu* Cooper & Maxwell, 2022) form a clade supported by three homoplastic characters (c.45 peg like anterior process of maxilla absent; c.51 teeth of outer dental arcade form two rows, with large teeth lingually and small teeth labially; c.188 basal scutes on fins). **Node H3:** *Orthocormus* and *Hypsocormus* – the macrophageous toothed clade – are united by two uniquely derived characters (c.247 parietals form a single midline ossification, c.248 paramedial fangs on rostrodermethmoid present). **Node H4** *Saurostomus* forms a clade with the SFC supported by two uniquely derived characters: (c.242 infraorbitals absent; c.244 hypural plate short and deep) and one homoplastic character (c.33 suborbitals absent). **Node H5:** *Martillichthys*, *Bonnerichthys* and *Rhinoconichthys* - the suspension feeding clade (SFC) - is supported by four homoplastic characters (c.17 parietals rectangular; c.42 teeth on maxilla absent; c.47 supramaxilla absent; c.50 teeth on dentary absent). **Node H6:** *Bonnerichthys* and *Rhinoconichthys* form a clade supported by one homoplastic character (c.53 one infradentary - angular only). **Node I:** Pholidophoriformes and “More Advanced Teleosts” form a clade supported by six homoplastic characters (c.7 1; c.58 1; c.68 1; c.124 0; c.130 1; c.171 1). **Node I1:** Pholidophoriformes is supported by four homoplastic characters (c.13 1; c.20 1, c.41 1; c.226 0). **Node I2:** *Dorsetichthys* and Pholidophoridae form a clade supported by three homoplastic characters (c.23 parietal fused to dermopterotic; c.60 dentary with a well-developed, lateral bony ridge separating the dental and splenial regions; c. 213 jaw articulation not ventral to orbit). **Node I3:** Pholidophoridae are supported by one uniquely derived character (c.48 supramaxillae with scarce ganoine ornamentation) and four homoplastic characters (c. 17 0; 85 1; 114 0; 176 1). **Node J:** “More Advanced Teleosts” form a clade supported by three homoplastic characters (c.2 1; c.54 1; c.163 1). **Node K:** Ichthyodectids and crown teleosts form a clade united by six homoplastic characters (c.20 1 c.58 0 c.130 0 c.154 0 c.171 0 c.198 1). **Node K1:** Ichthyodectids are supported by one uniquely derived character (c.194 step-like sutures between segments of caudal fin rays) and nine homoplastic characters (c.16 1; c.62 1; c.71 1; c.72 1; c.72 0; c.131 1; c.168 1; c.187 1; c.192 0; c.194 1; c.199 0). **Node L:** The teleost crown group is supported by three homoplastic characters (c.104 basisphenoid absent or reduced; c.124 buccohypophyseal canal does not pierce parasphenoid c.204 four ural neural arches modified as uroneurals).

## 4.6 DISCUSSION

### 4.6.1 Updates to previous descriptions: *Pachycormus*

This three-dimensionally preserved, articulated specimen provides previously unobserved anatomical information, clarifies the position and identify of disarticulated material, and suggests revisions to existing schemes of anatomical evolution within pachycormids.

**Braincase:** Rayner (1984: pg. 312, Lehman (1949: pg. 29) and Mainwaring (1978: pg. 45) all identified residual sutures between the fused basioccipital and exoccipital. Patterson (1975) did not recognise any sutures during his redescription of the same material. Sutures in the occipital region of the braincase are not visible in either tomograms or segmented models in BRLSI M1311, and there is no indication of weaker areas of ossification between presumed basioccipital and exoccipital components. This study agrees with Patterson's observations.

Previous interpretations of the braincase have suggested that the basisphenoid in *Pachycormus* is extensive, continuing into the orbit anterior to the posterior myodome (Lehman, 1949: pg. 30). Reinvestigation shows that the pituitary fossa is not developed in this ossification, and it is better interpreted as part of the orbitosphenoid, with the basisphenoid ossification very reduced.

**Circumorbital Series:** Infraorbitals in previously examined specimens of *Pachycormus* are often lost, displaced or difficult to differentiate, and their number is frequently estimated (Lehman, 1949, Cawley *et al.*, 2019). The left infraorbital series is complete and articulated in BRLSI M1311, and a total of twelve are present, including the lachrymal. The suspension feeding clade, including transitional members

such as *Saurostomus*, lack circumorbital elements, lending support to the placement of *Pachycormus* outside of this radiation.

**Upper Jaw and Palate:** The dermopalatines are rarely preserved or visible in most pachycormids, and their morphology is typically only described in passing. The dermopalatines series of BRLSI M1311 reveals the presence of large fang-like teeth, which have not been previously recognised in *Pachycormus*. These superficially resemble the large fangs of *Hypsocormus* (Lehman, 1949: pg. 35), although those of the latter taxon originate from the vomer.

The quadratojugal has previously been described as reduced in *Pachycormus* (Patterson, 1973). Mainwaring (1978: pg. 27,31) disputed this and suggested that independent quadratojugal was not only present, but formed a distinct, elongate posterodorsal process. This feature is illustrated but undescribed by Rayner (1948: fig. 17) earlier work. In agreement with Mainwaring, this study finds that the quadratojugal process is well developed as a broad process that extends past the posterodorsal corner of the quadrate.

**Lower jaw:** Previous descriptions (e.g., Mainwaring, 1978: pg. 21) found that the coronoid plates in *Pachycormus* are progressively smaller posteriorly. The anatomy of BRLSI M1311 allows this observation to be clarified: there are nine plates in total, and although the posterior process of each coronoid grows progressively smaller posteriorly, the coronoid plates themselves are more variable in size and morphology. An inflated anterior coronoid plate is a common feature among macrophageous pachycormids (e.g., *Protosphyraena*, Lambers, 1988; *Australopachycormus,* Kear, 2010; *Kaykay*, Gouiric-Cavalli & Arratia 2022) and is also known in *Saurostomus* (Cooper & Maxwell, 2022), but has previously been coded as

absent in *Pachycormus* (e.g., Friedman *et al.*, 2010; Cooper & Maxwell, 2022). This chapter finds an inflated anterior coronoid plate is present in BRLSI M1311, and that the anterior coronoid also bears two large, conical, fangs. This feature has not been recognised previously in *Pachycormus,* but a similar condition is known in *Australopachycormus hurleyi* (Kear, 2010; the validity of this taxon has been questioned: Gouiric-Cavalli & Arratia, 2022) and *Orthocormus teyleri* (Tyborowski, 2017). While these features suggest a proximal to the toothed macrophageous clade, most are unique to pachycormids, so provide limited broader grouping information within Neopterygii.

A coronoid process has variably been considered absent (Wenz, 1968), or formed from the articular (Patterson, 1973; Mainwaring, 1975). BRLSI M1311 clarifies that a small coronoid process is present and is formed exclusively by the prearticular.

**Hyoid arch:** While an interhyal is known in some pachycormid taxa (e.g., *Martillichthys*: Dobson *et al.,* 2021), it is rarely mineralised in *Pachycormus*, being present only on one side in a single one of several individuals examined by Mainwaring (1978: pg. 33). Therefore, the absence of this element in BRLSI M1311 is not surprising. Mainwaring also reported that some specimens exhibited fragments of toothplates close to the medial surface of the anterior ceratohyal, although she was unsure whether this was their true life-position. Here, the articulated nature of BRLSI M1311 confirms that there are no toothplates present on the ceratohyal, but a short row is associated with the medial surface of the hyomandibula.

In contrast to previous work in which the dorsal margin of the anterior ceratohyal is described as smooth (Lehman, 1949: pg. 34; Mainwaring, 1978: pg. 34), the dorsal margin of the anterior ceratohyal of BRLSI M1311 is distinctly notched. Superficially

similar features are known in some extant teleosts, e.g., *Callichthys callichthys* (Arratia & Schultze, 1990), but this feature is absent or unknown in other taxa on the teleost stem.

**Gill skeleton:** In previous descriptions of *Pachycormus* (Mainwaring, 1978) the fourth epibranchial has been described as bearing an elongate “rod” to articulate directly with the parasphenoid, but this feature is absent on both the left and right fourth epibranchials of BRLSI M1311. In addition, the fifth ceratobranchial exhibits an unusual tube-like process along its dorsal margin, but this feature is only present on one side of the specimen. In the absence of additional tomography-aided descriptions of pachycormid gill skeletons, it is not possible to determine whether this feature is unique to this specimen or of diagnostic use. No suprapharyngobranchials are observed in the dorsal gill arch, contrasting Patterson (1975 pg. 398) but supporting observations by Mainwaring.

The gill rakers are very robust, suggested an enhanced role in supporting the filtration of ingested material (Friedman, 2012). Although the anterior rakers are relatively short, those that are more posteriorly positioned approach the elaborate morphology seen in suspension-feeding pachycormids such as *Martillichthys* (Dobson *et al.,* 2021), although individual tooth cusps are less pronounced.

This study also confirms the presence of numerous elongate median toothplates associated with the basibranchial. These were previously recognised by Mainwaring (1978) and are evidence of the missing unossified/ cartilaginous basibranchials. Conversely, Mainwaring (1978) also identified a urohyal which I find no evidence in this specimen.

**Pectoral fin:** The endoskeletal pectoral girdle of *Pachycormus* is poorly described as it is usually concealed and therefore difficult to access (e.g., Cawley *et al.*, 2019: pg. 296). This chapter finds the lepidotrichia fused to the propterygium in *Pachycormus*. This important synapomorphy strengths the placement of Pachycormidae within Teleostei, and was previously identified in *Pachycormus, Orthocormus and Hypsocormus* by Friedman *et al.*, 2010, Friedman, 2012. However, its presence was contested by Arratia & Lambers 1996; Arratia & Schultze 2013. This chapter supports the former. Although Maxwell *et al. (*2020) remarked that the feature is well distributed among toothed pachycormids, it is very poorly known among the suspension feeding clade (Gouiric-Cavalli & Arratia, 2022: pg. 1539). Additionally, previous work has identified a total of four paired proximal radials on the pectoral fin (Jessen, 1972; Mainwaring, 1978). Here, there are a total of five paired proximal radials, and the fifth radial appears to be bifurcated.

**Axial skeleton:** As reviewed by Cooper & Maxwell, 2022, previous descriptions report a paired row of supraneurals in *Pachycormus* (Wenz, 1968; Bartsh, 1988). Here I find the supraneurals form a single median row, matching the recently revised condition of the supraneurals in *Saurostomus* (Cooper & Maxwell, 2022).

### 4.6.2 Phylogenetic relationships within Aspidorhynchidae

*Richmondichthys* is resolved in a nested position within Aspidorhynchidae, as sister to *Vinctifer*. Although *Richmondichthys* has not been included in any previous phylogenetic analyses, this result agrees with qualitative assessments of aspidorhynchid taxonomy. As reviewed by Bogan *et al. (*2011), Bartholomai (2004) recognised several shared specialisations in the upper jaw and rostrum of *Vinctifer* and *Richmondichthys*. This chapter supports this interpretation, recovering multiple

shared features of the braincase, such as a closed occipital fissure and an almost completely ossified braincase. Other similarities are apparent in the morphology of the posterior myodome, which is short in both *Vinctifer* (Maisey, 1991) and *Richmondichthys*. This contrasts with the condition in more crownward stem teleosts such as *Dorsetichthys*, where the myodome extends to the basioccipital (Patterson, 1975, see Chapter 2). In *Richmondichthys*, and likely other aspidorhynchids where the condition is observed, the space directly posterior to the myodome is occupied by the saccular chambers, which meet on the midline.

Other features of the aspidorhynchid braincase are at odds with characters previously suggested to unite the teleost crown (e.g., López-Arbarello & Sferco, 2018; Giles *et al.*, 2023), suggesting either that examples of early aspidorhynchid morphology are lacking or that schemes of character evolution need revisiting. For example, stem teleosts typically possess dermal basipterygoid processes of the parasphenoid, e.g., *Dorsetichthys, Pholidophorus* and *Leptolepis* (Patterson, 1975, see also previous chapters). This derived feature is lost in crown teleosts (e.g., *Elops*, *Hiodon*) but is also absent in all aspidorhynchids, including *Richmondichthys*. Likewise, the buccohypophyseal canal is absent from the parasphenoid of aspidorhynchids (Maisey 1991, 1999, Brito, 1992, Bogan, *et al*., 2011). This feature is found across most stem teleosts, including those closely related to the teleost crown such as ichthyodectids, but is lost in the crown itself.

This pattern extends to the endocast. Aspidorhynchids are united alongside other teleosts by the posterior portion of the horizontal canal being engulfed by the posterior ampulla and possessing a relatively shallow utricular. However, while crown teleosts are marked by the loss of the lateral cranial canal (Argyriou *et al.*, 2018, Giles

*et al.*, 2023) both *Vinctifer* and *Richmondichthys* converge upon the loss of the lateral cranial canal much earlier in teleost phylogeny.

### 4.6.3 Phylogenetic relationships within Pachycormidae

This study recovers *Pachycormus* within a monophyletic Pachycormidae (Fig. 4.32). In contrast to some recent results (Friedman, 2012; Cooper & Maxwell, 2022; Gouiric-Cavalli & Arratia, 2022, Fig. 4.33B, C), *Pachycormus* is not supported as the sister taxon to the suspension feeding clade (SFC) or the macrophageous toothed clade (MTC), the two main groups of pachycormids, but rather as the sister taxon to a broader clade that contains both the suspension feeding clade (SFC) and the macrophageous toothed clade (MTC) (Fig. 4.33D). This result has also been reported by Friedman *et al.* (2010), though as a polytomy (Fig. 4.33A).

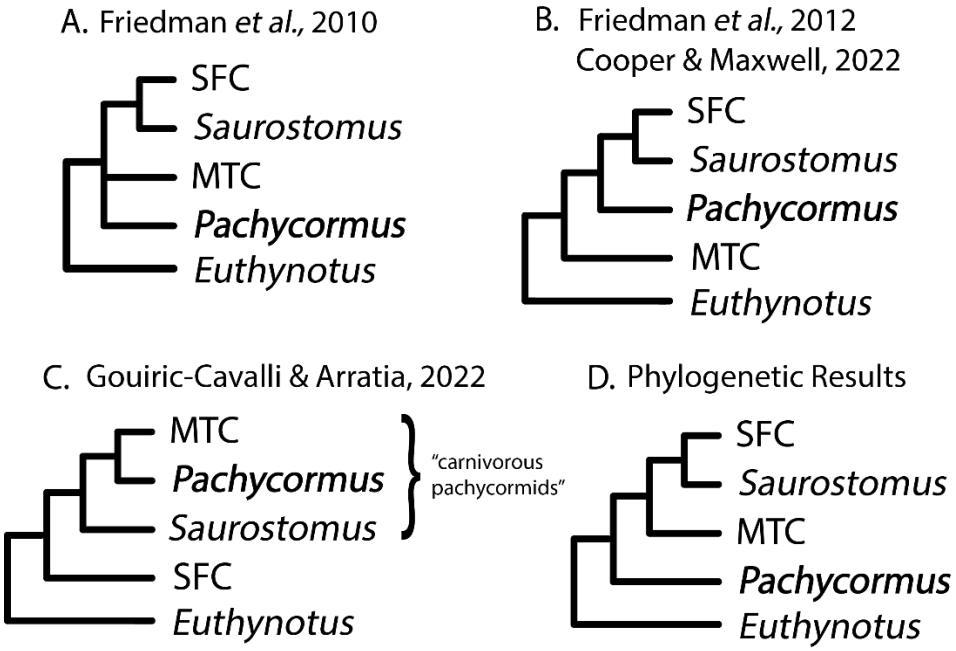


**Figure 4.33: Comparison of phylogenetic results with previously recovered cladograms** *Abbreviations: MTC, macrophageous toothed clade; SFC, suspension feeding clade.*

*Euthynotus* is recovered as sister taxon to all other pachycormids. This has been recovered frequently (e.g., Cooper & Maxwell, 2022; Gouiric-Cavalli & Arratia, 2022, Fig. 4.33A, B, C) and is well supported by its lack of uniquely derived characters but is not well described (Cooper & Maxwell, 2022); *Euthynotus* represents an important avenue for future investigations and would assist in optimising characters outside of the two major clades.

*Pachycormus* is united to the SFC and MTC by one uniquely derived character (c.246 posterior boss) and only one homoplastic character (c.199) short caudal fin lobe. The relatively shorter caudal lobe of the tail reflects some of the specialisations acquired in the tails that typify pachycormiforms. *Pachycormus* is excluded from the suspension feeding clade primarily by the presence of teeth on its maxilla and dentary. The suspension feeding clade is highly specialised and are entirely edentulous. This character transition is well supported, however, Liston *et al. (*2022) found that omitting tooth-related characters from an analysis resulted in highly unusual placements, such as *Protosphyraena* being well nested in the suspension feeding clade. This exposes how this clade relies upon these characters, and that limitations in available material can potentially undermine phylogenetic results. Transitional suspension feeders (i.e., *Saurostomus*) are toothed but also lack ossified orbital bones (Cooper & Maxwell, 2022). *Pachycormus* has orbital bones, so this strongly suggests that it is not nested within the SFC.

*Orthocormus* and *Hypsocormus* (the macrophageous toothed clade) – are united by two uniquely derived characters (c.247 parietals form a single midline ossification, c.248 paramedial fangs on rostrodermethmoid present). These are robust characters, sufficient to place *Pachycormus* outside of the MTC also. However, redescription of *Pachycormus* reveals additional teeth not recognised in these genera

(Lehman, 1949). It is possible that there are perhaps better tooth characters that have not been fully implemented due to a lack of data.

Finally, it has also been suggested that pachycormiform interrelationships may be improved by the inclusion of underappreciated taxa. Pachycormiforms are distributed globally but specimens from western Europe overshadow most work, while taxa representing Gondwana (e.g., *Kaykay*) are rarely included in phylogenies (Gouiric-Cavalli & Arratia, 2022).

### 4.6.4 Validity of Aspidorhynchoidei

In this phylogenetic analysis, Aspidorhynchidae are recovered in a clade with Pachycormidae. This relatively novel grouping, Aspidorhynchoidei (Nelson *et al.,* 2016), represents the earliest diverging group of the teleost stem and was first recovered by Arratia (2013). The same arrangement has since been found by Gouiric-Cavalli (2016); Arratia (2017) and López-Arbarello & Sferco (2018). However, the number of characters that support its monophyly, particularly those that do not exhibit homoplasy elsewhere in the analysis, have been gradually whittled down. Even the often cited supramaxilla positioned posterior to the maxilla (e.g. Arratia, 2013; López-Arbarello & Sferco, 2018) is recovered as homoplastic when incorporated into a broader analysis, occurring also in some pycnodonts. Here, only a single uniquely derived character – absence of epural bones – supports this node. and this distribution of this character in neopterygians is not straightforward.

The development and homologies of the epural bones is very poorly understood (Doosey & Wiley, 2014; López-Arbarello & Sferco 2018). Epurals (*sensu* Arratia & Schultze, 1992) are median caudal elements developed posterior to the most distal

neural spine, dorsal to the neural arches of the preural and ural centra, homologous to detached neural spines. The epurals in teleosts (i.e., pholidophorids, leptolepids, *Dorsetichthys*, *Elops*) are not homologous to the 'epurals' of pachycormids (Arratia & Schultze, 1992; Schultze & Arratia, 2013), and are interpreted as developed from the neural arches and spines instead (Patterson, 1968). This character does not provide concrete support for this clade because the state of the "absence" in both characters does not convey equivalent conditions for aspidorhynchids and pachycormids; in the former, epurals or equivalents are absent entirely. Ultimately, their shared "absence" span potentially diverse conditions (see Brazeau, 2011). It is uncertain how they compare, as the caudal fin is highly specialised in both assemblages (e.g., the hypural plate) so comparison of these regions is very difficult and it is not clear how the state came about compared to the stepwise acquisition of shared present features.

The homoplastic characters that unite aspidorhynchids and pachycormids into a single clade also offer equivocal support. Two of which (c.105 opisthotic larger than pterotic; c.108 forward extension of the exoccipital around the vagus nerve) concern relative braincase ossifications that are homoplastic throughout this dataset. This is also true of 'c.158 The leading margin of dorsal and anal fins without fringing fulcra' and 'c.211 suborbitals extend ventral to orbit'. 'c.162 anterior ceratohyal with no medial constriction' may also problematic as in its current state this character does not capture the dorsal notch identified in *Pachycormus*. Finally, 'c.231 supramaxillae positioned posterior to maxilla' was previously interpreted as a uniquely derived character (Arratia, 2013), however Gouiric-Cavalli & Arratia (2022: supplement 2) have suggested that "supramaxilla" may not be homologous between pachycormiforms and aspidorhynchiforms. Overall, these characters are also not reliable and do not strongly support Aspidorhynchoidei.

Notably, while tomography-aided investigations of the braincase and endocast in *Richmondichthys* and a near-complete and articulated specimen of *Pachycormus macropterus* have highlighted a range of previously unknown anatomical details, few – if any – of these lend support for a close relationship between pachycormiforms and aspidorhynchiforms. Both are highly specialised and extremely different from one another, including the braincase and endocast. In most aspidorhynchiforms (with the exception of *Aspidorhynchus*) the braincase is fully ossified – closing the vestibular fontanelle and rendering individual ossification as undifferentiated. The braincase of pachycormiforms on the other hand is very weakly ossified. In aspidorhynchiforms, the olfactory nerve forms a single tract in the within the orbitosphenoid, while in pachycormiforms it appears to form paired tracts. In *Richmondichthys* the vagus nerve emits a supratemporal branch vertically into the skull roof, in *Pachycormus,* the supratemporal branch is short and emerges within the intercalar. In addition, the symplectic and jaw joint display extremely different morphologies. The aspidorhynchid symplectic is a thin, rod-like element positioned posterior to the quadrate (Brito, 1988), the pachycormid symplectic is broad and closely applied to the quadrae medial surface. Characters related to the braincase, endocast and inner ear have proven rich sources of anatomical data to support relationships between other neopterygian groups. Here, there are very few related derived features of the braincase shared by aspidorhynchids and pachycormids, which would suggest that they are not as closely related as is currently proposed. However, even with the addition of improved character coding of internal anatomical features, this is not well resolved.

## 4.6 Conclusion

This chapter presents a detailed redescription of two outstanding specimens of key early diverging stem teleosts. Through high resolution CT and synchrotron

scanning, a detailed description of the dermal skull, braincase, including the first pachycormiform endocast, palatoquadrate, gill skeleton, pectoral girdle and partial axial skeleton from a single exceptionally preserved individual of *Pachycormus macropterus* from the Strawberry Bank Lagerstätte is presented. This chapter also reveals the first digital reconstruction of an aspidorhynchiform endocast (*Richmondichthys sweeti*). Using this new information, this chapter presents a novel phylogenetic hypothesis of early neopterygians.

# 5. SUMMARY AND FUTURE DIRECTIONS

## 5.1 Summary

This thesis illustrates the use of CT and synchrotron scanning to describe novel anatomical features of three-dimensionally preserved examples of iconic fossil neopterygians and presents a new hypothesis of early neopterygian relationships.

Chapter 1 reviews the history of stem teleost research. Existing phylogenies of stem teleosts (Gardiner *et al.*, 1960; Brito, 1997; Stewart, 1999; Poyato-Ariza & Wenz, 2002; Alvarado-Ortega, 2005; Hurley *et al.*, 2007; Zu & Wu, 2012; Arratia, 2017; López-Arbarello & Sferco, 2018 and Latimer & Giles, 2018) recover conflicting and often unstable tree shapes.

Chapter 2 (Atterby *et al.*, 2024, in review) presents a CT based redescription of *Dorsetichthys bechei*, a key taxon in investigating anatomy and relationships of early fossil neopterygians, based on two specimens from Lyme Regis: one of substantial historic significance (NHMUK PV P 1052, Rayner, 1948; Patterson, 1975), and one newly described (NHMUK PV P 73995). A comprehensive and up-to-date three-dimensional description of *D. bechei* now exists. In redescribing this important and iconic taxon, a long-standing issue regarding the reconciliation of flattened dermal skeletons (Nybelin, 1966) and three-dimensionally preserved braincase (Rayner, 1948; Patterson, 1975) specimens was clarified and novel anatomical features to support a revision of this taxon's phylogeny and ecology were discovered. Furthermore, this study enabled the clarification of the presence of features previously undescribed but proposed as diagnostic of Dorsetichthyiformes (Arratia, 2013; 2017) such as the quadratojugal process and surangular bone. Conversely, the inverse of key character states used to previously resolve *D. bechei* outside of

Pholidophoriformes (Arratia, 2013; 2017) and closer to the teleost crown were also found, including the absence of a postarticular process and the presence of a prearticular. In contrast to recent analyses (e.g., López-Arbarello & Sferco 2018, Gouiric-Cavalli & Arratia, 2022) these results suggest that *D. bechei* may still belong to Pholidophoriformes. Previous work has also inferred the presence of a mobile upper jaw. Here, this feature was confirmed with evidence of a foramen in the ethmoid to accommodate the anterior processes of the maxilla and premaxilla. Furthermore, elaborate gill rakers were observed in *D. bechei* for the first time, including rakers associated with the medial surface of the hyomandibular, suggests the presence of a pseudobranch. These novel observations of the upper jaw and gill skeleton indicate that *D. bechei* was capable of suspension filter feeding, which supports a brief observation by Rayner (1948, pg. 328) that the small teeth of *D. bechei* suggest it may have been planktivorous.

Chapter 3 presents a CT and synchrotron based redescription of NHMUK PV P 9843 and 9844; two enigmatic isolated braincases previously referred to *“Aspidorhynchus”* (Woodward, 1918; Rayner, 1948). The braincase and – for first time for NHMUK PV P 9843 – the endocast of both specimens were described. Though both specimens have been described in detail previously (Rayner, 1948; Patterson, 1975), NHMUK PV P 9843 and 9844 have been excluded from phylogenetic analyses due to their incompleteness (Gardiner *et al.*, 1996). Here, the specimens were introduced (as a single terminal) to a revised phylogenetic matrix based on Giles *et al.* (2023), which incorporates a broad set of braincase and endocast characters. Following recent qualitative assessments of their affinity (Maisey, 1991; 1999; Gardiner *et al.*, 1996) based on the presence of an infraorbital canal-bearing innerorbital process and an elongate dermopterotic, this study finds specimens likely

represent a new genus of Ionoscopidae. However, in contrast to the same studies, this new genus is recovered as sister to *“Ionoscopus” cyprinoides* as opposed to *Oshunia brevis*. This is based on several shared features of both the braincase and endocast, including the presence of a pterotic bone, the distal position of the innerorbital flange and a posterior diverticulum on the posterior semi-circular canal – a relatively novel feature recognised in NHMUK PV P 9844 by Giles *et al.* (2018) and now known in NHMUK PV P 9843 and *“I” cyprinoides* (NHMUK PV OR 37795a). Furthermore. character distribution within Ionoscopiformes was found to be poorly optimised due to a lack of overlapping anatomy within this assemblage; *“I.” cyprinoides* and *O. brevis* are known from a combination of well-preserved braincases and associated dermal skeletons, the remaining skeleton of NHMUK PV P 9843 and 9844 is unknown while other related taxa are known exclusively from poorly preserved dermal remains (i.e., *Ionoscopus petrarojae* and *Spathiurus dorsalis* (Hossney *et al.*, 2020), which has limited the analysis resolution. Recent work has also proposed that *“I.” cyprinoides* does not belong to *Ionoscopus* (Maisey, 1999; Taverne & Capasso, 2016; Ebert (2018). Hossney *et al.*, 2020 also found that *I. petrarojae* and *S. dorsalis* form a clade to the omission of *“I.” cyprinoides* as is also recovered here. However, a specific clade/ new genus for *“I.” cyprinoides* has not yet been identified. Here, the proposed sister relationship between NHMUK PV P 9843 and 9844 and *“I.” cyprinoides* may suggest that these specimens form a new genus.

Chapter 4 presents a CT and synchrotron based redescription of the first aspidorhynchid braincase *(Richmondichthys sweeti)* to be described in the literature (Etheridge and Woodward, 1891) and presents the first digital reconstruction of an aspidorhynchiform endocast. This revealed key character transitions in the endocast of one of the earliest diverging teleosts, such as the loss of the lateral cranial canal, a

loss which is convergent within some crown teleosts such as *Elops* and *Hiodon*. Chapter 4 also presents a detailed description of an exceptionally preserved, articulated specimen of *Pachycormus macropterus*, clarifying the arrangement and number of small, often disarticulated elements such as coronoids from past anatomical descriptions (e.g., Lehman, 1949; Patterson, 1975, Mainwaring, 1978, Cawley *et al.*, 2019) Furthermore, in contrast to Friedman *et al.* (2010) and Cooper & Maxwell (2022), an inflated anterior coronoid and large fang-like teeth on the anterior dermopalatines and coronoids are observed for the first time, challenging previous claims of an affinity with the SFC. Lehman, (1949) and Mainwaring (1978) described smooth dorsal margins of the anterior ceratohyals, here, a distinct notch which has not been recognised previously was also recognised. This chapter also clarifies the morphology of the endoskeletal pectoral fin and axial skeleton, including its visualisation in three-dimensions for the first time. In contrast to past work (Jessen, 1972; Mainwaring, 1978) a total of five paired proximal radials were observed, and it was found that the supraneurals form a single medial row as opposed to a pair of rows, as previously inferred from flattened specimens (Bartsh, 1988; Wenz, 1968, Cooper & Maxwell, 2022). These data were introduced to a revised phylogenetic model of early Neopterygii, revealing very limited support for Aspidorhynchoidei – a recently recovered clade uniting aspidorhynchiforms and pachycormiforms.

Chapter 5 summarises the thesis and explores future directions in the field by quantifying some of the challenges which continue to effect stem teleost research. inappropriate outgroups leading to difficulty in polarising character states, incomplete taxon sampling within the ingroup, and poorly constructed characters. Furthermore, incomplete anatomical descriptions hamper a complete understanding of character transformation within groups of interest. Improved descriptions of known taxa are

needed to feed into an expanded and revised character-by-taxon matrix combined with updated phylogenetic analyses to investigate patterns of relationships and future macroevolutionary of the teleost stem.

The results of this work corroborate the use of CT scanning as a key tool to developing a better understanding of the anatomy and therefore relationships of three-dimensionally preserved fossil specimens in palaeoichthology (Schultze, 1991; Maisey, 2001; 2005; Tapanila & Pruitt, 2013; Friedman *et al.*, 2015; Dearden *et al.*, 2023) but under-utilised in study of early teleosts (e.g., Cawley *et al.*, 2019, pg. 296).

## 5.2 Future Work and Directions

### 5.2.1 Anatomical innovations

This thesis provides a major step forward in the three-dimensional visualisation of the internal anatomy of key stem teleost taxa by providing detailed models of articulated anatomical features. Previous research has focused primarily on external anatomy (e.g., Arratia. 2013, 2017) and/or rely upon the compositing of scant three-dimensionally preserved specimens with two-dimensionally preserved, flattened specimens. This work demonstrates the exceptional value of CT and synchrotron scanning as a tool for investigating the anatomy and relationships of early neopterygians. However, there remain countess taxa which contain specimens viable for scanning. Future work should continue to scan viable specimens to identify hidden novel features. By acquiring new anatomical data, it is possible to find phylogenetically valuable and informative features which can provide new grouping information. This thesis demonstrates that CT and Synchrotron scanning of even historic specimens is an ideal avenue to improve understanding of the teleost stem.

It was long understood that recovering the endocast was the only way to visualise the neuroanatomy of fossil fishes, even though the endocast was only an approximation of the brain. However, in 2023, Figueroa *et al.,* uncovered the oldest preserved actinopterygian brain in *Coccocephalus wildi*. They concluded that while the endocast gives a generally accurate impression of the brain, there can be a major discrepancy in volume between an endocast and the brain itself (Figueroa *et al.* (2023, fig. 3). While fossilised brains are an exceptional rarity, so cannot be relied upon as readily as endocasts, it is possible that interest in endocasts could wane as more exceptionally preserved specimens are identified.

### 5.2.2 Visualising Patterns of Uncertainty

This thesis attempts to overcome some of the numerous challenges that have given rise to numerous conflicting phylogenetic positions of taxa associated with the teleost stem, which were outlined in Chapter 1. Chapter 5 attempts to further quantify some of these challenges, in order to demonstrate why stem teleosts are contentious and are an important area for future study:

- Are taxa associated with the teleost stem of equal interest? Or are some taxa studied more frequently than others?
- Do existing analyses feature a wide breadth of taxa? Are certain taxa studied in isolation? Are some taxa regularly ignored? Are groups represented by a single species or multiple species?
- Are there anatomical biases? Are certain regions of anatomy over or underrepresented in existing analyses?

**Compiling Character Matrices**

To investigate potential sources of uncertainty, 11 character-by-taxon matrices from a range of physical and digital sources have been collated and standardised into NEXUS and TNT formats using Mesquite (Maddison & Maddison, 2019). Matrices were chosen purely for their relevance to investigating the relationships of taxa associated with the teleost stem (Table 5.1). Minor adjustments were made to several datasets to ensure the token for expressing an unknown or multistate character was consistent. Here, a “token” refers to the integer or symbol used to represent a morphological character’s state (*sensu* Brazeau, 2011).

**Table 5.1: Representation of taxa allied with the teleost stem within the 11 matrices investigated.** Blank cells indicate the absence of said group, cells shaded blue highlight where just one taxon is used to represent the given group and cells shaded dark blue indicate where more than one taxon is representing the said group; number of taxa is also given. Asterisk (*) indicates inclusion of hypothetical taxa in the outgroup.

| | Latimer & Giles, 2018 | López-Arbarello & Sferco, 2018 | Arratia, 2017 | Friedman, 2012 | Xu & Wu, 2012 | Hurley *et al.*, 2007 | Alvarado-Ortega, 2005 | Poyato-Ariza & Wenz, 2002 | Stewart, 1999 | Brito, 1997 | Gardiner *et al.*, 1996 |
|---|---|---|---|---|---|---|---|---|---|---|---|
| **dapediids** | 9 | 3 | | | 1 | 1 | | | | | 1 |
| **pycnodonts** | 6 | | | | | 1 | | 28 | | | 1 |
| **pachycormids** | | 1 | 6 | 15 | | 1 | 1 | | | 1 | 1 |
| **aspidorhynchids** | | 1 | 3 | | | | | | | 3 | |
| **ichthyodectids** | | 1 | | | | | 20 | | 10 | | |
| **leptolepids** | 1 | 1 | 1 | | 1 | | | | 1 | | |
| **pholidophorids** | | 7 | 9 | | 1 | 1 | | | 1 | | 1 |
| ***Dorsetichthys*** | 1 | 1 | 1 | 1 | | | | | | 1 | |
| ***Hulettia*** | 1 | | | | | 1 | | | | | |
| ***Prohalecites*** | | | 1 | | | | | | | | |
| **Total no. of taxa** | 110 | 99 | 42 | 29 | 15 | 31 | 23* | 33* | 15 | 14 | 12 |

**Taxa:** In order to examine the representation of taxa in previous phylogenetic analyses, the frequency of key taxon across 11 gathered matrices were recorded (Table 5.1). While a broad range of taxa associated with the teleost stem are represented in the literature, taxonomic representation within individual matrices is often sparse. There were very few studies that united and integrated taxa from across the stem into a single analysis. In existing literature, broad groups are more often studied in near total isolation of the broader stem. For example, Poyato-Ariza & Wenz (2002, 2015), Alvarado-Ortega (2005) and Friedman *et al.* (2012) only target the interrelationships of pycnodonts, ichthyodectids and pachycormids respectively. Furthermore, analyses that do incorporate a range of groups usually rely on a single exemplary specimen to represent the assemblage. For example, in López-Arbarello & Sferco's (2018) comprehensive reassessment of neopterygian characters and interrelationships, pachycormids are only represented by *Pachycormus*, aspidorhynchids are only represented by *Aspidorhynchus*, ichthyodectids are only represented by *Thrissops* and leptolepids are only represented by *Leptolepis*.

Also of note is the choice of outgroups in these examples, which range from *Entelognathus* (Latimer & Giles, 2018) – a late Silurian stem gnathostome (Zhu *et al.*, 2013) – to *Pholidophorus* (Stewart, 1999) – the mid-Triassic type genus of Pholidophoridae. The most commonly used outgroup is *Pteronisculus* (Brito, 1997 and López-Arbarello & Sferco, 2018) – an early Triassic stem actinopterygian of uncertain phylogenetic affinities (Xu *et al.*, 2014; Ren & Xu 2021; Cavicchini *et al*., 2024). Most notable is that the Poyato-Ariza & Wenz (2002) and Alvarado-Ortega (2005) analyses both feature hypothetical taxa as their outgroups.

**Characters**: In order to compare the distribution of characters across multiple matrices, each character list was subdivided into 11 discrete partitions. Each partition represents a distinct anatomical region (Table 5.2).

**Table 5.2: Character partitions used to divide the 11 matrices investigated in this review.**

| Partition | Description |
|---|---|
| dermal skull | Dermal cranial bones, e.g., rostral, frontals, parietals, and orbitals. |
| jaws and palate | Upper and lower jaws, palate, and dentition, e.g., maxilla, dentary, coronoids, and vomers. |
| operculogular system | Opercular series, as well as gulars and cheek bones. |
| braincase & endocast | Braincase, such the presence of individual ossifications, and the endocast, such as the bony labyrinth. |
| hyoid arch | Hyomandibula, ceratohyal, interhyoid elements, and hypohyal. |
| gill skeleton | Gill arches and branchial bones. |
| dermal shoulder girdle | Cleithrum, clavicles and scapulocoracoid. |
| paired fins | Endo- and exoskeletal characters relating to the pectoral and pelvic fins. |
| median fins | Any character relating to the dorsal, anal, and caudal fins. |
| postcranial | Characters of the vertebrae and body scales, as well as some miscellaneous characters such as overall body shape and length. |
| soft tissue | Any characters concerning soft tissue, such as organs and musculature. |

The dermal skull, jaws and palate and braincase and endocast are generally the most character dense partitions. The dermal skull accounts for ~25% of the character list in the five most recent matrices, while the braincase and endocast often form the largest partition by far, even in the older studies, yielding 41% of the total character list in Gardiner *et al.* (1996). However, the Poyato-Ariza & Wenz, (2002) matrix, which is based almost exclusively on pycnodont morphology, forms a major exception, with only 1% of its characters pertaining to the braincase and endocast. Many partitions only contain a handful of characters. The hyoid arch and gill skeleton

constitute a very minor part of most matrices, e.g., Gardiner *et al.* (1996), Brito (1997) and Stewart (1999). The least character dense partition is soft tissue, as only Arratia (2017) uses soft tissue characters to support relationships among extant crown taxa.

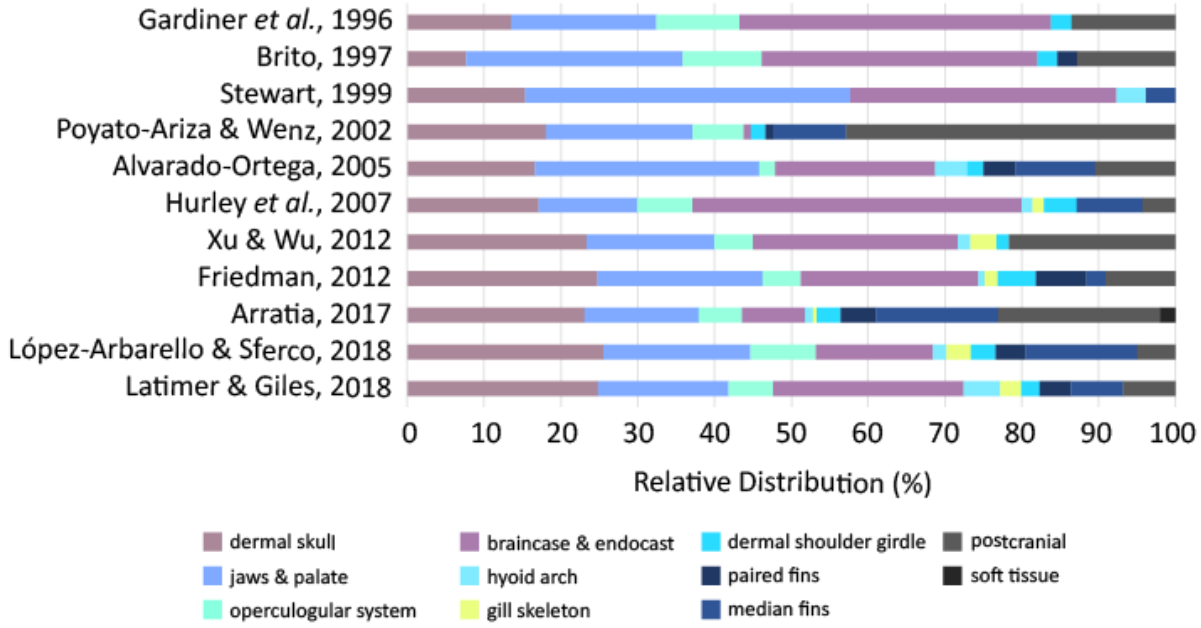


**Figure 5.1: Distribution and proportion of characters per anatomical partition in previously published character matrices.**

### Character Completeness Metric

To investigate which anatomical regions are best preserved/ known in stem teleosts, the Character Completeness Metric (CCM), as first proposed by Mannion & Upchurch (2010), was used to quantify how frequently each character was adequately preserved such that it could be coded. Ideally, CCM would be calculated in tandem with the actual Skeletal Completeness Metric, however that is beyond the scope of this investigation. The CCM provides an approximate analogue for the skeletal completeness of each taxon, and while CCM methods have previously been used to successfully quantify the completeness of a wide range of vertebrates, it has seen no previous application with ray-finned fishes. The CCM was determined for each species across all eleven

matrices by dividing the total number of missing characters by the total number of scored and missing characters per taxon. By manually ensuring the consistent use of tokens across each matrix, it was possible to omit non-applicable characters from this test (i.e., characters that cannot be scored due to logical incongruities, such as the length of an element that was already scored as absent), to avoid any subsequent dependent characters overinflating a taxon's incompleteness (as highlighted by Maddison, 1993).

Here, the completeness of each taxon per character, and each character per taxon was calculated, revealing that certain genera and anatomical partitions were far better preserved than others (Table 5.3). On average, the dermal skull and jaws and palate were the best-preserved anatomical partitions, followed closely by the operculogular system and braincase and endocast. By far the least well-preserved partitions are the gill skeleton, hyoid arch and, unsurprisingly, soft tissue.

**Table 5.3: Average character completeness per partition across each matrix.**

| | Latimer & Giles, 2018 | López-Arbarello & Sferco, 2018 | Arratia, 2017 | Friedman, 2012 | Xu & Wu, 2012 | Hurley *et al.*, 2007 | Alvarado-Ortega, 2005 | Poyato-Ariza & Wenz, 2002 | Stewart, 1999 | Brito, 1997 | Gardiner *et al.*, 1996 | AVERAGE |
|---|---|---|---|---|---|---|---|---|---|---|---|---|
| **Dermal Skull** | 76.7 | 81.9 | 92 | 73 | 94.2 | 87.4 | 75.9 | 78.5 | 76.7 | 100 | 94.4 | **84.6** |
| **Jaws and Palate** | 59.7 | 72.8 | 84.4 | 70.7 | 88.7 | 84.3 | 87.1 | 77.5 | 88.5 | 99.4 | 84.6 | **81.6** |
| **Operculogular System** | 80.2 | 85.9 | 98.3 | 83.2 | 97.8 | 93.1 | 70.8 | 58.8 | 0 | 100 | 0 | **69.8** |
| **Braincase and Endocast** | 30.4 | 37.3 | 66.5 | 50.7 | 70.4 | 61.4 | 73.8 | 91.2 | 75.6 | 93.9 | 74 | **65.9** |
| **Hyoid Arch** | 37.3 | 40.4 | 63.1 | 58.6 | 86.7 | 82.8 | 64.6 | 0 | 80 | 0 | 69.2 | **53** |
| **Gill Skeleton** | 29.3 | 19.8 | 66.7 | 29.3 | 66.7 | 51.7 | 0 | 0 | 0 | 0 | 0 | **24** |
| **Dermal Shoulder Girdle** | 56.1 | 59 | 77.6 | 62.1 | 93.3 | 70.1 | 0 | 86.8 | 0 | 100 | 0 | **55** |
| **Paired Fins** | 50.2 | 61.4 | 75.1 | 73.6 | 0 | 0 | 83.3 | 73.5 | 0 | 100 | 0 | **47** |
| **Median Fins** | 52 | 66.6 | 83.6 | 64.4 | 0 | 81 | 70.8 | 80 | 86.7 | 0 | 0 | **53.2** |
| **Postcranial** | 56.3 | 47.6 | 76.2 | 76.5 | 92.8 | 72.4 | 73.3 | 80.2 | 0 | 92.9 | 81.3 | **68.1** |
| **Soft Tissue** | 0 | 0 | 14.3 | 0 | 0 | 0 | 0 | 0 | 0 | 0 | 0 | **1.3** |

## Leaf Stability

Finally, in order to assess the impact of character completeness on previously recovered relationships, the maximum and residual maximum leaf stability of taxa in the Latimer & Giles (2018) and Arratia (2017) datasets were examined. Phylogenetic analyses were conducted in TNT v. 1.5 (Goloboff & Catalano, 2016), and exclusively used pre-existing morphological character-based data. To procure the leaf stability of individual taxa, a bootstrap analysis was performed with 1000 pseudoreplicates and 10 internal replications of a TBR (tree dissection reconnection) algorithm. A custom script (A.4.2) was used to complete the analysis to ease data handling, by outputting all 4030 bootstrap trees into a single, continuous file from which subsamples could be

made. Using R v. 4.0.3. (R Core Team, 2020), 30 subsamples of 100 randomly selected trees were produced. Each subsample (i.e., each individual packet of 100 bootstrap trees in Newick format) were uploaded to the web version of RogueNaRok (Aberer *et al.*, 2013). RogueNaRok identifies wandering taxa and calculates maximum leaf stability. The maximum leaf stability of each taxon across all 30 subsamples was taken, and an average stability was calculated in Excel. This was plotted against taxon age (Figs. 5.2A, 5.3A) to compare the stability of taxa associated with the teleost stem with Palaeozoic and Cenozoic actinopterygians.

More completely coded taxa may be expected to have higher leaf stability values. To counter this, the maximum leaf stability was corrected for taxonomic incompleteness by calculating the residuals of a linear regression between the average maximum leaf stability and the CCM of each taxon (Figs. 5.2B, 5.3B) – using the R package 'Ape' (Paradis & Schliep, 2019). Each taxon was also assigned an approximate midpoint age, and then separated into a 24-Myr bins, allowing both the maximum and residual maximum leaf stability as well as the moving average for both plots to be mapped over geological time. This was achieved with the R package Geoscale (Bell, 2015).

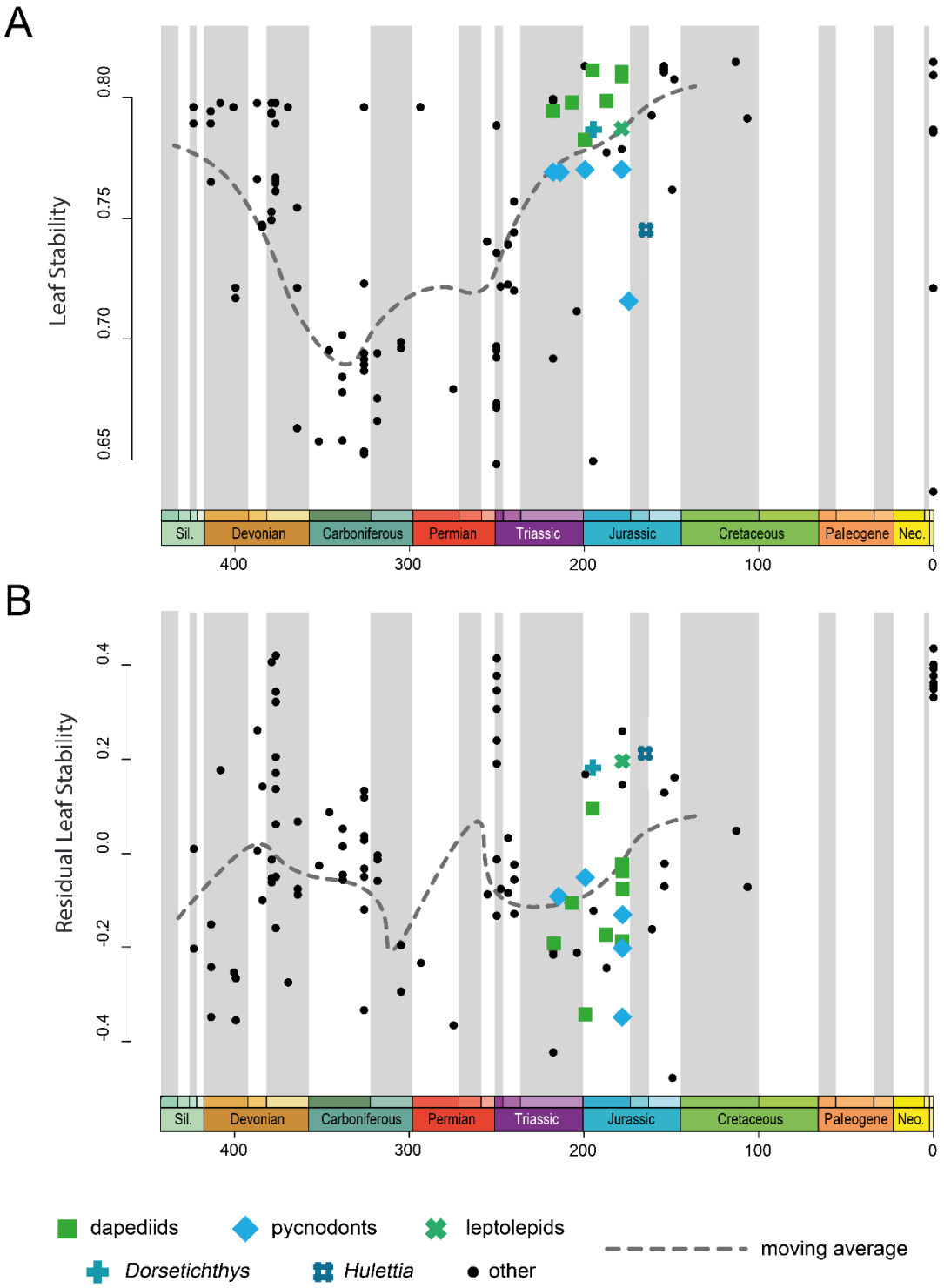


**Figure 5.2: Stability of taxa associated with the teleost stem, Latimer & Giles (2018)** (A) Raw maximum leaf stability plotted against taxon age (B). Residuals from a linear regression of maximum leaf stability against CCM, plotted by taxon age.

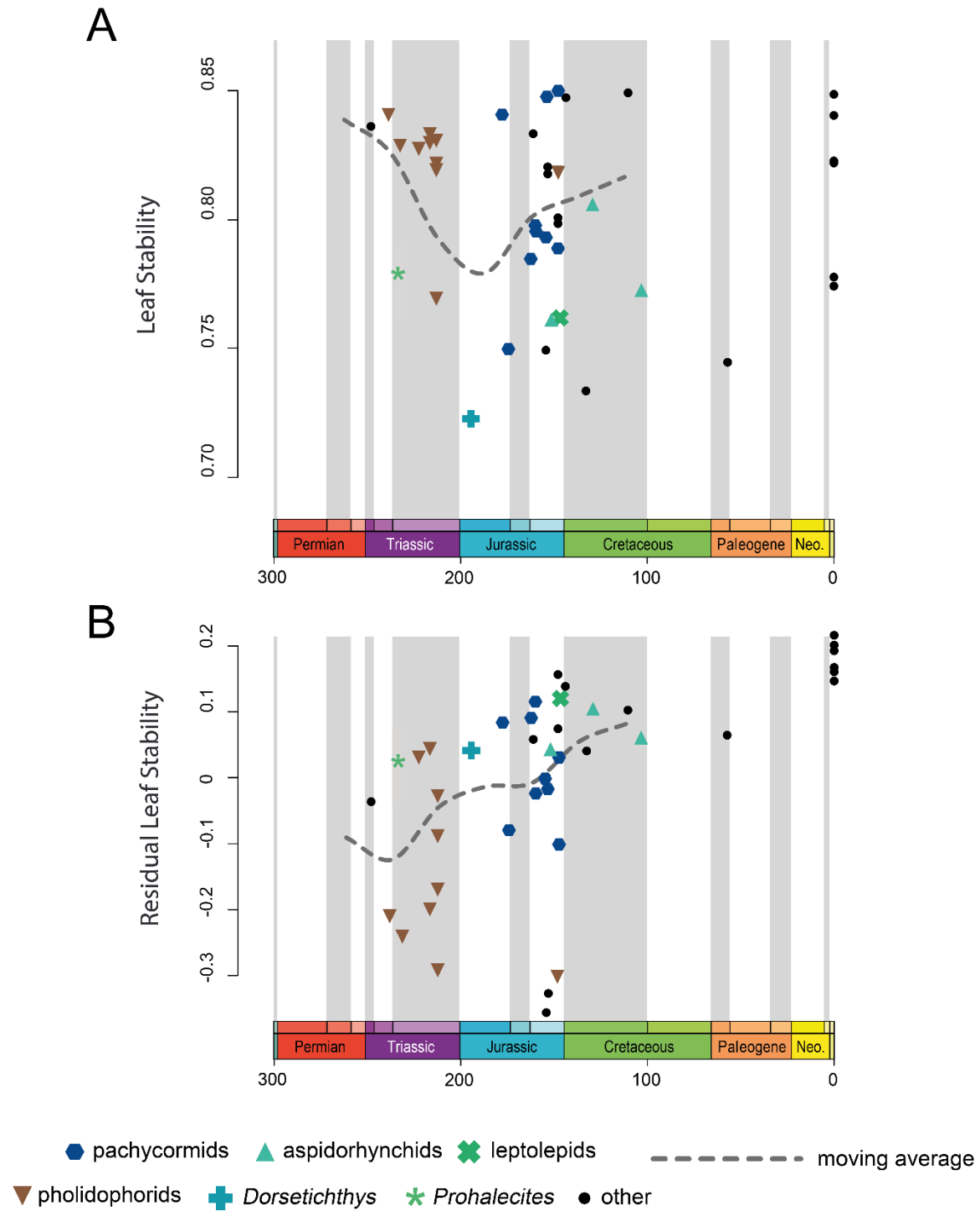


**Figure 5.3: Stability of taxa associated with the teleost stem, Arratia (2017)** (A) Raw maximum leaf stability plotted against taxon age (B). Residuals from a linear regression of maximum leaf stability plotted against CCM, plotted by taxon age.

Taxa previously associated with the teleost stem form only a small portion of the Latimer & Giles (2018) dataset, and initially appear stable (Fig. 5.2A). Dapediids are especially stable, falling above the moving average, while pycnodonts are comparatively less stable, falling below the moving average. In contrast, the Arratia (2017) dataset is composed primarily of taxa associated with the teleost stem. Triassic taxa, including pholidophorids and *Prohalecites* are relatively stable. There is an apparent notable dip in leaf stability in Jurassic taxa, such as pachycormids and *Dorsetichthys* (Fig. 5.3A). However, once character completeness is accounted for (Figs. 5.2B, 5.3B), taxa previously associated with the teleost stem are revealed to be very unstable in both data sets. Conversely, other (non-teleost) taxa are revealed to be more stable the raw leaf stability suggests.

## 5.3 Discussion: Persistent Problems on The Teleost Stem

### 5.3.1 Anatomical Inconsistencies

**Trends in Anatomical Preservation and Representation**

There are major biases and gaps in the understanding of anatomy on the teleost stem. Although certain groups allied with the teleost stem are disproportionately prone to disarticulation, such as the giant pachycormids (Friedman, 2010), this is only a minor aspect of the greater issue. There are numerous well preserved, three-dimensional specimens readily available, but most of them lack up-to-date, complete descriptions. In particular, some recent descriptions of stem teleost braincases are quite stylised (e.g., Arratia, 2017) or given limited consideration (e.g., López-Arbarello & Sferco, 2018). As a result, potentially phylogenetically informative material is being lost.

There are several possible factors responsible for the uneven appreciation of stem teleost anatomy. The most complete anatomical partitions (Tables 5.2; 5.3), such as the dermal skull, jaws and palate, and operculogular system, tend to comprise

large, well ossified, externally visible features, including robust, plate-like elements, such as the skull roof, nasal, maxilla, dentary and operculum. In contrast, the least complete partitions, i.e., the gill skeleton and hyoid arch, consist of delicate, internal features that are less readily accessible unless the specimen has undergone CT or synchrotron scanning, or destructive preparation. This suggests there may be two main biases influencing the apparent completeness of taxa associated with the teleost stem; (1) the least complete anatomical partitions contain elements more likely to be lost to taphonomic processes (Smith *et al*., 1988), This could also account for the smaller discrepancies in incompleteness between the dermal skull and the jaws and palate, as the jaws and palate partition also includes delicate elements such as the vomers, prearticulars and coronoids. On the other hand, (2) the under of certain partitions suggests there may also be a bias in collection and research. Fossil fishes bearing externally visible features are more attractive to collectors (Hunter & Donovan, 2005; Cleary *et al*., 2015; Nanglu & Cullen, 2023) and more easily described, while smaller, internal features are less likely to be observed by a researcher.

Numerous geological and taphonomic biases have been proposed to account for the current state of several fossil assemblages, previously quantified by character or skeletal completeness metrics of other vertebrate groups (e.g., Cleary *et al.*, 2015; Tutin & Butler, 2017; Brown *et al.*, 2019; Cashmore & Butler, 2020; Schnetz *et al.*, 2022, 2024). However, this investigation is the first use of CCM with actinopterygians, Furthermore, without a solid phylogenetic foundation, accurately determining the possible taphonomic and anthropogenic factors and biases responsible for stem teleost completeness over time is difficult.

As expected, these trends point more towards an underuse of internal characters. This is exemplified by the braincase and endocast partition. Despite being

one of the most character dense anatomical partitions in many analyses (Fig. 5.1), the braincase and endocast are notably less complete than similarly character dense partitions, such as the dermal skull (Table 5.3), suggesting a tangible gap in the appreciation for these characters. This is because, unless the specimen was already disarticulated or heavily prepared (e.g., Mainwaring, 1975; Patterson, 1975) internal anatomical features are best observed with x-ray imaging methods. In addition, even in less well ossified or immature individuals, the braincase may be only partially mineralised and may therefore not be preserved in the fossil (Friedman & Giles, 2016).

As discussed, in contrast to early members of other key vertebrate radiations (e.g., Porro *et al.* 2015; Coates *et al.*, 2017) stem teleosts have received very little CT-based study, despite proving very successful in investigating early actinopterygians (Giles *et al.*, 2015, 2017, 2018; Argyriou *et al.*, 2018; Latimer & Giles, 2018; Schwarzhans *et al.*, 2018; Figueroa *et al.*, 2019, 2023). These studies have also revealed new morphologies, including potential synapomorphies, and new hypotheses of relationships. CT scanning therefore represents an important avenue in pursuing further issues on the teleost stem by providing additional morphological characters, improving their anatomical resolution and therefore strengthening support for phylogenetic hypotheses of relationships (Puttick *et al.,* 2016).

**Poorly Constructed Characters**

Although revealing new anatomical features and providing additional characters can improve an analysis, an abundance of characters does not negate the need for good character construction and implementation (Simões *et al.*, 2017). Recent decades have seen a wealth of literature on how to carefully construct phylogenetic characters (e.g., Patterson, 1982; Hawkins *et al.*, 1997; Forey & Kitching, 2000; Jenner, 2002; Wiens, 2003a, 2003b; Sereno, 2007; Brazeau, 2011; Brazeau & Friedman, 2014; Vogt,

2016; Vogt *et al.*, 2017; Simões *et al.*, 2017; Goloboff *et al.,* 2021). This thesis introduced a new phylogenetic analysis featuring a broad range of taxa associated with the teleost stem. However, although efforts were made to amend existing characters, there are instances of problematic character conceptualisation which this thesis relies upon that may limit its reliability, representing an area for improvement and further work. For example, c.4: “Premaxilla contributes to orbital margin [0] absent [1] present” (ch. 7 in Giles *et al.*, 2023) may be an unreliable character. Here, the “absent” state could encompass a wide range of conditions, which a phylogenetic analysis assumes to be equivalent (see Brazeau, 2011). Likewise, c.43: Teeth on maxilla [0] homogenous or irregular [1] increasing in size posteriorly (ch. 65 in Arratia, 2017) compresses two different states, “homogenous” and “irregular” into a single character state.

Furthermore, there are several characters that are subjective and/or ambiguous, such as c.240 Lachrymal [0] significantly smaller than orbit [1] equal in size to orbit appears self explanatory for most taxa, but there is ambiguity for taxa with large lachrymals. In some phylogenies, e.g., Friedman (2012), the elongate pectoral fins of pachycormids are coded as “scythe-like” or “sickle-like”. However, these are subjective descriptors. Liston *et al.* (2019) argued that this terminology is not appropriate; it is far better for accessibility and reproducibility to describe the morphology with precision, such as an aspect ratio. Character descriptions should generally employ precise, undated language to best ensure their accuracy and longevity. One of the best ways to ensure this is to sample taxa from across the stem and build characters that adequately reflect their diverse morphologies. These issues are likely the result of studying key taxa independently from other related

assemblages. Were analyses to include a wider breadth of taxa, it could force characters to be written more precisely and inclusively.

### 5.3.2 Inconsistent Relationships

**Non-Exhaustive Taxon Sampling**

The inadequate representation of relevant taxa in existing analyses may also contribute to the lack of consensus regarding the topology of the teleost stem. Once more, there is extensive literature about taxon sampling (e.g., Lecointre *et al.* 1993; Zwick & Hillis 2002; Hill 2005; Hedtke *et al.*2006; Heath *et al.* 2008), however there are persistent issues in how stem teleost taxa are represented in most phylogenies.

Many published trees only explore the interrelationships of one major taxonomic group at a time (Table 5.1), the interrelationships of which are usually already well supported. For instance, the internal arrangement and monophyly of pycnodonts is relatively well established (Nursall, 1996b; Poyato-Ariza, 1998; Kriwet, 2000, Poyato-Ariza & Wenz, 2002, 2005, 2015; Martin-Abad & Poyato-Ariza, 2013, 2015, Ebert & Kölbl-Ebert, 2018), but their relationships to other neopterygian assemblages, including other deep-bodied radiations such as dapediids, remain controversial. There is only one recent analysis (Latimer & Giles, 2018) where both dapediids and pycnodonts are relatively well represented in a broad analysis. Though clade-specific work is still invaluable, it does not address broader phylogenetic questions.

Conversely, studies that explicitly consider a wide range of neopterygian groups usually represent speciose assemblages only by a single, exemplar taxa. For example, although the interrelationships of pachycormids have received much study (e.g., Kear, 2010; Liston, 2008; Friedman, 2010, 2012; Wretman *et al.*, 2016), their

occurrence in most wider analyses is usually reduced to a single taxon, typically *Pachycormus macropterus*. Though this can reduce the computational workload of an analysis and compensate for a lack of taxa (Rosenberg & Kumar, 2001), employing a sole representative taxon in place of a more diverse sample of specimens can impart serious biases into an analysis (Mansion *et al.*, 2012). While *P. macropterus* is arguably the best known pachycormid, its phylogenetic position remains somewhat contested (Cawley *et al.*, 2019) and it is not morphologically or ecologically exemplary of pachycormids as a whole. While new character data and improving existing character definitions has an equal if not greater positive impact on an analysis than adding new taxa (Huelsenbeck, 1991), a fully articulated, exceptionally preserved specimen of any taxon cannot perfectly represent an entire assemblage, as any different taxon in its place could result in an entirely different outcome (Nylander, 2001). Furthermore, condensing a complex group to one potentially problematic taxon can propagate errors across tree topologies, can unintentionally draw unrelated taxa together and vice versa and ultimately reducing the accuracy of a given phylogenetic analysis (Hedtke *et al.*, 2006; Heath *et al.*, 2008). In the absence of a broad, overarching analysis, in which key members associated with the teleost stem are poorly sampled, understanding of teleost stem phylogeny is incomplete and is therefore worth addressing in future work.

**Inappropriate or hypothetical outgroups**

The choice of outgroup can radically alter the result of a phylogenetic analysis, therefore, selecting an appropriate outgroup is exceptionally important. The methodology of outgroup selection has been discussed extensively (e.g., Watrous & Wheeler, 1981; Maddison *et al.*, 1998; Nixon & Carpenter; 1993; Lyons-Weiler *et al.*, 1998) but issues persistent in the study of stem teleosts. Typically, the choice of

outgroup should be sufficiently removed from the ingroup to allow character polarity to be adequately determined (Maddison *et al.*, 1984). However, Maddison's doublet rule is limited in that it assumes the ingroup is monophyletic and that the outgroup is fully resolved (Nixon & Carpenter; 1993).

Given the general lack of broad, overarching analyses of the teleost stem, existing analyses of taxa associated with the stem use outgroups that are very closely related to the ingroup. Stewart (1999) uses *Pholidophorus*, which is very closely related to the ingroup (ichthyodectids) and has a contested phylogenetic position. The stem gnathostome *Entelognathus*, as used by Giles *et al*. (2023) a more suitable outgroup when assessing patterns of relationship within actinopterygians, as it does not belong to the immediate sister group (i.e. sarcopterygians) of the ingroup, and the next closest outgroup (i.e. chondrichthyans) display many inapplicable character scores, presenting difficulties when assessing character polarity (Maddison *et al.*, 1998). However, if the outgroup is too distantly related to the ingroup, subsequent characters may be needed to sufficiently represent its disparate morphology that would otherwise be inapplicable for much of the remaining ingroup at the root of the tree. As such, this thesis uses *Mimipiscis* and *Moythomasia* as outgroup taxa - Devonian actinopterygians in which the endo- and exoskeletal morphology is very well known.

Some authors polarise their analyses on one or more hypothetical outgroup taxa (e.g., Poyato-Ariza & Wenz, 2002; Alvarado-Ortega, 2005). However, this can force problematic constraints on tree topology and is a practice best avoided (Bryant, 1997). Arratia (1999, 2001, 2004) tested the use of hypothetical outgroups and demonstrated the instability of neopterygian interrelationships by running multiple analyses with different outgroups. Using *Watsonulus*, an early Triassic parasemionotid

(holostean) (Olsen, 1984) is often used as an outgroup in investigations of teleost phylogeny a clade containing pachycormids and dapediids was resolved as the closest sister group to crown teleosts within the data set. However, switching to a hypothetical outgroup and excluding *Watsonulus* recovered a clade of pycnodonts and aspidorhynchids in this position instead, a result not previously recovered in any other analysis. Due to their potential to produce wildly variable results, hypothetical outgroups should be generally avoided.

### 5.3.3 Patterns of macroevolution

Due to a lack of consensus on their phylogeny, the exact timings of speciation events on the teleost stem are in constant flux. As a result, macroevolutionary patterns cannot be confidently explored. There are a handful of preliminary studies but with limited results. For example, aspidorhynchid fossils are almost globally distributed, suggests aspidorhynchids were once distributed across Pangea early in its breakup, before being separated by continental drift throughout the Mesozoic Brito (1997). Conversely, Cavin (2008) investigated palaeobiogeographic patterns of dispersal and vicariance in multiple stem teleosts and related taxa, including, pachycormids, aspidorhynchids, ichthyodectids and pycnodonts, but was unable to find any strong palaeogeographic signal using previous phylogenies (Lambers. 1992; Brito, 1997; Poyato-Ariza & Wenz, 2002; Cavin & Forey, 2008). Perhaps a broad phylogeny may enable more fruitful investigations into stem teleost macroevolution.

Another active area of study that demands further attention is the study of the driving factors behind teleost evolution, to understand how their vast modern diversity and array of unique adaptations came about. An important intrinsic factor that has been implicated is whole genome duplication. Davesne *et al.* (2021) examined osteocyte cavities in the fossil bone of several stem teleosts, including *Eubiodectes*

and *Leptolepis*, to estimate genome sizes and locate when the teleost WGD had occurred. The authors discovered that WGD occurred earlier on the stem than previously thought – prior to the diversification of Mesozoic stem teleosts, the relationships and divergence time estimates of which were based on a composite phylogeny of previously published trees (e.g., Brito 1997; Poyato-Ariza & Wenz, 2002; Arratia, 2017; Latimer & Giles, 2018; López-Arbarello & Sferco, 2018). They concluded that WGD was not the immediate driving force in teleost diversification, and that teleosts did not undergo rapid body shape evolution or ecological diversification until at the late Jurassic/ early Cretaceous. This suggests that additional, possible extrinsic pressures played a greater role in the teleost radiation however they are unknown, and further work is needed.

An improved phylogeny would also help clarify macroevolutionary studies in which stem teleosts are themselves potentially exerting pressure on other groups. The so-called Mesozoic Marine Revolution (MMR) for instance, is a theoretical evolutionary arms race, in which the emergence of durophageous predators coincided with a major faunal turnover in benthic marine molluscs throughout the Mesozoic. It has been proposed that the first appearance of durophageous predatory teleosts directly contributed to the preferential survival of sturdier, shelled molluscs, leading to a gradual shift towards infaunalisation (McRoberts, 2001; Mariusz & Salamon, 2008; Salamon *et al.,* 2012).

These studies provide only a glimpse into the vast potential for studying macroevolutionary patterns in stem teleosts, but with the aid of an improved phylogenetic model, new insights could be gained. Given that the branching patterns, divergence times and affinities of these taxa are highly prone to change and can easily be altered depending on the character and taxon sampling and choice of outgroup,

producing a revised phylogeny that uses well-constructed characters, encompasses a wide range of available taxa, and uses appropriate outgroups would it improve confidence in existing macroevolutionary analyses, but would open the door for future macroevolutionary analyses to be performed. Stem teleosts are in essence an untapped reserve of potential studies, but few analyses can be carried out, until the foundation of a solid phylogeny is in place.

This thesis has produced a new phylogenetic hypothesis for early neopterygians, incorporating novel internal anatomical data of the elusive and enigmatic teleost stem. These results serve as a solid foundation to underlie future analyses. This new model, incorporating new data, helps build a comprehensive picture of the patterns of divergence of the most successful living vertebrate group.

# LIST OF REFERENCES


Abel, O. (1914) *Die vorzeitlichen säugetiere*. G. Fischer.

Agassiz, L. (1832) “Untersuchungen über die fossilen Fische der Lias-Formation,” *Neues Jahrbuch für Mineralogie, Geognosie, Geologie und Petrefaktenkunde*, 3, pp. 139–149.

Agassiz, L. (no date) “1833–1844. Recherches sur les Poissons Fossiles, Vols. 1–5,” *Imprimerie de Petitpierre, Neuchâtel, Switzerland* [Preprint].

Ali, M.-A. *et al.* (1976) “Descriptions,” *Retinas of Fishes: An Atlas*, pp. 17–253.

Allis, E.P. (1922) “The Cranial Anatomy of Polypterus, with Special Reference to Polypterus bichir.,” *Journal of anatomy*, 56(Pt 3-4), pp. 189-294.43.

Alvarado Ortega, J. (2005) *Sistematica de los peces Ichthyodectiformes de la cantera Tlayua, Puebla, Mexico*.

Alvarado-Ortega, J. and Brito, P.M. (2010) “A new ichthyodectiform (Actinopterygii, Teleostei) from the Lower Cretaceous Marizal Formation, north-east Brazil,” *Palaeontology*, 53(2), pp. 297–306. Available at: https://doi.org/10.1111/j.1475-4983.2010.00935.x.

Alvarado-Ortega, J. and Espinosa-Arrubarrena, L. (2008) “A new genus of ionoscopiform fish (Halecomorphi) from the Lower Cretaceous (Albian) lithographic limestones of the Tlayúa Quarry, Puebla, Mexico,” *Journal of Paleontology*, 82(1), pp. 163–175. Available at: https://doi.org/10.1666/04-152.1.

Amalfitano, J. *et al.* (2017) “A reappraisal of the Italian record of the Cretaceous pachycormid fish Protosphyraena Leidy, 1857,” *Rivista Italiana di Paleontologia e Stratigrafia*, 123, pp. 475–485.

Amores, A. *et al.* (1998) “Zebrafish *hox* Clusters and Vertebrate Genome Evolution,” *Science*, 282(5394), pp. 1711–1714. Available at: https://doi.org/10.1126/science.282.5394.1711.

Argyriou, T. *et al.* (2018) “Internal cranial anatomy of Early Triassic species of †Saurichthys (Actinopterygii: †Saurichthyiformes): implications for the phylogenetic placement of †saurichthyiforms,” *BMC Evolutionary Biology*, 18(1), p. 161. Available at: https://doi.org/10.1186/s12862-018-1264-4.

Arratia, G. (1998) “Basal Teleosts and Teleostean Phylogeny: Response to C. Patterson,” *Copeia*, 1998(4), p. 1109. Available at: https://doi.org/10.2307/1447369.

Arratia, G. (1999) “The monophyly of Teleostei and stem-group teleosts,” in *Mesozoic Fishes*. Verlag Dr. F. Pfeil München, pp. 265–334.

Arratia, G. (2001) “The sister-group of Teleostei: consensus and disagreements,” *Journal of Vertebrate Paleontology*, 21(4), pp. 767–773.

Arratia, G. (2004) “Mesozoic halecostomes and the early radiation of teleosts,” in *Mesozoic Fishes*. Verlag Dr. F. Pfeil München, pp. 279–315.

Arratia, G. (2008a) “Actinopterygian postcranial skeleton with special reference to the diversity of fin ray elements, and the problem of identifying homologies,” *Mesozoic fishes*, 4, pp. 49–101.

Arratia, G. (2008b) “Remarkable teleostean fishes from the Late Jurassic of southern Germany and their phylogenetic relationships,” *Fossil Record*, 3(1), pp. 137–179. Available at: https://doi.org/10.1002/mmng.20000030108.

Arratia, G. (2013) “Morphology, taxonomy, and phylogeny of Triassic pholidophorid fishes (Actinopterygii, Teleostei),” *Journal of Vertebrate Paleontology*, 33(sup1), pp. 1–138. Available at: https://doi.org/10.1080/02724634.2013.835642.

Arratia, G. (2015) “Complexities of early Teleostei and the evolution of particular morphological structures through time,” *Copeia*, 103(4), pp. 999–1025.

Arratia, G. (2016) “New remarkable Late Jurassic teleosts from southern Germany: Ascalaboidae n. fam., its content, morphology, and phylogenetic relationships,” *Fossil Record*, 19(1), pp. 31–59. Available at: https://doi.org/10.5194/fr-19-31-2016.

Arratia, G. (2017) “New Triassic teleosts (Actinopterygii, Teleosteomorpha) from northern Italy and their phylogenetic relationships among the most basal teleosts,” *Journal of Vertebrate Paleontology*, 37(2), p. e1312690. Available at: https://doi.org/10.1080/02724634.2017.1312690.

Arratia, G. *et al.* (2021) “The intriguing Atacamichthys fish from the middle Jurassic of Chile-an amiiform or a teleosteomorph},” in *Ancient Fishes and their Living Relatives: A Tribute to John Maisey*. Verlag Dr. F. Pfeil Munich, pp. 19–36.

Arratia, G. (2022) “The outstanding suction-feeder Marcopoloichthys furreri new species (Actinopterygii) from the Middle Triassic Tethys Realm of Europe and its implications for early evolution of neopterygian fishes,” *Fossil Record*, 25(2), pp. 231–261.

Arratia, G. and Hikuroa, D.C.H. (2010) “Jurassic fishes from the Latady Group, Antarctic Peninsula, and the oldest teleosts from Antarctica,” *Journal of Vertebrate Paleontology*, 30(5), pp. 1331–1342. Available at: https://doi.org/10.1080/02724634.2010.501448.

Arratia, G. and Lambers, P. (1996) “The caudal skeleton of pachycormiforms: Parallel evolution,” in *Mesozoic Fishes*. Verlag Dr. F. Pfeil München, pp. 191–218.

Arratia, G. and Schultze, H. (1990) “The urohyal: development and homology within osteichthyans,” *Journal of Morphology*, 203(3), pp. 247–282.

Arratia, G. and Schultze, H. (1991) “Palatoquadrate and its ossifications: development and homology within osteichthyans,” *Journal of morphology*, 208(1), pp. 1–81.

Arratia, G. and Schultze, H. (1992) “Reevaluation of the caudal skeleton of certain actinopterygian fishes: III. Salmonidae. Homologization of caudal skeletal structures,” *Journal of Morphology*, 214(2), pp. 187–249. Available at: https://doi.org/10.1002/jmor.1052140209.

Arratia, G. and Schultze, H.-P. (2024) “The oldest teleosts (Teleosteomorpha): Their early taxonomic, phenotypic, and ecological diversification during the Triassic,” *Fossil Record*, 27(1), pp. 29–53.

Arratia, G., Schultze, H.-P. and Tischlinger, H. (2019) “On a remarkable new species of Tharsis, a Late Jurassic teleostean fish from southern Germany: its morphology and phylogenetic relationships,” *Fossil Record*, 22(1), pp. 1–23.

Arratia, G. and Thies, D. (2008) “A new teleost (Osteichthyes, Actinopterygii) from the Early Jurassic Posidonia shale of Northern Germany,” *Fossil Record*, 4(1), pp. 167–187. Available at: https://doi.org/10.1002/mmng.20010040111.

Arratia, G. and Tintori, A. (1999) “The caudal skeleton of the Triassic actinopterygian† Prohalecites and its phylogenetic position,” in *Mesozoic Fishes*. Verlag Dr. F. Pfeil München, pp. 121–142.

Atterby, J., Friedman, M. and Giles, S. (2024) “Micro-CT Based Description of *Dorsetichthys bechei* (Actinopterygii: Teleostei): Cranial Anatomy of an Iconic Early Teleost.” Available at: https://doi.org/10.1101/2024.05.10.593503.

Bardack, D. (1965) “New Upper Cretaceous teleost fish from Texas.”

Bartholomai, A. (2004) “The large aspidorhynchid fish, Richmondichthys sweeti (Etheridge Jnr and Smith Woodward, 1891) from Albian marine deposits of Queensland, Australia,” *Memoirs of the Queensland Museum*, 49(2), pp. 521–536.

Bartsch, P. (1988) “Funktionelle Morphologie und Evolution des Axialskeletts und der Caudalis urspr{\"u}nglicher Knochenfische,” *Palaeontographica. Abteilung A, Paläozoologie, Stratigraphie*, 204(4–6), pp. 117–226.

Bechly, G. and Stockar, R. (2011) “The first Mesozoic record of the extinct apterygote insect genus Dasyleptus (insecta: archaeognatha: Monura: dasyleptidae) from the triassic of Monte San giorgio (Switzerland),” *Palaeodiversity*, 4, pp. 23–37.

Bell, M.A. (2015) “Package ‘geoscale’.” Available at cran. r-project. org/web/packages/geoscale/index. html.

Benton, M.J. (2000) “Stems, nodes, crown clades, and rank-free lists: is Linnaeus dead?,” *Biological Reviews*, 75(4), pp. 633–648.

Berg, L.S. (1940) “Classification of fishes, both recent and fossil,” *Trav. Inst. Zool. Acad. Sci. SSSR*, 5, pp. 87–517.

Bermúdez-Rochas, D.D. and Poyato-Ariza, F.J. (2015) “A new semionotiform actinopterygian fish from the Mesozoic of Spain and its phylogenetic implications,” *Journal of Systematic Palaeontology*, 13(4), pp. 265–285. Available at: https://doi.org/10.1080/14772019.2014.881928.

Berrell, R.W. *et al.* (2014) “The first record of the ichthyodectiform fish Cladocyclus from eastern Gondwana: a new species from the Lower Cretaceous of Queensland, Australia,” *Acta Palaeontologica Polonica*, 59(4), pp. 903–920.

Betancur-R., R. *et al.* (2013) “The Tree of Life and a New Classification of Bony Fishes,” *PLoS Currents* [Preprint]. Available at: https://doi.org/10.1371/currents.tol.53ba26640df0ccaee75bb165c8c26288.

Bogan, S., Taverne, L. and Agnolin, F.L. (2011) “Description of a new aspidorhynchid fish, Belonostomus lamarquensis sp. nov.(Halecostomi, Aspidorhynchiformes), from the continental Upper Cretaceous of Patagonia, Argentina,” *Bull. Instit. Roy. Sci. Nat. Belgique*, 81, pp. 235–245.

Brazeau, M.D. (2011) “Problematic character coding methods in morphology and their effects,” *Biological Journal of the Linnean Society*, 104(3), pp. 489–498. Available at: https://doi.org/10.1111/j.1095-8312.2011.01755.x.

Brazeau, M.D. and Friedman, M. (2014) “The characters of Palaeozoic jawed vertebrates,” *Zoological Journal of the Linnean Society*, 170(4), pp. 779–821. Available at: https://doi.org/10.1111/zoj.12111.

Brito, P.M. (1988) “La structure du suspensorium de Vinctifer, Poisson Actinoptérygien Mésozoique: Remarques sur les implications phylogénétiques.,” *Geobios*, 21(6), pp. 819–823.

Brito, P.M. (1997) “Révision des Aspidorhynchidae (Pisces, Actinopterygii) du Mésozoïque: ostéologie, relations phylogénétiques, données environnementales et biogéographiques,” *Geodiversitas*, 19(4), pp. 681–772.

Brito, P.M. (1999) “Description of Aspidorhynchus arawaki from the Late Jurassic of Cuba (Actinopterygii: Halecostomi,” in *Mesozoic Fishes*. Verlag Dr. F. Pfeil Munich, pp. 239–248.

Brito, P.M. and Ebert, M. (2009) “A new aspidorhynchid fish (Teleostei: Aspidorhynchiformes) from the Upper Jurassic of Ettling, Solnhofen, Bavaria, Germany,” *Comptes Rendus Palevol*, 8(4), pp. 395–402. Available at: https://doi.org/10.1016/j.crpv.2008.12.003.

Brito, P.M. and Meunier, F.J. (2000) “The morphology and histology of the scales of Aspidorhynchidae (Actinopterygii, Halecostomi),” *Geobios*, 33(1), pp. 105–111.

Brito, P.M. and Yabumoto, Y. (2011) “An updated review of the fish faunas from the Crato and Santana formations in Brazil, a close relationship to the Tethys fauna,” *Bulletin of the Kitakyushu Museum of Natural History and Human History, Series A (Natural History)*, 9, pp. 107–136.

Bronn, H. (1830) “Ueber zwei fossile Fischarten: Cyprinus coryphaenoides und Tetragonolepis semicinctus aus dem Gryphitenkalke bei Donau-Eschingen,” *Jahrbuch für Mineralogie, Geognosie, Geologie und Petrefaktenkunde*, 1(1), pp. 14–30.

Brough, J. (1939) “The Triassic fishes of Besano, Lombardy,” *British Museum (Natural History)*, p. 117.

Brown, E.E. *et al.* (2019) “Quantifying the completeness of the bat fossil record,” *Palaeontology*, 62(5), pp. 757–776. Available at: https://doi.org/10.1111/pala.12426.

Bryant, H. (1997) “Hypothetical Ancestors and Rooting in Cladistic Analysis,” *Cladistics*, 13(4), pp. 337–348. Available at: https://doi.org/10.1006/clad.1997.0048.

Bürgin, T. (1992) *Basal ray-finned fishes (Osteichthyes; Actinopterygii) from the middle Triassic of Monte San Giorgio (Canton Tessin, Switzerland): Systematic palaeontology with notes on functional morphology and palaeoecology*. Birkhäuser.

Caine, H. and Benton, M.J. (2011) “Ichthyosauria from the Upper Lias of Strawberry Bank, England,” *Palaeontology*, 54(5), pp. 1069–1093. Available at: https://doi.org/10.1111/j.1475-4983.2011.01093.x.

Campbll, K.W. and Phuoc, L.D. (1983) “A Late Permian actinopterygian fish from Australia,” *Palaeontology;(United Kingdom)*, 26(1).

Cantalice, K.M., Alvarado-Ortega, J. and Brito, P.M. (2018) “On the occurrence of Vinctifer ferrusquiai sp. nov.(Actinopterygii, Aspidorhynchiformes) in the Kimmeridgian (Late Jurassic) deposits near Tlaxiaco, Oaxaca, southern Mexico,” *Revista mexicana de ciencias geológicas*, 35(2), pp. 179–187.

Carroll, R.L. (1988) *Vertebrate paleontology and evolution*. WH Freeman.

Cashmore, D.D. and Butler, R.J. (2019) “Skeletal completeness of the non-avian theropod dinosaur fossil record,” *Palaeontology*, 62(6), pp. 951–981. Available at: https://doi.org/10.1111/pala.12436.

Cavicchini, I. *et al.* (2024) “A Portrait of a Young Fish: Redescription of Pteronisculus gunnari (Nielsen, 1942) from a juvenile specimen from the Early Triassic of East Greenland, with implications for ontogenetic development in early actinopterygians,” *bioRxiv*, pp. 2024–2027.

Cavin, Lionel (2008) “Palaeobiogeography of Cretaceous bony fishes (Actinistia, Dipnoi and Actinopterygii),” *Geological Society, London, Special Publications*, 295(1), pp. 165–183. Available at: https://doi.org/10.1144/SP295.11.

Cavin, L. and Berrell, R.W. (2019) “Revision of *Dugaldia emmilta* (Teleostei, Ichthyodectiformes) from the Toolebuc Formation, Albian of Australia, with comments on the jaw mechanics,” *Journal of Vertebrate Paleontology*, 39(1), p. e1576049. Available at: https://doi.org/10.1080/02724634.2019.1576049.

Cavin, L., Forey, P.L. and Giersch, S. (2013) “Osteology of *Eubiodectes libanicus* (Pictet & Humbert, ) and some other ichthyodectiformes (Teleostei): phylogenetic implications,” *Journal of Systematic Palaeontology*, 11(2), pp. 115–177. Available at: https://doi.org/10.1080/14772019.2012.691559.

Cawley, J.J. *et al.* (2019) “The stem group teleost Pachycormus (Pachycormiformes: Pachycormidae) from the Upper Lias (Lower Jurassic) of Strawberry Bank, UK,” *PalZ*, 93(2), pp. 285–302. Available at: https://doi.org/10.1007/s12542-018-0431-7.

Choo, B. (2012) “Revision of the actinopterygian genus Mimipiscis (= Mimia) from the Upper Devonian Gogo Formation of Western Australia and the interrelationships of the early Actinopterygii,” *Earth and Environmental Science Transactions of the Royal Society of Edinburgh*, 102(2), pp. 77–104.

Choo, B. (2015) “A new species of the Devonian actinopterygian Moythomasia from Bergisch Gladbach, Germany, and fresh observations on M. durgaringa from the Gogo Formation of Western Australia,” *Journal of Vertebrate Paleontology*, 35(4), p. e952817.

Claeson, Kerin M., Bemis, W.E. and Hagadorn, J.W. (2007) “New interpretations of the skull of a primitive bony fish *Erpetoichthys calabaricus* (Actinopterygii: Cladistia),” *Journal of Morphology*, 268(11), pp. 1021–1039. Available at: https://doi.org/10.1002/jmor.10567.

Claeson, K.M. and Hagadorn, J.W. (2008) “The occipital region in the basal bony fish Erpetoichthys calabaricus (Actinopterygii: Cladistia),” *Journal of fish biology*, 73(4), pp. 1075–1082.

Clarke, J.T. and Friedman, M. (2018) “Body-shape diversity in Triassic–Early Cretaceous neopterygian fishes: sustained holostean disparity and predominantly gradual increases in teleost phenotypic variety,” *Paleobiology*, 44(3), pp. 402–433.

Clarke, J.T., Lloyd, G.T. and Friedman, M. (2016) “Little evidence for enhanced phenotypic evolution in early teleosts relative to their living fossil sister group,” *Proceedings of the National Academy of Sciences*, 113(41), pp. 11531–11536. Available at: https://doi.org/10.1073/pnas.1607237113.

Cleary, Terri J. *et al.* (2015) “The fossil record of ichthyosaurs, completeness metrics and sampling biases,” *Palaeontology*, 58(3), pp. 521–536. Available at: https://doi.org/10.1111/pala.12158.

Coates, M.I. *et al.* (2017) “A symmoriiform chondrichthyan braincase and the origin of chimaeroid fishes,” *Nature*, 541(7636), pp. 208–211. Available at: https://doi.org/10.1038/nature20806.

Collazo, A. (1996) “Evolutionary Correlations Between Early Development and Life History in Plethodontid Salamanders and Teleost Fishes,” *American Zoologist*, 36(2), pp. 116–131. Available at: https://doi.org/10.1093/icb/36.2.116.

Collazo, A., Bolker, J.A. and Keller, R. (1994) “A Phylogenetic Perspective on Teleost Gastrulation,” *The American Naturalist*, 144(1), pp. 133–152. Available at: https://doi.org/10.1086/285665.

Cooper, S.L.A. *et al.* (2022) “A New Large †Pachycormiform (Teleosteomorpha: †Pachycormiformes) from the Lower Jurassic of Germany, with Affinities to the Suspension-Feeding Clade, and Comments on the Gastrointestinal Anatomy of Pachycormid Fishes,” *Diversity*, 14(12), p. 1026. Available at: https://doi.org/10.3390/d14121026.

Cooper, S.L.A. and Maxwell, E.E. (2022) “Revision of the pachycormid fish *Saurostomus esocinus* Agassiz from the Early Jurassic (Toarcian) of Europe, with new insight into the origins of suspension-feeding in Pachycormidae,” *Papers in Palaeontology*, 8(6). Available at: https://doi.org/10.1002/spp2.1467.

Costa, O.G. (1853) *Ittiologia fossile Italiana, opera da servire di supplemento alle richerche sui Pesci fossile de L. Agassiz, &c*.

Crook, A.R. (1892) “Über einige fossile Knochenfische aus der mittleren Kreide von Kansas,” *Palaeontographica*, 39, pp. 107–124.

Damsgaard, C. *et al.* (2019) “Retinal oxygen supply shaped the functional evolution of the vertebrate eye,” *Elife*, 8, p. e52153.

Danil’chenko, P. and Y.V. (1964) “Order Pholidophorida,” in *Fundamentals of Paleontology*. Obruchev, DV, pp. 599–603.

Darwin, C. (1859) *The Origin of Species*. John Murray, London. Available at: https://doi.org/10.1017/CBO9780511694295.

Davesne, D. *et al.* (2021) “Fossilized cell structures identify an ancient origin for the teleost whole-genome duplication,” *Proceedings of the National Academy of Sciences*, 118(30). Available at: https://doi.org/10.1073/pnas.2101780118.

Dearden, R.P. *et al.* (2023) “The oldest three-dimensionally preserved vertebrate neurocranium,” *Nature*, 621(7980), pp. 782–787. Available at: https://doi.org/10.1038/s41586-023-06538-y.

Deecke, W. (1889) “Ueber Fische aus verschiedenen Horizonten der Trias,” *Palaeontographica*, pp. 97–138.

Dobson, C. (2019) *Morphology, systematics and palaeoecology of pachycormid fishes [PhD thesis]*.

Dobson, C. *et al.* (2021) “Cranial osteology of the Middle Jurassic (Callovian) *Martillichthys renwickae* (Neopterygii, Pachycormiformes) with comments on the evolution and ecology of edentulous pachycormiforms,” *Papers in Palaeontology*, 7(1), pp. 111–136. Available at: https://doi.org/10.1002/spp2.1276.

Doosey, M.H. and Wiley, E.O. (2015) “Epural bones in teleost fishes: a problem of phylogenetic homology,” *Ichthyological Research*, 62(2), pp. 131–144. Available at: https://doi.org/10.1007/s10228-014-0413-z.

Ebert, M. (2014) “The genus Belonostomus Agassiz, 1834 (Neopterygii, Aspidorhynchiformes) in the Late Jurassic of the Solnhofen Archipelago, with a focus on Belonostomus kochii Münster, 1836 from Ettling (Germany,” *Archaeopteryx*, 32, pp. 15–43.

Ebert, M. (2018) “*Cerinichthys koelblae* , gen. et sp. nov., from the Upper Jurassic of Cerin, France, and its phylogenetic setting, leading to a reassessment of the phylogenetic relationships of Halecomorphi (Actinopterygii),” *Journal of Vertebrate Paleontology*, 38(1), p. e1420071. Available at: https://doi.org/10.1080/02724634.2017.1420071.

Ebert, M. and Kölbl-Ebert, M. (2018) “Neues zur Systematik der Oberjurassischen Fische der Neo-Tethys,” *Archaeopteryx*, 35, pp. 18–26.

Eschmeyer W.N and Fricke R (2012) *Catalog of Fishes electronic version*, *San Francisco California Academy of Sciences*.

Etheridge, R. and Woodward, A. (1891) “On the occurrence of the genus Belonostomus in the Rolling Downs Formation (Cretaceous) of Central Queensland,” *Transactions of the Royal Society of Victoria*, 2, pp. 1–7.

Figueroa, R.T. *et al.* (2023) “Exceptional fossil preservation and evolution of the ray-finned fish brain,” *Nature*, 614(7948), pp. 486–491. Available at: https://doi.org/10.1038/s41586-022-05666-1.

Figueroa, R.T., Friedman, M. and Gallo, V. (2019) “Cranial anatomy of the predatory actinopterygian *Brazilichthys macrognathus* from the Permian (Cisuralian) Pedra de Fogo Formation, Parnaíba Basin, Brazil,” *Journal of Vertebrate Paleontology*, 39(3), p. e1639722. Available at: https://doi.org/10.1080/02724634.2019.1639722.

Flannery Sutherland, J.T. *et al.* (2017) “Leptolepid otoliths from the Hauterivian (Lower Cretaceous) Lower Weald Clay (southern England),” *Proceedings of the Geologists’ Association*, 128(4), pp. 613–625. Available at: https://doi.org/10.1016/j.pgeola.2017.05.001.

Forey, P.L. (1973) “A revision of elopiform fishes, fossil and Recent.,” *Bull. Br. Mus.(Nat. Hist.), Geol., Suppl.*, 10, pp. 1–222.

Forey, P.L. (2016) “Smith Woodward’s ideas on fish classification,” *Geological Society, London, Special Publications*, 430(1), pp. 115–127. Available at: https://doi.org/10.1144/SP430.1.

Foster, J. *et al.* (2018) “Paleontology, taphonomy, and sedimentology of the Mygatt-Moore Quarry, a large dinosaur bonebed in the Morrison Formation, western Colorado—Implications for Upper Jurassic dinosaur preservation modes,” *Geology of the Intermountain West*, 5, pp. 23–93.

Frey, E., Meyer, C.A. and Tischlinger, H. (2011) “The oldest azhdarchoid pterosaur from the Late Jurassic Solnhofen Limestone (Early Tithonian) of Southern Germany,” *Swiss Journal of Geosciences*, 104(S1), pp. 35–55. Available at: https://doi.org/10.1007/s00015-011-0073-1.

Frey, E. and Tischlinger, H. (2012) “The Late Jurassic Pterosaur Rhamphorhynchus, a Frequent Victim of the Ganoid Fish Aspidorhynchus?,” *PLoS ONE*, 7(3), p. e31945. Available at: https://doi.org/10.1371/journal.pone.0031945.

Friedman, M. *et al.* (2010) “100-Million-Year Dynasty of Giant Planktivorous Bony Fishes in the Mesozoic Seas,” *Science*, 327(5968), pp. 990–993. Available at: https://doi.org/10.1126/science.1184743.

Friedman, M. (2010) “Explosive morphological diversification of spiny-finned teleost fishes in the aftermath of the end-Cretaceous extinction,” *Proceedings of the Royal Society B: Biological Sciences*, 277(1688), pp. 1675–1683.

Friedman, M. (2012) “Parallel evolutionary trajectories underlie the origin of giant suspension-feeding whales and bony fishes,” *Proceedings of the Royal Society B: Biological Sciences*, 279(1730), pp. 944–951. Available at: https://doi.org/10.1098/rspb.2011.1381.

Friedman, M. *et al.* (2013) “Geographic and stratigraphic distribution of the Late Cretaceous suspension-feeding bony fish *Bonnerichthys gladius* (Teleostei, Pachycormiformes),” *Journal of Vertebrate Paleontology*, 33(1), pp. 35–47. Available at: https://doi.org/10.1080/02724634.2012.713059.

Friedman, M. (2015) “The early evolution of ray-finned fishes,” *Palaeontology*, 58(2), pp. 213–228.

Friedman, M. *et al.* (2016) “The English Chalk and London Clay: two remarkable British bony fish *Lagerstätten*,” *Geological Society, London, Special Publications*, 430(1), pp. 165–200. Available at: https://doi.org/10.1144/SP430.18.

Friedman, M. and Giles, S. (2016) “Actinopterygians: the ray-finned fishes – an explosion of diversity,” in J. Clack, R. Far, and P. Arthur (eds) *Evolution of the vertebrate ear: Evidence from the fossil record*. Springer, pp. 17–49.

Gardiner B, Maisey J and Littlewood D (1996) “Interrelationships of basal neopterygians,” in Stiassney M.LJ., Parenti L.R., and Johnson G.D. (eds) *Interrelationships of fishes*. San Diego: Academic Press, pp. 117–146.

Gardiner, Brian George (1960) *A revision of certain actinopterygian and coelacanth fishes, chiefly from the Lower Lias*. British Museum (Natural History).

Gardiner, B.G., Maisey, J.G. and Littlewood, D.T.J. (1996) “Interrelationships of basal neopterygians. In ‘“Interrelationships of Fishes”’(MLJ Stiassny, LR Parenti, and GD Johnson, Eds.).” Academic Press, San Diego.

Gardiner, B.G. and Schaeffer, B. (1989) “Interrelationships of lower actinopterygian fishes,” *Zoological Journal of the Linnean Society*, 97(2), pp. 135–187.

Gardiner, B.G., Schaeffer, B. and Masserie, J.A. (2005) “A review of the lower actinopterygian phylogeny,” *Zoological Journal of the Linnean Society*, 144(4), pp. 511–525.

Gaudant, J (1978) “Essai de révision taxonomique des «Pholidophorus»(Poissons Actinoptérygiens) du Jurassique supérieur de Cerin (Ain).,” *Publications du musée des Confluences*, 16(1), pp. 101–121.

Gibson, R.N. and Ezzi, I.A. (1990) “Relative importance of prey size and concentration in determining the feeding behaviour of the herring Clupea harengus,” *Marine Biology*, 107(2), pp. 357–362.

Gibson, S.Z. (2016) “Redescription and Phylogenetic Placement of †Hemicalypterus weiri Schaeffer, 1967 (Actinopterygii, Neopterygii) from the Triassic Chinle Formation, Southwestern United States: New Insights into Morphology, Ecological Niche, and Phylogeny,” *PLOS ONE*, 11(9), p. e0163657. Available at: https://doi.org/10.1371/journal.pone.0163657.

Giles, S. *et al.* (2017) “Early members of ‘living fossil’ lineage imply later origin of modern ray-finned fishes,” *Nature*, 549(7671), pp. 265–268. Available at: https://doi.org/10.1038/nature23654.

Giles, S. *et al.* (2022) “A Late Devonian actinopterygian suggests high lineage survivorship across the end-Devonian mass extinction,” *Nature Ecology & Evolution*, 7(1), pp. 10–19. Available at: https://doi.org/10.1038/s41559-022-01919-4.

Giles, S., Friedman, M. and Brazeau, M.D. (2015) “Osteichthyan-like cranial conditions in an Early Devonian stem gnathostome,” *Nature*, 520(7545), pp. 82–85. Available at: https://doi.org/10.1038/nature14065.

Giles, S., Rogers, M. and Friedman, M. (2018) “Bony labyrinth morphology in early neopterygian fishes (Actinopterygii: Neopterygii),” *Journal of Morphology*, 279(4), pp. 426–440. Available at: https://doi.org/10.1002/jmor.20551.

Glasauer, S.M.K. and Neuhauss, S.C.F. (2014) “Whole-genome duplication in teleost fishes and its evolutionary consequences,” *Molecular Genetics and Genomics*, 289(6), pp. 1045–1060. Available at: https://doi.org/10.1007/s00438-014-0889-2.

Goloboff, P.A. and Catalano, S.A. (2016) “TNT version 1.5, including a full implementation of phylogenetic morphometrics,” *Cladistics*, 32(3), pp. 221–238. Available at: https://doi.org/10.1111/cla.12160.

Goodrich, E.S. (1988) “Studies on the Structure and Development of Vertebrates,” *Journal of the History of Biology*, 12(2).

Gouiric-Cavalli, S. (2016) “A new Late Jurassic halecomorph fish from the marine Vaca Muerta Formation, Argentina, southwestern Gondwana,” *Fossil Record*, 19(2), pp. 119–129. Available at: https://doi.org/10.5194/fr-19-119-2016.

Gouiric-Cavalli, S. (2017) “Large and Mainly Unnoticed: The First Lower Tithonian Record of a Suspension-Feeding Pachycormid from Southern Gondwana,” *Ameghiniana*, 54(3), pp. 283–289. Available at: https://doi.org/10.5710/AMGH.16.11.2016.3029.

Gouiric-Cavalli, S. and Arratia, G. (2021) “A new †Pachycormiformes (Actinopterygii) from the Upper Jurassic of Gondwana sheds light on the evolutionary history of the group,” *Journal of Systematic Palaeontology*, 19(21), pp. 1517–1550. Available at: https://doi.org/10.1080/14772019.2022.2049382.

Grande L. (2010) “An empirical synthetic pattern study of gars (Lepisosteiformes) and closely related species, based mostly on skeletal anatomy. The resurrection of Holostei. ,” *Ichthyology & Herpetology*, 10(2).

Grande, L. and Bemis, W.E. (1998) “A Comprehensive Phylogenetic Study of Amiid Fishes (Amiidae) Based on Comparative Skeletal Anatomy. an Empirical Search for Interconnected Patterns of Natural History,” *Journal of Vertebrate Paleontology*, 18(sup1), pp. 1–696. Available at: https://doi.org/10.1080/02724634.1998.10011114.

Greenwood, P.H. *et al.* (1966) “Phyletic studies of teleostean fishes, with a provisional classification of living forms. Bulletin of the AMNH; v. 131, article 4.”

Greenwood, P.H., Miles, R.S. and Patterson, C. (1973) “Interrelationships of holosteans,” in Greenwood PH, Miles RS, and Patterson C (eds) *Interrelationships of holosteans*. London: Academic Press, pp. 233–305.

Griffith, J. (1977) “the Upper triassic fishes from Polzberg bei Lunz, Austria,” *Zoological Journal of the Linnean society*, 60(1), pp. 1–93.

Griffith, J and Patterson, C. (1963) “The structure and relationships of the Jurassic fish. Ichthyokentema purbeckensis,” *Bulletin of British Natural History Museum, Geology*, 8.

Hamel, M.-H. and Poplin, C. (2008) “The braincase anatomy of Lawrenciella schaefferi, actinopterygian from the Upper Carboniferous of Kansas (USA),” *Journal of Vertebrate Paleontology*, 28(4), pp. 989–1006.

Havelka, M. *et al.* (2013) “Extensive genome duplications in sturgeons: new evidence from microsatellite data,” *Journal of Applied Ichthyology*, 29(4), pp. 704–708. Available at: https://doi.org/10.1111/jai.12224.

Heath, T.A., Hedtke, S.M. and Hillis, D.M. (2008) “Taxon sampling and the accuracy of phylogenetic analyses,” *Journal of Systematics and Evolution*, 46(3), pp. 239–257.

Heckel, J.J. (1849) “1846–1849. Index. Addenda et Corrigenda,” *Russegger, J. Reisen in Europa, Asien und Afrika, mit besonderer Rücksicht auf die naturwissenschaftlichen Verhältnisse der betreffenden Länder, unternommen in den Jahren*, pp. 347–360.

Hedtke, S.M., Townsend, T.M. and Hillis, D.M. (2006) “Resolution of Phylogenetic Conflict in Large Data Sets by Increased Taxon Sampling,” *Systematic Biology*, 55(3), pp. 522–529. Available at: https://doi.org/10.1080/10635150600697358.

Hennig, W. (1969) “Die stammesgeschichte der Insekten,” *Verlag von Waldemar Kramer*

Hill, R. v. (2005) “Integration of Morphological Data Sets for Phylogenetic Analysis of Amniota: The Importance of Integumentary Characters and Increased Taxonomic Sampling,” *Systematic Biology*, 54(4), pp. 530–547. Available at: https://doi.org/10.1080/10635150590950326.

Hilton, E.J. (2002) “Osteology of the extant north American fishes of the genus Hiodon Lesueur, 1818 (Teleostei: Osteoglossomorpha: Hiodontiformes),” *Publication (Field Museum of Natural History), 1520* [Preprint].

Hilton, E.J., Grande, L. and Bemis, W.E. (2011) “Skeletal anatomy of the shortnose sturgeon, Acipenser brevirostrum Lesueur, 1818, and the systematics of sturgeons (Acipenseriformes, Acipenseridae),” *Fieldiana Life and Earth Sciences*, 2011(3), pp. 1–168.

Hoegg, S. *et al.* (2004) “Phylogenetic Timing of the Fish-Specific Genome Duplication Correlates with the Diversification of Teleost Fish,” *Journal of Molecular Evolution*, 59(2), pp. 190–203. Available at: https://doi.org/10.1007/s00239-004-2613-z.

Holmgreen, N. and Stensiö, E. (1936) “Kranium Und Visceralskelett Der Akranier, Cyclostomen Und Fische,” in L. Göppert, E. Kallius, and W. Lubosch (eds) *Handbuch Der Vergleichenden Anatomie Der Wirbeltiere*. Berlin, Wien (Urban & Schwarzenberg), pp. 233–500.

el Hossny, T. *et al.* (2020) “Spathiurus dorsalis Davis, 1887, from the Upper Cretaceous of Haqel, Lebanon, and the evolutionary history of Ionoscopiformes,”

*Cretaceous Research*, 116, p. 104619. Available at: https://doi.org/10.1016/j.cretres.2020.104619.

Huelsenbeck, J.P. (1991) “Tree-length distribution skewness: an indicator of phylogenetic information,” *Systematic Biology*, 40(3), pp. 257–270.

Hunter, A. and Donovan, S. (2005) “Field sampling bias, museum collections and completeness of the fossil record,” *Lethaia*, 38(4), pp. 305–314.

Hurley, I.A. *et al.* (2007) “A new time-scale for ray-finned fish evolution,” *Proceedings of the Royal Society B: Biological Sciences*, 274(1609), pp. 489–498. Available at: https://doi.org/10.1098/rspb.2006.3749.

Inoue, J.G. *et al.* (2003) “Basal actinopterygian relationships: a mitogenomic perspective on the phylogeny of the ‘ancient fish,’” *Molecular Phylogenetics and Evolution*, 26(1), pp. 110–120. Available at: https://doi.org/10.1016/S1055-7903(02)00331-7.

Jain, S.L. (1973) “New specimens of Lower Jurassic holostean fishes from India.”

Jain, S.L. and Robinson, P.L. (1963) “Some new specimens of the fossil fish Lepidotes from the English Upper Jurassic,” in *Proceedings of the Zoological Society of London*. Wiley Online Library, pp. 119–135.

Jenner, R.A. (2002) “Boolean logic and character state identity: pitfalls of character coding in metazoan cladistics,” *Contributions to Zoology*, 71(1–3), pp. 67–91. Available at: https://doi.org/10.1163/18759866-0710103006.

Jessen, H.L. (1972) “Schultergürtel und Pectoralflosse bei Actinopterygiern,” in, pp. 1–101. Available at: https://doi.org/10.18261/8200092887-1972-01.

Jordan, D.S. (1919) “New genera of fossil fishes from Brazil,” *Proceedings of the Academy of Natural Sciences of Philadelphia*, 71(3), pp. 208–210.

Kear, B. P. (2007) “First Record of a Pachycormid Fish (Actinopterygii: Pachycormiformes) from the Lower Cretaceous of Australia,” *Journal of Vertebrate Paleontology*, 27(1), pp. 1033–1038. Available at: http://www.jstor.org/stable/30117467.

Kikugawa, K. *et al.* (2004) “Basal jawed vertebrate phylogeny inferred from multiple nuclear DNA-coded genes,” *BMC Biology*, 2(1), p. 3. Available at: https://doi.org/10.1186/1741-7007-2-3.

Kogan, I. and Romano, C. (2016) “Redescription of Saurichthys madagascariensis Piveteau, 1945 (Actinopterygii, Early Triassic), with implications for the early saurichthyid morphotype,” *Journal of Vertebrate Paleontology*, 36(4), p. e1151886.

Kölbl-Ebert, M. *et al.* (2018) “A Piranha-like Pycnodontiform Fish from the Late Jurassic,” *Current Biology*, 28(21), pp. 3516-3521.e2. Available at: https://doi.org/10.1016/j.cub.2018.09.013.

Konwert, M. and Hörnig, M. (2018) “*Grimmenichthys ansorgei* , gen. et sp. nov. (Teleostei, ‘Pholidophoriformes’), and other ‘pholidophoriform’ fishes from the early Toarcian of Grimmen (Mecklenburg-Western Pomerania, Germany),” *Journal of Vertebrate Paleontology*, 38(3), p. e1451871. Available at: https://doi.org/10.1080/02724634.2018.1451871.

Konwert, M. and Stumpf, S. (2017) “Exceptionally preserved Leptolepidae (Actinopterygii, Teleostei) from the late Early Jurassic Fossil-Lagerstätten of Grimmen and Dobbertin (Mecklenburg-Western Pomerania, Germany).,” *Zootaxa*, 4243(2), pp. 249–296.

Kottelat, M. *et al.* (2006) “*Paedocypris* , a new genus of Southeast Asian cyprinid fish with a remarkable sexual dimorphism, comprises the world’s smallest vertebrate,” *Proceedings of the Royal Society B: Biological Sciences*, 273(1589), pp. 895–899. Available at: https://doi.org/10.1098/rspb.2005.3419.

Kriwet, J. (2000) “Revision of Mesturus cordillera Martill et al., 1998 (Actinopterygii, Pycnodontiformes) from the Oxfordian (Upper Jurassic) of northern Chile,” *Journal of Vertebrate Paleontology*, 20(3), pp. 450–455. Available at: https://doi.org/10.1671/0272-4634(2000)020[0450:ROMCME]2.0.CO;2.

Kriwet, J. (2004) “A new pycnodont fish genus (Neopterygii: Pycnodontiformes) from the Cenomanian (Upper Cretaceous) of Mount Lebanon,” *Journal of Vertebrate Paleontology*, 24(3), pp. 525–532.

Kriwet, J. (2005) “A comprehensive study of the skull and dentition of pycnodont fishes,” *Zitteliana*, 45, pp. 135–188.

Kuljian, C. (2024) “Scientific racism: Histories, legacies and ethics Steve Biko Bioethics Lecture, 12 September 2023,” *South African Journal of Bioethics and Law*, 17(1), pp. 16–21.

de la Beche, H.T. (1822) “II.—Remarks on the Geology of the South Coast of England, from Bridport Harbour, Dorset, to Babbacombe Bay, Devon.,” *Transactions of the Geological Society of London*, 1(1), pp. 40–47.

Lambers, P.H. (1988) “Orthocormus teyleri, nov. spec., the first pachycormid from the Kimmeridge lithographic limestone at Cerin (Ain), France; with remarks on the genus Orthocormus Weitzel,” *Proceedings of the Koninklijke Nederlandse Akademie Van Wetenschappen Series B-palaeontology Geology Physics Chemistry Anthropology*, 91(4), pp. 369–391.

Lambers, P.H. (1992) “On the ichthyofauna of the Solnhofen lithographic limestone (Upper Jurassic, Germany).”

Latimer, A.E. and Giles, S. (2018) “A giant dapediid from the Late Triassic of Switzerland and insights into neopterygian phylogeny,” *Royal Society Open Science*, 5(8), p. 180497. Available at: https://doi.org/10.1098/rsos.180497.

Lauder, G. v (1983) “Functional design and evolution of the pharyngeal jaw apparatus in euteleostean fishes,” *Zoological Journal of the Linnean Society*, 77(1), pp. 1–38.

Laurent, P. and Dunel-Erb, S. (1984) “9 The Pseudobranch: Morphology and Function,” in *Fish physiology*. Elsevier, pp. 285–323.

Lecointre, G. *et al.* (1993) “Species sampling has a major impact on phylogenetic inference,” *Molecular phylogenetics and evolution*, 2(3), pp. 205–224.

Lehman, J.P. (1947) “Étude d’un Pachycormus du Lias de Normandie,” *Kungliga Svenska Vetenskaps Akademiens Handlingar*, 1, pp. 1–44.

Lehman, J.P. (1966) “Dipnoi, inPIVETEAU J.(ed.), Traité de paléontologie 4 (3).” Masson, Paris.

Lidgard, S. and Love, A.C. (2021) “The living fossil concept: reply to Turner,” *Biology & Philosophy*, 36(2), p. 13.

Liston, J. *et al.* (2013) “Growth, age and size of the Jurassic pachycormid Leedsichthys problematicus (Osteichthyes: Actinopterygii),” in G., Arratia, H. Schultze, and M. Wilson (eds) *Mesozoic Fishes*. Verlag Dr. Friedrich Pfeil.

Liston, J.J. *et al.* (2019) “Scythes, sickles and other blades: defining the diversity of pectoral fin morphotypes in Pachycormiformes,” *PeerJ*, 7, p. e7675. Available at: https://doi.org/10.7717/peerj.7675.

Lombardo, C. and Tintori, A. (2005) “Feeding specializations in Late Triassic fishes,” *Sezione di Museologia Scientifica e Naturalistica*, pp. 25–32.

López-Arbarello, A. (2012) “Phylogenetic Interrelationships of Ginglymodian Fishes (Actinopterygii: Neopterygii),” *PLoS ONE*, 7(7), p. e39370. Available at: https://doi.org/10.1371/journal.pone.0039370.

López-Arbarello, A., Maxwell, E.E. and Schweigert, G. (2020) “New halecomorph (Actinopterygii, Neopterygii) from the Nusplingen Lithographic Limestone (Upper Jurassic, Late Kimmeridgian), Germany,” *Journal of Vertebrate Paleontology*, 40(2), p. e1771348. Available at: https://doi.org/10.1080/02724634.2020.1771348.

López-Arbarello, A. and Schröder, K.M. (2014) “The species of Aspidorhynchus Agassiz, 1833 (Neopterygii, Aspidorhynchiformes) from the Jurassic plattenkalks of Southern Germany,” *Paläontologische Zeitschrift*, 88(2), pp. 167–185. Available at: https://doi.org/10.1007/s12542-013-0187-z.

López-Arbarello, A. and Sferco, E. (2011) “New semionotiform (Actinopterygii: Neopterygii) from the Late Jurassic of southern Germany,” *Journal of Systematic Palaeontology*, 9(2), pp. 197–215. Available at: https://doi.org/10.1080/14772019.2010.493751.

López-Arbarello, A. and Sferco, E. (2018) “Neopterygian phylogeny: the merger assay,” *Royal Society Open Science*, 5(3), p. 172337. Available at: https://doi.org/10.1098/rsos.172337.

Lord, A.R. and Davis, P.G. (2010) *Fossils from the Lower Lias of the Dorset coast*.

Lyons-Weiler, J., Hoelzer, G.A. and Tausch, R.J. (1996) “Relative apparent synapomorphy analysis (RASA). I: The statistical measurement of phylogenetic signal,” *Molecular Biology and Evolution*, 13(6), pp. 749–757. Available at: https://doi.org/10.1093/oxfordjournals.molbev.a025635.

Macqueen, D.J. and Johnston, I.A. (2014) “A well-constrained estimate for the timing of the salmonid whole genome duplication reveals major decoupling from species diversification,” *Proceedings of the Royal Society B: Biological Sciences*, 281(1778), p. 20132881. Available at: https://doi.org/10.1098/rspb.2013.2881.

Maddison, W.P., Donoghue, M.J. and Maddison, D.R. (1984) “Outgroup analysis and parsimony,” *Systematic biology*, 33(1), pp. 83–103.

Maddison, W.P. and Maddison, D.R. (1992) “macclade,” *Sinauer, Sunderland, MA* [Preprint].

Maddison WP and Maddison DR (2019) “Mesquite: a modular system for evolutionary analysis. .” http://mesquiteproject.org.

Mainwaring, A.J. (1978) “Anatomical and systematic review of the Pachycormidae, a family of Mesozoic fossil fishes.”

Maisey, J.G. (1991) “Santana fossils: an illustrated atlas,” *(No Title)* [Preprint].

Maisey, J.G. (1999) “The supraotic bone in neopterygian fishes (Osteichthyes, Actinoptergii). American Museum novitates; no. 3267.”

Maisey, J.G. (2001) “CT-scan reveals new cranial features in Devonian chondrichthyan ‘Cladodus’ wildungensis,” *Journal of Vertebrate Paleontology*, 21(4), pp. 807–810.

Maisey, J.G. (2005) “Braincase of the Upper Devonian shark Cladodoides wildungensis (Chondrichthyes, Elasmobranchii), with observations on the braincase in early chondrichthyans,” *Bulletin of the American Museum of Natural History*, 2005(288), pp. 1–103.

Mannion, P.D. and Upchurch, P. (2010) “Completeness metrics and the quality of the sauropodomorph fossil record through geological and historical time,” *Paleobiology*, 36(2), pp. 283–302.

Martin, R. (2019) “Fossil Thoughts: Thoreau, Arrowheads, and Radical Paleontology,” *ESQ: A Journal of Nineteenth-Century American Literature and Culture*, 65(3), pp. 424–468.

Martin-Abad, H. and Poyato-Ariza, F.J. (2013) “Historical patterns of distribution in Pycnodontiform and Amiiform fishes in the context of moving plates,” *Geologica Belgica* [Preprint].

Maxwell, E. *et al.* (2020) “Re-evaluation of pachycormid fishes from the Late Jurassic of Southwestern Germany,” *Acta Palaeontologica Polonica*, 65(3), pp. 429–453.

McClain, C.R. *et al.* (2015) “Sizing ocean giants: patterns of intraspecific size variation in marine megafauna,” *PeerJ*, 3, p. e715.

Meyer, A. and van de Peer, Y. (2005) “From 2R to 3R: evidence for a fish-specific genome duplication (FSGD),” *Bioessays*, 27(9), pp. 937–945.

Meyer, A. and Zardoya, R. (2003) “Recent advances in the (molecular) phylogeny of vertebrates,” *Annual Review of Ecology, Evolution, and Systematics*, 34(1), pp. 311–338.

Michelis, I. *et al.* (1996) *Die Vertebratenfauna des Calloviums (Mittlerer Jura) aus dem Steinbruch Störmer (Wallücke, Wiehengebirge)*. Landschaftsverband Westfalen-Lippe.

Moy-Thomas, J.A. and Dyne, M.B. (1938) “XVII.—The Actinopterygian Fishes from the Lower Carboniferous of Glencartholm, Eskdale, Dumfriesshire,” *Earth and Environmental Science Transactions of The Royal Society of Edinburgh*, 59(2), pp. 437–480.

Müller, J. (1845) “Uber den Bau und die Grenzen der Ganoiden, and iiber das naturliche System der Fische,” *Berlin Akademie Wissenschaften Berlin*, 1844, pp. 67–85.

Nanglu, K. and Cullen, T.M. (2023) “Across space and time: a review of sampling, preservational, analytical, and anthropogenic biases in fossil data across macroecological scales,” *Earth-Science Reviews*, 244, p. 104537.

Near, T.J. *et al.* (2012) “Resolution of ray-finned fish phylogeny and timing of diversification,” *Proceedings of the National Academy of Sciences*, 109(34), pp. 13698–13703.

Near, T.J. *et al.* (2014) “Boom and bust: ancient and recent diversification in bichirs (Polypteridae: Actinopterygii), a relictual lineage of ray-finned fishes,” *Evolution*, 68(4), pp. 1014–1026.

Nelson, G. (1989) “Phylogeny of major fish groups.,” *The hierarchy of life*, pp. 325–336.

Nelson, G.J. (1969) “Origin and diversification of teleostean fishes,” *Annals of the New York Academy of Sciences*, 167(1), pp. 18–30.

Nelson, J.S., Grande, T.C. and Wilson, M.V.H. (2016) *Fishes of the World*. John Wiley & Sons.

Nelson, J.S., Schultze, H.-P. and Wilson, M.V.H. (2010) “Origin and phylogenetic interrelationships of teleosts,” *New York* [Preprint].

Nicholson, H.A. and Lydekker, R. (1889) *A Manual of Palaeontology*. 2nd edn. Blackwood and Sons, Edinburgh and London.

Nielsen, E. (1949) *Studies on triassic fishes from East Greenland I-II*.

Nixon, K. and Carpenter, J. (1993) “On Outgroups,” *Cladistics*, 9(4), pp. 413–426. Available at: https://doi.org/10.1006/clad.1993.1028.

Nursall, J.R. (1996a) “Distribution and ecology of pycnodont fishes,” in *Mesozoic Fishes*. Verlag Dr. Friedrich Pfeil München, pp. 115–124.

Nursall, J.R. (1996b) “The phylogeny of pycnodont fishes,” in *Mesozoic Fishes*. Verlag Dr. Friedrich Pfeil Munich, pp. 125–152.

Nursall, J.R. (1999) “The family† Mesturidae and the skull of pycnodont fishes,” *Mesozoic fishes*, 2, pp. 153–188.

Nursall, J.R. (2010) “The case for pycnodont fishes as the fossil sister-group of teleosts,” in *Origin and phylogenetic interrelationships of teleosts*, pp. 37–60.

Nybelin, O. (1966) *On Certain Triassic and Liassic Representatives of the Family Pholidophoridae S Str*. Trustees of the British Museum (Natural History).

Nybelin, O. (1974) *A revision of the leptolepid fishes.* Kungl. Vetenskaps- och vitterhets-samhället.

Olsen, P.E. (1984) “The skull and pectoral girdle of the parasemionotid fish Watsonulus eugnathoides from the Early Triassic Sakamena Group of Madagascar, with comments on the relationships of the holostean fishes,” *Journal of Vertebrate Paleontology*, 4(3), pp. 481–499.

Olsen, P.E. and McCune, A.R. (1991) “Morphology of the Semionotus elegans species group from the Early Jurassic part of the Newark Supergroup of Eastern North America with comments on the family Semionotidae (Neopterygii),” *Journal of Vertebrate Paleontology*, 11(3), pp. 269–292.

Paradis, E. and Schliep, K. (2019) “ape 5.0: an environment for modern phylogenetics and evolutionary analyses in R,” *Bioinformatics*, 35(3), pp. 526–528.

Patterson, C. (1967) “Teleostei; Elasmobranchii,” *The Fossil Record*, pp. 654–683.

Patterson, C. (1968) “The caudal skeleton in Lower Liassic pholidophorid fishes,” . *Bulletin of the British Museum (Natural History) Geology*, 16, pp. 201–239.

Patterson, C. (1973) “Interrelationships of holosteans.,” in Greenwood PH, Miles RS, and Patterson C (eds) *Interrelationships of holosteans*. London: Academic Press, pp. 233–305.

Patterson, C. (1975) “The braincase of pholidophorid and leptolepid fishes, with a review of the actinopterygian braincase,” *Philosophical Transactions of the Royal Society of London. B, Biological Sciences*, 269(899), pp. 275–579.

Patterson, C. (1977) “The contribution of paleontology to teleostean phylogeny,” *Major patterns in vertebrate evolution*, pp. 579–643.

Patterson, C. (1982) “Morphology and interrelationships of primitive actinopterygian fishes,” *American Zoologist*, 22(2), pp. 241–259.

Patterson, C. (1984) “Chanoides, a marine Eocene otophysan fish (Teleostei: Ostariophysi),” *Journal of Vertebrate Paleontology*, 4(3), pp. 430–456.

Patterson, C. and Rosen, D.E. (1977) “Review of ichthyodectiform and other Mesozoic teleost fishes, and the theory and practice of classifying fossils. ; v. 158, article 2,” *Bulletin of the AMNH*, 158.

van de Peer, Y., Taylor, J.S. and Meyer, A. (2003) *Are all fishes ancient polyploids?* Springer Netherlands.

de Pinna, M. (1996) “Teleostean monophyly,” in M.L.J. Stiassny, L.R. Parenti, and G.D. Johnson (eds) *Interrelationships of fishes*. San Diego: Academic, pp. 147–162.

Poplin, C. (1974) *Étude de quelques paléoniscidés pennsylvaniens du Kansas*. FeniXX.

Poplin, M.C. and Véran, M. (1996) “A revision of the actinopterygian fish Coccocephalus wildi from the Upper Carboniferous of Lancashire,” *Special Papers in Palaeontology*, 52, pp. 7–30.

Porro, L.B., Rayfield, E.J. and Clack, J.A. (2015) “Computed tomography, anatomical description and three-dimensional reconstruction of the lower jaw of Eusthenopteron foordi Whiteaves, 1881 from the Upper Devonian of Canada,” *Palaeontology*, 58(6), pp. 1031–1047.

Poyato-Ariza, F.J. *et al.* (1998) “First isotopic and multidisciplinary evidence for nonmarine coelacanths and pycnodontiform fishes: palaeoenvironmental implications,” *Palaeogeography, Palaeoclimatology, Palaeoecology*, 144(1–2), pp. 65–84.

Poyato-Ariza, F.J. (2015) “Studies on pycnodont fishes (I): evaluation of their phylogenetic position among actinopterygians,” *Rivista Italiana di Paleontologia e Stratigrafia*, 121(3), pp. 329–343.

Poyato-Ariza, F.J. and Martín-Abad, H. (2016) “The Cretaceous in the evolutionary history of the Actinopterygii,” *Cretaceous period: biotic diversity and biogeography. New Mexico Museum of Natural History and Science Bulletin*, 71, pp. 275–286.

Poyato-Ariza, F.J. and Wenz, S. (2002) “A new insight into pycnodontiform fishes,” *Geodiversitas*, 24(1), p. 139.

Poyato-Ariza, F.J. and Wenz, S. (2005) “Akromystax tilmachiton gen. et sp. nov., a new pycnodontid fish from the Lebanese Late Cretaceous of Haqel and En Nammoura,” *Journal of Vertebrate Paleontology*, 25(1), pp. 27–45.

Rayner, D.H. (1941) “The structure and evolution of the holostean fishes,” *Biological Reviews*, 16(3), pp. 218–237.

Rayner, D.H. (1948) “The structure of certain Jurassic holostean fishes, with special reference to their neurocrania,” *Philosophical Transactions of the Royal Society of London. Series B, Biological Sciences*, 233(601), pp. 287–345.

Redmond, A.K. *et al.* (2023) “Independent rediploidization masks shared whole genome duplication in the sturgeon-paddlefish ancestor,” *Nature Communications*, 14(1), p. 2879.

Regan, C.T. (1923) “The skeleton of Lepidosteus, with remarks on the origin and evolution of the lower neopterygian fishes,” in *Proceedings of the Zoological Society of London*. Wiley Online Library, pp. 445–461.

Ren, Y. and Xu, G.-H. (2021) “A new species of Pteronisculus from the Middle Triassic (Anisian) of Luoping, Yunnan, China, and phylogenetic relationships of early actinopterygian fishes,” *Vertebrata Palasiatica*, 59, pp. 169–199.

Richard, L. (2000) “The new actinopterygian order Guildayichthyiformes from the Lower Carboniferous of Montana (USA),” *Geodiversitas*, 22(2).

Rosenberg, M.S. and Kumar, S. (2001) “Incomplete taxon sampling is not a problem for phylogenetic inference,” *Proceedings of the National Academy of Sciences*, 98(19), pp. 10751–10756.

Rosindell, J. *et al.* (2024) “Phylogenetic biodiversity metrics should account for both accumulation and attrition of evolutionary heritage,” *Systematic Biology*, 73(1), pp. 158–182.

Ross, A.J. and Cook, E. (1995) “The stratigraphy and palaeontology of the Upper Weald Clay (Barremian) at Smokejacks Brickworks, Ockley, Surrey, England,” *Cretaceous Research*, 16(6), pp. 705–716.

Saint-Seine, P. de (1949) “Les poissons des calcaires lithographiques de Cerin (Ain),” *Publications du musée des Confluences*, 2(1), pp. 3–79.

Santini, F. *et al.* (2009) “Did genome duplication drive the origin of teleosts? A comparative study of diversification in ray-finned fishes,” *BMC evolutionary biology*, 9, pp. 1–15.

Sallan, L.C. (2014) “Major issues in the origins of ray-finned fish (A ctinopterygii) biodiversity,” *Biological Reviews*, 89(4), pp. 950–971.

Schaeffer, B. (1955) “Mendocinia, a subholostean fish from the Triassic of Argentina. American Museum novitates; no. 1737.”

Schaeffer, B. (1967) “Late Triassic fishes from the western United States. Bulletin of the AMNH; v. 135, article 6.”

Schaeffer, B. and McDonald, N.G. (1978) “Redfieldiid fishes from the Triassic-Liassic Newark Supergroup of eastern North America. Bulletin of the AMNH; v. 159, article 4.”

Schaeffer, B. and Patterson, C. (1984) “Jurassic fishes from the western United States, with comments on Jurassic fish distribution,” *American Museum novitates*, 2796.

Schaeffer, B. and Scott, G. (1971) “The braincase of the holostean fish Macrepistius, with comments on neurocranial ossification in the Actinopterygii. American Museum novitates; no. 2459.”

Schneider, C.A., Rasband, W.S. and Eliceiri, K.W. (2012) “NIH Image to ImageJ: 25 years of image analysis,” *Nature methods*, 9(7), pp. 671–675.

Schnetz, L. *et al.* (2022) “Skeletal and soft tissue completeness of the acanthodian fossil record,” *Palaeontology*, 65(4), p. e12616.

Schnetz, L. *et al.* (2024) “The skeletal completeness of the Palaeozoic chondrichthyan fossil record,” *Royal Society Open Science*, 11(1), p. 231451.

Schröder, K.M., López-Arbarello, A. and Ebert, M. (2012) “Macrosemimimus, gen. nov.(Actinopterygii, Semionotiformes), from the Late Jurassic of Germany, England, and France,” *Journal of Vertebrate Paleontology*, 32(3), pp. 512–529.

Schultze, H. and Arratia, G. (1988) “Reevaluation of the caudal skeleton of some actinopterygian fishes: II. Hiodon, Elops, and Albula,” *Journal of Morphology*, 195(3), pp. 257–303.

Schultze, H.-P. (1991) “CT scan reconstruction of the palate region of Latimeria chalumnae,” *Environmental biology of fishes*, 32, pp. 183–192.

Schultze, H.-P. and Arratia, G. (2013) “The caudal skeleton of basal teleosts, its conventions, and some of its major evolutionary novelties in a temporal dimension,” *Mesozoic fishes*, 5, pp. 187–246.

Schumacher, B.A. *et al.* (2016) “Highly specialized suspension-feeding bony fish Rhinconichthys (Actinopterygii: Pachycormiformes) from the mid-Cretaceous of the United States, England, and Japan,” *Cretaceous Research*, 61, pp. 71–85.

Schwarzhans, W. *et al.* (2018) “Computed tomography scanning as a tool for linking the skeletal and otolith-based fossil records of teleost fishes,” *Palaeontology*, 61(4), pp. 511–541.

Sereno, P.C. (2005) “The logical basis of phylogenetic taxonomy,” *Systematic Biology*, 54(4), pp. 595–619.

Sereno, P.C. (2007) “Logical basis for morphological characters in phylogenetics,” *Cladistics*, 23(6), pp. 565–587.

Silva, J.L. e *et al.* (2023) “Presence of the Aspidorhynchidae Vinctifer longirostris in the Early Cretaceous of the Araripe Basin,” *Historical Biology*, 35(8), pp. 1297–1307.

Simões, T.R. *et al.* (2018) “Giant taxon-character matrices II: a response to Laing et al.(2017),” *Cladistics*, 34(6), pp. 702–707.

Smith, G.R., Stearley, R.F. and Badgley, C.E. (1988) “Taphonomic bias in fish diversity from Cenozoic floodplain environments,” *Palaeogeography, Palaeoclimatology, Palaeoecology*, 63(1–3), pp. 263–273.

Smithwick, F.M. (2015) “Feeding ecology of the deep-bodied fish Dapedium (Actinopterygii, Neopterygii) from the Sinemurian of Dorset, England,” *Palaeontology*, 58(2), pp. 293–311.

Stensiö, E.A. (1932) *Triassic Fishes from East Greenland: Collected by the Danish Expeditions in 1929-31:[de Østgrønlandske Expeditioner Til Kong Christian Den X’s Land Udført i Aarene 1926-27 Od 1929-30 Under Ledelse Af Lauge Koch]*. Reitzel.

Stewart, J.D. (1999) “A new genus of Saurodontidae (Teleostei: Ichthyodectiformes) from Upper Cretaceous rocks of the Western Interior of North America,” *Mesozoic fishes*, 2, pp. 335–360.

Stiassny ML *et al.* (1996) “Teleostean monophyly,” in Stiassny ML, Parenti LR, and Johnson GD (eds) *Interrelationships of fishes*. San Diego: Academic Press, pp. 147–162.

Stumpf, S. *et al.* (2017) “Early Jurassic diversification of pycnodontiform fishes (Actinopterygii, Neopterygii) after the end-Triassic extinction event: evidence from a new genus and species, Grimmenodon aureum,” *Journal of Vertebrate Paleontology*, 37(4), p. e1344679.

Sytchevskaya, E.K. (1999) “Freshwater fish fauna from the Triassic of Northern Asia,” *Mesozoic fishes*, 2, pp. 445–468.

Szabó, M. and Pálfy, J. (2020) “Dapedium sp. from the Toarcian (Lower Jurassic) Úrkút Manganese Ore Formation (Bakony Mts., Hungary) and an overview of diversity of dapediiform fishes,” *Palaeobiodiversity and Palaeoenvironments*, 100(1), pp. 179–195.

Tapanila, L. and Pruitt, J. (2013) “Unraveling species concepts for the Helicoprion tooth whorl,” *Journal of Paleontology*, 87(6), pp. 965–983.

Taverne, L. (1975) “Considérations sur la position systématique des genres fossiles Leptolepis et Allothrissops au sein des Téléostéens primitifs,” *Bulletins de l’Académie Royale de Belgique*, 61(1), pp. 336–371.

Taverne, L. (2011) “Ostéologie et relations de Catervariolus (Teleostei,‘Pholidophoriformes’) du Jurassique moyen de Kisangani (Formation de Stanleyville) en République Démocratique du Congo,” *Bulletin de l’Institut Royal des Sciences Naturelles de Belgique, Sciences de la Terre*, 81, pp. 175–212.

Taverne, L. (2018) “The Mesozoic fish genus Pholidophorus (Teleostei, Pholidophoriformes), with an osteological study of the type-species Pholidophorus latiusculus. Comments on some problems concerning the ‘pholidophoriform’ fishes,” *Geo-Eco-Trop*, 42(1), pp. 89–116.

Taverne, L. and Capasso, L. (2016) “Revision of Ionoscopus petrarojae (Ionoscopiformes, Osteichthyes) from the Albian of Petraroja (Campania, Southern Italy),” *Thalassia Salentina*, 38, pp. 65–79.

Taverne, L. and Capasso, L. (2017) “Osteology and relationships of Caeus (‘Chanos’) leopoldi (Teleostei, Gonorynchiformes, Chanidae) from the marine Albian (Early Cretaceous) of Pietraroja (Campania, southern Italy),” *Bollettino dem Museo Civico di Storia Naturale di Verona, Geologia Paleontologia Preistoria*, 41, pp. 3–20.

Taverne, L. and Steurbaut, E. (2017) “Osteology and relationships of Luxembourgichthys (‘Pholidophorus’) friedeni gen. nov.(Teleostei,‘Pholidophoriformes’) from the Lower Jurassic of Belgium and the Grand Duchy of Luxembourg,” *Geologica Belgica* [Preprint].

Thies, D. (1991) “The osteolog of the bony fish Tetragonalepis semicincta BRONN 1830 (Actinopterygii+ Semionotiformes) from the Early Jurassic (Lower Toarcian) of Germany,” *Geologica et Palaeontologica*, (25), pp. 251–297.

Thies, D. and Hauff, R.B. (2011) “A new species of Dapedium Leach, 1822 (Actinopterygii, Neopterygii, Semionotiformes) from the Early Jurassic of South Germany,” *Palaeodiversity*, 4, pp. 185–221.

Thies, D., Hauff, R.B. and Herzog, A. (2008) “A neotype for Dapedium caelatum Quenstedt, 1858 (Actinopterygii, Neopterygii, Semionotiformes) from the Early Jurassic (Early Toarcian) of South Germany,” *Geologica et Palaeontologica*, 42, pp. 23–38.

Thies, D. and Herzog, A. (1999) “New information on† Dapedium LEACH 1822 (Actinopterygii,† Semionotiformes),” *Mesozoic fishes*, 2, pp. 143–152.

Thies, D. and Waschkewitz, J. (2015) “Redescription of Dapedium pholidotum (Agassiz, 1832)(Actinopterygii, Neopterygii) from the Lower Jurassic Posidonia Shale, with comments on the phylogenetic position of Dapedium Leach, 1822,” *Journal of Systematic Palaeontology*, 14(4), pp. 339–364.

Tintori, A. (1981) “Two new Pycnodonts (Pisces)”

Tintori, A. (1983) “Hypsisomatic Semionoidae (Pisces, Actinopterygii) from the Upper Triassic of Lombard (N. Italy),” *Riv. Ital. Palaeontol. Strat.*, 88(3), pp. 417–442.

Tintori, A. (1990) “The actinopterygian fish Prohalecites from the Triassic of Northern Italy,” *Palaeontology*, 33(1), pp. 155–174.

Tintori, A. *et al.* (2008) “New specialized basal neopterygians (Actinopterygii) from Triassic of the Tethys realm,” *Geologia Insubrica* [Preprint].

Tintori, A. *et al.* (2015) “Oldest stem Teleostei from the late Ladinian (Middle Triassic) of southern China,” *Rivista Italiana di Paleontologia e Stratigrafia*, 121(3), pp. 285–296.

Tintori, A. and Renesto, S. (1983) “The Macrosemiidae (Pisces, Actinopterygii) from the Upper Triassic of Lombardy (N. Italy),” *Rivista Italiana di Paleontologia e Stratigrafia*, 89(2).

Tutin, S.L. and Butler, R.J. (2017) “The completeness of the fossil record of plesiosaurs, marine reptiles from the Mesozoic,” *Acta Palaeontologica Polonica*, 62(3), p. 563.

Tyborowski, D. (2017) “Large predatory actinopterygian fishes from the Late Jurassic of Poland studied with X-ray microtomography,” *Neues Jahrbuch für Geologie und Paläontologie, Abhandlungen*, 283(2), pp. 161–172.

Vavrek, M.J., Murray, A.M. and Bell, P.R. (2014) “Xiphactinus audax Leidy 1870 from the Puskwaskau Formation (Santonian to Campanian) of northwestern Alberta, Canada and the distribution of Xiphactinus in North America,” *Vertebrate Anatomy Morphology Palaeontology*, 1, pp. 89–100.

Venkatesh, B., Erdmann, M. v and Brenner, S. (2001) “Molecular synapomorphies resolve evolutionary relationships of extant jawed vertebrates,” *Proceedings of the National Academy of Sciences*, 98(20), pp. 11382–11387.

Vogt, L. (2017) “Assessing similarity: on homology, characters and the need for a semantic approach to non-evolutionary comparative homology,” *Cladistics*, 33(5), pp. 513–539.

Volff, J.N. (2005) “Genome evolution and biodiversity in teleost fish,” *Heredity*, 94(3), pp. 280–294.

Voss, M. *et al.* (2019) “Stomach contents of the archaeocete Basilosaurus isis: apex predator in oceans of the late Eocene,” *PLoS One*, 14(1), p. e0209021.

Watrous, L.E. and Wheeler, Q.D. (1981) “The out-group comparison method of character analysis,” *Systematic Biology*, 30(1), pp. 1–11.

Weitzel, K. (1930) “Drei Riesenfische aus den Solnhofener Schiefern von-Langenaltheim.”

Wenz, S. (1967) *Compléments à l'étude des poissons actinoptérygiens du Jurassique français*. Éditions du Centre national de la recherche scientifique.

Werth, A.J. and Shear, W.A. (2014) "The evolutionary truth about living fossils," *American Scientist*, 102(6), pp. 434–443.

Wiens, J.J. (2003a) "Incomplete taxa, incomplete characters, and phylogenetic accuracy: is there a missing data problem?," *Journal of Vertebrate Paleontology*, 23(2), pp. 297–310.

Wiens, J.J. (2003b) "Missing data, incomplete taxa, and phylogenetic accuracy," *Systematic biology*, 52(4), pp. 528–538.

Wiley, E.O. and Schultze, H.-P. (1984) "Family Lepisosteida (gars) as living fossils," in *Living fossils*. Springer, pp. 160–165.

Wittbrodt, J., Meyer, A. and Schartl, M. (1998) "More genes in fish?," *BioEssays*, 20(6), pp. 511–515.

Woodward, A.S. (1889) *Catalogue of the Fossil Fishes in the British Museum (Natural History.)*. Taylor & Francis.

Woodward, A.S. (1890) "A synopsis of the fossil fishes of the English Lower Oolites," *Proceedings of the Geologists' Association*, 11(6), pp. 285-IN1.

Woodward, A.S. (1895) *Catalogue of the fossil fishes in the British Museum (Natural History)*. British Museum.

Woodward, A.S. (1896) "On the Fossil Fishes of the Upper Lias of Whitby, Part II.," *Proceedings of the Yorkshire Geological Society*, 13(2), pp. 155–170.

Woodward, A.S. (1897) "III.—Observations on Señor Ameghino's 'Notes on the Geology and Palæontology of Argentina,'" *Geological Magazine*, 4(1), pp. 20–23.

Woodward, A.S. (1918) "The Fossil Fishes of the English Wealden and Purbeck Formations. Part II. Pages 49–104, Plates XI—XX," *Monographs of the Palaeontographical Society*, 70(336), pp. 49–104.

Woodward, A.S. (1919) *The fossil fishes of the English Wealden and Purbeck formations*. Palaeontographical Society.

Woodward, A.S. (1929) "The Upper Jurassic Ganoid Fish Heterostrophus.," in *Proceedings of the Zoological Society of London*. Wiley Online Library, pp. 561–566.

Woodward, A.S. (1941) "VIII.—The mesozoic ganoid fishes of the genus Pholidophorus Agassiz," *Journal of Natural History*, 8(44), pp. 88–91.

Woodward, A.S. (1942) "LXXI.—The Beginning of the Teleostean Fishes," *Journal of Natural History*, 9(60), pp. 902–912.

Wretman, L., Blom, H. and Kear, B.P. (2016) “Resolution of the Early Jurassic actinopterygian fish Pachycormus and a dispersal hypothesis for Pachycormiformes,” *Journal of Vertebrate Paleontology*, 36(5), p. e1206022.

Xu, G. and Wu, F. (2012) “A deep-bodied ginglymodian fish from the Middle Triassic of eastern Yunnan Province, China, and the phylogeny of lower neopterygians,” *Chinese Science Bulletin*, 57, pp. 111–118.

Xu, G.-H. (2019) “Osteology and phylogeny of Robustichthys luopingensis, the largest holostean fish in the Middle Triassic,” *PeerJ*, 7, p. e7184.

Xu, G.-H. and Gao, K.-Q. (2011) “A new scanilepiform from the Lower Triassic of northern Gansu Province, China, and phylogenetic relationships of non-teleostean Actinopterygii,” *Zoological Journal of the Linnean Society*, 161(3), pp. 595–612.

Xu, G.-H., Gao, K.-Q. and Finarelli, J.A. (2014) “A revision of the Middle Triassic scanilepiform fish Fukangichthys longidorsalis from Xinjiang, China, with comments on the phylogeny of the Actinopteri,” *Journal of Vertebrate Paleontology*, 34(4), pp. 747–759.

Xu, G.-H., Zhao, L.-J. and Coates, M.I. (2014) “The oldest ionoscopiform from China sheds new light on the early evolution of halecomorph fishes,” *Biology letters*, 10(5), p. 20140204.

Zambelli, R. (1975) “Note sui Pholidophoriformes: VI contribto: Pholidopborinae subfamiglia nuova del tiassico Superiore,” *Rio. Mus. cia. Sc. Nat. Bergamo*, 10, pp. 3–49.

Zhang, H. *et al.* (2020) “Extinction of one of the world’s largest freshwater fishes: Lessons for conserving the endangered Yangtze fauna,” *Science of the Total Environment*, 710, p. 136242.

Zhu, M. *et al.* (2013) “A Silurian placoderm with osteichthyan-like marginal jaw bones,” *Nature*, 502(7470), pp. 188–193.

Zuoyu, S. *et al.* (2017) “A new non-parasemionotiform order of the Halecomorphi (Neopterygii, Actinopterygii) from the Middle Triassic of Tethys,” *Journal of Systematic Palaeontology*, 15(3), pp. 223–240.

# APPENDICES

## A.1 List of Taxa

| No. | Taxon Name | Character coding based on… |
|---|---|---|
| 1 | **"Pholidophorus germanicus"* | **Patterson, 1973; Patterson, 1975** |
| 2 | ****"Aspidorhynchus"*** | Rayner, 1948; Patterson, 1975 |
| 3 | ****"Ionoscopus" cyprinoides*** | Grande & Bemis 1998 |
| 4 | ***Acipenser brevirostrum*** (shortnose sturgeon) | Hilton, *et al.* 2011 |
| 5 | ***Aetheolepis mirabilis*** | Woodward, 1895. |
| 6 | ****Allothrissops mirabilis*** | Patterson & Rosen 1977 |
| 7 | ***Amia calva*** (bowfin) | Grande & Bemis 1998 |
| 8 | ****Ankylophorus*** | Saint-Seine, 1949 |
| 9 | ****Annaichthys pontegiurinensis*** | Arratia, 2013 |
| 10 | ***Arduafrons sp.*** | Nursall, 1999 |
| 11 | ****Ascalabos voithii*** | Arratia, 2016 |
| 12 | ****Aspidorhynchus acutirostris*** | Brito, 1999; Brito & Ebert, 2009 |
| 13 | ****Aspidorhynchus arawaki*** | Brito, 1999; Brito & Meunier, 2000; |
| 14 | ****Aspidorhynchus sanzenbacheri*** | Arratia, 2008b |
| 15 | ***Atractosteus spatula*** (alligator gar) | Grande, 2010 |
| 16 | ***Australosomus kochi*** | Nielsen, 1949 |
| 17 | ***Beishanichthys brevicaudalis*** | Xu & Gao, 2011 |
| 18 | ****Belonostomus kochii*** | Bogan *et al.*, 2011 |
| 19 | ****Belonostomus lamarquensis*** | Ebert, 2014 |
| 20 | ***Birgeria groenlandica*** | Nielsen, 1949 |
| 21 | ***Bobasatrania groenlandica*** | Stensiö. 1932 |
| 22 | ***Boreosomus piveteaui*** | Nielsen, 1942 |
| 23 | ***Brembodus ridens*** | Tintori, 1981 |
| 24 | ****Bonnerichthys gladius*** | Friedman *et al.,* 2010 |
| 25 | ***Caturus furcatus*** | Patterson,1975; Grande & Bemis 1998 |
| 26 | ***Chanoides macropoma*** | Patterson, 1984. |
| 27 | ****Cladocyclus gardneri*** | Patterson & Rosen, 1977; Forey & Cavin, L., 2007; Berrell *et al.*, 2014 |
| 28 | ***Coccocephalus wildi*** *(=Coccocephalichthys)* | Poplin, 1974; Poplin & Véran, 1996; Figueroa, *et al*. 2023 |
| 29 | ***Dandya ovalis*** | Tintori, 1983 |
| 30 | ***Dapedium caelatum*** | Thies & Herzog, 1999; Thies & Hauff, 2008 |
| 31 | ***Dapedium noricum*** | Thies & Herzog, 1999; Thies & Hauff, 2011; Thies & Waschkewitz, 2015 |
| 32 | ***Dapedium pholidotum*** | Thies & Herzog, 1999; Thies & Hauff, 2011; Thies & Waschkewitz, 2015 |
| 33 | ***Dapedium punctatum*** | Thies & Herzog, 1999; Thies & Hauff, 2011; Thies & Waschkewitz, 2015 |
| 34 | ***Dapedium sp Lias*** | Latimer & Giles, 2018 |
| 35 | ***Dapedium stollorum*** | Thies & Herzog, 1999; Thies & Hauff, 2011; Thies & Waschkewitz, 2015 |
| 36 | ***Dipteronotus ornatus*** | Bürgin, 1992 |
| 37 | ***Discoserra pectinodon*** | Lund, 2000 |
| 38 | ***Dorsetichthys bechei*** | Patterson, 1975 |
| 39 | ***Ebenaqua ritchei*** | Campbell & Phouc, 1983 |
| 40 | ***Ebertichthys*** | Arratia, 2016 |

| | | |
|---|---|---|
| **41** | ***Elops hawaiensis*** (Hawaiian ladyfish) | Forey, 1973; Schultze & Arratia, 1988 |
| **42** | ***Eomesodon liassicus*** | Gardiner, 1960 |
| **43** | ***Erpetoichthys calabaricus*** | Claeson *et al.,* 2007; Claeson & Hagadorn, 2008. |
| **44** | ****Eubiodectes libanicus*** | Cavin, *et al.,* 2013 |
| **45** | ****Eurycormus speciosus*** | Arratia & Schultze, 2007 |
| **46** | ****Euthynotus sp.*** | Arratia & Schultze, 2007 |
| **47** | ***Evenkia eunoptera*** | Sytchevskaya, 1999 |
| **48** | ***Fukangichthys longidorsalis*** | Xu, Gae & Finarelli, 2014. |
| **49** | ***Gibbodon cenensis*** | Tintori, 1981 |
| **50** | ***Hemicalypterus weiri*** | Schaeffer, 1967 |
| **51** | ***Heterostrophus phillipsi*** | Woodward, 1929 |
| **52** | ***Hiodon alosoides* (goldeye)** | Hilton, 2002 |
| **53** | ***Hulettia americana*** | Schaeffer & Patterson, 1984 |
| **54** | ****Hypsocormus posterodorsalis*** | Maxwell, *et al.,* 2020 |
| **55** | ***Ichthyokentema purbeckensis*** | Griffith & Patterson, 1963 |
| **56** | ****Ionoscopus petrarojae*** | Taverne & Capasso, L., 2016 |
| **57** | ***Lawrenciella schaefferi*** | Hamel & Poplin, 2008 |
| **58** | ****Lehmanophorus segusianus*** | Gaudant, 1978 |
| **59** | ***Lepisosteus osseus*** (longnose gar) | Grande, 2010 |
| **60** | ***Leptolepis bronni*** | Konwert & Stumpf, 2017 |
| **61** | ****Leptolepis coryphaenoides*** | Patterson, 1975 |
| **62** | ****Lombardichthys gervasutti*** | Arratia, 2017 |
| **63** | ***Macrepistius arenatus*** | Schaeffer & Scott, 1971 |
| **64** | ***Macrosemimimus lennieri*** | Jain & Robinson, 1963; Schröder *et al.,* 2012 |
| **65** | ***Macrosemius rostratus*** | Bartram, 1977 |
| **66** | ****Malingichthys nimaiguensis*** | Tintori, *et al.,* 2015 |
| **67** | ****Marcopoloichthys furreri*** | Tintori, *et al.,* 2008; Arratia, 2022 |
| **68** | ****Martillichthys renwickae*** | Dobson, *et al*., 2022 |
| **69** | ***Mesturus sp*** | Nursall, 1999 |
| **70** | ***Mesturus verrucosus*** | Nursall, 1999 |
| **71** | ***Mimipiscis bartrami*** | Choo, 2011 |
| **72** | ***Mimipiscis toombsi*** | Choo, 2011 |
| **73** | ***Moythomasia durgaringa*** | Choo, 2015 |
| **74** | ***Obaichthys decoratus*** | Grande, 2010 |
| **75** | ****Orthocormus cornutus*** | Lambers, 1988 |
| **76** | ****Orthocormus roeperi*** | Lambers, 1988 |
| **77** | ****Orthocormus teyleri*** | Arratia & Schultze, 2013 |
| **78** | ****Oshunia brevis*** | Maisey, 1991 |
| **79** | ****Pachycormus macropterus*** | Cawley *et al.,* 2019 |
| **80** | ***Paradapedium egertoni*** | Jain, 1973 |
| **81** | ****Parapholidophorus nybelini*** | Arratia, 2013 |
| **82** | ***Peltopleurus lissocephalus*** | Bürgin, 1992 |
| **83** | ****Pholidoctenus sanpellegrinensis*** | Arratia, 2017 |
| **84** | ****Pholidoctenus serianus*** | Arratia, 2013 |
| **85** | ****Pholidophorus latiusculus*** | Arratia, 2013 |
| **86** | ****Pholidorhynchodon malzannii*** | Arratia, 2017 |
| **87** | ***Platysomus superbus*** | Moy-Thomas & Dyne, 1938 |
| **88** | ***Polypterus bichir*** (Nile bichir) | Grande, 2010 |
| **89** | ***Propterus elongatus*** | Bartram, 1977 |

| | | |
|---|---|---|
| **90** | ***Pteronisculus stensioi*** | Nielsen, 1942 |
| **91** | ****Rhinconichthys purgatoirensis*** | Schumacher *et al.,* 2016 |
| **92** | ****Richmondichthys sweeti*** | Bartholomai, 2004 |
| **93** | ****Robustichthys luopingensis*** | Xu, 2019 |
| **94** | ***Saurichthys madagascarensis*** | Kogan & Romano, 2016 |
| **95** | ****Saurostomus esocinus*** | Cooper & Maxwell, 2022 |
| **96** | ***Scanilepis dubia*** | Lehman, 1980 |
| **97** | ***Scopulipiscis saxciput*** | Latimer & Giles, 2018 |
| **98** | ****Siemensichthys macrocephalus*** | Arratia, 2000 |
| **99** | ****Siemensichthys siemensi*** | Arratia, 2000 |
| **100** | ****Spathiurus dorsalis*** | El Hossny *et al.,* 2020 |
| **101** | ***Tanaocrossus kalliokoskii*** | Schaeffer & McDonald, 1978 |
| **102** | ***Tetragonolepis oldhami*** | Jain, 1973 |
| **103** | ***Tetragonolepis semicincta*** | Thies, 1991 |
| **104** | ****Tharsis elleri*** | Arratia *et al.,* 2019 |
| **105** | ****Vinctifer comptoni*** | Brito, 1997; Cantalice *et al.,* 2018; |
| **106** | ****Vinctifer longirostris*** | Silva, *et al.,* 2023 |
| **107** | ***Watsonulus eugnathoides*** | Grande & Bemis, 1998 |
| **108** | ****Zambellichthys bergamensis*** | Arratia, 2013 |

46 new species (*) were introduced to a heavily modified version of Giles ***et al***., 2023.

## A.2 List of Characters

| | |
|---|---|
| **1** | Fusion of skull roofing bones (parietals, postparietals, autosphenotics, and dermopterotics) (emended from A 1) [0] unfused [1] partial fusion [2] all fused into a continuous plate |
| **2** | Antero-lateral margin of frontal (emended from A 6) [0] smooth, without process [1] with process |
| **3** | [G 4] Premaxillae, contact at midline [0] present [1] absent |
| **4** | [G 5] Premaxilla fused at midline [0] absent [1] present |
| **5** | [G 7] Premaxilla contributes to orbital margin [0] absent [1] present |
| **6** | [G 8] Teeth on premaxillae [0] present [1] absent |
| **7** | [G 9] Mobile premaxilla [0] absent [1] present |
| **8** | [G 10] Olfactory nerve pierces premaxilla [0] absent [1] present |
| **9** | [G 11] Nasal process of premaxilla [0] absent [1] short [2] long, reaches skull roof |
| **10** | [G 17] Nasal bone as single consolidated ossification (i.e. bone(s) carrying supraorbital canal between premaxilla and anterior margin of frontals) [0] absent [1] present |
| **11** | [G 15] Median rostal [0] plate-like [1] tube-like |
| **12** | [G 18] Contact of nasals on midline [0] separated by dermal bones [1] contacting or separated by gap unfilled by bone |
| **13** | [G 19] Nasal contributes to orbital margin [0] absent [1] present |
| **14** | Contact between nasal and antorbital (emended from A 26) [0] absent [1] present |
| **15** | Mesial margin of nasal (emended from G 20) [0] not notched [1] notched |
| **16** | [G 21] Posterior nostril in complete communication with orbital fenestra [0] absent [1] present |
| **17** | [G 27] Shape of parietals (sarcopterygian postparietals): [0] rectangular, with long axis parallel to midline [1] quadrate |
| **18** | [G 29] Frontals broad posteriorly and tapering anteriorly [0] absent [1] present |
| **19** | [G 30] Anterior pit line [0] absent [1] present |
| **20** | [G 32] Junction between supraorbital and infraorbital canals [0] absent [1] present |
| **21** | [G 33] Anterior branch of infraorbital sensory canal [0] absent [1] present |
| **22** | [G 36] Number of bones carrying otic portion of lateral line canal between dermosphenotic and posterior edge of skull roof. [0] at least two (i.e. intertemporal and supratemporal) [1] one (i.e. dermopterotic) |
| **23** | [G 41] Parietal fused to dermopterotic [0] absent [1] present |
| **24** | [G 43] Number of paired extrascapulars [0] one pair [1] two pairs [2] three or more pairs |
| **25** | [G 45] Single median extrascapular [0] present [1] absent |
| **26** | [G 46] Extrascapulae contact each other at midline [0] absent [1] present |
| **27** | [A 20] Extrascapula with large rollerover bony layer at anterior margin [0] absent [1] present |
| **28** | [G 49] Antorbital bone [0] absent [1] present |
| **29** | [G 50] Tube-like canal bearing anterior arm of antorbital: [0] absent [1] present |
| **30** | [G 51] Infraorbitals [0] one [1] two [2] more than two |
| **31** | [G 52] Anterior expansion of infraorbital 1 (lacrimal) [0] absent [1] present |
| **32** | Posterior margin of infraorbital 3 (jugal) (emended from A 47) [0] confined anterior to the suborbital [1] extending beyond the suborbital |
| **33** | [G 54] Suborbitals (non-canal bearing ossifications separating jugal and maxilla) [0] absent [1] one [2] two [3] three or more |
| **34** | [G 58] Supraorbital [0] absent [1] one or two [2] three or more |
| **35** | [G 59] Anterior-most infraorbital anterior to orbit (i.e. does not contribute to orbital margin) [0] absent [1] present |
| **36** | [G 60] Three or more lachrymals [0] absent [1] present |
| **37** | [G 61] Circumorbital ring [0] Supraorbitals do not contact infraorbitals at the anterior rim of the orbit. [1] Supraorbitals contact infraorbitals, closing the orbit. |
| **38** | Canal between preopercule and infraorbitals (emended from G 62) [0] absent [1] present |
| **39** | [G 63] Dermohyal [0] absent [1] present |
| **40** | [G 68] Expanded dorsal lamina of maxilla [0] absent [1] present |
| **41** | [G 69] Contribution by maxilla to posterior margin of cheek [0] absent [1] present |
| **42** | [G 71] Teeth on maxilla [0] present [1] absent |
| **43** | [A 65] Teeth on maxilla [0] homogenous or irregular [1] increasing in size posteriorly |
| **44** | [G 72] Mobile maxilla in cheek [0] absent [1] present |
| **45** | [G 73] Peg-like anterior process of maxilla [0] absent [1] present |
| **46** | [G 74]Posterior maxillary notch [0] absent [1] present |

**47** [G 75] Supramaxilla [0] absent [1] one [2] two
**48** [A 82] Supramaxilla(e): with scarce ganoine ornamentation [0] absent [1] present
**49** [G 79] Relative length of dentary [0] long (constitutes most of the length of the lower jaw) [1] short (constitutes less than half of jaw length)
**50** [G 80] Teeth on dentary [0] present [1] absent
**51** [G 84] Teeth of outer dental arcade [0] several rows of disorganized teeth [1] two rows, with large teeth lingually and small teeth labially [2] single row of teeth
**52** [G 87] Plicidentine [0] absent [1] present
**53** [G 89] Number of infradentaries [0] more than two [1] two (angular and surangular) [2] one (angular only)
**54** [G 90] Coronoids (sensu stricto, excluding parasymphysial tooth whorl or anterior coronoid) [0] present [1] absent
**55** [G 92] Posterior coronoid [0] morphologically similar to anterior coronoids [1] expanded
**56** [G 93] Coronoid process of lower jaw [0] absent [1] present
**57** [G 94] Coronoid process contributed to by [0] prearticular only [1] surangular only [2] dentary plus postdentary bones [3] angular only
**58** [G 95] Leptolepid notch [0] absent [1] present
**59** [A 66] Dorsal margin of maxilla [0] without supramaxillary process [1] with supramaxillary process
**60** [A 78] Dentary [0] with no seperation between dental and splenial regions [1] with a well developed, protruding lateral bony ridge seperating dental and splenial regions
**61** Predentary (emended from A 79) [0] absent [1] present
**62** [G 96] Symplectic involvement in jaw joint [0] absent [1] present
**63** [G 100] Palatoquadrate ossifications [0] comineralized [1] separate ossification centers
**64** [G 101] Lateral process of ectopterygoid [0] absent [1] present
**65** [G 102] Palatoquadrate symphysis [0] absent [1] present
**66** [G 103] Dorsal margin of palate [0] high posterior extension [1] flat dorsal margin
**67** [G 104] Metapterygoid posterior to quadrate [0] absent [1] present
**68** [A 89] Symplectic [0] posterior to posterior margin of quadrate [1] medial to posterior margin of quadrate
**69** [G 106] Prearticular [0] present [1] absent
**70** Retroarticular contributes to the articular facet (emended from C 32) [0] absent [1] present
**71** Angular contributes to articular facet for quadrate (emended from C 33) [0] absent [1] present
**72** [G 107] Vomers [0] paired [1] single
**73** [G 108] Vomer sutured to parasphenoid [0] absent [1] present
**74** Dermal component to ethmopalatine (emended from C 13) [0] absent [1] present
**75** [G 112] Anterodorsal process of suboperculum [0] absent [1] present
**76** [G 113] Anteroventral process of suboperculum [0] absent [1] present
**77** [G 114] Number of cheek bones bearing pre-opercular canal posterior to jugal [0] one [1] multiple [2] series of small ossicles
**78** [G 115] Preoperculum orientation [0] pronounced dorsal limb [1] vertical [2] pronounced ventral limb
**79** [A 101] Posterior margin of preopercle: [0] smooth [1] serrated
**80** [G 116] Junction between preopercular and more anterior cheek bones [0] Infraorbitals (including jugal) or suborbitals suture with or abut preopercular [1] Infraorbitals (including jugals) and suborbitals broadly overlap preopercular [2] completely obscure
**81** [G 117] Posterior border of preopeculum notched ventrally [0] absent [1] present
**82** [G 118] Interopercle [0] absent [1] present
**83** [A 121] Postcleithrum (delete if coding finds very little variation) [0] one or two [1] three or more [2] none
**84** [G 120] Lateral gulars [0] present [1] absent
**85** [G 122] Median gular [0] absent [1] present
**86** [G 127] Interorbital septum [0] broad [1] narrow
**87** [G 128] Optic foramen [0] dorsally positioned [1] ventrally positioned (i.e. abuts parasphenoid)
**88** [G 135] Anterodorsal myodome [0] paired [1] single [2] absent
**89** [G 136] Posterior myodome [0] absent [1] paired [2] median
**90** [G 138] Endoskeletal spiracular canal [0] open [1] partial closure of spiracular bar [2] complete enclosure in canal

**91** [G 139] Basipterygoid process [0] present [1] absent
**92** [G 141] Dermal component to basipterygoid process [0] absent [1] present
**93** [G 142] Hyoid facet [0] directed posteroventrally [1] horizontal
**94** [G 143] Fossa bridgei [0] absent [1] present
**95** [G 145] Vestibular fontanelle [0] absent [1] present
**96** [G 146] Ventral cranial fissure and vestibular fontanelle [0] separated by bridge of bone [1] confluent
**97** Otoccipital fissure (emended from G 148 absent/present to present/closed) [0] present [1] closed
**98** Dorsal aorta (emended from G 151, split into two characters) [0] open in groove [1] closed
**99** Dorsal aorta canal notched posteriorly (emended from G 151, split into two characters) [0] present [1] absent
**100** [G 152] Dorsal aorta pierced by canal/s for exit of eff.a.2 [0] absent [1] present
**101** [G 153] Dorsal aorta pierced by canal/s for exit of eff.a.1 [0] absent [1] present
**102** [G 155] Birfurcation of dorsal aorta into lateral dorsal aortae [0] open [1] enclosed in canal
**103** [G 156] Braincase ossifications differentiated [0] absent [1] present
**104** [G 157] Basisphenoid [0] present [1] absent or very reduced
**105** [G 158] Opisthotic-pterotic relationship [0] opisthotic larger than subotic [1] opisthotic and pterotic equal in size
**106** [C 1] Epioccipital crest [0] absent [1] present
**107** [G 159] Epioccipital [0] present [1] absent
**108** [G 160] Forward extension of the exoccipital around the vagus nerve [0] absent [1] present
**109** [G 161] Spenotic with small dermal component [0] absent [1] present
**110** [G 162] Pterotic [0] present [1] absent
**111** [G 163] Opisthotic bone [0] present [1] absent
**112** [G 164] Intercalar [0] present [1] absent
**113** Intercaler contributes to hyomandibular facet (emended from C 6) [0] absent [1] present
**114** [G 165] Supraoccipital bone [0] absent [1] present
**115** [C 2] Supraoccipital crest [0] absent [1] present
**116** Median Supraotic [0] absent [1] present (cf. Patterson, 1975; Maisey, 1999)
**117** [G 166] Membranous outgrowth of intercalar [0] absent [1] present
**118** [G 167] Post-temporal fossa [0] absent [1] present
**119** [G 168] Sub-temporal fossa [0] absent [1] present
**120** [G 169] Dilatator fossa [0] absent [1] present
**121** [G 170] Parasphenoid [0] absent [1] present
**122** [G 171] Parasphenoid [0] terminates at/anterior to ventral otic fissure [1] extends across ventral otic fissure [2] extends to basioccipital
**123** [G 172] Ascending process of the parasphenoid [0] absent [1] present
**124** [G 174] Buccohypophyseal canal pierces parasphenoid [0] present [1] absent
**125** [G 175] Parasphenoid teeth [0] small [1] large [2] absent
**126** [G 176] Parasphenoid pierced by internal carotid artery [0] absent [1] present
**127** [G 177] Parasphenoid pierced by efferent pseudobranchial artery [0] absent [1] present
**128** [G 178] Aortic notch in parasphenoid [0] absent [1] present
**129** [A 9] Large compound rostrodermethmoid [0] absent [1] present
**130** [A 11] Laterodermethmoids [0] without teeth [1] bearing teeth
**131** [A 37] Foramen for glossopharyngeal nerve (may need to change this to account for braincases that are fully fused) [0] in prootic-exoccipital suture [1] in exoccipital region
**132** Middle pit-line groove (emended from A 41) [0] on parietal [1] on dermopterotic [2] absent
**133** [G 180] Anterolaterally divergent olfactory tracts [0] absent [1] present
**134** [G 181] Elongate olfactory tract(s) [0] absent [1] present
**135** [G 182] Olfactory nerves carried in a single tract [0] present [1] absent
**136** [G 183] Hypophyseal chamber [0] projects posteroventrally [1] projects ventrally or anteroventrally
**137** [G 184] Optic lobes [0] narrower than cerebellum [1] same width or wider than cerebellum
**138** [G 185] Optic lobes [0] smaller than telencephalon [1] larger than telencephalon
**139** [G 186] Optic tectum divided into bilateral halves [0] absent [1] present
**140** [G 187] Cerebellar corpus [0] absent [1] present
**141** [G 188] Cerebellar corpus [0] divided bilaterally [1] undivided
**142** [G 189] Position of cerebellar corpus [0] enters fourth ventricle [1] arches above fourth ventricle

**143** [G 190] Cerebellar corpus with median anteriorly projecting portion [0] absent [1] present

**144** [G 191] Horizontal semicircular canal [0] joins vestibular region dorsal to ampulla for the posterior semicircular canal [1] joins vestibular region level with ampulla for the posterior semicircular canal

**145** [G 192] Junction between ampulla of posterior semicircular canal and cranial cavity [0] separated by short length of canal [1] confluent

**146** [G 193] Crus commune of anterior and posterior semicircular canal [0] dorsal to endocranial roof [1] ventral to endocranial roof

**147** [G 194] Lateral cranial canal [0] absent [1] present

**148** [G 195] Lateral cranial canal connects to cranial cavity anteriorly [0] absent [1] present

**149** [G 196] in part; G 147] Enameloid on dermal bones and scales [0] absent [1] present

**150** [G 198] Enamel [0] single-layered [1] multi-layered

**151** [G 199] Enamel layers [0] applied directly to one another [1] separated by layers of dentine

**152** [G 200] Scales on body [0] present [1] absent

**153** [G 201] Scales [0] micromeric [1] macromeric

**154** [G 202] Scales with 'peg and socket articulation' [0] absent [1] present

**155** [G 204] Anterodorsal process on scale [0] absent [1] present

**156** [G 206] Small scales below dorsal fin [0] absent [1] present

**157** [A 130] Leading margin of paired fins (G 208 split into two characters) [0] Without fringing fulcra [1] With fringing fulcra

**158** [A 130] Leading margin of dorsal and anal fins (G 208 split into two characters) [0] Without fringing fulcra [1] With fringing fulcra

**159** [A 140] Leading margin of caudal fin [0] Without fringing fulcra [1] With fringing fulcra

**160** [G 211] Opercular process [0] absent [1] present

**161** [G 212] Ceratohyal [0] single ossification [1] two ossifications

**162** [G 213] Anterior ossification of ceratohyal [0] no medial constriction [1] medial constriction (hourglass-shaped)

**163** Hypohyal [0] single ossification [1] two ossifications

**164** [G 214] Anterior ceratohyal [0] no groove [1] groove for afferent hyoidean artery

**165** [G 215] Interhyal [0] absent [1] present

**166** [G 216] Symplectic [0] absent [1] present

**167** [G 217] Symplectic shape [0] tube/splint like [1] hatchet [2] I-shaped

**168** [G 221] Number of ceratobranchials [0] five [1] four

**169** [G 222] Number of hypobranchials [0] three [1] four [2] five

**170** [G 223] Uncinate processes on epibranchials [0] absent [1] present

**171** [G 224] Endoskeletal urohyal [0] absent [1] present

**172** [G 225] Urohyal formed as a tendon bone of the sternohyoideus muscle [0] absent [1] present

**173** [G 226] Presupracleithrum [0] absent [1] present

**174** [G 227] Presupracleithrum [0] single [1] multiple

**175** [G 229] Medial wing on cleithrum [0] absent [1] present

**176** Postcleithrum (emended from G 230) [0] one [1] two [2] three or more [3] absent

**177** [G 231] Clavicle [0] present as a broad plate [1] much reduced or absent

**178** [G 232] Serrated organ [0] absent [1] present

**179** [G 233] Interclavicle [0] present [1] absent

**180** [G 234] Triradiate scapulocoracoid [0] absent [1] present

**181** [A 119] Posttemporal [0] without a dorsal process [1] with a distinct dorsal process to articulate with the cranium

**182** [G 235] Perforate propterygium [0] absent [1] present

**183** [G 236] Anterior rays embrace propterygium [0] absent [1] present [2] fused

**184** [G 237] Propterygium fused to first ray [0] absent [1] present

**185** [G 238] Pectoral fin endoskeleton [0] extends far beyond body wall (fins lobate) [1] barely extends beyond body wall (fins not lobate)

**186** Pelvic Fins (emended from G 244) [0] present [1] absent

**187** [G 245] Pelvic fin insertion [0] shorter than fin depth (short based) [1] longer than fin depth (long based)

**188** [G 246] Basal scutes on fins [0] absent [1] present

**189** [G 247] Dorsal scutes anterior to dorsal fin [0] absent [1] few limited to region immediately anterior to fin (basal fulcra only) [2] many, extending to posterior of skull roof (complete set of dorsal ridge scales)

**190** [G 248] Ventral scutes between hypochordal lobe of caudal fin and anal fin [0] absent [1] present

**191** [G 249] Ventral scutes anterior to anal fin [0] absent [1] present

**192** [G 251] Relative positions of anal and (second) dorsal fin [0] anal shifted anteriorly relative to dorsal [1] fins opposite one another [2] anal shifted posteriorly relative to dorsal

**193** [G 252] Median fins (except caudal fin) [0] rays more numerous than radials [1] rays andradials equal

**194** Step-like' sutures between segments of caudal fin rays (emended from C 67) [0] absent, straight or sigmoidal sutures [1] present

**195** Articular surfaces of segments of the epaxial principal caudal rays joined by Z-like articulations (emended from A 176) [0] absent [1] present

**196** [G 253] Proximal and middle radials of dorsal fin [0] proximal and middle radials of similar size [1] proximal radials substantially enlarged

**197** Proximal radial of the first dorsal fin pterygiophore basally forked (emended from C 55) [0] absent [1] present

**198** [G 254] Posteriormost proximal radial of dorsal fin [0] absent [1] present

**199** [G 257] Caudal fin geometry [0] long chordal lobe [1] short chordal lobe

**200** [G 258] Posterior margin of caudal fin [0] forked [1] unforked

**201** [G 259] Diplospondyly in mid-caudal region [0] absent [1] present

**202** [G 260] Median neural spines in caudal region [0] absent [1] present

**203** [G 261] Uroneural [0] absent [1] present

**204** Number of ural neural arches modified as uroneurals (emended from A 152) [0] Absent [1] Three or less [2] Four [3] Five [4] Six or more

**205** [G 262] Division of hypurals into dorsal and ventral groups (i.e., is there a pace (hypural diastema) between hypurals 1 and 2) (emended from A 161) [0] absent [1] present

**206** [G 263] Number of caudal lepidotrichs borne per hypural [0] multiple [1] single

**207** [G 264] Opistocoelous vertebrae [0] absent [1] present

**208** [G 265] Ossified ribs [0] present [1] absent

**209** [G 267] Infraorbitals fragmented [0] absent [1] present

**210** [G 268] Suborbitals fragmented [0] absent [1] present

**211** [G 269] Suborbitals extend ventral to orbit [0] absent [1] present

**212** [G 270] Coronoids contribute to lateral dentition field [0] absent [1] present

**213** [G 271] Jaw articulation ventral to orbit [0] absent [1] present

**214** [G 272] Parasphenoid wings around basiocciput [0] absent [1] present

**215** [G 273] Dorsal extension of parasphenoid between orbits [0] absent [1] present

**216** [G 274] Ligament pit on posterior face of braincase [0] absent [1] present

**217** [G 275] 'Hem-like' median fins [0] absent [1] present

**218** [G 276] Anal fin insertion [0] short [1] long

**219** [G 277] Denticulate ridge scales [0] absent [1] present

**220** [G 278] Ossified centra [0] absent [1] present

**221** Cordacentrum surrounded laterally by growth of dorsal and ventral arcocentra that fuse to each other (archocentral type) [emended from A 106] [0] absent [1] present

**222** [G 279] Supratemporal commissure in parietal [0] absent [1] present

**223** [G 280] Enlarged vomerine teeth [0] absent [1] present

**224** [G 281] Enlarged prearticular teeth [0] absent [1] present

**225** [G 282] Prearticular symphysis [0] absent [1] present

**226** [G 284] Preoperculum taller than operculum [0] shorter [1] taller

**227** [G 285] Preoperculum wider than operculum [0] narrower [1] wider

**228** [G 286] Branchiostegals contact next in sequence [0] absent [1] present

**229** [G 288] Parasphenoid inflected ventrally below orbit [0] absent [1] present

**230** [G 289] Sagittal flange on neural spine [0] absent [1] present

**231** (A 69) Supramaxillae positioned [0] dorsal to maxilla [1] posterior to maxilla

**232** [GB 63] Innerorbital flange of dermosphenotic bearing sensory canal tube [0] absent [1] present [cf. Gardiner c.33, Grande Bemis c.63)

**233** Descending lamina of dermosphenotic (innerorbital flange) [0] fused to sphenotic/ preorbital wall [1] free distally (new)

**234** (LA&S 18) Ventral surface of infraorbital bones intensely pitted [0] absent [1] present

**235** (LA&S 265) Epural bones [0] absent [1] present

**236** Relative length of predentary [0] short (constitutes less than half the length of the lower jaw) [1] elongate (constitutes more than half of jaw length)

**237** Toothed predentary [0] present [1] absent (endentulate) (cf. Ebert, 2014)
**238** Notch in second infraorbital for supramaxilla [0] absent [1] present (cf. Xu et al. 2014)
**239** (LA&S 220) Lateral line canal in maxilla [0] absent [1] present (cf. Gardiner et al. 1996)
**240** (LA&S 102) Lachrymal [0] significantly smaller than orbit [1] nearly equal in side to orbit
**241** Tooth rows on coronoids [0] two or more [1] one row
**242** Infraorbitals [0] present [1] absent
**243** [C&M 102] Hypural plate [0] absent [1] present
**244** [C&M 128] Hypural plate [0] short and deep, with anterior margins orientated close to dorsoventral plane [1] more anteroposteriorly elongate with anterior margins angled posteriorly.
**245** Posterodorsal diverticulum on posterior semicircular canal [0] absent [1] present
**246** Posterior boss [0] absent [1] present
**247** Parietals [0] paired [1] single medline ossification
**248** Paramedial fangs on rostrodermethmoid (0) absent (1) present
**249** Dermopterotic more than double the length of the longer the parietal [0] absent [1] present (new)

Origin of character indicated in parentheses: G = Giles, S., Feilich, K., Warnock, R.C., Pierce, S.E. and Friedman, M., 2023. A Late Devonian actinopterygian suggests high lineage survivorship across the end-Devonian mass extinction. Nature Ecology & Evolution, 7(1), pp.10-19; A = Arratia, G., 2017. New Triassic teleosts (Actinopterygii, Teleosteomorpha) from northern Italy and their phylogenetic relationships among the most basal teleosts. Journal of Vertebrate Paleontology, 37(2), p.e1312690; LA&S = López-Arbarello, A. and Sferco, E., 2018. Neopterygian phylogeny: the merger assay. Royal Society Open Science, 5(3), p.172337; C&M = Cooper, S.L. and Maxwell, E.E., 2022. Revision of the pachycormid fish Saurostomus esocinus Agassiz from the Early Jurassic (Toarcian) of Europe, with new insight into the origins of suspension-feeding in Pachycormidae. Papers in Palaeontology, 8(6), p.e1467; C =Cavin, L., Forey, P.L. and Giersch, S., 2013. Osteology of Eubiodectes libanicus(Pictet & Humbert,) and some other ichthyodectiformes (Teleostei): phylogeneticimplications. Journal of Systematic Palaeontology, 11(2), pp.115-177.

*e.g., '[G 4]' = this character is equivalent to the 4$^{th}$ character of the Giles et al. (2023) matrix, and has not been modified; 'emended from A 1' = This character is an updated/revised version of the 1$^{st}$ character of the Arratia (2017) matrix, etc.*

*Otherwise, individual characters are referenced where clarification may be needed.*

# A.3 Character by Taxon Matrix

A.3 Character by Taxon Matrix

```
1.  "Pholidophorus" germanicus

1  1  1  0  0  0  1  ?  1  ?  ?  ?  0  1  ?  ?  ?  ?  ?  ?  ?  ?  ?  ?  ?  ?  1  0  2  1  ?
?  1  0  0  0  ?  ?  ?  ?  0  0  1  ?  ?  ?  ?  0  0  2  ?  1  1  -  1  2  ?  ?  0  0  0  1  ?
0  ?  ?  1  0  ?  ?  ?  ?  ?  ?  ?  ?  0  2  0  1  0  ?  ?  ?  ?  ?  ?  ?  2  2  0  ?  1  1  1  ?
0  0  -  -  -  -  1  0  1  0  0  0  ?  0  0  0  0  1  0  1  1  1  ?  ?  1  2  1  0  0  1  1  1
0  1  0  ?  ?  ?  ?  ?  ?  ?  ?  ?  ?  ?  ?  ?  ?  ?  ?  ?  ?  ?  ?  ?  ?  1  1  1  ?  ?  ?  ?  ?
1  ?  1  ?  ?  1  0  ?  ?  ?  ?  ?  ?  0  ?  ?  ?  ?  ?  ?  ?  ?  ?  ?  ?  ?  ?  ?  ?  ?  ?  ?  ?
?  ?  ?  ?  ?  ?  ?  ?  ?  ?  ?  ?  ?  ?  ?  0  ?  0  0  1  ?  ?  0  0  0  ?  ?  ?  ?  ?  ?  0  0
0  1  0  1  ?  ?  ?  ?  -  ?  ?  -  -  0  0  0  -  0  ?  ?  ?  ?  ?  -  ?

2.  "Aspidorhynchus"

1  ?  ?  ?  ?  ?  ?  ?  ?  ?  ?  ?  ?  ?  ?  ?  ?  0  0  ?  ?  ?  ?  0  ?  ?  ?  ?  ?  ?  ?  ?  ?
?  ?  ?  ?  ?  ?  ?  ?  ?  ?  ?  ?  ?  ?  ?  ?  ?  ?  ?  ?  ?  ?  ?  ?  ?  ?  ?  ?  ?  ?  ?  ?
?  ?  ?  ?  ?  ?  ?  ?  ?  ?  ?  ?  ?  ?  ?  ?  ?  ?  ?  ?  ?  ?  1  0  1  2  2  1  -  1  1  0  -
1  0  ?  ?  ?  1  1  0  0  0  0  1  0  0  0  0  0  0  0  1  1  1  1  1  1  2  1  1  0  0  0  1
0  0  1  ?  0  ?  1  1  0&1  0&1  1  1  0&1  ?  0  0  0  0  1  1  ?  ?  ?  ?  ?  ?  ?  ?  ?  ?  ?
?  ?  ?  ?  ?  ?  ?  ?  ?  ?  ?  ?  ?  ?  ?  ?  ?  ?  ?  ?  ?  ?  ?  ?  ?  ?  ?  ?  ?  ?  ?  ?
?  ?  ?  ?  ?  ?  ?  ?  ?  ?  ?  ?  ?  ?  ?  ?  ?  ?  ?  ?  ?  ?  ?  ?  0  0  0  ?  ?  ?  ?  ?  0
?  ?  ?  ?  ?  ?  0  ?  ?  1  1  ?  ?  ?  ?  ?  ?  ?  ?  ?  ?  ?  1  0  0  -  1

3.  "Ionoscopus" cyprinoides

1  ?  0  0  0  0  ?  ?  1  1  0  1  ?  ?  0  0  0  0  ?  1  1  1  0  0  1  ?  0  1  1  2  ?  1
2  1  ?  ?  ?  0  0  0  0  0  0  1  0  0  1  0  0  0  2  ?  1  ?  ?  1  2  0  0  0  0  1  1  ?
0  ?  ?  0  0  0  0  0  1  0  ?  0  0  2  0  0  0  1  0  ?  1  1  0  1  2  ?  1  -  1  ?  0  -
1  0  -  -  -  ?  1  0  0  0  0  0  0  0  0  0  0  0  0  1  1  1  1  1  1  2  1  1  0  0  0  1
0  0  1  ?  ?  ?  ?  ?  ?  ?  ?  1  1  ?  ?  0  0  0  1  1  ?  ?  ?  0  1  0  -  ?  1  1  1  ?
1  0  ?  ?  ?  1  1  ?  ?  ?  ?  ?  ?  0  -  ?  ?  ?  ?  ?  ?  0  ?  ?  ?  ?  0  ?  ?  ?  ?  ?  ?
?  0  0  ?  ?  ?  1  0  0  1  0  ?  0  1  0  0  0  0  ?  ?  ?  0  0  0  ?  ?  ?  ?  ?  ?  1  ?
?  1  0  1  0  0  0  1  1  1  1  -  -  1  1  1  ?  0  0  -  1  0  0  -  1

4.  Acipenser brevirostrum

1  1  -  -  -  -  -  -  -  0  ?  0  0  -  -  1  0  0  -  1  0  1  0  1  0  -  0  ?  ?  1  ?  -
0  1  ?  ?  0  0  0  -  -  -  -  -  -  -  -  -  -  0  1  -  ?  -  1  -  0  -  0  -  0  0  -  1  0
1  1  -  -  1  0  -  1  0  0  0  0  2  -  -  -  -  0  -  1  0  1  0  2  0  2  0  ?  0  1  0  -
1  0  -  -  -  -  1  0  ?  0  1  0  0  ?  0  1  ?  0  -  -  -  0  0  0  1  2  1  1  2  0  0  1
0  0  1  2  1  0  1  0  0  0  0  1  1  0  1  ?  ?  ?  ?  0  -  -  -  1  -  -  -  0  0  0  1  0
1  1  0  0  1  0  -  0  0  0  0  0  0  -  0  0  0  0  0  1  0  0  1  ?  1  0  0  1  2  1  1  2
0  0  0  0  0  0  0  0  0  1  0  -  0  0  0  1  0  -  -  -  0  0  0  0  0  0  0  0  -  0  0  -
-  -  -  1  0  0  -  0  -  0  1  -  -  0  -  ?  -  0  0  -  ?  0  0  -  0

5.  Aetheolepis mirabilis

?  ?  ?  ?  ?  ?  ?  ?  ?  ?  ?  ?  ?  -  0  ?  ?  ?  ?  ?  ?  ?  ?  ?  ?  ?  ?  ?  ?  ?  ?  ?
?  ?  ?  ?  ?  ?  ?  ?  ?  ?  ?  ?  ?  ?  ?  ?  ?  ?  ?  ?  ?  ?  ?  ?  ?  ?  ?  ?  ?  ?  ?  ?
?  ?  ?  ?  ?  ?  ?  ?  ?  -  ?  ?  ?  ?  ?  ?  ?  ?  ?  ?  ?  ?  ?  ?  ?  ?  ?  ?  ?  ?  ?  ?
?  ?  ?  ?  ?  ?  ?  ?  ?  ?  ?  ?  ?  ?  ?  ?  ?  ?  ?  ?  ?  ?  ?  ?  ?  ?  ?  ?  ?  ?  ?  ?
?  ?  ?  ?  ?  ?  ?  ?  ?  ?  ?  ?  ?  ?  ?  ?  ?  ?  ?  ?  ?  ?  ?  0  1  1  0  ?  ?  1  1  ?
?  ?  ?  ?  ?  ?  ?  ?  ?  ?  ?  ?  ?  -  ?  ?  ?  ?  ?  ?  ?  ?  ?  ?  1  0  0  ?  ?  ?  ?  ?
?  ?  ?  ?  0  ?  ?  ?  ?  ?  ?  ?  ?  ?  ?  ?  ?  ?  1  ?  1  ?  ?  ?  1  1  0  0  -  ?  ?  ?
?  0  0  1  ?  ?  ?  ?  -  ?  ?  ?  ?  ?  ?  ?  ?  ?  ?  ?  ?  ?  ?  ?  ?

6.  Allothrissops

0  1  0  0  0  0  1  0  0  1  0  0  0  0  0  1  0  1  1  1  1  1  0  0  1  0  0  1  0  2  1  -
0  1  0  0  0  0  0  0  0  0  0  1  1  0  2  0  0  0  2  ?  2  ?  ?  1  2  0  0  0  0  1  1  ?
?  ?  ?  1  ?  ?  1  0  1  0  0  0  0  2  0  0  0  1  0  ?  ?  1  0  ?  2  ?  0  1  ?  ?  ?  ?
?  ?  ?  ?  ?  ?  1  ?  ?  0  0  ?  ?  ?  ?  0  0  1  0  0  0  1  ?  ?  1  1  ?  ?  0  ?  1  1
0  0  1  0  ?  ?  ?  ?  ?  ?  ?  ?  ?  ?  ?  ?  ?  ?  ?  ?  ?  ?  ?  ?  ?  0  1  0  -  ?  ?  ?  ?  1
1  0  1  1  1  1  0  1  ?  1  ?  ?  0  -  0  2  1  ?  ?  ?  ?  ?  ?  ?  ?  ?  0  1  ?  ?  ?  ?  0
```

0 1 1 ? 1 1 0 0 ? 1 1 4 1 ? 0 0 0 - - ? 1 ? 0 ? 0 1 0 1 0 0 0 0
0 1 0 1 0 0 0 0 - 0 1 - - 0 0 0 ? 0 0 - ? 0 0 - 0

7. Amia calva

1 0 0 ? 0 0 0 1 2 1 0 1 0 1 0 0 1 0 1 1 0 1 0 0 1 1 0 1 1 0 0 -
0 0 0 0 ? 0 0 0 0 0 0 0 1 1 1 1 0 0 0 2 ? 1 0 0 1 2 0 1 0 0 1 1 ?
0 1 0 0 0 0 0 0 1 0 1 0 0 2 0 1 0 1 0 1 1 ? 0 1 2 2 1 - 1 1 0 -
1 0 - - - - 1 1 - 0 0 0 1 1 1 0 0 0 - - 0 1 0 1 1 2 1 1 0 0 0 1
0 - 1 0&1 0 0 1 1 1 0 1 1 1 1 1 0 0 1 0 - 0 - - 0 1 0 - ? 0 0 0
1 1 0 0 0 1 1 1 0 1 1 0 0 0 - 0 0 1 1 1 0 1 0 1 0 1 0 0 0 0 0 0
2 1 0 0 1 0 1 1 1 1 1 0 - 0 1 0 0 0 - - 0 0 0 0 0 0 ? 0 1 0 0 1
0 0 1 0 1 0 0 0 0 - 0 1 - - - 0 0 0 0 0 - 0 0 0 - 0

8. Ankylophorus

0 1 ? ? 0 0 1 ? 1 1 0 0 0 1 0 0 1 1 1 0 ? 1 0 0 1 1 0 1 0 2 1 1
1 1 0 0 0 ? 0 0 0 0 0 0 1 1 0 2 0 0 0 2 ? ? 1 - ? ? ? ? 0 0 ? 1 ?
0 ? 0 1 ? ? ? ? ? ? ? 0 0 0 2 0 1 0 1 0 ? ? 1 0 ? ? ? ? ? ? ? ? ?
? ? ? ? ? ? ? ? ? ? ? ? ? ? ? ? ? ? ? ? ? ? ? ? ? ? ? ? ? ? ? ? ?
0 1 ? 0&1 ? ? ? ? ? ? ? ? ? ? ? ? ? ? ? ? ? ? ? ? ? ? ? ? ? ? 1 1 1
? ? ? ? ? ? ? ? ? ? ? ? ? ? ? ? ? ? ? ? ? ? ? 0 ? ? ? ? ? ? ? ? ? ?
? ? ? ? ? ? ? ? ? ? ? ? ? ? ? ? ? ? 0 0 1 ? 1 ? 0 ? ? ? ? ? 1 ? ?
? ? 1 0 1 0 ? 0 0 - ? ? - - 0 0 0 - 0 ? ? ? 0 0 - 0

9. Annaichthys pontegiurinensis

2 0 1 ? 0 0 ? ? 0 1 - 0 1 0 0 1 - 1 ? ? 1 1 1 0 1 ? ? 1 0 2 1 1
2 ? 0 0 ? 0 0 0 ? 0 0 ? 1 0 2 1 0 ? ? ? 1 ? - ? - ? 0 1 0 ? ? ?
? ? 1 ? ? ? 0 ? ? - 1 0 0 2 0 1 1 1 1 ? ? ? ? ? ? ? ? ? ? ? ? ?
? ? - ? ? ? ? ? ? ? ? ? ? ? ? ? ? 0 - - ? ? ? ? 1 ? ? ? ? ? ? ?
0 1 ? - ? ? ? ? ? ? ? ? ? ? ? ? ? ? ? ? ? ? ? ? ? 0 ? 1 ? - 0 ? 1 ?
? ? ? ? ? ? ? ? ? ? ? ? 0 - ? ? 1 0 1 ? ? ? ? ? ? ? 0 0 ? ? 0 ? ?
- - 0 - ? - 1 0 ? ? ? ? ? ? ? ? 0 0 0 - 1 ? 0 ? ? ? ? 1 0 ? - -
- 1 0 1 ? ? 0 0 - 0 ? - - 0 0 0 ? 0 ? ? ? ? - - -

10. Arduafrons

1 0 0 0 0 0 0 0 1 - - - - - - 0 0 0 ? ? ? - 1 ? ? ? ? 0 - ? ? ?
0 0 ? ? ? ? 0 0 0 0 0 1 ? ? 0 - 0 0 2 ? ? ? ? ? ? ? ? ? ? ? ? ?
? ? ? ? 0 ? ? ? ? ? ? - - ? 2 0 0 0 0 ? ? 0 ? ? ? ? ? ? ? ? ? ? ?
? ? ? ? ? ? ? ? ? ? ? ? ? ? ? ? ? ? ? ? ? ? ? ? ? ? ? ? ? ? ? ? ?
? ? ? ? ? ? ? ? ? ? ? ? ? ? ? ? ? ? ? ? ? ? ? ? ? ? ? ? ? ? ? ? ?
? ? ? ? ? ? ? ? ? ? ? ? ? ? ? ? ? ? ? ? ? ? ? ? ? 0 1 1 1 ? 0 0 0 0
? ? ? ? ? ? ? ? ? ? ? ? ? ? ? ? ? 1 ? ? ? ? ? ? ? ? ? ? ? 0 2 1 1 1
? ? ? ? ? ? 1 1 0 ? 1 ? ? ? ? ? ? ? ? ? 1 ? ? ? 0 1 1 0 - ? 1 ?
? 1 1 0 ? ? - ? - ? 1 ? ? ? 0 ? ? ? ? ? ? 0 0 ? 0

11. Ascalabos

0 ? ? ? 0 ? 1 0 0 ? 0 ? ? ? ? ? ? ? ? ? ? ? ? ? ? ? 0 ? ? 2 ? ?
0 ? 0 0 ? 1 0 0 0 0 1 1 1 0 2 0 0 0 2 ? 2 1 - 1 3 ? 0 0 0 0 1 ?
0 1 ? 1 1 0 0 ? ? ? 0 0 0 2 0 1 0 0 0 1 0 ? ? ? ? ? ? ? ? ? ? ?
? ? ? ? ? ? ? ? ? ? ? ? ? ? ? ? ? ? 1 0 0 ? ? ? ? 1 ? 1 ? 2 ? ? ?
? ? 1 ? ? ? ? ? ? ? ? ? ? ? ? ? ? ? ? ? ? ? ? ? ? ? ? ? ? ? 0 0 0 ?
? ? ? ? ? 1 0 ? ? ? ? ? ? ? 0 2 ? 0 ? ? 1 ? ? 1 0 0 0 0 0 1 0 2
? 0 1 0 0 ? 1 0 0 1 1 4 ? 0 0 0 0 - - ? 1 ? 0 ? 0 1 ? 1 0 ? ? -
- ? 0 1 0 0 0 ? - 0 1 - - 0 0 ? - 0 ? ? ? ? ? ? ?

12. Aspidorhynchus acutirostris

2 0 0 1 0 0 0 0 0 1 1 0 0 - 0 0 - 1 - 0 0 1 1 0 1 1 0 0 - 2 0 0
2 1 0 0 0 0 0 1 0 0 0 1 1 0 1 0 0 0 2 ? 2 1 - 1 2 0 0 0 1 ? ? ?
? ? ? 0 1 0 0 ? ? - 0 0 0 2 0 0 0 1 0 1 0 1 0 1 2 2 0 0 1 ? 0 -
0 ? ? ? ? ? 1 0 0 0 0 1 ? 0 0 0 0 1 0 0 1 1 1 ? 1 2 1 1 0 0 1 1
0 0 1 ? ? ? ? ? ? ? ? ? ? ? ? ? ? ? ? ? ? ? ? ? ? 0 1 1 0 0 0 0 1 0
1 1 0 0 0 1 0 ? ? ? ? ? 0 - 0 3 1 0 1 ? 0 ? 0 0 0 0 0 0 0 0 0 0 0
1 0 0 1 0 ? 1 0 ? 0 1 1 1 ? 0 0 0 0 1 - 1 0 0 0 0 1 0 ? 1 0 0 -
- 1 0 1 0 ? 1 0 - 0 0 0 0 0 0 0 - 0 0 - ? ? - - -

**13. Aspidorhynchus arawaki**

? 0 0 1 0 0 0 0 ? 1 1 0 0 - 0 0 ? ? ? 0 ? 1 ? 0 1 ? 0 0 - 2 ? ?
2 1 ? ? 0 0 ? 1 0 0 0 1 ? 0 1 0 0 0 2 ? 2 1 - 1 2 0 0 0 1 0 1 0
0 1 0 0 1 0 0 1 1 - 0 0 0 2 0 0 0 ? 0 1 0 1 ? 1 1 ? ? ? 1 ? ? ?
? ? ? ? ? ? 1 0 0 ? ? ? ? 0 ? ? ? ? ? ? ? ? ? ? 1 ? 1 ? 0 0 1 ?
0 0 ? ? ? ? ? ? ? ? ? ? ? ? ? ? ? ? ? ? ? ? ? ? 0 1 1 0 0 ? ? ? 0
1 1 ? 0 0 1 0 ? ? ? ? ? ? 0 - 0 3 ? ? ? ? 0 ? ? ? 0 0 0 ? ? ? ? ?
? ? ? ? ? ? 1 0 ? ? ? ? 1 ? ? ? 0 0 1 - 1 0 0 ? ? 1 0 ? ? 0 0 -
- 1 0 ? 0 ? 1 0 - 0 ? 0 0 0 0 ? - 0 0 - ? ? ? - ?

**14. Aspidorhynchus sanzenbacheri**

2 0 0 1 0 0 0 0 0 1 1 0 0 - 1 0 - 1 - 0 0 1 1 0 1 1 0 0 - 2 0 0
2 1 0 0 0 ? ? 1 0 0 0 1 1 0 1 0 0 0 2 ? 2 1 - 1 2 0 0 0 1 0 ? ?
? ? ? ? 1 0 0 ? ? - 0 0 0 2 0 0 0 1 0 1 0 1 ? ? ? ? ? ? ? ? ? ?
? ? ? ? ? ? ? ? ? ? ? ? ? ? ? ? ? ? ? ? ? ? ? ? 1 ? ? ? ? ? ? ?
0 0 ? ? ? ? ? ? ? ? ? ? ? ? ? ? ? ? ? ? ? ? ? ? 0 1 1 0 0 ? ? 1 0
1 0 0 0 0 1 0 ? ? ? ? ? 0 - 0 3 ? ? ? ? 0 ? ? 0 0 0 0 0 0 0 0 0 0
1 0 0 1 0 ? 1 0 ? ? ? ? 1 ? ? ? 0 0 1 - 1 ? 0 ? ? 1 0 ? 1 0 ? -
- 1 0 1 0 ? 1 0 - 0 0 0 0 0 0 0 - 0 0 - ? ? - - -

**15. Atractosteus spatula**

0 0 0 0 0 0 ? 1 2 1 1 1 0 1 0 0 1 0 1 1 1 1 0 2 1 1 0 1 1 2 ? 1
3 1 1 1 1 0 1 0 0 0 0 0 1 0 0 - 0 0 1 1 1 0 0 1 2 0 0 0 0 0 1 0
0 1 1 0 0 0 0 0 1 0 1 0 0 2 0 1 0 0 0 1 0 1 0 2 2 2 0 1 1 1 0 -
1 0 - - - - 1 1 - 0 0 1 1 1 1 1 ? 0 - - - 1 0 1 1 2 1 1 0 0 0 1
0 - 1 0 ? ? ? ? ? ? ? ? ? ? ? ? ? ? ? ? ? 1 1 ? 0 1 1 0 0 1 1 1 1
1 1 0 0 1 1 2 0 1 1 0 0 0 - 1 0 1 1 1 0 0 0 1 0 0 0 0 0 0 0 0 1
1 0 0 1 0 1 1 1 0 1 0 - 0 1 1 0 0 1 0 0 1 0 0 0 0 0 - 1 0 0 0 0
0 0 0 1 0 0 - 0 - 0 1 - - 0 0 ? 0 0 0 - ? 0 0 - 0

**16. Australosomus kochi**

0 1 ? ? ? ? ? ? ? ? 0 0 ? - ? ? 0 0 1 0 0 1 0 0 1 0 0 ? ? 0 ? -
0 0 ? ? ? 0 1 1 0 0 0 0 0 0 0 0 - 0 0 2 ? 1 1 - 0 - 0 0 0 0 - 0 0
0 0 0 - 0 0 0 0 0 0 0 0 0 0 1 0 0 0 0 0 0 0 1 1 0 2 2 2 1 - ? 1 1 1
0 1 1 0 0 0 0 1 ? ? ? ? ? ? ? ? ? ? 0 - - - 0 ? 1 1 0 1 1 2 0 0 0
0 ? 0 2 0 1 1 1 1 1 0 ? ? ? ? 1 1 1 0 - ? ? ? 0 1 1 1 0 0 ? 0 1
0 0 0 1 1 0 - 0 0 1 0 0 0 - 0 3 0 0 1 1 0 0 ? 0 0 0 0 0 0 0 0 0 0
0 0 0 1 ? 0 1 0 0 1 0 - 0 0 0 1 0 - - - 0 - 0 0 0 1 - 1 0 0 0 0
0 1 0 1 0 0 - 0 - 0 1 - - - 0 ? - 0 0 - 0 0 0 - 0

**17. Beishanichthys brevicaudalis**

0 0 0 ? 1 0 0 0 ? 1 0 0 1 - 1 1 1 0 ? ? ? 1 0 1 1 ? ? 0 - 1 0 0
2 2 0 ? 0 0 1 1 0 0 0 0 0 0 0 - 0 0 2 ? 2 ? ? 1 ? 0 0 ? 0 ? ? ?
? ? ? ? ? ? ? ? ? - 0 0 0 0 0 0 0 0 0 0 ? ? ? ? ? ? ? ? ? ? ? ? ?
? ? - ? ? ? ? ? ? ? ? ? ? ? ? ? ? ? ? ? ? ? ? ? ? ? 1 ? ? ? ? ? ? ?
? ? ? ? ? ? ? ? ? ? ? ? ? ? ? ? ? ? ? ? ? ? ? ? 0 1 1 1 ? 0 0 0 ?
? ? ? ? ? 0 - ? ? ? ? ? 0 - ? 0 ? ? ? ? 0 ? ? ? ? 0 0 0 0 0 0 2
? ? ? ? 0 ? 1 1 ? ? ? ? ? ? ? ? 0 0 0 ? 0 ? ? ? 0 1 - ? ? 0 ? ?
? 1 0 1 0 ? - 0 - 0 ? - - 0 0 0 ? 0 ? ? ? 0 0 ? 0

**18. Belonostomus kochii**

0 0 0 1 0 0 0 0 0 1 1 0 0 - 0 0 0 1 ? ? ? 1 1 0 1 1 0 0 - 2 0 0
3 1 0 0 1 0 0 1 0 0 0 1 0 1 0 0 0 0 2 ? 2 1 - 1 2 0 0 0 1 0 1 0
0 ? ? 0 1 0 0 1 ? 0 ? 0 0 2 0 0 0 0 0 1 0 ? ? ? ? ? ? ? ? ? ? ?
? ? ? ? ? ? ? ? ? ? ? ? ? ? ? ? ? ? ? ? ? ? ? ? 1 ? 1 ? ? ? ? ?
0 0 ? ? ? ? ? ? ? ? ? ? ? ? ? ? ? ? ? ? ? ? ? ? 0 1 1 0 0 0 0 1 0
1 0 0 ? 0 ? ? ? ? ? ? ? 0 - 0 0 ? ? ? ? 0 ? 0 0 0 0 0 0 0 0 0 0
1 0 0 ? 0 ? 1 0 ? ? 1 1 1 ? 0 ? 0 0 1 - 1 0 0 0 0 0 0 ? 1 ? 0 -
- 1 0 1 0 ? 1 0 - 0 0 1 0 0 0 0 - 0 0 - ? 0 0 - 0

**19. Belonostomus lamarquensis**

0 0 ? ? ? ? ? ? ? ? ? ? ? ? ? ? 0 1 ? ? ? ? ? ? ? ? ? ? ? ? ?
? ? ? ? ? ? ? ? ? ? ? ? ? 1 ? ? 0 0 2 ? ? ? ? ? ? ? ? 0 1 ? ? ?
? ? ? ? ? ? ? ? ? ? ? ? ? ? ? ? ? ? ? ? ? ? ? 0 1 2 ? 0 0 1 1 0 -
0 ? ? ? ? ? 0 0 ? 0 ? 1 ? ? ? 0 0 1 0 0 1 1 ? ? 1 2 1 1 0 1 1 ?
0 ? 1 ? ? ? ? ? ? ? ? ? ? ? ? ? ? ? ? ? ? ? ? ? 0 1 1 0 ? ? ? ? ?
? ? ? ? ? ? ? ? ? ? ? ? ? ? ? ? ? ? ? ? ? ? ? 0 ? ? ? ? ? ? ? ? ? ? ?
? ? ? ? ? ? ? ? ? ? ? ? ? ? ? 0 ? ? ? ? ? ? 0 0 ? ? ? ? ? ? ? ? ?
? ? ? ? ? ? ? ? ? ? ? 1 0 ? ? ? ? ? ? ? ? 0 0 - 0

**20. Birgeria groenlandica**

0 0 0 1 0 0 0 0 1 1 0 0 1 1 1 0 ? 0 1 0 0 1 0 0 1 0 0 1 0 2 0 1
3 2 0 0 0 0 0 1 0 0 0 0 0 0 0 - 0 0 1 ? 1 ? ? 1 1 0 0 0 0 - 1 0
0 0 0 - 0 0 0 - - - 0 0 0 0 0 0 0 0 0 0 1 1 0 ? 2 2 ? ? 0 1 ? ?
0 ? ? ? ? ? 1 0 - ? ? - 0 ? ? ? ? ? ? ? - 0 0 0 1 2 1 1 2 0 0 1
0 ? ? 0 ? ? ? ? ? ? ? ? ? ? ? ? ? ? ? ? ? 0 ? ? ? 1 1 ? ? 0 0 0 0 0
0 0 0 ? 1 0 - ? 0 ? 0 0 0 - 0 3 0 0 1 0 0 0 - - 0 0 0 0 0 0 0 2
0 0 0 0 0 0 0 0 0 1 0 - 0 0 0 1 0 1 0 0 0 1 0 0 0 0 - 0 - ? - 0
0 1 0 1 0 0 - 0 - 0 1 - - 0 0 0 ? 0 0 - ? ? ? - 0

**21. Bobasatrania groenlandica**

0 0 - - - - - - - 1 0 0 1 - 1 1 1 0 ? 0 0&1 1 0 0 1 1 0 0 - 2 1
- 0 0 0 0 ? 0 0 0 0 1 - 1 0 0 0 - 0 1 - ? 2 ? ? 0 - ? ? ? ? - ?
? ? ? 0 - ? ? 0 ? ? - - - 1 1 0 0 0 0 0 ? 0 1 0 ? ? ? 0 ? ? ? ?
? ? ? ? ? ? ? ? 1 ? ? ? ? ? ? ? ? ? ? ? ? ? ? ? ? ? 1 2 1 ? 2 ? ?
? ? ? ? 2 ? ? ? ? ? ? ? ? ? ? ? ? ? ? ? ? ? ? ? ? ? 0 1 1 ? 0 0 1 1
1 0 1 ? 0 ? 0 - ? ? ? ? ? 0 - 0 0 1 ? ? ? 0 ? ? ? ? 0 0 0 1 0 1
2 1 0 0 0 0 ? 0 0 ? ? ? ? ? ? ? 1 0 - - 0 0 ? ? ? 1 1 0 0 - 0 0
0 ? 0 0 ? 0 ? - 0 - 0 ? ? ? 0 0 0 ? 0 ? ? ? 0 0 ? 0

**22. Bonnerichthys gladius**

2 ? 0 1 0 1 0 ? 0 0 - - ? 1 ? ? - 0 ? ? ? 1 ? ? ? ? ? 1 0 - - -
0 0 - - - - ? 0 0 1 - 1 0 0 ? ? 0 1 - - 2 ? ? ? ? 0 0 0 0 ? 1 0
0 1 ? ? 0 ? ? ? ? ? 0 0 0 ? ? ? ? ? ? ? ? ? ? ? ? ? ? ? 1 ? ? ?
? ? ? ? ? ? ? ? ? ? ? ? ? ? ? ? ? ? ? ? ? ? ? ? ? 1 2 1 ? 2 1 ? 1
1 ? ? 2 ? ? ? ? ? ? ? ? ? ? ? ? ? ? ? ? ? ? ? ? ? ? ? ? ? ? ? ? 1
1 0 0 0 ? ? ? ? ? ? ? ? ? ? 0 ? ? ? ? 1 ? 0 ? ? 0 ? ? ? ? ? ? ?
? ? ? ? ? ? ? ? ? ? ? ? ? - ? ? ? - ? ? ? 0 0 0 0 0 ? ? ? ? ? ? ?
? ? ? ? 0 ? ? ? ? ? ? - - - 0 - ? 1 1 0 ? ? - - -

**23. Boreosomus piveteaui**

0 0 0 1 1 1 0 0 0 1 0 1 1 - 1 1 0 0 1 0 1 1 0 1 0 - ? 0 - 2 0 1
3 0 0 0 ? 1 1 1 1 0 0 0 0 0 0 - 0 0 1 0 1 0 0 0 - 0 0 0 0 - 0 0
0 0 1 - 1 0 0 0 0 0 0 0 0 1 0 0 0 0 0 0 1 1 0 1 2 2 0 1 0 1 1 0
0 1 1 1 1 0 0 0 ? ? ? ? ? ? ? ? ? ? ? ? - 0 0 0 1 0 1 1 0 1 0 0
0 ? 0 0 0 1 0 1 1 1 1 1 1 0 0 ? ? 1 1 0 ? ? ? 0 1 1 1 0 1 1 1 1
1 1 0 ? 1 0 - ? ? 0 0 ? 0 - 0 2 0 0 1 1 ? ? ? ? 0 0 0 0 0 1 0 2
0 0 0 0 0 ? 0 0 0 0 0 - 0 ? 0 1 0 0 0 0 0 - 0 0 0 0 - 0 - 0 0 -
- 1 0 1 0 ? - 0 - 0 1 - - 0 0 0 ? 0 0 - ? 0 0 - 0

**24. Brembodus ridens**

1 1 0 0 0 0 0 0 1 - - - - - - 0 1 0 0 ? ? - 1 - - - - 0 - 0 ? ?
1 0 ? ? ? ? 0 ? ? ? ? 1 ? ? ? ? 1 0 2 ? 2 ? ? ? ? ? ? 0 0 ? ? ?
? ? ? ? 0 0 ? 1 1 0 - - 0 2 0 0 0 0 0 1 ? ? ? ? ? ? 0 ? ? ? ? ?
? ? - ? ? ? ? ? ? ? ? ? ? ? ? ? ? ? 0 0 1 ? ? ? ? 1 2 1 ? ? 0 ? ?
0 ? ? 1 ? ? ? ? ? ? ? ? ? ? ? ? ? ? ? ? ? ? ? ? ? 0 1 1 ? 0 1 1 1 1
? ? ? ? ? ? ? ? ? ? ? ? ? 0 - ? ? 1 ? 1 ? ? ? 0 0 0 0 0 0 2 ? 1 2
1 0 0 ? 0 ? 1 1 0 1 0 - ? 0 0 0 0 0 0 ? 1 1 1 ? 0 1 1 0 - 1 1 1
1 1 1 1 1 1 ? ? - ? 1 - - - ? ? ? 0 ? ? ? 0 0 - 0

**25. Caturus furcatus**

1 ? 0 0 0 0 0 1 ? 1 1 1 0 0 0 0 1 0 0 1 1 1 0 0 1 1 0 1 1 2 1 1
2 2 0 0 1 0 0 0 0 0 0 0 1 1 1 1 0 0 0 2 ? 1 0 0 1 2 0 0 0 0 1 1 0
0 1 ? 0 0 0 ? 0 1 0 1 0 0 2 0 1 0 ? 0 1 1 1 0 ? ? 2 1 - 1 ? 0 -

0 0 - ? ? ? 1 0 ? 0 0 0 0 1 1 0 0 0 - - 0 1 ? ? 1 2 1 1 0 0 0 0
0 ? ? ? ? ? ? ? ? ? ? ? ? ? ? ? ? ? ? 0 1 ? ? ? ? ? ? ? 0 0 0 0 1
1 0 0 0 1 1 1 ? ? 1 ? ? 1 0 0 1 ? 1 ? 0 1 ? ? ? ? 0 0 0 0 0 0 2
1 0 0 1 0 1 1 0 ? 1 0 - 0 0 0 0 0 0 0 0 0 0 0 ? 0 0 0 0 - 0 1 0
0 0 0 ? 0 0 0 0 - 0 1 - - 0 0 0 ? 0 0 - ? 0 0 - 0

**26. Chanoides macropoma**

0 1 ? 0 0 1 1 0 0 1 0 0 0 0 0 0 1 1 1 1 1 1 0 ? 1 ? ? 1 0 2 1 ?
0 1 0 0 0 0 0 0 0 1 - 1 1 0 1 0 0 1 - - 2 1 - 1 2 0 1 0 0 0 1 0
0 1 1 1 1 0 0 1 1 0 0 0 0 2 0 0 0 1 1 1 0 ? ? ? ? ? 0 0 ? ? ? ?
? ? - ? ? ? 1 1 ? 0 0 ? ? 0 ? ? ? ? 0 ? ? ? ? ? 1 2 1 1 0 1 1 1
0 0 ? 0 ? ? ? ? ? ? ? ? ? ? ? ? ? ? ? ? ? ? ? ? ? 0 1 0 - 0 0 0 0 1
? ? ? ? ? 1 0 ? ? ? ? ? 0 - 0 2 1 0 1 0 1 0 1 1 1 0 0 0 0 0 0 2
1 0 1 1 0 1 1 0 0 1 1 1 - 0 0 0 0 - - - 1 0 0 ? 0 1 - 1 0 0 0 -
- 1 1 1 0 0 0 0 - 0 1 - - 0 0 0 - 0 0 - ? 0 0 - 0

**27. Cladocyclus**

0 1 0 0 0 0 1 ? 0 ? 0 ? ? ? ? 1 0 1 1 1 ? 1 0 0 1 0 0 1 0 2 0 0
1 1 0 0 0 0 ? 0 0 0 0 1 1 0 2 0 0 0 2 ? 2 ? ? 1 2 0 0 0 0 1 1 0
0 0 1 1 ? 1 1 0 1 1 0 0 0 2 0 0 0 1 0 ? ? 1 0 ? 2 ? 0 1 0 ? ? ?
? ? ? ? ? ? 1 0 ? 1 0 1 ? 0 1 0 1 1 1 0 1 ? ? 1 1 2 1 0 2 1 1 1
0 0 1 0 ? ? ? ? ? ? ? ? ? ? ? ? ? ? ? ? ? ? ? ? ? 0 1 0 ? - ? ? ? 1
? ? 1 ? 0 1 1 ? ? ? ? ? ? 0 - 0 2 ? ? ? ? ? ? ? ? ? ? 0 ? ? ? ? ? ?
? 1 1 ? 0 ? ? ? ? 1 1 4 1 ? 0 0 0 0 ? ? 1 0 0 0 ? ? ? 1 0 0 0 0
0 0 0 ? 0 ? 0 0 - 0 1 - - 0 0 0 ? 0 0 - ? 0 0 - 0

**28. Coccocephalus wildi**

0 1 ? ? 0 ? ? ? ? 1 ? 0 1 1 0 1 0 0 1 0 1 1 0 1 0 - ? 1 ? 2 0 -
0 1 0 ? 0 1 ? 1 1 0 0 0 ? 0 0 - 0 0 1 ? 1 ? ? 1 1 0 0 0 0 ? 0 0
0 0 0 ? 0 0 0 ? 0 - 1 ? 0 0 0 0 0 0 0 ? ? 1 0 0 2 2 0 0 0 1 1 0
0 0 - 1 0 1 0 0 ? ? ? ? ? ? ? ? ? ? ? ? 1 0 0 0 1 0 1 1 0 0 0 0
0 ? 1 0 0 1 0 1 0 1 1 0 - - - 1 0 0 1 0 ? ? ? 0 1 ? ? ? ? ? ? 1
0 1 0 1 1 0 - 0 0 1 0 0 1 0 0 0 ? 0 ? 1 0 1 0 0 ? 0 ? ? ? ? ? ? ?
? ? ? ? ? ? ? ? ? ? ? ? ? ? ? ? ? 0 - - 0 0 - 0 ? ? ? ? ? ? 0 ? 0
0 1 0 ? 0 ? - 0 - 0 ? - - 0 0 0 ? 0 0 - 0 0 0 - ?

**29. Dandya ovalis**

1 ? ? ? ? 0 0 ? ? 1 0 1 ? - 0 ? 1 0 1 1 ? 1 0&1 2 1 1 0 ? ? 2 ?
0 3 ? 0 0 ? ? 0 0 0 1 - 1 ? 0 ? ? ? 0 2 ? ? ? ? ? ? ? 0 0 0 ? ?
? ? ? ? ? ? ? ? ? ? - 1 0 1 2 0 2 0 1 ? ? ? ? ? ? ? ? 0 1 ? ? ?
? ? ? - ? ? ? ? ? ? ? ? ? ? ? ? ? ? ? ? ? ? ? ? ? ? ? 1 ? 1 ? ? ? ?
? ? ? ? 0&1 ? ? ? ? ? ? ? ? ? ? ? ? ? ? ? ? ? ? ? ? ? 0 1 1 ? ? 1 1
0 ? ? ? ? ? ? ? ? ? ? ? ? ? ? 0 - ? 0 ? ? ? ? 0 ? ? ? ? 0 0 0 ? ?
? 2 ? ? ? ? ? ? 1 1 ? ? ? ? ? ? ? ? ? 0 0 1 ? 1 ? ? ? 1 1 ? 0 - 0
1 ? ? 0 0 1 ? 0 ? 0 - ? ? - - 0 0 ? ? 0 0 - ? 0 0 ? ?

**30. Dapedium caelatum**

0 0 0 0 0 0 0 0 ? 1 0 1 0 1 0 0 1 0 1 ? 1 1 0 ? ? ? ? 1 0 2 ? 0
3 1 0 0 0 0 0 0 0 1 - 1 1 0 ? ? 1 0 2 ? 0 0 0 1 2 0 0 0 0 ? 1 ?
? ? ? ? ? ? ? 0 ? 0 0 0 0 2 0 1 0 1 0 1 1 ? ? ? ? ? 0 1 1 ? 0 -
1 0 - ? ? 1 0 - ? ? ? ? ? ? ? ? ? ? ? ? ? - ? ? ? 1 2 1 ? 2 ? ? ?
0 ? ? 0&1 ? ? ? ? ? ? ? ? ? ? ? ? ? ? ? ? ? ? ? ? ? 0 1 1 ? 1 1 1 0
? ? ? ? ? ? ? ? ? ? ? ? ? ? ? - ? 0&1 1 ? 1 ? 0 ? ? ? 1 0 1 0 2 0
? 2 ? ? ? ? 0 ? 1 1 ? ? ? ? ? ? ? ? ? 1 ? 1 1 1 1 1 ? 1 1 0 ? ? ?
0 ? ? 0 0 1 0 ? ? 0 - 0 ? - - 0 0 ? ? 0 ? ? ? 0 0 - ?

**31. Dapedium noricum**

1 0 ? 0 0 0 0 ? ? 1 0 1 ? - 0 ? 0 0 1 ? ? 1 0 2 1 1 0 ? ? 2 ? 0
3 1 0 0 ? ? 0 0 0 1 - 1 ? 0 0 - ? 0 2 ? ? 0 ? ? ? ? 0 0 0 ? ? ?
? ? ? ? ? ? ? ? ? - 1 0 0 2 0 2 0 1 0 1 1 ? ? ? ? ? ? ? ? ? ? ? ?
? ? ? ? ? ? ? ? ? ? ? ? ? ? ? ? ? ? ? ? ? ? ? ? ? ? 1 ? ? ? 0&2 ? ?
? 0 ? ? 0&1 ? ? ? ? ? ? ? ? ? ? ? ? ? ? ? ? ? ? ? ? ? ? ? 0 1 1 ? ? 1 1
1 ? ? ? ? ? ? ? ? ? ? ? ? ? ? ? - ? ? ? ? ? ? ? ? ? ? ? 1 0 0 0 ? ?

? 2 ? ? ? ? ? ? 1 1 ? ? ? ? ? ? ? ? 0 0 1 1 1 ? ? ? 1 1 0 0 - 0
? ? ? 0 0 1 ? ? - 0 - ? ? - - 0 0 ? ? 0 ? ? ? 0 0 - 0

**32. Dapedium pholidotum**

2 0 0 1 0 0 0 0 1 1 0 1 0 1 1 0 - - ? 0 1 - 1 2 1 1 0 1 0 2 ? 0
3 2 0 0 0 1 0 0 0 0 0 0 1 ? 0 1 0 1 0 2 ? 0 0 0 1 2 0 0 0 0 ? 0 ?
0 ? 0 ? 0 0 0 0 1 0 0 0 0 2 0 2 0 1 0 1 1 ? ? ? ? ? ? ? 1 ? ? ?
1 ? - ? ? ? 0 - ? ? ? ? ? ? ? ? ? ? ? ? - ? ? ? ? ? ? ? ? ? ? ?
? ? ? - ? ? ? ? ? ? ? ? ? ? ? ? ? ? ? ? ? ? ? ? 0 1 1 ? 1 1 1 1 1
? 1 ? 0 ? 1 ? ? ? ? ? ? ? 1 0 ? 2 1 ? 1 ? 0 ? ? ? 1 0 0 0 2 0 1 2
1 0 0 ? 0 ? 1 1 ? ? ? ? ? ? ? ? ? 1 1 1 1 1 ? ? ? 1 1 0 ? ? 0 ? ?
? 0 0 1 ? ? 0 ? - 0 ? - - 0 0 ? 0 0 ? ? ? ? - ? -

**33. Dapedium punctatum**

2 0 ? 0 0 0 0 0 ? 1 0 1 0 1 0 0 - - ? ? ? - 1 2 1 1 0 1 0 2 ? 0
3 1 1 0 1 ? 0 0 0 0 0 1 1 0 ? ? 1 0 2 ? 0 ? ? ? ? ? 0 0 0 ? ? ?
? ? ? ? ? ? ? ? ? - 0 0 1 2 0 1 0 1 0 ? ? ? ? ? ? ? ? ? ? ? ? ?
1 0 - ? ? ? ? ? ? ? ? ? ? ? ? ? ? ? ? ? ? ? ? ? ? 1 ? ? ? ? ? ? ?
0 ? ? - ? ? ? ? ? ? ? ? ? ? ? ? ? ? ? ? ? ? ? ? 0 1 1 ? 1 1 1 1 1
? ? ? ? ? ? ? ? ? ? ? ? ? 1 0 ? 0 1 ? ? ? 0 ? ? ? 1 ? ? 0 2 0 ? 2
? ? ? ? 0 ? 1 1 ? ? ? ? ? ? ? ? ? 1 1 1 1 1 ? ? ? 1 1 0 ? ? ? ? ?
? 0 0 1 0 ? ? ? - ? ? - - 0 0 ? ? 0 ? ? ? ? - - -

**34. Dapedium sp Lias**

2 0 0 1 0 0 0 0 1 1 0 1 0 ? ? 0 - - 0 ? ? - 1 1 1 1 0 1 0 2 ? ?
3 1 0 0 0 ? 0 0 0 0 0 1 1 0 1 0 1 0 2 ? ? 0 0 1 2 0 ? ? ? ? ? ?
0 ? ? ? 0 0 ? ? ? - 1 0 0 2 0 1 0 1 ? 1 1 1 0 1 2 ? 0 1 1 1 0 -
1 1 1 0 0 ? 0 - ? ? ? ? ? ? ? ? ? 0 - - - 1 1 1 1 2 1 1 2 1 0 0
? ? ? ? 0 0 1 1 1 1 ? ? ? ? ? 1 1 0 1 1 ? ? ? 0 1 1 ? ? ? ? ? 1
? ? ? ? ? 1 0 ? ? ? ? ? 1 0 ? ? 1 ? 1 ? ? ? ? ? ? ? 0 0 ? ? ? ? ?
? ? ? ? ? ? 1 1 ? 1 ? ? 0 ? ? 0 1 1 1 1 1 1 1 1 1 1 0 ? ? 0 ? ?
? 0 0 1 ? ? 0 ? - ? ? ? ? 0 0 ? ? 0 0 - 0 ? - ? -

**35. Dapedium stollorum**

0 0 1 ? ? 0 0 0 1 1 0 1 0 0 1 0 1 0 1 0 1 1 0 2 1 1 0 1 0 2 ? 0
3 1 0 0 0 1 1 0 0 0 0 0 1 1 0 1 ? 1 0 2 ? 0 0 0 ? ? 0 0 0 0 ? 1 ?
? ? ? ? ? ? ? ? ? - 1 0 0 2 0 1 0 1 0 1 1 ? ? ? ? ? ? ? ? ? ? ? ?
? ? - ? ? ? 0 ? ? ? ? ? ? ? ? ? ? ? ? ? ? ? ? ? ? ? ? ? ? ? ? ? ?
0 ? ? 0&1 ? ? ? ? ? ? ? ? ? ? ? ? ? ? ? ? ? ? ? ? ? 0 1 1 ? 1 1 1 1
? ? ? ? ? ? ? ? ? ? ? ? ? ? 1 0&1 ? 2 1 ? 1 ? 0 ? ? ? 1 0 0 0 2 0
1 2 ? ? ? ? 0 ? 1 1 ? ? ? ? ? ? ? ? ? 1 1 1 1 1 ? ? ? 1 1 0 ? ? ?
? ? ? 0 0 1 ? ? 0 0 - 0 ? - - 0 0 ? ? 0 ? ? ? 0 0 - ?

**36. Dipteronotus ornatus**

0 0 ? ? 0 0 0 0 ? 1 0 0 0 1 1 0 1 0 ? 0 0 1 ? ? ? ? ? 1 ? 0 ? -
0 1 ? ? 1 ? ? 0 0 0 0 0 0 0 0 - 0 0 2 ? ? 1 ? ? ? 0 ? ? 0 ? 1 ?
? ? ? ? ? ? ? ? ? - 0 0 0 1 0 0 0 0 0 1 ? ? ? ? ? ? ? ? 1 ? ? ?
? ? - ? ? ? ? ? ? ? ? ? 0 ? ? ? ? ? ? ? ? ? ? ? ? 1 1 1 1 2 0 0 ?
? ? ? ? ? ? ? ? ? ? ? ? ? ? ? ? ? ? ? ? ? ? ? ? ? ? 0 1 ? ? ? 0 1 1 ?
? ? ? ? ? ? ? ? ? ? ? ? ? ? ? ? ? ? ? ? ? ? ? ? ? ? ? 0 0 0 2 ? 1 2
? ? ? ? 0 ? 1 0 ? 1 0 - 0 ? ? ? 0 - - - 0 - 0 ? 0 1 0 0 - ? 0 ?
? 1 0 1 0 0 - 0 - 0 1 - - - 0 ? - 0 0 - ? 0 0 ? ?

**37. Discoserra pectinodon**

0 0 0 0 1 0 0 0 0 1 0 0 1 - 1 1 1 0 ? 0 0 1 0 2 1 0 0 0 - 2 0 0
3 1 0 0 0 0 0 0 0 0 0 ? 0 0 0 - 0 0 2 ? 2 0 ? 0 - 0 0 0 0 - 1 ?
? ? 0 - 0 0 0 ? ? - - - 1 2 0 0 0 0 0 0 0 ? 0 0 2 2 ? ? 1 1 0 -
? ? ? ? ? ? 0 - ? ? ? ? ? ? ? ? ? 0 - - - 1 ? ? 1 2 1 0 ? 0 ? ?
? ? ? ? ? ? ? ? ? ? ? ? ? ? ? ? ? ? ? ? ? ? ? ? 0 1 1 ? 1 0 0 0 ?
0 0 ? 0 1 0 - ? ? ? ? ? 1 1 ? 0 1 ? 1 ? 0 ? ? 0 0 0 0 0 2 0 1 2
0 0 0 0 0 0 1 1 ? 1 0 - ? ? ? 1 0 1 1 0 1 ? ? ? 0 1 1 0 - 0 ? 0
0 0 0 1 0 0 - 0 - 0 1 - - 0 0 0 ? 0 ? ? ? 0 0 ? 0

**38. Dorsetichthys bechei**

0&2 0 0 0 0 0 1 0 0 1 0 0 1 1 0 0 1 1 1 1 1 1 1 0 1 ? 0 1 0 2 1
1 1&2 1&2 0 0 0 ? 0 0 1 0 1 1 1 0 2 0 0 0 2 ? 2 1 ? 1 2 1 0 1 0
0 1 0 0 1 0 1 0 0 0 1 1 0 0 0 0 2 0 1 0 1 0 1 0 1 0 ? 2 2 0 1 1
1 1 - 0 0 - - - - 0 0 1 0 1 0 0 0 0 0 0 1 0 0 1 1 1 1 1 2 1 0 2
1 1 1 0 1 1 1 1 1 0 1 1 1 ? 0 - - - 1 1 1 1 0 ? ? ? 0 1 1 ? ? 1
1 1 1 1 1 0 0 1 1 0 ? 0 1 1 ? 0 - ? 0 ? ? ? ? 0 ? ? 1 0 0 0 0 0
0 0 2 ? ? 0 ? 0 ? 1 0 1 1 0 - 1 0 0 0 0 0 0 0 0 0 0 0 0 0 - 1 0
0 0 - - 0 0 1 0 0 0 0 - 0 1 - - 0 0 0 - 0 0 - 0 0 0 - 0

**39. Ebenaqua ritchei**

0 0 - - - 1 - - - 1 0 0 1 - 0 1 1 0 ? 0 0 1 0 1 1 1 0 0 - 2 ? -
0 0 0 0 ? 0 0 0 0 1 - 1 ? 0 0 - 0 1 - ? 2 0 0 0 - 0 0 0 0 ? ? ?
? ? ? ? ? ? ? ? ? - 0 0 1 1 0 0 0 0 0 0 0 ? ? ? ? ? ? 1 ? ? ? ?
? ? - ? ? ? ? ? ? ? ? ? ? ? ? ? ? ? ? ? ? ? ? ? 1 ? 1 ? ? ? ? ?
? ? ? ? ? ? ? ? ? ? ? ? ? ? ? ? ? ? ? ? ? ? ? 0 1 1 ? 0 1 1 ? ?
0 1 ? ? ? ? ? ? ? ? ? ? 1 1 ? ? 1 ? ? ? 0 ? ? ? ? 0 0 0 2 1 1 1
? ? ? ? 0 1 0 1 ? ? ? ? ? ? ? ? ? 0 - - 0 1 ? ? ? 0 1 0 0 - 0 ? ?
? 0 0 ? ? ? - 0 - 0 ? - - 0 0 ? ? 0 ? ? ? 0 0 ? ?

**40. Ebertichthys**

0 0 0 0 0 0 1 0 0 1 0 0 0 0 ? 0 0 0 ? 0 1 1 0 0 1 ? 0 1 0 2 1 -
0 1 0 0 0 1 0 0 0 0 1 1 1 0 2 0 0 0 2 ? 2 1 - 1 3 ? 0 0 0 0 1 ?
0 1 0 1 1 0 0 1 ? 0 ? 0 0 2 0 1 0 1 1 1 0 1 ? ? ? ? ? ? ? ? ? ?
? ? ? ? ? ? ? ? ? ? ? ? ? ? ? ? ? ? 0 ? ? ? ? ? 1 ? ? ? 2 ? ? ?
0 1 ? ? ? ? ? ? ? ? ? ? ? ? ? ? ? ? ? ? ? ? ? ? ? 0 1 ? ? 0 0 0 0 1
1 1 1 1 ? 1 0 ? ? ? 1 ? 0 - 0 2 ? 0 ? ? 1 ? 1 1 1 0 0 0 ? ? ? 1
0 0 1 1 0 0 1 0 0 1 1 ? 1 0 0 0 0 - - - 1 ? 0 ? 0 1 0 1 0 0 0 -
- 1 0 1 0 0 0 0 - 0 1 - - 0 0 0 - 0 0 - ? 0 0 - ?

**41. Elops hawaiensis**

0 1 1 ? 0 0 1 0 2 1 0 0 0 0 0 0 1 1 0 1 1 1 0 0 1 1 0 1 0 2 1 -
0 1 0 0 0 1 0 0 1 0 0 1 1 0 2 0 0 0 0 0 2 1 - 1 2 0 0 0 0 0 1 0
0 1 0 1 1 0 0 1 1 0 0 1 0 2 0 1 0 1 ? 1 1 1 0 ? 2 0 1 - 1 1 0 -
1 0 - - - - 1 1 ? 0 0 1 0 0 1 0 0 1 0 0 1 1 1 1 1 2 0 1 0 1 0 1
0 0 0 2 ? ? ? ? ? ? ? ? ? ? ? ? ? ? 0 - 0 - - 0 0 0 - 0 1 1 1 1
1 1 1 1 ? 1 0 0 0 0 ? 1 0 - 0 0 1 0 1 0 1 0 1 1 1 0 0 0 0 0 0 2
1 0 1 1 0 1 1 0 0 1 1 2 1 0 0 0 0 - - - 0 0 0 0 0 0 - 1 0 0 0 -
- 1 0 1 0 0 0 0 - 0 1 - - 0 0 0 - 0 0 - ? 0 0 - 0

**42. Eomesodon liassicus**

0 0 0 0 0 0 0 0 1 - - - - - - 0 0 0 0 0 0 - 1 - - - - 0 - 0 ? -
0 0 ? ? ? ? 0 ? ? ? ? 1 ? ? ? ? 0 0 2 ? 2 ? ? ? ? 0 0 0 0 1 1 ?
? 0 1 0 0 0 0 1 1 0 - - 1 2 0 0 0 0 0 1 0 ? ? ? ? ? ? ? ? ? ? ?
? ? - ? ? ? ? ? ? ? ? ? ? ? ? ? ? 0 0 1 ? ? ? ? 1 2 ? ? ? ? ? ?
0 ? ? ? ? ? ? ? ? ? ? ? ? ? ? ? ? ? ? ? ? ? ? ? 0 1 1 ? 0 0 0 ? 0
? ? ? ? ? 1 ? ? ? ? ? ? 0 - ? 0 1 ? 1 ? ? ? 0 0 0 ? ? 0 2 ? 1 2
1 0 0 ? 0 ? 1 1 0 1 0 - 0 0 0 0 0 - - ? 1 ? 1 ? 0 1 1 0 - 1 1 1
1 1 1 0 1 0 ? ? - ? 1 - - - ? ? ? 0 0 - ? 0 0 - 0

**43. Erpetoichthys calabaricus**

0 1 1 ? 1 0 0 0 0 0 0 0 0 - 0 1 0 0 1 1 0 - - 2 1 1 0 0 - 1 0 ?
3 0 0 0 ? 0 1 1 0 0 0 0 0 0 0 0 - 0 0 2 0 2 0 0 1 0 0 0 0 0 - 1 1
0 1 0 - 0 0 0 1 0 0 - - 0 0 0 0 0 0 0 0 0 0 1 0 0 1 1 - 0 0 1 -
1 1 1 0 0 1 1 0 ? ? ? ? 0 ? 0 0 0 0 - - 0 0 0 0 1 2 1 1 0 0 0 1
0 0 1 2 1 0 1 0 1 0 1 1 0 0 0 0 0 1 1 ? 0 1 ? ? 0 1 1 1 0 0 0 0 1
0 0 0 0 1 0 - 1 1 0 0 1 0 - 0 0 0 0 0 1 ? 1 ? ? ? 0 1 - ? ? ? ? -
? ? ? 1 ? 1 1 1 ? ? ? ? ? 1 ? 0 0 0 0 0 0 0 0 ? 0 0 0 0 - 0 0 0
0 1 0 0 ? ? - ? - 0 ? - - 0 0 0 0 0 ? ? 0 0 0 - 0

**44. Eubiodectes**

0 1 0 0 0 0 1 ? 0 ? 0 ? 0 ? ? ? 0 1 1 1 ? 1 0 0 1 - 0 1 0 ? ? ?
? 1 ? ? ? ? 0 0 0 0 0 1 1 0 2 0 0 0 2 ? 2 ? ? 1 2 ? 0 0 0 1 1 0
0 0 1 1 ? 1 1 0 1 0 ? 0 0 2 0 ? 0 1 0 ? ? 1 0 ? 2 ? 0 1 1 ? ? ?
? ? ? ? ? ? 1 ? ? 1 0 ? ? 0 ? 0 1 1 1 0 1 ? ? 1 1 1 1 0 2 ? ? ?
0 0 ? 0 ? ? ? ? ? ? ? ? ? ? ? ? ? ? ? ? ? ? ? 0 1 0 - ? 1 ? 0 1
? ? 1 ? 0 1 ? 1 ? 1 0 ? 0 - 0 2 ? ? ? ? ? ? ? ? ? 1 0 1 ? ? ? ? 0
0 1 1 1 0 1 0 0 ? 1 1 3 1 0 ? 0 ? ? ? ? 1 ? 0 0 0 1 ? 1 0 0 0 0
0 1 0 1 0 ? 0 0 - ? 1 - - ? 0 ? ? ? 0 - ? 0 0 - ?

**45. Eurycormus speciosus**

1 0 1 ? 1 0 1 0 0 1 0 0 1 1 0 0 1 1 ? 1 1 1 0 0 1 1 0 1 0 2 1 1
3 1 0 0 0 ? 0 0 1 0 0 1 1 0 2 0 0 0 2 ? 2 0 0 0 - 1 0 0 0 1 1 0
0 ? ? 1 0 0 ? 1 1 0 0 0 0 2 0 1 0 1 0 0 0 ? ? ? ? ? ? ? ? ? ? ?
? ? ? ? ? ? ? ? ? ? ? ? ? ? ? ? ? ? ? ? ? ? ? ? 1 ? ? ? ? ? ? ?
0 1 0 2 ? ? ? ? ? ? ? ? ? ? ? ? ? ? ? ? ? ? ? ? 0 1 1 ? ? 1 1 1 0
? ? 0 ? ? ? ? ? ? ? ? ? 0 - ? 0 0 0 ? ? 0 ? 1 1 0 ? ? ? ? ? ? 2
? ? 1 ? ? ? 0 0 ? 1 1 4 1 ? ? 0 0 0 0 0 1 ? ? ? 0 1 0 1 0 0 0 -
- 0 1 1 ? 0 0 0 - 0 1 - - 0 0 0 ? 0 0 - ? 0 0 - 0

**46. Euthynotus sp**

1 ? 1 0 0 0 0 ? ? 1 - 0 ? ? ? ? ? ? ? ? ? ? ? ? ? ? 1 ? ? ? ?
2 0 ? ? - ? ? ? 0 0 0 1 ? ? 1 0 0 0 2 ? ? ? ? 0 - 0 ? 0 0 0 ? ?
? ? ? 0 ? ? ? ? ? ? ? ? ? ? ? ? ? ? ? ? ? ? ? ? ? ? ? ? ? ? ? ?
? ? ? ? ? ? ? ? ? ? ? ? ? ? ? ? ? ? ? ? ? ? ? ? ? ? ? ? ? ? ? ?
1 ? ? ? ? ? ? ? ? ? ? ? ? ? ? ? ? ? ? ? ? ? ? ? 0 1 0 0 ?   ? ?
? ? ? ? 1 0 ? ? ? ? ? ? ? 0 ? ? ? ? ? ? ? ? ? ? 0 0 0 0 ? ? ? 2 0
0 0 0 0 ? 1 0 ? 0 0 - - - 0 0 0 0 ? ? 0 ? ? ? 0 1 ? ? ? ? ? ? ?
? ? ? ? ? 1 0 - - 0 - - ? 0 ? ? ? 1 1 ? 0 0 - ?

**47. Evenkia eunoptera**

1 0 ? 0 1 0 0 0 0 0 ? ? 0 - 1 ? 1 0 0 1 1 - - ? ? ? ? 0 ? 2 0 0
2 2 0 0 0 0 1 1 0 0 0 0 0 0 0 - ? 0 2 ? 1 ? ? ? ? 0 0 0 0 ? ? ?
? ? ? ? ? ? ? ? ? - 0 1 0 0 0 0 0 0 0 0 ? ? ? ? ? ? ? ? ? ? ? ? ?
? ? - ? ? ? ? ? ? ? ? ? ? ? ? ? ? ? ? ? ? ? ? ? ? ? ? ? ? ? ? ? ?
0 ? ? 2 ? ? ? ? ? ? ? ? ? ? ? ? ? ? ? ? ? ? ? ? 0 1 1 ? 1 0 0 0 ?
? ? ? ? ? ? ? ? ? ? ? ? 1 0 ? 1 ? ? ? ? 0 ? ? ? 0 0 0 0 0 ? 1 2
? ? ? ? 0 ? 0 ? ? ? ? ? ? ? ? ? 0 1 0 ? 0 ? ? ? 0 1 - ? ? 0 ? ?
? 1 0 1 ? ? - ? - 0 ? - - 0 0 0 ? 0 ? ? ? 0 0 - ?

**48. Fukangichthys longidorsalis**

0 0 0 0 1 0 0 0 ? 1 0 ? 1 - 1 1 1 0 ? 1 0 1 0 1 1 1 0 ? ? ? ? 0
3 2 0 ? 0 ? 1 1 1 0 0 0 0 0 0 0 - 0 0 2 0 1 ? ? 1 0 0 0 0 0 ? 1 1
0 1 0 ? 0 0 0 1 0 0 0 0 0 0 0 0 0 0 0 0 1 0 1 ? ? ? ? 1 ? ? ? ?
? ? - ? ? ? ? ? ? ? ? ? ? ? ? ? ? ? ? ? ? ? ? ? ? ? 1 ? 1 0 0 0 0 ?
0 ? ? 0 ? ? ? ? ? ? ? ? ? ? ? ? ? ? ? ? ? ? ? ? ? ? 0 1 1 ? 0 1 0 0 1
0 0 ? 0 ? 0 - 1 ? 1 ? ? ? - 0 ? ? ? ? ? ? 0 ? ? ? ? ? 0 0 0 0 0 0 2
? ? ? ? 0 ? 1 1 ? ? ? ? ? ? ? ? ? 0 0 0 0 0 ? 0 ? 0 1 - ? ? 0 1 0
0 1 0 1 0 ? - 0 - ? ? - - ? 0 ? ? ? ? ? ? ? 0 0 - ?

**49. Gibbodon cenensis**

0 0 0 0 0 0 0 0 ? ? ? ? ? ? - 0 1 0 0 ? ? - 1 - - - - 0 - 0 ? ?
1 0 ? ? ? ? 0 0 0 1 - 1 ? ? ? ? 1 0 2 ? 2 ? ? ? ? ? ? 0 0 ? ? ?
? ? ? ? 0 0 ? 1 ? 0 - - 0 2 0 0 0 0 ? 1 ? ? ? ? ? ? ? ? ? ? ? ?
? ? - ? ? ? ? ? ? ? ? ? ? ? ? ? ? ? 1 0 1 ? ? ? ? ? ? ? ? ? ? ? ?
0 ? ? 0 ? ? ? ? ? ? ? ? ? ? ? ? ? ? ? ? ? ? ? ? ? 0 1 1 ? 0 0 1 1 ?
? ? ? ? ? ? ? ? ? ? ? ? 0 - ? ? 1 ? 1 ? ? ? ? ? ? ? ? ? 1 2 1 1 2
? ? ? ? 0 ? 1 1 ? ? ? ? ? ? ? ? ? 0 0 0 ? 1 ? ? ? 1 1 1 ? ? ? 1 1
? 0 1 1 ? ? ? ? - 0 ? - - - 0 ? ? 0 ? ? ? 0 0 - ?

**50. Hemicalypterus weiri**

0 1 0 0 0 0 0 0 1 1 - 1 0 ? ? ? 0 0 0 0 1 1 0 2 1 1 0 1 1 2 1 1
3 1 0 0 1 0 0 0 0 1 - 1 1 0 0 - ? 0 2 ? 1 ? ? 1 ? ? 0 0 0 ? 1 ?
? ? ? ? ? ? ? ? ? - 1 0 ? 2 0 1 0 1 0 1 1 ? ? ? ? ? ? ? ? ? ? ?

? ? - ? ? ? ? ? ? ? ? ? ? ? ? ? ? ? ? ? ? ? ? ? ? ? ? ? ? ? ?
? ? ? ? ? ? ? ? ? ? ? ? ? ? ? ? ? ? ? ? ? ? ? 0 1 1 ? - 1 0 1 ?
? ? ? ? ? ? ? ? ? ? ? ? 0&1 0 ? 0 1 ? 1 ? 0 ? ? ? 1 0 0 0 2 - 1
2 1 0 0 ? 0 1 1 1 ? ? ? ? ? 1 ? ? 0 0 1 0 1 ? ? ? 1 1 1 0 - 0 ?
? ? 0 0 1 ? ? - 0 - 0 ? - - 0 0 0 ? 0 ? ? ? 0 0 ? ?

**51. Heterostrophus phillipsi**

1 0 ? 0 0 0 0 0 ? 1 0 1 ? 1 1 ? 0 0 ? ? ? 1 0 ? ? ? ? 1 0 2 ? 0
3 1 0 0 ? ? 0 0 0 0 0 1 1 0 0 - 0 0 2 ? 1 ? ? ? ? ? 0 0 0 ? ? ?
? ? ? ? ? ? ? ? ? - 1 0 0 2 0 1 1 1 0 1 1 ? ? ? ? ? ? ? ? ? ? ?
? ? - ? ? ? ? ? ? ? ? ? ? ? ? ? ? ? ? ? ? ? ? ? ? 1 ? ? ? ? ? ? ?
0 ? ? - ? ? ? ? ? ? ? ? ? ? ? ? ? ? ? ? ? ? ? ? ? 0 1 1 1 ? ? ? ?
? ? ? ? ? ? ? ? ? ? ? ? 1 0 ? ? 1 ? 1 ? ? ? ? ? 1 0 0 0 ? 0 1 ?
? ? ? ? ? ? 1 1 ? ? ? ? ? ? ? 0 ? 1 1 0 1 ? ? ? 1 1 0 0 - ? ? ?
? 0 0 1 0 ? - 0 - 0 ? - - 0 0 ? ? 0 ? ? ? 0 0 - 0

**52. Hiodon alosoides**

0 1 0 0 0 0 1 0 0 1 0 1 0 - 0 0 1 0 1 0 1 1 1 0 1 0 0 0 - 2 0 -
0 0 0 0 ? 0 0 0 0 0 0 1 1 0 0 - 0 0 2 ? 2 1 - 1 2 0 0 0 0 0 1 ?
0 1 0 1 1 0 0 1 0 0 0 0 0 2 0 1 0 0 ? 1 0 ? ? ? 2 1 1 - 1 1 0 -
1 0 - - - - 1 1 - 0 0 1 0 0 1 0 0 1 0 0 1 1 ? 1 1 2 1 1 1 0 0 1
0 0 0 2 ? ? ? ? ? ? ? ? ? ? ? ? 1 1 1 0 - 0 - - 0 1 0 - 0 0 0 0 1
1 1 1 0 1 1 0 0 0 1 0 1 0 - 0 0 1 0 1 0 1 0 1 1 1 0 1 0 0 0 0 1
1 0 1 1 0 1 1 0 0 1 1 2 1 0 0 0 0 - - - 0 0 0 0 0 1 - 1 0 0 0 -
- 1 1 ? 0 0 - 0 - 0 1 - - 0 0 0 - 0 0 - 0 0 ? - 0

**53. Hulettia americana**

0 0 0 0 0 0 0 0 1 1 0 0 0 0 0 0 ? 0 1 0 0 1 0 0 1 1 0 1 0 2 ? 1
3 2 0 0 0 0 0 0 0 0 0 0 1 1 0 0 - 0 0 2 ? 1 0 ? 1 2 0 0 0 0 0 1 0
0 1 0 0 ? ? 0 1 ? - 1 0 0 2 0 1 0 1 0 1 0 ? ? ? ? 2 0 1 1 ? ? -
0 0 - - - - 1 0 1 0 0 ? 0 0 0 0 0 0 - - 0 ? 0 ? 1 1 1 0 2 1 1 0
? ? 0 0&1 ? ? ? ? ? ? ? ? ? ? ? ? ? ? ? ? ? 1 ? ? 0 1 1 ? 0 1 1 1
1 1 1 0 0 ? 1 0 ? ? 1 ? 0 0 - ? 1 1 0 1 ? 0 ? ? ? ? 0 0 0 1 0 1
2 1 0 0 1 0 1 1 0 1 0 0 - 0 0 0 0 0 0 0 0 1 - 0 0 0 0 0 1 0 0 0
? ? 1 0 1 0 0 - 0 - 0 1 - - 0 0 ? 0 0 0 - ? ? 0 ? ?

**54. Hypsocormus posterodorsalis**

1 ? ? ? ? ? ? ? ? ? ? ? ? ? ? ? 1 ? ? ? ? 1 0 ? 1 - - ? ? ? ? ?
2 ? ? ? ? ? ? 0 0 0 0 1 0 0 ? ? 0 0 1 ? 1 ? ? 0 - 0 0 0 0 0 1 0
0 ? ? ? 0 0 ? ? ? ? ? ? 0 ? ? ? ? ? ? ? ? ? ? ? ? ? ? 1 - 1 ? 1 ?
? ? ? ? ? ? 1 0 0 ? ? ? ? 0 0 0 0 ? ? ? 1 1 ? 1 1 1 1 ? ? 1 ? ?
1 ? ? ? ? ? ? ? ? ? ? ? ? ? ? ? ? ? ? ? ? ? ? ? ? 0 1 0 0 0 0 0 1 1
1 ? ? ? ? ? ? ? ? ? ? ? ? ? ? ? 1 1 0 ? 1 1 ? ? 1 0 0 0 1 1 ? ? 2
0 0 0 0 ? ? 0 0 ? 1 0 - - ? 0 0 ? 0 1 ? 0 0 0 0 0 1 0 ? 0 0 ? ?
? ? ? ? 0 ? ? ? ? ? ? 0 - - ? 0 ? ? 0 1 1 ? 1 1 1 0

**55. Ichthyokentema purbeckensis**

0 1 1 ? 0 0 1 0 0 1 0 1 0 1 0 0 1 1 1 0 0 1 0 0 1 0 0 1 0 2 1 1
1 2 0 0 0 1 0 0 0 0 0 0 1 1 0 1 0 0 0 2 ? 2 0 ? 1 2 1 0 0 0 0 1 0
0 0 0 1 ? ? 0 1 1 0 1 0 0 2 0 1 0 1 0 1 1 1 0 ? 2 ? 0 1 1 1 1 -
1 0 - - - ? 1 1 1 0 0 1 ? 0 0 0 0 1 0 0 1 1 1 1 1 2 1 0 1 1 0 0
0 1 0 1 ? ? ? ? ? ? ? ? ? ? ? ? ? ? ? ? ? ? 1 0 - 0 1 1 1 ? 1 1 1 ?
1 0 ? 1 ? 1 0 ? ? ? ? ? 0 - 0 ? 1 0 1 1 ? ? ? ? 1 0 0 0 1 0 ? ?
1 0 ? ? 0 ? 1 0 ? 1 1 ? ? ? 0 0 0 0 0 0 1 0 0 0 0 0 0 1 0 0 0 ?
? 1 0 1 0 0 0 0 - 0 1 - - 0 0 0 0 0 0 - ? 0 0 - 0

**56. Ionoscopus petrarojae**

1 ? 0 0 0 0 ? ? 1 1 0 1 0 1 1 ? 1 ? ? 1 1 1 0 0 1 1 0 1 1 2 ? 0
2 ? ? ? ? 0 0 0 0 0 0 ? ? ? 1 0 1 0 2 ? 1 ? ? 1 2 0 ? 0 0 1 ? ?
? ? ? 0 ? ? ? ? ? ? ? 0 0 2 0 0 0 1 0 ? 1 1 ? ? ? ? ? ? ? ? ? ?
? ? ? ? ? ? ? ? ? ? ? ? ? ? ? ? ? ? ? ? ? ? ? ? ? ? ? ? ? ? ? ?
? ? ? ? ? ? ? ? ? ? ? ? ? ? ? ? ? ? ? ? ? ? ? ? ? ? ? ? ? ? ? ?
? ? ? ? ? ? ? ? ? ? ? ? ? ? ? ? ? ? ? ? ? ? ? ? 0 1 0 - 1 0 1 1 ?
1 0 ? 0 ? 1 1 ? ? ? ? ? 0 - ? ? ? ? ? ? ? ? ? 1 0 0 0 0 0 0 0 0 2

1 0 0 ? 0 ? 1 0 0 1 0 0 0 1 0 0 0 0 ? ? 1 ? ? ? 0 0 ? 1 0 ? ? ?
? 1 0 1 ? ? 0 ? ? 1 1 - - ? 1 ? ? 0 0 - ? 0 ? ? 1

**57. Lawrenciella schaefferi**

? ? ? ? ? ? ? ? ? ? ? ? ? - ? ? ? ? ? ? ? ? ? ? ? ? ? ? ? ? ? ?
? ? ? ? ? ? ? ? ? ? ? ? ? ? ? ? ? ? ? ? ? ? ? ? ? ? ? ? ? ? ? ?
? ? ? ? ? ? ? ? 0 - ? ? ? ? ? ? ? ? ? ? ? 1 0 0 2 2 0 1 0 1 1 0
0 1 0 1 0 1 0 0 ? ? ? ? ? ? ? ? ? ? ? ? ? - 0 0 0 1 0 1 1 0 0 0 0
0 - ? ? 0 1 0 0 1 1 ? 1 1 0 0 1 1 1 1 0 ? ? ? ? ? ? ? ? ? ? ? ? ?
? ? ? ? ? ? ? ? ? ? ? ? ? ? - ? ? ? ? ? ? ? ? ? ? ? ? 0 ? ? ? ? ? ?
? ? ? ? ? ? ? ? ? ? ? ? ? ? ? ? ? ? ? ? ? ? ? ? - 0 0 ? ? ? ? ? ? ?
? ? ? ? ? ? ? ? - ? ? ? ? ? 0 ? ? ? ? ? 0 ? 0 - 0

**58. Lehmanophorus**

0 1 ? ? 1 0 1 ? 1 1 ? 0 0 1 0 0 0 1 1 0 ? 1 0 0 1 0 0 1 0 0 - -
0 1 0 0 0 ? 0 0 0 0 0 1 1 0 2 0 0 0 2 ? ? 1 - ? - ? ? 1 0 ? 1 ?
0 ? ? ? ? ? ? 1 1 ? 0 0 0 2 0 - 0 1 0 ? ? 1 0 ? ? ? ? ? ? ? ? ?
? ? ? ? ? ? ? ? ? ? ? ? ? ? ? ? ? ? ? ? ? ? ? ? ? ? 1 ? ? ? ? ? ? ?
0 1 ? 1 ? ? ? ? ? ? ? ? ? ? ? ? ? ? ? ? ? ? ? ? ? ? ? ? ? ? 1 1 ?
? ? ? ? ? ? ? ? ? ? ? ? ? ? ? ? ? ? ? ? ? ? 0 ? ? ? ? ? ? ? ? ? ?
? ? ? ? ? ? ? ? ? ? ? ? ? ? ? ? ? 0 0 - - 1 ? 0 ? ? ? ? ? 1 ? 0 ?
? 0 1 1 0 ? 0 0 - ? 1 - - - 0 - - 0 ? ? ? 0 0 - ?

**59. Lepisosteus osseus**

0 1 0 0 0 0 ? 1 2 0 1 1 0 1 1 0 0 0 1 1 1 1 0 2 1 1 0 1 1 2 ? 1
3 1 1 1 1 0 1 0 0 0 0 0 1 0 0 - 0 0 1 1 1 0 0 1 2 0 0 0 0 0 1 0
0 1 1 0 0 0 0 0 1 0 1 0 0 2 0 1 0 0 0 1 0 ? 0 2 2 2 0 1 1 1 1 -
1 0 - - - - 1 1 - 0 0 1 1 1 1 1 ? 0 - - - 0 0 1 1 2 0 1 0 0 0 1
0 - 1 0&1 0 1 1 1 1 0 1 1 1 1 1 0 1 1 1 0 1 1 0 0 1 1 1 0 1 1 1
1 1 1 0 0 1 1 2 0 1 1 0 0 0 - 1 0 1 1 1 0 0 0 1 0 0 0 0 0 0 0 0
0 1 0 0 1 0 1 1 1 0 1 0 - 0 1 1 0 0 0 0 0 1 0 0 0 0 0 - 1 0 0 0
0 0 1 1 1 0 0 - 0 - 0 1 - - 0 0 ? 0 0 0 - 0 0 0 - ?

**60. Leptolepis bronni**

0 1 0 0 0 0 1 0 1 1 0 0 0 - ? ? 1 1 1 0 1 1 0 0 0 - 0 0 - 2 ? 1
1 1 0 0 0 0 0 0 0 1 - 1 1 0 2 0 0 0 2 ? 2 ? ? 1 2 1 0 0 0 ? 1 0
0 1 0 ? 1 0 0 1 ? 0 0 0 0 2 0 1 0 1 0 1 1 1 ? ? ? ? ? ? ? ? ? ?
? ? ? ? ? ? ? ? ? ? ? ? ? ? ? ? ? ? ? ? ? ? ? ? ? ? ? ? ? ? ? ?
0 ? ? ? ? ? ? ? ? ? ? ? ? ? ? ? ? ? ? 1 1 ? ? ? ? ? ? 0 0 0 0 1
1 1 0 1 1 1 ? ? ? ? 1 1 0 - ? 0 1 1 1 ? ? ? ? 1 ? 0 0 0 0 0 0 2
1 0 0 1 1 0 1 0 0 1 1 ? 1 0 0 0 0 0 0 0 1 0 0 0 0 0 - ? ? 0 ? -
- 1 0 1 0 0 0 0 - 0 1 - - 0 0 ? ? 0 0 - ? 0 ? - 0

**61. Leptolepis coryphaenoides**

0 0 ? 0 0 0 1 ? ? 1 0 ? 0 - ? ? ? 1 ? 0 1 1 ? 0 0 - 0 0 - 2 1 1
1 1 0 0 0 0 0 0 0 0 0 1 1 0 1 0 0 0 2 ? 2 1 - 1 2 1 0 0 0 0 1 ?
0 1 0 1 1 0 0 ? ? ? 0 0 0 2 0 1 0 1 0 1 1 ? 0 ? 2 ? 0 1 1 ? 1 -
1 1 1 1 1 ? 1 0 ? ? ? 0 0 0 0 0 ? 1 0 0 1 1 ? ? 1 2 1 0 ? 1 1 1
0 ? 0 0 ? ? ? ? ? ? ? ? ? ? ? ? ? ? ? ? ? ? ? ? ? ? ? ? ? ? ? 1
1 1 0 1 ? 1 0 ? ? ? ? ? ? - 0 0 1 ? 1 ? 0 ? ? ? ? ? ? ? ? ? ? ?
? ? ? ? ? ? 1 0 0 ? ? ? 1 0 0 ? 0 0 0 ? 1 ? ? ? ? ? ? ? ? ? ? -
- 1 0 1 ? ? 0 0 - 0 ? - - 0 0 0 - 0 0 - ? ? - - ?

**62. Lombardichthys gervasutti**

2 0 1 ? 0 0 ? ? 0 1 ? 0 0 ? 0 0 - 1 1 1 ? 1 1 1 1 ? 1 1 ? 2 1 0
1&2 1 0 0 0 ? 0 0 1 0 0 ? 1 1 2 1 0 0 2 ? 1 ? ? 1 1 1 0 1 0 0 ?
? ? ? 0 ? 1 0 0 ? ? - 1 0 0 2 0 0 1 1 0 ? 1 ? ? ? ? ? ? ? ? ? ?
? ? ? - ? ? ? ? ? ? ? ? ? ? ? ? ? ? ? 0 - - ? ? ? ? 1 ? ? ? ? ? ?
? 0 1 0 1 ? ? ? ? ? ? ? ? ? ? ? ? ? ? ? ? ? ? ? ? ? ? 0 ? 1 ? 0 1 1 1
? 1 1 0 0 1 1 0 ? ? ? ? ? ? 0 - ? 1 1 0 1 ? ? ? ? ? ? ? 0 0 ? 0 1 ?
2 1 0 0 1 0 1 1 0 1 1 ? ? ? ? ? ? 0 0 0 0 - 0 ? ? ? ? ? ? ? ? 0 -
- - 0 0 1 ? ? 0 0 - 0 ? - - 0 0 0 ? 0 ? ? ? ? 0 - -

**63. Macrepistius arenatus**

0 0 ? ? 0 0 0 1 ? ? ? ? 0 ? ? 0 1 0 ? ? ? 0 - 0 1 1 0 1 1 2 ? 1
3 2 0 0 1 0 0 0 0 0 0 0 1 ? 0 ? ? 0 0 2 ? 1 0 ? 1 ? 0 0 0 0 ? ? ?
? ? ? ? ? ? ? 0 ? 0 1 0 0 2 0 1 0 1 0 ? ? 1 0 1 2 ? 0 1 1 ? 0 -
1 0 - ? ? ? 1 0 1 0 0 0 1 0 0 0 0 0 - - 1 1 1 1 1 2 1 1 2 1 0 0
0 ? ? ? ? ? ? ? ? ? ? ? ? ? ? ? ? ? ? ? 1 ? ? 0 1 ? ? ? ? 1 1 ?
? ? ? ? ? ? ? - ? ? ? ? 0 - ? 0 1 ? ? ? ? ? ? ? ? ? 0 ? ? ? ? ? ?
? ? ? ? ? ? 1 0 ? ? ? ? ? ? ? ? 0 0 1 0 1 1 0 0 ? ? ? 1 0 ? ? ?
? 1 0 1 0 ? 0 ? - 0 ? - - 0 0 ? 0 0 ? ? ? 0 0 - ?

**64. Macrosemimimus lennieri**

1 0 0 0 0 0 0 ? ? 1 1 1 0 1 ? 0 1 0 ? ? ? 1 0 0 0 - ? 1 1 2 ? 1
1 2 1 1 1 ? 0 0 0 0 0 1 1 0 0 - 0 0 2 ? 1 0 ? ? ? 0 0 0 0 0 1 0
0 0 0 0 ? ? 0 ? ? - 1 0 0 2 0 1 0 1 0 ? ? ? 0 ? 2 2 0 1 ? ? 0 -
1 0 - - - ? 1 1 - 0 0 1 0 ? 1 1 ? 0 - - - 1 1 ? 1 2 1 0 ? 0 ? 1
0 ? ? ? ? ? ? ? ? ? ? ? ? ? ? ? ? ? ? 1 0 ? ? ? 0 1 1 ? 0 0 ? ? ?
? ? ? ? ? 1 0 ? ? ? ? ? 0 - ? 2 1 ? 1 ? ? ? ? ? 1 0 0 0 0 0 0 2
? ? ? ? ? ? ? ? ? ? ? ? ? ? ? ? ? 0 0 1 0 1 ? ? ? ? ? - ? ? ? ? ?
? 1 0 1 ? ? - 0 - 0 ? - - 0 0 ? 0 0 ? ? ? 0 0 - ?

**65. Macrosemius rostratus**

1 1 0 0 0 0 0 1 2 1 ? ? 0 ? 0 ? 1 1 0 ? 1 1 0 0 1 0 0 1 1 2 ? -
0 0 0 1 ? ? 0 0 1 0 0 1 1 0 0 - 0 0 2 ? 1 0 0 1 2 0 0 0 0 ? 1 ?
0 0 0 ? 0 0 0 0 0 1 0 1 0 0 2 0 - 1 1 0 1 0 ? ? ? 2 ? 0 1 1 ? 0 -
1 ? - ? ? ? 1 1 - 0 0 1 0 0 1 1 ? ? ? ? - 1 ? 0 1 2 1 ? ? 0 0 ?
0 ? 1 2 ? ? ? ? ? ? ? ? ? ? ? ? ? ? ? 1 ? ? ? ? 0 1 1 ? ? 0 0 1 1
1 1 0 ? 1 ? ? ? ? 1 ? 0 0 - 1 ? 1 0 1 0 0 0 0 ? ? 0 0 0 ? 1 0 2
1 0 0 1 ? 1 1 1 0 ? 0 - 0 ? 0 0 0 - - 0 1 0 0 0 1 0 ? 1 0 1 1 1
0 1 0 1 - ? - 0 - 0 1 - - 0 0 ? 0 0 0 - ? 0 0 - ?

**66. Malingichthys nimaiguensis**

1 0 ? ? ? ? ? ? ? 1 - 1 1 1 1 ? 0 1 1 ? ? 1 0 0 1 1 0 1 0 2 ? 1
1 2 ? ? 0 ? 0 0 1 0 0 1 1 0 ? 1 0 0 2 ? 2 ? ? ? ? ? 1 1 0 ? ? ?
? ? ? ? ? ? 0 ? ? ? 0 0 0 2 0 1 0 1 0 ? ? ? ? ? ? ? ? ? ? ? ? ?
? ? ? ? ? ? ? ? ? ? ? ? ? ? ? ? ? ? ? ? ? ? ? ? ? ? ? ? ? ? ? ?
0 ? ? 0 ? ? ? ? ? ? ? ? ? ? ? ? ? ? ? ? ? ? ? ? 0 1 1 0 ? 1 1 1 ?
? ? ? ? ? ? ? ? ? ? ? ? 0 - 0 1 0 ? ? ? 0 ? ? 1 0 0 0 0 0 0 0 2
1 0 0 1 0 ? 1 0 ? ? ? ? 1 0 ? ? 0 0 0 ? ? ? ? ? 0 0 ? ? ? 0 ? -
- 1 0 1 ? ? ? 0 - 0 ? - - 0 0 ? ? 0 0 - ? 0 0 - 0

**67. Marcopoloichthys furreri**

0 1 ? 0 0 1 1 0 0 0 0 0 0 ? 0 0 1 1 ? ? ? 1 1 0 1 ? ? 1 0 2 0 0
1 0 0 0 ? ? 0 0 0 0 0 1 1 0 0 - 0 1 - ? 1 0 ? 1 2 0 0 0 0 0 1 0
0 1 ? 1 1 0 ? 1 ? 0 0 0 0 2 0 0 0 1 0 1 ? 1 ? ? ? ? ? ? ? ? ? ?
? ? - ? ? ? ? ? ? ? ? ? ? ? ? ? ? ? 0 - - ? ? ? ? 1 ? 1 ? ? ? ? ?
0 0 0 ? ? ? ? ? ? ? ? ? ? ? ? ? ? ? ? ? ? ? ? ? ? 1 - - - - 0 0 1 1
? ? 0 ? ? 1 0 ? ? ? ? ? 0 - 0 2 0 0 1 0 1 0 1 1 1 0 0 0 0 0 0 2
1 0 0 1 0 1 1 0 0 1 1 2 1 0 0 0 0 0 0 ? 1 ? 0 ? 0 0 0 1 0 ? 0 -
- 1 1 1 0 0 - 0 - 0 1 - - 0 0 0 ? 0 0 - ? 0 0 - 0

**68. Martillichthys renwickae**

1 1 1 0 ? ? ? ? ? 1 - 0 ? ? ? ? 0 0 0 0 ? 1 0 - 1 - - 1 ? 2 ? ?
2 ? ? 0 ? ? 0 0 0 1 - 1 1 0 0 - 0 1 - - 1 0 ? 0 - 0 0 0 0 0 1 0
0 ? 1 1 0 0 0 1 1 0 ? ? ? ? ? ? ? ? ? 1 1 ? ? ? ? ? 1 - 1 ? ? ?
? 0 - - - - ? ? ? ? ? ? ? ? ? ? ? ? ? 0 ? ? ? ? 1 1 ? ? 2 ? ? 1
1 ? ? 2 ? ? ? ? ? ? ? ? ? ? ? ? ? ? ? ? ? ? ? ? ? ? ? ? ? ? ? ? 1
1 0 0 1 1 1 1 0 ? ? ? ? ? ? ? ? ? ? ? ? ? ? ? ? ? ? ? ? ? ? ? ? ?
? ? ? ? ? ? ? ? ? ? ? ? ? ? ? ? ? 0 0 ? 0 ? 0 ? ? ? ? ? ? ? 0 0
0 ? ? 1 ? ? ? ? ? ? ? - - ? 0 ? ? 0 ? ? ? 1 0 0

**69. Mesturus sp**

1 0 ? ? ? ? ? ? ? ? ? ? ? - ? ? 0 0 0 ? ? ? 1 ? ? ? ? ? ? ? ? ?
? ? ? ? ? ? ? ? ? ? ? ? ? ? ? ? ? ? ? ? ? ? ? ? ? ? ? ? ? ? ? ? ?
? ? ? ? ? ? ? ? ? - ? ? ? ? ? ? ? ? ? ? ? ? ? - 0 ? 2 ? 0 1 1 ? 0 -
0 ? - ? ? ? 1 0 1 0 0 0 0 0 0 0 0 0 - - 0 1 1 1 1 2 1 1 2 1 1 1
? ? ? 2 ? ? ? ? ? ? ? ? ? ? ? ? ? ? ? ? ? ? ? ? ? ? ? ? ? ? ? ? ?
? ? ? ? ? ? ? ? ? ? ? ? ? ? - ? ? ? ? ? ? ? ? ? ? ? ? 0 ? ? ? ? ? ?
? ? ? ? ? ? ? ? ? ? ? ? ? ? ? ? ? ? ? ? ? ? ? ? 1 1 ? ? ? ? ? ? ? ?
? ? ? ? 1 ? ? ? - ? 1 ? ? ? ? ? ? ? ? ? ? ? 0 0 -

**70. Mesturus verrucosus**

0 0 0 0 0 0 0 0 1 - - - - - - 0 0 0 0 ? ? ? 1 ? ? ? ? 0 - ? ? -
0 0 ? ? ? ? 0 0 0 1 - 1 1 0 0 - 0 0 2 ? 2 ? ? 1 0 0 0 0 0 ? ? ?
? ? ? ? 0 0 ? 1 ? 0 - - - 2 0 0 0 0 0 1 0 ? ? ? ? ? ? ? ? ? ? ?
? ? ? ? ? ? ? ? ? ? ? ? ? ? ? ? ? ? ? ? ? ? ? ? ? ? ? ? ? ? ? ? ?
0 ? ? 2 ? ? ? ? ? ? ? ? ? ? ? ? ? ? ? ? ? ? ? ? ? 0 1 1 ? 0 ? ? 0 0
1 1 ? 0 ? ? ? ? ? ? ? ? ? - ? ? 1 ? ? ? ? ? ? 0 0 0 0 ? 0 2 ? ? ?
1 0 0 ? ? ? 1 1 0 1 ? ? ? ? 0 0 - - - ? 1 ? ? ? 0 1 1 0 - ? 1 1
1 1 1 0 ? 1 - ? - - ? - - - 0 ? ? ? ? ? ? 0 0 - 0

**71. Mimipiscis bartrami**

1 1 0 0 1 0 0 0 0 1 0 0 1 - 1 1 0 0 1 0 1 0 - 0 1 1 0 0 - 1 0 -
0 0 0 0 ? 0 1 1 1 0 0 0 0 0 0 0 - 0 0 1 0 2 0 0 0 - 0 0 0 0 - 0 0
0 0 0 - 0 0 0 0 0 0 1 0 0 0 0 0 0 0 0 0 1 1 0 ? 0 1 0 0 0 0 1 0
0 1 1 0 0 0 0 0 ? ? ? ? ? ? ? ? ? ? ? ? ? - 0 0 0 1 0 0 0 0 0 0 -
0 0 ? 0 ? 1 1 ? ? ? ? ? ? ? ? ? ? ? ? 1 ? ? ? ? 0 1 1 1 0 1 1 1 ?
0 0 ? 1 1 0 - 0 1 0 0 0 1 0 0 0 0 0 ? ? 0 1 ? 0 1 0 0 0 2 1 1 2
0 0 0 ? 0 0 0 0 0 0 0 - 0 ? 0 1 0 - - 0 0 - 0 0 0 0 0 0 - 0 0 0
0 1 0 1 0 0 - 0 - 0 1 - - 0 0 0 0 0 0 - ? 0 0 - 0

**72. Mimipiscis toombsi**

1 1 0 0 1 0 0 0 0 1 0 0 1 - 1 1 0 0 1 0 1 0 - 0 1 1 0 0 - 1 0 -
0 0 0 0 ? 0 1 1 1 0 0 0 0 0 0 - 0 0 1 0 2 0 0 0 - 0 0 0 0 - 0 0
0 0 0 - 0 0 0 0 0 0 1 0 0 0 0 0 0 0 0 0 1 1 0 0 0 1 0 0 0 0 1 0
0 1 1 0 0 0&1 0 0 ? ? ? ? ? ? ? ? ? ? ? ? ? - 0 0 0 1 0 0 0 0 0 0
- 0 0 ? 0 1 1 1 0 0 1 0 0 - - - 1 0 0 1 0 1 1 0 0 1 1 1 0 1 1 1
0 0 0 ? 1 1 0 - 0 1 0 0 0 1 0 0 0 0 0 0 1 0 1 1 0 1 0 0 0 2 1 1
1 0 0 0 ? 0 0 0 0 0 0 0 - 0 ? 0 1 0 - - 0 0 - 0 0 0 0 0 0 - 0 0
0 0 1 0 1 0 0 - 0 - 0 1 - - 0 0 0 ? 0 0 - 0 0 0 - 0

**73. Moythomasia durgaringa**

1 0 1 ? 1 0 0 0 ? 1 0 0 1 - 1 1 1 0 1 0 1 0 - 1 ? ? ? 0 - 1 1 -
0 0 0 0 ? 0 1 1 1 0 0 0 0 0 0 - 0 0 1 0 1 0 0 0 - 0 0 0 0 - 0 0
0 0 0 - 0 0 0 0 0 0 1 0 0 0 0 0 0 0 0 0 1 1 0 0 1 1 0 0 0 0 1 0
0 1 0 0 0 0 0 0 ? ? ? ? ? ? ? ? ? ? ? ? ? - 0 0 0 1 0 1 0 0 0 0 0
0 ? ? 0 ? ? 1 ? ? ? ? ? ? ? ? ? ? ? ? 1 ? 1 1 0 0 1 1 1 0 1 1 1 0
0 0 ? 1 1 0 - 0 1 0 0 0 1 0 0 0 0 0 0 1 0 1 1 ? 1 0 0 0 2 1 1 1
0 0 0 ? 0 ? ? 0 0 1 0 - 0 ? 0 1 0 - - 0 0 - 0 0 0 0 0 0 - 0 0 0
0 1 0 1 0 0 - 0 - 0 1 - - 0 0 0 ? 0 0 - ? 0 ? - 0

**74. Obaichthys decorates**

1 ? ? 0 0 0 0 ? 2 ? ? ? 0 - 1 ? 0 0 ? ? ? 1 0 1 1 0 0 ? ? 2 ? 1
3 1 1 1 1 ? 0 0 0 0 0 0 1 1 0 0 - 0 0 2 0 1 0 ? 1 2 0 0 0 0 0 1 0
0 ? 1 0 0 0 0 0 1 0 1 0 0 2 0 1 0 1 0 1 0 ? ? ? ? ? 0 1 ? ? 0 -
1 0 - - - - 1 ? - ? ? 1 1 1 1 1 ? 0 - - - ? ? ? 1 2 0 1 0 ? ? 1
0 - 1 ? ? ? ? ? ? ? ? ? ? ? ? ? ? ? ? ? ? ? ? ? ? 0 1 1 1 0 1 1 ? ?
1 1 0 0 ? 1 2 ? ? 1 ? ? 0 - 1 0 0 1 1 ? ? 0 ? 0 0 0 0 0 0 0 0 0 1
? ? ? ? 0 ? 1 ? 0 1 ? ? 0 ? 1 0 0 0 0 0 1 0 0 ? 0 0 - 1 0 0 ? ?
? 1 0 1 ? 0 - 0 - 0 ? - - 0 0 ? 0 0 0 - ? 0 ? - ?

**75. Orthocormus cornutus**

1 ? 1 0 0 0 0 ? 0 1 - 0 1 1 0 0 ? ? ? ? ? 1 1 - 1 - - 1 0 2 ? 0
1 0 0 0 - ? 0 0 0 0 0 1 ? 0 1 0 0 0 1 ? ? 0 ? ? ? ? 0 0 0 ? ? ?
? ? ? ? ? ? ? ? ? ? ? ? 0 ? ? 1 ? ? ? ? ? ? ? ? ? ? ? ? ? ? ? ?

? ? ? ? ? ? ? ? ? ? ? ? ? ? ? ? ? ? ? ? ? ? ? ? 1 ? ? ? ? ? ? ?
1 0 ? ? ? ? ? ? ? ? ? ? ? ? ? ? ? ? ? ? ? ? ? ? ? 0 1 ? ? ? ? 0 0 ?
1 ? ? ? ? ? ? ? ? ? ? ? ? ? ? ? ? ? 0 ? ? ? ? 0 1 0 0 0 1 1 ? ? 2
0 0 0 0 0 ? 0 0 ? ? 0 - ? ? 0 0 ? 0 1 ? 0 ? ? ? 0 0 ? ? 0 ? ? ?
? ? 0 ? ? ? 1 0 - 0 0 - - 0 0 0 ? 0 ? ? ? ? ? 1 ?

**76. Orthocormus roeperi**

1 ? 1 0 0 0 0 ? 0 1 - 0 1 1 0 0 ? ? ? ? ? 1 1 - 1 - - ? ? 2 ? ?
1 0 ? 0 - ? 0 0 0 0 0 1 ? 0 1 0 0 0 1 ? ? 0 ? ? ? ? 0 0 0 ? ? ?
? ? ? ? ? ? ? ? ? ? ? ? ? ? ? ? ? ? ? ? ? ? ? ? ? ? ? ? ? ? ? ?
? ? ? ? ? ? ? ? ? ? ? ? ? ? ? ? ? ? ? ? ? ? ? ? 1 ? ? ? ? ? ? ?
1 0 ? ? ? ? ? ? ? ? ? ? ? ? ? ? ? ? ? ? ? ? ? ? 0 1 0 0 ? 1 1 0 ?
? ? ? ? ? ? ? ? ? ? ? ? ? ? ? ? ? 1 0 ? ? ? ? 0 1 0 0 0 1 1 1 ? 2
0 0 0 0 0 0 0 0 ? 1 0 - - ? 0 0 ? 0 1 ? 0 ? ? ? 0 1 ? 1 0 ? ? ?
? ? 0 1 ? ? 1 0 - 0 0 - - 0 0 0 ? 0 1 1 ? 1 1 1 ?

**77. Orthocormus teyleri**

1 ? 1 0 0 0 0 1 0 1 - ? ? ? ? ? ? ? ? ? ? 1 1 - 1 - - 1 0 2 ? ?
2 0 ? ? - ? ? 0 0 0 0 1 0 0 ? ? 0 0 1 ? ? ? ? ? ? ? 0 0 0 ? 1 0
0 ? 0 0 0 0 0 0 ? 0 ? ? 0 ? 0 1 ? ? 0 1 1 ? ? ? ? ? ? ? ? ? ? ?
? ? ? ? ? ? ? ? ? ? ? ? ? ? ? ? ? ? ? ? ? ? ? ? 1 ? ? ? ? ? ? ?
1 0 ? ? ? ? ? ? ? ? ? ? ? ? ? ? ? ? ? ? ? ? ? ? 0 1 ? ? ? ? 0 0 ?
1 1 0 ? ? 1 ? ? ? ? ? ? ? ? 0 1 ? 0 ? ? ? ? ? 1 0 0 0 ? ? ? ? ?
? ? ? ? ? ? ? ? ? ? ? ? ? ? ? ? ? ? 0 1 ? 0 ? ? ? 0 ? ? ? ? ? ? ?
? ? ? ? ? ? 1 0 - 0 ? - - 0 0 ? ? 0 ? ? ? 1 1 1 ?

**78. Oshunia brevis**

1 1 0 ? 0 0 ? ? 1 1 0 1 0 1 1 0 0 0 ? 1 1 1 0 ? ? ? ? 1 1 2 1 0
1 0 0 0 - ? 0 0 0 0 0 1 1 0 1 0 0 0 2 0 1 0 ? ? ? 0 0 0 0 1 1 ?
0 ? ? 0 0 ? 0 0 1 0 1 0 0 2 0 1 0 1 0 ? 1 1 0 0 2 0 0 ? 1 ? ? ?
1 ? ? ? ? ? 1 0 - 0 0 0 ? 1 0 0 0 0 0 1 1 1 ? ? 1 2 1 1 0 1 1 1
0 0 1 ? ? ? ? ? ? ? ? ? ? ? ? ? ? ? ? ? ? ? ? ? ? 0 1 0 - 1 1 1 1 ?
1 0 0 0 ? 1 ? ? ? ? ? ? ? 0 - ? ? ? ? ? ? ? 1 ? ? ? 0 0 0 ? 0 0 0 2
1 0 0 1 0 ? 1 0 0 1 ? ? 0 1 1 ? 0 0 1 ? 1 0 0 0 0 0 ? 1 ? ? 1 ?
? 1 0 ? 0 ? - 1 0 1 1 - - 1 1 1 0 0 0 - ? 0 0 - 1

**79. Pachycormus macropterus**

1 1 1 0 0 0 0 0 0 1 - 0 1 1 1 ? 1 0 0 0 0 1 0 - 1 - - 1 0 2 1 1
2 0 0 0 - 0 0 0 0 0 0 1 1 0 1 0 0 0 2 ? 1 0 0 0 - 0 0 0 0 0 1 0
0 0 0 1 0 0 0 0 1 0 0 0 0 0 0 1 0 1 0 1 1 0 0 1 2 1 1 - 1 1 1 ?
0 0 - - - - 1 0 0 0 0 1 0 0 0 0 0 0 1 0 0 1 1 ? 1 1 1 1 1 2 1 1 1
1 1 1 2 1 1 1 ? 1 1 ? ? ? ? ? ? ? ? ? ? ? ? ? ? ? 0 1 0 - 0 1 ? ? 1
1 0 0 1 1 1 0 0 2 1 0 - 1 0 0 1 1 0 1 1 ? 0 ? 1 0 1 - 0 ? ? ? 2
0 0 0 ? ? ? 0 0 ? 1 0 - - ? 0 0 0 0 1 0 0 0 0 0 0 1 0 1 0 0 1 0
0 1 0 1 0 0 1 0 - - 0 - - 0 0 0 0 0 1 1 ? 1 - 0 1

**80. Paradapedium egertoni**

0 0 ? 0 0 0 0 0 ? 1 0 1 0 - 0 0 0 0 1 ? ? 1 0 2 1 1 ? ? ? 2 ? 0
3 ? 0 0 ? ? 0 ? 0 0 0 1 ? ? ? ? 0 0 2 ? ? 0 ? ? 2 ? 0 0 0 ? 1 0
? 1 0 ? 0 0 0 ? ? - 1 0 0 2 0 1 0 1 0 ? ? ? ? ? ? ? ? ? ? ? ? ? ?
? ? - ? ? ? ? ? ? ? ? ? ? ? ? ? ? ? ? ? ? ? ? ? ? ? ? ? ? ? ? ? ?
? ? ? 0&1 ? ? ? ? ? ? ? ? ? ? ? ? ? ? ? ? ? ? ? ? ? 0 1 1 ? 1 1 1 1
1 ? ? ? ? ? ? ? ? ? ? ? ? ? 0 - ? ? 1 ? ? ? ? ? ? ? 1 0 0 0 2 1 1
2 1 0 0 ? 0 1 1 1 ? ? ? ? ? ? ? ? ? ? ? ? ? ? ? ? ? ? ? 1 ? ? ? ?
0 ? 0 0 1 ? ? ? 0 - 0 ? - - 0 0 ? ? 0 ? ? ? 0 0 ? ?

**81. Parapholidophorus nybelini**

2 1 ? 0 0 0 ? ? 0 1 0 0 1 1 0 1 - 1 1 1 1 1 1 1 1 1 1 1 0 2 1 1
1&2 1&2 0 0 0 0 0 0 1 0 0 ? 1 0 2 1 0 0 ? ? 1 0 ? ? ? 1 1 1 0 1
? ? ? ? 1 1 ? ? 0 ? ? - 1 0 0 2 0 0 0 1 1 ? 1 ? ? ? ? ? ? ? ? ?
? ? ? ? - ? ? ? ? ? ? ? ? ? ? ? ? ? ? 0 - - ? ? ? ? 1 ? ? ? ? ?
? ? 0 0 0 - ? ? ? ? ? ? ? ? ? ? ? ? ? ? ? ? ? ? ? ? ? 0 ? 1 ? - 1 1
1 1 1 ? ? ? ? 1 0 ? ? ? ? ? 0 - 0 1 0 1 ? ? 0 ? ? ? 1 0 0 ? ? 1

? ? - - ? - ? - 1 0 1 1 0 0 1 0 0 ? 0 0 0 - 1 ? ? ? ? ? ? 1 0 0
- - - 1 0 1 ? ? 0 0 - 0 ? - - 0 0 0 ? 0 0 - ? 0 - - -

**82. Peltopleurus lissocephalus**

0 0 ? 0 1 1 0 0 0 1 0 0 1 - 1 0 1 0 1 0 0 1 0 0 0 - ? 0 - 1 0 1
2 2 0 0 1 0 1 0 0 1 - 0 0 0 0 - 0 0 2 ? ? 0 ? ? ? 0 0 0 0 ? ? ?
? ? ? ? ? ? ? ? ? - 0 0 0 1 0 0 0 0 0 1 ? ? ? ? ? ? ? ? ? ? ? ?
? ? - ? ? ? ? ? ? ? ? ? 0 ? ? ? ? ? ? ? ? ? ? ? ? ? ? ? ? ? ? ?
0 ? ? 0 ? ? ? ? ? ? ? ? ? ? ? ? ? ? ? ? ? ? ? ? 0 1 ? ? ? 0 1 0 ?
? ? ? ? ? ? ? - ? ? ? ? 0 - 0 3 1 ? 1 ? ? ? ? ? 1 0 0 0 0 0 1 2
? ? ? ? 0 ? 0 0 ? ? ? ? ? ? ? ? 0 0 0 0 0 ? ? ? 0 0 0 ? ? 0 ? 0
0 1 0 1 ? ? - 0 - 0 ? - - 0 0 0 ? 0 ? ? ? 0 - - ?

**83. Pholidoctenus sanpellegrinensis**

2 0 ? 0 0 ? 1 ? 0 1 0 1 1 1 1 0 - 1 1 1 ? 1 1 0 1 1 1 1 0 2 1 1
2 1 0 0 0 ? ? 0 1 0 0 ? 1 1 2 1 0 ? ? ? 2 ? ? 1 ? 0 1 1 0 ? ? ?
? ? ? ? ? ? ? ? ? - 0 0 ? 0 1 1 0 1 ? 1 1 ? ? ? ? ? ? ? ? ? ? ?
? ? - ? ? ? ? ? ? ? ? ? ? ? ? ? ? ? 0 - - ? ? ? ? ? ? ? ? ? ? ?
0 0 0 - ? ? ? ? ? ? ? ? ? ? ? ? ? ? ? ? ? ? ? ? ? 0 1 1 ? ? 1 1 1 ?
? ? ? ? ? ? ? ? ? ? ? ? 0 - ? 1 0 ? ? ? 0 ? ? ? 1 0 0 ? ? ? ? ?
1 0 0 ? ? ? 1 0 0 ? ? ? ? ? ? ? ? 0 0 0 ? 0 ? ? ? ? ? ? ? ? - ? -
- 1 0 ? ? ? 0 0 - 0 ? - - 0 0 0 ? 0 ? ? ? 0 - - -

**84. Pholidoctenus serianus**

2 0 ? 0 0 1 1 ? 0 1 0 1 1 1 1 0 - 1 1 1 ? 1 1 0 1 1 1 1 0 2 1 1
2 1 0 0 0 ? 0 0 1 0 0 1 1 0 2 1 0 0 2 ? 2 ? ? ? ? ? 0 1 0 ? 1 ?
0 ? ? ? ? ? ? ? ? ? 0 0 0 2 1 1 0 1 0 1 1 ? ? ? ? ? ? ? ? ? ? ?
? ? ? ? ? ? ? ? ? ? ? ? ? ? ? ? ? ? ? ? ? ? ? ? ? ? 1 ? 1 ? 2 ? ? ?
0 0 ? - ? ? ? ? ? ? ? ? ? ? ? ? ? ? ? ? ? ? ? ? 0 1 1 ? ? 1 1 1 ?
? ? ? ? ? 1 0 ? ? ? ? ? ? 0 - 1 1 ? ? ? ? 0 ? ? ? 1 0 0 0 ? ? ? 2
1 0 0 1 0 ? 1 0 0 1 0 - 1 ? 0 ? 0 0 0 ? 0 ? ? ? ? ? 0 ? ? ? - ? -
- 1 0 1 0 0 0 0 - 0 1 - - 0 0 0 ? 0 0 - ? 0 0 - -

**85. Pholidophorus latiusculus**

2 0 - - - - - - - ? ? ? ? - - ? - 1 1 ? ? 1 ? ? ? - 1 ? ? 2 ? 1
1 1 ? ? ? ? ? 0 1 1 - ? ? 0 2 1 ? ? ? ? ? ? ? ? ? 1 0 1 0 ? ? ?
? ? ? ? ? ? ? ? ? - 0 0 ? 0 0 0 1 1 1 ? ? ? ? ? ? ? ? - ? ? ? ?
? ? - ? ? ? ? ? ? ? ? ? ? ? ? ? ? ? 0 - - ? ? ? ? ? ? ? ? ? ? ?
? ? ? - ? ? ? ? ? ? ? ? ? ? ? ? ? ? ? ? ? ? ? ? ? 0 ? 1 ? 1 1 1 1 ?
? ? ? ? ? ? ? ? ? ? ? ? ? - ? 0 ? ? ? ? ? ? ? ? ? ? ? 0 ? 1 0 ? 2
1 0 0 ? 0 ? 1 0 ? ? ? ? ? ? ? ? ? 0 0 0 ? ? ? ? ? ? ? ? ? ? ? ? ?
? 1 0 ? ? ? 0 0 - 0 ? - - 0 0 ? ? 0 0 - ? 0 0 ? -

**86. Pholidorhynchodon malzannii**

2 0 1 ? 0 0 ? ? 0 1 ? 0 1 1 0 1 0 1 1 1 1 1 0 1 1 ? 1 1 ? 2 0 1
1&2 1&2 0 0 0 0 0 0 1 0 0 ? 1 0 2 1 0 0 1 ? 1 0 ? 1 2 1 0 1 0 0
? ? ? ? ? ? 1 0 ? ? ? - 1 0 0 2 0 0 1 1 1 ? 1 ? ? ? ? ? 0 ? ? ?
? ? ? ? - ? ? ? ? ? ? ? ? ? ? ? ? ? ? 0 - - ? ? ? ? 1 1 1 0 2 1
1 1 0 1 0 - ? ? ? ? ? ? ? ? ? ? ? ? ? ? ? ? ? ? ? ? ? 0 ? 1 ? 0 1 1
1 1 ? ? 0 ? ? ? ? ? ? ? ? ? 0 - 0 1 0 0 1 ? 0 ? ? ? 1 0 0 ? 1 ?
? - 1 0 0 1 0 0 ? ? ? ? ? ? ? ? ? ? ? 0 0 0 0 0 0 0 ? ? ? ? 1 0 0
- - - 0 0 1 ? ? 0 0 - 0 1 - - 0 0 0 ? 0 ? ? ? 0 0 - 0

**87. Platysomus superbus**

0 ? ? ? 0 ? ? - - 1 0 0 1 - 1 1 1 0 1 0 0 1 0 1 1 1 0 0 - 1 0 -
0 0 0 0 ? 0 0 1 1 ? ? 0 0 0 0 - 0 ? 2 ? 2 ? ? ? ? 0 0 0 0 ? ? ?
? ? ? ? ? ? ? ? ? - 0 0 0 1 0 0 0 0 0 0 ? ? ? ? ? ? 0 1 ? ? ? ?
? ? - ? ? ? ? ? ? ? ? ? ? ? ? ? ? ? ? ? ? ? ? ? ? ? 1 2 1 0 ? 0 0 1
? ? ? 0 ? ? ? ? ? ? ? ? ? ? ? ? ? ? ? ? ? ? ? ? ? 0 1 1 1 ? 1 1 1 ?
? ? ? ? ? ? ? ? ? ? ? ? 0 - ? 3 0 ? ? ? ? ? ? ? ? 0 0 0 0 0 0 0 2
? ? 0 ? 0 ? 0 ? ? ? ? ? ? ? ? ? ? 0 - - ? 0 ? ? ? 0 1 0 ? ? 0 ? ?
? 1 0 1 0 ? - 0 - 0 ? - - 0 ? 0 ? 0 ? ? ? 0 0 ? 0

**88. Polypterus bichir**

0 1 0 0 1 0 0 0 0 0 0 0 0 - 0 1 0 0 1 1 0 - - 2 1 1 0 0 - 1 0 ?
3 0 ? ? ? 0 1 1 0 0 0 0 0 0 0 0 - 0 0 2 0 2 0 0 1 0 0 0 0 0 - 1 1
0 1 0 - 0 0 0 1 0 0 1 0 0 0 0 0 0 0 0 0 0 0 1 0 0 1 1 - 0 0 1 -
1 ? - ? ? ? 1 0 ? ? ? ? 0 ? 0 0 0 0 - - 0 0 0 0 1 2 1 1 0 0 0 1
0 0 1 1 1 0 1 0 1 0 1 1 0 0 0 ? ? ? ? ? 1 1 0 0 1 1 1 0 0 0 0 1
0 0 0 0 1 0 - 1 1 0 0 1 0 - 0 3 0 0 1 0 1 0 0 0 0 0 0 0 ? 0 0 2
0 0 0 1 0 1 1 1 0 1 0 - 0 1 0 0 0 0 0 0 0 0 0 0 0 0 0 - 0 - 0 0 0
0 1 1 ? 0 0 - ? - 0 ? - - 0 0 0 0 0 0 - ? 0 0 - 0

**89. Propterus elongates**

1 1 0 0 0 0 ? ? ? 1 1 1 0 1 0 ? 0 1 1 1 0 1 0 ? ? ? ? 1 1 2 ? -
0 2 0 1 0 ? 0 0 1 0 0 1 1 0 0 - 0 0 2 ? ? ? ? ? ? 0 0 0 0 ? 1 ?
0 ? 0 ? ? ? 0 0 ? 0 1 0 0 2 0 - 1 0 1 1 0 ? ? ? ? ? 0 1 ? ? ? ?
? ? - ? ? ? ? ? ? ? ? ? 0 ? ? ? ? ? ? ? ? ? ? ? 1 ? ? ? ? ? ? ?
0 ? ? 0 ? ? ? ? ? ? ? ? ? ? ? ? ? ? ? ? ? ? ? ? 0 1 1 ? ? 1 1 1 ?
1 1 0 ? ? ? 0 ? ? ? ? ? ? 0 - 0 3 0 1 1 0 0 ? ? 0 ? 0 0 0 ? ? ? 2
? ? ? 1 ? 1 1 0 ? 1 ? ? ? 1 0 0 0 - - 0 1 0 0 ? 0 0 0 1 0 1 1 ?
? 1 0 1 0 0 - 0 - 0 ? - - 0 0 ? ? 0 ? ? ? 0 0 - 0

**90. Pteronisculus stensioi**

1 1 0 0 1 0 0 0 0 1 0 0 1 1 1 1 1 0 1 0 0 1 0 1 1 0 0 1 0 2 0 1
2 0 0 0 ? 0 1 1 1 0 0 0 0 0 0 - 0 0 1 0 1 0 0 0 - 0 0 0 0 - 0 0
0 0 0 - 0 0 0 0 0 0 0 0 0 0 0 0 0 0 0 0 0 1 1 0 0 2 2 0 1 0 1 1 1
0 1 1 1 0 1 0 0 ? ? ? ? ? ? ? ? ? ? ? ? ? - 0 0 0 1 0 1 1 0 0 0 0
0 ? 0 0 1 1 1 1 1 1 1 1 1 0 0 1 1 1 1 0 ? ? ? 0 1 1 1 0 ? ? ? 1
0 1 0 1 1 0 - 0 1 0 0 0 1 0 0 0 0 0 1 1 ? ? 1 0 1 0 0 0 1 1 1 2
0 0 0 0 0 0 0 0 0 0 0 - 0 ? 0 1 0 0 0 0 0 0 - 0 0 0 0 0 0 0 - 0 0 0
0 1 0 1 0 0 - 0 - 0 ? - - 0 0 0 0 0 0 - 0 0 - - 0

**91. Rhinconichthys purgatoirensis**

1 1 ? ? ? ? ? ? ? ? - ? ? ? ? ? 0 0 0 ? ? 1 0 ? 1 ? ? 1 0 - - -
? ? - - - - 0 0 1 1 - 1 0 0 1 0 0 1 - - 2 ? ? ? ? 0 0 0 0 ? 1 0
0 ? 0 0 0 0 0 ? ? 0 0 0 0 1 0 ? 0 ? ? ? 1 ? ? ? ? ? ? ? ? ? ? ?
? ? ? ? ? ? ? ? ? ? ? ? ? ? ? ? ? ? ? ? ? ? ? ? ? ? ? ? ? ? ? ?
1 ? ? 2 ? ? ? ? ? ? ? ? ? ? ? ? ? ? ? ? ? ? ? ? ? ? ? ? ? ? ? 0
1 1 0 ? ? 1 0 ? ? ? 0 - ? ? 0 ? ? ? ? 1 ? 0 0 1 ? 1 ? ? ? ? ? ?
? ? ? ? ? ? ? ? ? ? ? ? ? ? ? ? ? - ? ? ? 0 ? ? ? ? ? ? ? ? 0 ? ?
? ? 0 ? ? ? 0 0 - - 0 - - - 0 - ? 1 ? ? ? 1 0 0 ?

**92. Richmondichthys sweeti**

1 0 0 1 0 1 0 ? ? 1 ? 0 0 - 0 0 - - ? ? - 1 0 0 1 1 0 0 - 2 1 0
2 1 0 0 1 ? 0 1 0 1 - 1 0 0 0 - 0 1 - ? 2 1 ? 0 - 0 0 0 1 0 1 ?
0 ? 1 ? 1 1 1 ? ? ? 0 0 0 2 0 0 0 0 ? ? 0 1 0 1 2 2 0 0 1 1 0 -
1 0 - ? ? ? 0 0 ? 0 ? 1 ? ? ? 0 0 1 0 0 1 1 0 ? 1 2 1 1 2 1 1 1
0 0 1 ? 0 1 0 1 1 1 1 1 0 1 0 1 0 0 0 - ? ? ? 0 1 1 0 ? ? ? ? 0
1 ? ? ? 0 ? ? ? ? ? ? ? 0 - 0 ? ? 0 1 ? 0 ? ? ? ? ? ? ? ? ? ? ?
? ? ? ? ? ? ? ? ? ? ? ? ? ? ? ? 0 0 0 1 ? 1 0 0 0 ? ? 0 ? ? ? 0 -
- 1 0 ? 0 ? - 0 - 0 ? 0 1 0 0 0 - 0 ? 0 0 0 - 0

**93. Robustichthys luopingensis**

0 1 0 0 0 0 ? 0 1 0 1 1 0 1 1 0 0 0 1 1 1 1 0 0 1 ? 0 1 1 2 0 0
3 1 0 0 0 ? 0 1 0 0 0 1 1 0 1 0 0 0 2 ? 1 0 ? 1 2 0 0 0 0 1 1 1
0 ? 0 0 0 0 0 0 1 0 ? 0 0 2 0 0 0 1 0 ? 1 ? ? ? ? ? ? ? ? ? ? ?
? ? ? ? ? ? ? ? ? ? ? ? ? ? ? ? ? ? ? ? ? ? ? ? ? 1 ? 1 ? 0 ? ? ?
0 0 ? 0&1 ? ? ? ? ? ? ? ? ? ? ? ? ? ? ? ? ? ? ? ? ? 0 1 0 - 1 1 1 1
1 1 1 0 0 1 1 1 0 1 ? 0 0 1 0 0 2 ? ? ? ? 1 ? ? ? 0 0 0 0 0 0 0
2 1 0 0 1 0 ? 1 0 0 1 ? ? 0 ? ? 0 0 1 1 0 1 0 0 ? 0 0 0 ? ? 0 1
1 0 1 0 1 0 ? 0 1 0 1 ? - - 0 0 0 0 0 0 - ? 0 0 - ?

**94. Saurichthys madagascarensis**

1 1 ? ? 0 0 - - - 1 - 0 1 1 0 0 0 1 0 ? ? 1 0 0 1 1 0 1 - ? 0 0
1 1 0 0 0 0 1 1 1 0 0 0 0 0 0 0 - 0 0 2 ? 1 ? ? ? ? 0 0 0 0 ? 0 0
0 0 0 ? ? ? 0 0 0 0 - - 0 0 0 0 0 0 0 0 1 0 1 0 ? 2 2 1 - ? 1 0 -
0 ? - ? ? ? 0 ? ? ? ? ? ? ? ? ? ? ? ? ? ? - ? ? 0 1 2 1 0 0 ? ? ?
0 ? ? 0 0 1 1 0 1 1 1 ? ? ? ? ? ? ? ? ? ? ? ? ? ? 0 1 0 0 0 1 1 1 ?
? ? ? ? ? ? ? ? ? ? ? ? ? 0 - 0 ? 0 0 1 1 1 ? 1 0 0 0 0 0 2 1 1 1
0 0 0 1 0 1 1 1 ? ? ? ? ? 0 ? ? 1 0 0 0 0 0 ? ? ? 0 0 0 0 - ? 0 0
0 1 0 ? 0 0 - 0 - ? ? - - ? 0 0 ? ? 0 - ? 0 0 - ?

**95. Saurostomus esocinus**

1 1 1 0 0 0 0 0 0 1 - 0 1 1 1 ? 1 0 0 ? ? 1 0 - 1 - - 1 0 - - -
0 0 - - - - 0 0 0 0 0 1 0 0 1 0 0 0 1 ? 1 0 1 0 - 0 0 0 0 0 1 0
0 ? 0 0 0 0 0 0 1 0 0 0 0 2 0 - 0 1 0 1 1 ? ? ? ? ? 1 - ? ? ? ?
? ? ? ? ? ? ? ? ? ? ? ? ? ? ? ? ? ? ? ? ? ? ? ? ? 1 ? 1 1 2 1 1 1
1 ? ? 2 ? ? ? ? ? ? ? ? ? ? ? ? ? ? ? ? ? ? ? ? ? 0 1 0 0 0 0 0 1 1
1 0 0 ? 0 1 1 2 ? ? 0 - 0 - 0 1 ? 0 1 1 0 0 1 1 0 1 - 1 1 1 1 2
0 0 0 0 0 0 0 0 ? 1 0 - - ? 0 0 - - - ? 0 0 0 ? 0 1 0 ? 0 0 0 0
0 1 0 1 0 0 1 0 - - 0 - - - 0 - 0 1 1 0 ? 1 0 0 ?

**96. Scanilepis dubia**

0 0 ? ? 1 0 ? ? ? 1 ? ? 0 - ? ? 0 0 1 ? ? 1 0 1 1 ? ? ? ? 1 ? 1
3 2 0 ? 0 ? 1 1 1 0 0 0 ? 0 0 - 0 0 2 ? ? ? ? ? ? 0 0 0 0 ? ? ?
? ? ? ? ? ? ? ? ? - 0 ? 0 0 0 0 0 0 0 0 ? ? ? ? ? ? ? ? ? ? ? ? ?
? ? - ? ? ? ? ? ? ? ? ? ? ? ? ? ? ? ? ? ? ? ? ? ? ? ? ? ? ? ? ? ?
? ? ? 0 ? ? ? ? ? ? ? ? ? ? ? ? ? ? ? ? ? ? 1 1 0 0 1 1 1 1 0 0 0 ?
? ? ? ? ? ? ? ? ? ? ? ? ? 0 - ? 3 ? ? ? ? 0 ? ? ? ? 0 0 0 ? ? ? 2
? ? ? ? ? ? ? ? ? ? ? ? ? ? ? ? ? 0 0 0 ? 0 ? ? ? ? 1 0 ? ? ? ? ?
? 0 0 ? ? ? - 0 - 0 ? - - 0 0 ? ? 0 ? ? ? 0 0 ? 0

**97. Scopulipiscis saxciput**

0 0 ? ? ? ? ? ? ? ? ? ? ? - ? ? 1 0 ? 0 ? 1 0 ? ? ? ? ? ? ? ? ?
? ? ? ? ? ? ? ? ? ? ? ? ? ? ? ? ? ? ? ? ? ? ? ? ? ? ? ? ? ? ? ? ?
? ? ? ? ? ? ? ? ? - ? ? ? ? ? ? ? ? ? ? ? 1 0 ? 2 2 0 1 1 1 0 -
1 1 1 0 0 ? ? 0 ? ? ? ? ? ? ? ? ? ? ? ? ? 1 1 1 1 2 1 0 2 1 0 0
? ? ? ? ? ? ? 1 1 1 ? ? ? ? ? 1 1 0 1 0 ? ? ? ? ? ? ? ? ? ? ? ? ?
? ? ? ? ? ? ? ? ? ? ? ? ? ? - ? ? ? ? ? ? ? ? ? ? ? ? ? ? ? ? ? ?
? ? ? ? ? ? ? ? ? ? ? ? ? ? ? ? ? ? ? ? ? ? ? 1 1 1 ? ? ? ? 1 0 ? ?
? ? ? ? 0 ? ? 0 - 0 ? ? ? ? ? ? ? ? ? ? 0 0 ? ? 0

**98. Siemensichthys microcephalus**

1 1 ? 0 ? 0 1 ? 0 1 0 0 1 1 0 0 0 1 ? ? ? ? ? 0 1 ? 0 1 ? 2 1 -
0 1 0 0 ? ? 0 0 0 0 0 1 1 0 1 0 0 0 2 ? 1 1 - ? ? ? 0 1 0 ? ? ?
? ? ? ? ? ? 0 1 1 0 0 0 0 2 0 1 0 1 ? 1 0 1 0 ? 2 2 0 ? 1 ? 1 -
1 0 - - - - 1 0 0 ? ? 0 0 0 0 0 0 1 ? ? 1 ? 1 1 1 2 1 0 2 1 ? 1
0 1 0 0 ? ? ? ? ? ? ? ? ? ? ? ? ? ? ? ? ? ? ? ? ? 0 1 1 1 ? ? ? ? ?
1 0 1 ? 1 ? ? ? ? ? ? ? ? 0 - ? ? 1 0 1 ? ? ? ? ? ? ? ? ? ? ? ? ? ?
? ? 1 ? ? ? ? ? ? ? ? ? ? ? ? ? ? ? 0 - - ? ? 0 0 0 ? ? ? ? 1 0 0 ?
? 1 1 1 0 ? 0 ? - 0 ? - - 0 0 0 - 0 ? ? ? 0 0 - 0

**99. Siemensichthys siemensi**

? ? ? ? ? ? ? ? ? ? 0 ? ? ? ? ? ? 1 ? ? ? ? ? 0 1 ? 0 1 0 2 1 0
1 ? 0 0 ? ? 0 0 0 0 0 1 1 0 1 0 0 0 2 ? 1 1 - 1 2 ? 0 1 0 0 1 ?
0 1 ? 1 0 0 0 ? ? ? ? ? 0 2 0 1 0 ? 0 1 0 ? ? ? ? ? ? ? ? ? ? ? ?
? ? ? ? ? ? ? ? ? ? ? ? ? ? ? ? ? ? ? ? ? ? ? ? ? ? ? ? ? ? ? ? ?
0 1 ? ? ? ? ? ? ? ? ? ? ? ? ? ? ? ? ? ? ? ? ? ? 0 1 1 ? ? 1 1 1 ?
1 ? 1 ? 1 1 0 ? ? ? ? ? 0 - ? 0 ? 0 ? ? ? ? ? ? 1 0 0 0 0 0 0 2
? ? 1 ? ? ? 1 0 ? ? ? ? ? ? ? ? 0 0 0 - 1 ? ? ? ? ? ? ? ? ? ? 0
0 ? 1 1 ? ? 0 ? - 0 ? - - 0 0 0 - 0 ? ? ? ? ? - ?

**100. Spathiurus dorsalis**

1 1 0 0 0 1 ? ? 1 1 0 1 0 1 1 0 1 1 ? ? ? 1 0 0 1 1 ? 1 ? 2 0 ?
? 2 0 0 0 ? ? 0 0 0 0 1 1 0 1 0 0 0 2 ? 1 0 0 1 2 0 0 0 0 1 1 ?
? ? ? 0 ? 0 0 ? ? ? 0 0 0 2 0 ? 0 1 0 ? 1 ? ? ? ? ? ? ? ? ? ? ?

? ? ? ? ? ? ? ? ? ? ? ? ? ? ? ? ? ? ? ? ? ? ? ? ? ? ? ? ? ? ? ?
? ? ? ? ? ? ? ? ? ? ? ? ? ? ? ? ? ? ? ? ? ? ? ? ? 0 ? ? ? ? 0 1 1 ?
? ? ? ? ? 1 1 ? ? ? ? ? ? 0 - ? ? ? ? ? ? ? ? ? 1 ? 0 0 0 ? ? ? ? 2
? ? ? ? ? ? 1 0 0 1 0 0 0 1 0 0 0 0 ? 0 1 ? ? ? ? ? ? ? ? ? ? ? ? ?
? 1 0 ? ? ? 0 ? ? ? 1 - - 1 1 1 1 0 0 - ? 0 ? ? 0

**101. Tanaocrossus kalliokoskii**

? ? ? ? ? ? ? ? ? ? ? ? ? - ? ? ? ? ? ? ? ? 1 ? 1 ? ? ? ? ? ? ? ? ?
? ? ? ? ? ? ? 1 ? ? ? ? ? ? 0 - ? ? ? ? ? ? ? ? ? ? ? ? ? ? ? ? ? ?
? ? ? ? ? ? ? ? ? - 0 ? ? ? ? ? 0 0 0 ? ? ? ? ? ? ? ? ? ? ? ? ? ? ?
? ? ? ? ? ? ? ? ? ? ? ? ? ? ? ? ? ? ? ? ? ? ? ? ? ? ? ? ? ? ? ? ? ?
? ? ? ? ? ? ? ? ? ? ? ? ? ? ? ? ? ? ? ? ? ? ? ? ? ? ? ? 1 ? 1 ? ? ? ?
? ? ? ? ? ? ? ? ? ? ? ? ? - ? ? ? ? ? ? ? ? ? ? ? ? 0 0 ? ? ? ? ?
? ? ? ? ? ? 1 1 ? ? ? ? ? ? ? ? ? ? ? ? ? ? ? ? ? 0 0 0 ? ? ? ? ?
? 1 0 1 ? ? - 0 - ? ? ? ? ? ? ? ? ? ? ? ? ? ? 0 ? ?

**102. Tetragonolepis oldhami**

0 0 ? ? 0 0 0 ? ? ? 0 0 ? ? ? ? ? 0 ? ? ? 1 0 0 ? ? ? ? ? ? ? ? ?
3 ? ? ? ? ? 0 ? 0 0 0 1 ? ? ? ? ? 0 0 2 ? ? ? ? ? ? ? ? ? 0 0 ? ? ?
? ? ? ? ? ? ? ? ? - 0 1 0 2 0 1 0 1 0 1 1 ? ? ? ? ? ? ? ? ? ? ? ? ?
? ? - ? ? ? ? ? ? ? ? ? ? ? ? ? ? ? ? ? ? ? ? ? ? ? ? ? ? ? ? ? ? ?
? ? ? ? ? ? ? ? ? ? ? ? ? ? ? ? ? ? ? ? ? ? ? ? ? ? 0 1 1 ? ? 0 0 1 ?
? ? ? ? ? ? ? ? ? ? ? ? ? ? - ? 3 1 ? 1 ? ? ? ? ? 1 0 0 0 2 ? 1 2
1 0 0 ? 0 1 1 1 ? ? ? ? ? ? ? ? 0 ? ? 1 ? 1 ? ? ? ? 1 1 1 ? ? 0 1 ?
? 0 0 1 ? ? - 0 - ? ? - - ? 0 ? ? ? ? ? ? ? ? 0 ? ?

**103. Tetragonolepis semicincta**

0 0 0 0 0 0 0 0 1 1 0 0 0 1 1 0 0 0 ? 0 1 1 0 0 1 0 0 1 0 2 1 0
3 1 0 0 0 0 0 0 0 0 0 0 1 1 0 0 - 0 0 2 ? 1 0 ? ? ? 0 0 0 0 0 1 0
0 1 0 0 ? ? 0 1 ? 0 1 0 0 2 0 1 0 1 0 1 1 1 0 ? ? 2 0 1 1 ? 0 -
1 ? - ? ? ? 0 ? ? ? ? ? ? ? ? ? ? 0 - 1 ? ? ? ? 1 ? 1 ? 2 1 1 ?
? ? ? 2 ? ? ? ? ? ? ? ? ? ? ? ? ? ? ? ? ? ? ? ? ? 0 1 1 ? 0 1 0 1 1
? 1 0 0 0 1 1 ? ? ? ? ? 0 - 0 3 1 0 1 ? 0 1 1 0 1 0 0 0 2 0 1 2
1 0 0 1 0 1 1 1 ? 1 0 - 0 0 0 0 0 0 1 0 1 ? ? ? 1 1 1 1 0 1 1 ?
? 1 0 1 0 0 - 0 - 0 ? - - 0 0 0 0 0 0 - ? 0 - ? 0

**104. Tharsis elleri**

0 ? 0 0 0 0 1 0 0 1 0 0 0 - ? 0 0 0 ? 0 1 ? ? 0 1 ? 0 ? ? 2 1 ?
0 1 1 0 0 1 0 0 0 0 0 1 1 0 2 0 0 0 2 ? 2 1 - 1 3 1 0 0 0 ? 1 0
0 ? 0 1 ? ? 0 ? ? ? ? ? ? 0 2 0 1 0 1 0 ? ? 1 ? ? ? ? ? ? ? ? ? ?
? ? - ? ? ? ? ? ? ? ? ? ? ? ? ? ? - 1 0 0 ? ? ? ? 1 ? ? ? 2 ? ? ?
? ? 0 0 ? ? ? ? ? ? ? ? ? ? ? ? ? ? ? ? ? ? ? ? ? 0 1 1 1 ? 1 ? 0 1
1 ? ? ? ? 1 0 ? ? ? 1 ? 0 - ? ? ? ? ? ? ? 1 ? ? ? 1 ? ? 0 1 ? ? ?
? 0 1 ? 0 ? 1 0 ? 1 1 4 1 0 0 0 0 0 0 0 1 ? 0 ? 0 ? 0 1 0 0 ? -
- 1 0 1 0 0 0 ? - 0 1 - - 0 0 0 - 0 0 - ? 0 - ? 0

**105. Vinctifer comptoni**

1 0 0 1 0 1 0 0 0 1 1 0 0 - 0 0 - 1 ? 0 0 1 1 0 1 1 0 0 - 2 0 1
2 1 0 0 1 ? 0 1 0 0 0 1 0 0 0 - 0 0 2 ? 2 ? ? 0 - 0 0 0 1 1 1 0
0 ? ? 0 1 0 0 1 1 0 0 0 0 2 0 0 0 0 0 1 0 1 0 ? 2 ? 0 0 1 1 0 -
1 ? ? ? ? ? 0 0 ? 0 ? 0 ? ? ? 0 0 1 0 0 ? 1 0 ? 1 2 1 1 2 1 1 ?
0 0 1 ? 1 1 0 1 1 1 1 1 0 1 0 1 0 0 0 - ? ? ? 0 1 1 0 ? 0 0 0 0
? ? 0 ? ? 1 0 ? ? ? ? ? 0 - 0 3 1 0 1 ? 0 ? ? 1 ? 0 0 0 0 0 0 1
1 ? ? ? 0 ? 1 0 ? ? ? ? 0 0 ? 0 0 0 1 ? 1 0 0 0 0 0 0 1 1 1 0 -
- 1 0 ? 0 ? - 0 - 0 0 0 0 0 0 0 ? 0 0 - 0 ? 0 - -

**106. Vinctifer longirostris**

1 0 0 1 0 1 0 0 0 1 1 0 0 - 0 0 - 1 ? 0 0 1 1 0 1 1 0 0 - 2 0 1
2 1 0 0 1 ? 0 1 0 0 0 1 0 0 0 - 0 0 2 ? 2 ? ? 0 - ? 0 0 1 1 1 0
0 ? 1 0 1 0 0 ? ? 0 0 0 0 2 0 0 0 0 0 ? ? ? ? ? ? ? ? ? ? ? ? ? ?
? ? ? ? ? ? ? ? ? ? ? ? ? ? ? ? ? ? ? ? ? ? ? ? ? 1 ? ? ? 2 1 ? ?
0 0 ? ? ? ? ? ? ? ? ? ? ? ? ? ? ? ? ? ? ? ? ? ? ? 0 1 1 0 ? 0 0 0 0
? ? ? ? ? 1 0 ? ? ? ? ? ? ? ? 3 ? ? ? ? 0 ? ? ? ? ? ? ? ? 0 0 0 1

? ? ? ? 0 ? 1 0 ? ? ? ? 0 0 ? ? 0 0 1 ? 1 ? 0 ? 0 0 0 1 1 1 ? -
- 1 0 ? 0 ? - ? ? 0 0 0 0 0 0 0 ? 0 0 - ? ? - - -

**107. Watsonulus eugnathoides**

0 1 0 0 0 0 1 1 1 1 1 0 0 0 0 0 1 0 0 0 1 1 0 0 0 1 0 1 1 2 1 -
0 1 0 0 1 0 0 0 1 0 0 1 1 1 1 0 0 0 2 ? 1 0 0 1 2 0 1 0 0 1 1 ?
0 1 0 0 0 0 0 ? 1 - 1 0 0 1 0 1 0 1 1 0 1 1 ? 1 2 2 0 1 1 ? 1 1
0 0 - - - - 1 0 1 0 0 0 1 ? 0 0 0 0 - - 0 1 1 1 1 2 1 1 0 0 0 0
0 0 ? 0&1 ? ? ? ? ? ? ? ? ? ? ? ? ? ? ? 1 0 ? ? ? 0 1 ? ? ? ? ? ?
1 1 0 0 0 ? 1 0 ? ? ? 0 ? 1 0 0 0 0 ? 1 1 1 ? ? ? 1 0 0 0 0 0 0
2 ? ? 0 - 0 ? 1 0 ? ? 0 - 0 ? 0 0 0 - - 0 0 0 0 ? 0 ? - 1 0 0 0
0 0 1 0 1 0 ? 0 0 - 0 ? - - 0 0 0 0 0 0 - ? 0 0 - 0

**108. Zambellichthys bergamensis**

2 0 ? 0 0 0 ? ? 0 1 - 0 1 1 1 1 - 1 1 1 0 1 ? 0 1 ? 1 1 0 2 0 1
3 ? 0 0 ? 0 0 0 1 0 0 ? 1 ? 2 1 0 ? ? ? 1 ? ? 1 2 ? 0 1 0 0 ? ?
? ? ? ? 1 0 ? ? ? - 1 0 0 2 0 0 1 1 1 ? 1 ? ? ? ? ? ? ? ? ? ? ?
? ? - ? ? ? 0 ? ? ? ? ? ? ? ? ? ? 0 - - ? ? ? ? 1 ? 1 ? ? ? ? ?
0 0 0 - ? ? ? ? ? ? ? ? ? ? ? ? ? ? ? ? ? ? ? ? 0 ? 1 ? - 1 ? ? ?
? ? ? ? ? ? ? ? ? ? ? ? 0 - 0 ? 1 0 1 ? ? ? ? ? 1 ? ? ? ? ? ? ?
- - 0 - ? - ? ? ? ? ? ? ? ? ? ? 0 0 0 - 0 ? ? ? ? ? ? ? ? 0 - -
- 0 0 1 ? ? 0 0 - 0 1 - - 0 0 0 ? 0 ? ? ? ? ? - -

## A.4 Annotated TNT Command Scripts

### A.4.1 TNT script used to perform phylogenetic analyses in Chapter 3 and Chapter 4

```
mxram1000;

##File, Open Input File

hold100000;

outgroup 72;

##Nb. TNT can only set one taxon as an outgroup. TNT starts
counting taxa from 0. Here, the outgroup taxon is 72:
Moythomasia_durgaringa.

ccode+52+97+98+121;

##Converting the NEXUS file to TNT will removes ordered
characters, so they need to be re-added here. TNT starts
counting characters from 0 too.

xmult=level10;

##generates starting trees

bbreak=fillonly;

##runs the complete analysis

nelsen*;

##generates the consensus tree

export -[FILENAME].tre;

##The final tree file in this file is the consensus tree

export= [FILENAME].tre;
```

### A.4.2 TNT script used to generate bootstrap trees in Chapter 5:

```
macro=;
var:
;
tsave* boottrees.tre;
resample boot repl 1000 freq allow
[
     mult 10;
     save;
]
;
ts/;
k0;
proc boottrees.tre;
##generates list of bootstrap trees
log LSI.out;
##creates and outputs LSI file, for use in R and RogueNaRok
quote Terminal LSI;
log/;
log+ LSI.out;
taxcode+;
tcomp !!;
log/;
proc/;
```

## A.5 Approximate reconstruction of NHMUK PV OR 37795 A and B (counterpart) specimens.

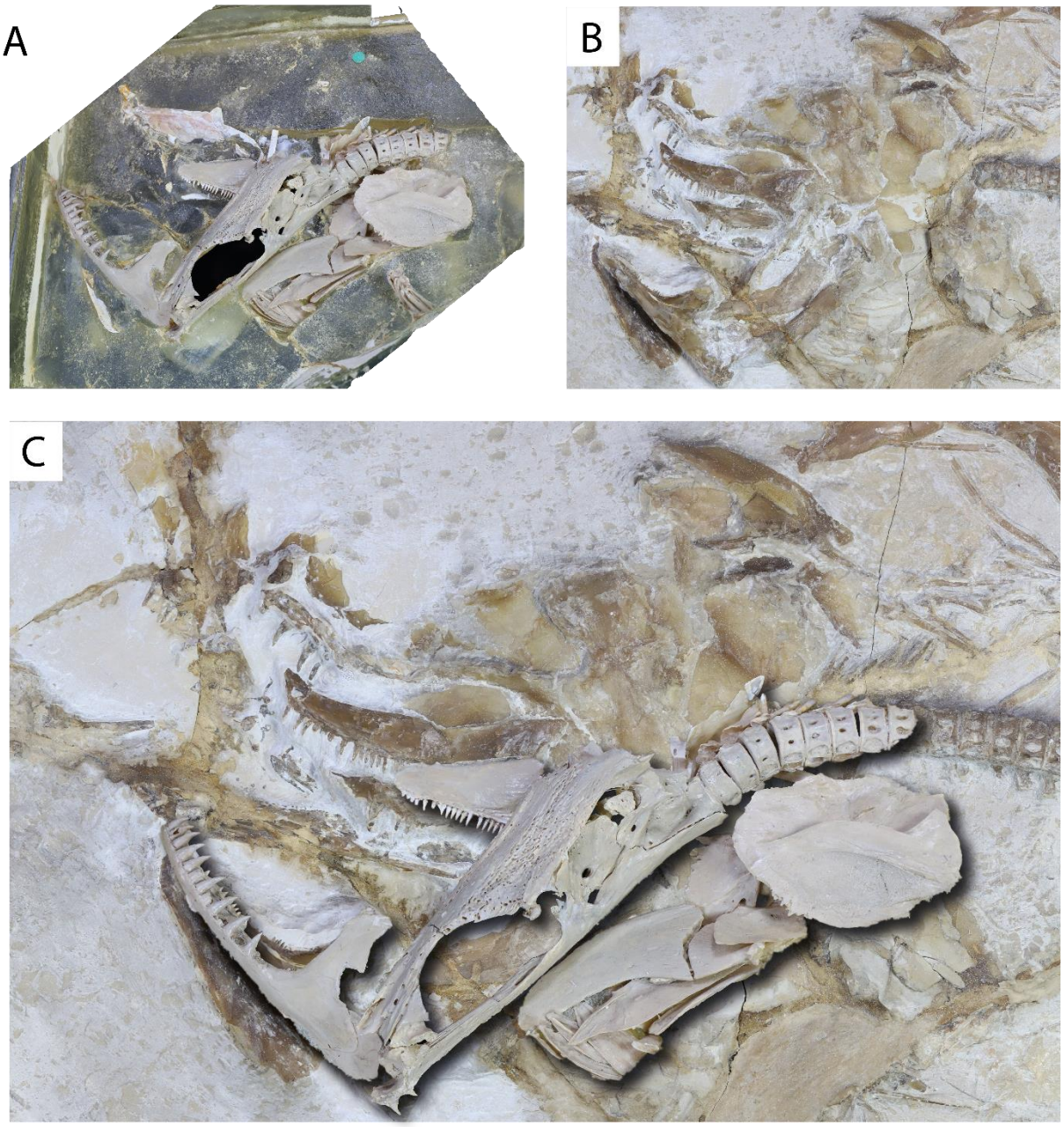


**Approximate reconstruction of NHMUK PV OR 37795A and NHMUK PV OR 37795AB (counterpart) specimens.** The most complete elements from the acid prepared A specimen (A) were digitally masked and superimposed over the remaining B specimen (B), using the position of the spine and coronoid process as guides to prove that both specimens are the same individual (C).

## A.6 List of Figures

### Chapter 1



### Chapter 2

Chapter 3



Chapter 4

## A.7 List of Tables

Chapter 5